Srinivasan Chandrasekaran

Dynamic Analysis and Design of Offshore Structures

Second Edition

Springer

Ocean Engineering & Oceanography

Volume 9

Series editors

Manhar R. Dhanak, Florida Atlantic University SeaTech, Dania Beach, USA
Nikolas I. Xiros, New Orleans, USA

Srinivasan Chandrasekaran

Dynamic Analysis and Design of Offshore Structures

Second Edition

Springer

Srinivasan Chandrasekaran
Department of Ocean Engineering
Indian Institute of Technology Madras
Chennai, Tamil Nadu
India

To
My parents, teachers, family members
and friends

Foreword

I consider it a great privilege to write a "Foreword" for this excellent book authored by Prof. Chandrasekaran of Indian Institute of Technology Madras. He has succeeded in closing a very evident gap namely unavailability of a suitable textbook dealing with the dynamic analysis and design of offshore structures for undergraduate and graduate students. As he has included elements of recent research into the topics, this book becomes ideal for research students also. Inclusion of large number of worked examples, objective/subjective type exercises with solution keys and MATLAB programs make it more valuable. I have recommended this book to undergraduate students in civil engineering majoring on "offshore structures", postgraduate students doing M.Sc. in "offshore engineering" as well as postgraduate research students working on related topics at my University.

Chapter 1 on "Introduction to Offshore Platforms" is very much informative dealing with all basic information needed. The excellent quality of illustrative figures and the large number of objective and subjective exercises with solutions make it very much valuable. Chapter 2 deals with "Environmental Forces". The various components of wind, wave, current, ice/snow, marine growth, earthquake loads as well as the mass/additional mass/damping effects have been dealt with. All other loads such as dead, live, fabrication, installation, lifting, load-out, transportation, launching, upending, and accidental components are explained. The chapter on "Introduction to Structural Dynamics" is exhaustive starting from the fundamentals and covering all aspects related to the dynamic equations and solutions. There are about 90 solved numerical examples and two MATLAB programs along with many additional exercises and examples to facilitate the understanding. The important aspect of "Damping" is covered in Chap. 4. "Hydrodynamic Response of Perforated Offshore Members" is covered in Chap. 5, where results of experimental and numerical studies are explained and compared in detail. The chapter on "Stochastic Dynamics" deals with very important topics like response spectrum, reliability, fatigue, and stress concentration factor. The final chapter on "Applications" describes detailed studies on Triceratops as well as TLP, dealing with the significance of springing and ringing responses. The experimental

investigations on VIV suppression systems and Buoyant Leg Storage and Regasification Platforms are of great research interest recently.

Based on my 50 years of academic/research/consultancy experience, I am very glad to recommend this book for the senior undergraduate and postgraduate students of civil, structural, applied mechanics, mechanical, naval arch, ocean, offshore, and marine engineering programs. Also, this book will serve as a very good reference book for practicing engineers working on related topics.

Prof. Dr. Kurian V. John, Director
Deep Water Technology Research Cluster
Universiti Teknologi PETRONAS
Bandar Seri Iskandar
Perak, Malaysia

Preface to Second Edition

The book titled Dynamic Analysis and Design of Offshore Structures: Second Edition is updated with recent advancements in the field of research in deep-water offshore platforms. The author felt the necessity to update the contents by including experimental and numerical investigations carried out on new-generation offshore platforms. This edition includes many solved examples and exercise for self-learning, in addition to computer codes for various applications in dynamic analyses. Basic intention is to make it a widely accepted textbook for the senior under graduate and postgraduate students of civil, structural, applied mechanics, mechanical, aerospace, naval arch, and ocean engineering program. This new edition will also have valuable contents with respect to new and recent research carried out by the author in structural dynamics. Each chapter is updated with a section of frequently asked Q&A in the form of exercise, which is likely to enhance understanding of this complex subject, through easy and self-explanatory text.

To encourage easy learning and a better tool for classroom teaching, this edition is also supported with slide presentation to conduct the course in a complete classroom mode. This edition is also an outcome of a few short courses conducted by the author in the recent past, which were well attended by practicing engineers, both from India and abroad. New sections in almost all chapters are included with authentic research findings, which are verified by wide publications in various journals in the recent past.

My sincere thanks are due to my research scholars, colleagues, and my students who have given their valuable input and feedback to develop the contents of this book. In particular, I wish to express my thanks to Ms. Indira, Mr. Lognath, Mr. Kiran, and Ms. Nagavinothini for their editorial assistance and graphic art support extended during the preparation of manuscript of the book.

Chennai, India   Srinivasan Chandrasekaran

Preface to First Edition

Offshore structures are unique in the field of engineering, as they pose many challenges in the development and conceptualization of the design. As innovative platform geometries are envisaged to alleviate the encountered environmental loads efficiently, detailed understanding of their analysis and basic design becomes inevitable. Structural dynamics, being an important domain of offshore engineering, require an intensive teaching and guidance to illustrate the fundamental concepts as applied to ocean structures in particular. With the vast experience of teaching this subject and guiding research, a humble attempt is made to present the basics in a closed form, which will be useful for the graduate students and researchers. The chapters in the book are organized such that the reader gets an overall idea of various types of offshore plants, basic engineering requirements, fundamentals of structural dynamics and their applications to preliminary design. Numerical examples and application problems are chosen to illustrate the use of experimental, numerical, and analytical studies in the design and development of new structural form for deep-water oil exploration. This book is a repetitive effort in the direction of capacity building of practicing and consulting offshore structural engineers who need to understand the basic concepts of dynamic analysis of offshore structures through a simple and straightforward approach.

Video lectures of the courses available at the following websites: (i) http://nptel. ac.in/courses/114106035; (ii) http://nptel.ac.in/courses/114106036; and (iii) http:// nptel.ac.in/courses/114106037, which also substitute the classroom mode of understanding of the contents of this book.

My sincere thanks are due to my professors, colleagues, and my students who have given their valuable input and feedback to develop the contents of this book. In particular, I wish to express my thanks to Ms. Ezhil, Ms. Indira, and Ms. Madhavi for their editorial assistance and graphic art support extended during the preparation of manuscript of the book.

I also owe a lot of thanks to all the authors and publishers who have earlier attempted to publish books on structural dynamics and allied topics, based on which I developed my concepts on the said subject.

<div align="right">Srinivasan Chandrasekaran</div>

Contents

About the Author

Srinivasan Chandrasekaran is a Professor in the Department of Ocean Engineering at the Indian Institute of Technology Madras, Chennai, India. He has 23 years of teaching, research, and industrial experience, during which he has supervised many sponsored research projects and offshore consultancy assignments both in India and abroad. His current areas of research are dynamic analysis and design of offshore platforms, development of geometric forms of compliant offshore structures for ultra-deep water oil exploration and production, subsea engineering, rehabilitation and retrofitting of offshore platforms, structural health monitoring of ocean structures, seismic analysis and design of structures, and risk analyses and reliability studies of offshore and petroleum engineering plants. He has also been a Visiting Fellow at the invitation of the Ministry of Italian University Research to the University of Naples Federico II, Italy, for a 2-year period, during which he conducted research on the advanced nonlinear modeling and analysis of structures under different environment loads with experimental verifications. He has published 110 research papers in international journals and refereed conferences organized by professional societies around the world. He has also authored three textbooks which are quite popular among graduate students of civil and ocean engineering. He is a member of many national and international professional bodies and has delivered many invited lectures and keynote addresses at international conferences, workshops, and seminars organized in India and abroad.

Abbreviations

API	American Petroleum Institute
BLS	Buoyant Leg Structure
BOP	Blow Out Preventer
CDF	Cumulative distribution function
CFD	Computational Fluid Dynamics
DBE	Design basis earthquake
DNV	Det Norske Veritas
DPS	Dynamic Position Keeping Systems
FEED	Front-End Engineering Design
FFFP	Film Forming Fluoro Protein
FLS	Fatigue Limit State
FOSM	First-Order Second Moment Method
FPS	Floating Production Systems
FPSO	Floating Production, Storage and Offloading
FPU	Floating Production Unit
FSI	Fluid Structure Interaction
FSO	Floating Storage and Offloading
FSRU	Floating, Storage and Regasification Units
GBS	Gravity-Based Structure
GoM	Gulf of Mexico
ISSC	International Ship Structures Congress
JONSWAP	Joint North Sea Wave Project
KT	Kanani-Tajimi
LNG	Liquid Natural Gas
LRFD	Load Resistance Factor Design
MARIN	Maritime Research Institute Netherlands
MATLAB	Matrix Laboratory
MCE	Maximum credible earthquake
MF	Magnification Factor
MSL	Mean Sea Level
ODE	Ordinary Differential Equation

PC	Perforated Cover
PDF	Probability Density Function
PLS	Progressive Collapse Limit State
PM	Pierson Moskowitz
SALM	Single Anchor Leg Mooring system
SCF	Stress Concentration factor
SDOF	Single Degree of Freedom System
SHM	Simple Harmonic Motion
SLS	Serviceability Limit State
SSS	Subsea systems
THT	Tetra-hydrothiophene
TLP	Tension Leg Platform
ULS	Ultimate Limit State
VIV	Vortex induced Vibration
WSI	Wave Structure Interaction

Symbols

A	Cross-sectional area in mm^2
α	Philip's constant
$\bar{\alpha}$	Modified Philip's constant
a_n	Acceleration of water particle
β	Reliability Index
c	Damping element
C_c	Critical damping
C_H	Force coefficient in horizontal direction
C_V	Force coefficient in vertical direction
C_w	Wind pressure coefficient
C_D	Drag Coefficient
C_L	Lift Coefficient
$C_x(\tau)$	Auto-covariance function
d	Water depth
dA	Exposed area
dV	Disposed volume of water per unit length
D	Diameter of the ice cone
D_{max}	Maximum Dynamic amplification factor
D_g	Fatigue damage
δ	Surface drag coefficient/drag coefficient
δ_a	Crack growth
Δx	Centre-to-Centre distance between the column members of TLP
Δt	Dynamic tether tension variation
E	Young's modulus of steel
F	Cyclic frequency
F_i	Inertia force
F_w	Wind force
F_D	Drag Force
F_g	Average gust factor
F_L	Lift Force
F_r	Froude Number
Φ	Velocity Potential

f_H	Force on horizontal cylinder
$\overline{F}_o$	Force amplitude on the structure
$F(t)$	Excitation force
g	Acceleration due to gravity
$g(x)$	Limit state function
γ	Peakedness parameter
γ_R	Resistance factor
$\overline{F}_0$	Force amplitude on the structure
H	Wave Height
H_s	Significant Wave Height
h	Ice thickness
$h_{FX(t)}$	Impulse Response function
$H(\omega)$	Transfer function or frequency response function
K	Wave Number
k	Stiffness
Λ	Wavelength
L	Live loads
L_u	Integral length scale
L_b	Ice-breaking length
L_c	Characteristic length of ice
M	Margin of Safety
m	Mass element
M_o, M_1	Spectral moments
m_n	nth moment
μ	Coefficient of absolute viscosity of the film
$N(t)$	Number of upcrossings
n_g	Number of cycles
ω	Circular frequency
ω_d	Damped vibration frequency
ω_p	Peak frequency
ω_g	Natural frequency of the ground
P	Permanent loads
p_f	Probability of failure
R	Resistance of the structure
r	Radius of the cylinder
$R_x(\tau)$	Autocorrelation function
ρ	Density of fluid
ρ_a	Mass density of air (1.25 kg/m³)
ρ_w	Density of water
S	Load effects
$S_F^+(\omega)$	One-sided power spectral density function
$S_U^+(\omega)$	Wind spectrum
S_0	Intensity of earthquake
σ_g^2	Variance of the ground acceleration

σ_u^2	Variance of wind speed at a reference height of 10 m
$\bar{\sigma}$	Spectral width parameter
σ_f	Bending strength of ice
T	Wave period
T_p	Peak Wave period
$\bar{T}'$	Period of ice
t_f	Time of first failure
Θ	Phase angle
$\bar{U}_{10}$	Mean wind speed at a height of 10 m above Mean Sea Level
$\dot{u}$	Horizontal water particle velocity
$\ddot{u}$	Horizontal water particle acceleration
u_c	Current velocity
u_w	Mean wave period
$\dot{v}$	Vertical water particle velocity
$\ddot{v}$	Vertical water particle acceleration
V	Submerged volume of the structure
v	Velocity of air in m/s
v_n	Velocity of water particle
V_{S1}, V_{S2}	Load factors
v_{10}	Wind speed at 10 m above MSL
v_z	Wind speed at an elevation of z m above MSL
$\bar{v}$	Mean wind velocity in m/s
$v(t)$	Gust component
$\dot{x}$	Velocity of the structure
$\ddot{x}$	Acceleration of the structure
$x(t)$	Instantaneous response vector of TLP
$x_\mathrm{g}(t)$	Ground displacement vector
x_{1g}	Horizontal ground displacement
x_{3g}	Vertical ground displacement
Z_s	Thickness of the surface layer
ξ	Damping ratio
Y	Crack and geometry-dependent factor
ζ_g	Damping of the ground

List of Figures

List of Tables

Chapter 1
Introduction to Offshore Platforms

Abstract This chapter deals with the evolution of platform and various types of offshore platforms and their structural action under different environmental loads. The newly evolved structural forms and their discrete characteristics are discussed in this chapter. This chapter also gives the reader a good understanding about the structural action of different forms in the offshore. An overview of the construction stages of offshore plants and their foundation systems is presented.

Keywords Offshore structures · Bottom-supported structures · Compliant platforms · Tension leg platforms · Buoyant leg structures · Triceratops · Semisubmersibles · Drill ships · Floating · Storage and regasification platforms · Subsea systems

1.1 Introduction

Offshore structures are being challenged to counteract the depletion of oil resources with the new set of discoveries. By 2010, increase in drilling platforms induced the demand for offshore structures in deep sea. Hence, the quest on the research and development of the deepwater structures has resulted in the recent advancement and thrust in this area. Expansion of the structures from shallow to deep waters makes the accessibility difficult, and hence the structures demand higher deck areas consisting of additional space for third-party drilling equipment. Specific challenges in Arctic regions in shallow waters that arise due to low temperature, remoteness, ice conditions, eco system, and safety necessitate an adaptive design of offshore platforms addressing these factors.

Development of offshore platforms depends on various factors:

- Structural geometry with a stable configuration
- Easy to fabricate, install, and decommission
- Low CAPEX

- Early start of production
- High return on investment by increased and uninterrupted production.

Newly generated structural forms do not have any precedence to compare and understand their behavior and complexities. It is, therefore, important to understand the response of the structure and then select the structure that is most suitable to the environment. This is one of the essential features of the Front-End Engineering Design (FEED) (Devon and Jablokow 2010). Figure 1.1 shows a drilling semisubmersible for deepwater drilling with vertical riser storage.

1.2   Types of Offshore Platforms

Offshore platforms fall under three major categories: (i) fixed platforms; (ii) compliant platforms; and (iii) floating platforms. They are further classified as follows:

(i) *Fixed Platforms*

   (a) Jacket Platform
   (b) Gravity Platform
   (c) Jack-up rigs

(ii)   *Compliant Platforms*

    (a) Guyed Tower
    (b) Articulated Tower
    (c) Tension Leg Platform

(iii)   *Floating Platforms*

    (a) Semisubmersible
    (b) Floating Production Unit (FPU)
    (c) Floating Storage and Offloading (FSO)
    (d) Floating Production, Storage, and Offloading (FPSO) System
    (e) Spar

1.3   Bottom-Supported Structures

Energy is the driving force of the progress of civilization. Industrial advancements were first stoked by coal and then by oil and gas. Oil and gas are essential commodities in world trade. Oil exploration that initially started ashore has now moved to much deeper waters owing to the paucity of the resources at shallow waters (Bhattacharyya et al. 2003; GustoMSC 2010). Until now, there are more than 20,000 offshore platforms of various kinds installed around the world. Geologists and geo-physicists search for the potential oil reserve within the ground under ocean sea floor, and engineers take the responsibility of transporting the oil from the offshore site to the shore location (Dawson 1983). There are five major areas of operation from exploration to transportation of oil: (i) exploration; (ii) exploration drilling; (iii) development drilling; (iv) production operations; and (v) transportation (Chandrasekaran and Bhattacharyya 2011; Clauss et al. 1992; Clauss and Birk 1996). Ever since the first offshore structure was constructed, more advanced design technologies emerged for building larger platforms that cater to deeper water requirements; each design is unique to the specific site (Ertas and Eskwaro 1991). A precise classification of the offshore platform is difficult because of the large variety of parameters involved, such as functional aspects, geometric form, construction and installation methods, etc. However, in general, the platforms are broadly classified based on the geometric configurations (Chandrasekaran and Yuvraj 2013, Chandrasekaran and Nannaware 2013, Chandrasekaran et al. 2013). Offshore installations are constructed for varied purposes: (i) exploratory and production drilling; (ii) preparing water or gas injection into reservoir; (iii) processing oil and gas; (iv) cleaning the produced oil for disposal into sea; and (v) accommodation facilities (DOE-OG 1985). They are not classified on the basis of their functional use but based on their geometric (structural) *form* (Sadehi 1989,

2001, 2007; Sarpkaya and Isaacson 1981). As the platforms are aimed for greater water depths, their structural *form* changes significantly; alternatively the same *form* cannot be used at a different water depth. It means that the geometric evolution of the platform needs to be adaptive to counteract the environmental loads at the chosen water depths (Patel 1989). Furthermore, the technological complexities faced by new offshore platforms including analysis and design, topside details, construction, and installation are not available in the open domain; they are protected and owned by the respective companies/agencies as part of their copyright. Because of such practices, knowledge on the complexities in designing the offshore plants is not available to the practicing young engineers, in particular. Hence, prior to the knowledge of FEED, it is necessary to understand different structural *forms* of offshore structures, which are successful in the past. As it is well known that each platform is unique in many ways, learning about their structural configurations, limitations with respect to the sea states and water depth, construction complexities, decommissioning issues and their structural action will be an important stage in the pre-FEED (Hsu 1981; Paik et al. 2007). The present trend is to design and install offshore platforms in regions that are inaccessible and difficult to use the existing technologies (Anagnostopoulos 1982). The structural *form* of every platform is largely derived on the basis of structural innovativeness but not on the basis of the functional advantages. Revisiting the existing platforms constructed around the world will impart decent knowledge to offshore engineers (Gerwick 1986; Graff 1981a, b).

Major components of offshore platforms are

 (i) Superstructure: It consists of deck and equipment for functioning of the platform.
 (ii) Substructure: It supports the deck and transmits the load from substructure to foundation.
(iii) Foundation: It supports the substructure and superstructure; it also transmits the load to the seabed.
(iv) Mooring system: It is used for station keeping.

Offshore platforms are classified either as bottom-supported or floating. Bottom-supported platforms can be further classified as fixed or compliant-type structures; *compliant* means flexible (mobility). Compliancy changes the dynamic behavior of such platforms. Floating structures are classified as neutrally buoyant type (e.g., semisubmersibles, FPSO, mono-column spars) and positively buoyant type (e.g., tension leg platforms). It is important to note that buoyancy plays a very important role in floating-type offshore structures, as the classifications are based on buoyancy (Bea et al. 1999). In bottom-supported structures, base of the structure is fixed rigidly to the seabed. The structure attracts more forces due to its rigidity, but the response to the wave loads is very less.

1.4   Jacket Platforms

Fixed type platforms are also called as template-type structures, which consist of the following:

- A jacket or a welded space frame, which is designed to facilitate pile driving and also acts as a lateral bracing for the piles
- Piles, which are permanently anchored to the seabed to resist the lateral and vertical loads that are transferred from the platform
- A superstructure consisting of the deck to support other operational activities.

Table 1.1 shows the list of fixed offshore platforms constructed worldwide (Chandrasekaran and Jain 2016).

With reference to the Table 1.1, it is seen that a large bunch of platforms were initiated in USA and Europe. A typical jacket platform (Bullwinkle platform) is shown in Fig. 1.2. A typical jacket platform consists of process, wellhead, riser, flare support, and living quarters.

Table 1.1 Fixed offshore platforms around the world

S. No.	Platform name	Water depth (m)	Location
North America			
1	East Breaks 110	213	USA
2	GB 236	209	USA
3	Corral	190	USA
4	EW910-Platform A	168	USA
5	Virgo	345	USA
6	Bud Lite	84	USA
7	Falcons' Nest production	119	USA
8	South Timbalier 301	101	USA
9	Ellen	81	USA
10	Elly	81	USA
11	Eureka	213	USA
12	Harmony	365	USA
13	Heritage	328	USA
14	Hondo	259	USA
15	Enchilada	215	USA
16	Salsa	211	USA
17	Cognac	312	USA
18	Pompano	393	USA
19	Bullwinkle	412	USA
20	Canyon Station	91	USA
21	Amberjack	314	USA

Table 1.1 (continued)

S. No.	Platform name	Water depth (m)	Location
22	Bushwood	***	USA
23	Hebron	92	Canada
24	Hibernia	80	Canada
25	Alma	67	Canada
26	North Triumph	76	Canada
27	South Venture	23	Canada
28	Thebaud	30	Canada
29	Venture	23	Canada
30	KMZ	100	Mexico
South America			
1	Peregrino Wellhead A	120	Brazil
2	Hibiscus	158	Trin and Tobago
3	Poinsettia	158	Trin and Tobago
4	Dolphin	198	Trin and Tobago
5	Mahogany	87	Trin and Tobago
6	Savonette	88	Trin and Tobago
7	Albacora	***	Peru
Australia			
1	Reindeer	56	
2	Yolla	80	
3	West Tuna	***	
4	Stag	49	
5	Cliff Head	**	
6	Harriet Bravo	24	Australia
7	Blacktip	50	Australia
8	Bayu-Undan	80	Australia
9	Tiro Moana	102	New Zealand
10	Lago	200	Australia
11	Pluto	85	Australia
12	Wheatstone	200	Australia
13	Kupe	35	New Zealand
South America			
1	Peregrino Wellhead A	120	Brazil
2	Hibiscus	158	Trin and Tobago
3	Poinsettia	158	Trin and Tobago
4	Dolphin	198	Trin and Tobago
5	Mahogany	87	Trin and Tobago
6	Savonette	88	Trin and Tobago
7	Albacora	***	Peru

(continued)

Table 1.1 (continued)

S. No.	Platform name	Water depth (m)	Location
Asia			
1	QHD 32-6	20	China
2	Peng Lai	23	China
3	Mumbai High	61	India
4	KG-8 Well head	109	India
5	Bua Ban	***	Thailand
6	Bualuang	60	Thailand
7	Arthit	80	Thailand
8	Dai Huang Fixed Well head	110	Vietnam
9	Ca Ngu Vang	56	Vietnam
10	Chim Sao	115	Vietnam
11	Oyong	45	Indonesia
12	Kambuna	40	Indonesia
13	Gajah Baru	***	Indonesia
14	Belumut	61	Malaysia
15	Bukha	90	Oman
16	West Bukha	90	Oman
17	Al Shaheen	70	Qatar
18	Dolphin	***	Qatar
19	Zakum Central complex	24	UAE
20	Mubarek	61	UAE
21	Sakhalin I	***	Russia
22	Lunskoye A	48	Russia
23	Molikpaq	30	Russia
24	Piltun-Astokhskoye-B	30	Russia
25	LSP-1	13	Russia
26	LSP-2	13	Russia
27	Gunashli Drilling and Production	175	Azerbaijan
28	Central Azeri	120	Azerbaijan
29	Chirag PDQ	170	Azerbaijan
30	Chirag-1	120	Azerbaijan
31	East Azeri	150	Azerbaijan
32	West Azeri	118	Azerbaijan
33	Shah Deniz Production	105	Azerbaijan
Europe			
1	Brage	140	Norway
2	Oseberg A	100	Norway
3	Oseberg B	***	Norway
4	Oseberg C	***	Norway
5	Oseberg D	100	Norway

Table 1.1 (continued)

S. No.	Platform name	Water depth (m)	Location
6	Oseberg South	100	Norway
7	Gullfaks A	138	Norway
8	Gullfacks B	143	Norway
9	Gullfacks C	143	Norway
10	Sleipner A	80	Norway
11	Sleipner B	**	Norway
12	Sleipner C	***	Norway
13	Valhall	70	Norway
14	Ekofisk Center	75	Norway
15	Varg Wellhead	84	Norway
16	Hyperlink	303	Norway
17	Draugen	250	Norway
18	Statfjord A	150	Norway
19	Statfjord B	***	Norway
20	Statfjord C	290	Norway
21	Beatrice Bravo	290	UK
22	Jacky	40	UK
23	Ula	40	UK
24	Inde AC	70	UK
25	Armada	23	UK
26	Auk A	88	UK
27	Fulmar A	84	UK
28	Clipper South	81	UK
29	Clair	24	UK
30	East Brae	140	UK
31	Lomond	113	UK
32	East Brae	86	UK
33	Alwyn North A	126	UK
34	Alwyn North B	126	UK
35	Cormorant Alpha	126	UK
36	Dunbar	145	UK
37	Nelson	***	UK
38	Schooner	100	UK
39	Andrew	117	UK
40	Forties Alpha	107	UK
41	Forties Bravo	107	UK
42	Forties Charlie	107	UK
43	Forties Delta	107	UK
44	Forties Echo	107	UK
45	Eider	159	UK

Table 1.1 (continued)

S. No.	Platform name	Water depth (m)	Location
46	Elgin	93	UK
47	Elgin PUQ	93	UK
48	Franklin	93	UK
49	Babbage	42	UK
50	Alba North	158	UK
51	Alba South	138	UK
52	Judy	80	UK
53	Amethyst	30	UK
54	Buzzard	100	UK
55	Brigantine BG	29	UK
56	Brigantine BR	***	UK
57	Cecilie Wellhead	60	Denmark
58	Nini East	***	Denmark
59	Nini Wellhead	58	Denmark
60	South Arne	60	Denmark
61	Galata	34	Bulgaria

*Data not available

Fig. 1.2 Bullwinkle steel jacket
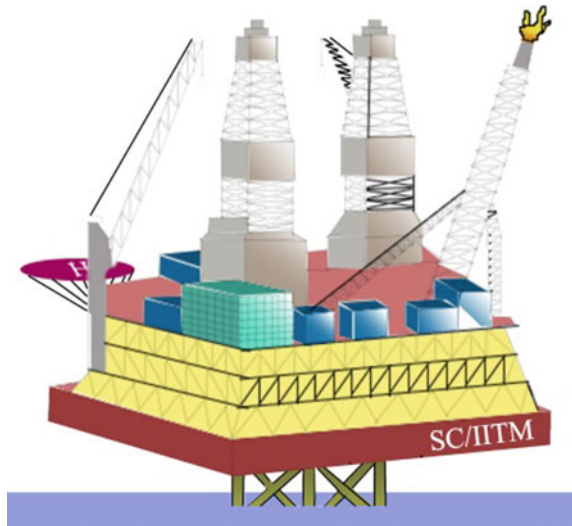
The platform leg braces the piles and serves as guides for driving the piles; hence called "jacket structure". It is a truss-based system, which remains fixed to the seabed and transparent to wave loads. Platform is designed mainly for production purposes and suitable up to a depth of 400 m. The different components of a jacket platform are

(i) **Superstructure**: It is called "topsides". It is divided into deck and deck modules.

Deck: The upper part of the platform that houses most of the equipment related to process, mechanical, electrical, piping, and instrumentation. It consists of three components—drilling deck, wellhead/production deck, and cellar deck. These decks are supported on a grid work of girders, trusses, and columns. The deck structure is usually made up of Warren trusses.

Deck modules: The arrangement of deck modules into the available space on the deck structure is carefully planned during the preliminary design. Modules are fabricated with connecting pipe joints and it includes drilling equipment, production equipment, gas turbine, pumps, generating sets, compressors, gas flare stack, helideck, revolving camera, survival crafts, and living quarters. It weighs about 40,000 tons.

Crane pedestal: A large structural tube that supports an offshore crane for lifting purposes. Crane pedestal also serves as diesel storage tanks as they are of very large in diameter and capable of housing enough fuel.

Helideck: It is a raised level on the platform to facilitate helicopter landing. Solar panels are mounted just below the helideck to facilitate auxiliary power.

Flare boom: It is a long truss that supports a vent or a flare line that releases a part of hydrocarbon gas (about one-third of production) at a greater height.

(ii) **Substructure**:

Jacket: It is a supporting frame of the platform that supports the topsides and is generally submerged below the waterline. Its design is mainly governed by the wave loads.

Transition piece: It is a structural member in the form of cone that connects the topside and the jacket. It is a type of cup and cone joint. Cone-shaped design is preferable as leg size of topsides is smaller in diameter as compared to that of the jacket legs.

Legs: The jacket legs are usually battered in elevation to provide larger base for the jacket at the mudline so as to assist the overturning loads more effectively.

Braces: Main legs of the jacket are interconnected by horizontal and diagonal braces for improving their stability against lateral loads.

Buoyancy tanks: They provide adequate clearance between the seabed surface and the lowest point of the launched structure.

Conductors: These are long hollow vertical or curved tubes of 1 m diameter driven through guide rings below the mud line. The wells are drilled through conductor tubes positioned in an array which can be reached by sliding the drilling derrick from location to location across the deck. To support the long length of the tube, conductor framings are provided to act as a lateral support guide to the conductors.

Risers: These are vertical tubes of 0.4 m diameter located within the jacket framework for pumping seawater into decks, for heat exchange and to carry the

crude or partially processed oil/gas to another location for many other processing functions. Risers are generally clamped to the jacket structure.

Boat landings: Two boat landings at different levels are provided on each longitudinal side of the platform for embarking and disembarking.

Barge bumpers: These are provided on all jacket legs to accommodate landing/unloading in a variety of sea conditions and to facilitate a smooth berthing.

Riser guards: A riser guard protects the oil/gas carrying risers. They are designed for accidental vessel impacts.

Launch truss: Sometimes, the jacket structures are very large and cannot be lifted even with large cranes. Permanent structures like launch truss are provided on one side of the jacket to facilitate the loading out onto the barge. If the jacket is designed for buoyancy, the jacket is launched in the sea after reaching its position for a natural upend and leveling. When the jacket is launched, it floats due to buoyancy. The jacket legs are then sequentially flooded to make it upright and stand over the seabed before the piles are driven through the legs to fix it to the sea bed. The launch truss helps in skidding the jacket from the barge to the sea. It is provided to avoid damage in the main members of the truss while launching. Rollers are provided to adjust the overlapping distance between the launch truss and the tower.

Joint Cans: It is provided to facilitate welding and expansion during the installed condition. The stress concentration at the joints is very high and termed as "hot spot stresses". At increased stresses, connections are generally damaged, which needs replacement. Number of joints in a leg member should be optimum as longer members are susceptible to buckling, causing a premature failure.

 (iii) **Foundation**:

Piles: The topside loads are directly taken by piles and transferred to the soil. In this structure, the superstructure loads are taken by the jacket structure and transferred to the piles through grouted sleeves. Piles support the platform in its worst in-service condition.

1. End bearing pile: pile resting on rocky strata. It transfers the load by bearing.
2. Skin friction pile: longer than end bearing pile. It transfers load by friction.
3. Combined end bearing and skin friction pile.

Skirt piles: When the structure becomes heavier due to increased water depths, improved jacket configurations known as skirt pile jackets are required. The number of skirt piles to be established depends upon bottom soil conditions. Usually, they are placed in concentric circles around the base of the legs in rows of 4, 6, 8, or more. The skirt pile sleeves are incorporated in the jacket structure between the two lowest levels of horizontal bracing. The sleeves are sufficiently offset from the plane of the jacket side through pile guides. In deepwater applications, the skirt piles are clustered around enlarged corner legs, to provide greater uplift resistance. Skirt piles are required when the soil is very weak and the existing number of piles formed by the geometry of the platform is not adequate.

The translational movement occurs in the platform due to improper fitting of fasteners and increase in the flexibility of the piles in due course of time.

Mud mat: It is provided at the bottom of the jacket to provide suitable additional area to resist initial fluidization of the top layer of the seabed. They are provided to keep the platform stable and in a vertical upright position against the lateral forces before the piles are driven through the legs. They are usually made of heavy timbers or light steel plates and fastened across the corners of the jacket, immediately beneath the lowest level of horizontal bracing. It is similar to large raft made up of timber. It helps the platform to sink deeper if the soil is too soft near the top layer of the sea bed. It provides adequate resistance to overturning.

The steps involved in the construction process are load-out, towing, launching, floating, upending, vertical position, piling, and deck mating. Dry towing is always preferred against wet towing as the later is severely affected by the sea state during installation. Most common procedure for installation is to let the jacket slide from the barge into the sea following a trajectory, which finally allows the jacket to float almost horizontal. Buoyancy tanks provide adequate clearance. From this naturally floating horizontal position, an upending operation is carried out to bring the structure to its vertical (desired) position. Then the structure is flooded to set down in its final position and secured by driving piles into the seafloor. The advantages of offshore jacket platforms are as follows: (i) support large deck loads; (ii) possibility of being constructed in sections and transported; (iii) suitable for large field and long-term production (supports a large number of wells); (iv) piles used for foundation result in good stability; and (v) not influenced by seafloor scour. Few disadvantages are as follows: (i) cost increases exponentially with increase in water depth; (ii) high initial and maintenance costs; (iii) not reusable and (iv) steel structural members are subjected to corrosion, causing material degradation in due course of service life, (v) installation process is time consuming and expensive.

1.5 Gravity Platforms

In addition to steel jackets, concrete was also prominently used to build some offshore structures. These structures are called gravity platforms or gravity-based structures (GBS). A gravity platform relies on the weight of the structure to resist the encountered loads instead of piling (API-RP 2A 2000; Hitchings et al. 1976; Hoeg 1976; Tromans et al. 2006). In regions where driving piles become difficult, structural forms are designed to lie on its own weight to resist the environmental loads (Hove and Foss 1974). Gravity platforms are the large bottom mounted reinforced concrete structures that are capable of supporting large topside loads during tow-out, which minimizes the hook-up work during installation (Young et al. 1975). Additional large storage spaces for hydrocarbons add up to their advantage. The major components of gravity platform are as follows:

  (i) *Foundation*: These structures have foundation element that contributes significantly to the required weight and spreads over a large area of the seafloor to prevent failure due to overturning moments caused by lateral loads. Shape of foundation shall be circular, square, hexagonal, or octagonal.

 (ii) *Caissons*: They are the hollow concrete structures located at the bottom of the platform. They provide the structure with natural buoyancy and used for storage purposes as well. This enables the platform to float to field development location. After installation, void spaces are used as storage compartments for crude oil or filled with permanent iron or ballast. Height of the caissons is usually about one-third of the height of the platform.

(iii) *Steel Skirts*: The steel skirts are provided around the periphery of the main legs to improve stability against lateral movement of the platform against sliding; they also act as erosion-resistant members. In addition, they assist in grouting the caisson base. In addition to steel skirts, dowels are also provided, which extend about 4 m below the level of steel skirts. They help to prevent damage to steel skirts during touchdown operation.

 (iv) *Modular Deck*: The deck supports drilling derrick, engine room, pipe rack, living quarters, processing equipment, and heliport. The main load carrying members are plate girders, box girders, or trusses.

  (v) *Cellar Deck*: They are used for placing the machinery and should be provided between the topside module and deck to improve stability of the platform. The base of the platform is constructed in dry dock after which it is floated and moored in a sea harbor. The construction is then completed by slip forming the large towers in a continuous operation until they are topped off. The structure is then ballasted (void spaces are flooded) and a steel prefabricated deck is floated over the structure and attached to its top (topside modules are mounted). When the caissons are filled with oil or ballast, the center of gravity of the platform moves towards the bottom, which in turn makes the platform to sink. This is called "**well sinking**". The construction of gravity platforms obviously requires deep harbors and deep tow-out channels.

The large weight of the structure causes enormous soil erosion at the bottom. This also results in unequal settlement due to which the structure tilts. Furthermore, tilting causes shift in the center of gravity of the platform, which creates an overturning moment at the base. The overturning moment increases with the increase in the lateral forces arise from waves, causing failure. In addition, a few geotechnical problems associated with GBS platforms cause large horizontal and vertical displacements. The geotechnical problems associated with GBS are namely:

- Sliding, which occurs due to the change in the soil characteristics (friction) and lower resistance to wind and wave loads.
- Bearing capacity failure, which occurs due to over weight of the structure (punching failure) where the weight of the platform becomes greater than the bearing capacity of the soil. The massive weight of the structure initiates local failure.

- Rocking, which occurs due to unequal settlement and causes moment at the bottom of the platform.
- Liquefaction, which occurs due to poor soil condition and saturation level.

Their salient advantages include: (i) constructed onshore and transported; (ii) towed to the site of installation; (iii) quick installation by flooding; (iv) no special foundation is required; and (v) use of traditional methods and labor for installation. Table 1.2 shows the list of gravity platforms constructed worldwide. These platforms are also known to be responsible for seabed scouring due to large foundations, causing severe environmental impact (Chandrasekaran 2015a, b, c, 2016a, b).

Gravity platforms had serious limitations namely: (i) not suitable for sites of poor soil conditions, as this would lead to significant settlement of foundation; (ii) long construction period which thereby delays the early start of production; and

Table 1.2 Gravity platforms constructed worldwide

S. No.	Name of the platform	Water depth (m)
1	Ekofisk 1	70
2	Beryl A	119
3	Brent B	140
4	Frigg CDP1	98
5	Frigg TP 1	104
6	Frigg MCP01	94
7	Brent D	142
8	Statfjord A	145
9	Dunlin A	153
10	Frigg TCP2	103
11	Ninian	136
12	Brent C	141
13	Cormorant	149
14	Statfjord B	145
15	Maureen	95.6
16	Stafjord C	145
17	Gulfaks A	133.4
18	GulfaksB	133.4
19	GulfaksC	214
20	Oseberg	100
21	Slebner	80
22	Oseberg North	100
23	Draugen	280
24	Heidrun	280
25	Troll	330

Courtesy Pennwell Publishing Co.

(iii) natural frequencies falling within the range of significant power of the input wave spectrum (Boaghe et al. 1998). Gravity structures are constructed with reinforced cement concrete and consist of large cellular base, surrounding several unbraced columns that extend upward from the base to support the deck and equipment above the water surface (Reddy and Arockiasamy 1991). Gravity platforms consist of production risers as well as oil supply and discharge lines, contained in one of the columns; the corresponding piping system for exchange of water is installed in another; and drilling takes place through the third column. This particular type is referred as CONDEEP (concrete deep water) structure and was designed and constructed in Norway. The construction of gravity platforms obviously requires deep harbors and deep tow-out channels. The floatation chambers are used as storage tanks, and platform stability is ensured through skirts. Steel gravity platforms exist off Nigeria, where the presence of rock close to sea floor ruled out the possibility of using piles to fix the structures to the seabed. Figure 1.3 shows the Hibernia gravity base structure. The platform is a steel gravity base structure with a
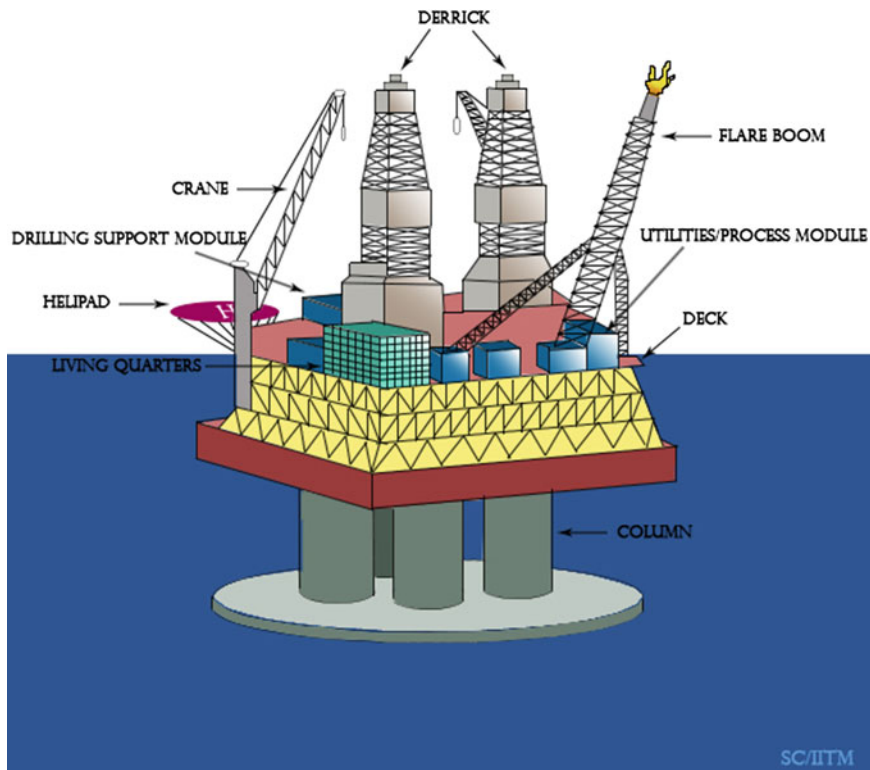
Fig. 1.3 Hibernia gravity base structure

weight of 112,000 ton, height of 241 m, and has steel skirts for penetration into the seabed.

Advantages of gravity platforms over jacket platforms are namely: (i) Greater safety for people on board and topside; (ii) Towing to site with deck is possible, which minimizes installation time and cost; (iii) Low maintenance cost because concrete submerged in water will have lesser problems than that of steel structure; (iv) Adjustable crude oil capacity; (v) Capability to support large deck areas; (vi) Risers are protected as they are placed inside the central shaft; and (vii) Possible access to sea floor from the cell compartment in the foundation, resulting in healthy monitoring.

1.6   Jack-Up Rigs

Jack-up (rigs) platforms are temporary structures, meant for exploratory drilling. They are similar to barges with movable legs. They are mobile as their hulls have the requisite floating characteristics to enable towing from site to site. When the legs are projecting upwards, the rig can be easily towed from one location to another location. Jacking system provides an effective method to quickly lower or raise the hull. The legs are lattice, truss-type, and transparent to wave loads. When the jack-up is being towed to the site for exploratory drilling, the legs will be projecting upwards from the deck. On installation, the legs will be pushed inside the sea bed while the deck is lifted up. Hence called "Jack-up rig". After installation, one-third height of the leg should be left above the hull for maintaining the stability of the platform. The failure in the platform occurs during sailing when the legs are completely above the hull due to overturning moment caused by the wind load and by spud can pull off. The latter may cause serious damage to the drill pipes and risers but the system will remain floating. The spud can foundation is not an ideal hinged joint. It offers partial fixity to the structure so that the structure may also fail under bending. The jack-up rigs are capable of working under harsh environments of wave heights up to 24 m and wind speed exceeding 100 knots.

The components of Jack-up rig include the following:

Derrick: The derrick has a shape of frustum of cone and tubular members are used for the construction. The derrick moves over the rails in the hull to house more number of wells. This movement will not affect the functionality of the platform.

Draw works: It is the assembly of pipes used for drilling. The drilling takes place through the center pipe and the oil comes out under pressure through the circumferential pipes. The center pipe is also loaded with drilling mud, which acts as a counter weight to balance the bottom pressure and it avoids the movement of drill bit vertically upwards during the drilling process.

Drill floor: It is the floor where the drilling derrick is located.

Drill pipe: It is used for oil extraction.

Drill string: The sharp wedge-shaped tip of the drill pipe used for drilling is called drill string.

Cantilever: The derrick moves over the cantilever projection. This is called "Offset drilling" by which the center of gravity of the hull in the trapezoidal cross section will be shifted towards center of the hull. Since drilling is performed on the cantilever projection, there is a least disturbance to the deck and other processes.

Legs: The legs are lattice truss-type. Length of the legs should be larger than 1.4 times the water depth. Lacing and battens on the legs provide additional stability.

Hull: it houses all the facilities, which includes living quarters and helideck.

Spud can: It is a shallow conical underside footing used for placing the leg on the seafloor. When the spud can is pushed into the sea bed under greater pressure, partial vacuum will be created inside the spud can. Due to suction force, the clay fills the void space and it is fixed to the seabed. Once fixed, high pull-out force is required for extraction. Diameter varies from 2.5 to 4 m, while depth of immersion is about 1–2 m. In order to remove the spud can, soil in the circumferential area should be excavated enabling soil inside the spud can to flow out.

Moon pool: It is the vent provided for the passage of drilling rig in the hull.

Advantages of the platform include (i) high mobility; (ii) low cost and efficient; (iii) easy fabrication and repair; (iv) easy decommissioning; and (v) simple construction. These platforms also have some serious limitations such as (i) suitable only for shallow depth; (ii) subjected to sea bed scouring which leads to differential settlement; (iii) not suitable for rocky stratum. The name *jack-up* is assigned as the legs will be pulled up while they are transported from one site to another. On reaching the installation site, legs will be driven into the seabed for a better stability. Jack-up rigs have significant mobility but the geometric configuration is comparable to that of a fixed-base structure. Figure 1.4 shows a schematic view of a typical jack-up rig.

The rig will be preloaded to test whether the foundation of the legs has reached the desired level of lateral stability. Once the preloaded test is completed, deck is further lifted to obtain the desired air gap that is required for safe operation. Air gap is provided to ensure that the deck is not interfered with the tides during operation. Foundation of jack-up rig is vital to ensure its stability against lateral loads caused by waves and wind. Lattice tower-type legs of jack-up rigs are supported on spud can. It is a shallow, conical shaped cup, which is provided underside of the footing of each leg. Figure 1.5 shows schematic view of a spud can used in the foundation of each of the legs of jack-up rigs. Spud cans are suitable for stiff, clay, and sand but not for rocks.
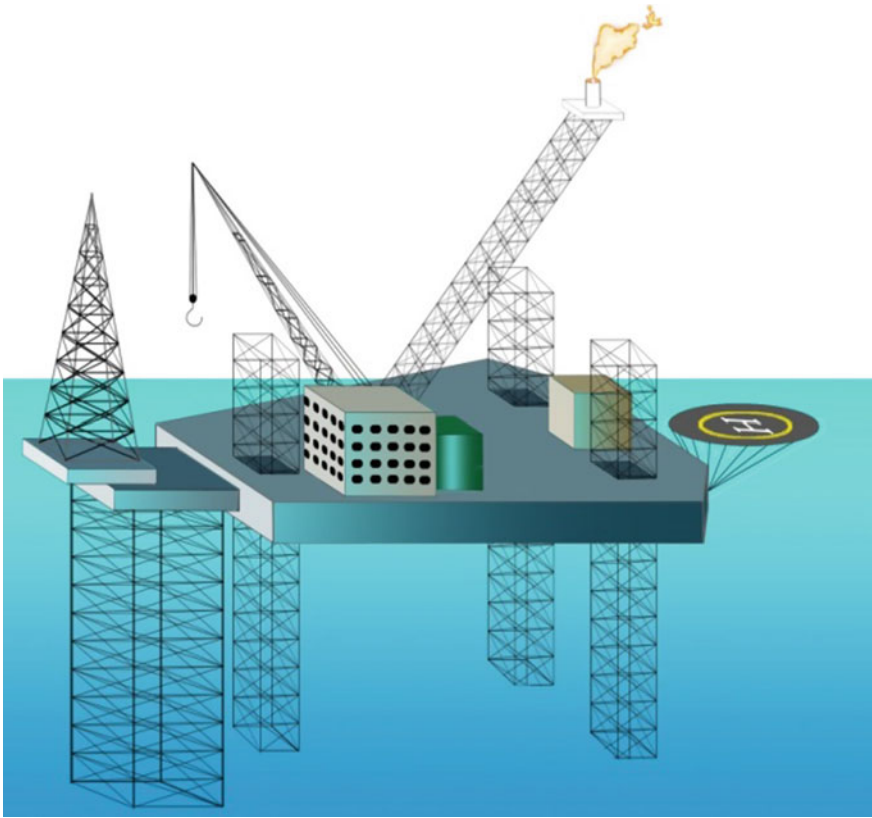
Fig. 1.4 Jack-up platforms (Rigs)
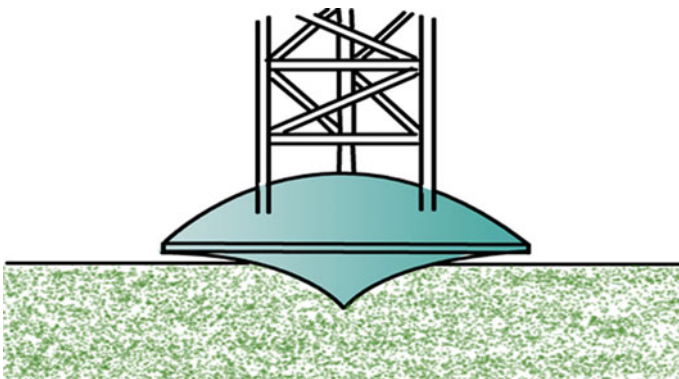
Fig. 1.5 Spud can (Chandarsekaran and Jain 2016)

1.7   Compliant Structures

To overcome the above negative factors, one should design a structural *form*, which should attract fewer forces and remain flexible to withstand the cyclic forces. The structural action and the *form* are corrected based on the "mistakes" learnt from the fixed type platforms. This is a special kind of reverse engineering, which makes offshore platforms unique. This leads to continuous improvement from one platform to the other. Hence, FEED is on a constant update as new structural forms are being tried for oil and gas exploration in deep and ultra-deep waters (Chandrasekaran 2014; Stansberg et al. 2002). Fixed type offshore structures became increasingly expensive and difficult to install in greater water depths. Hence, modified design concept evolved for structures in water depths beyond 500 m. A compliant offshore tower is similar to that of a traditional platform, which extends from surface to the sea bottom and transparent to waves. A compliant tower is designed to flex with the forces of waves, wind, and current. Classification under compliant structure includes those structures that extend to the ocean bottom and are anchored directly to the seafloor by piles and/or guidelines (Mather 2000). Guyed towers, articulated tower, and tension leg platform fall under this category. The structural action of complaint platforms is significantly different from that of the fixed ones, as they resist lateral loads not by their weight but by the relative movement. In fact, instead of resisting the lateral loads, the structural geometry enables the platform to move in line with the wave forces. To facilitate the production operation, they are position-restrained by cables/tethers or guy wires. By attaching the wires to the complaint tower, majority of the lateral loads will be counteracted by the horizontal component of the tension in the cables; the vertical component adds to the weight and improves stability (Chakrabarti 1994; Dawson 1983; de Boom et al. 1984).

1.8   Guyed Towers

Guyed tower is a slender structure made up of truss members that rest on the ocean floor and is held in place by a symmetric array of catenary guy lines. The foundation of the tower is supported with the help of spud can arrangement, which is similar to the inverted cone placed under suction. The structural action of the guyed tower makes its innovation more interesting, which is one of the successful improvements in the structural *form* in the offshore structural design. The upper part of the guy wire is a lead cable, which acts as a stiff spring in moderate seas. The lower portion is a heavy chain, which is attached with clump weights called touch-down point. The clump weights are provided to drag down the cables to the seabed and drag anchors are provided to avoid lifting up of clump weight due to scour. Under normal operating conditions, the weights will remain at the bottom, and the tower deck motion will be nearly insignificant. However, during a severe

storm, the weights on the storm-ward side will lift off the bottom, softening the guying system and permitting the tower and guying system to absorb the large wave loads. Since the guy lines are attached to the tower below mean water level close to the center of applied environmental forces, large overturning moments will not be transmitted through the structure to the base. This feature has allowed the tower to be designed with a constant square cross section along its length, reducing the structural steel weight as compared with that of a conventional platform (Moe and Verley 1980). Guyed towers are considered as pinned-pinned beam in analysis. In guy lines, the initial axial force is zero. It invokes the force only on larger displacement. The length of the guy wire is 2.5–3 times the water depth. The guy wires are provided circumferentially around the tower (possibly symmetrical) and they are connected to the top of the deck by "top tension risers". The tower is supported by spud can, which is an inverted cone-shaped foundation system that resists the lateral force by suction pressure. The failure may occur due to spud can pull off and either at fair lead or touchdown point.

Exxon in 1983 installed the first guyed tower named Lena Guyed Tower in the Mississippi Canyon Block in a 300 m water depth. Figure 1.6 shows the schematic view of the Lena tower. Though the structural *form* resembles a jacket structure, it is compliant and is moored by catenary anchor lines. The tower has a natural period of 28 s in sway mode while bending, and torsion modes have a period of 3.9 and 5.7 s, respectively. The tower consists of 12 buoyancy tanks of diameter 6 m and length of about 35 m. Around 20 guy lines are attached to the tower with clump weights of about 180 ton to facilitate the holding of the tower in position. The advantages of guyed towers are (i) low cost (lower than steel jacket); (ii) good
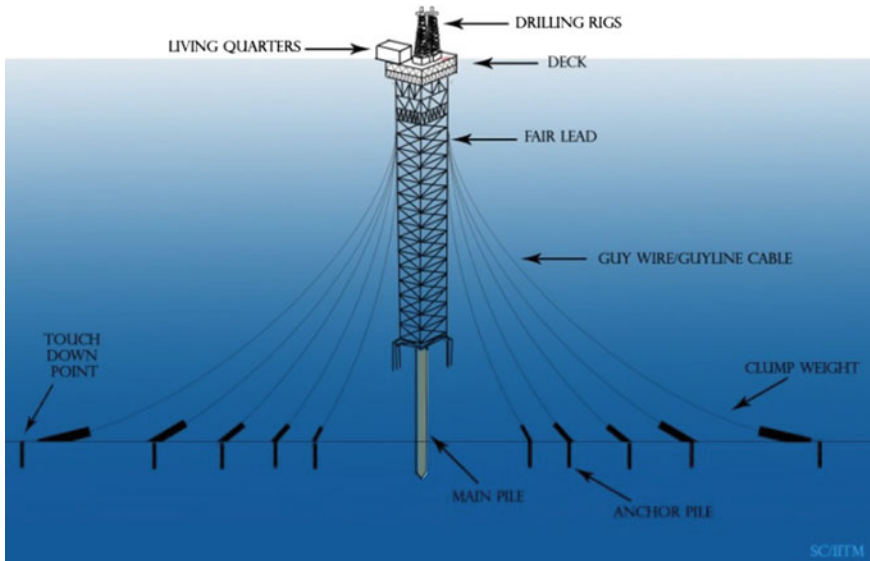
Fig. 1.6 Lena guyed tower

stability as guy lines and clump weights improve restoring force; and (iii) possible reuse. The disadvantages are as follows: (i) high maintenance costs; (ii) applicable to small fields only; (iii) exponential increase in cost with increase in water depth; and (iv) difficult mooring. These factors intuited further innovation in the platform geometry, which resulted in articulated towers (Choi and Lou 1991).

1.9   Articulated Towers

One of the earliest compliant structures that started in relatively shallow waters and slowly moved into deep water is the articulated tower. An articulated tower is an upright tower that is hinged at its base with a universal joint, which enables free rotation about the base. When there was a need to improve the structural *form* from fixed to compliant, researchers thought of both modes of compliancy namely: (i) rotational and (ii) translational. Enabling large translational motion could make the platform free from position-restrained, and hence rotational compliancy was attempted. In such geometric *forms*, it is important to note that the design introduces a single-point failure deliberately, which is the universal joint (Helvacioglu and Incecik 2004). The tower is ballasted near the universal joint and has a large buoyancy tank at the free surface to provide large restoring force (moment). Buoyancy chamber acts as a large container to store crude oil and the lower ballast chamber is filled with permanent iron ore or ballast, which is used for shifting the center of gravity towards the bottom to provide more stability to the tower. Due to the lateral force, the structure tilts, which causes a shift of buoyancy (variable submergence). Depending upon location and size, the buoyancy chamber keeps on giving extra force in upward direction, which will cause a couple in anticlockwise directions. This will restore the platform to its normal position. This is achieved by the dynamic change in water plane area or variable submergence of the member. In addition, the compliancy of the articulated tower avoids the concentration of high overturning moments and the resulting stress.

The tower extends above the free surface and accommodates a deck and a fluid swivel. In deeper water, it is often advantageous to introduce double articulation, the second one being at a mid-depth (Nagamani and Ganapathy 2000). Provision of more articulation reduces the bending moment along the tower (Nazrul and Suhail 2003). Fatigue is an important criterion for this type of system design as the universal joints are likely to fail under fatigue loads. The time period varies from 40 to 90 s, which results in dynamic amplification factor lesser than that of the fixed platforms. The advantages of articulated towers are as follows: (i) low cost; (ii) large restoring moments due to high center of buoyancy; and (iii) protection of risers by tower. There are few disadvantages: (i) suitable only for shallow water as the tower shows greater oscillations for increased water depth; (ii) cannot operate in bad weather; (iii) limited to small fields; and (iv) fatigue of universal joint leads to a single-point failure (Chandrasekaran and Pannerselvam 2009; Chandarsekaran et al. 2010a, b). They are used only for anchoring, storage and repairing works and not as
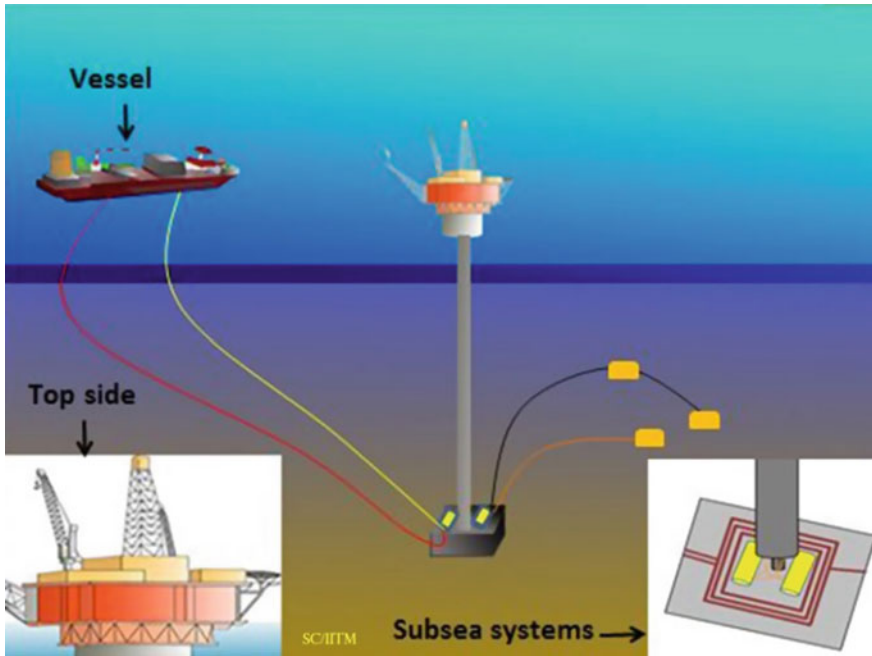
Fig. 1.7 Articulated tower

permanent production structures and hence called single anchor leg mooring system (SALM). Figure 1.7 shows a typical articulated tower, supporting the storage activities of a vessel.

In both the above structural *forms* of complaint towers namely guyed tower and articulated tower, it can be seen that the tower extends through the water depth, making it expensive for deep waters. Therefore, successive structural *forms* are intuited towards the basic concept of not extending the tower to the full water depth but only to retain it near the free surface level as far as possible. In such kinds of structural geometry, it is inevitable to make the platform weight dominant. To improve the installing features and decommissioning procedures, the geometry is attempted to be buoyancy dominant instead of weight dominant (buoyancy force exceeds the weight by manifold). While this enabled easy fabrication and installation, it also demanded skilled labor and high expertise for installation and commissioning of such platforms. The evolved structural geometry is tension leg platforms (Vannucci 1996; Yan et al. 2009; Yoneya and Yoshida 1982; Demirbilek 1990).

1.10   Tension Leg Platform

A tension leg platform (TLP) is a vertically moored compliant platform (Zeng et al. 2007). Figure 1.8 shows a typical TLP, highlighting its various components. Taut mooring lines vertically moor the floating platform, with its excess buoyancy; they are called tendons or tethers. The structure is vertically restrained, while it is compliant in the horizontal direction permitting surge, sway, and yaw motions. The structural action resulted in low vertical force in rough seas, which is the key design factor (Chandrasekaran and Jain 2002a, b; Rijken and Neidzwecki 1991; Roitman et al. 1992). Columns and pontoons in TLP are constructed with tubular members due to which the buoyancy force exceeds the weight of the platform. The excess buoyancy created is balanced by the pretension in the taut moorings. Substantial pretension is required to prevent the tendons from falling slack even in the deepest trough, which is achieved by increasing the free-floating draft (Chandrasekaran et al. 2006a, b; Basim et al. 1996; Kawanishi et al. 1987, 1993). As the requirement of pretension is too high, pretension cannot be imposed in tethers by any mechanical means. During commissioning, void chambers (columns and pontoon members) are filled with ballast water to increase the weight; this slackens the tendons. After tendons are securely fastened to the foundation in the seabed, de-ballasting is carried out to impose necessary pretension in the tendons. Under static equation of equilibrium, the following relationship holds good:

$$W + T_o = F_B, \tag{1.1}$$
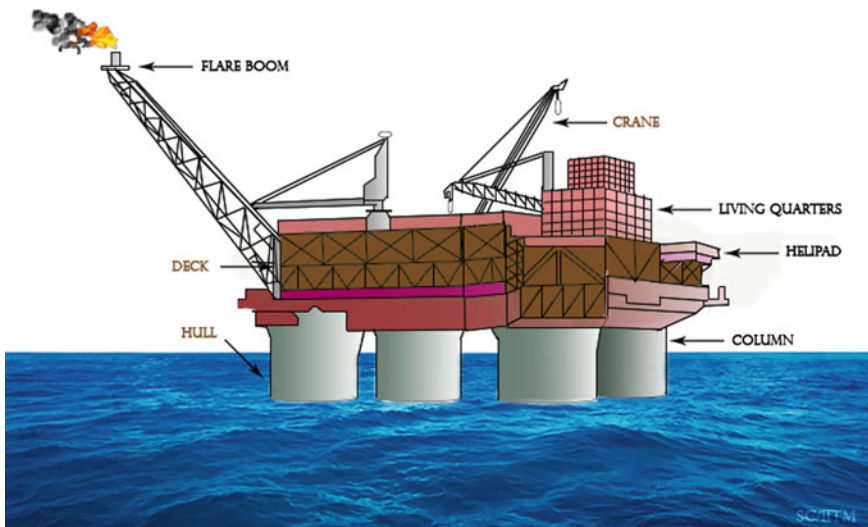
Fig. 1.8 Tension leg platform

where W is weight of the platform, T_o is initial pretension in tethers, which is usually about 20% of the total weight and F_B is the buoyancy force. Pinned connection is provided between the deck and the mooring lines to hold-down the platform in the desired position. Due to lateral forces, the platform moves along the wave direction. Horizontal movement is called **offset**. Due to horizontal movement, the platform also has the tendency to have increased immerse volume of members. Thus, the platform will undergo **set-down** effect. The lateral movement increases the tension in the tethers. The horizontal component of tensile force counteracts the wave action and the vertical component increases the weight, which will balance the additional weight imposed by set-down.

TLP is hybrid structure with two groups of natural periods. Typical natural periods of the TLP are kept away from the range of wave excitation periods and typically for TLP resonance periods of 132 s (surge/sway) and 92 s (yaw) as well as 3.1 s (heave) and 3.5 s (pitch/roll), which are achieved through proper design (Nordgren 1987). The main challenge for the TLP designers is to keep the natural periods in heave and pitch below the range of significant wave energy, which is achieved by an improved structural *form* (Paik and Roesset 1996; Kobayashi et al. 1987; Low 2009). The failure may occur either due to tether pull-out or fatigue effect on the tethers. TLP mechanism preserves many of the operational advantages of a fixed platform while reducing the cost of production in water depths up to about 1500 m (Iwaski 1981; Haritos 1985; Chandrasekaran et al. 2004, 2007a, b, c, d; Chandrasekaran and Jain 2004). Its production and maintenance operations are similar to those of fixed platforms. TLPs are weight sensitive but have limitations in accommodating heavy payloads (Tabeshpour et al. 2006; Yoshida et al. 1984; Ertas and Lee 1989). Usually, a TLP is fabricated and towed to an offshore well site wherein the tendons are already installed on a prepared seabed. Then, the TLP is ballasted down so that the tendons may be attached to the TLP at its four corners. The mode of transportation of TLP allows the deck to be joined to the TLP at dockside before the hull is taken offshore (Bar-Avi 1999; Gadagi and Benaroya 2006).

Advantages of TLPS are as follows: (i) mobile and reusable; (ii) stable as the platform has minimal vertical motion; (iii) low increase in cost with increase in water depth; (iv) deepwater capability; and (v) low maintenance cost. Few disadvantages are namely: (i) high initial cost; (ii) high subsea cost; (iii) fatigue of tension legs; (iv) difficult maintenance of subsea systems; and (v) little or no storage. Table 1.3 highlights a few of TLPs constructed worldwide (Chandrasekaran and Jain 2016).

Table 1.3 Tension leg platforms constructed worldwide

S. No.	Platform name	Water depth (m)	Location
USA			
1	Shenzi	1333	USA
2	Auger	872	USA
3	Matterhorn	869	USA
4	Mars	896	USA
5	Marlin	986	USA
6	Brutus	1036	USA
7	Magnolia	1433	USA
8	Marco Polo	1311	USA
9	Ram Powell	980	USA
10	Prince	454	USA
11	Neptune	1295	USA
12	Ursa	1222	USA
13	Morpeth	518	USA
14	Alllegheny	1005	USA
15	Jolliet	542	USA
Europe			
1	Snorre A	350	Norway
2	Heidrun	351	Norway
Africa			
1	Okume/Ebano	500	Equatorial Guniea
2	Oveng	280	Equatorial Guniea

1.11   Floating Platforms

Semisubmersibles, FPSO systems, FPUs, FSO systems, and spar platforms are grouped under this category.

1.11.1   Semisubmersibles

Semisubmersible marine structures are well known in the oil and gas industries and belong to the category of neutrally buoyant structure. These structures are typically moveable only by towing. These semisubmersibles have a relatively low transit draft, with a large water plane area, which allows them to be floated to a stationing location. On location, it is ballasted, usually by seawater, to assume a relatively deep draft or semi-submerged condition, with a smaller water plane area, for operation. Semisubmersible platforms have the principal characteristic of remaining in a
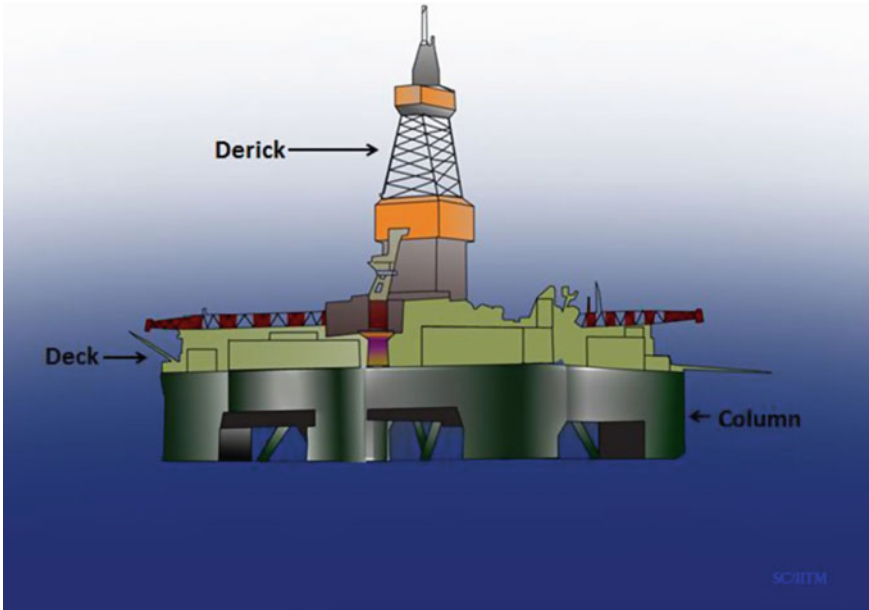
Fig. 1.9 Semisubmersible

substantially stable position and have minimal motions in all the degrees of freedom due to environmental forces such as the wind, waves, and currents. The main parts of the semisubmersibles are the pontoons, columns, deck, and the mooring lines. The columns bridge the deck and the pontoons, i.e., the deck is supported by columns. Flotation of semisubmersibles is accomplished with pontoons. The pontoons provide a relatively large water plane area, as is desirable for transit. When submerged for stationing and operations, the columns connecting the pontoons to the upper deck present a lower water plane area, thereby attracting less wave loads and thus reducing the motions. Generally, dynamic position keeping systems (DPS) are deployed to hold the semisubmersibles in position while production and drilling (Witz et al. 1986). Figure 1.9 shows a typical semisubmersible. The advantages of semisubmersibles are as follows: (i) mobility with high transit speed (~ 10 knots); (ii) stable as they show minimal response to wave action; and (iii) large deck area. Few disadvantages are (i) high initial and operating costs; (ii) limited deck load (low reserve buoyancy); (iii) structural fatigue; (iv) expensive to move large distances; (v) availability of limited dry-docking facilities; and (vi) difficult to handle mooring systems and land BOP stack and riser in rough seas. Table 1.4 shows a list of semisubmersibles commissioned worldwide (Chandrasekaran and Jain 2016).

Table 1.4 Semisubmersibles commissioned worldwide

S. No.	Platform name	Location	Water depth (m)	Year of commissioning
Europe				
1	Argyll FPU	UK	150	1975
2	Buchan A	UK	160	1981
3	Deep sea Pioneer FPU	UK	150	1984
4	Balmoral FPV	UK	150	1986
5	AH001	UK	140	1989
7	Janice A	UK	80	1999
8	Northern producer FPF	UK	350	2009
9	Asgard B	Norway	320	2000
10	Kristin FPU	Norway	320	2005
11	Gjoa	Norway	360	2010
12	Veslefrikk B	Norway	175	1989
13	Troll B FPU	Norway	339	1995
14	Njord A	Norway	330	1997
15	Visund	Norway	335	1999
16	Troll C FPU	Norway	339	1999
17	Snorre B FPDU	Norway	350	2001
USA				
1	Innovator	North America	914	1996
2	Nakika	North America	969	2003
3	Atlantis	North America	2156	2006
4	ATP Innovator	North America	914	2006
5	Thunder Horse	North America	1849	2008
6	Blind Faith	North America	1980	2008
7	Thunder Hawk	North America	1740	2009
8	P-09	Brazil	230	1983
9	P-15	Brazil	243	1983
10	P-12	Brazil	100	1984
11	P-21	Brazil	112	1984
12	P-22	Brazil	114	1986
13	P-07	Brazil	207	1988
14	P-20	Brazil	625	1992
15	P-08	Brazil	423	1993
16	P-13	Brazil	625	1993
17	P-14	Brazil	195	1993
18	P-18	Brazil	910	1994
19	P-25	Brazil	252	1996
20	P-27	Brazil	533	1996

Table 1.4 (continued)

S. No.	Platform name	Location	Water depth (m)	Year of commissioning
21	P-19	Brazil	770	1997
22	P-26	Brazil	515	2000
23	P-36	Brazil Campos basin	1360	2000
24	P-51	Brazil Campos basin	1255	2001
25	SS-11	Brazil	145	2003
26	P-40	Brazil	1080	2004
27	P-52	Brazil	1795	2007
28	P-56	Brazil	1700	2010
29	P-55	Brazil	1707	2012
Asia				
1	Tahara	Indian Ocean	39	1997
2	Nan Hia Tiao Zhan	South China sea	300	1995
3	Gumusut Kakap	Malaysia	1220	2011

1.11.2 Floating Production, Storage, and Offloading (FPSO) Platform

FPSO is an acronym for Floating Production, Storage and Offloading systems. Offloading of the crude oil is usually to a shuttle tanker. Typically converted or newly built tankers are custom-made for production and storage of hydrocarbons. These stored hydrocarbons are subsequently transported by other vessels to terminals or deepwater ports. The design variants of FPSO are FPS and FSO. FPS is an acronym for Floating Production Systems devoid of storage facility. Now, it is a universal term to refer to all production facilities that float rather than structurally supported by the seafloor, and typical examples include TLPs, spars, semisubmersibles, shipshape vessels, etc. FSO is an acronym for Floating, Storage, and Offloading system. Like the FPSO, these are typically converted or newly built tankers, and they differ from the FPSO by not incorporating the processing equipment for production; the liquids are stored for shipment to another location for processing. Offloading indicates transfer of produced hydrocarbons from an offshore facility into shuttle tankers or barges for transport to terminals or deepwater ports. Figure 1.10 shows a typical FPSO used in oil and gas exploration. An FPSO relies on subsea technology for the production of hydrocarbons and typically involves pipeline export of produced gas with shuttle tanker (offloading) transport of produced liquids (Leffler et al. 2011). FPSOs are usually ship-shaped structures and are relatively insensitive to water depth. Mooring systems of FPSOs are classified as "permanent mooring" or "turret mooring". Majority of FPSOs deployed worldwide are permanently moored, i.e., the FPSOs with their moorings
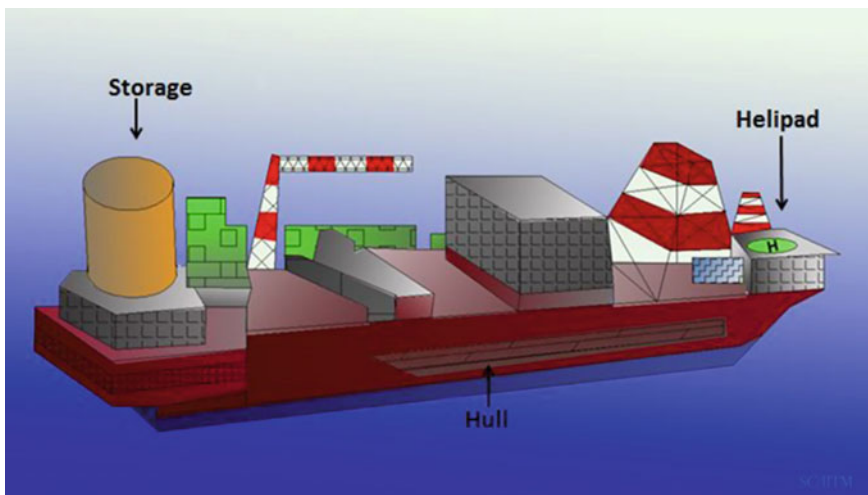
Fig. 1.10 FPSO platform

and riser systems are capable of withstanding extreme storms in the field. On the other hand, disconnect able FPSOs have attracted more attention recently. They are typically turret moored. Disconnect able turret is designed for FPSO to be able to disconnect to avoid certain extreme environments. Salient advantages of the FPSOs are as follows: (i) low cost; (ii) mobile and reusable; (iii) reduced lead time; (iv) quick disconnecting capability, which can be useful in iceberg-prone areas; (v) little infrastructure required; and (vi) turret mooring system enables FPS (converted ship type) to head into the wind/waves reducing their effect. Few disadvantages are (i) limited to small fields; (ii) low deck load capacity; (iii) damage to risers due to motion; (iv) poor stability in rough seas; and (v) little oil storage capabilities. Table 1.5 shows details of FPSOs commissioned worldwide (Chandrasekaran and Jain 2016).

Table 1.5 Details of FPSO commissioned worldwide

S. No	Platform	Water depth (m)	Location
Australia			
1	Maersk Ngujima-Yin	400	Australia
2	Stybarrow Venture	825	Australia
3	Pyrenees Venture	200	Australia
4	Glass Dowr	344	Australia
5	Front Puffin	110	Australia
6	Crystal Ocean	170	Australia
7	Ningaloo Vision	380	Australia

Table 1.5 (continued)

S. No	Platform	Water depth (m)	Location
8	Cossak Pioneer	80	Australia
9	Umurao	120	New Zealand
10	Raroa	102	New Zealand
North America			
1	Terra Nova	95	Canada
2	Sea Rose	122	Canada
3	Yuum K'ak'naab	100	US
Egypt			
1	Zaafarana	60	Egypt
2	PSVM	2000	Angola
3	Kizomba A	1241	Angola
4	Kizomba B	1163	Angola
5	Pazfor	762	Angola
6	CLOV	1365	Angola
7	Girassol	1350	Angola
8	Dalia	1500	Angola
9	Gimboa	700	Angola
10	Kuito	414	Angola
11	Petroleo Nautipa	137	Gabon
12	Knock Allan	50	Gabon
13	Abo	550	Nigeria
14	Bonga	1030	Nigeria
15	Armada Perkasa	13	Nigeria
16	Armada Perdana	350	Nigeria
17	Erha	1200	Nigeria
18	Usan	750	Nigeria
19	Agbami	1462	Nigeria
20	Akpo	1325	Nigeria
21	Ukpokiti	***	Nigeria
22	Kwame Nkrumah MV 21	***	Ghana
23	Sendje Ceiba	90	Equatorial Guinea
24	Aseng	945	Equatorial Guinea
25	Zafiro	***	Equatorial Guinea
26	Chinguetti Berge Helene	800	Mauritania
27	Baobab	1219	Cote d'Ivoire
Europe			
1	Huntington	91	UK
2	BW Athena	134	UK
3	Global producer III	140	UK
4	Bleo Holm	105	UK

Table 1.5 (continued)

S. No	Platform	Water depth (m)	Location
5	Aoka Mizu	110	UK
6	Kizomba	1341	UK
7	Humming bird	120	UK
8	Petrojarl Foinaven	461	UK
9	Maersk Curlew	76	UK
10	Schiehallion	400	UK
11	North Sea Producer	125	UK
12	Caption	106	UK
13	Norne	380	Norway
14	Alvheim	130	Norway
15	Petrojarl I	100	Norway
16	Skarv	391	Norway
17	Goliat	400	Norway
18	Asgard A	300	Norway
19	Petrojarl Varg	84	Norway
South America			
1	Cidade de Rio das Ostras	977	Brazil
2	Cidade de Sao Mateus	763	Brazil
3	P-63	1200	Brazil
4	Frade	1128	Brazil
5	Cidade de Victoria	1400	Brazil
6	Peregrino	120	Brazil
7	Espadarte I	1100	Brazil
8	Espadarte II	850	Brazil
9	Golfinho	1400	Brazil
10	Marlim Sul (south)	1430	Brazil
11	Espirito Santo	1780	Brazil
12	Cidadde de Angra	2149	Brazil
13	Cidade de Niteroi MV18	1400	Brazil
14	Cidade de Santos MV20	1300	Brazil
Asia			
1	Bohai Shi Ji	20	China
2	Bohai Ming Zhu	31	China
3	Song Doc MV19	55	Vietnam
4	Ruby II	49	Vietnam
5	Ruby Princess	50	Vietnam
6	Arthit	80	Thailand
7	Bualuang	60	Thailand
8	Anoa Natuna	253	Indonesia
9	Kakap Natuna	88	Indonesia
10	Dhirubhai I	1200	India

1.12 Spar Platform

Spar platform belongs to the category of neutrally buoyant structures and consists of a deep draft floating caisson. This caisson is a hollow cylindrical structure similar to a very large buoy. Its four major components are hull, moorings, topsides, and risers. The spar relies on a traditional mooring system, i.e., anchor-spread mooring or catenaries mooring system, to maintain its position. The spar design is now being used for drilling, production, or both. The distinguishing feature of a spar is its deep draft hull, which produces very favorable motion characteristics. The hull is constructed by using normal marine and shipyard fabrication methods, and the number of wells, surface wellhead spacing, and facilities weight dictate the size of the center well and the diameter of the hull. Figure 1.11 shows a typical spar platform. In the classic or full cylinder hull forms, the whole structure is divided into upper, middle and lower sections. The upper section is compartmentalized around a flooded center well housing different type of risers namely production riser, drilling riser, and export/import riser. This upper section provides buoyancy for the spar. The middle section is also flooded but can be configured for oil storage. The bottom section, called keel, is also compartmentalized to provide buoyancy during transport and to contain any field-installed, fixed ballast. The mooring lines are a combination of spiral strand wire and chain. Taut mooring system is possible due to small motions of the spar and has a reduced scope, defined as the ratio of length of the mooring
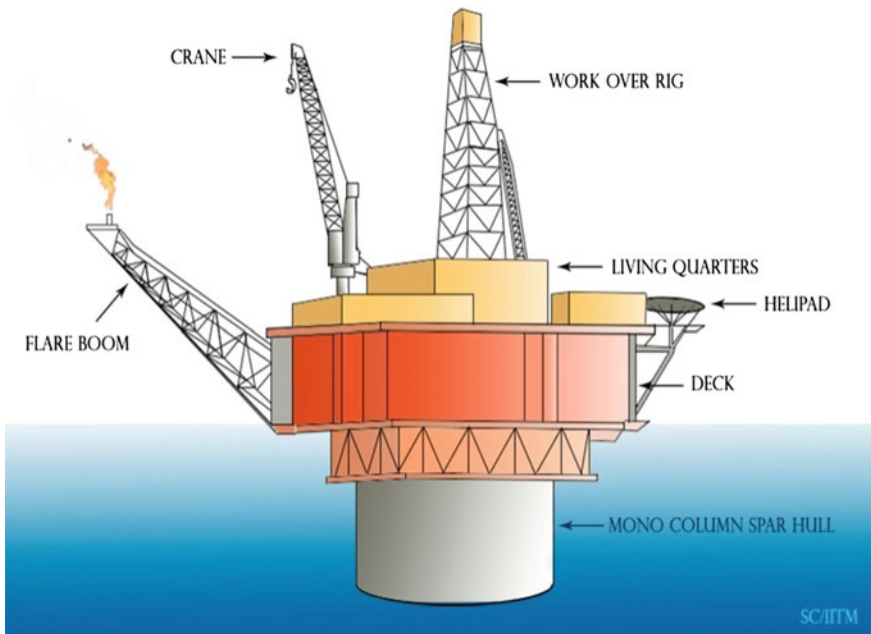
Fig. 1.11 SPAR platform
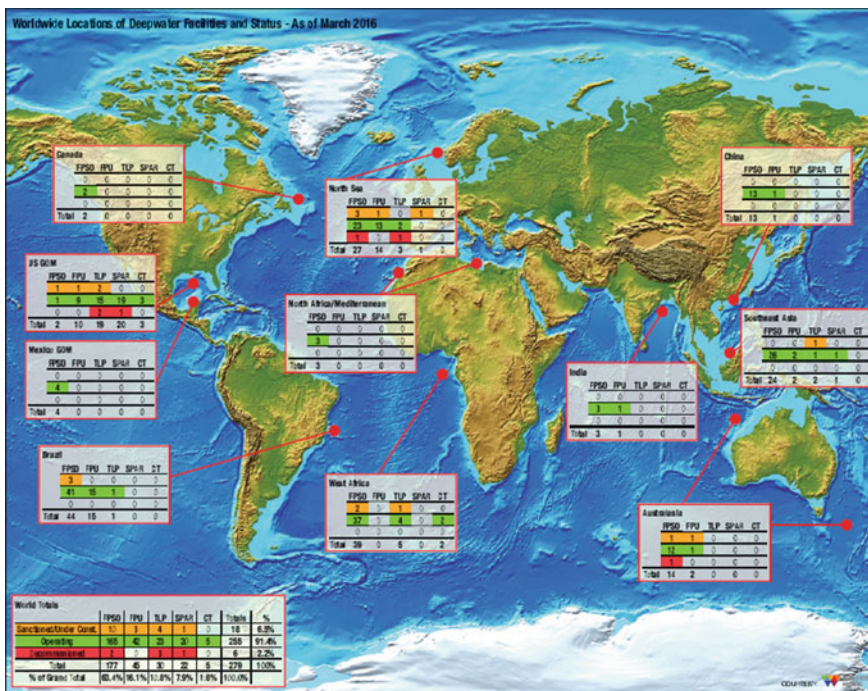
Fig. 1.12 Deepwater facilities worldwide (*Courtesy* Offshore Magazine, May 2016)

line to water depth, and cost compared with a full catenary system. Mooring lines are anchored to the seafloor with a driven or suction pile. Different types of spars include: (i) Classical spar, which has a cylindrical hull with heavy ballast at the bottom of the cylinder. (ii) Truss spar, which has a shorter cylinder called hard tank. Truss is further connected to its bottom to a soft tank, which houses ballast material. (iii) Cell spar, which has a large central cylinder surrounded by smaller cylinders of alternating lengths. Soft tank is attached to the bottom of longer cylinder to house ballast material.

Advantages of spar platforms are as follows: (i) low heave and pitch motion compared to other platforms; (ii) use of dry trees (i.e., on surface); (iii) ease of fabrication; (iv) unconditional stability as its center of gravity is always lower than the center of buoyancy, resulting in a positive GM (metacentric height); and (v) derive no stability from its mooring system and hence does not list or capsize even when completely disconnected from its mooring system. Few disadvantages include the following: (i) installation is difficult as the hull and the topsides can only be combined offshore after the spar hull is upended; (ii) have little storage capacity which brings along the necessity of a pipeline or an additional FSO; and (iii) have no drilling facilities. Figure 1.12 shows worldwide deepwater facilities as on March 2016.

1.13 New Generation Offshore Platforms

As the availability of oil and gas reserves moves towards higher waters depths, oil, and gas exploration is targeted at deep and ultra-deep waters. As the encountered environmental loads are more severe in greater water depths, the geometric *form* of offshore platforms proposed for deep and ultra-deep waters needs special attention. Apart from being cost-effective, the proposed geometric form shall also have better motion characteristics under the encountered forces arising from the rough sea. Offshore structures that are found suitable for deep and ultra-deep waters are shown in Fig. 1.13.

1.14 Buoyant Leg Structure (BLS)

Buoyant leg structures (BLSs) are tethered spars with single or group of cylindrical water-piercing hulls; these are alternative structural forms to TLPs and conventional spars. They are positively buoyant wherein the buoyancy exceeds the mass of the structure. Although being positively buoyant, positive metacentric height is maintained to ensure the desired structural stability even after the removal of tethers from the structure. This characteristic ensures high stability and deep draft, which makes the structural form relatively insensitive to increased water depth (Copple and Capanoglu 1995). Since the BLS is a deep draft structure, the exposed structural part near the free surface is reduced, the forces exerted on the structure reduces when compared with the conventional TLPs. Since the risers are inside the moon pool of the BLS, the forces exerted on the risers are also minimized, but below the keel of the BLS, some forces like wave or current act. Halkyard et al. (1991) initially proposed the concept of a tension buoyant tower, which was subsequently

Tension leg platform   Gravit base semi submersible   Deep draft floating buoy   Spar   FPSO   Buoyant leg structure   Triceratops   Circular FPSO

SC/IITM
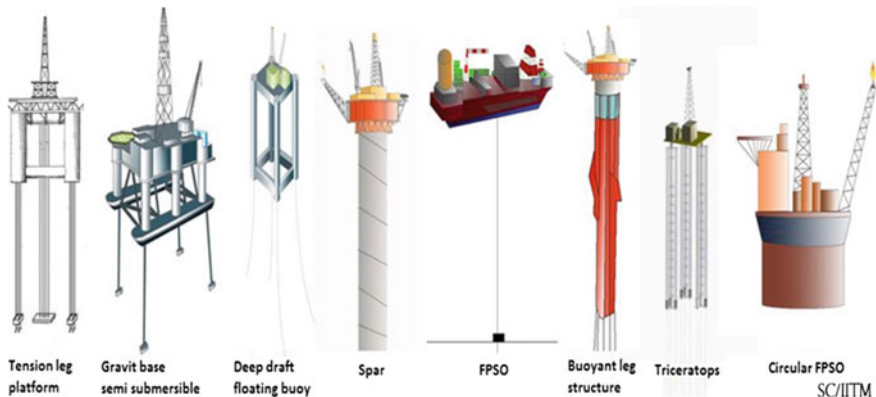
Fig. 1.13 Different types of ultra-deepwater structures

Fig. 1.14 Buoyant tower in the fabrication yard
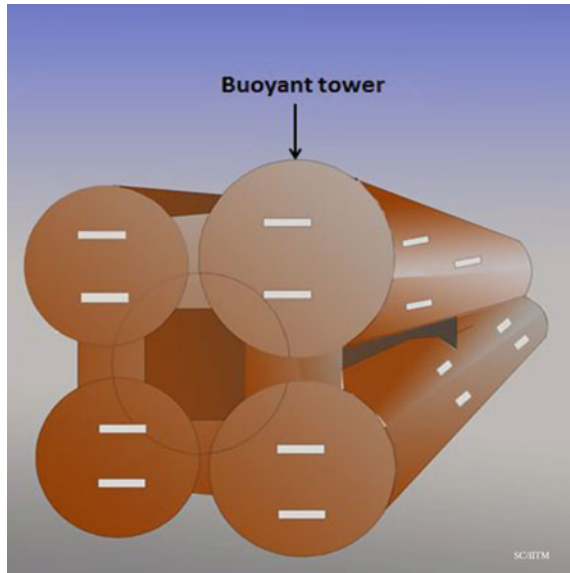
modified by other researchers (Copple and Capanoglu 1995; Perryman et al. 1995). The structural form of BLS is evolved by combining the advantageous features of spars and TLPs where its deep draft hull limits the vertical motion to a significant extent (Shaver et al. 2001); BLS resembles spar due to its shape and deep-draft feature, and its response behavior is similar to that of a TLP due to its restoring system. BLS is simple to fabricate, easy to load-out, tow, and install (Capanoglu et al. 2002). Figure 1.14 shows the views of buoyant tower in the fabrication yard, while different stages of installation of BLS are shown in Fig. 1.15.

Installation process of BLS is the combination of the installation procedures of spar and TLP. Since spar is a stable structure, it is installed simply by free-floating, while TLP is generally installed by achieving required pretension in tethers using the following techniques: (i) ballast; (ii) pull-down; or (iii) both pull-down and ballast methods. During the installation of BLS, the structure can be free-floated using its permanent ballast. Pretension in the tethers can be achieved by the above-mentioned procedure. In the ballast method, the structure will be additionally ballasted until it achieves the required draft; tethers are then attached from the structure to the seafloor. Additional ballast will be removed from the structure to enable pretension in the tethers. In the pull-down method, free-floating structure will be pulled down until it achieves the required draft; excess buoyancy that is transferred to the tethers helps to achieve the desired pretension. Pull-down and ballast method is the combination of the above-mentioned procedures. BLS imposes improved motion characteristics and more convenient riser systems, as they consist of simple hulls in comparison to spars or TLPs. BLS is more economic than TLPs or spars due to the reduced cost of commissioning. The first buoyant tower drilling production platform, CX-15 for Peru's Corvina offshore field was
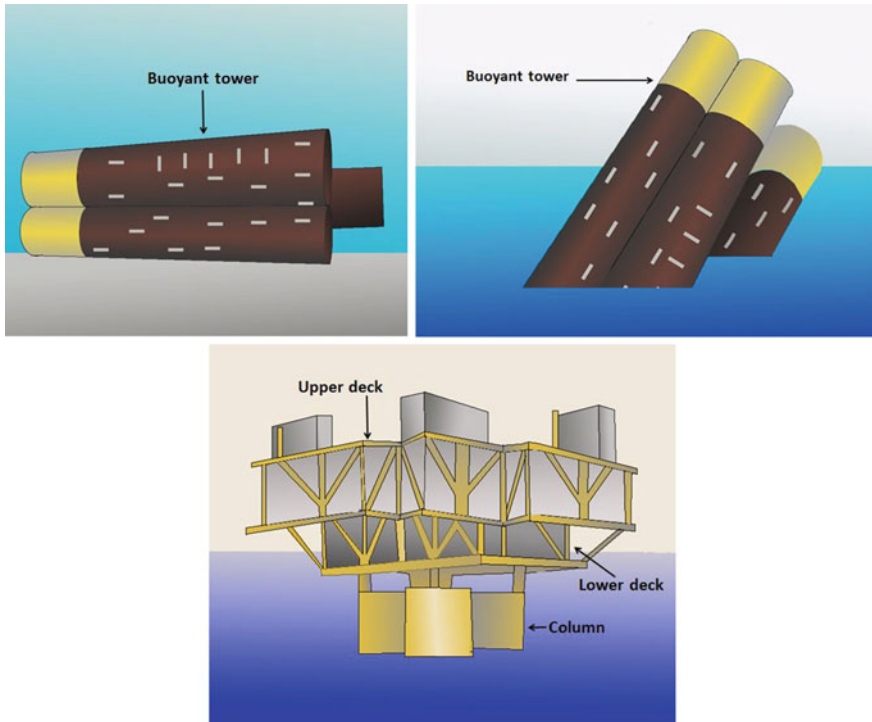
Fig. 1.15 Load-out and installed structure in offshore field

installed in September 2012 at a water depth of more than 250 m with a production capacity of 12,200 barrels per day.

1.15   Triceratops

More innovative geometric forms of offshore platforms are evolved in the recent past to improve the motion characteristics of these platforms under deep and ultra-deep waters. Triceratops, non-ship-shaped FPSOs, Min Doc are few of them. The conceptual idea of a triceratops discussed in literature indicated favorable characteristics of the platform under deep and ultra-deep waters (White et al. 2005); Fig. 1.16 shows the conceptual view of the triceratops. Geometric innovativeness imposed in the design by the introduction of ball joints between the deck and BLS makes triceratops different from other new generation offshore platforms. Triceratops consist of three BLS units, deck, three ball joints between the BLS units and deck, and restoring system either with restraining leg or with the tethers. Ball joints transfer all translation but not rotation about any axis, making the platform different from other classic types of offshore structures; the distinct motion
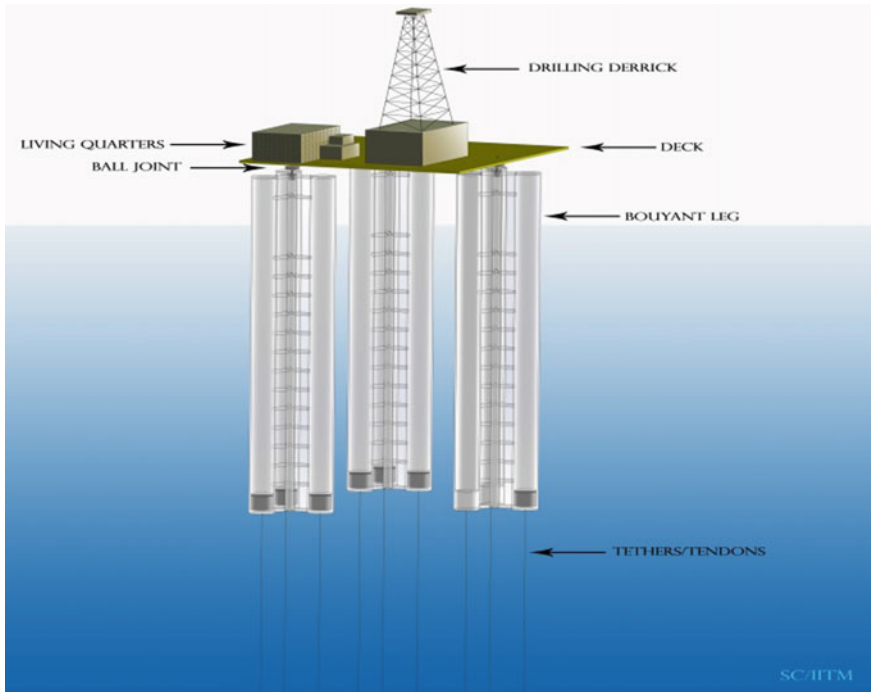
Fig. 1.16 Conceptual view of triceratops

characteristics of its structural members such as BLS and deck provide uniqueness to its structural behavior under lateral loads. Common types of offshore platforms have rigid body motion due to the rigid connection between the members; this makes the platform to respond as a single unit. As triceratops is integrated with different structural elements, it behaves as a rigid body in all translations but not in rotations about any axis due to the presence of the ball joints; rotational responses of BLS differ from that of the deck.

Studies focusing their response behavior become interesting as the responses of BLS and deck are to be dealt separately, which is not a common practice in most of the offshore platforms. In addition, the derived geometric form has few advantages: (i) reduction in forces exerted on the platform due to the decrease in the exposed part of the structure near the free surface; and (ii) protection of risers from lateral forces as they are located inside the moon pool of the BLS. The presence of ball joints between the deck and BLS restrains the transfer of the rotational motion of the deck from BLS; translation and rotation motion of BLS under the encountered environmental loads are significantly high. However, due to the deep draft of the BLS, there is more possibility of unusual corrosion. Corrosion challenges can be overcome by few techniques such as (i) frequent inspection using corrosion testing probes; (ii) use of sacrificial anodes; (iii) anticorrosive coatings; and (iv) use of cathodic protection. The salient advantages are (i) better motion characteristics;

(ii) suitable for deep waters; (iii) improved dynamics in comparison to TLPs and spars; (iv) wells within protected environment and are laterally supported; (v) simple structure; (vi) simple station keeping; (vii) easy to install and decommission (Installation can be part by part or as a whole structure); (viii) reusable and relocated; (ix) simple restraining system (does not require high strength systems like TLPs); (x) highly stable structure; and (xii) relatively low cost.

1.16   Floating, Storage and Regasification Units (FSRUs)

Transportation of unprocessed crude from the drilling/exploratory platform to the onshore site involves expensive systems like transportation through pipes, large vessels, etc., which makes the oil production more expensive. In particular, the offshore platforms located far offshore prove to be highly uneconomical. Key components of FSRU consist of regasification equipment that transforms LNG at -160 °C and high-pressure, storage tanks, loading arms for receiving LNG, export manifolds, and sea water pumps that uses sea water to re-gasify the LNG. FSRU is the more cost-effective alternative to meet the lower demand of LNG than traditional, land-based terminals. It contains regasification unit, gas turbine with generator, air compressors, fuel pumps, fire water and foam systems, fresh water systems, cranes, lubrication oil system, life boats, and helipad.

The LNG is stored at $-160°$ in double-walled insulated tanks to limit boil-off. The outer walls of the tank are made of prestressed reinforced concrete or steel to limit the temperature during storage period. Despite the high-quality insulation, a small amount of heat still penetrates the LNG tanks, causing minor evaporation. The resulting boil-off gas is captured and fed back into the LNG tank using compressor and recondensing systems. This recycling process prevents any natural gas from escaping the terminal under normal operating conditions. The LNG is subsequently extracted from the tanks, pressurized and re-gasified using heat exchangers. The tanks are equipped with submerged pumps that transfer the LNG towards other high-pressure pumps. The compressed LNG (at around 80 times atmospheric pressure) is then turned back into a gaseous state in vaporizers. Once returned to its gaseous state, the natural gas is treated in a number of ways, including metering and odorizing, before it is fed into the transmission network.

LNG is simply warmed using the heat from seawater. This is done in a heat exchanger (with no contact between the gas and the sea water), resulting in a slight drop in the temperature of the sea water, which reaches 6 °C at the end of the discharge pipe, quickly becoming imperceptible once diluted. Natural gas is odorless. Although nontoxic, it is inflammable and is therefore odorized to ensure even the slightest leak can be identified. This is done by injecting tetra-hydrothiophene (THT), which is an odorant detectable in very small doses, at the terminal before the natural gas is distributed. Gas turbine equipped at the topside of the FSRU uses multiple units of generating capacity of up to 10–12 MW. The instrument air system provides air for the plant and the instrument air in process

control and maintenance. Inert gas (nitrogen) will be generated on demand by a membrane package using dry, compressed air. A backup inert gas supply system consisting of compressor seals, cooling medium, expansion drums, and utility stations also has to be provided. The oil pump provides high-pressure oil to the engine. The fuel is pumped from the fuel tank to the primary fuel filter/water separator, which is then pressurized to 650 kPa gauge pressure by the fuel transfer pump. The pressurized fuel is then sent through the secondary/tertiary fuel filter. Water supply for the fire-fighting systems is supplied by fire water pumps at a pumping rate of about 600–5000 m^3/h at the discharge flange at a pressure of about 18 bar. A film-forming fluro protein (FFFP) concentrate system is provided to enhance the effectiveness of the deluge water spray that protects the separator module, which has high potential for hydrocarbon pool fires. FFFP is a natural protein foaming agent that is biodegradable and nontoxic. The fresh water maker system will utilize a reverse osmosis process to desalinate the sea water at the rate of 5 m^3/h. The saline effluent from the fresh water will be directed overboard through the seawater discharge caissons, while the fresh water will be stored in a fresh water tank. Water delivered to the accommodation module will be further sterilized in a UV sterilization plant before stored in a potable water header tank. The lubrication system contains an oil cooler, oil filter, gear driven oil pump, pre-lube-pump and an oil pan that meets offshore tilt requirements. The internal lubrication system is designed to provide a constant supply of filtered, high-pressure oil. This system meets the tilt requirements for nonemergency offshore operations. Lubrication oil should have special features in offshore requirements such as (i) water solubility; (ii) non-sheering on water surface; (iii) excellent lubrication properties; (iv) biodegradable; and (v) nontoxic to aquatic environment.

1.17   Drill Ships

Drill ship is an adaptation of a standard sea going ship of mono-hull form, additions are substructure containing a moon pool and cantilevers from which drilling operations may be carried out. Drill ships are designed to carry out drilling operations in deep sea conditions that are quite turbulent and susceptible to wave action. A typical drillship has a drilling platform and derrick located at the middle of its deck. Drill ships contain a hole called moon pool, extending right through the ship, down the hull. They are relatively unstable and liable to be tossed by waves and currents. They use Dynamic Positioning System (DPS) and moorings for station keeping. The major components of DPS include controller, sensor system, thrusters and power system. DPS comprises of electric motors on the underside of the ship hull and they are capable of propelling the ship any direction. Propeller motors are integrated with the computer system of the ship. It uses the satellite positioning system technology, in conjunction with sensors located on the drilling template to ensure that the ship is directly above the drill site at all times. DPS activates thrusters to move the ship back to original position. The controllers command the

action of the thrusters installed at the bottom of the ship hull and it keeps the platform within a tolerance radius of about 2–6% of the water depth. DPS controls displacement in surge, sway and yaw motion. In mooring system, 8 to 10 anchor lines are required and hence uneconomical. Drill ships have the following advantages compared to semisubmersibles: (i) ship-shaped hull; (ii) subjected to longer period of down time under wind and wave action; (iii) used in smooth waters; and (iv) large load carrying capacity.

1.18 Subsea Production Systems

Subsea systems (SSS) are multicomponent seafloor systems which allow the production of hydrocarbons in water depths where conventional fixed or bottom founded platforms cannot be installed (Bai 2001). Subsea system can be located many miles away in deeper water and tied back to existing host facilities like FPS. The components of SSS are (i) Array of subsea wells; (ii) manifolds; (iii) central umbilical; and (iv) flow lines. The different layouts of subsea systems are single-well satellite, multi-well satellite, cluster well system, template system, and combinations of the above. The various components are as follows:

Subsea production tree: It is an arrangement of valves, pipes, fittings, and connections placed on a top of a wellbore. They are common for all type of drilling platforms. The height varies about 30 m and it requires a counter weight to regulate the flow under pressure. The orientation of the valve can be done in the horizontal bore or in the vertical outlet of the tree, comparatively horizontal outlet is safe. The valves can be operated by electrical or hydraulic signals or manually by diver.

Pipeline and flow line: These are the conduits to transport fluid from one location to another. Pipelines are used over a large area for transporting oil, gas, sulfur and produced water from two separate facilities. The length varied from 1 m to 1000 km and the diameter of the pipeline is about 450 mm. The flow lines are installed within the confines of the platforms or manifold. These are the diversion lines for routing the subsea manifold into the processing equipment (Guo et al. 2005).

Subsea Manifold: These are gravity-based stand-alone or integrated structures, containing valves, pipes, and fittings. It serves as a central gathering point for production from subsea wells. It redirects the combined flow to host facility. They are rectangular or circular with a height of about 9 m. These are anchored to the seabed by piles. The size of the manifold depends upon the pattern and number of wells.

Umbilical: It connects the host and the subsea system. These are the bundled arrangement of tubing, piping and electrical conductors of 25 mm diameter. An armored sheath is provided for the purpose of insulation. It transmits the control fluid and electric current in order to control the functions of the subsea production and safety equipment. These are the dedicated tubes to monitor pressure and inject fluids.

Jumper: These are the check arrangement for the umbilical, used to connect various subsea equipments. The offset distance between the components governs the length of the jumper. They are classified as production jumper, hydraulic jumper, and electrical jumper. They are provided at the terminal. Flexible jumper system provides versatility, unlike rigid jumper system that limits the space and the handling capacity.

Termination unit: it is an equipment to facilitate the interface of the pipeline or flow line with the subsea manifold. It is positioned near the manifolds and it can be used for the electric/hydraulic control, equipped with an installation arm to brace it during lowering process.

Production risers: It is a portion of flow line that resides between the host facility and the seabed adjacent to the host. The length of the riser depends upon the water depth and the riser configuration can be of the following forms: (i) free hanging; (ii) lazy S; (iii) lazy wave; (iv) steep S; and (v) steep wave. They are designed to withstand all type of forces.

Template: It is a fabricated structure that houses the subsea equipment. It accommodates multiple trees in tight clusters, manifold, piping equipment, and chemical treatment equipment.

Exercise
Part A: **Objective type questions**

1. Offshore platforms are broadly classified based on _____.
2. The structural form of every platform is largely derived on the basis of _____ but not on the basis of _____.
3. Compliancy changes _____ behavior of offshore platforms.
4. _____ plays a very important role in floating-type structures.
5. Floating structures are classified as _____.
6. Fixed platforms with a welded space frame is also called _____.
7. A jacket platform complex consists of _____, _____, _____, _____, and _____.
8. TLP is _____ type floating platform.
9. Compliancy means _____.
10. Compliant platforms are meant for _____ drilling.
11. The design objective of GBS platform is _____.
12. The net relative response is greatly reduced in _____platforms.
13. Compliant structures have high degree of _____.
14. The compliant structures vibrate due to _____ because of its flexibility.
15. Compliant structures are position-restrained by _____.
16. The compliant structures rely on _____ to maintain the stability.
17. The ability of the system to regain its original position by virtue of its displacement is called _____.
18. Complaint platforms resist the lateral load by _____.
19. In jacket platforms, _____ cross-section members are used.

20. Jacket platforms are influenced by _____.
21. The deck is usually made up of _____ type truss.
22. The structural member in the form of cone that connects the topside and the jacket is _____.
23. The horizontal and diagonal members in the jacket structure are called _____ and they provide _____ to the structures.
24. The long hollow tubes that are embedded into the seabed through which drilling is performed is called _____.
25. The long slender tube that carries the crude or partially processed oil gas to another location for further processing is called _____.
26. _____ protects the oil/gas carrying risers.
27. _____ is provided to facilitate welding and expansion.
28. _____ provides greater uplift resistance to the jacket platform.
29. _____ helps the platform to sink deeper if the soil is too soft near the top layer of the sea bed.
30. _____ towing is always preferred during the construction of the jacket platform.
31. Gravity platforms are responsible for _____ due to _____.
32. The construction of gravity platforms requires _____ and _____.
33. The foundation of GBS prevents failure due to _____ caused by _____.
34. _____ are the hollow concrete structures at the bottom of the platform to provide the structure with natural buoyancy.
35. _____ helps to prevent damage to steel skirts during touchdown by properly anchoring the caisson.
36. Machinery should be placed in _____ deck.
37. _____ occurs due to unequal settlement, which causes coupled moment at the bottom of the platform.
38. Jack-up rigs are used for _____.
39. The legs of jack-up rigs are _____ type.
40. _____ members are used for the construction of drilling derrick.
41. Jack-up rigs are _____ at bottom.
42. The sharp wedge-shaped tip of the drill pipe used for drilling is called _____.
43. _____ is used as a counter weight during drilling.
44. The shallow underside footing used in jack-up platform is called _____.
45. The vent provided in the hull of offshore platforms for drilling to take place is called _____.
46. _____ in the jack-up platforms leads to differential settlement.
47. In compliant platforms, majority of lateral loads are counteracted by _____.
48. In compliant platforms, the vertical component of tension in tendons adds to _____ and improves _____.

49. Guyed towers are held in place by _____ guy lines.
50. The upper part of the guy wire is called _____, which acts as a _____ in moderate seas
51. The guyed towers are considered as _____ in analysis.
52. The point where the mooring line touches the floor is called _____.
53. _____ are provided to avoid lifting up of clump weight due to scouring.
54. The guy wires are connected to the top by _____.
55. An articulated tower is an upright tower that is hinged at its base with a _____.
56. The tower is ballasted near _____ and has a large buoyancy tank at _____.
57. The buoyancy tank is provided near the free surface to improve _____.
58. The universal joints are likely to fail under _____ loads.
59. Dynamic amplification factor of articulated tower is _____ than that of fixed type platforms.
60. The articulated towers restore its original position due to _____.
61. Buoyancy chamber is _____ than the ballast chamber.
62. Tension leg platforms are position-restrained by _____.
63. Tension leg platforms are _____ restrained and complaint in _____.
64. Pretensioning of tendons is achieved by increasing _____.
65. In TLP, the natural periods in heave and pitch should be kept _____ the range of significant wave energy.
66. _____ connection is provided between the deck and the mooring lines to maintain _____.
67. The horizontal movement of TLP due to lateral forces is called _____.
68. The vertical movement of TLP due to _____ is called _____.
69. Tethers are susceptible to _____ failure due to _____.
70. TLP is flexible in _____ and rigid in _____.
71. The pontoons provide a _____, as is desirable for transit.
72. The columns connecting the pontoons to the upper deck present a _____, thereby attracting _____ wave loads.
73. _____ are used to hold the semisubmersibles in position during drilling and operation.
74. An FPSO relies on _____ for the production of hydrocarbons.
75. Mooring systems of FPSOs are classified as _____ and _____.
76. FPSO is meant for _____ and not for _____.
77. _____ is designed for FPSO to be able to disconnect to avoid certain extreme environments.
78. A spar consists of _____ caisson.
79. _____ is a hollow cylindrical structure similar to a very large buoy.
80. The distinguishing feature of a spar is its _____, which produces very favorable motion characteristics.
81. The bottom section of classical spar is called _____ and it is also compartmentalized to provide _____ during transport.

82. Mooring lines are anchored to the seafloor with a _____.
83. The mooring lines are a combination of _____.
84. In truss spar, ballast material is provided in _____.
85. _____ spar has a large central cylinder surrounded by smaller cylinders of alternating length.
86. SPAR platforms have low _____ compared to other platforms.
87. In SPAR platforms, the center of gravity is _____ than that of center of buoyancy.
88. SPAR has a _____ metacentric height.
89. _____, _____, and _____ platforms are suitable for ultra-deepwater condition.
90. Buoyant leg structures are _____ spars.
91. Buoyant leg structures are alternative forms of _____ and _____.
92. BLS are _____ wherein the buoyancy _____ the mass of the structure.
93. In BLS, _____ is maintained to ensure the desired structural stability even after the removal of tethers from the structure.
94. The force exerted on BLS is _____ comparatively, due to _____.
95. The shape of BLS resembles _____ and its structural action resembles _____.
96. Pretension in TLP is achieved by _____, _____ and _____ methods.
97. In triceratops, the BLS units and the deck are connected by _____.
98. Ball joints transfer _____, but restrains _____.
99. Triceratops behaves as _____ in translation motion.
100. _____ and _____of BLS results in relative insensitivity to water depth.
101. New generation deepwater structures that are easily relocatable are _____ and _____.
102. In triceratops, the rotational response is _____ and translational response is _____.
103. _____ is the more cost-effective alternative to meet the lower demand of LNG than traditional, land-based terminals.
104. The LNG is stored at _____ in double-walled insulated tanks to limit boil-off.
105. _____ is provided to enhance the effectiveness of the deluge water spray that protects the separator module, which has high potential for hydrocarbon pool fires.
106. _____ is an adaptation of a standard sea going ship of mono-hull form.
107. Drill ships are designed to carry out drilling operations in _____ conditions.
108. In DPS, _____ generates forces and moments to counteract the environmental forces.
109. _____ system is preferred for station keeping in drill ships.
110. _____ keeps the platform within a tolerance radius of about _____ of the water depth.

111. _____ allow the production of hydrocarbons in water depths where conventional fixed or bottom founded platforms cannot be installed.
112. _____ is an arrangement of valves, pipes, fittings and connections placed on a top of a wellbore.
113. _____ are the diversion lines for routing the subsea manifold into the processing equipment.
114. The length of the pipeline in SSS varies from _____.
115. _____ serves as a central gathering point for production from subsea wells.
116. _____ are the dedicated tubes to monitor pressure and inject fluids.
117. _____ is provided for the purpose of insulation in the umbilical.
118. The length of the riser depends upon _____.
119. _____ is a fabricated structure that houses the subsea equipment.
120. Termination unit is an equipment to facilitate the interface of the _____ with the _____.

Part B: Subjective type questions

1. What are the five major areas of operation from exploration to transportation of oil?
2. Define FEED.
3. Name any three floating platforms.
4. What are the functions of offshore platforms?
5. List the factors based on which the offshore platforms are developed.
6. What is the importance of pre-FEED in offshore structures?
7. Name few neutrally buoyant type floating platforms.
8. Name few positively buoyant type floating platforms.
9. Mention the reasons for less number of offshore installations.
10. What are the major components of offshore platforms?
11. What are the differences between fixed platforms and compliant platforms?
12. Why offshore structures are unique?
13. What are the salient features of fixed type platform?
14. What do you understand by recentering and equilibrium?
15. Define GBS.
16. What are the advantages and disadvantages of jacket platforms?
17. What are the three components of deck?
18. What are the functions of a crane pedestal?
19. What is a flare boom?
20. What is the transition piece?
21. What is the function of barge bumpers?
22. Why launch truss is provided in jacket platforms?
23. What is the function of mudmat?
24. List the steps involved in the construction of the jacket platform.
25. What is a CONDEEP?
26. Why caissons are provided at the bottom of GBS?

27. What are the functions of steel skirts?
28. Mention the components of the modular deck.
29. What is well sinking? Where it is used?
30. How failure occurs in GBS?
31. Explain the geotechnical problems associated with GBS.
32. Is GBS advantageous over jacket platforms? Explain.
33. Draw a neat sketch of jacket platform and name the components.
34. List the advantages and disadvantages of GBS.
35. What is a draw work?
36. What do you mean by Offset drilling?
37. What is a spud can?
38. Mention the advantages and disadvantages of jack-up rigs.
39. Explain the structural action of guyed tower.
40. Is the statement true or false: Guy lines are attached to the tower above mean sea level. If true, explain.
41. Why the guyed towers are designed with constant square section along its length?
42. Mention the salient features of Lena Guyed Tower.
43. State the advantages and disadvantages of guyed towers.
44. Why clump weights and drag anchors are provided in guyed towers?
45. Draw a neat sketch of guyed tower and mark the components.
46. How failure occurs in jack-up rigs?
47. Compare the restoration moment developed due to buoyancy in guyed tower and articulated tower.
48. What is the advantage of providing more articulations in the tower?
49. Mention the advantages and disadvantages of articulated towers.
50. Define SALM.
51. What are the functions of buoyancy chamber and ballast chamber?
52. Explain the structural action of articulated towers.
53. Why buoyancy chamber is not provided at the bottom of the articulated tower?
54. Why buoyancy chamber is larger than the ballast chamber?
55. What do you understand by the term single-point failure?
56. What is the key design factor in TLP?
57. Explain the steps involved the installation of TLP.
58. What are the advantages and disadvantages of TLP.
59. What type of connection is provided between the deck and mooring lines? Explain
60. Explain the structural action of TLP.
61. How failure occurs in TLP?
62. How pretension is imposed in tendons?
63. Why TLP is more advantageous than articulated towers?
64. What are the major components of semisubmersible?
65. Explain the structural action of a semisubmersible?

66. What are the advantages and disadvantages of semisubmersibles?
67. What are the design variants of FPSO?
68. What do you understand by the term FPSO?
69. What is offloading?
70. Differentiate permanent mooring and turret mooring.
71. Mention the advantages and disadvantages of FPSO.
72. What are the major components of SPAR?
73. Explain the form of classical SPAR.
74. What type of mooring system is preferred in SPAR?
75. Name different types of SPAR?
76. What is a BLS?
77. What characteristic of BLS provides it with increased stability?
78. Compare the forces acting on TLP and BLS.
79. Why BLS is considered as an alternate form of SPAR and TLP?
80. Compare the installation procedure of SPAR and TLP.
81. What is ballast method?
82. What is pull-down method?
83. What are the major components of triceratops?
84. List the advantages of triceratops.
85. Name few techniques to overcome the corrosion challenges in triceratops.
86. What is the function of ball joint in triceratops?
87. Comment on the wave forces exerted on the risers in BLS.
88. What is the unique motion characteristics of triceratops?
89. What is FSRU? Why are they necessary?
90. What are the key components of FSRU?
91. List the components present in FSRU.
92. How natural gas is prevented from escaping through the terminals by minor evaporation?
93. State the importance of odorizing the natural gas before distribution.
94. What are the salient features of lubrication oil?
95. What is a drill ship?
96. What are the components of drill ships?
97. What do you understand by DPS?
98. What are the advantages of drill ships over semisubmersibles?
99. What are the major components of DPS?
100. What is the function of the controllers in DPS?
101. What is SSS?
102. List the different layout of subsea systems.
103. Differentiate pipeline and flow line.
104. Write a short note on subsea production tree.
105. What are the functions of subsea manifold system?
106. Write a short note on Umbilicals.
107. What are the different types of jumpers?

108. Compare flexible and rigid jumper system.
109. Name the different riser configurations.
110. Write short notes on Termination unit.

Key to Exercise
Part A: **Objective questions**

1. Geometric form.
2. Structural innovativeness, the functional advantages.
3. Dynamic.
4. Buoyancy
5. Neutrally buoyant type and positively buoyant type.
6. Template-type structure.
7. Process, wellhead, riser, flare support, and living quarters.
8. Positive buoyant.
9. Flexible.
10. Exploratory.
11. Production.
12. Compliant.
13. Flexibility.
14. Self-induced motion.
15. Mooring system.
16. Restoring buoyancy forces.
17. Recentering capability.
18. Relative movement.
19. Tubular.
20. Seabed scour.
21. Warren.
22. Transition piece.
23. Braces, lateral stability.
24. Conductors.
25. Risers.
26. Riser guards.
27. Joint can.
28. Skirt piles.
29. Mudmat.
30. Dry.
31. Seabed scouring, large foundation.
32. Deep harbors and deep tow-out channels.
33. Overturning moment, lateral loads.
34. Caissons.
35. Dowel bars.
36. Cellar.
37. Rocking.

38. Exploratory drilling.
39. Lattice truss.
40. Tubular.
41. Hinged.
42. Drill string.
43. Drilling mud.
44. Spud can.
45. Moon pool.
46. Sea bed scouring.
47. Horizontal component of tension in the tendons.
48. Weight, stability.
49. Catenary.
50. Lead cable, stiff spring.
51. pinned-pinned beam.
52. Touch-down point.
53. Drag anchors.
54. Top tension risers.
55. Universal joint.
56. Universal joint, the free surface.
57. Restoring moment.
58. Fatigue.
59. Lower.
60. Buoyancy effect/variable submergence effect.
61. Larger.
62. Tendons/tethers/taut mooring lines.
63. Heave, horizontal (surge, sway and yaw).
64. Free-floating draft.
65. Below.
66. Pinned, the horizontal position of the structure.
67. Offset.
68. Variable submergence, set-down.
69. Fatigue, tether tension variation.
70. Horizontal, vertical.
71. Relatively large water plane area.
72. Lower water plane area, less.
73. Dynamic position keeping systems.
74. Subsea technology.
75. "Permanent mooring" and "Turret mooring".
76. Exploratory drilling, production drilling.
77. Disconnectable turret.
78. Deep-draft floating.
79. Caisson.
80. Deep-draft hull.

 81. Keel, buoyancy.
 82. Driven or suction pile.
 83. Spiral strand wire and chain.
 84. Soft tank.
 85. Cell.
 86. Heave and pitch motions.
 87. Lower.
 88. Positive.
 89. BLS, triceratops, FSRU.
 90. Tethered.
 91. TLP and conventional SPAR.
 92. Positively buoyant, exceeds.
 93. Positive metacentric height.
 94. Reduced, reduction in exposed part near the surface.
 95. SPAR, TLP.
 96. Ballast, pull-down, both ballast, and pull-down.
 97. Ball joints.
 98. Translation, rotation.
 99. Rigid body.
100. Deep-draft and high stability.
101. Tension buoyant tower and non-ship-shaped FPSOs.
102. Isolithic and monolithic.
103. FSRU.
104. $-160°$.
105. A film-forming fluoro protein (FFFP) concentrate system.
106. Drill ship.
107. Deep sea.
108. Thruster.
109. DPS.
110. Controllers, 2–6%.
111. Subsea systems.
112. Subsea production tree.
113. Flow lines.
114. 1 m to 1000 km.
115. Subsea manifold.
116. Umbilical.
117. Armored sheath.
118. Water depth.
119. Template.
120. Pipeline or flow line, subsea manifold.

Part B: **Subjective type questions**

  1. (i) exploration; (ii) exploration drilling; (iii) development drilling; (iv) pro-
      duction operations; and (v) transportation.

2. Newly generated structural forms do not have any precedence to compare and understand their behavior and complexities. It is, therefore, important to understand the response of the structure and then select the structure that is most suitable to the environment. This is one of the essential features of the Front-End Engineering Design (FEED).

3. Semisubmersible, Floating Production Unit (FPU), Floating Storage and Offloading (FSO), Floating Production, Storage, and Offloading (FPSO) System, Spar.

4. (i) exploratory and production drilling; (ii) preparing water or gas injection into reservoir; (iii) processing oil and gas; (iv) cleaning the produced oil for disposal into sea; and (v) accommodation facilities.

5. Structural geometry with a stable configuration, easy to fabricate, install and decommission, low CAPEX, early start of production, and high return on investment by increased and uninterrupted production.

6. As it is well known that each platform is unique in many ways, learning about their structural configurations, limitations with respect to the sea states and water depth, construction complexities, decommissioning issues, and their structural action will be an important stage in the pre-FEED.

7. Semisubmersibles, FPSO, mono-column spars.

8. Tension leg platforms.

9. Inaccessible, high cost, technological complexity, safety issues, and high risk.

10. The major components of offshore platforms are
    Superstructure: It consists of deck and equipment for functioning of the platform.
    Substructure: It supports the deck and transmits the load from substructure to foundation.
    Foundation: It supports the substructure and superstructure; it also transmits the load to the seabed.
    Mooring system: It is used for station keeping.

11. Fixed and compliant platforms:

Fixed	Compliant
Stiff	Flexible
Attracts more forces	Attracts less forces
Massive	Low mass
Failure due to strength parameters	Failure due to displacement
Time period: <6 s	Time period: above 30 s
Suitable for shallow water depth	Suitable for deepwater depth
High frequency	Low frequency
Displacement is restrained	Displacement is allowed
Equilibrium condition	Recentering capability
Resists lateral loads by self-weight	Resists lateral load by relative movement

12. Offshore structures are form driven. Choosing the form involves complexity. Every form is site specific, not function specific. Structural form is realtered based on the structural performance. It is governed by the location where it is installed.

13. The base of the structure is fixed to the sea bed, Stiff or rigid structure, tendency to attract more forces, they are subjected to cyclic forces which leads to fatigue failure, Less response to the lateral loads, high and sudden damage, massive structure.

14. Recentering capability—the ability to regain its original position by virtue of its displacement.
    Equilibrium—the restoration happens under the action of forces.

15. BBS—Gravity-Based Structure.
    The platform relies on its own weight to resist the lateral load. Hence named as "Gravity platforms". They are large bottom mounted reinforced concrete structures.

16. The advantages of offshore jacket platforms are as follows: (i) support large deck loads; (ii) possibility of being constructed in sections and transported; (iii) suitable for large field and long-term production (supports a large number of wells); (iv) piles used for foundation result in good stability; and (v) not influenced by seafloor scour. Few disadvantages are as follows: (i) cost increases exponentially with increase in water depth; (ii) high initial and maintenance costs; (iii) not reusable; and (iv) steel structural members are subjected to corrosion, causing material degradation in due course of service life.

17. Drilling deck, wellhead/production deck and cellar deck.

18. A large structural tube that supports an offshore crane for lifting purpose. Crane pedestals also functions diesel storage tanks since their diameter is large enough to house fuel.

19. A long truss that supports a vent or a flare line that releases a part of hydrocarbon gas (about one-third of production) at a greater height.

20. It is a structural member in the form of cone that connects the topside and the jacket. It is a type of cup and cone joint. Cone-shaped design is preferable as leg size of topsides is smaller in diameter as compared to that of the jacket legs.

21. These are provided on all jacket legs to accommodate landing/unloading in a variety of sea conditions and to facilitate a smooth berthing.

22. The jacket structures are very large and cannot be lifted even with large cranes. Permanent structures like launch truss are provided on one side of the jacket to facilitate the loading out onto the barge. If the jacket is designed for buoyancy, the jacket is launched in the sea after reaching its position for a natural upend and leveling. When the jacket is launched, it floats due to buoyancy. The jacket legs are then sequentially flooded to make it upright and stand over the seabed before the piles are driven through the legs to fix it to the sea bed. The launch truss helps in skidding the jacket from the barge to the sea. It is

provided to avoid damage in the main members of the truss while launching. Rollers are provided to adjust the overlapping distance between the launch truss and the tower.

23. Mudmat is provided at the bottom of the jacket to provide suitable additional area to resist initial fluidization of the top layer of the seabed. They are provided to keep the platform stable and in a vertical upright position against the lateral forces before the piles are driven through the legs.

24. The steps involved in the construction process are load-out, towing, launching, floating, upending, vertical position, piling, and deck mating.

25. Gravity structures are constructed with reinforced cement concrete and consists of large cellular base, surrounding several un-braced columns that extend upward from the base to support the deck and equipment above the water surface (Reddy and Arockiasamy 1991). Gravity platforms consist of production risers as well as oil supply and discharge lines, contained in one of the columns; the corresponding piping system for exchange of water is installed in another; and drilling takes place through the third column. This particular type is referred as CONDEEP (concrete deep water) structure and was designed and constructed in Norway.

26. They are the hollow concrete structures at the bottom of the platform to provide the structure with natural buoyancy and may also be used for storage purpose. This enables the platform to float to field development location.

27. The steel skirts are provided around the periphery of the system to improve the foundation stability of the platform. They also act as erosion-resistant members. They assist in grouting the caisson base. It provides lateral resistance to the platform against sliding.

28. The deck supports drilling derrick, engine room, pipe rack, living quarters, processing equipment and heliport. The main load carrying members are plate girders, box girders or trusses.

29. When the caissons are filled with oil or ballast, the center of gravity of the platform moves towards the bottom, which in turn makes the gravity platform to sink. This is called "well sinking".

30. The large weight of the structure causes enormous soil erosion at the bottom, which causes unequal settlement due to which the structure tilts. The tilting causes shift in the center of gravity of the platform which creates an overturning moment. The moment gets increased due to the action of lateral forces which leads to failure. Soil erosion also causes horizontal and vertical displacement in the platform.

31. Sliding: occurs due to the change in the soil characteristics (friction) and lower resistance to wind and wave loads.
    Bearing capacity failure: occurs due to over weight of the structure (punching failure) where the weight of the platform becomes greater than the bearing capacity of the soil. The massive weight of the structure initiates local failure.

Rocking: occurs due to unequal settlement which causes coupled moment at the bottom of the platform.

Liquefaction: due to poor soil condition and saturation level.

32. Yes.

 (i) Greater safety for people on board and topside, (ii) Towing to site with deck is possible which minimizes installation time and cost, (iii) Low maintenance cost because concrete submerged in water will have lesser problems than that of steel structure, (iv) Adjustable crude oil capacity, (v) Capability to support large deck areas, (vi) Risers are protected as they are placed inside the central shaft and (vii) Possible access to sea floor from the cell compartment in the foundation. Thus, healthy monitoring.

33. Jacket Platform.

34. Salient advantages of GBS include: (i) constructed onshore and transported; (ii) towed to the site of installation; (iii) quick installation by flooding; (iv) no special foundation is required and (v) use of traditional methods and labor for installation. Gravity platforms had serious limitations namely: (i) not suitable for sites of poor soil conditions, as this would lead to significant settlement of foundation; (ii) long construction period which thereby delays the early start of production; and (iii) natural frequencies falling within the range of significant power of the input wave spectrum.

35. It is the assembly of pipes used for drilling. The drilling takes place through the center pipe and the oil comes out under pressure through the circumferential pipes. The center pipe is also loaded with drilling mud which acts as a counter weight to balance the bottom pressure and it avoids the movement of drill bit vertically upwards during the drilling process.

36. The derrick moves over the cantilever projection. This is called "Offset drilling" by which the center of gravity of the hull in the trapezoidal cross section will be shifted towards center of the hull. Since drilling is performed on the cantilever projection, there is a least disturbance to the deck and other processes.

37. It is a shallow conical underside footing used for placing the leg on the seafloor. When the spud can is pushed into the sea bed under greater pressure, partial vacuum will be created inside the spud can. Due to suction force, the clay fills the void space and it is fixed to the seabed. Once fixed, high pull-out force is required for extraction.

38. The advantages of the platform include (i) high mobility; (ii) low cost and efficient; (iii) easy fabrication and repair; (iv) easy decommissioning; and (v) simple construction. These platforms also have some serious limitations such as (i) suitable only for shallow depth; (ii) subjected to sea bed scouring which leads to differential settlement; (iii) not suitable for rocky stratum.

39. The structural action of the guyed tower makes its innovation more interesting, which is one of the successful form improvements in the offshore structural design. The upper part of the guy wire is a lead cable, which acts as a stiff spring in moderate seas. The lower portion is a heavy chain, which is attached with clump weights. Under normal operating conditions, the weights will

remain at the bottom, and the tower deck motion will be nearly insignificant. However, during a severe storm, the weights on the storm-ward side will lift off the bottom, softening the guying system and permitting the tower and guying system to absorb the large wave loads.

40. Since the guy lines are attached to the tower below mean water level close to the center of applied environmental forces, large overturning moments will not be transmitted through the structure to the base.

41. Since the guy lines are attached to the tower below mean water level close to the center of applied environmental forces, large overturning moments will not be transmitted through the structure to the base. This feature has allowed the tower to be designed with a constant square cross section along its length, reducing the structural steel weight as compared with that of a conventional platform.

42. Exxon in 1983 installed the first guyed tower named Lena Guyed Tower in the Mississippi Canyon Block in a 300 m water depth. Though the structural form resembles a jacket structure, it is compliant and is moored by catenary anchor lines. The tower has a natural period of 28 s in sway mode while bending, and torsion modes have a period of 3.9 and 5.7 s, respectively. The tower consists of 12 buoyancy tanks of diameter 6 m and length of about 35 m. Around 20 guy lines are attached to the tower with clump weights of about 180 ton to facilitate the holding of the tower in position.

43. The advantages of guyed towers are (i) low cost (lower than steel jacket); (ii) good stability as guy lines and clump weights improve restoring force; and (iii) possible reuse. The disadvantages are as follows: (i) high maintenance costs; (ii) applicable to small fields only; (iii) exponential increase in cost with increase in water depth; and (iv) difficult mooring.

44. The clump weights are provided to drag down the cables to the seabed and drag anchors are provided to avoid lifting up of clump weight due to scour.

45. Sketch of guyed tower
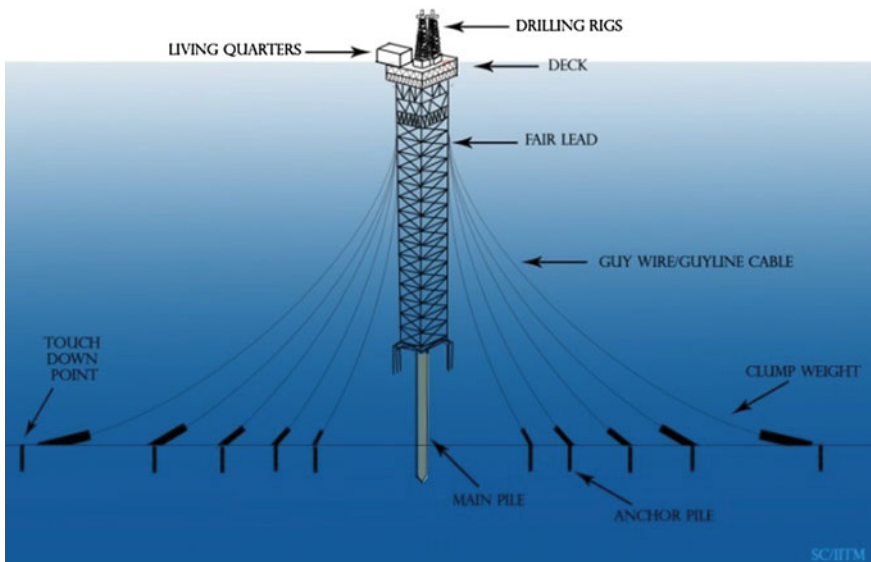
46. The failure in the platform occurs during sailing when the legs are completely above the hull due to overturning moment caused by the wind load and by spud can pull off. The latter may cause serious damage to the drill pipes and risers but the system will remain floating. The spud can foundation is not an ideal hinged joint. It offers partial fixity to the structure so that the structure may also fail under bending.

47. Comparatively, the restoration moment developed in guyed tower is low because the cross section of the tower is less.

48. In deeper water, it is often advantageous to introduce double articulation, the second one being at a mid-depth. Provision of more articulation reduces the bending moment along the tower.

49. The advantages of articulated towers are as follows: (i) low cost; (ii) large restoring moments due to high center of buoyancy; and (iii) protection of risers by tower. There are few disadvantages: (i) suitable only for shallow water as the tower shows greater oscillations for increased water depth; (ii) cannot operate in bad weather; (iii) limited to small fields; and (iv) fatigue of universal joint leads to a single-point failure

50. Articulated towers are used only for anchoring, storage and repairing works and not as permanent production structures and hence called Single Anchor Leg Mooring system (SALM).

51. The tower is ballasted near the universal joint and has a large buoyancy tank at the free surface to provide large restoring force (moment). Buoyancy chamber acts as a large container to store crude oil and the lower ballast chamber is filled with permanent iron ore or ballast which is used for shifting the center of gravity towards the bottom to provide more stability to the tower.

52. Due to the lateral force, the structure tilts which causes a shift of buoyancy (variable submergence). Depending upon location and size, the buoyancy chamber keeps on giving extra force in upward direction which will cause a couple in anticlockwise direction. This will restore the platform to its normal position. This is achieved by the dynamic change in water plane area or variable submergence of the member. In addition, the compliancy of the articulated tower avoids the concentration of high overturning moments and the resulting stress.

53. Buoyancy is associated with variable submergence. There should be variation in level of submergence. If it is provided at bottom, it is completely submerged.

54. The buoyancy force should be greater than the ballast force. Because the couple produced should be anticlockwise for counteracting the lateral load.

55. Articulation needs to be lubricated, else it develops self-friction which leads to fatigue failure. Thus, a joint susceptible to failure is deliberately introduced. This is called single-point failure.

56. The structural action resulted in low vertical force in rough seas, which is the key design factor.

57. Usually a TLP is fabricated and towed to an offshore well site wherein the tendons are already installed on a prepared seabed. Then the TLP is ballasted down so that the tendons may be attached to the TLP at its four corners. The mode of transportation of TLP allows the deck to be joined to the TLP at dockside before the hull is taken offshore

58. The advantages of TLPS are as follows: (i) mobile and reusable; (ii) stable as the platform has minimal vertical motion; (iii) low increase in cost with increase in water depth; (iv) deepwater capability; and (v) low maintenance cost. Few disadvantages are namely: (i) high initial cost; (ii) high subsea cost; (iii) fatigue of tension legs; (iv) difficult maintenance of subsea systems; and (v) little or no storage.

59. Pinned connection is provided between the deck and the mooring lines to maintain the horizontal position of the structure.

60. Due to lateral forces, the platform moves along the wave direction. Horizontal movement is called offset. Due to horizontal movement, the platform also has the tendency to have increased immerse volume of members. Thus, the platform will undergo set-down effect. The lateral movement increases the tension in the tethers. The horizontal component of tensile force counteracts the wave action and the vertical component increases the weight, which will balance the additional weight imposed by set-down.

61. The failure may occur either due to tether pull off or fatigue effect on the tethers.

62. Pretension in cables cannot be imposed by any mechanical means because the requirement of pretension is too high. It is done ballasting the structure. Initially, the structure has to be built as a void chamber. After commissioning, the void chamber is filled with ballast to increase the weight, which the tethers loose. Then the tethers are tightened and the ballast is removed. Now the tension will get transferred to the tethers.

63. There is no critical point in TLP. The disadvantage of articulated towers of putting an articulation is eliminated in this form. TLP has no proportion with the water depth, because the design is based only on weight and buoyancy. Weight depends upon the plan and function of the platform. The buoyancy force depends upon the submerged volume. Thus, the form is independent of water depth.

64. The main parts of the semisubmersibles are the pontoons, columns, deck and the mooring lines. The columns bridge the deck and the pontoons, i.e., the deck is supported by columns. Flotation of semisubmersibles is accomplished with pontoons.

65. The pontoons provide a relatively large water plane area, as is desirable for transit. When submerged for stationing and operations, the columns connecting the pontoons to the upper deck present a lower water plane area, thereby attracting less wave loads and thus reducing the motions.

66. The advantages of semisubmersibles are as follows: (i) mobility with high transit speed (~ 10 knots); (ii) stable as they show minimal response to wave action; and (iii) large deck area. Few disadvantages are (i) high initial and

operating costs; (ii) limited deck load (low reserve buoyancy); (iii) structural fatigue; (iv) expensive to move large distances; (v) availability of limited dry-docking facilities; and (vi) difficult to handle mooring systems and land BOP stack and riser in rough seas.

67. The design variants of FPSO are FPS and FSO. FPS is an acronym for Floating Production Systems devoid of storage facility. FSO is an acronym for Floating, Storage and Offloading system.

68. FPSO is an acronym for Floating Production, Storage, and Offloading systems. Offloading of the crude oil is usually to a shuttle tanker. Typically converted or newly built tankers are custom-made for production and storage of hydro-carbons. These stored hydrocarbons are subsequently transported by other vessels to terminals or deepwater ports.

69. Offloading indicates transfer of produced hydrocarbons from an offshore facility into shuttle tankers or barges for transport to terminals or deepwater ports.

70. Mooring systems of FPSOs are classified as "permanent mooring" or "turret mooring". Majority of FPSOs deployed worldwide are permanently moored, i.e., the FPSOs with their moorings and riser systems are capable of with-standing extreme storms in the field. On the other hand, disconnect able FPSOs have attracted more attention recently. They are typically turret moored. Disconnect able turret is designed for FPSO to be able to disconnect to avoid certain extreme environments.

71. The advantages of the FPSOs are as follows: (i) low cost; (ii) mobile and reusable; (iii) reduced lead time; (iv) quick disconnecting capability, which can be useful in iceberg-prone areas; (v) little infrastructure required; and (vi) turret mooring system enables FPS (converted ship type) to head into the wind/waves reducing their effect. Few disadvantages are (i) limited to small fields; (ii) low deck load capacity; (iii) damage to risers due to motion; (iv) poor stability in rough seas; and (v) little oil storage capabilities.

72. The four major components of spar are hull, moorings, topsides, and risers. The spar relies on a traditional mooring system, i.e., anchor-spread mooring or catenaries mooring system, to maintain its position.

73. In the classic or full cylinder hull forms, the whole structure is divided into upper, middle, and lower sections. The upper section is compartmentalized around a flooded center well housing different type of risers namely produc-tion riser, drilling riser and export/import riser. This upper section provides buoyancy for the spar. The middle section is also flooded but can be con-figured for oil storage. The bottom section, called keel, is also compartmen-talized to provide buoyancy during transport and to contain any field-installed, fixed ballast.

74. Taut mooring system is possible due to small motions of the spar and has a reduced scope, defined as the ratio of length of the mooring line to water depth, and cost compared with a full catenary system.

75. The different types of spars include: (i) Classical spar, which has a cylindrical hull with heavy ballast at the bottom of the cylinder. (ii) Truss spar, which has a shorter cylinder called hard tank. Truss is further connected to its bottom to a soft tank, which houses ballast material. (iii) Cell spar which has a large central cylinder surrounded by smaller cylinders of alternating lengths. Soft tank is attached to the bottom of longer cylinder to house ballast material.

76. Buoyant leg structures (BLSs) are tethered spars with single or group of cylindrical water-piercing hulls; these are alternative structural forms to TLPs and conventional spars.

77. They are positively buoyant wherein the buoyancy exceeds the mass of the structure. Although being positively buoyant, positive metacentric height is maintained to ensure the desired structural stability even after the removal of tethers from the structure. This characteristic ensures high stability and deep draft, which makes the structural form relatively insensitive to increased water depth.

78. Since the BLS is a deep-draft structure, the exposed structural part near the free surface is reduced, the forces exerted on the structure reduces when compared with the conventional TLPs. Since the risers are inside the moon pool of the BLS, the forces exerted on the risers are also minimized, but below the keel of the BLS, some forces like wave or current act.

79. BLS resembles spar due to its shape and deep-draft feature, and its response behavior is similar to that of a TLP due to its restoring system.

80. Since spar is a stable structure, it is installed simply by free-floating, while TLP is generally installed by achieve required pretension in tethers using the following techniques: (i) ballast; (ii) pull-down; or (iii) both pull-down and ballast methods.

81. In the ballast method, the structure will be additionally ballasted until it achieves the required draft; tethers are then attached from the structure to the seafloor. Additional ballast will be removed from the structure to enable pretension in the tethers.

82. In the pull-down method, free-floating structure will be pulled down until it achieves the required draft; excess buoyancy that is transferred to the tethers helps to achieve the desired pretension.

83. Triceratops consists of three BLS units, deck, three ball joints between the BLS units and deck and restoring system either with restraining leg or with the tethers.

84. (i) reduction in forces exerted on the platform due to the decrease in the exposed part of the structure near the free surface; and (ii) protection of risers from lateral forces as they are located inside the moon pool of the BLS.

85. Corrosion challenges can be overcome by few techniques such as (i) frequent inspection using corrosion testing probes; (ii) use of sacrificial anodes; (iii) anti-corrosive coatings; and (iv) use of cathodic protection

86. The presence of ball joints between the deck and BLS restrains the transfer of the rotational motion of the deck from BLS.

87. As risers are located inside the buoyant legs, the wave forces on risers are reduced.
88. Ball joints transfer all translation but not rotation about any axis, making the platform different from other classic types of offshore structures; the distinct motion characteristics of its structural members such as BLS and deck provide uniqueness to its structural behavior under lateral loads.
89. FSRU—Floating, Storage, Regasification unit.
    Transportation of unprocessed crude from the drilling/exploratory platform to the onshore site involves expensive systems like transportation through pipes, large vessels, etc., which makes the oil production more expensive. In particular, the offshore platforms located far offshore prove to be highly uneconomical.
90. Key components of FSRU consists of regasification equipment that transforms LNG at −160 °C to has at high-pressure, storage tanks, loading arms for receiving LNG, export manifolds and sea water pumps that uses sea water to re-gasify the LNG.
91. It contains regasification unit, gas turbine with generator, air compressors, fuel pumps, fire water and foam systems, fresh water systems, cranes, lubrication oil system, life boats, and helipad.
92. Despite the high-quality insulation, a small amount of heat still penetrates the LNG tanks, causing minor evaporation. The resulting boil-off gas is captured and fed back into the LNG tank using compressor and recondensing systems. This recycling process prevents any natural gas from escaping the terminal under normal operating conditions.
93. Natural gas is odorless. Although nontoxic, it is inflammable and is therefore odorized to ensure even the slightest leak can be identified. This is done by injecting tetra-hydrothiophene (THT), which is an odorant detectable in very small doses, at the terminal before the natural gas is distributed.
94. Lubrication oil should have special features in offshore requirements such as (i) water solubility; (ii) non-sheering on water surface; (iii) excellent lubrication properties; (iv) biodegradable; and (v) nontoxic to aquatic environment.
95. Drill ship is an adaptation of a standard sea going ship of mono-hull form, additions are substructure containing a moon pool and cantilevers from which drilling operations may be carried out.
96. A typical drillship has a drilling platform and derrick located at the middle of its deck. Drill ships contain a hole called moon pool, extending right through the ship, down the hull.
97. Dynamic Positioning System (DPS). DPS comprises of electric motors on the underside of the ship hull and they are capable of propelling the ship any direction. Propeller motors are integrated with the computer system of the ship. It uses the satellite positioning system technology, in conjunction with sensors located on the drilling template to ensure that the ship is directly above the drill site at all times.

98. Drill ships have the following advantages compared to semisubmersibles: (i) ship-shaped hull; (ii) subjected to longer period of down time under wind and wave action; (iii) used in smooth waters; and (iv) large load carrying capacity.

99. The major components of DPS includes controller, sensor system, thruster and power system.

100. The controllers command the action of the thrusters installed at the bottom of the ship hull and it keeps the platform within a tolerance radius of about 2–6% of the water depth.

101. Subsea systems (SSS) are multicomponent seafloor systems which allow the production of hydrocarbons in water depths where conventional fixed or bottom founded platforms cannot be installed.

102. The different layouts of subsea systems are single-well satellite, multi-well satellite, cluster well system, template system and combinations of the above.

103. These are the conduits to transport fluid from one location to another. Pipelines are used over a large area for transporting oil, gas, sulfur, and produced water from two separate facilities. The length varied from 1 m to 1000 km and the diameter of the pipeline is about 450 mm. The flow lines are installed within the confines of the platforms or manifold. These are the diversion lines for routing the subsea manifold into the processing equipment.

104. Subsea production tree is an arrangement of valves, pipes, fittings, and connections placed on a top of a wellbore. They are common for all type of drilling platforms. The height varies about 30 m and it requires a counter weight to regulate the flow under pressure. The orientation of the valve can be done in the horizontal bore or in the vertical outlet of the tree, comparatively horizontal outlet is safe. The valves can be operated by electrical or hydraulic signals or manually by diver.

105. It serves as a central gathering point for production from subsea wells. It redirects the combined flow to host facility.

106. It connects the host and the subsea system. These are the bundled arrangement of tubing, piping and electrical conductors of 25 mm diameter. An armored sheath is provided for the purpose of insulation. It transmits the control fluid and electric current in order to control the functions of the subsea production and safety equipment. These are the dedicated tubes to monitor pressure and inject fluids.

107. Production jumper, hydraulic jumper, and electrical jumper.

108. Flexible jumper system provides versatility, unlike rigid jumper system that limits the space and the handling capacity.

109. (i) free hanging; (ii) lazy S; (iii) lazy wave; (iv) steep S; and (v) steep wave.

110. Termination unit is an equipment to facilitate the interface of the pipeline or flow line with the subsea manifold. It is positioned near the manifolds and it can be used for the electric/hydraulic control, equipped with an installation arm to brace it during lowering process.

Chapter 2
Environmental Forces

Abstract This chapter deals with different types of environmental loads on off-shore structures. It also includes code information regarding the loads. Step-by-step method for load estimate on a cylindrical member and an example structure is detailed. The procedure for estimating wave loads is illustrated through examples. Computer codes are included for load estimates; simple MATLAB program is used to illustrate the code. Exercise is given at the end along with the key for self-learning.

Keywords Wind forces · Wave forces · Aerodynamic admittance function · Current forces · Wave theories · Ice and snow loads · Earthquake loads · Accidental loads · General design requirements

2.1 Introduction

Loads for which an offshore structure must be designed can be classified into the following categories:

- Permanent loads or dead loads
- Operating loads or live loads
- Other environmental loads including earthquake loads
- Construction and installation loads
- Accidental loads

While the design of buildings onshore is influenced mainly by the permanent and operating loads, the design of offshore structures is dominated by environmental loads, especially waves, and the loads arising in the various stages of construction and installation. In civil engineering, earthquakes are normally regarded as accidental loads. But in offshore engineering, they are treated as environmental loads. Environmental loads are those caused by environmental phenomena that are random in nature. These include wind, waves, current, tides, earthquakes, temperature, ice, seabed movement, and marine growth. Their

characteristic parameters, defining design load values, are determined in special studies on the basis of available data. According to U.S. and Norwegian regulations (or codes of practice), the mean recurrence interval for the corresponding design event must be 100 years, while according to the British rules it should be 50 years or greater. The different load to be considered while designing the structure are wind loads, wave load, mass, damping, ice load, seismic load, current load, dead load, live load, impact load, etc.

2.2 Wind Force

Wind forces on offshore structures is caused by complex fluid-dynamics phenomenon, which is generally difficult to calculate with high accuracy. Most widely used engineering approaches to estimate wind forces on offshore structures based on few observations as listed below

- When stream of air flows with constant velocity (v), it will generate force on the flat plate of area (A).
- The plate will be placed orthogonal to the flow direction.
- This force will be proportional to (Av^2).
- The proportionality constant is independent of the area, which is verified by experimental studies.

Hence, the wind force on a plate orthogonal to the wind flow direction can be determined by the net wind pressure as given below

$$p_w = \frac{1}{2}\rho_a C_w v^2 \tag{2.1}$$

where, ρ_a is mass density of air (1.25 kg/m^3), and C_w is wind pressure coefficient. It is important to note that the mass density of air increases due to the water spray (splash) up to a height of 20 m above MSL. Hence, the total wind induced force, on the plate is given by:

$$F_w = p_w A \tag{2.2}$$

If the plate has an angle has an angle (θ) with respect to the wind direction, then the appropriate projected area, normal to the flow direction should be used in the above equation. The wind pressure coefficient C_w is determined under controlled stationary wind flow conditions in a wind tunnel. It depends on the Reynolds number; typical values of 0.7–1.2 are used for cylindrical members. Natural wind has two components: (i) mean wind component (which is static component); and (ii) fluctuating, gust component (which is a dynamic component). The gust component is generated by the turbulence of the flow field in all the three spatial directions. For offshore locations, mean wind speed is much greater than the gust

component, which means that in most of the design cases, a static analysis will suffice. The wind velocity is given by

$$v(t) = \bar{v} + v(t) \tag{2.3}$$

where, $\bar{v}\sqrt{a^2 + b^2}$ the mean wind velocity and $v(t)$ is the gust component. The spatial dependence of the mean component is only through the vertical coordinate, while $v(t)$ is homogeneous in both space and time. Wind forces in the directions parallel (drag force) and normal to the wind direction (lift force) are given by

$$F_D = \frac{1}{2} \rho C_D \bar{v}_z A$$
$$F_L = \frac{1}{2} \rho C_L \bar{v}_z A \tag{2.4}$$

Wind spectrum above water surface is given by one-seventh power law, which is

$$v_z = V_{10} \left[\frac{z}{10} \right]^{\frac{1}{7}} \tag{2.5}$$

where, v_z is the wind speed at elevation of z m above MSL, V_{10} is the wind speed at 10 m above MSL, and 10 m is called the reference height. Power law is purely empirical and most widely used. It is tested with the actual field measurements and found to be in good agreement. As Eq. (2.5) gives mean wind component, the gust component can be obtained by multiplying a gust factor with the sustained wind speed. Average gust factor (F_g) is in the range of 1.35–1.45; variation of the gust factor along the height is negligible. The sustained wind speed, which is to be used in the design, is the *one minute average wind speed*, according to the U.S. Weather Bureau. The product of sustained wind speed and the gust factor will give the *fastest mile velocity*. 200 year sustained wind velocity of 125 miles per hour is to be used for the design of offshore structures.

Wind produces a low-frequency excitation. The fluctuating component is modeled probabilistically. Drag force on the members will be caused by the encountered waves and wind. Wave forces alone acting on the member will cause inertia and drag forces, while earthquake forces cause only inertia forces on the members. Hence, vibration of the structure induced by wind and waves are different from that caused by earthquakes. For the design of members under wind loads, most of the international codes prefer quasi-static analysis. Very slender and flexible structures are wind-prone; for members under wave action, de-amplification takes place in flexible structures due to compliancy. While considering wind as a dynamic process, the following parameters are important:

- Length of the record: The record can be continuous, intermittent or select record whose values are above the threshold value. For the record to be continuous, average values of the wind velocity is lesser than that of the intermittent because of the longer length of the record when compared with the former.

- Wind spectrum: It is used as input for the structural analysis, which defines the fluctuating wind component.
- Gust component: It is approximated by the *aerodynamic admittance function*.

2.2.1 Aerodynamic Admittance Function

Aerodynamic admittance function is an intelligent way to define the cross-spectrum in the analysis, indirectly. There are two reasons for using the aerodynamic admittance function: (i) to bypass the rigorous random analysis; and (ii) possibility of an accurate measurement of this function through wind tunnel experiments. In this manner, the spatial variations of wind velocity are handled intelligently in the design. Force due to wind is given by

$$
\begin{aligned}
F_{\mathrm{w}}(t) &= \frac{1}{2}\rho_{\mathrm{a}}C_{\mathrm{w}}v^2 A \\
&= \frac{1}{2}\rho_{\mathrm{a}}C_{\mathrm{w}}A[\bar{v} + v(t)]^2 \\
&= \frac{1}{2}\rho_{\mathrm{a}}C_{\mathrm{w}}A[\bar{v}^2 + (v(t))^2 + 2\bar{v}v(t)]
\end{aligned}
\tag{2.6}
$$

by neglecting higher powers of gust component,

$$
\cong \overline{F}_{\mathrm{w}} + \rho_{\mathrm{a}}C_{\mathrm{w}}A\bar{v}v(t)
$$

In the above equation, wind force is expressed as a sum of mean component and the gust component. Wind is considered an ergodic process; the (one-sided) power spectral density of the wind process is then related to the wind spectrum as

$$
S_{\mathrm{F}}^{+}(\omega) = [\rho_{\mathrm{a}}C_{\mathrm{w}}A\bar{v}]^2 S_{\mathrm{U}}^{+}(\omega)
\tag{2.7}
$$

Substituting Eq. (2.2) in Eq. (2.7) and rearranging the terms, we get

$$
S_{\mathrm{F}}^{+}(\omega) = \frac{4\left[\overline{F}_{\mathrm{w}}\right]^2}{[\bar{v}]^2}\left[\chi\left\{\frac{\omega\sqrt{A}}{2\pi\bar{v}}\right\}\right]^2 S_{\mathrm{U}}^{+}(\omega)
\tag{2.8}
$$

In the above equation, force and the response spectra are connected by the *aerodynamic admittance function*, which varies as below

$$
\begin{aligned}
\text{for } \frac{\omega\sqrt{A}}{2\pi\bar{v}} &\Rightarrow 0, \quad \chi\left\{\frac{\omega\sqrt{A}}{2\pi\bar{v}}\right\} \Rightarrow 1 \\
\text{for } \frac{\omega\sqrt{A}}{2\pi\bar{v}} &\Rightarrow \infty, \quad \chi\left\{\frac{\omega\sqrt{A}}{2\pi\bar{v}}\right\} \Rightarrow 0
\end{aligned}
\tag{2.9}
$$

Aerodynamic admittance function is found empirically, as proposed below (Davenport 1961):

$$\chi(x) = \left\{ \frac{1}{[1 + (2x)^{4/3}]} \right\} \tag{2.10}$$

2.2.2   Wind Data

Wind observations were made for maximum wind speed, mean wind direction, and mean wind speed. The standard wind data represents 10 min average speed measured on mean sea level (DNV 1982). Wind instruments are mounted on light houses, ships, at fixed positions at sea approximately 4 m above sea level. The visual observations were made to find the wind directions. Instrumental wind data are collected by anemometers and the wind directions may also be measured by wind vane.

2.3   Wind Spectra

Wind spectra for the design of offshore structures are listed below with the details. For the reference height of $z = 10$ m, wind spectra as applied to offshore structures are expressed in terms of circular frequency as given below

$$S_u^+(\omega) = fG_u^+(f) \tag{2.11}$$

where, $S_u^+(\omega)$ is the wind spectral density and f is the frequency.

(i) *Davenport spectrum*

Davenport spectrum is focused on the high-frequency portion of the wind data, with the adjustment of a single site-specific parameter. The power in a frequency band is described by this parameter as a complex function of average wind velocity.

$$\frac{\omega S_u^+(\omega)}{\delta \overline{U}_p^2} = \frac{4\theta^2}{\left(1 + \theta^2\right)^{4/3}} \tag{2.12}$$

(ii) *Harris spectrum*

Steady wind forces are calculated from time averaged wind speed. However, fluctuating gust component may lead to resonating oscillations in offshore

structures. Harris spectrum considered the spatial correlation of gust effects and mean wind velocity variation. This is not recommended for frequencies less than 0.1 Hz.

$$\frac{\omega S_u^+(\omega)}{\delta \overline{U}_p^2} = \frac{4\theta}{\left(2 + \theta^2\right)^{5/6}} \tag{2.13}$$

Derivable variable θ is given by

$$\theta = \frac{\omega L_u}{2\pi \overline{U}_{10}} = \frac{\delta L_u}{\overline{U}_{10}}, \quad 0 < \theta < \infty \tag{2.14}$$

where, L_u is integral length scale (=1200 m for Davenport and 1800 m for Harris spectrum), δ is surface drag coefficient referred to $\overline{U}_{10}$. For offshore locations, $\delta = 0.001$. $\overline{U}_{10}$ is the mean wind speed at a height of 10 m. It is important to note that none of these spectrum used in the analysis of wind speed is recorded offshore; they are based on onshore records. Hence these applications to offshore locations are questionable. They have serious problem when used for low-frequency flexible structures.

Alternatively, for large floating structures, following spectra are recommended (Dyrbye and Hassen 1997).

(a) *Kaimal spectrum*

Kaimal spectrum may give a better fit to empirical observations of atmospheric turbulence.

$$\frac{\omega S_u^+(\omega)}{\sigma_u^2} = \frac{6.8\theta}{\left(1 + 10.2\theta\right)^{5/3}} \tag{2.15}$$

where, σ_u^2 is the variance of $U(t)$ at reference height of 10 m. The derivable variable is given by

$$\theta = \frac{\omega}{\omega_p}$$

where, ω_p is the peak frequency.

(b) *API (2000) spectrum*

$$\frac{\omega S_u^+(\omega)}{\sigma_u(z)^2} = \frac{\left(\omega/\omega_p\right)}{\left[1 + 1.5\left(\omega/\omega_p\right)\right]^{5/3}} \tag{2.16}$$

where, ω_p is peak frequency and σ_z^2 is the variance of $U(t)$, which is not assumed as independent.
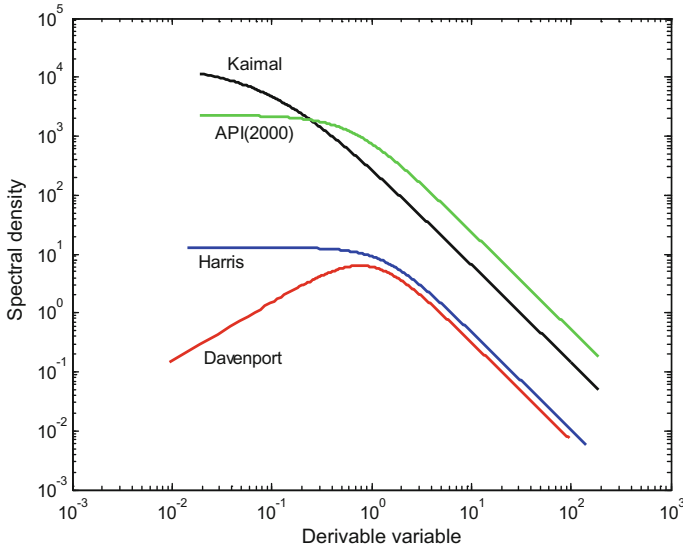
Fig. 2.1 Wind spectra

$$0.01 \leq \frac{\omega_p z}{\overline{U}(z)} \leq 0.1 \tag{2.17}$$

Usually, a value of 0.025 is obtained in lieu of the values computed from the above equation. Standard deviation and speed is given by

$$\sigma_u(z) = \begin{cases} 0.15\overline{U}(z)\left(\dfrac{Z_s}{Z}\right)^{0.125} : Z \leq Z_s \\ 0.15\overline{U}(z)\left(\dfrac{Z_s}{Z}\right)^{0.275} : Z > Z_s \end{cases} \tag{2.18}$$

where, Z_s is the thickness of the surface layer, which is usually taken as 20 m. The spectral density plot showing different wind spectra for mean wind speed of 20 m/s and time period 12 s at a reference height of 10 m is given in Fig. 2.1.

2.4 Computer Code for Wind Spectra

The MATLAB program for plotting the wind spectra is given below. The variables are mean wind speed and time period.

```
%%wind spectra plot---- spectral density versus theta
%%davenport spectrum
um=20; %mean wind speed at a height of 10 m
```

```
del=0.001; %surface drag coefficient
lu=1200; %integral length for davenport spectrum in m
w=0.001:0.001:10; %frequency is the varying component
theta=(w*lu)/(2*pi*um);
a=4*((theta).^2);
b=(1+(theta.^2)).^(4/3);
x=a./b;
y=(x*del*(um^2));
su=y./w;
%%harris spectrum
um=20; %mean wind speed at a height of 10 m
del=0.001; %surface drag coefficient
lu=1800; %integral length for harris spectrum in m
w=0.001:0.001:10; %frequency is the varying component
theta1=(w*lu)/(2*pi*um);
a=4*theta1;
b=(2+(theta1.^2)).^(5/6);
x=a./b;
y=x*del*(um^2);
su1=y./w;
%%Kaimal spectrum
t=12; %time period in seconds
w=0.01:0.001:100; %frequency is the varying component
wp=(2*pi)/t; %frequency in radians per second
z=10; %reference height is 10 m
zs=20; %the surface height usually taken as 20 m
uz=(wp*z)/0.025;
if z<=zs
   sigma=0.15*uz*((zs/z)^0.125);
else
   sigma=0.15*uz*((zs/z)^0.275);
end
theta2=w./wp;
a=6.8*theta2;
b=(1+(10.2*theta2)).^(5/3);
x=a./b;
y=x.*(sigma^2);
su2=y./w;
%%API(2000) spectrum
t=12; %time period in seconds
w=0.01:0.001:100; %frequency is the varying component
wp=(2*pi)/t; %frequency in radians per second
z=10; %reference height is 10 m
zs=20; %the surface height usually taken as 20 m
uz=(wp*z)/0.025;
```

```
if z<=zs
  sigma=0.15*uz*((zs/z)^0.125);
else
  sigma=0.15*uz*((zs/z)^0.275);
end
theta3=w./wp;
b=1+(1.5*(theta3)).^(5/3);
x=theta3./b;
y=x.*(sigma^2);
su3=y./w;
loglog(theta,su,'r','linewidth',2);%Davenport Spectrum
hold on;
loglog(theta1,su1,'b:','linewidth',2);%Harris spectrum
hold on;
loglog(theta2,su2,'k-.', 'linewidth',2);%Kaimal
hold on;
loglog(theta3,su3,'c--','linewidth',2);
xlabel('Derivable variable');
ylabel('Spectral density');
title('WIND SPECTRA (Mean wind speed=20m/s,  Reference  Height=10m,  Time
period=12s)');
```

2.5 Wave Forces

Wind-generated sea surface waves can be represented by a combination of regular waves. Regular waves of different magnitude and wave lengths from different directions are combined to represent the sea surface elevation. Water particle kinematics of regular waves is expressed by the sea surface elevation by various wave theories (Chandrasekaran and Bhattacharyya 2011).

2.6 Wave Theories

Wave theories serve to calculate the particle velocities, accelerations, and the dynamic pressure as functions of the surface elevation of the waves. For long-crested regular waves, the flow can be considered two-dimensional and are

characterized by parameters such as wave height (H), period (T), and water depth (d), as shown in Fig. 2.2. $k(=2\pi/L)$ denotes the wave number, $\omega = 2\pi/T$ denotes the wave circular frequency and $f(=1/T)$ denotes the cyclic frequency. Different wave theories available are as follows:

- Linear or first-order or Airy theory
- Stokes fifth-order theory
- Solitary wave theory
- Cnoidal theory
- Dean's stream function theory
- Numerical theory by Chappelear

Figure 2.3 shows the chart for the selection of the most appropriate theory, based on the parameters, H, T, and d. For example, linear wave theory can be applied when $H/gT^2 < 0.01$ and $d/GT^2 > 0.05$, besides other ranges, as shown in the figure.

2.6.1 Airy's Wave Theory

Among all the theories, Airy's wave theory is commonly used because it assumes linearity between the kinematic quantities and the wave height, which makes the wave theory simple. Airy's theory assumes a sinusoidal wave form of wave height (H), which is small in comparison to the wave length (λ) and water depth (d) as given below
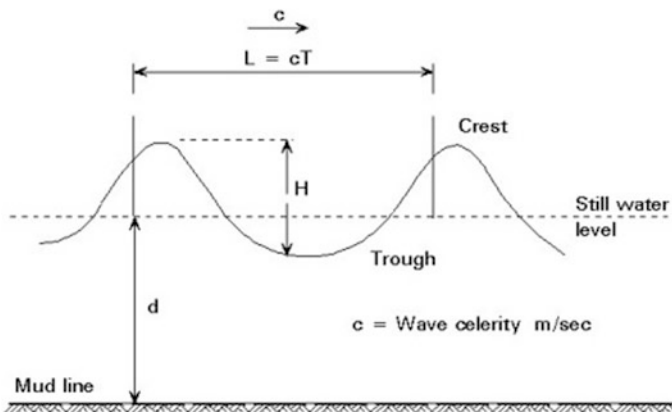
Fig. 2.2 Definition of wave parameters

Fig. 2.3 Wave theory chart (Sarpakaya and Issacson 1981)
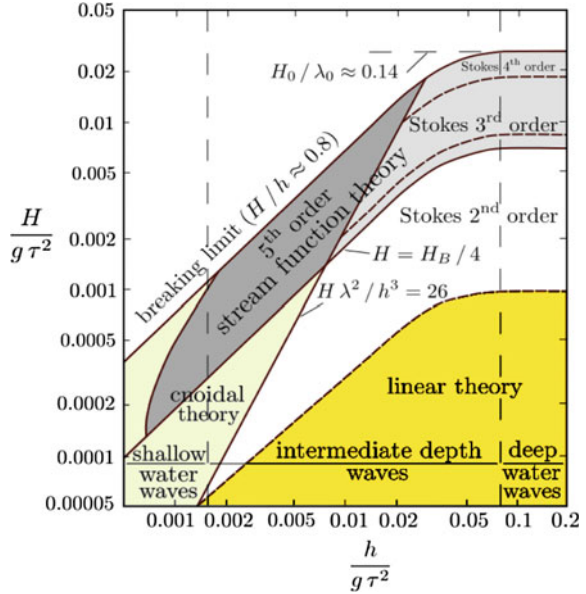
$$\eta(x,t) = \frac{H}{2}\cos(kx - \omega t)$$

$$k = \frac{2\pi}{\lambda}$$

$$\dot{u}(x,t) = \frac{\omega H}{2}\frac{\cosh(ky)}{\sinh(kd)}\cos(kx - \omega t)$$

$$\dot{v}(x,t) = \frac{\omega H}{2}\frac{\sinh(ky)}{\sinh(kd)}\sin(kx - \omega t) \qquad (2.19)$$

$$\ddot{u}(x,t) = \frac{\omega^2 H}{2}\frac{\cosh(ky)}{\sinh(kd)}\sin(kx - \omega t)$$

$$\ddot{v}(x,t) = -\frac{\omega^2 H}{2}\frac{\sinh(ky)}{\sinh(kd)}\cos(kx - \omega t)$$

The waves are classified according to depth as shallow, intermediate, and deep-water waves depending on the ratio of the water depth to wavelength. Variations in horizontal and vertical water particle velocities for different water depth conditions are shown in Fig. 2.4.

Airy's theory is valid up to mean sea level only. However, due to the variable submergence effect, the submerged length of the members will be continuously changing. This will attract additional forces due to their variable submergence at any given time. To compute the water particle kinematics up to the actual level of submergence, stretching modifications suggested by various researchers are used.

Fig. 2.4 Variations in
vertical and horizontal water
particle velocities
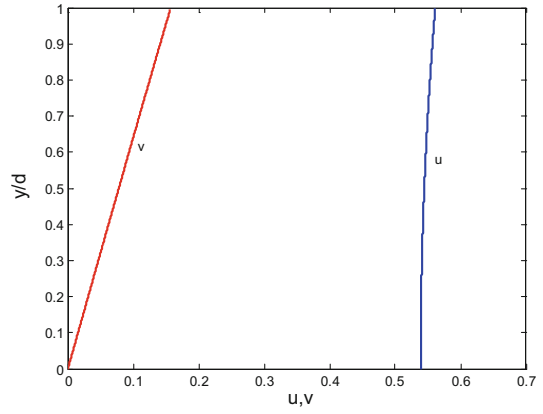
(a) Shallow water condition
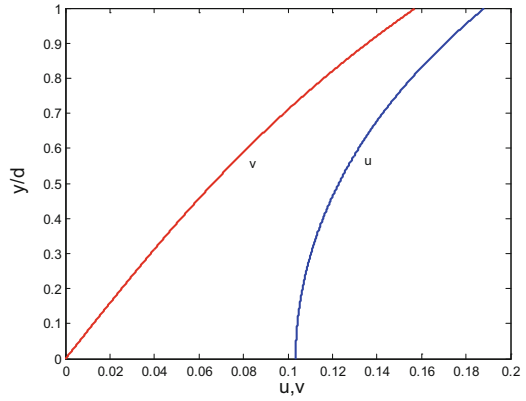
(b) Intermediate water condition
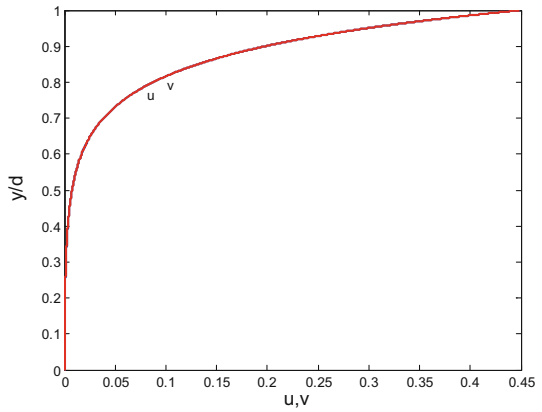
(c) Deep water condition

Wheeler suggested the following modifications in the horizontal water particle velocity and acceleration to include the actual level of submergence of the member:

$$\dot{u}(x,t) = \frac{\omega H}{2} \frac{\cosh\left(ky\left[\frac{d}{d+\eta}\right]\right)}{\sinh(kd)} \cos(kx - \omega t)$$

$$\ddot{u}(x,t) = \frac{\omega^2 H}{2} \frac{\cosh\left(ky\left[\frac{d}{d+\eta}\right]\right)}{\sinh(kd)} \sin(kx - \omega t)$$

(2.20)

Chakrabarti suggested the modifications as given below

$$\dot{u}(x,t) = \frac{\omega H}{2} \frac{\cosh(ky)}{\sinh(k(d+\eta))} \cos(kx - \omega t)$$

$$\ddot{u}(x,t) = \frac{\omega^2 H}{2} \frac{\cosh(ky)}{\sinh(k(d+\eta))} \sin(kx - \omega t)$$

(2.21)

Variations in the horizontal water particle velocity for the intermediate water depth condition, based on the modifications are shown in Fig. 2.5. As seen from the figure, horizontal water particle velocity variation increases with the increase in the wave height. The same variation is observed in deep and shallow water conditions also. At a wave height less than 1 m, the variations due to Wheeler's and Chakrabarti's modifications were found to be very small.

2.6.2 Stoke's Fifth-Order Theory

Airy's theory is the simplified theory, which is applicable only for waves of small heights. Stoke's theory extended the range covered by the Airy theory to the waves of greater steepness (Stokes 1880). The coefficients in the series involving five terms are complicated which restricts the usage of this theory widely. The Stoke's coefficients and equations are listed below

$$s = \sinh kd$$
$$c = \cosh kd$$
$$C_o^2 = g \tanh kd$$

Fig. 2.5 Horizontal water
particle velocity variation in
intermediate water condition
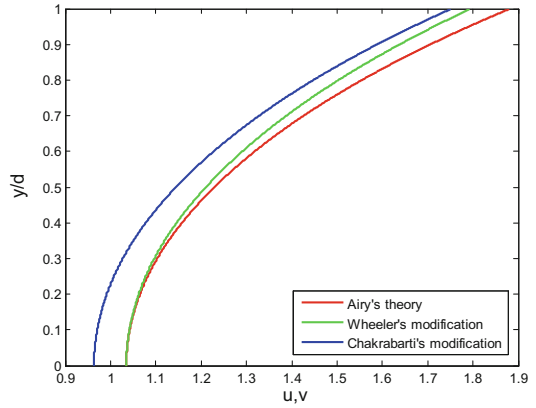
(a) Wave height = 10 m
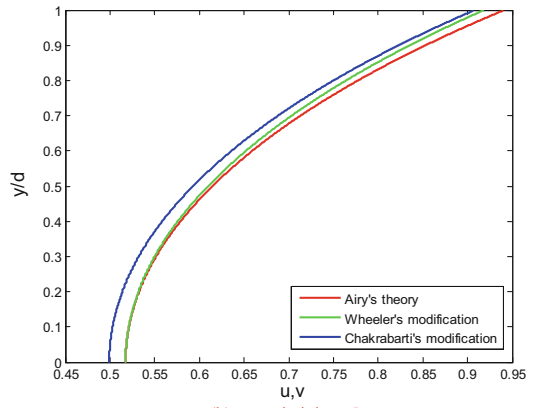
(b) wave height = 5m
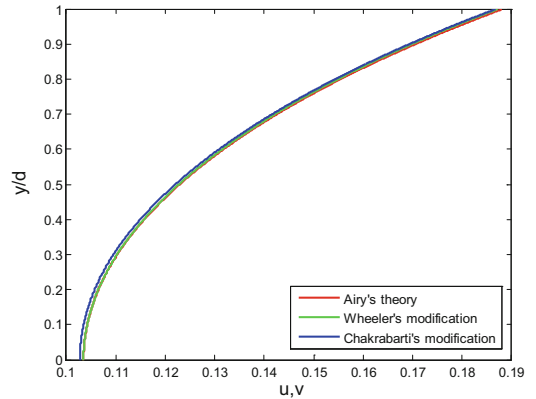
(c) wave height = 1m

$$A_{11} = \frac{1}{s}$$

$$A_{13} = \frac{-c^2(5c^2 + 1)}{8s^5}$$

$$A_{15} = \frac{-(1184c^{10} - 1440c^8 - 1992c^6 + 2641c^4 - 249c^2 + 18)}{1536s^{11}}$$

$$A_{22} = \frac{3}{8s^4}$$

$$A_{24} = \frac{(192c^8 - 42c^6 - 312c^4 + 480c^2 - 17)}{768s^{10}}$$

$$A_{33} = \frac{(13 - 4c^2)}{64s^7}$$

$$A_{35} = \frac{(512c^{12} + 4224c^{10} - 6880c^8 - 12808c^6 + 16704c^4 - 315c^2 + 107)}{4096s^{13}(6c^2 - 1)}$$

$$A_{44} = \frac{(80c^6 - 816c^4 + 1338c^2 - 197)}{1536s^{10}(6c^2 - 1)}$$

$$A_{55} = \frac{(2880c^{10} - 72480c^8 + 324000c^6 - 432000c^4 + 163470c^2 - 16245)}{61440s^{11}(6c^2 - 1)(8c^4 - 11c^2 + 3)}$$

$$B_{22} = \frac{(2c^2 + 1)c}{4s^3}$$

$$B_{24} = \frac{c(272c^8 - 504c^6 - 192c^4 + 322c^2 + 21)}{8384}$$

$$B_{33} = \frac{3(8c^6 + 1)}{64s^6}$$

$$B_{35} = \frac{(88128c^{14} - 208224c^{12} + 70848c^{10} + 54000c^8 - 21816c^6 + 6264c^4 - 54c^2 - 81)}{12288s^{12}(6c^2 - 1)}$$

$$B_{44} = \frac{(764c^{10} - 448c^8 - 48c^6 + 48c^4 + 106c^2 - 21)c}{384s^9(6c^2 - 1)}$$

$$B_{55} = \frac{(192000c^{16} - 262720c^{14} + 83680c^{12} + 20160c^{10} - 7280c^8 + 7160c^6 - 1800c^4 - 1050c^2 + 225)}{12288s^{10}(6c^2 - 1)(8c^4 - 11c^2 + 3)}$$

$$C_1 = \frac{(8c^4 - 8c^2 + 91)}{8s^4}$$

$$C_2 = \frac{(3840c^{12} - 4096c^{10} + 2592c^8 - 1008c^6 + 5944c^4 - 1830c^2 + 147)}{512s^{10}(6c^2 - 1)}$$

$$C_3 = \frac{1}{4sc}$$

$$C_4 = \frac{(12c^8 + 36c^6 - 162c^4 + 141c^2 - 27)}{192cs^9}$$

The water particle velocities are given by

$$u = C \sum_{n=1}^{5} n F_n \cos n\theta \cosh nkS$$

$$w = C \sum_{n=1}^{5} n F_n \sin n\theta \sinh nkS$$

2.6.3 Wave Data

Wave data are approximately collected for 20 min every 3 h and assumed to represent the stationary sea state between the measurements. The sea state is defined by significant wave height, significant wave period, peak period, and wave direction. Data collection is done by visual investigation and instrumental observations by buoys, radars, lasers, and satellites. The sea state, in a short term, which is typically 3 h, is assumed as zero mean, ergodic Gaussian process. This can be defined completely by a wave spectrum. For North Sea, JONSWAP spectrum is recommended. For open sea conditions, Peirson-Moskowitz (PM) spectrum is recommended. In a long term, variation of sea state is slower than the short-term fluctuations. It is often approximated by a series of stationary, nonzero-mean Gaussian process, which is specified by the significant wave height (H_s) and peak wave period (T_p). Following are a few relevant spectra, applicable in the design of offshore platforms.

2.7 Wave Spectra

The wave spectrum describes the energy distribution of different frequencies of a sea state. The spectrum should be selected based on the frequency characteristics of the wave environment (Boaghe et al. 1998; Issacson and Det 1982).

(a) *PM spectrum for wave loads*

PM spectrum is a one parameter spectrum and it used for fully developed sea condition as generated by relatively moderate winds over large fetches.

$$S^+ (\omega) = \frac{\alpha g^2}{\omega^5} \exp \left[-1.25 \left(\frac{\omega}{\omega_0} \right)^{-4} \right] \tag{2.22}$$

where, α is Phillips constant $\cong 0.0081$.

(b) *Modified PM spectrum (2 parameters H_s, ω_0)*

This is a two parameter spectrum which was developed to account for the wave height. This spectrum is suitable for fully developed sea condition and it is usually employed to describe the tropical storm waves generated by hurricanes. It has a greater frequency bandwidth.

$$S^+(\omega) = \frac{5}{16} H_s \frac{\omega_0^4}{\omega^5} \exp\left[-1.25\left(\frac{\omega}{\omega_0}\right)^{-4}\right] \tag{2.23}$$

(c) *ISSC spectrum (International Ship Structures Congress) (2 parameters H_s, $\bar{\omega}$)*

ISSC spectrum is slight modification of Bretschneider spectrum and it recommended for fully developed sea condition. This spectral equation is true only for a narrow-banded spectrum and the wave elevation follows a Gaussian distribution.

$$S^+(\omega) = 0.1107 H_s \frac{\omega^{-4}}{\omega^5} \exp\left[-0.4427\left(\frac{\omega}{\bar{\omega}}\right)^{-4}\right] \tag{2.24}$$

$$\bar{\omega} = \frac{M_1}{M_0}$$

where, M_1 and M_0 are spectral moments.

(d) *JONSWAP (Joint North Sea Wave Project) spectrum (Five parameters H_s, ω_{0o},*
   γ, τ_a, τ_b).

JONSWAP spectrum is a modified form of PM spectrum and it is recommended for use in the reliability analysis. This spectrum is applicable only for limited fetch and it is used to describe the winter storm waves of the North Sea.

$$S^+(\omega) = \frac{\bar{\alpha} g^2}{\omega^5} \exp\left[-1.25\left(\frac{\omega}{\omega_0}\right)^{-4}\right] \gamma^{a(\omega)} \tag{2.25}$$

where, γ is the peakedness parameter. The value of 3.3 yields a mean spectrum for a specified wind speed and a given fetch length. The variation of the peakedness parameter depends upon the duration of the wind and stage of growth and decay of the storm. This value follows a normal probability distribution.

$$a(\omega) = \exp\left[-\frac{(\omega - \omega_0)^2}{2\bar{\sigma}^2 \omega_0^2}\right] \tag{2.26}$$

where, $\bar{\sigma}$ is spectral width parameter or shape parameter and is given by

$$\bar{\sigma}_a = 0.07, \omega \leq \omega_0 \tag{2.27}$$

$$\bar{\sigma}_b = 0.09, \omega > \omega_0 \tag{2.28}$$

The modified Phillips constant is given by

$$\bar{\alpha} = 3.25 \times 10^{-3} H_s^2 \omega_0^4 [1 - 0.287 \ln(\gamma)] \tag{2.29}$$

$$\gamma = 5 \quad \text{for} \quad \frac{T_p}{\sqrt{H_s}} \leq 3.6 \tag{2.30}$$

$$= \exp\left[5.75 - 1.15 \frac{T_p}{\sqrt{H_s}}\right] \quad \text{for} \quad \frac{T_p}{\sqrt{H_s}} > 3.6 \tag{2.31}$$

$$H_s = 4\sqrt{m_0} \tag{2.32}$$

where, γ varies from 1 to 7.

The wave spectra plot, as shown in Fig. 2.6 illustrates comparison for significant mean wind speed 20 m/s, wave height 5 m, and time period 10 s. It is seen from the figure that Modified PM spectrum and ISSC spectrum have the same spectral distribution while JONSWAP spectrum shows the high energy peak.
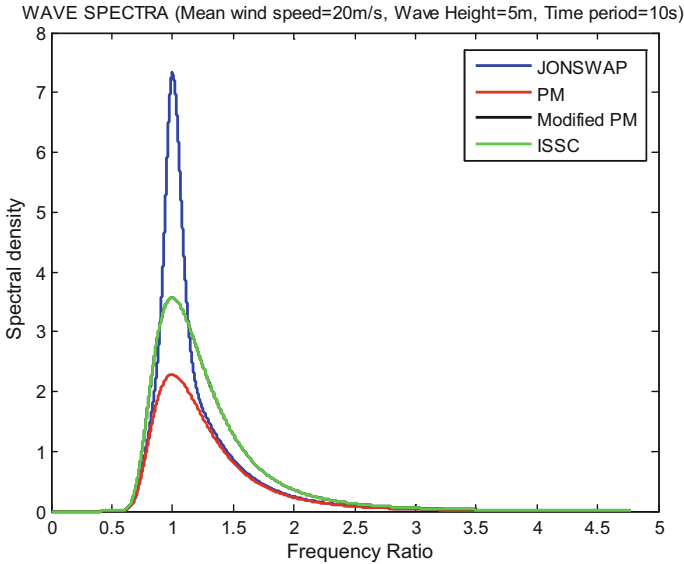
Fig. 2.6 Comparison of wave spectra

2.7.1   Computer Code for Wave Spectra Plots

The MATLAB program for the wave spectra plot is given below. The variables are
mean wind speed, significant wave height and time period.

```
%%WAVE SPECTRA plot ---- spectral density versus frequency ratio
%%Jonswap spectrum
hs=5; %wave height in m
t=10; %time period in seconds
v=3; %peakedness factor chosen between 1 to 7
g=9.81; %gravitational constant
w=0:0.000001:3; %frequency is the varying component
n=length(w);
wo=(2*pi)/t;
alpha=3.25*(10^-3)*(hs^2)*(wo^4)*(1-(0.287*(log(v))));
for i=1:n
if w(i)<=wo
   sigma(i)=0.07;%spectral width parameter
else
   sigma(i)=0.09;
end
x(i)=-((w(i)-wo)^2)/(2*(sigma(i)^2)*((wo)^2));
y(i)=-1.25*((w(i)/wo)^(-4));
aw(i)=exp(x(i));
z(i)=exp(y(i))*(v^aw(i))*alpha*(g^2);
s(i)=z(i)/(w(i)^5);
p(i)=w(i)/wo;
i=i+1;
end
%%PM spectrum
hs=5; %wave height in m
t=10; %time period in seconds
g=9.81; %gravitational constant
v=20; %mean wind speed in m/s
wo=(2*pi)/t;
w=0:0.0001:3; %frequency is the varying component
n=length(w);
for i=1:n
x(i)=-1.25*((w(i)/wo)^(-4));
a(i)=exp(x(i));
b(i)=1/((w(i))^5);
s1(i)=0.0081*a(i)*b(i)*(g)^2;
p1(i)=w(i)/wo;
i=i+1;
```

```
end
%%Modified PM spectrum
hs=5; %wave height in m
t=10; %time period in seconds
wo=(2*pi)/t;
w=0:0.0001:3; %frequency is the varying component
n=length(w);
for i=1:n
y(i)=(-1.25)*((w(i)/wo)^(-4));
a(i)=exp(y(i));
b(i)=(wo^4)/((w(i))^5);
s2(i)=0.3125*((hs^2)*a(i)*b(i));
p2(i)=w(i)/wo;
i=i+1;
end
%%ISSC spectrum
hs=5; %wave height in m
t=10; %time period in seconds
wo=(2*pi)/t;
w=0:0.0001:3; %frequency is the varying component
n=length(w);
for i=1:n
y(i)=-1.2489*((w(i)/wo)^(-4));
a(i)=exp(y(i));
b(i)=(wo^4)/((w(i))^5);
s3(i)=0.3123*((hs^2)*a(i)*b(i));
p3(i)=w(i)/wo;
i=i+1;
end
plot(p,s,'k'); %jonswap spectrum
hold on;
plot(p1,s1,'r');%Modified PM spectrum
hold on;
plot(p2,s2,'b'); %Bretschneider spectrum
hold on;
plot(p3,s3,'g'); %ISSC spectrum
xlabel('Frequency Ratio');
ylabel('Spectral density');
title
('WAVE SPECTRA (Mean wind speed=20m/s, Wave Height=5m, Time period=10s)');
```

2.8 Wave Force on Cylinders

Main force components, rising from the wave loads are grouped as follows: (i) *Froude-Krylov force*, which is caused by the pressure effects due to the undisturbed incident waves; (ii) *diffraction force*, which is caused by the pressure effects due to the presence of the structure in the fluid-flow domain; (iii) *hydrodynamic added mass and potential damping forces*, which is caused by the pressure effects due to the motion of the structural components in ideal fluid; and (iv) *viscous drag force*, which is caused by the pressure effects due to the relative velocity between the water particle and the structural component. For slender structures, *Froude-Krylov force and diffraction forces* are idealized by a single inertia term. Velocity and acceleration do not differ significantly from the values of the cylinder axis when $D/\lambda < 0.2$. When the waves act on the slender structures, the structure oscillates, which will set up waves radiating away from it. Reaction forces are then set up in the fluid, which will be proportional to the acceleration and velocity of the structure. Reaction force proportional to the acceleration of the structure will result in an added mass term, contributing to the inertia force. Reaction force proportional to the velocity results in the potential damping force. If the structure is compliant, the added mass forces associated with the relative acceleration between the fluid particles and the structures are included. Drag force will be computed by replacing the water particle velocity with the relative velocity term. The total force acting normal to the axis of the member is given by

$$
\begin{aligned}
q_n &= \rho \mathrm{d}V.a_n + (C_m - 1)\rho \mathrm{d}V(a_n - \ddot{x}_n) + \frac{1}{2}\rho C_d \mathrm{d}A(v_n - \dot{x}_n)|v_n - \dot{x}_n| \\
&= C_m \rho \mathrm{d}V.a_n - (C_m - 1)\rho \mathrm{d}V\ddot{x}_n + \frac{1}{2}\rho C_d \mathrm{d}A(v_n - \dot{x}_n)|v_n - \dot{x}_n|
\end{aligned}
\tag{2.33}
$$

where, ρ is density of fluid, (C_d, C_m) are the drag and inertia coefficients, (v_n, a_n) are velocity and acceleration of the water particle normal to the axis of the member, $\dot{x}, \ddot{x}$ are the velocity and acceleration of the structure, and $(\mathrm{d}A, \mathrm{d}V)$ are exposed area and displaced volume of water per unit length, respectively.

The above equation has two main issues: first, the relative motion formulation is valid only if the structure motion is of large amplitude; second, the relative velocity formation of the drag produces both excitation and damping forces. In the above equation, the most critical aspect is the evaluation of the drag and inertia coefficients, which is dependent on flow conditions, Keulegan–Carpenter number and Reynolds number. The recommended value of drag coefficient is 0.6–1.2, while that of the inertia coefficient is 1.2–2.0, as seen in the literature (APR RP 2A). As in the case of bottom-supported structures (gravity platforms), when the diameter of the member is very large, incident waves are disturbed by the presence of the structure.

In such cases, viscous force becomes less significant due to the smaller values of the ratio of wave height to member diameter ($H/D \ll 1$). In such cases, the above equations cannot be applied; it is recommended that the analyzer should use numerical methods to determine the forces on the members. The variation of forces at the mean sea level with respect to phase angle is shown in Fig. 2.7, where a wave height of 5 m, period of 10 s, water depth of 50 m and diameter of the member of 1 m is used for the plot.

The variation of the total force with respect to depth is shown in Fig. 2.8. Force variation shown in the plot corresponds to the maximum phase angle.

Offshore structures have large plane area. Larger topside is required for accommodating the equipment layout as discussed in the previous chapter. As the deck will be supported on a few column members in order to reduce the interference of the waves by the presence of column members, their spacing plays an important role. For a large spacing of *c/c* distance of column members, there can be cancelation of forces. Let us consider an example of the tension leg platform (TLP). For a typical size of topside of 90 m × 90 m, resting on four columns, phase angle (θ) is given by the following relationship:

$$\theta = \frac{2\pi\Delta x}{\lambda} \tag{2.34}$$
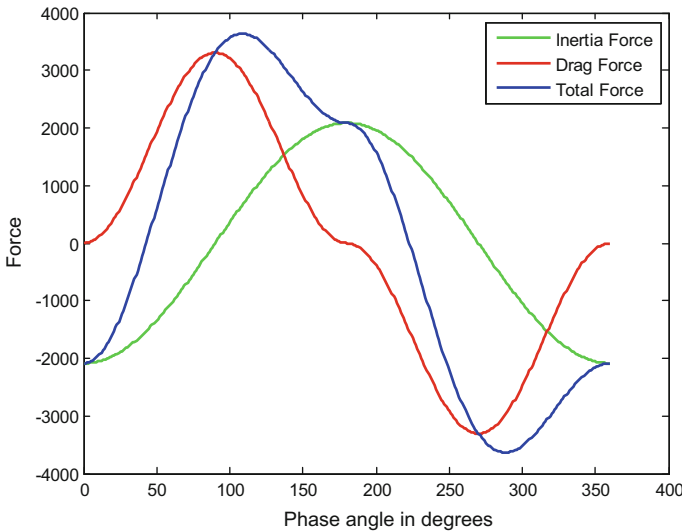
Fig. 2.7 Force variation with respect to phase angle
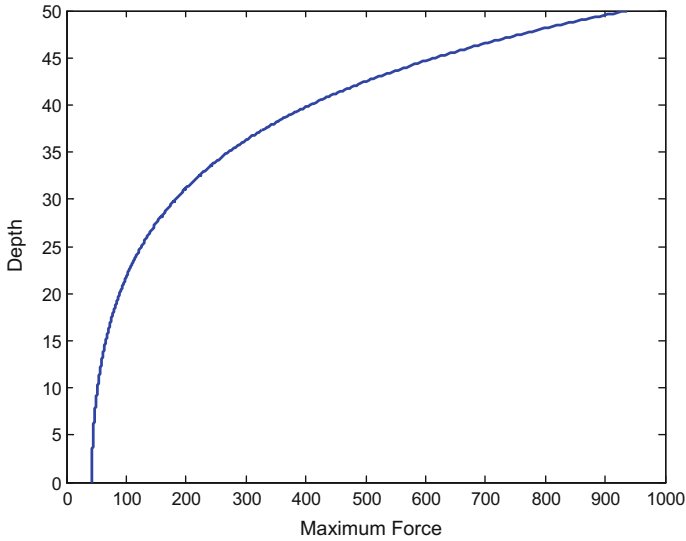
Fig. 2.8 Force variation with respect to depth

where, Δx the is *c/c* distance between the column members (leg spacing) and λ is the wave length. For the spacing between the columns of 90 m and wave period of 10 s, the phase angle will be 1.2π, which can cause cancelation of forces on members. It is important to note that the spacing of the members are chosen in such a manner that the force cancelation effects at the dominant wave frequencies are expected to have close to the natural frequency of the platform. The forces on a submerged structure in waves appear from the pressure distribution on its surface. For a small structure, Morison equation is valid because the flow structure is complex. However, for large structures (relative to the wavelength) the flow remains essentially attached to the surface. It is therefore easier to compute this pressure field. If the computation of the scattered wave potential is waived and its effect is incorporated by a force coefficient, then this force is called the *Froude-Krylov* force. Thus, the calculation of the force is performed assuming that the structure does not distort the wave field in its vicinity. The force is computed by a pressure area method using the incident wave pressure that is acting on the submerged surface of the structure. Then a force coefficient is used to account for the wave diffraction.

For a few basic shapes of the structural forms, a closed form expression may be obtained by the Froude-Krylov theory: (i) horizontal cylinder, (ii) horizontal half-cylinder, (iii) vertical cylinder, (iv) sphere, (v) hemisphere and (vi) rectangular barge.

(a) Force on a horizontal cylinder is given by

$$f_H = r\ell \int\limits_{0}^{2\pi} p\cos\theta d\theta \qquad (2.35)$$

(b) Force on a vertical cylinder:

Consider a vertical cylinder placed on the ocean bottom and extended above the still water level, as shown in Fig. 2.9

Velocity potential is given by

$$\varphi = \frac{gH}{2\omega}\frac{\cosh(ks)}{\cos h(kd)}\sinh(kx - \omega t) \qquad (2.36)$$

Dynamic pressure is given by

$$\begin{aligned} p &= \rho\frac{\partial\varphi}{\partial t} \\ &= \rho g\frac{H}{2}\frac{\cosh(ks)}{\cosh(kd)}\cos(kx - \omega t) \end{aligned} \qquad (2.37)$$

Variation of dynamic pressure at a depth of 10 m with significant wave height 5 m and the total water depth is 20 m is shown in Fig. 2.10.

Fig. 2.9 Bottom-supported cylinder
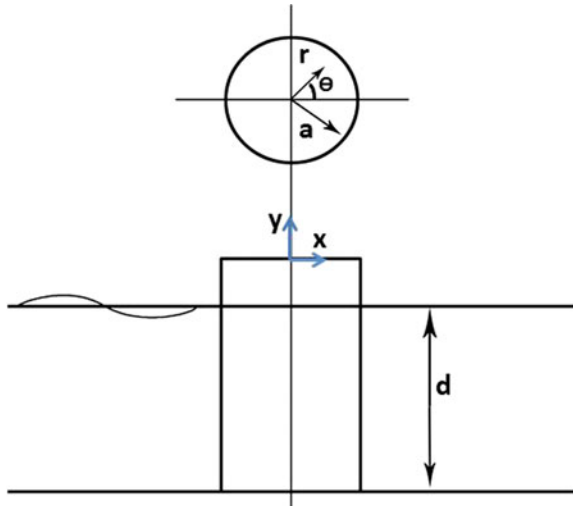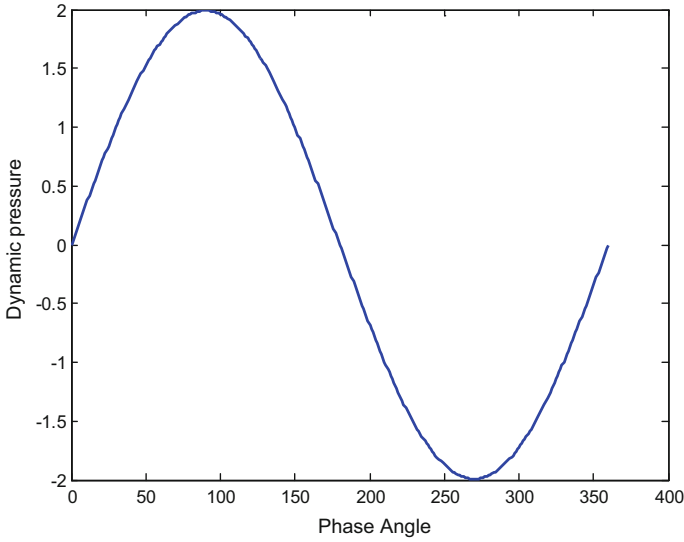
Fig. 2.10 Dynamic pressure variation

Horizontal force per unit length is given by

$$f_x = \rho \int\limits_{0}^{2\pi} \int\limits_{-d}^{0} \frac{\partial \varphi_0}{\partial t} a \cos \theta \, d\theta \, d\ell$$

$$f_x = \frac{\rho g a H}{2 \cosh(kd)} \int\limits_{-d}^{0} \cos h(ks) ds \int\limits_{0}^{2\pi} \cos[ka \cos \theta - \omega t] \cos \theta \, d\theta \tag{2.38}$$

This reduces the following form, which accounts for diffraction effect:

$$f_x = C_H \frac{\pi \rho g H a}{k} J_1(ka) \tanh(kd) \sin \omega t \tag{2.39}$$

The above method of computing the forces by the incident wave alone is known as Froude-Krylov theory. It does not give the correct value of the force, as the phase value is accounted for in the equation. It is due to this fact a force coefficient is used in the expression as a multiplier. For a vertical cylinder, the horizontal force coefficient is taken as 2; for small values of ka; the value changes as ka increases. Table 2.1 shows the equations for forces using Froude-Krylov theory for different geometric shapes of members. Numerical values of C_1–C_4 depend on the diffraction

Table 2.1 Forces on members of different geometric shapes using Froude-Krylov theory

Basic shape	Horizontal force	C_H	Vertical force	C_V	K_a range
Horizontal cylinder	$C_H \rho V \dot{u}_0$	2.0	$C_V \rho V \dot{v}_0$	2.0	0–1.0
Horizontal half-cylinder	$C_H \rho V [\dot{u}_0 + C_1 \omega v_0]$	2.0	$C_V \rho V [\dot{v}_0 + C_2 \omega u_0]$	1.1	0–1.0
Vertical cylinder	$C_H \rho V \dfrac{2 J_1(ka)}{ka} \dfrac{\sinh\left[\frac{k\ell_1}{2}\right]}{\left[\frac{k\ell_1}{2}\right]} \dot{u}_0$	2.0	–	–	–
Rectangular block	$C_H \rho V \dfrac{\sinh\left[\frac{k\ell_3}{2}\right]}{\left[\frac{k\ell_3}{2}\right]} \dfrac{\sinh\left[\frac{k\ell_1}{2}\right]}{\left[\frac{k\ell_1}{2}\right]} \dot{u}_0$	1.5	$C_V \rho V \dfrac{\sinh\left[\frac{k\ell_3}{2}\right]}{\left[\frac{k\ell_3}{2}\right]} \dfrac{\sinh\left[\frac{k\ell_1}{2}\right]}{\left[\frac{k\ell_1}{2}\right]} \dot{v}_0$	6.0	0–5.0
Hemi sphere	$C_H \rho V [\dot{u}_0 + C_3 \omega v_0]$	1.5	$C_V \rho V [\dot{v}_0 + C_4 \omega u_0]$	1.1	0–0.8
Sphere	$C_H \rho V \dot{u}_0$	1.5	$C_V \rho V \dot{v}_0$	1.1	0–1.75

Where V = submerged volume of the structure; C_H and C_V are force coefficients in the horizontal and vertical directions, respectively; subscript zero indicates that the amplitude of the water particle velocity or acceleration is computed at the center of the geometric shape; l_1 and l_3 are the length and underwater depth of the rectangular block, respectively

Table 2.2 Numerical values of C_1–C_4

ka	C_1	C_2	C_3	C_4
0.1	0.037	15.019	0.042	12.754
0.2	0.075	7.537	0.085	6.409
0.3	0.112	5.056	0.127	4.308
0.4	0.140	3.825	0.169	3.268
0.5	0.186	3.093	0.210	2.652
0.6	0.223	2.612	0.252	2.249
0.7	0.259	2.273	0.292	1.966
0.8	0.295	2.024	0.332	1.760
0.9	0.330	1.834	0.372	1.603
1.0	0.365	1.685	0.411	1.482
1.5	0.529	1.273	0.591	1.156
2.0	0.673	1.105	0.745	1.034
2.5	0.792	1.031	0.867	0.989
3.0	0.886	0.999	0.957	0.977
3.5	0.955	0.989	1.015	0.978
4.0	1.000	0.087	1.945	0.985

parameter ka and are given Table 2.2. The forces in Table 2.1 are given in terms of the water particle acceleration and velocity at the center of the structure wherever possible. The force coefficients shown are applicable over a small range of diffraction parameter. If the values of ka are much different from the range given in the table, values of the force coefficients are to be used with caution.

2.9   Current Forces

The presence of current in water produces the following distinct effects: Current velocity should be added vectorially to the horizontal water particle velocity before computing the drag force, because drag force depends on the square of the water particle velocity. Current decreases slowly with the increase in depth, but even a small magnitude of current velocity can cause significant drag force. The opposing current will increase the force on the member and the superposed current will decrease the total force. The effect of current on the variation of total force with respect to phase angle is shown in Fig. 2.11.

This effect is insignificant and generally neglected. Current makes the structure itself to generate waves, which in turn creates diffraction forces. However, these values are negligible for realistic value of current acting on the normal-sized members. The presence of current is alternatively accounted by increasing the wave height to 10–15% and neglect the presence of current per se.

2.10   Earthquake Loads

Offshore platforms, which do not have stiff connection with the seabed are indirectly influenced by earthquakes; those which are bottom-supported are affected by earthquakes directly. Compliant structures that are position-restrained by tethers will be subjected to dynamic tether tension variations under the presence of
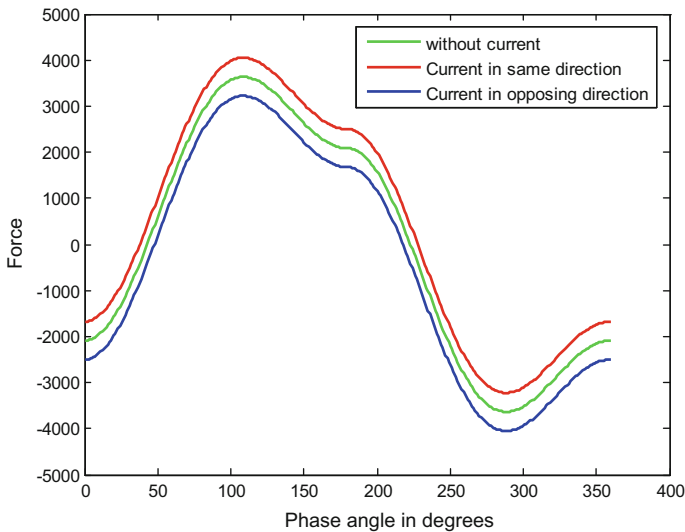
Fig. 2.11 Variation of the total force due to current

earthquake forces, which in turn shall affect the response of the platform under lateral loads. Earthquakes give rise to the horizontal and vertical motions for a typical duration of 15–30 s. Earthquake acceleration exhibits random characteristics due to (i) the nature of the mechanism causing earthquakes; (ii) wave propagation; (iii) reflection; and (iv) deflection. Earthquakes can result in inertia forces due to the acceleration and damping forces due to the motion of the water particles. In case of the analysis of compliant structures like TLPs, earthquake forces are handled in an indirect manner. Water waves generated due to the ground motion are neglected. Stiffness of TLP tether is modeled as axial tension members; slackening of tethers is neglected. The dynamic tether tension variation, caused by the horizontal motion of the earthquakes, is used to update the stiffness matrix of the TLP using the following equation (Chandrasekaran and Gaurav 2008):

$$\Delta T = \frac{AE}{\ell}\left[x(t) - x_g(t)\right] \tag{2.40}$$

where, $x(t)$ is the instantaneous response vector of TLP and $x_g(t)$ is the ground displacement vector, which is given by:

$$x_g(t) = \begin{Bmatrix} x_{1g}(t) \\ 0 \\ x_{3g}(t) \\ 0 \\ 0 \\ 0 \end{Bmatrix} \tag{2.41}$$

where, x_{1g}, x_{3g} is the horizontal and vertical ground displacements, respectively. Ground motions can be generated using Kanai-Tajimi ground acceleration spectrum (K-T spectrum), which is given by

$$S_{\ddot{x}_g\ddot{x}_g}(\omega) = \left[\frac{\omega_g^4 + 4\xi_g^2\omega_g^2\omega^2}{\left(\omega_g^2 - \omega^2\right)^2 + 4\xi_g^2\omega_g^2\omega^2}\right]S_0$$

$$S_0 = \frac{2\xi_g\sigma_g^2}{\pi\omega_g(1 + 4\xi_g^2)} \tag{2.42}$$

where, S_0 is the intensity of earthquake, ω_g is the natural frequency of the ground, ξ_g is the damping of the ground and σ_g^2 is the variance of the ground acceleration. These are the three parameters on which K-T spectrum depends on, which need to be chosen for any analytical studies on TLP under seismic action. The above three parameters should be estimated from the representative earthquake records by established estimation processes (Chandrasekaran et al. 2006a, b). For example, an earthquake occurred in GoM, approximately at 250 miles WSW of Anna Maria, Florida on 10 September 2006 at 14:56:07 (coordinated universal time). The signal
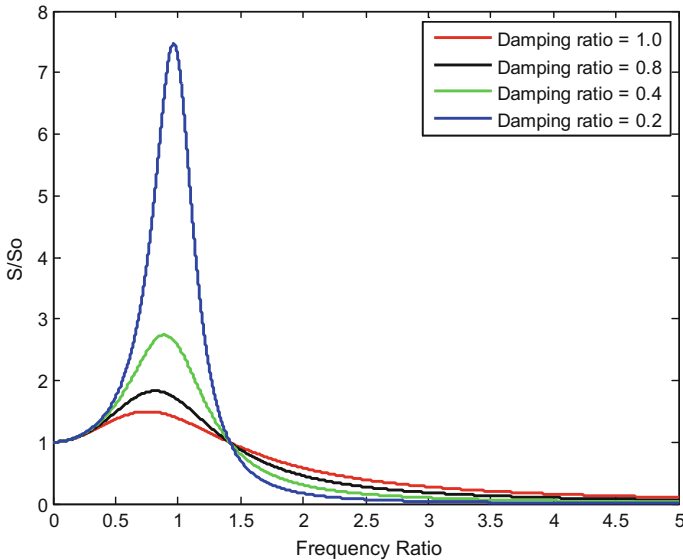
Fig. 2.12 Kanai-Tajimi ground acceleration spectrum

was epicentered 26.34N, 86.57W. Incidentally MARS TLP was operating in the
Mississippi Canyon Block, which is also located in GoM. The three parameters S_0,
ω_g and ξ_g are chosen such that the real earthquake is simulated for analysis pur-
poses (Chandrasekaran and Gaurav 2008). Studies showed that the dynamic tether
tension variations caused by the earthquake forces are in the order of about 65%
more than that of the normal values. Even structures with rigid degrees of freedom
like heave are excited, which may result in the loss of functionality of the platform.
The ground acceleration spectrum is shown in Fig. 2.12. The curves are plotted for
different damping ratios. It is seen from the figure that amplitude of the spectral
density function tends to decrease with the increase in damping ratio.

2.11   Ice and Snow Loads

Ice loads are dominant in offshore structures in the Arctic regions. Prediction of ice
loads is associated with a significant degree of uncertainty, as there are various ice
conditions that exist in the service life of an offshore platform. They are level ice,
broken ice, ice ridges, and icebergs. Offshore structures show different types of
failure under ice loads namely creep, cracking, buckling, spalling, and crushing. Ice
loads exhibit random variations in both space and time. They are classified into:
(i) total or global loads and (ii) local loads or pressure. Global loads affect the
overall motion and stability of the platform, while local loads affect the members at

connections. In the level ice condition, frequency of interaction between the structure and ice is important; number of interactions per unit time is important to quantify the ice loads on offshore platforms. Total ice force can result in a periodic loading and can cause dynamic amplification in flexible/slender structures. Current codes include equations for the extreme static ice loads, which depend on the geometric shape of the structure. Studies show that ice loads in a conical structure are lesser than that of the cylindrical structure. This is because a well-designed cone shape can change the ice-failure mode from crushing to bending. Estimating (predicting) ice forces on offshore platforms has a lot of uncertainties. Ice forces often control the design of the platform in operational conditions, in particular. The design ice loads use varying factors for level ice, first-year ridge ice and multi-year ridge ice; the factored values are 2, 5, and 7, respectively.

There are four approaches for addressing ice forces on offshore platforms: (a) experimental studies on scaled models; (b) numerical studies; (c) field studies; and (d) data mining. Experimental studies use scaling laws to determine the ice loads and ice-structure interaction. This method claims many advantages due to the capability of testing many types of structural shapes in large testing facilities. However, such tests are expensive apart from a strong disagreement of the model ice not being accurately scaled as of the sea ice. As the ice failure is dependent on the geometric shape significantly, ice-failure behavior cannot be accurately studied. This may result in over-prediction of ice loads. Numerical modeling uses high-end software to model ice forces for different interaction scenarios, which makes it very cost-effective and instructive. However, limited validation of results with that of the experiments is reported in the literature. The more practical way to estimate ice loads is from data mining. Previous platforms can be visited to determine the ice loads through field measurements. This will give a real picture of the ice loads. In the frequency domain approach, excitation caused by ice loads is modeled as sinusoidal pseudo-excitation, and the response is characterized by the transfer function. Ice force spectrum on a narrow conical structure is given by

$$S^+(f) = \frac{A\overline{F}_0^2 \overline{T}^{(-\delta)}}{f^\gamma} \exp\left[-\frac{B}{\overline{T}^{(\alpha)} f^\beta}\right] \qquad (2.43)$$

where, A (=10), B (=5.47) are constants; $\overline{F}_0$ is the force amplitude on the structure; $\overline{T} = L_b/v$ is the period of ice; L_b is ice-breaking length, which is typically 4–10 times of thickness of ice; v is the velocity; $\alpha, \beta, \gamma, \delta$ are constants whose values are typically 0.64, 0.64, 3.5, and 2.5, respectively. Force amplitude on the structure is given by

$$\overline{F}_0 = C\sigma_f h^2 \left(\frac{D}{L_c}\right)^{0.34} \qquad (2.44)$$
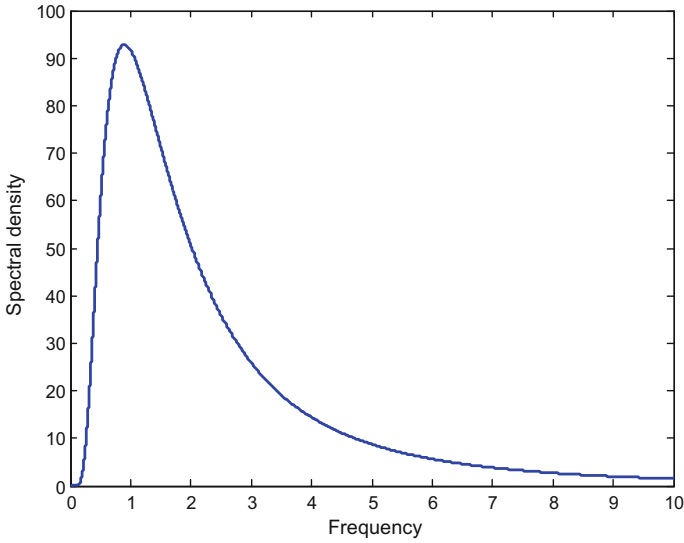
Fig. 2.13 Ice spectrum for Bohai Gulf region

where C is the constant (usually taken as 3.4); σ_f is bending strength of ice
(0.7 MPa); h is the ice thickness; D is the diameter of the ice cone and L_c is the
characteristic length of ice, which is given by the following equation:

$$L_c = \left[\frac{Eh^3}{12g\rho_w}\right]^{0.25} \tag{2.45}$$

where, E is Young's modulus of ice (=0.5 GPa) and ρ_w is density of water. As a
sample application, spectral density plot for Bohai Gulf region is shown in
Fig. 2.13. The spectrum is plotted with the variables in the above equations for the
ice characteristics in the Bohai Gulf region. The variables chosen were ice thick-
ness, velocity of ice cap and the diameter of the ice core.

2.12   Marine Growth

Marine growth or bio-fouling is the ubiquitous attachments of soft and hard
bio-particles on the surface of a submerged structure. It ranges from seaweeds to
hard-shelled barnacles. Its growth on the surface of the structure increases its
diameter and affects its roughness. Its main effect is to increase the wave forces on
the members by increasing not only exposed areas and volumes, but also the drag
coefficient due to higher surface roughness. In addition, it increases the unit mass of
the member, resulting in higher gravity loads and in lower member frequencies.

Depending upon the geographic location, the thickness of marine growth can reach 0.3 m or more. It is accounted for in the design through appropriate increases in the diameters and masses of the submerged members.

2.13 Mass

Mass is contributed by the structural mass and hydrodynamic added mass of the structure. For a slender structure, mass of the displaced volume of the structure will be significant and should be considered in the analysis. Added mass depends on the submerged volume of the platform, which also varies with respect to period of vibration. This is due to the variation in buoyancy, which in turn changes the tether tension variation that affects the natural frequency of motion. Based on the equipment layout plan and the chosen structural form, one can compute the mass of the platform readily. It is also important to establish the fact that a desired proportion between center of buoyancy and center of mass is maintained to ensure stability under free-floating conditions. This is important to enable smooth construction process in case of floating.

2.14 Damping

For steel offshore structures, structural damping is usually considered to vary from 0.2 to 0.5% of that of the critical damping (Adams and Baltrop 1991). For concrete structures, it can be of the order 0.5–1.5%. Hydrodynamic damping originates from the radiation damping and viscous damping effects. Radiation damping is determined using potential theory. It exhibits a strong dependence on frequency and submergence effects. Literature shows that the drag damping is lower for structures with large diameter column members ($\sim 0.1\%$). Damping ratio for offshore structures (wet structures), including the effects of added mass, can be expressed as a ratio of that of the dry structures, as given below

$$\xi_{\text{wet}} = \xi_{\text{wet}} \frac{(m^*_{\text{dry}})(\omega^*_{\text{dry}})}{(m^*_{\text{wet}})(\omega^*_{\text{wet}})} \qquad (2.46)$$

where, m^*, ω^* are generalized mass and frequency, respectively (Naess and Moan 2013). Literature shows that the total damping ratio is about 2% for the first three modes of bottom-supported structures.

2.15   Dead Load

Dead load is the weight of the overall platform in air, which includes piling, superstructure, jacket, stiffeners, piping, conductors, corrosion anodes, deck, railing, grout, and other appurtenances. Dead load excludes the following: weight of the drilling equipment placed on the platform including the derrick, draw works, mud pumps, mud tanks, etc.; weight of production or treatment equipment located on the platform including separators, compressors, piping manifolds and storage tanks; weight of drilling supplies that cause variable loads during drilling such as drilling mud, water, fuel, casing, etc.; weight of treatment supplies employed during production such as fluid in the separator, storage in the tanks; drilling load, which is approximate combination of derrick load, pipe storage, rotary table load, etc.

2.16   Live Load

Live loads are acting in addition to the equipment loads. They include load caused by impacts of vessels and boats on the platform. Dynamic amplification factor is applied to such loads to compute the enhanced live loads. Live loads are generally designated as factor times of the applied static load. These factors are assigned by the designer depending on the type of platform. Table 2.3 gives the live load factors that are used in the platform design.

2.17   Impact Load

For structural components which experience impact under live loads, the stipulated live loads in Table 2.3 should be increased by an impact factor, as given in Table 2.4. Deck floor loads can be taken as 11.95 kN/m^2 in the drilling rig area, 71.85 kN/m^2 in the derrick area and 47.9 kN/m^2 for pipe racks, power plants and living and accommodation areas.

Table 2.3 Typical live load values used in platform design (Graff 1981a, b)

Description	Uniform load on decks (kN/m^2)	Concentrated load on deck	Concentrated load on beams
Walkway, stair	4.79	4.38 kN/m^2	4.45 kN/m^2
Areas > 40 m^2	3.11	–	–
Areas for light use	11.9	10.95 kN/m^2	267 kN

Table 2.4 Impact factor for live loads

Structural item	Load direction	
	Horizontal	Vertical
Rated load in craned	20%	100%
Drilling hook loads	–	–
Supports of light machinery	–	20%
Supports of rotating machinery	50%	50%
Boat landings (kN)	890	890

2.18 General Design Requirements

Design methodology of offshore platforms differs with different types of offshore structures. For example, vertical deformation will be lesser in case of bottom-supported structures like jacket platform, GBS, etc. Such platforms are highly rigid and tend to attract more forces. Hence the design criteria should be to limit the stresses in the members. Displacement of the members under the applied loads will be insignificant. On the contrary, compliant structures are more flexible, as they all displaced more under wave action. They also create more disturbances in the waves. Hence the design criteria will be to control displacement instead of limiting the stresses in the members. Orientation of the platform is another important aspect in the design. Preferred orientation is that members are oriented to have less projected area to the encountered wave direction. This induces lesser response on the members. Predominant wave direction for the chosen site is made available to the designer based on which the platform orientation is decided (Chandrasekaran and Bhattacharyya 2011). Following are the list of data required for the design of offshore structures:

- Land topographical survey of sufficient area covering the chosen site for platform installation
- Hydrographical survey of the proposed location (hydrographic charts are used for this purpose)
- Information regarding silting at the site
- Wind rose diagram showing information on wind velocities, duration, predominant direction round the year
- Cyclonic tracking data showing details of the past cyclonic storm such that wind velocities, direction, peak velocity period, etc., are indicated
- Oceanographic data including general tide data, tide table, wave data, local current, seabed characteristics, temperature, rainfall, and humidity
- Seismicity level and values of acceleration
- Structural data of existing similar structures, preferably in the close vicinity
- Soil investigation report

2.18.1   Steel Structures

The analysis of an offshore structure is an extensive task, embracing consideration of the different stages, i.e., execution, installation, and in-service stages, during its life. Many disciplines such as structural, geotechnical, naval architecture, and metallurgy are involved. The analytical models used in offshore engineering are in some respects similar to those adopted for other types of steel structures. Only the salient features of offshore models are presented here. The same model is used throughout the analysis with only minor adjustments to suit the specific conditions, e.g., at supports in particular, relating to each analysis. Stick models (beam elements assembled in frames) are used extensively for tubular structures (jackets, bridges, flare booms) and lattice trusses (modules, decks). Each member is (normally) rigidly fixed at its ends to other elements in the model. If more accuracy is required, particularly for the assessment of natural vibration modes, local flexibility of the connections may be represented by a joint stiffness matrix. In addition to its geometrical and material properties, each member is characterized by hydrodynamic coefficients, e.g., relating to drag, inertia, and marine growth, to allow wave forces to be automatically generated. Integrated decks and hulls of floating platforms, involving large bulkheads, are described by plate elements. The characteristics assumed for the plate elements depend on the principal state of stress to which they are subjected. Membrane stresses are taken when the element is subjected merely to axial load and shear. Plate stresses are adopted when bending and lateral pressure is to be taken into account. After developing a preliminary model for analysis, member stresses are checked for preliminary sizing under different environmental loads.

Verification of an element consists of comparing its characteristic resistance(s) to a design force or stress. It includes (i) a strength check where the characteristic resistance is related to the yield strength of the element; and (ii) a stability check for elements in compression where the characteristic resistance relates to the buckling limit of the element. An element (member or plate) is checked at typical sections (at least both ends and mid span) against resistance and buckling. This verification also includes the effect of water pressure for deep-water structures. Tubular joints are checked against punching under various load patterns. These checks may indicate the need for local reinforcement of the chord using over-thickness or internal ring-stiffeners. Elements should also be verified against fatigue, corrosion, temperature or durability wherever relevant.

2.18.2   Allowable Stress Method

This method is presently specified by American codes. The loads remain unfactored and a unique coefficient is applied to the characteristic resistance to obtain an allowable stress as shown in Table 2.5.

Table 2.5 Coefficient for resistance to stresses

Condition	Axial	Strong axis bending	Weak axis bending
Normal	0.60	0.66	0.75
Extreme	0.80	0.88	1.00

"Normal" and "extreme" respectively represent the most severe conditions under which (a) the plant is to operate without shutdown; and (b) the platform is to endure over its lifetime.

2.18.3   Limit State Method

This method is enforced by European and Norwegian authorities and has now been adopted by American Petroleum Institute (API) as it offers a more uniform reliability. Partial factors are applied to the loads and to the characteristic resistance of the element as given in Table 2.6. They reflect the amount of confidence placed in the design value of each parameter and the degree of risk accepted under a limit state as discussed below

- Ultimate limit state (ULS), which corresponds to an ultimate event considering the structural resistance with appropriate reserve.
- Fatigue limit state (FLS), which relates to the possibility of failure under cyclic loading.

Table 2.6 Load factors

Limit state	Load categories				
	P	L	D	E	A
ULS (normal)	1.3	1.3	1.0	0.7	0.0
ULS (extreme)	1.0	1.0	1.0	1.3	0.0
FLS	0.0	0.0	0.0	1.0	0.0
PLS (accidental)	1.0	1.0	1.0	1.0	1.0
PLS (post-damage)	1.0	1.0	1.0	1.0	0.0
SLS	1.0	1.0	1.0	1.0	0.0

Where, the following explanations are applicable
P represents permanent loads (structural weight, dry equipment, ballast, hydrostatic pressure)
L represents live loads (storage, personnel, liquid)
D represents deformations (out-of-level supports, subsidence)
E represents environmental loads (wave, current, wind, earthquake)
A represents accidental load (dropped object, ship impact, blast, fire). The material partial factors for steel are normally taken equal to 1.15 for ULS and 1.00 for PLS and SLS design. Guidance for classifying typical conditions into typical limit states is given in Table 2.7

Table 2.7 Conditions specified for various limit states

Conditions	Loadings				Design criterion
	P/L	E	D	A	
Construction	P				ULS, TSLS
Load-out	P	Reduced wind	Support displacement		ULS
Transport	P	Transport wind and wave			ULS
Tow-out (accidental)	P			Flooded compartment	PLS
Launch	P				ULS
Lifting	P				ULS
In-Place (normal)	P + L	Wind, wave and snow	Actual		ULS, SLS
In-Place (extreme)	P + L	Wind and 100 year wave	Actual		ULS, SLS
In-Place (exceptional)	P + L	Wind and 10,000 year wave	Actual		PLS
Earthquake	P + L	10^{-2} quake			ULS
Rare earthquake	P + L	10^{-4} quake			PLS
Explosion	P + L			Blast	PLS
Fire	P + L			Fire	PLS
Dropped object	P + L			Drill collar	PLS
Boat collision	P + L			Boat impact	PLS
Damaged structure	P + reduced L	Reduced wave and wind			PLS

- Progressive collapses limit state (PLS), which reflects the ability of the structure to resist collapse under accidental or abnormal conditions.
- Serviceability limit state (SLS), which corresponds to the criteria for normal use or durability (often specified by the plant operator).

The analysis of the offshore platform is an iterative process, which requires progressive adjustment of the member sizes with respect to the forces they transmit, until a safe and economical design is achieved. It is therefore of utmost importance to start the main analysis from a model which is close to the final optimized one. The simple rules given below provide an easy way of selecting realistic sizes for the

main elements of offshore structures in moderate water depth (up to 80 m) where dynamic effects are negligible.

Jacket Pile Sizes

- Calculate the vertical resultant (dead weight, live loads, and buoyancy), the overall shear and the overturning moment (environmental forces) at the mudline.
- Assuming that the jacket behaves as a rigid body, derive the maximum axial and shear force at the top of the pile.
- Select a pile diameter in accordance with the expected leg diameter and the capacity of pile-driving equipment.
- Derive the penetration from the shaft friction and tip bearing diagrams.
- Assuming an equivalent soil sub grade modulus and full fixity at the base of the jacket, calculate the maximum moment in the pile and derive its wall thickness.

Deck Leg Sizes

- Adapt the diameter of the leg to that of the pile.
- Determine the effective length from the degree of fixity of the leg into the deck (depending upon the height of the cellar deck).
- Calculate the moment caused by wind loads on topsides and derive the appropriate thickness.

Jacket Bracings

- Select the diameter in order to obtain a span/diameter ratio between 30 and 40.
- Calculate the axial force in the brace from the overall shear and the local bending caused by the wave assuming partial or total end restraint.
- Derive the thickness such that the diameter/thickness ratio lies between 20 and 70 and eliminate any hydrostatic buckle tendency.

Deck Framing

- Select spacing between stiffeners (typically 500–800 mm).
- Derive the plate thickness from formulae accounting for local plastification under the wheel footprint of the design forklift truck.
- Determine by straight beam formulae the sizes of the main girders under "blanket" live loads and/or the respective weight of the heaviest equipment.

The static in-place analysis is the basic and generally the simplest of all analyses. The structure is modeled as it stands during its operational life and subjected to pseudo-static loads. This analysis is always carried at the very early stage of the project, often from a simplified model, to size the main elements of the structure. The main model should account for eccentricities and local reinforcements at the joints. For example, a typical model for North Sea jacket may feature over 800 nodes and 4000 members. The contribution of appurtenances like risers, J-tubes, caissons, conductors, boat-fenders, etc., to the overall stiffness of the structure is normally neglected. They are therefore analyzed separately and their reactions applied as loads at the interfaces with the main structure. Since their behavior is

nonlinear, foundations are often analyzed separately from the structural model. They are represented by an equivalent load-dependent secant stiffness matrix; coefficients are determined by an iterative process where the forces and displacements at the common boundaries of structural and foundation models are equated. This matrix may need to be adjusted to the mean reaction corresponding to each loading condition. The static in-place analysis is performed under different conditions where the loads are approximated by their pseudo-static equivalent. The basic loads relevant to a given condition are multiplied by the appropriate load factors and combined to produce the most severe effect in each individual element of the structure. A dynamic analysis is normally mandatory for every offshore structure, but can be restricted to the main modes in the case of stiff structures.

2.19   Fabrication and Installation Loads

These loads are temporary and arise during fabrication and installation of the platform or its components. During fabrication, various structural components generate lifting forces, while in the installation phase forces are generated during platform load-out, transportation to the site, launching and upending, as well as during lifts related to installation. According to the Det Norske Veritas (DNV 1982) rules, the return period for computing design environmental conditions for installation and fabrication loads is three times as that of the duration of the corresponding phase. API-RP2A, on the other hand, leaves this design return period up to the owner, while the BS6235 rules recommend a minimum recurrence interval of 10 years for the design environmental loads associated with transportation of the structure to the offshore site.

2.20   Lifting Force

Lifting forces are functions of the weight of the structural component being lifted, the number and location of lifting eyes used for the lift, the angle between each sling and the vertical axis and the conditions under which the lift is performed, as shown in Fig. 2.14. All members and connections of a lifted component must be designed for the forces resulting from static equilibrium of the lifted weight and the sling tensions. Moreover, API-RP2A recommends that in order to compensate for any side movements, lifting eyes and the connections to the supporting structural members should be designed for the combined action of the static sling load and a horizontal force equal to 5% this load, applied perpendicular to the member at the center of the pinhole. All these design forces are applied as static loads if the lifts are performed in the fabrication yard. If, however, the lifting derrick or the structure to be lifted is on a floating vessel, then dynamic load factors should be applied to the static lifting forces. A factor of 2 is applied for members and connections and 1.35 for all other secondary members. For load-out at sheltered locations, the

(a) Derrick and structure on land

(b) Derrick on land, structure on floating
      barge

(c) Derrick and structure in
      the sea
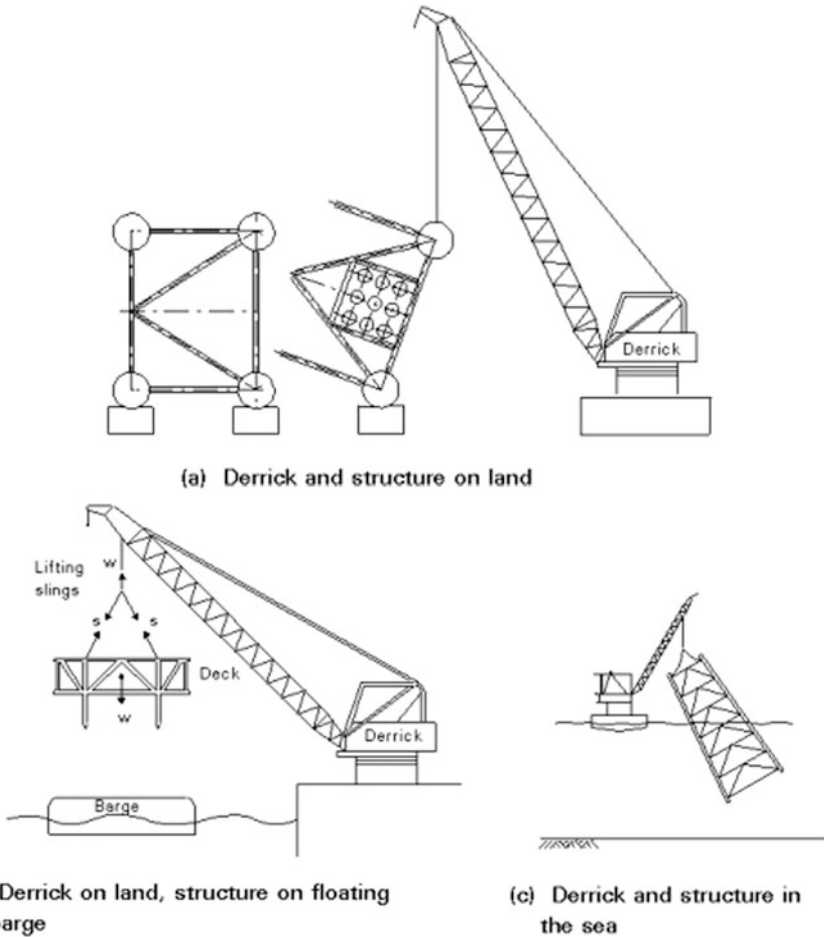
Fig. 2.14 Lifts under different conditions

corresponding minimum load factors for the two groups of structural components
are 1.5 and 1.15, respectively.

2.21 Load-Out Force

These are forces generated when the jacket is loaded from the fabrication yard onto
the barge. If the load-out is carried out by direct lift, then, unless the lifting
arrangement is different from that to be used for installation, lifting forces need not
be computed. This is because lifting in the open sea creates a more severe loading
condition, which requires higher dynamic load factors. If load-out is done by
skidding the structure onto the barge, a number of static loading conditions must be

considered, with the jacket supported on its side. Such loading conditions arise from the different positions of the jacket during the load-out phases as shown in Fig. 2.15. Since movement of the jacket is slow, all loading conditions can be taken as static.

Typical values of friction coefficients for the calculation of skidding forces are: (i) steel on steel without lubrication (0.25); (ii) steel on steel with lubrication (0.15); (iii) steel on Teflon (0.10); and (iv) Teflon on Teflon (0.08). A typical ballast and displacement values are indicated in the figure.
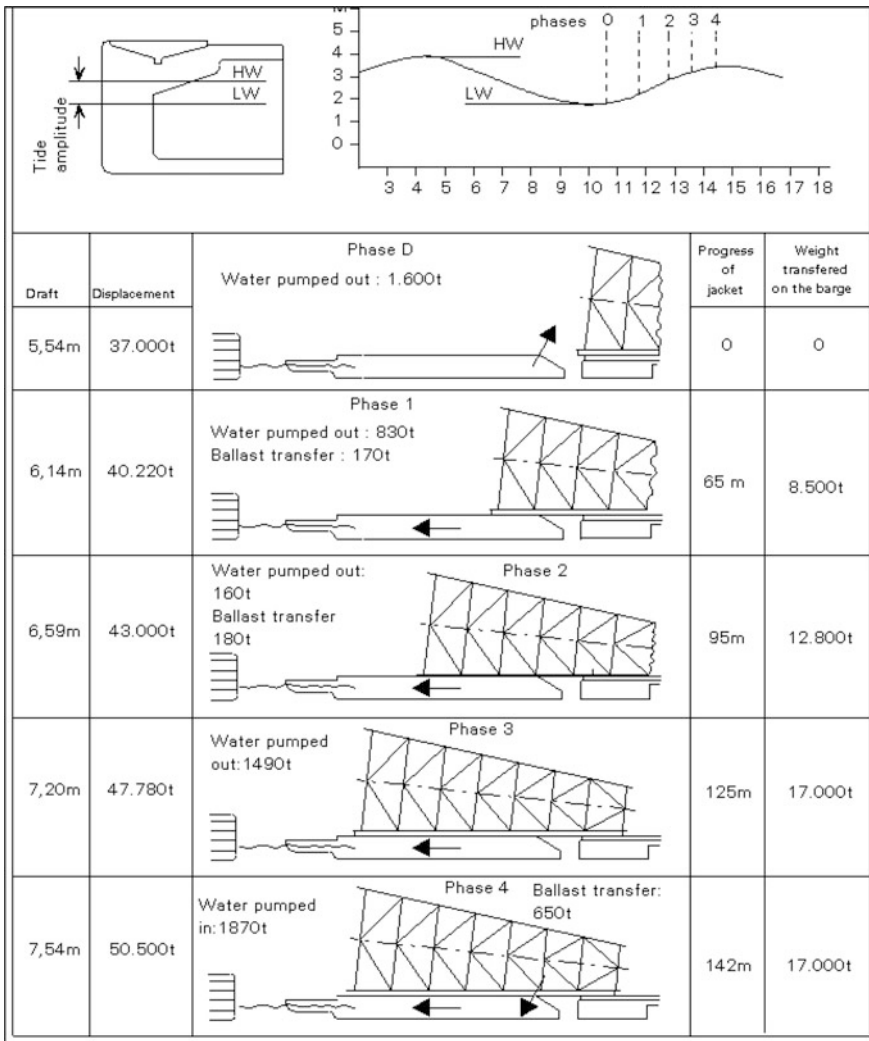
Fig. 2.15 Different phases of jacket load-out by skidding

2.22   Transportation Forces

These forces are generated when platform components (jacket, deck) are transported offshore on barges or self-floating. They depend upon the weight, geometry and support conditions of the structure (by barge or by buoyancy) and also on the environmental conditions (waves, winds, and currents) that are encountered during transportation. The types of motion that a floating structure may experience are shown schematically in Fig. 2.16.

In order to minimize the associated risks and secure safe transport from the fabrication yard to the platform site, it is important to plan the operation carefully by considering the following (API-RP2A):

- Previous experience along the tow route
- Exposure time and reliability of predicted "weather windows"
- Accessibility of safe havens

Fig. 2.16 Motion of floating objects during installation
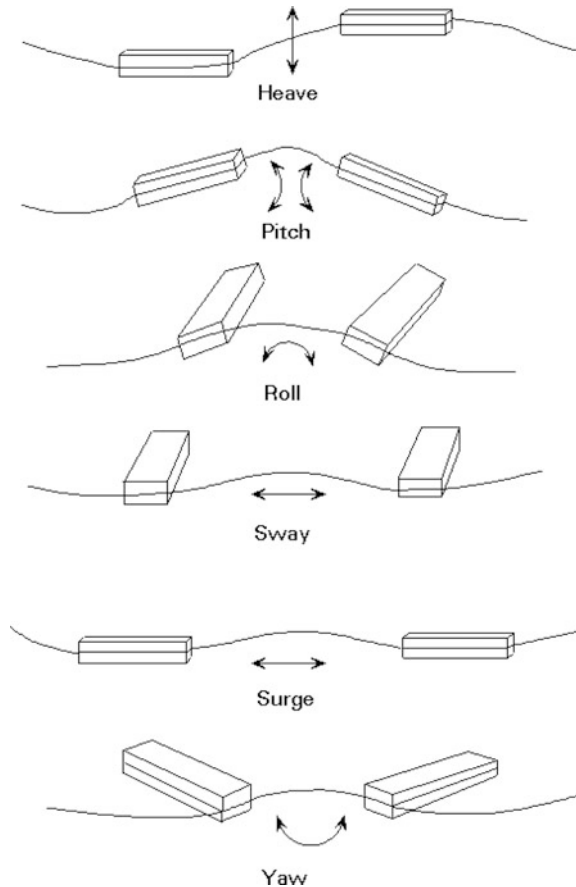
- Seasonal weather system
- Appropriate return period for determining design wind, wave and current conditions, taking into account the characteristics of the tow such as size, structure, sensitivity and cost.

The motion of the tow, i.e., the structure and supporting barge, generates transportation forces. They are determined from the design winds, waves and currents. If the structure is self-floating, the loads are calculated directly. According to API-RP2A, towing analyses must be based on the results of model basin tests or appropriate analytical methods and must consider wind and wave directions parallel, perpendicular and at 45° to the tow axis. Inertial loads shall be computed from a rigid body analysis of the tow by combining roll and pitch with heave motions, when the size of the tow, magnitude of the sea state and experience make such assumptions reasonable. For open sea conditions, typical values are 20° (for single amplitude roll motion) and 10° for single amplitude pitch motion. The period of roll or pitch is taken as 10 s, while heave acceleration is taken as 0.2 g. When transporting a large jacket by barge, stability against capsizing is a primary design consideration because of the high center of gravity of the jacket. Moreover, the relative stiffness of jacket and barge may need to be taken into account together with the wave slamming forces that could result during a heavy roll motion of the tow, as shown in Fig. 2.17. Structural analyses are carried out for designing the tie-down braces and the jacket members affected by the induced loads.

Fig. 2.17 View of launch barge and jacket undergoing motion

F = Component of gravity plus inertia
G_1 = Centre of gravity of jacket
G_2 = Centre of gravity of the tow
M = Metacentre of the tow
A = Areas of potential impact
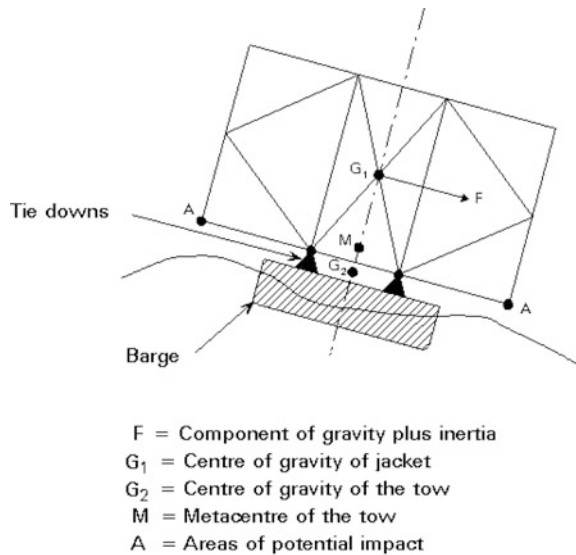
2.23   Launching and Upending Force

These forces are generated during the launch of a jacket from the barge into the sea and during the subsequent upending into its proper vertical position to rest on the seabed. A schematic view of the five stages the operation can be seen in Fig. 2.18.

Five stages in a launch-upending operation are (i) jacket slides along the skid beams; (ii) jacket rotates on the rocker arms; (iii) jacket rotates and slides simultaneously; (iv) detaches completely and comes to its floating equilibrium position; and (v) jacket is upended by a combination of controlled flooding and simultaneous lifting by a derrick barge. Both the static and dynamic loads for each stage of the above under the action of wind, waves and current need to be included in the analysis. To start the launch, the barge must be ballasted to an appropriate draft and trim angle and subsequently the jacket must be pulled towards the stern by a winch. Sliding of the jacket starts as soon as the downward force (gravity component and winch pull) exceeds the friction force. As the jacket slides, its weight is supported on the two legs that are part of the launch trusses. The support length keeps decreasing and reaches a minimum, equal to the length of the rocker beams, when rotation starts. It is generally at this instant that the most severe launching forces develop as reactions to the weight of the jacket. During the last two stages, variable hydrostatic forces arise, which have to be considered at all members affected. Buoyancy calculations are required for every stage of the operation to ensure fully controlled, stable motion. Computer programs are available to perform the stress analyses required for launching and upending and also to portray the whole operation graphically.
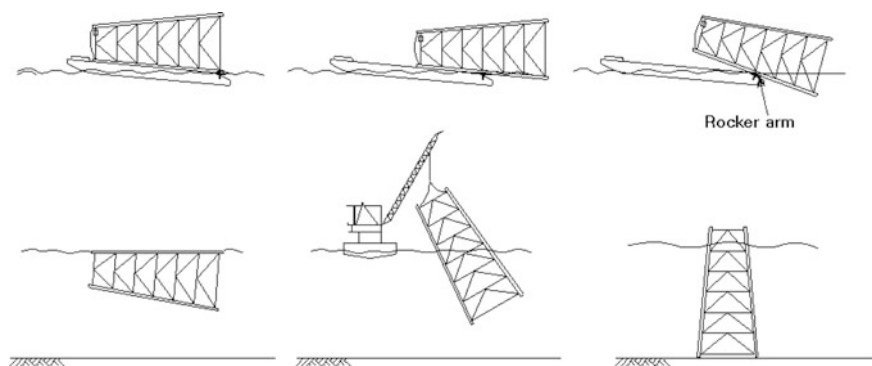
Fig. 2.18 Launching and upending

2.24   Accidental Load

According to the DNV rules, accidental loads are ill-defined with respect to intensity and frequency, which may occur as a result of an accident or exceptional circumstances. Examples of accidental loads are loads due to collision with vessels, fire or explosion, dropped objects, and unintended flooding of buoyancy tanks. Special measures are normally taken to reduce the risk from accidental loads. For example, protection of wellheads or other critical equipment from a dropped object can be provided by specially designed, impact resistant covers. An accidental load can be disregarded if its annual probability of occurrence is less than 10^{-4}. This number is the estimate of order of magnitude and is extremely difficult to compute.

Exercise
PART A

1. The design of offshore structures are dominated by _____.
2. Earthquakes are normally regarded as _____ loads in offshore engineering.
3. The mean recurrence interval of a design event is called _____.
4. The wind pressure coefficient is calculated from _____.
5. The coefficient of wind pressure depends upon _____.
6. The gust component of wind is generated by _____.
7. Wind force in the direction parallel and normal to the wind direction are called _____ and _____ respectively.
8. The one minute average wind speed according to U.S. weather bureau is called _____.
9. The one-seventh power law is used to calculate _____ of wind speed.
10. Wave forces causes _____ and _____, while earthquake forces causes _____ on the members.
11. In slender and flexible members, the de-amplification takes place due to _____.
12. _____ is used to define the cross-spectrum in the analysis.
13. Aerodynamic admittance function connects _____ and _____.
14. For the analysis of high-frequency wind data, _____ spectrum is used.
15. Harris spectrum is not recommended for the frequencies _____.
16. _____ gives a better fit to empirical observations of atmospheric turbulence.
17. Linear theory is applied when H/gT^2 is _____.
18. Airy's theory is valid only up to _____.
19. PM spectrum is recommended for _____ conditions.
20. For North Sea, _____ spectrum is recommended.
21. The sea state in short term is assumed as _____.
22. _____ describes the energy distribution of different frequencies of a sea state.

23. PM spectrum is used for _____ condition, which is neither _____, nor _____.

24. _____ spectrum has a greater frequency bandwidth compared to PM spectrum.

25. Bredneidger spectrum is usually used to describe _____ waves, generated by _____.

26. _____ spectrum is a modification of Bredneidger spectrum, and is true only for _____.

27. JONSWAP spectrum is recommended for use in _____ analysis.

28. Peakedness parameter follows _____ distribution.

29. _____ is caused by the pressure effects due to undisturbed incident waves.

30. _____ is caused by the pressure effects due to the presence of the structure in the fluid domain.

31. _____ and _____ is cause by the pressure effects due to the motion of the structural components in _____.

32. _____ is caused by the pressure effects due to the relative velocity between the water particle and the structural component.

33. For slender structures, _____ and _____ are idealized as a single inertia term.

34. Reaction forces developed due to acceleration and velocity results in _____ and _____ respectively.

35. The relative velocity of the structure in the fluid produces _____ and _____.

36. In large diameter members, _____ becomes less significant.

37. Force is calculated by _____ method using the incident wave pressure that is acting on the _____ of the structure.

38. The opposing current will _____ the wave height and _____ the wave length.

39. The superposing current will _____ the wave height and _____ the wave length.

40. The opposing current will _____ the force and supposing current will _____ the force on the member.

41. Current affects the _____ force component only.

42. Current force should be added vectorially to _____ before calculating _____.

43. Current causes the structure to generate _____, which inturn creates _____.

44. Compliant structures that are position-restrained by tethers will be subjected to _____ under the presence of earthquake forces.

45. Earthquake will cause motion for a typical duration of _____.

46. Earthquake can result in _____ due to _____ and _____.

47. Dynamic tether tension variation caused by the earthquake forces are in the order of about _____ more than that of the normal values.

48. _____ is important to quantify the ice loads n the offshore structure.
49. Total ice force can result in _____ and can cause _____ in flexible structures.
50. Extreme static ice loads depends upon _____ of the structure.
51. Ice loads in _____ are lesser than that of the cylindrical structure.
52. Well-defined cone shape can change the ice-failure mode from _____ to _____.
53. _____ is the most practical way to estimate the ice loads.
54. In the frequency domain approach, excitation caused by ice loads is modeled as _____, and the response is characterized by the _____.
55. Marine growth increases _____ and _____ of the structure.
56. Marine growth results in _____ gravity loads.
57. Marine growth _____ drag coefficient due to _____.
58. Added mass depends upon _____ of the platform.
59. Mass is contributed by _____ and _____ of the structure.
60. In slender structures, _____ should be considered in the analysis.
61. For steel offshore structures, structural damping varies from _____ of that of the critical damping.
62. For concrete offshore structures, structural damping varies from _____ of that of the critical damping.
63. Hydrodynamic damping originated from _____ and _____.
64. Radiation damping is determined based on _____ and it depends upon _____ and _____.
65. Drag damping is lower for _____.
66. Total damping ratio is about _____ for the first three modes of bottom-supported structures.
67. Dead load excludes _____, _____, _____ and _____.
68. Dynamic amplification factor is applied to _____.
69. _____ is lesser in bottom-supported structures.
70. In bottom-supported structures, the design criteria is to control _____.
71. In compliant structures, the design criteria is to control _____.
72. Orientation of the platform is altered to reduce _____ and _____.
73. _____ should be considered when the elements are subjected to axial load and shear.
74. When the elements are subjected to bending and lateral pressure, _____ should be considered in the analysis.
75. Tubular joints in steel offshore platforms should be checked for _____ under various load patterns.
76. Fatigue limit state relates the possibility of failure under _____.
77. _____ corresponds to the criteria for normal use or durability.
78. _____ is the basic simplest analysis procedure, where the loads are approximated by _____.

79. According to BS6235, the mean recurrence interval associated with the transportation of the structure is _____.
80. According to DNV, the return period for computing design environmental conditions for installation and fabrication is _____.
81. Lifting forces on the structures are functions of _____, _____, _____ and _____.
82. The members and connections of the lifted component must be designed for the forces resulting from _____ and _____.
83. If the structure is lifted in fabrication yard, the design forces are applied as _____.
84. The minimum load factors that must be considered for the members and connections for load-out at sheltered locations are _____ and _____ respectively.
85. Lifting in open sea creates _____ which requires _____.
86. Load-out is carried out by _____ and _____.
87. Transportation forces depends upon _____, _____ and _____ of the structure.
88. The offshore structures are transported by _____ and _____.
89. During floating transportation, the structure will undergo _____.
90. According to API-RP2A, the period of roll or pitch in towing analysis is _____.
91. _____ is the primary consideration while transporting a large jacket by barge, because of the _____.
92. _____ and _____ should be considered while transporting the jacket platforms.
93. _____ is considered important in every stage of launch operation for fully controlled stable motion.
94. Accidental loads occurs sue to _____, _____, _____ and _____.
95. Fire resistance to structures are provided in the form of _____.
96. An accidental load can be disregarded if its annual probability of occurrence is _____.

PART B

1. List type of loads that act on offshore structures.
2. List various environmental loads that act on offshore structure.
3. How wind forces are estimated on offshore structures?
4. What are the two components of wind?
5. In offshore structures, static wind analysis is sufficient. State true or false with reason.
6. Explain the spatial dependence of the components of wind.
7. Mention the law, used to calculate the wind speed. Explain why it is widely used?

8. How the mean and gust components of wind speed were calculated?
9. What is fastest mile velocity?
10. The effect of waves and earthquake on the structure is different. Why?
11. What are the parameters to be considered while considering wind as a dynamic process?
12. Name the function which is used to handle the spatial variations of the wind velocity. State the importance of the function.
13. How the standard wind data is measured?
14. Name few wind spectra used in the design of offshore structures.
15. State the importance of gust component of wind speed in offshore structures.
16. The application of Davenport spectrum and Harris spectrum to offshore structures is questionable. Why?
17. Plot the variation of spectral density for wind spectra and state the inferences.
18. How the wind-generated sea surface is represented?
19. List the different wave theories.
20. Why Airy's wave theory is commonly used?
21. How the additional forces due to variable submergence are accounted for, in Airy's theory?
22. How the wave data is collected?
23. How the sea state is assumed in short-term- and long-term processes?
24. Under what conditions, PM spectrum is used?
25. Where will you recommend the usage of JONSWAP spectrum?
26. Compare the different wave spectra and state the inferences.
27. How the compliancy of the structure is considered while calculating the wave forces?
28. Mention the parameters based on which the drag and inertia components are calculated?
29. Mention the recommended values of drag and inertia coefficients according to API RP 2A.
30. Why Morison equation is not recommended for large diameter structures?
31. Why the spacing between the columns in offshore structures is considered to be very important?
32. Find the phase angle for the typical topside of 100×100 m, resting on four columns. The wave period is 12 s. State whether cancelation of forces will occur or not.
33. Wave force is calculated by assuming that the structure does not distort the wave field in its vicinity. Why?
34. What are the effects of current in the wave forces?
35. How the presence of the current is accounted in the design alternatively?
36. Show the variation of the total force in the presence and absence of current and state the inferences.
37. How earthquake affects the fixed and compliant structures?
38. Why earthquakes are considered to be random in nature?

39. Explain how earthquake forces are handled in the analysis of compliant structures?
40. Spectral density peak of earthquake forces increases with the decrease in the damping ratio. Validate the statement.
41. Mention the different forms of ice.
42. What are the different types of failure of offshore structures under ice loads?
43. Mention the classification of ice loads.
44. Why ice loads in conical structure are lesser than that of the cylindrical structure?
45. Mention the factors used for the design ice loads.
46. What are the advantages and disadvantages of the experimental analysis of structures subjected to ice loads?
47. What are the effects of the marine growth on the offshore structures?
48. How marine growth is accounted for in the design of the structure?
49. What is the significance of added mass in the analysis of the structure?
50. How stability is ensured during free-floating conditions? Why is it important?
51. Mention the different types of damping.
52. How to calculate the damping ratio for offshore structures?
53. Mention the dead loads acting on an offshore platform.
54. How live loads on offshore structures are designated?
55. Explain why the design methodology of the offshore platform differs based on the different types?
56. State the design criteria in bottom-supported and compliant structures.
57. How orientation of members plays an important role in the design?
58. How to check the safety of the steel structure?
59. List the different limit states considered in the design of offshore structures.
60. What are the steps involved in the calculation of the jacket pile sizes?
61. How to arrive at the optimum size of leg member in an offshore platform?
62. How jacket bracings are designed in offshore platforms?
63. List the fabrication and installation loads developed in the offshore structures.
64. How the members of the lifted components should be designed?
65. Mention the recommendations from API-RP2A for the design of the lifted structure.
66. How the design forces are applied, when the structure is lifted from a floating vessel?
67. What do you understand by load-out force?
68. How load-out analysis is performed under direct lift and skidding conditions?
69. Mention the recommendations from API for secure transport of the offshore structures.
70. What is the consequence of heave roll motion of the tow during transportation?
71. What are the steps involved in the installation of jacket platforms?
72. Hoe launching and upending forces are generated in the offshore structure?
73. What are the stages involved in the launch-upending operation?

74. What are the loads to be considered in the launch-upending operation?
75. When will the maximum launching force acts on a structure?

Key to Exercise
PART A

1. Environmental loads.
2. Environmental loads.
3. Return period.
4. Wind tunnel experiment.
5. Reynolds number.
6. Turbulence of the flow field.
7. Drag force and lift force.
8. Sustained wind speed.
9. Mean component.
10. Inertia and drag, inertia.
11. Compliancy.
12. Aerodynamic admittance function.
13. Force and response spectra.
14. Davenport.
15. Less than 0.1 Hz.
16. Kaimal spectrum.
17. Less than 0.01.
18. Mean sea level.
19. Opens sea.
20. JONSWAP.
21. Zero-mean ergodic process.
22. Wave spectra.
23. Fully developed sea, fetch limited, duration limited.
24. Bredsneidger.
25. Tropical storm, hurricanes.
26. ISSC, narrow-banded spectrum.
27. Reliability.
28. Normal probability.
29. Froude-Krylov forces.
30. Diffraction force.
31. Hydrodynamic added mass and potential damping force, ideal fluid.
32. Viscous drag force.
33. Froude-Krylov forces and Diffraction force.
34. Inertia force and potential damping force.
35. Excitation and damping forces.
36. Viscous force.
37. Pressure area method, submerged surface.
38. Increase, decrease.

39. Decrease, increase.
40. Increase, decrease.
41. Drag.
42. Horizontal water particle velocity, drag force.
43. Waves, diffraction forces.
44. Dynamic tether tension variations
45. 15–30 s.
46. Inertia forces, acceleration and damping.
47. 65%
48. Number of interactions per unit time.
49. Periodic loading, dynamic amplification.
50. Geometric shape.
51. Conical structure.
52. Crushing, bending.
53. Data mining.
54. Sinusoidal pseudo-excitation, transfer function.
55. Diameter, roughness.
56. Higher.
57. Increases, roughness.
58. Submerged volume.
59. Structural mass, hydrodynamic added mass.
60. Mass of the displaced volume.
61. 0.2–0.5%.
62. 0.5–1.5%.
63. Radiation and viscous damping.
64. Potential theory, frequency and submergence effects.
65. Large diameter column members.
66. 2%.
67. Weight of drilling equipment, production equipment, drilling supplies and treatment supplies.
68. Live loads.
69. Vertical deformation.
70. Stresses.
71. Displacement.
72. Projected area, response.
73. Membrane stresses.
74. Plate stresses.
75. Punching.
76. Cyclic loads.
77. Serviceability limit state.
78. Static in-place analysis, pseudo-static equivalent.
79. 10 years.
80. Three times as that of the duration of the corresponding phase.

81. Weight of the structure, number and location of lifting eyes, angle of lifting and conditions under which the lift is performed.
82. Static equilibrium of the lifted weight and sling tensions.
83. Static loads.
84. 1.5 and 1.15.
85. Severe loading condition, higher load factors.
86. Direct lift and skidding.
87. Weight, geometry and support conditions of the structure.
88. Derrick barges and self-floating.
89. Surge, sway, heave, roll, pitch and yaw.
90. 10 s.
91. Stability against capsizing, high center of gravity of the jacket.
92. Relative stiffness of jacket and barge, wave slamming forces.
93. Buoyancy.
94. Collision with vessels, fire or explosion, dropped objects and unintended flooding of buoyancy tanks.
95. Passive fire protection.
96. Less than 10^{-4}.

PART B

1. Permanent loads or dead loads, Operating loads or live loads, Other environmental loads including earthquake loads, Construction and installation loads and Accidental loads.
2. Wind, waves, current, tides, earthquakes, temperature, ice, seabed movement and marine growth.
3. Most widely used engineering approaches to estimate wind forces on offshore structures are based on few observations as listed below

   - When stream of air flows with constant velocity (v), it will generate force on the flat plate of area (A).
   - The plate will be placed orthogonal to the flow direction.
   - This force will be proportional to (Av^2).
   - The proportionality constant is independent of the area, which is verified by experimental studies.

4. Natural wind has two components: (i) mean wind component (which is static component); and (ii) fluctuating, gust component (which is a dynamic component).
5. For offshore locations, mean wind speed is much greater than the gust component, which means that in most of the design cases, a static analysis will suffice.
6. The spatial dependence of the mean component is only through the vertical coordinate, while $v(t)$ is homogeneous in both space and time.
7. Wind spectrum above water surface is given by one-seventh power law, which is

$$v_z = V_{10} \left[\frac{z}{10} \right]^{\frac{1}{7}} \tag{2.5}$$

where v_z is the wind speed at elevation of z m above MSL, V_{10} is the wind speed at 10 m above MSL, and 10 m is called the reference height. Power law is purely empirical and most widely used. It is tested with the actual field measurements and found to be in good agreement.

8. One-seventh power law is used to calculate the mean component of wind speed. The gust component can be obtained by multiplying a gust factor with the sustained wind speed. Average gust factor (F_g) is in the range of 1.35–1.45; variation of the gust factor along the height is negligible.

9. The product of sustained wind speed and the gust factor will give the *fastest mile velocity*.

10. Wave forces alone acting on the member will cause inertia and drag forces, while earthquake forces cause only inertia forces on the members. Hence, vibration of the structure induced by wind and waves are different from that caused by earthquakes.

11. While considering wind as a dynamic process, the following parameters are important:

   - Length of the record: The record can be continuous, intermittent or select record whose values are above the threshold value. For the record to be continuous, average values of the wind velocity is lesser than that of the intermittent because of the longer length of the record when compared with the former.
   - Wind spectrum: It is used as input for the structural analysis, which defines the fluctuating wind component.
   - Gust component: It is approximated by the *aerodynamic admittance function*.

12. There are two reasons for using the aerodynamic admittance function: (i) to bypass the rigorous random analysis; and (ii) possibility of an accurate measurement of this function through wind tunnel experiments. In this manner, the spatial variations of wind velocity are handled intelligently in the design.

13. The standard wind data represents 10 min average speed measured on mean sea level (DNV report). Wind instruments are mounted on light houses, ships, at fixed positions at sea approximately 4 m above sea level.

14. Davenport, Harris, Kaimal and API (2000) spectrum.

15. Steady wind forces are calculated from time averaged wind speed. However, fluctuating gust component may lead to resonating oscillations in offshore structures.

16. It is important to note that none of these spectrum used in the analysis of wind speed is recorded offshore; they are based on onshore records. Hence these applications to offshore locations are questionable. They have serious problem when used for low-frequency flexible structures.

17. Wind spectra plot

WIND SPECTRA (Mean wind speed=20m/s, Reference Height=10m, Time period=12s)
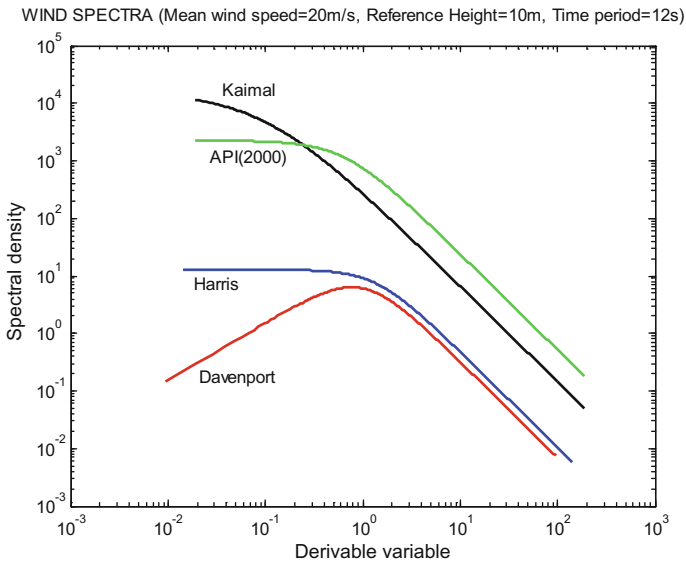
18. Wind-generated sea surface waves can be represented by a combination of regular waves. Regular waves of different magnitude and wave lengths from different directions are combined to represent the sea surface elevation.
19. Linear or first-order or Airy theory
    Stokes fifth-order theory
    Solitary wave theory
    Cnoidal theory
    Dean's stream function theory
    Numerical theory by Chappelear
20. Among all the theories, Airy's wave theory is commonly used because it assumes linearity between the kinematic quantities and the wave height, which makes the wave theory simple.
21. Airy's theory is valid up to mean sea level only. However, due to the variable submergence effect, the submerged length of the members will be continuously changing. This will attract additional forces due to their variable submergence at any given time. To compute the water particle kinematics up to the actual level of submergence, stretching modifications suggested by various researchers are used.

- Wheeler suggested the following modification in the horizontal water particle velocity and acceleration to include the actual level of submergence of the member

$$\dot{u}(x,t) = \frac{\omega H}{2} \frac{\cosh\left(ky\left[\frac{d}{d+\eta}\right]\right)}{\sinh(kd)} \cos(kx - \omega t)$$

$$\ddot{u}(x,t) = \frac{\omega^2 H}{2} \frac{\cosh\left(ky\left[\frac{d}{d+\eta}\right]\right)}{\sinh(kd)} \sin(kx - \omega t)$$

- Chakrabarti suggested the modification as given below

$$\dot{u}(x,t) = \frac{\omega H}{2} \frac{\cosh(ky)}{\sinh(k(d+\eta))} \cos(kx - \omega t)$$

$$\ddot{u}(x,t) = \frac{\omega^2 H}{2} \frac{\cosh(ky)}{\sinh(k(d+\eta))} \sin(kx - \omega t)$$

22. Wave data are collected are approximately collected for 20 min every 3 h and assumed to represent the stationary sea state between the measurements. The sea state is defined by significant wave height, significant wave period, peak period, and wave direction. Data collection is done by visual investigation and instrumental observations by buoys, radars, lasers, and satellites.

23. The sea state, in a short term, which is typically 3 h, is assumed as zero mean, ergodic Gaussian process. In a long term, variation of sea state is slower than the short-term fluctuations. It is often approximated by a series of stationary, nonzero-mean Gaussian process, which is specified by the significant wave height (H_s) and peak wave period (T_p).

24. PM spectrum is a one parameter spectrum and it used for fully developed sea condition as generated by relatively moderate winds over large fetches.

25. JONSWAP spectrum is a modified form of PM spectrum and it is recommended for use in the reliability analysis. This spectrum is applicable only for limited fetch and it is used to describe the winter storm waves of the North Sea.

26. Wave spectra plot

WAVE SPECTRA (Mean wind speed=20m/s, Wave Height=5m, Time period=10s)
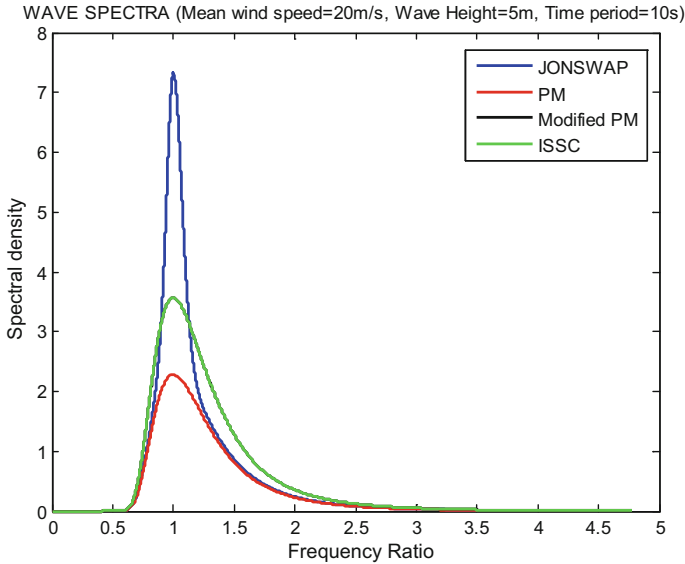
27. If the structure is compliant, the added mass forces associated with the relative acceleration between the fluid particles and the structures are included. Drag force will be computed by replacing the water particle velocity with the relative velocity term.

28. flow conditions, Keulegan–Carpenter number and Reynolds number.

29. The recommended value of drag coefficient is 0.6–1.2, while that of the inertia coefficient is 1.2–2.0, as seen in the literature (APR RP 2A).

30. As in the case of bottom-supported structures (gravity platforms), when the diameter of the member is very large, incident waves are disturbed by the presence of the structure. In such cases, viscous force becomes less significant due to the smaller values of the ratio of wave height to member diameter ($H/D \ll 1$). In such cases, the above equations cannot be applied; it is recommended that the analyzer should use numerical methods to determine the forces on the members.

31. Offshore structures have large plane area. Larger topside is required for accommodating the equipment layout as discussed in the previous chapter. As the deck will be supported on a few column members in order to reduce the interference of the waves by the presence of column members, their spacing plays an important role. For a large spacing of c/c distance of column members, there can be cancelation of forces.

32. Phase angle (θ) is given by the following relationship:

$$\theta = \frac{2\pi\Delta x}{\lambda}$$

Phase angle = 0.89π. Hence there is no cancelation effect.

33. For a small structure, Morison equation is valid because the flow structure is complex. However, for large structures (relative to the wavelength) the flow remains essentially attached to the surface. It is therefore easier to compute this pressure field. If the computation of the scattered wave potential is waived and its effect is incorporated by a force coefficient, then this force is called the *Froude-Krylov* force. Thus, the calculation of the force is performed assuming that the structure does not distort the wave field in its vicinity.

34. Current decreases slowly with the increase in depth, but even a small magnitude of current velocity can cause significant drag force. The opposing current will increase the force on the member and the superposed current will decrease the total force. The effect of current on the variation of total force with respect to phase angle is shown in the figure.

35. The presence of current is alternatively accounted by increasing the wave height to 10–15% and neglect the presence of current per second.

36. Influence of phase angle.
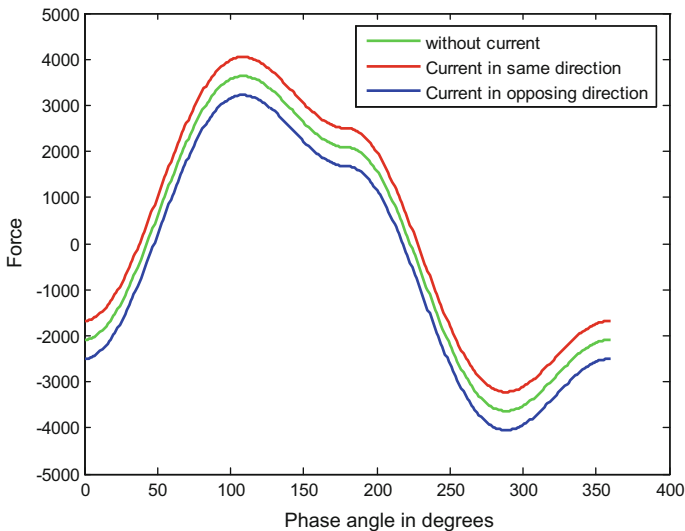
37. Offshore platforms which do not have stiff connection with the seabed are indirectly influenced by earthquakes; those which are bottom-supported are affected by earthquakes directly. Compliant structures that are position-restrained by tethers will be subjected to dynamic tether tension variations under the presence of earthquake forces. This will give rise to the

dynamic tether tension variations, which in turn shall affect the response of the platform under lateral loads.

38. Earthquake acceleration exhibits random characteristics due to (i) the nature of the mechanism causing earthquakes; (ii) wave propagation; (iii) reflection; and (iv) deflection.

39. In case of the analysis of compliant structures like TLPs, earthquake forces are handled in an indirect manner. Water waves generated due to the ground motion are neglected. Stiffness of TLP tether is modeled as axial tension members; slackening of tethers is neglected. The dynamic tether tension variation, caused by the horizontal motion of the earthquakes, is used to update the stiffness matrix of the TLP using the following equation (Chandrasekaran and Gaurav 2008):

$$\Delta T = \frac{AE}{\ell}\left[x(t) - x_{\mathrm{g}}(t)\right]$$

40. The spectrum plot shows the variation.
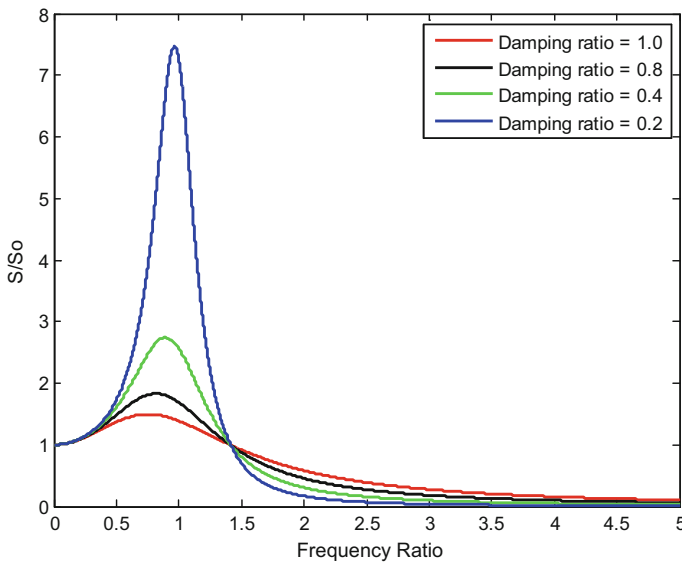
41. Level ice, broken ice, ice ridges, and icebergs.

42. Creep, cracking, buckling, spalling, and crushing.

43. (i) Total or global loads and (ii) local loads or pressure. Global loads affect the overall motion and stability of the platform, while local loads affect the members at connections.

44. Studies show that ice loads in a conical structure are lesser than that of the cylindrical structure. This is because a well-designed cone shape can change the ice-failure mode from crushing to bending.
45. The design ice loads use varying factors for level ice, first-year ridge ice and multi-year ridge ice; the factored values are 2, 5, and 7, respectively.
46. Experimental studies use scaling laws to determine the ice loads and ice–structure interaction. This method claims many advantages due to the capability of testing many types of structural shapes in large testing facilities. However, such tests are expensive apart from a strong disagreement of the model ice not being accurately scaled as of the sea ice. As the ice failure is dependent on the geometric shape significantly, ice-failure behavior cannot be accurately studied. This may result in over-prediction of ice loads.
47. Marine growth or bio-fouling is the ubiquitous attachments of soft and hard bio-particles on the surface of a submerged structure. It ranges from seaweeds to hard-shelled barnacles. Its growth on the surface of the structure increases its diameter and affects its roughness. Its main effect is to increase the wave forces on the members by increasing not only exposed areas and volumes, but also the drag coefficient due to higher surface roughness. In addition, it increases the unit mass of the member, resulting in higher gravity loads and in lower member frequencies.
48. It is accounted for in the design through appropriate increases in the diameters and masses of the submerged members.
49. Added mass depends on the submerged volume of the platform, which also varies with respect to period of vibration. This is due to the variation in buoyancy, which in turn changes the tether tension variation that affects the natural frequency of motion.
50. It is also important to establish the fact that a desired proportion between center of buoyancy and center of mass is maintained to ensure stability under free-floating conditions. This is important to enable smooth construction process in case of floating.
51. 1. Structural damping
    2. Hydrodynamic damping: Radiation and viscous damping.
52. Damping ratio for offshore structures (wet structures), including the effects of added mass, can be expressed as a ratio of that of the dry structures, as given below

$$\xi_{\text{wet}} = \xi_{\text{wet}} \frac{(m^*_{\text{dry}})(\omega^*_{\text{dry}})}{(m^*_{\text{wet}})(\omega^*_{\text{wet}})}$$

where m^*, ω^* are generalized mass and frequency, respectively.
53. Dead load is the weight of the overall platform in air, which includes piling, superstructure, jacket, stiffeners, piping, conductors, corrosion anodes, deck, railing, grout and other appurtenances.

54. Live loads are generally designated as factor times of the applied static load. These factors are assigned by the designer depending on the type of platform.

55. Design methodology of offshore platforms differs with different types of offshore structures. For example, vertical deformation will be lesser in case of bottom-supported structures like jacket platform, GBS, etc. Such platforms are highly rigid and tend to attract more forces. Hence the design criteria should be to limit the stresses in the members. Displacement of the members under the applied loads will be insignificant. On the contrary, compliant structures are more flexible, as they all displaced more under wave action. They also create more disturbances in the waves. Hence the design criteria will be to control displacement instead of limiting the stresses in the members.

56. In bottom-supported structures, design criteria should be to limit the stresses in the member. In compliant platforms, the design criteria will be to control displacement.

57. Preferred orientation is that members are oriented to have less projected area to the encountered wave direction. This induces lesser response on the members. Predominant wave direction for the chosen site is made available to the designer based on which the platform orientation is decided.

58. Following are the list of data required for the design of offshore structures:

   • Land topographical survey of sufficient area covering the chosen site for platform installation.
   • Hydrographical survey of the proposed location (hydrographic charts are used for this purpose).
   • Information regarding silting at the site.
   • Wind rose diagram showing information on wind velocities, duration, predominant direction round the year.
   • Cyclonic tracking data showing details of the past cyclonic storm such that wind velocities, direction, peak velocity period, etc., are indicated.
   • Oceanographic data including general tide data, tide table, wave data, local current, seabed characteristics, temperature, rainfall, and humidity.
   • Seismicity level and values of acceleration.
   • Structural data of existing similar structures, preferably in the close vicinity.
   • Soil investigation report.

59. The verification of an element consists of comparing its characteristic resistance(s) to a design force or stress. It includes (i) a strength check where the characteristic resistance is related to the yield strength of the element; and (ii) a stability check for elements in compression where the characteristic resistance relates to the buckling limit of the element. An element (member or plate) is checked at typical sections (at least both ends and mid span) against resistance and buckling. This verification also includes the effect of water pressure for deep-water structures.

60. Ultimate limit state (ULS), which corresponds to an ultimate event considering the structural resistance with appropriate reserve

- Fatigue limit state (FLS), which relates to the possibility of failure under cyclic loading.
- Progressive collapses limit state (PLS), which reflects the ability of the structure to resist collapse under accidental or abnormal conditions.
- Service limit state (SLS), which corresponds to the criteria for normal use or durability (often specified by the plant operator).

61. 1. Calculate the vertical resultant (dead weight, live loads, and buoyancy), the overall shear and the overturning moment (environmental forces) at the mud line.
    2. Assuming that the jacket behaves as a rigid body, derive the maximum axial and shear force at the top of the pile.
    3. Select a pile diameter in accordance with the expected leg diameter and the capacity of pile-driving equipment.
    4. Derive the penetration from the shaft friction and tip bearing diagrams.
    5. Assuming an equivalent soil sub grade modulus and full fixity at the base of the jacket, calculate the maximum moment in the pile and derive its wall thickness.

62. Adapt the diameter of the leg to that of the pile, determine the effective length from the degree of fixity of the leg into the deck (depending upon the height of the cellar deck) and calculate the moment caused by wind loads on topsides and derive the appropriate thickness.

63. Select the diameter in order to obtain a span/diameter ratio between 30 and 40, calculate the axial force in the brace from the overall shear and the local bending caused by the wave assuming partial or total end restraint and derive the thickness such that the diameter/thickness ratio lies between 20 and 70 and eliminate any hydrostatic buckle tendency.

64. These loads are temporary and arise during fabrication and installation of the platform or its components. During fabrication, various structural components generate lifting forces, while in the installation phase forces are generated during platform load-out, transportation to the site, launching and upending, as well as during lifts related to installation.

65. All members and connections of a lifted component must be designed for the forces resulting from static equilibrium of the lifted weight and the sling tensions.

66. The lifting derrick or the structure to be lifted is on a floating vessel, then dynamic load factors should be applied to the static lifting forces. A factor of 2 is applied for members and connections and 1.35 for all other secondary members.

67. These are forces generated when the jacket is loaded from the fabrication yard onto the barge.

68. If the load-out is carried out by direct lift, then, unless the lifting arrangement is different from that to be used for installation, lifting forces need not be computed. This is because lifting in the open sea creates a more severe loading condition, which requires higher dynamic load factors. If load-out is done by

skidding the structure onto the barge, a number of static loading conditions must be considered, with the jacket supported on its side. Such loading conditions arise from the different positions of the jacket during the load-out phases.

69. In order to minimize the associated risks and secure safe transport from the fabrication yard to the platform site, it is important to plan the operation carefully by considering the following (API-RP2A):

   - Previous experience along the tow route
   - Exposure time and reliability of predicted "weather windows"
   - Accessibility of safe havens
   - Seasonal weather system
   - Appropriate return period for determining design wind, wave and current conditions, taking into account the characteristics of the tow such as size, structure, sensitivity, and cost.

70. It causes wave slamming forces.
71. Transporting, launching, floating, upending, straight position, pile-driving, and deck mating.
72. These forces are generated during the launch of a jacket from the barge into the sea and during the subsequent upending into its proper vertical position to rest on the seabed.
73. Five stages in a launch-upending operation are (i) jacket slides along the skid beams; (ii) jacket rotates on the rocker arms; (iii) jacket rotates and slides simultaneously; (iv) detaches completely and comes to its floating equilibrium position; and (v) jacket is upended by a combination of controlled flooding and simultaneous lifting by a derrick barge.
74. Both the static and dynamic loads for each stage of the above under the action of wind, waves, and current need to be included in the analysis.
75. As the jacket slides, its weight is supported on the two legs that are part of the launch trusses. The support length keeps decreasing and reaches a minimum, equal to the length of the rocker beams, when rotation starts. It is generally at this instant that the most severe launching forces develop as reactions to the weight of the jacket.

Chapter 3
Introduction to Structural Dynamics

Abstract This chapter deals with introduction to structural dynamics and its application to offshore structures. Basics of single-degree of freedom are discussed to highlight the conventional mathematical model of single-degree of freedom. Free vibration analysis and forced vibration analysis are discussed with focus on few important dynamic characteristics of the single and multi-degrees of freedom models. Solved numerical examples of determining natural frequencies and mode shapes of different mathematical model of single and multi-degrees of freedom systems are included.

Keywords Single-degree of freedom · Multi-degrees of freedom · Undamped free vibration · Damped free vibration · Forced vibration · Structural damping · Half-power method · Influence coefficient method · Dunkerley method · Stodola method · Mode superposition · Static correction · Missing mass correction

3.1 Introduction

For understanding the advantages of the offshore structural forms and action, it is necessary to convert the structure into simple basic mathematical models for dynamic analysis. However, it is important to note that complexities arising from the mechanical and process equipment that forms a major part of topside activity of offshore structures pose serious limitation to such idealized mathematical models considered for dynamic analysis.

Dynamic loads are defined as time-varying loads whose magnitude, direction of application, or position varies continuously with time. As repose to these applied loads, response of the structure also varies with respect to time. Basic approaches to evaluate the response of structures to such dynamic loads are (i) deterministic and (ii) nondeterministic. In *deterministic approach*, in which the time history of the loading is fully known with the highly varying and irregular load magnitude, loading can be classified as prescribed dynamic loading. In *nondeterministic approach*, in which the time history of the loading is not completely known but can be defined in

statistical sense, the loading is termed as random dynamic loading. Deterministic analyses lead to displacement time history corresponding to the given (completely known) load time history. Other aspects like stress, strain, and internal forces are derived from the established displacement patterns. In case of nondeterministic analyses, results obtained will provide statistical information of the displacement pattern under the action of a statistically defined loading (random loads). Other aspects like stress, strain, and internal forces like bending moment and shear must be computed directly by similar independent nondeterministic analyses rather than from deriving them from the displacement results as in the earlier case. In dynamic analysis, deterministic loads are classified into periodic and non-periodic loading. Periodic loading repeats after same interval of time, while non-periodic loadings vary from short duration impulse loads to long duration loadings. Essential characteristics of dynamic loading are their time-varying nature and presence of inertia force. Inertia force is the force, which resists acceleration, which is the most essential characteristic of dynamic analysis as they represent a significant portion of the total load. As the applied load is time-varying, dynamic analysis is never a single solution like static analysis and the response is then evaluated.

3.2   Glossary

All bodies having mass and elasticity are capable of vibration. Mass is an inherent property of a body, and elasticity causes relative motion of the parts. Due to an external force, the body is vibrated, and the internal inherent forces in the form of elastic energy are developed, and this tries to bring back the structure to its original position. At equilibrium, the total energy is converted to kinetic energy, and then the body continues to move in the opposite direction. Then kinetic energy is converted into strain or elastic energy due to which the body returns to its equilibrium position. By this way, the vibratory motion is repeated indefinitely with the exchange of energy. Thus, any motion, which repeats itself after an interval of time, is called *vibration.* The major factors that cause vibration are the unbalanced centrifugal force in the system, elastic property of the system and external excitation.

Before getting into the subject, it is necessary to understand some terminologies. A motion, which repeats itself after an equal interval of time, is called *periodic motion.* The time taken to complete one cycle is called the *period*, and the number of cycles per unit time is called *frequency. Free vibration is* caused due to initial displacement in the absence of any external force, and their frequency is called *natural frequency*. The mode, which has the lowest natural frequency is called the *fundamental mode of vibration.* When the frequency of the external vibration matches with that of the natural frequency of the vibrating body, amplitude of vibration becomes excessively large; this is known as resonance. *Degree of freedom* is defined as the number of independent displacement components of a structural system that are necessary at any given time to represent the effect of all significant

inertia forces present in the system. Systems with infinite number of degrees of freedom, are called *continuous systems*, and those with finite number of degrees of freedom are called *discrete* or *lumped mass systems*.

3.3 Mathematical Model of Structural System

Idealization of offshore structures to simple mathematical models is the most essential part of dynamic analysis. Generally, analysis is carried out by not considering the serious limitations and complexities arising from the topside equipment (and their dynamic loads). More accurate analysis, incorporating the required details of dynamic response behavior of machineries (under static condition and under operation) shall be carried out to understand the platform behavior in more detail; this is beyond the scope of this chapter. Structural idealizations originate from defining the degrees of freedom for the idealized mathematical model. Inertia forces are mass proportional, and an approximate method of understanding degree of freedom shall be oriented toward the number of locations where the mass is assumed to be concentrated. Figure 3.1 shows an idealized mathematical model of single-degree of freedom (SDOF) system. As the mass is lumped at one point and contained to move in only direction (marked by an arrow direction), the shown model is an idealized case of single-degree of freedom system. Basic and essential characteristics of the single-degree of freedom system are namely: (i) mass element [*m*] representing the inertial characteristics of the system; (ii) spring element represented by stiffness [*k*] that identifies the presence of elastic restoring force and potential energy of the system; (iii) damping element [*c*] or dashpot representing frictional characteristics of energy loss or dissipation of energy in the system; and (iv) an excitation force [*f(t)*] representing the external force acting on the system. Energy is stored by the mass in the form of kinetic energy $\left(\frac{1}{2}m\ddot{x}^2\right)$, in spring in the form of potential energy $\left(\frac{1}{2}kx^2\right)$. Dissipation energy will always act in the opposite direction.

In the idealized SDOF system, it is not necessary that all the four parameters need to be present. The most important are the mass element and spring element; inertial force is characterized by mass element, which is one of the most important features of dynamic analysis, and restoration to the mean position of the vibrating mass under any given external/internal action of forces is characterized by spring element. A system can be termed as undamped system if damping element is not

Fig. 3.1 Single-degree of freedom model
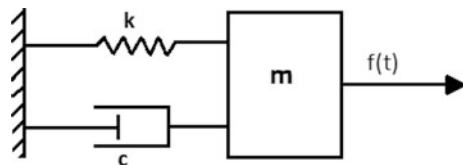
present, and if the system is not excited by external force, it is called as free vibration. As the system is constrained so that it can vibrate only in one direction, it is termed as single-degree of freedom model.

3.4   Single-Degree of Freedom Model

The simplest vibratory system can be described by a single mass connected to a spring (and possibly a dashpot). The mass is allowed to displace only along the direction of spring elongation. Restoration will be attained by the spring force of stiffness (k) applied opposite to that of the external force. Figure 3.2 shows the free body diagram of the single-degree of freedom under external force $f(t)$. Forces acting on the body under the free state are namely: (i) external force $f(t)$ acting to the right as shown; (ii) internal restoration force offered by the spring acting in the direction opposite to that of the applied external force; and (iii) damping force offered by the dashpot acting in the direction opposite to that of the external force. Equilibrium of these set of forces can be arrived by employing Newton's second law of motion. Using appropriate sign conventions for the force directions and by equating the net force to the inertial force, we get a second-order, nonhomogeneous ordinary differential equation as given below:

$$m\ddot{x} + c\dot{x} + kx = f(t) \tag{3.1}$$

With the initial conditions as $x(t = 0) = x_0$ and $\dot{x}(t = 0) = \dot{x}_0$, the above equation can be solved.

3.5   Equation of Motion

Equations of motion are equations that describe the behavior of a physical system in terms of its motion as a function of time. The equation of motion can be obtained by the employing various methods namely: (i) Simple harmonic motion method; (ii) Newton's method; (iii) Energy method; (iv) Rayleigh's method; and (v) D'Alembert's principle. Consider the spring–mass system of simple pendulum, which is constrained to move in the rectilinear manner along the axis of the spring. Springs of stiffness (k), which is fixed at one end carries a mass (m) at its free end.

Fig. 3.2 Free body diagram of single-degree of freedom model
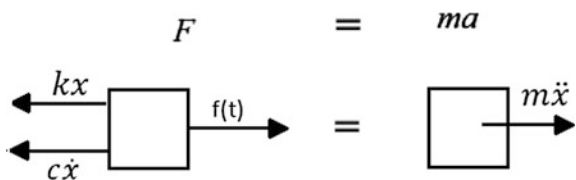
The body is displaced from its equilibrium position vertically downwards. The equilibrium position is called static equilibrium. In equilibrium position, the gravitational pull W is balanced by the force in the spring such that $mg = W = k\delta$.

3.5.1 Simple Harmonic Motion Method (SHM Method)

The equation of motion using the SHM method involves three important considerations: (i) acceleration will be always proportional to its displacement or the particle/body measured along the path; (ii) the body will always be directed toward the equilibrium position (fixed point); (iii) direction is opposite always toward its motion.

$$\ddot{x} \infty -(x)$$

$$\ddot{x} = -kx$$

where k is the proportionality constant. Hence, equation reduces to the form:

$$\ddot{x} + kx = 0$$

3.5.2 Newton's Law

The equation of motion using the Newton's law of motion is derived by equating the forces.
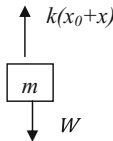
$$W - k(x_0 + x) = m\ddot{x}$$

$$W = k(x_0)$$

$$m\ddot{x} + k(x) = 0$$

3.5.3 Energy Method

In a conservative system, the total sum of the energy is constant. In the vibratory system, the energy is partly potential and partly constant. The kinetic energy is a function of the velocity, and the potential energy is a function of displacement.

$$\text{K.E.} = \frac{1}{2}m\dot{x}^2$$

$$\text{P.E.} = \frac{1}{2}kx^2$$

$$\frac{d}{dt}\left(\frac{1}{2}m\dot{x}^2 + \frac{1}{2}kx^2\right) = 0$$

$$\dot{x}[m\ddot{x} + kx] = 0$$

$$m\ddot{x} + kx = 0$$

3.5.4 Rayleigh Method

It is assumed that maximum kinetic energy at the mean position is equal to the maximum potential energy at the extreme position. If the motion is assumed to be simple harmonic, then

$$x = A\ \sin \omega_n t$$

where x = displacement of the body from mean position to the extreme position.

$$\dot{x} = \omega_n A\ \cos \omega_n t$$

Maximum velocity at mean position

$$\dot{x} = A\omega_n$$

So, maximum kinetic energy at the mean position $= \frac{1}{2}m\dot{x}^2 = \frac{1}{2}m\omega_n^2 A^2$.
Maximum Potential energy at the extreme position $= \frac{1}{2}kA^2$.

$$\frac{1}{2}m\omega_n^2 A^2 = \frac{1}{2}kA^2$$

$$\omega_n = \sqrt{\frac{k}{m}}$$

These methods are widely used for the determination of the natural frequency of the system.

3.5.5 D'Alembert's Principle

D'Alembert's principle states that if the resultant force acting on the body along with the inertia force is zero, then the body will remain in the equilibrium. In this approach, the dynamic problem is converted into a static problem. This methodology cannot be applied to the multi-degree problem without proper understanding of the constraints.

$$F + F_i = 0$$

where F is the resultant force acting on the system and F_i is the inertial force. It is important to note that inertial force and accelerating force are equal in magnitude but opposite in direction. The inertial force is an external force acting on the body. Mathematically, the equation of motion for the spring–mass system in vertical position can be written as

$$m\ddot{x} + kx = 0$$

3.6 Undamped Free Vibration

In the absence of external force $f(t)$, the vibratory motion set in the body shall be termed as free vibration. One may wonder how the body will vibrate in the absence of any external force; it is the initial displacement given to the body makes it to vibrate. Vibratory motion will be set also due to the presence of elastic restoring force (kx) that continuously attempts to bring the vibrating mass to original position. Such vibration induced by the initial displacement and not by the external force is termed as free vibration. The whole action of restoration may also be influenced by the presence of dashpot in the system. As explained earlier, there is no necessity of the presence of dashpot in an idealized mathematical model of single-degree of freedom system. In the absence of such damping force, the induced vibration is called undamped vibration. In the present case of undamped free vibration, there is no loss of energy due to friction or resistance to this motion in any other form. In simple terms, if there is no external force applied on the system making the statement $\{f(t) = 0\}$ true; therefore the system will experience free vibration. Motion of the system will be established by an initial disturbance (i.e., initial conditions). Furthermore, if there is no resistance or damping in the system making $C = 0$, the oscillatory motion will continue forever with constant amplitude. Such a system is shown in Fig. 3.3.
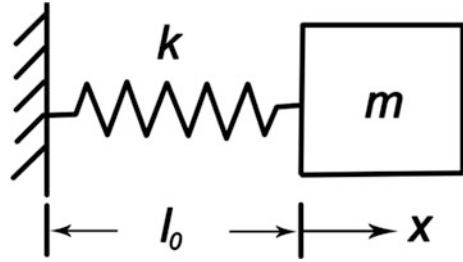
Based on the free body diagram explained earlier, equation of motion for undamped free system can be written as

$$m\ddot{x} + kx = 0 \tag{3.2}$$

Dividing by mass throughout, we get the following form:

$$\ddot{x} + \frac{k}{m} = 0$$

$$\ddot{x} + \omega^2 = 0$$

where $\omega^2 = \frac{k}{m}$.

For the second-order differential equation as shown above, auxiliary equation is given as

$$D^2 + \omega^2 = 0$$

$$D = \pm i\omega$$

Complimentary function is given by

$$x(t) = C_1 \cos \omega t + C_2 \sin \omega t \tag{3.3}$$

Using the initial condition as explained earlier, the above equation reduces to the following form:

$$x(t) = x_0 \cos \omega t + \frac{\dot{x}_0}{\omega} \sin \omega t \tag{3.4}$$

where x_0 and $\dot{x}_0$ are initial displacements and velocities, respectively, and ω_n is the natural frequency of the said vibrating motion. It can be easily seen that the natural frequency is dependent on the mass of the system and spring constant or restoring force coefficient of the system; it is independent of the said initial displacement given to preset the vibrating motion to the body.

3.7 Damped Free Vibration

While discussing the above case of free vibration of single-degree of freedom model, one may wonder about the duration of such vibration being setup by the given initial displacement. The duration of such vibration is hypothetically infinite, as no external (or) internal agency is responsible to control such induced vibration. However, in practice, one can notice that such vibrations do not extend for infinite time duration; the reason is that some external agency is responsible to stop such vibration. Hence, it is now necessary to update our existing mathematical model to include this factor in the analysis. In case of any external force being responsible for controlling the vibration, air will offer resistance to such motion. In case of offshore structures, waves contribute significantly toward this action, and hence damping should be included in the revised model. However, one may still consider the analysis under the absence of any external force $f(t)$. Hence, free vibration (no external force) of a single-degree of freedom system with damping is shown in Fig. 3.4. Damping force is commonly considered proportional to the magnitude of velocity of motion of the body, which shall be applied in the direction opposite to the direction of external force $f(t)$. This is termed as viscous damping. Alternatively, resistance to vibratory motion may also arise from friction between the following surfaces: (i) the plane on which the body is moving and (ii) the plane of the body itself that is in motion. Such forces arising purely from frictional resistance are termed as coulomb damping. In this case, damping force depends on the coefficient of friction between the two surfaces and remains independent of the velocity of motion of the body. It is customary practice to assume viscous damping in dynamic analysis of offshore structures. Damping that produces a damping force proportional to the mass's velocity is commonly referred to as "viscous damping", and is denoted graphically by a dashpot. Reasons for not considering coulomb damping are explained in the later part through a numerical example.

Damping is the resistance offered by a body to the motion of a vibratory system. The resistance may be applied by a liquid or solid internally or externally. If the value of the damping is small in the mechanical system, then it will have very less influence on natural frequency. The main advantage of providing damping in mechanical systems is just to control the amplitude of vibration so that the failure occurring because of resonance may be avoided.

Fig. 3.4 Damped free vibration of single-degree of freedom model
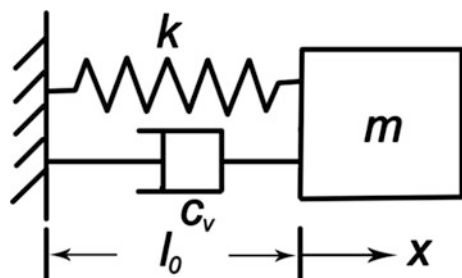
3.7.1   Viscous Damping

When the system is allowed to vibrate in a viscous medium, the damping is called viscous. Viscosity is the property of the fluid by virtue of which it offers a resistance to the motion of one layer over the adjacent one. When two plates are separated by fluid film of thickness t and the upper plate is allowed to move parallel to the fixed plate with a velocity $\dot{x}$, then the net force F required for maintaining the velocity $\dot{x}$ of the plate is expressed as

$$F = \frac{\mu A}{t}\dot{x}$$

where A is the area of plate, t is thickness of the fluid film and μ is coefficient of absolute viscosity of the film. The force can also be written as:

$$F = c\dot{x}$$

$$c = \frac{\mu A}{t}$$

where c is viscous damping coefficient.

3.7.2   Coulomb Damping

Coulomb damping results from the sliding of two dry surfaces. Displacement of a system in coulomb damping is shown in Fig. 3.5. Damping force is equal to the product of the normal force and the coefficient of friction μ and is assumed to be independent of the velocity once the motion is initiated. Because the sign of the damping force is always opposite to that of the velocity, the differential equation of motion for each sign is valid only for half-cycle intervals.

Fig. 3.5 Displacement of a system in coulomb damping
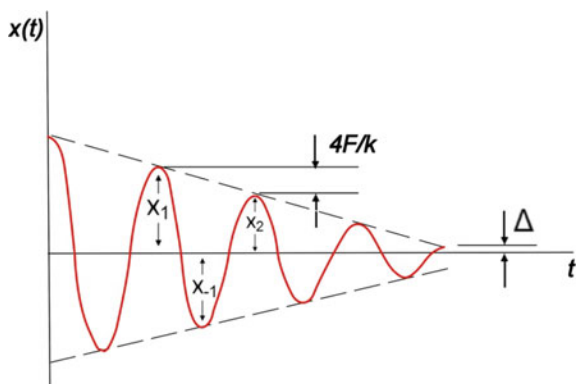
To determine the decay of amplitude, we resort to the work-energy principle of equating the work done to the change in kinetic energy. By choosing a half-cycle starting at the extreme position with velocity equal to zero and the amplitude equal to X_1, the change in the kinetic energy is zero and the work done on m is also zero.

$$\frac{1}{2}k\left(X_1^2 - X_{-1}^2\right) - F_d(X_1 + X_{-1}) = 0$$

or

$$\frac{1}{2}k(X_1 - X_{-1}) = F_d$$

where (X_{-1}) is the amplitude after the half-cycle, as shown in Fig. 3.5. By repeating this procedure for the next half-cycle, a further decrease in amplitude of $2F_d/k$ will be found, so that the decay in amplitude per cycle is a constant and is given by

$$X_1 - X_2 = \frac{4F_d}{k}$$

The motion will cease when the amplitude becomes less than Δ; at this position, spring force is insufficient to overcome the static friction force, which is generally greater than the kinetic friction force. It can also be shown that the frequency of oscillation is the same as that of the undamped system. Amplitude of the coulomb damping system decays linearly with time. For damped free vibration of single-degree of freedom system, equation of motion is given by

$$m\ddot{x} + c\dot{x} + kx = 0 \tag{3.5}$$

This is a second-order, homogeneous, ordinary differential equation (ODE). If all parameters (mass, spring stiffness and viscous damping) are constants, then the equation becomes linear with constant coefficients that can be solved by a simple characteristic equation method. The characteristic equation for this problem is given by

$$ms^2 + cs + k = 0 \tag{3.6}$$

This determines two independent roots that fall into one of the following three cases:

1. If $c^2 - 4mk < 0$, the system is termed under-damped. The roots of the characteristic equation are complex conjugates, corresponding to oscillatory motion with an exponential decay in amplitude.
2. If $c^2 - 4mk = 0$, the system is termed critically damped. The roots of the characteristic equation are repeated, corresponding to simple decaying motion with at most one overshoot of the system's resting position.

3. If $c^2 - 4mk > 0$, the system is termed over-damped. The roots of the characteristic equation are purely real and distinct, corresponding to simple exponentially decaying motion.

To simplify the solutions coming up, we define the critical damping C_c, the damping ratio ξ, and the damped vibration frequency ω_d as follows:

$$C_c = 2m\sqrt{k/m} = 2m\omega_n$$

$$\xi = c/C_c$$

$$\omega_d = \sqrt{1 - \xi^2}\,\omega_n$$

where ω_d is termed damped vibration frequency. This will be the same as the natural frequency for an undamped system. Solution in time domain is discussed below for each of the three cases.

3.7.3   Under-Damped Systems

When $c^2 - 4mk < 0$ (equivalent to $\xi < 1$ or $c < C_c$), the characteristic equation has a pair of complex conjugate roots. The displacement solution for this kind of system is given by

$$x(t) = e^{-\xi\omega_n t}[A\cos(\omega_d t) + B\sin(\omega_d t)] \tag{3.7}$$

With the initial conditions as $x(t = 0) = x(0)$ and $\dot{x}(t = 0) = \dot{x}$, Eq. (3.7) becomes

$$x(t) = e^{-\xi\omega_n t}\left[x_0\cos(\omega_d t) + \frac{\dot{x}_0 + \xi\omega_n x_0}{\omega_d}\sin(\omega_d t)\right] \tag{3.8}$$

The displacement plot of an under-damped system is shown in Fig. 3.6.

The damping ratio ξ can be experimentally determined from the free response by the logarithmic decrement method. To illustrate this approach, note from Eq. (3.8) that the period of damped oscillations is given by

$$T = \frac{2\pi}{\omega_d}$$
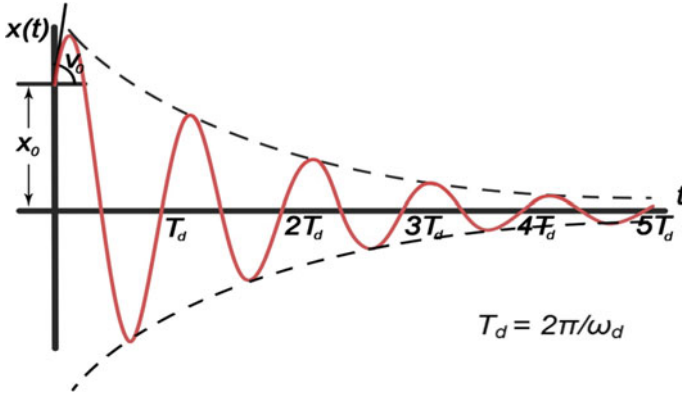
Fig. 3.6 Response of under-damped system

Evaluate Eq. (3.8) at $t = 0$ and $t = \frac{2\pi}{\omega_d}$

$$\text{At } t = 0, \quad x(t) = x_1 = x_0 \tag{3.9}$$

$$\text{At } t = \frac{2\pi}{\omega_d}, \quad x(t) = x_2 = e^{-\xi\omega_n\frac{2\pi}{\omega_d}}x_0 \tag{3.10}$$

x_1 and x_2 are the two consecutive positive peaks of the response. Dividing Eq. (3.9) by (3.10), we get the following form:

$$\frac{x_1}{x_2} = e^{-\xi\omega_n\frac{2\pi}{\omega_d}} = e^{\frac{2\pi\xi}{\sqrt{1-\xi^2}}}$$

$$\ln\frac{x_1}{x_2} = \frac{2\pi\xi}{\sqrt{1-\xi^2}} \tag{3.11}$$

Equation (3.11) is called logarithmic decrement and is denoted by δ.

$$\delta = \ln\frac{x_1}{x_2} = \frac{2\pi\xi}{\sqrt{1-\xi^2}} \tag{3.12}$$

Logarithmic decrement is also given by the following relationship:

$$\delta = \frac{1}{n}\ln\frac{x}{x_n} \tag{3.13}$$

where x is the amplitude at particular maxima and x_n represents the amplitude after further n cycles.

3.7.4 Critically Damped Systems

When $c^2 - 4mk = 0$ (equivalent to $\xi = 1$ or $c = C_c$), the characteristic equation has repeated real roots. Displacement time history is given by

$$x(t) = (A + Bt)e^{-\omega_n t} \tag{3.14}$$

Using the given initial conditions, equation reduces to the following form:

$$x(t) = e^{-\omega_n t}[x_0 + (\dot{x}_0 + \omega_n x_0)t] \tag{3.15}$$

The critical damping factor C_c can be interpreted as the minimum damping that result in non-periodic motion (i.e., simple decay). Displacement plot of a critically damped system with positive initial displacement and velocity is shown in Fig. 3.7.

3.7.5 Over-Damped Systems

When $c^2 - 4mk > 0$ (equivalent to $\xi > 1$ or $c > C_c$), the characteristic equation has two distinct real roots. Displacement time history is given by

$$x(t) = Ae^{\left[-\xi + \sqrt{\xi^2 - 1}\right]\omega_n t} + Be^{\left[-\xi - \sqrt{\xi^2 - 1}\right]\omega_n t} \tag{3.16}$$

Using the given initial conditions, equation reduces to the following form:

$$\begin{aligned}
x(t) = & \frac{x_0 \omega_n \left[\xi + \sqrt{\xi^2 - 1} + \right] + \dot{x}_0}{2\omega_n \sqrt{\xi^2 - 1}} e^{\left[-\xi + \sqrt{\xi^2 - 1}\right]\omega_n t} \\
& + \frac{-x_0 \omega_n \left[\xi - \sqrt{\xi^2 - 1} + \right] - \dot{x}_0}{2\omega_n \sqrt{\xi^2 - 1}} e^{\left[-\xi - \sqrt{\xi^2 - 1}\right]\omega_n t}
\end{aligned} \tag{3.17}$$

Fig. 3.7 Response of critically damped system
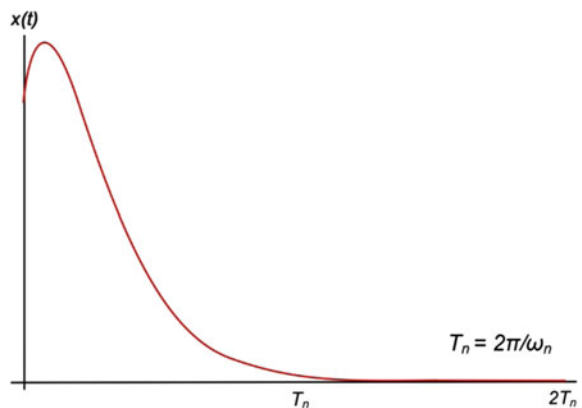
Fig. 3.8 Response of
over-damped system
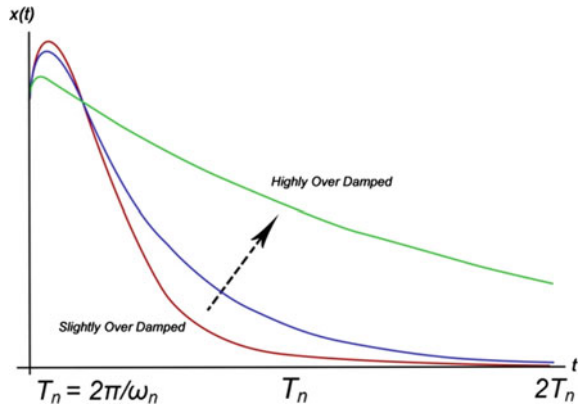
The displacement plot of an over-damped system is shown in Fig. 3.8.

The motion of an over-damped system is non-periodic, regardless of the initial conditions; larger the damping, longer the time to decay from an initial disturbance. If the system is heavily damped $\xi \gg 1$, the displacement solution takes the approximate form as given below:

$$x(t) \approx x_0 + \frac{\dot{x}_0}{2\xi\omega_n}\left(1 - e^{-2\xi\omega_n t}\right) \tag{3.18}$$

3.7.6 Half-Power Method

This is used to calculate the damping from the response of the amplitude as shown in Fig. 3.9. The first step is to locate the peak amplitude. Corresponding frequencies are notes as f_1 and f_2.

Fig. 3.9 Half power
bandwidth method
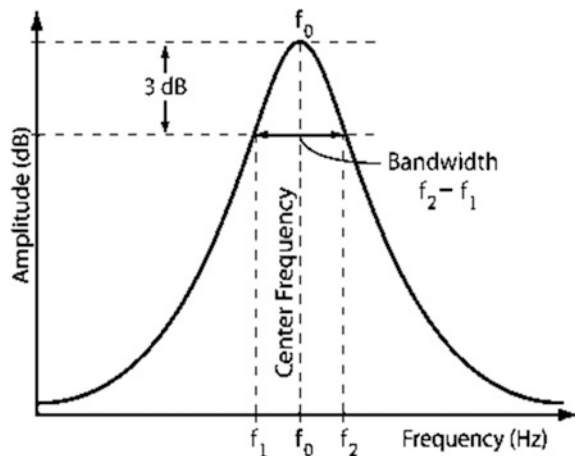
$$\frac{x_{st}}{\sqrt{\left(1-\beta^2\right)^2 + 2\beta\zeta}} = \frac{x_{st}}{\sqrt{2}\zeta} = \frac{1}{\sqrt{2}}\left(\frac{x_{st}}{2\zeta}\right)$$

Solving we get $\beta_1 = 1 - \zeta - \zeta^2$; $\beta_2 = 1 + \zeta - \zeta^2$. Simplifying and neglecting higher powers, we get $\zeta = \frac{\beta_2 - \beta_1}{2}$;

$$\zeta = \frac{1}{2}\left(\frac{\omega_2 - \omega_1}{\omega_n}\right) = \frac{1}{2}\left(\frac{f_2 - f_1}{f_n}\right)$$

The value of the ζ depends upon the quality of the graph. The area representing the energy should represent 50% of the area of the spectrum. This is used only for forced function. This is not related to degrees of freedom.

3.8 Forced Vibration

In the presence of external force $f(t)$, the resulting vibration is termed as force vibration. Such vibrations can be either undamped or damped as the case may be considered in the analysis. Examples of forced excitation include wave action on the offshore platform that is inherently and always present in the system. Equation of motion for forced vibration is given by

$$m\ddot{x} + c\dot{x} + kx = f(t) \tag{3.19}$$

Figure 3.10 shows damped single-degree of freedom system in the presence of external force $f(t)$. Subjecting the system to a harmonically varying load $f(t)$ amplitude p_o and circular frequency ω, equation of motion is given by

$$m\ddot{x} + c\dot{x} + kx = f(t) = p_o \sin \omega t \tag{3.20}$$

Response of the single-degree of freedom is further analyzed for two cases: (i) undamped and (ii) damped.

Fig. 3.10 Damped single-degree of freedom under external excitation
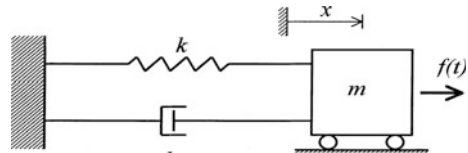
3.8.1 Undamped Forced Vibration

Equation of motion is further modified as given below:

$$m\ddot{x} + kx = f(t) = p_o \sin \omega t \tag{3.21}$$

Complete solution of the above equation contains two parts namely: (i) complementary solution and (ii) particular integral. Complementary solution to the equation is given by

$$x_c(t) = A \cos \omega t + B \sin \omega t \tag{3.22}$$

Particular solution depends on the form of dynamic loading. In case of harmonic excitation as considered in the present argument, it is simple to assume that the resulting response shall also be harmonic and in phase with the loading. Particular solution for the assumed conditions is given by

$$x_p(t) = C \sin \omega t \tag{3.23}$$

in which the amplitude C is to be evaluated. Substituting Eq. (3.23) in Eq. (3.21), we get

$$-m\omega^2 C \sin \omega t + k C \sin \omega t = p_o \sin \omega t$$

Dividing throughout by ($k \sin \omega t$) (which is nonzero in general) and $k/m = \omega^2$, we get the following form:

$$C = \frac{p_o}{k} \frac{1}{1 - \beta^2} \tag{3.24}$$

where β is defined as the ratio of frequency of the applied load to natural frequency of the system and is given by the following relationship:

$$\beta = \frac{\omega}{\omega_n}$$

Complete solution to the equation of motion is the sum of complementary solution and particular integral as given below:

$$x(t) = x_c(t) + x_p(t)$$

$$x(t) = A \cos \omega t + B \sin \omega t + \frac{p_o}{k} \frac{1}{\left[1 - \beta^2\right]} \sin \omega t \tag{3.25}$$

In the above equation, constants A and B depend on the initial conditions. For the system at rest $\{x(0) = \dot{x}(0) = 0\}$, it can be seen that

$$A = 0 \quad \text{and} \quad B = \frac{p_o}{k} \frac{\beta}{[1 - \beta^2]}$$

Substituting these in Eq. (3.25), we get

$$x(t) = \frac{p_o}{k} \frac{1}{[1 - \beta^2]} (\sin \omega t - \beta \sin \omega_n t) \tag{3.26}$$

where $p_o/k = x_{st}$ is termed as static displacement that is caused by the applied external load p_o and $1/(1 - \beta^2)$ is the magnification factor (MF) representing the amplification effect of the harmonically applied loading. Equation (3.26) contains two distinct terms:

 (i) $\sin \omega t$ term represents the response component at frequency of the applied loading which is called steady-state response
(ii) $\beta \sin \omega_n t$ represents the response component at natural frequency of vibration and is termed as transient response. This depends on the initial conditions assigned to the body and shall vanish eventually. It is interesting to note that this term will not vanish in case of hypothetical undamped system.

Therefore, in dynamic analysis, one is more interested in the steady-state response.

3.8.2   Damped Forced Vibration

Considering equation of motion including viscous damping, Eq. (3.20) is modified by dividing it by m and noting that $c/m = 2\xi\omega n$; modified form is given as below:

$$\ddot{x}(t) + 2\xi\omega n\dot{x}(t) + \omega^2 x(t) = \frac{p_0}{m} \sin \omega t \tag{3.27}$$

Complementary solution is given by

$$x_c(t) = [A \cos \omega_d t + B \sin \omega_d t] \exp(-\xi \omega nt) \tag{3.28}$$

Particular solution is of the following form:

$$x_p(t) = G1 \cos \omega t + G2 \sin \omega t \tag{3.29}$$

Equation (3.29) contains both the harmonic terms that are essential, as the response of a damped system shall not be in phase with the loading. Substituting in Eq. (3.27) and rearranging the terms, we get the following form:

$$\left[G1\omega^2 + G2\omega(2\xi\omega_n) + G1\omega_n^2\right]\cos\omega t + \left[-G2\omega^2 - G1\omega(2\xi\omega_n) + G2\omega^2 - \frac{p_0}{m}\right]\sin\omega t = 0$$

$$(3.30)$$

In order to satisfy this equation for all values of t, it is necessary that each of the two square bracket quantities equal zero; thus, it reduces to the form as given below:

$$G1(1 - \beta^2) + G2(2\xi\beta) = 0$$
$$G2(1 - \beta^2) - G1(2\xi\beta) = p_o/k$$

$$(3.31)$$

where, β is the frequency ratio. Solving these two equations simultaneously, we get:

$$G1 = \frac{p_o}{k}\left[\frac{-2\xi\beta}{\left(1 - \beta^2\right)^2 + (2\xi\beta)^2}\right]$$

$$G2 = \frac{p_o}{k}\left[\frac{1 - \beta^2}{\left(1 - \beta^2\right)^2 + (2\xi\beta)^2}\right]$$

$$(3.32)$$

Substituting the values and combining the results of complimentary solution, Eq. (3.28) reduces the following form:

$$x(t) = [A\cos\omega_d t + B\sin\omega_d t]\exp(-\xi\omega t) + \frac{p_o}{k}\left[\frac{1}{\left(1 - \beta^2\right)^2 + (2\xi\beta)^2}\right]$$

$$\left[(1 - \beta^2)\sin\omega t - (2\xi\beta)\cos\omega t\right]$$

$$(3.33)$$

First term on the right hand side of Eq. (3.33) represents transient response which damps out in accordance with $\exp(-\xi\omega_n t)$; second term represents the steady-state harmonic response, which will continue indefinitely. The constants A and B can be evaluated for any given initial conditions, $x(0)$ and $\dot{x}(0)$. As explained earlier, transient response will not be of primary inters, and therefore evaluation of constants A and B are not discussed further.

3.9   Steady-State Response

Steady-state response of equation of motion for a damped forced vibration, as presented in Eq. (3.33) is given below:

$$x_p(t) = \frac{p_o}{k} \left[\frac{1}{\left(1 - \beta^2\right)^2 + (2\xi\beta)^2} \right] \left[(1 - \beta^2) \sin\omega t - (2\xi\beta)\cos\omega t \right] \qquad (3.34)$$

This displacement can be interpreted easily by plotting two corresponding rotating vectors in the complex plane as shown in Fig. 3.11. Components along the real axis are identical to the terms of the above equation. Real component of the resultant vector gives the steady-state response in the following form:

$$x_p(t) = \rho \sin(\omega t - \theta) \qquad (3.35)$$

Amplitude of the response is given as below:

$$\rho = \frac{p_o}{k} \left[\left(1 - \beta^2\right)^2 + (2\xi\beta)^2 \right]^{-1/2} \qquad (3.36)$$

Phase angle by which the response lags behind the applied loading is given by

$$\theta = \tan^{-1} \left[\frac{2\xi\beta}{1 - \beta^2} \right] \qquad (3.37)$$

where $0 < \theta < 180°$ is the range. Ratio of the resultant harmonic response amplitude to the static displacement is termed as dynamic magnification factor and is given by

$$D = \frac{\rho}{p_o/k} \left[\left(1 - \beta^2\right)^2 + (2\xi\beta)^2 \right]^{-1/2} \qquad (3.38)$$
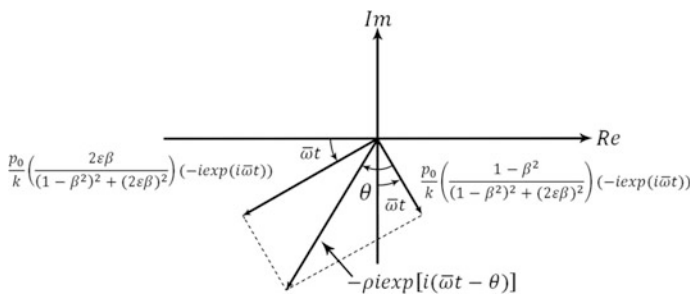
Fig. 3.11 Steady-state response of damped single-degree of freedom system

Fig. 3.12 Variation of frequency ratio with phase angle for damped vibration
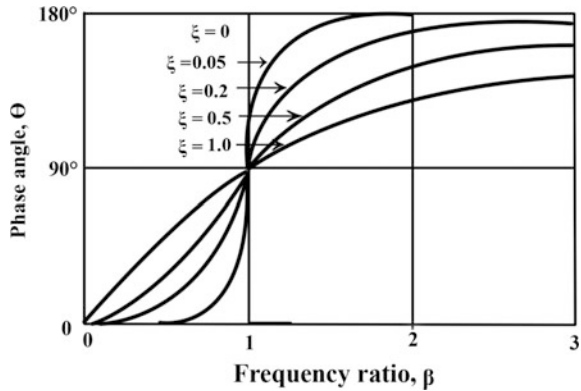
Fig. 3.13 Variation of dynamic magnification factor with frequency ratio for damped vibration
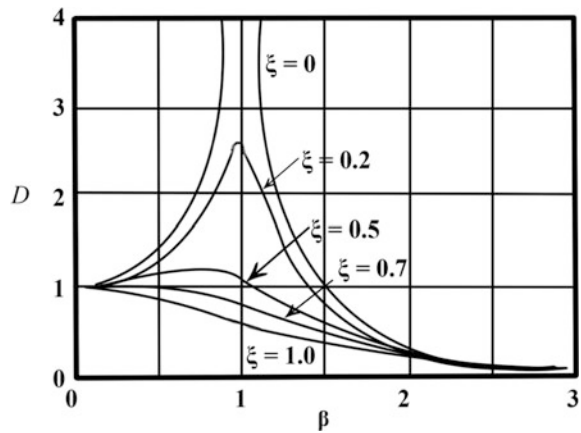
Figure 3.12 shows the variation of frequency ration with phase angle for different values of damping ratios. Figure 3.13 shows the variation of dynamic magnification factor with frequency ratio for different damping ratios.

3.10 Two-Degrees of Freedom Model

Systems that require two independent coordinates to specify their position during vibration are termed as two-degrees of freedom systems. In general, a system requiring n number of independent coordinates/parameters to specify its position is called a system with n degrees of freedom. Two-degrees of freedom system is therefore a specific case of a multi-degrees of freedom system. Number of degrees of freedom generally equals the number of discrete masses of the system, but this is not always true. Figure 3.14 shows two different forms of two-degrees of freedom models. Two masses connected by spring in series with stiffness k_1 and k_2 requires
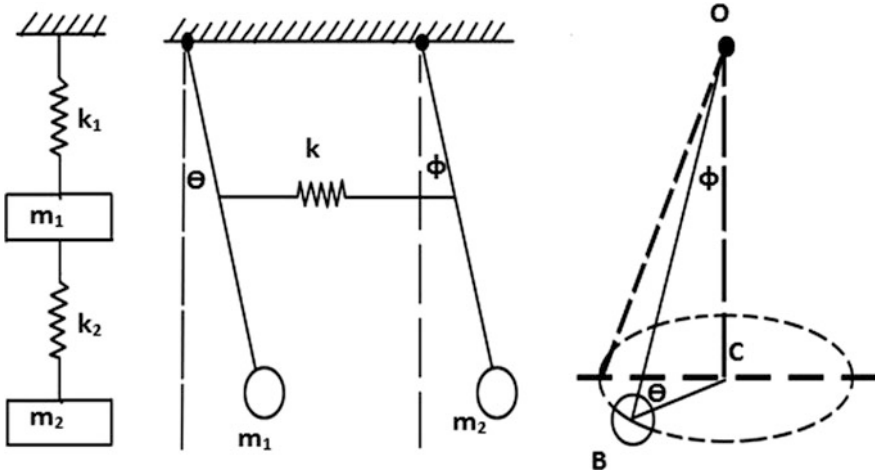
Fig. 3.14 Two-degrees of freedom system models. **a** Mass and stiffness in series; **b** two pendulums connected with a bar of stiffness k

two independent coordinates namely x_1 and x_2; the second system of two pendulums connected by a rod of known stiffness, k has two independent coordinates namely θ and Φ, respectively.

3.11   Undamped Free Vibrations and Principal Modes of Vibration

As a general rule, two-degrees of freedom system shall have two natural frequencies. Under certain condition, it is possible for both the masses to vibrate at any of these natural frequencies; this shall induce a definite relationship between the amplitudes of the two displacement coordinates. This resulting configuration is referred as principal mode of vibration; it is therefore easy to realize that a two-degrees of freedom model shall have two principal modes of vibrations. Under normal mode of vibration, both the masses pass through their respective mean equilibrium position simultaneously and reach their extreme position simultaneously as well. In case of forced harmonic excitation, resultant vibration of the masses takes place at the excitation frequency. Figure 3.15 shows a spring–mass undamped system with two degrees of freedom, x_1 and x_2, respectively. Masses are constrained to move only in the vertical direction; masses m_1 and m_2 have displacements x_1 and x_2, respectively, and are measured from their respective static equilibrium positions. Free body diagram of the system under the action of forces is also shown in Fig. 3.15.

Fig. 3.15 Spring–mass
undamped two-degrees of
freedom system
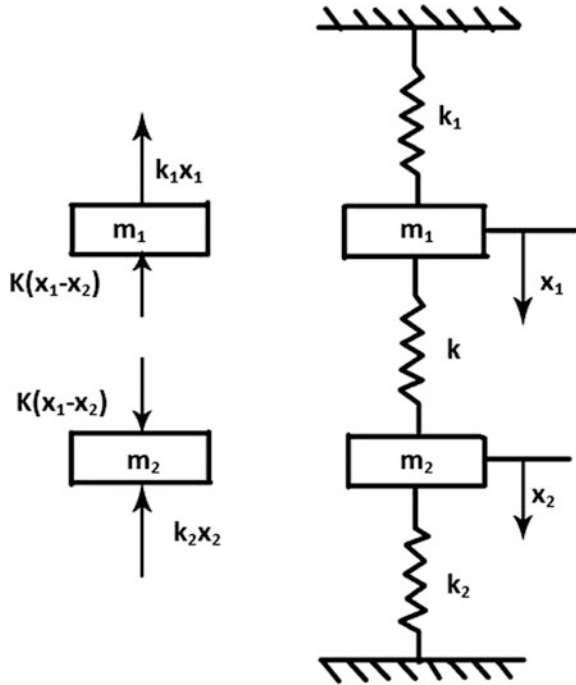
Equations of motion can be obtained by applying Newton's second law of
motion. Let the displacements and forces are measured positive when acting
downwards. Applying Newton's law to the free body diagrams of the two masses
m_1 and m_2, we get

$$m_1\ddot{x}_1 = -k_1x_1 - k(x_1 - x_2) \tag{3.39}$$

$$m_2\ddot{x}_2 = k(x_1 - x_2) - k_2x_2 \tag{3.40}$$

Rearranging and rewriting the above equations, we get

$$m_1\ddot{x}_1 + (k + k_1)x_1 - kx_2 = 0 \tag{3.41}$$

$$m_2\ddot{x}_2 + (k + k_2)x_2 - kx_1 = 0 \tag{3.42}$$

Considering that both the masses are vibrating at the same natural frequency ω
but with different amplitudes, solution of displacements is assumed as below:

$$x_1 = X_1 \sin \omega t \tag{3.43}$$

$$x_2 = X_2 \sin \omega t \tag{3.44}$$

Substituting for x_1, x_2 Eqs. (3.41) and (3.42) are rewritten as

$$-m_1 X_1 \omega^2 \sin \omega t + (k+k_1)x_1 \sin \omega t - kx_2 \sin \omega t = 0 \tag{3.45}$$

$$-m_2 X_2 \omega^2 \sin \omega t + (k+k_2)x_2 \sin \omega t - kx_1 \sin \omega t = 0 \tag{3.46}$$

Rearranging the terms in above equations, we get

$$\left\{ \left(k+k_1 - m_1\omega^2\right)X_1 - kX_2 \right\} \sin \omega t = 0 \tag{3.47}$$

$$\left\{ -kX_1 + \left(k+k_2 - m_2\omega^2\right)X_2 \right\} \sin \omega t = 0 \tag{3.48}$$

As assumed solutions involve $\sin \omega t$, the term $\sin \omega t$ cannot be equal to zero all the times. Therefore, Eqs. (3.47) and (3.48) simplify to the following:

$$\left(k+k_1 - m_1\omega^2\right)X_1 - kX_2 = 0 \tag{3.49}$$

$$-kX_1 + \left(k+k_2 - m_2\omega^2\right)X_2 = 0 \tag{3.50}$$

The above equations are homogeneous linear algebraic equations in X_1 and X_2. By carefully examining both the equations, it can be seen that two equations are connected through spring constant k, in the absence of which these equations will become independent. The spring k is, therefore, called a coupling spring. By employing Cramer's rule, these equations can be solved.

$$X_1 = \frac{\begin{vmatrix} 0 & -k \\ 0 & k+k_2 - m_2\omega^2 \end{vmatrix}}{\Delta\omega} \tag{3.51}$$

$$X_2 = \frac{\begin{vmatrix} k+k_1 - m_1\omega^2 & 0 \\ -k & 0 \end{vmatrix}}{\Delta\omega} \tag{3.52}$$

For solution other than the trivial one of $x_1 = x_2 = 0$, a necessary condition is given as

$$\Delta\omega = \begin{vmatrix} (k+k_1 - m_1\omega^2) & -k \\ -k & (k+k_2 - m_2\omega^2) \end{vmatrix} = 0 \tag{3.53}$$

The above equation is termed as characteristic equation from which the values of ω are established. Simplifying and rearranging, we get

$$m_1 m_2 \omega^4 - [(k+k_1)m_2 + (k+k_2)m_1]\omega^2 + (k+k_1)(k+k_2) - k^2 = 0 \tag{3.54}$$

Dividing by $m_1 m_2$, the above equation reduces to the following form:

$$\omega^4 - \left(\frac{k+k_1}{m_1} + \frac{k+k_2}{m_2}\right)\omega^2 + \frac{kk_1 + kk_2 + k_1 k_2}{m_1 m_2} = 0 \tag{3.55}$$

The above equation is a quadratic equation in ω^2 and can be solved for ω. Alternatively, another approach can be used to obtain the mode shapes of vibration. Mode shapes are the deflected profile of the vibrating masses indicating the relative position of the masses at any specific frequency at which mode shape is plotted. Hence, for every frequency of vibration, there exists a predefined pattern of displaced position of the mass, which is termed as mode shape. Mode shape is a graphical display of the relative amplitudes of two coordinates and their phase angle relationship. Apart from indicating the relative position of masses at any particular frequency of vibration, mode shapes also indicate the qualitative measure of the design of the system. For example, if the mode shape corresponding to the fundamental frequency show torsion, the system can be stated as unstable; in such cases, revision in the design is sought. Equations (3.49) and (3.50) can be rewritten as

$$\frac{X_1}{X_2} = \frac{k}{k+k_1 - m_1\omega^2} \tag{3.56}$$

$$\frac{X_1}{X_2} = \frac{k+k_2 - m_2\omega^2}{k} \tag{3.57}$$

Equating both, we get

$$\frac{k}{k+k_1 - m_1\omega^2} = \frac{k+k_2 - m_2\omega^2}{k} \tag{3.58}$$

$$m_1 m_2 \omega^4 - [(k+k_1)m_2 + (k+k_2)m_1]\omega^2 + (k+k_1)(k+k_2) - k^2 = 0 \tag{3.59}$$

The roots of the above quadratic equation may be written as

$$\omega^2 = \frac{1}{2}\left[\left(\frac{k+k_1}{m_1} + \frac{k+k_2}{m_2}\right) \pm \sqrt{\left(\frac{k+k_1}{m_1} + \frac{k+k_2}{m_2}\right)^2 - 4\frac{kk_1 + kk_2 + k_1 k_2}{m_1 m_2}}\right] \tag{3.60}$$

This can be further simplified as

$$\omega^2 = \frac{1}{2}\left[\left(\frac{k+k_1}{m_1} + \frac{k+k_2}{m_2}\right) \pm \sqrt{\left(\frac{k+k_1}{m_1} - \frac{k+k_2}{m_2}\right)^2 + 4\frac{k^2}{m_1 m_2}}\right] \tag{3.61}$$

It can be seen that roots of the above equation shall yield positive real values of ω. In the simplified form, above equation can be written as given below

$$\omega^2 = \frac{1}{2}\left(A \pm \sqrt{A^2 - 4B}\right) \tag{3.62}$$

Two finite positive values of the above equation, say for example, be denoted as ω_1^2 and ω_2^2. Out of the four values namely $(\pm\omega_1, \pm\omega_2)$, use of negative sign will simply change the signs of the arbitrary constants X_1 and X_2; it does not affect the solution. Lesser value of the above frequency is called fundamental frequency (or first harmonic frequency). The general solution is expressed as given below

$$x_1 = X_{11}\sin\omega_1 t + X_{12}\sin\omega_2 t \tag{3.63}$$

$$x_2 = X_{21}\sin\omega_1 t + X_{22}\sin\omega_2 t \tag{3.64}$$

where X_{11}, X_{12}, X_{21} and X_{22} are the arbitrary constants which can be determined by initial conditions. It is seen that mode shapes corresponding to each frequency indicates the relative position of mass at that corresponding frequency; it is therefore obvious that position of masses may not be the same. However, all masses can be made to vibrate at a specific frequency such that all the masses will pass their equilibrium position simultaneously and will reach their maximum displacements. Such a pattern of mode of vibration is called the principal mode of vibration. Fundamental mode of vibration is called first mode and the next successive mode is called second mode and so on. When the system vibrates in the first mode of vibration (i.e., When $\omega = \omega_1$), amplitude ratio in Eqs. (3.56) and (3.57) becomes

$$\frac{X_{11}}{X_{21}} = \frac{k}{k + k_1 - m_1\omega_1^2} = \frac{k + k_2 - m_2\omega_1^2}{k} = \frac{1}{\mu_1} \tag{3.65}$$

$$\frac{X_{12}}{X_{22}} = \frac{k}{k + k_1 - m_1\omega_2^2} = \frac{k + k_2 - m_2\omega_2^2}{k} = \frac{1}{\mu_2} \tag{3.66}$$

Constants μ_1 and μ_2 represent amplitude ratios to frequencies ω_1 and ω_2, respectively. Combining the above two expressions, we get

$$k\mu_{1,2} = k + k_1 - m\omega_{1,2}^2 \tag{3.67}$$

Substituting for $\omega_{1,2}^2$, we get

$$k\mu_{1,2} = \frac{m_1}{2}\left[\left(\frac{k + k_1}{m_1} - \frac{k + k_2}{m_2}\right) \pm \sqrt{\left(\frac{k + k_1}{m_1} - \frac{k + k_2}{m_2}\right)^2 + 4\frac{k^2}{m_1 m_2}}\right] \tag{3.68}$$

Since the quantity under the radical sign is greater than the quantity outside, the sign of expression on the right side of the above equation is decided by the sign of the quantity under the radical symbol. Hence, μ_1 and μ_2 are of opposite signs. When any of the amplitudes X_1 or X_2 in the amplitude ratio (X_1/X_2) is assumed to be unity, the mode of is called the normal mode of vibration.

3.12   Multi-degrees of Freedom

All the concepts introduced in the single and two degrees of freedom can be extended to multi-degrees of freedom systems. Equations of motion of a multi-degrees of freedom can be derived using Newton's second law of motion as described earlier. However, it is advantageous and necessary to know few more additional methods of writing equations of motion for multi-degrees of freedom. For a multi-degrees of freedom system with n degrees, there exist n natural frequencies, each associated with the corresponding mode shape. The method of determining these natural frequencies from the characteristic equation is also applicable to such systems. However, increase in the number of degrees of freedom will make the characteristic equation more complex. Thanks to the property of Orthogonality that is exhibited by mode shapes of multi-degrees of freedom system, analysis of such system is simplified.

3.12.1   *Equation of Motion for Multi-degrees of Freedom System*

Consider an undamped system shown in Fig. 3.16 having n degrees of freedom. Differential equation for each mass is written separately using Newton's second law. If $x_1, x_2, x_3, \ldots x_n$ are the displacements from the equilibrium position of the respective masses at any instant, then

$$
\begin{aligned}
m_1\,\ddot{x}_1 &= -k_1 x_1 - k_2(x_1 - x_2) \\
m_2\,\ddot{x}_2 &= k_2(x_1 - x_2) - k_3(x_2 - x_3) \\
m_3\,\ddot{x}_3 &= k_3(x_2 - x_3) - k_4(x_3 - x_4) \\
&\cdots \\
m_n\,\ddot{x}_n &= k_n(x_{n-1} - x_n)
\end{aligned}
\tag{3.69}
$$

Fig. 3.16 Undamped
multi-degrees of freedom
model
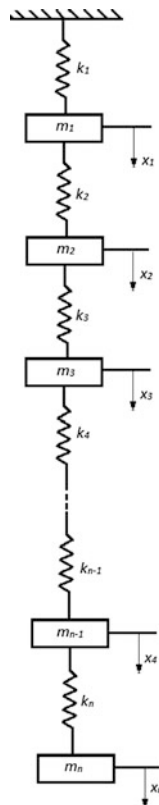
These equations can be arranged in the following forms.

$$m_1\ddot{x}_1 + k_1x_1 + k_2(x_1 - x_2) = 0$$
$$m_2\ddot{x}_2 - k_2(x_1 - x_2) + k_3(x_2 - x_3) = 0$$
$$m_3\ddot{x}_3 - k_3(x_2 - x_3) + k_4(x_3 - x_4) = 0 \qquad (3.70)$$
$$\cdots$$
$$m_n\ddot{x}_n - k_n(x_{n-1} - x_n) = 0$$

The above equation is the required equation of motion, which is written in the
matrix form as given below

$$
\begin{bmatrix}
m_1 & 0 & 0 & \ldots & 0 \\
0 & m_1 & 0 & \ldots & 0 \\
0 & 0 & m_1 & \ldots & 0 \\
\ldots & \ldots & \ldots & \ldots & \ldots \\
0 & 0 & 0 & \ldots & m_1
\end{bmatrix}
\begin{Bmatrix}
\ddot{x}_1 \\ \ddot{x}_2 \\ \ddot{x}_3 \\ \ldots \\ \ddot{x}_n
\end{Bmatrix}
+
\begin{bmatrix}
(k_1 + k_2) & 0 & 0 & \ldots & 0 \\
0 & (k_2 + k_3) & 0 & \ldots & 0 \\
0 & 0 & (k_3 + k_4) & \ldots & 0 \\
\ldots & \ldots & \ldots & \ldots & \ldots \\
0 & 0 & 0 & \ldots & k_n
\end{bmatrix}
\begin{Bmatrix}
x_1 \\ x_2 \\ x_3 \\ \ldots \\ x_n
\end{Bmatrix}
=
\begin{Bmatrix}
0 \\ 0 \\ 0 \\ \ldots \\ 0
\end{Bmatrix}
$$

$$(3.71)$$

$$[M]\{\ddot{x}\} + [K]\{x\} = \{0\} \tag{3.72}$$

where $[M]$ is a square matrix of nth order having only diagonal elements in this case; $[K]$ is a symmetric square stiffness matrix of order n and $\{x\}$ is a column matrix of n elements corresponding to the dynamic displacements of the respective n masses. Equation (3.72) is similar to that of the equation of motion of a single-degree of freedom except that $[M]$ and $[K]$ are a matrix of nth order where n is the degree of freedom.

3.13   Influence Coefficients

Equations of motion of a multi-degrees of freedom system can also be written in terms of influence coefficients that are extensively used in structural dynamics. For a linear spring, the force necessary to cause a unit elongation is called the spring constant. In more complex systems, we can express the relation between the displacement at a point and the forces acting at various other points of the system by means of influence coefficients. There are two types of influence coefficients namely (i) flexibility influence coefficients and (ii) stiffness influence coefficients. To illustrate the concept of an influence coefficient, let us consider the multi-degrees of freedom spring–mass system shown in Fig. 3.16.

Let the system be acted on by just one force F_j and let the displacement at point i (i.e., mass m_i) due to F_j be x_{ij}. The flexibility influence coefficient, denoted by a_{ij} is defined as the deflection at point i due to a unit load at point j. Since the deflection increases proportionately with the load for a linear system, we have the following relationship:

$$x_{ij} = a_{ij}F_j \tag{3.73}$$

If several forces $F_j(j = 1, 2, \ldots, n)$ act at different points of the system, then the total deflection at any point i can be found by summing up the contributions of all force F_j. This is given as below

$$x_i = \sum_{j=1}^{n} x_{ij} = \sum_{j=1}^{n} a_{ij}F_j \quad I = 1, 2, \ldots, n \tag{3.74}$$

Equation (3.74) can be expressed in matrix form as

$$\bar{x} = [a]\overline{F} \tag{3.75}$$

where $\bar{x}$ and $\overline{F}$ are displacement and force vectors and $[a]$ the flexibility matrix and is given by

$$[a] = \begin{bmatrix} a_{11} & a_{12} & -- & a_{1n} \\ a_{21} & a_{22} & -- & a_{2n} \\ -- & -- & -- & -- \\ a_{n1} & a_{n2} & -- & a_{nn} \end{bmatrix} \tag{3.76}$$

The stiffness influence coefficient, denoted by k_{ij}, is defined as the force at point i due to a unit displacement at point j when all the points other than the point j are restrained. Total force at point i, which is F_i, can be obtained by summing up the forces due to all such displacements $x_j (j = 1, 2, \ldots, n)$ and is given by

$$F_i = \sum_{j=1}^{n} k_{ij} x_j \quad i = 1, 2, \ldots, n \tag{3.77}$$

Equation (3.77) can be stated in matrix form as given below

$$\overline{F} = [k]\overline{x} \tag{3.78}$$

where $[k]$ is the stiffness matrix and is given by

$$[k] = \begin{bmatrix} k_{11} & k_{12} & -- & k_{1n} \\ k_{21} & k_{22} & -- & k_{2n} \\ -- & -- & -- & -- \\ k_{n1} & k_{n2} & -- & k_{nn} \end{bmatrix} \tag{3.79}$$

By comparing the Eqs. (3.75) and (3.78), following relationship can be deduced:

$$\overline{x} = [a]\overline{F} = [a][k]\overline{x} \tag{3.80}$$

It can be further seen that the following relationship also holds good.

$$[a][k] = [I] \tag{3.81}$$

where $[I]$ denotes the unit matrix. Equation (3.81) is equivalent to the following statement:

$$[k] = [a]^{-1} \quad \text{and} \quad [a] = [k]^{-1} \tag{3.82}$$

That is, the stiffness and flexibility influence coefficient matrices are inverse of one another. Further, more interesting observations can be made as listed below:

- Since deflection at point i due to a unit load at point j is the same as the deflection at point j due to a unit load at point i for a linear system (Maxwell's reciprocal theorem), we shall conclude that $a_{ij} = a_{ji}$ and $k_{ij} = k_{ji}$.
- Flexibility and stiffness influence coefficients can be calculated from the principles of basic structural mechanics.

- Influence coefficient matrix shall always be a square, symmetric matrix with positive leading diagonal elements.

3.14   Eigen Value Problem

Let us now consider a multi-degrees of freedom system shown in Fig. 3.16. Differential equations of motion for the system are given as below

$$
\begin{aligned}
&[m1\ddot{x}_1 + (k_1 + k_2)x_1] - k_2x_2 = 0 \\
&-k_2x_1 + [m_2\ddot{x}_2 + (k_2 + k_3)x_2] - k_3x_3 = 0 \\
&-k_3x_2 + [m_3\ddot{x}_3 + (k_3 + k_4)x_3] - k_4x_4 = 0 \\
&\qquad\qquad\qquad \cdots \\
&-k_nx_n - 1 + (m_n\ddot{x}_n + k_nx_n) = 0
\end{aligned}
\tag{3.83}
$$

For the principal mode of vibration, let us assume the solution as

$$
\begin{aligned}
x_1 &= X_1 \sin \omega t \\
x_2 &= X_2 \sin \omega t \\
x_3 &= X_3 \sin \omega t \\
&\cdots \\
x_n &= X_n \sin \omega t
\end{aligned}
\tag{3.84}
$$

Substituting Eq. (3.84) in Eq. (3.83) and canceling out the common terms, we get

$$
\begin{aligned}
&[(k_1 + k_2) - m_1\omega^2]X_1 - k_2X_2 = 0 \\
&-k_2X_1 + [(k_2 + k_3) - m_2\omega^2]X_2 - k_3X_3 = 0 \\
&-k_3X_2 + [(k_3 + k_4) - m_3\omega^2]X_3 - k_4X_4 = 0 \\
&\qquad\qquad\qquad \cdots \\
&-k_nX_{n-1} + (k_n - m_n\omega^2)X_n = 0
\end{aligned}
\tag{3.85}
$$

For the above equations, solution other than $X_1 = X_2 = X_3 = X_n = 0$ is possible only when the determinant composed of the coefficients of X's vanishes; this condition is expressed mathematically as below

$$
\begin{vmatrix}
[(k_1 + k_2) - m_1\omega^2] & -k_2 & -- & 0 & 0 \\
-k_2 & [(k_2 + k_3) - m_2\omega^2] & -k_3 & 0 & 0 \\
0 & -k_3 & -- & 0 & 0 \\
-- & -- & -- & -- & -- \\
-- & -- & -- & -k_n & (k_n - m_n\omega^2)
\end{vmatrix} = 0
$$

$$(3.86)$$

Solution to the above equation yields n values of ω^2 corresponding to n natural frequencies. Mode shapes can be obtained from Eq. (3.85).

3.15   Dynamic Matrix Method

Equation of motion of multi-degrees of freedom can be written in the matrix form as shown below

$$[M]\{\ddot{x}\} + [K]\{x\} = \{0\} \tag{3.87}$$

Pre-multiplying the above equation with $[M] - 1$, we get

$$[I]\{\ddot{x}\} + [D]\{x\} = \{0\} \tag{3.88}$$

where $[D] = [M] - [K]$ is termed as dynamic matrix. For free body vibrations, assuming displacement vector as a harmonic motion of frequency ω, we get

$$\{x\} = \{X\}\sin\omega t \tag{3.89}$$

$$\{\ddot{x}\} = -\omega^2\{x\} = \lambda\{x\} = -\lambda\{X\}\sin\omega t \tag{3.90}$$

where $\lambda = \omega^2$ is the Eigen value and $\{X\}$ is the column giving the amplitudes of respective masses i.e. eigenvectors. In other words, λ and $\{X\}$ are natural frequencies and the corresponding mode shapes, respectively. Equation (3.88) reduces to the form:

$$-\lambda[I]\{X\} + [D]\{X\} = \{0\}$$

$$[[D] - X[I]]\{X\} = \{0\} \tag{3.91}$$

The determinant formed from the above equation is given below

$$[[D] - A[I]] = 0 \tag{3.92}$$

The above equation is the frequency equation and gives n values of λ (for n degrees of freedom). Further by substitution, mode shapes can be obtained.

3.16   Dunkerley's Method

Dunkerley proposed an approximate method of determining fundamental frequency of vibrating system. It is known as lower bound method as Dunkerley's frequency will always be lower. For a multi-degrees of freedom system, following relationship is proposed by Dunkerley.

$$\frac{1}{\omega_n^2} = \frac{1}{\omega_1^2} + \frac{1}{\omega_2^2} + \frac{1}{\omega_3^2} + \cdots + \frac{1}{\omega_s^2} \tag{3.93}$$

where ω_n is the fundamental natural frequency of the system: $\omega_1, \omega_2, \omega_3 \ldots$ are the natural frequencies of the system with each mass acting separately at its point of application in the absence of other masses. This method shall be applicable only for discrete systems.

3.17   Matrix Iteration Method

This is one of the most commonly used methods among iterative methods for determining eigen values (natural frequencies) and eigenvectors (mode shapes). With the use of flexibility matrix $[A]$ in the differential equations, this method is used when only the lowest eigen value and eigenvector of multi-degrees of freedom system are desired. The advantage of this method is that the iterative process results in the principle mode of vibration of the system and the corresponding natural frequency simultaneously. Equation of motion in terms of flexibility matrix can be written as

$$[A][M][\ddot{x}] + \{x\} = \{0\} \tag{3.94}$$

Substituting $\{x\} = \{X\} \sin \omega t$, we get

$$\{X\} = \omega^2 [A][M]\{x\} \tag{3.95}$$

The above equation is rewritten as

$$\{X\} = \omega^2 [B]\{X\} \tag{3.96}$$

$$[B] = [A][M]$$

Equation (3.96) is of the following form:

$$
\begin{Bmatrix} X_1 \\ X_2 \\ \cdots \\ X_n \end{Bmatrix} = \omega^2 \begin{bmatrix} b_{11} & b_{12} & \cdots & b_{1n} \\ b_{21} & b_{22} & \cdots & b_{2n} \\ \cdots & \cdots & \cdots & \cdots \\ b_{n1} & b_{n1} & \cdots & b_{nn} \end{bmatrix} \begin{Bmatrix} X_1 \\ X_2 \\ \cdots \\ X_n \end{Bmatrix}
\tag{3.97}
$$

Iterative process is started by assuming a set of displacements for the right column of Eq. (3.97) and then expanding the right-hand side which results in a column of numbers. This is then normalized and compared with the new obtained value of the displacement vector. The procedure is repeated until the new set of displacements converges with that of the previous step of iteration. The iteration process with the use of Eq. (3.97) converges to the lowest value of $(1/\omega^2)$ so that the fundamental mode of vibration is obtained. For next higher modes and natural frequencies, Orthogonality principle is applied to obtain a modified matrix that is free from the lower modes.

3.18   Stodola's Method

This method is a quickly converging iterative process used for the calculating the fundamental natural frequency of undamped free vibrations for multi-degrees-of freedom systems. The procedure is to assume a reasonable deflection pattern for the given multi-degrees of freedom model. This shall be taken same as that of the static deflection curve as in Rayleigh's method. Determine inertia loading for the assumed deflection in terms of ω^2. For the system subjected to the inertia load, determine corresponding (new) deflection pattern; this shall also be in terms of ω^2. If the assumed deflection pattern of step 1 converges with that of the derived ones of step 3, then equate the two expressions of step 1 and step 3 which shall give the value of ω^2. If the deflection patterns do not match, then the derived deflection pattern obtained in step 3 is used as starting point for the next iteration. This process is repeated until the derived deflection pattern converges with the previous set of values. The method is independent of the amplitudes of initially assumed values of displacement pattern, and the convergence is very fast.

3.19   Mode Superposition Method

For multi-degrees of freedom system, equation of motion is given by

$$
[M]\{\ddot{x}\} + [C]\{\dot{x}\} + [K]\{x\} = \{F(t)\}
\tag{3.98}
$$

Any arbitrary vector $\{x\}$ in a nondimensional space can be represented as a linear combination of the mode shapes. Thus,

$$x = \sum_{r=1}^{N} q_r(t)\{\varphi^{(r)}\} = \Phi q \qquad (3.99)$$

where Φ is the modal matrix with each of its column representing mode shape and $\{q\}$ is the vector of modal coordinates related to the system coordinates. Now, the following operations are performed:

$$[M]\{\ddot{x}\} + [C]\{\dot{x}\} + [K]\{x\} = \{F(t)\}$$

pre-multiplying by Φ^{T} $\qquad\qquad\qquad (3.100)$

$$\Phi^{\mathrm{T}}M\,\Phi\,\ddot{q} + \Phi^{\mathrm{T}}C\,\Phi\,\dot{q} + \Phi^{\mathrm{T}}K\,\Phi q = \Phi^{\mathrm{T}}F$$

Since mode shape Φ are orthogonal with respect to $[M]$ and $[K]$, matrix triple products involving $[M]$ and $[K]$ will yield diagonal matrices.

$$\{\varphi^{(r)}\}^{\mathrm{T}}M\{\varphi^{(r)}\} = m_r^*$$
$$\{\varphi^{(r)}\}^{\mathrm{T}}C\{\varphi^{(r)}\} = c_r^*$$
$$\{\varphi^{(r)}\}^{\mathrm{T}}K\{\varphi^{(r)}\} = k_r^* \qquad (3.101)$$
$$\{\varphi^{(r)}\}^{\mathrm{T}}F = f_r^*$$

where m_r^* represents modal mass for mode r, c_r^* represents coefficient of viscous damping in rth mode, k_r^* represents modal stiffness for rth mode and f_r^* represents modal force in rth mode, respectively. If mode shapes are mass-orthogonalized, then the modal parameters reduce to the following:

$$m_r^* = 1.0$$
$$c_r^* = 2\xi_r\omega_r \qquad (3.102)$$
$$k_r^* = \omega_r^2$$

Modal participation factor for rth mode is given by

$$\Gamma_r = \frac{\{\varphi^r\}^{\mathrm{T}}M\,r}{\{\varphi^r\}^{\mathrm{T}}M\{\varphi^r\}} \qquad (3.103)$$

3.20   Mode Truncation

In a multi-degrees of freedom system, it is not necessary to include all modes to get rational estimate of the total response; higher modes can be truncated. Response vector $\{x\}$ can be written as

$$x = \sum_{r=1}^{\hat{N}} q_r(t)\{\varphi^{(r)}\} \tag{3.104}$$

where $\hat{N} \ll N$.

The number of modes to be included depends on: (i) all modes having frequency value lower than the highest frequency of the excitation force; and (ii) at least 90% of the total mass of the structural system.

3.20.1   Static Correction for Higher Mode Response

Let us consider modal contribution to the total response as the sum of two parts as shown below

$$x = \sum_{r=1}^{\hat{N}} \{\varphi^{(r)}\} q_r(t) + \sum_{S=\hat{N}+1}^{N} \{\varphi^{(S)}\} q_s(t) \tag{3.105}$$

where the second term of the modal summation represents the error term due to the truncation of the modal summation. Now,

$$M_s\ddot{q}_s(t) + C_s\dot{q}_s(t) + K_s q_s(t) = f_s$$
$$q_s(t) = \frac{f_s}{K_s} - \frac{\ddot{q}_s(t)}{\omega_s^2} - \frac{2\xi_s\dot{q}_s(t)}{\omega_s} \tag{3.106}$$

The first term in the above equation represents the response in sth mode if the load is applied statically. The other two terms represent the dynamic correction to the static response in the sth mode. It is also seen that the inertia term in inversely proportional to the square of the natural frequency and the damping term is inversely proportional to the natural frequency. Hence, in higher modes, contribution for the dynamic response terms becomes insignificant in comparison to that of the static response. Hence, the response in higher modes can be approximated only from the static response. Now the modal forces are given by

$$f_s = \{\varphi^{(s)}\}^{\mathrm{T}} f$$
$$x = \sum_{r=1}^{\hat{N}} \{\varphi^{(r)}\} q_r(t) + \sum_{S=\hat{N}+1}^{N} \frac{1}{K_S}\{\varphi^{(S)}\}\{\varphi^{(s)}\}^{\mathrm{T}} f$$
$$= \sum_{r=1}^{\hat{N}} \{\varphi^{(r)}\} q_r(t) + \sum_{S=\hat{N}+1}^{N} F_S f \tag{3.107}$$

where F_S represents the contribution of the sth mode toward the flexibility matrix f the system. It is important to note that the response of higher modes can be approximated by considering the static response only; still it is necessary to compute all the mode shapes in order to compute the contribution of higher modes to the structural flexibility.

$$\sum_{S=\hat{N}+1}^{N} \frac{1}{K_S} \{\varphi^{(S)}\} \{\varphi^{(s)}\}^{\mathrm{T}} = K^{-1} - \sum_{r=1}^{\hat{N}} \frac{1}{K_r} \{\varphi^{(r)}\} \{\varphi^{(r)}\}^{\mathrm{T}} = K^{-1} - \sum_{r=1}^{\hat{N}} F_r$$

$$(3.108)$$

The above equation shows that the higher mode contribution to the structural flexibility is computed by subtracting the contribution of the lower modes from the total structural flexibility matrix. Hence the total response is given by

$$x = \sum_{r=1}^{\hat{N}} \{\varphi^{(r)}\} q_r(t) + \left[K^{-1} - \sum_{r=1}^{\hat{N}} F_r \right] f \qquad (3.109)$$

The second term in the above equation is called *static correction* to account for the higher mode response. It is also called *missing mass correction*.

3.21   Rayleigh–Ritz Method—Analytical Approach

In the coordinate system, total energy at any instant of time during the vibration remains constant. We know that the total energy is the sum of potential energy (PE) and kinetic energy (KE). When the mass reaches maximum the maximum, the potential energy is maximum and the kinetic energy becomes zero. When mass crosses the equilibrium position, potential energy becomes zero and the kinetic energy becomes maximum. Considering this, the following equation is valid:

$$(PE)\mathrm{max} = (KE)\mathrm{max}$$

$$\frac{1}{2} M \int_0^l y^2 \mathrm{d}x \omega^2 = \frac{1}{2} \int_0^l EI \left(\frac{\mathrm{d}^2 y}{\mathrm{d}x^2} \right)^2 \mathrm{d}x$$

$$-\omega^2 = \frac{\int_0^l EI \left(\frac{\mathrm{d}^2 y}{\mathrm{d}x^2} \right)^2 \mathrm{d}x}{\frac{1}{2} M \int_0^l y^2 \mathrm{d}x} = \frac{U}{T} \qquad (3.110)$$

where ω be the frequency and m be the mass/unit volume.

Procedure suggested by Rayleigh is as follows:

1. Any shape resembling the fundamental mode shape can be assumed; boundary conditions should be satisfied.
2. By trial and error method, try many functions to get the lowest value of the frequency from Eq. (3.109).
3. Profile or the shape function assumed should correspond to fundamental mode; should satisfy the kinematics boundary condition.

In Ritz method, it is suggested that the shape function y is assumed such that it is linear combination of different function with unknown parameters. For example:
Let

$$y = a\varphi_1(x) + b\varphi_2(x) + c\varphi_3(x) + \cdots \tag{3.111}$$

The necessary condition is that Eq. (3.110) must completely satisfy all the BC. For, $(PE)\mathrm{max} = (KE)\mathrm{max}$;

$$\omega^2 = N \tag{3.112}$$

$$\text{that is } N = \frac{U}{T}; \quad \text{where } U = PE; \ T = KE \tag{3.113}$$

Partially differentiating with respect to a:

$$\frac{\partial N}{\partial a} = \frac{T(\partial u/\partial a) - u(\partial T/\partial a)}{T^2} = 0 \tag{3.114}$$

$$T(\partial u/\partial a) - u(\partial T/\partial a) = 0 \tag{3.115}$$

$$\partial u/\partial b - \frac{U}{T}\partial T/\partial b = 0 \tag{3.116}$$

$$\partial u/\partial c - \frac{U}{T}\partial T/\partial c = 0 \tag{3.117}$$

$$\partial u/\partial d - \frac{U}{T}\partial T/\partial d = 0 \tag{3.118}$$

The above homogeneous equations lead to eigen value problem. Also we know that $N = \frac{U}{T} = \omega^2$.
Hence, Eq. (3.117) becomes

$$\partial u/\partial d - \omega^2(\partial T/\partial d) = 0 \tag{3.119}$$

$$504EI - 6\omega^2 m.$$

Example 1 For a cantilever beam with uniformly distributed mass, determine the natural frequency. Take length of the beam as 1 m.
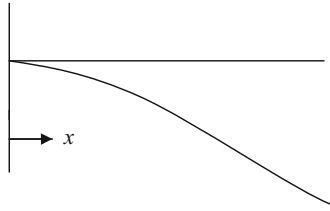
Step 1: *Boundary condition* At $x = 0$; $y = 0$; which is satisfied; At $x = 0$; $\frac{dy}{dx} = 0$; which is also satisfied

$$U = PE = 1/2 \int_0^l EI \left(\frac{d^2y}{dx^2}\right)^2 dx$$

$$\frac{dy}{dx} = 2ax + 3bx^2$$

$$\frac{d^2y}{dx^2} = 2a + 6bx$$

Step 2:

$$U = PE = 1/2 \int_0^l EI(2a + 6bx)^2$$

$$U = \frac{EI}{2} \int 4a^2l + 12b^2l^3 + 12abl^2$$

For unit length; $U = \frac{EI}{2} \int 4a^2 + 12b^2 + 12ab$

Step 3:

$$T = \frac{1}{2}m \int_0^l y^2 dx;$$

$$T = \frac{1}{2}m \int_0^l \left(ax^2 + bx^3\right)^2 dx;$$

$$T = \frac{1}{2}m\left(\frac{a^2 l^5}{5} + \frac{b^2 l^7}{7} + \frac{2ab l^6}{6}\right);$$

For unit length, $T = \frac{1}{2}m\left(\frac{a^2}{5} + \frac{b^2}{7} + \frac{2ab}{6}\right)$

Step 4:

$$\frac{\partial u}{\partial a} - \omega^2 \frac{\partial T}{\partial a} = 0$$

$$\frac{\partial u}{\partial a} = \frac{EI}{2}(8a + 12b)$$

$$\frac{\partial T}{\partial a} = \frac{m}{2}\left(\frac{2a}{5} + \frac{b}{3}\right)$$

$$\frac{EI}{2}(8a + 12b) - \omega^2\frac{m}{2}\left(\frac{2a}{5} + \frac{b}{3}\right) = 0 \qquad (3.120)$$

Step 5:

$$\frac{\partial u}{\partial b} = \frac{EI}{2}(24a + 12b)$$

$$\frac{\partial T}{\partial a} = \frac{m}{2}\left(\frac{2b}{7} + \frac{a}{3}\right)$$

$$\frac{EI}{2}(24a + 12b) - \omega^2\frac{m}{2}\left(\frac{2b}{7} + \frac{a}{3}\right) = 0 \qquad (3.121)$$

$$15EI(8a + 12b) - \omega^2 m(6a + 5b) = 0$$
$$21EI(12a + 24b) - \omega^2 m(7a + 6b) = 0$$
$$(120EI - 6\omega^2 m)a + (180EI - 5\omega^2 m)b = 0$$
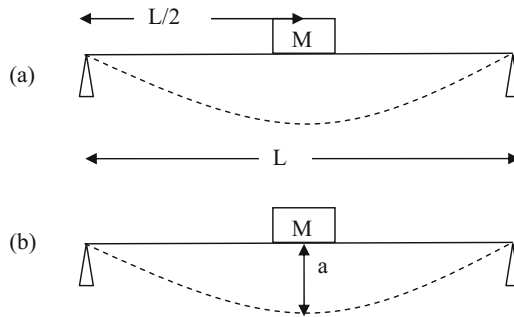$$(252EI - 7\omega^2 m)a + (504EI - 6\omega^2 m)b = 0$$
$$\begin{bmatrix} 120EI - 6\omega^2 m & 180EI - 5\omega^2 m \\ 252EI - 7\omega^2 m & 504EI - 6\omega^2 m \end{bmatrix}\begin{Bmatrix} a \\ b \end{Bmatrix} = \{0\}$$

$$(3.122)$$

It is in the form of $[A]\{X\} = 0$. The above equation can be solved to obtain the natural frequency.

Example 2 As a simple supported beam of length *L*, total mass *m* also carries a concentrated mass m at the center. Find its ω_n lowest of its transverse vibration.

(a) y = vertical deflection due to loads

$$\text{Let } U = \frac{EI}{2} \int\limits_0^l \left(\frac{d^2y}{dx^2}\right)^2 dx$$

$$y = a \, \sin\left(\frac{\pi x}{\ell}\right)$$

Boundary condition

$$\text{at } x = 0; \quad y = 0;$$

$$\text{at } x = \ell; \quad y = 0;$$

at $x = \ell/2$; $y = a$; which is all satisfied.

$$\frac{dy}{dx} = \left(\frac{\pi}{\ell}\right) a \, \cos\left(\frac{\pi x}{\ell}\right)$$

$$\frac{dy}{dx} = -\left(\frac{\pi}{\ell}\right)^2 a \, \sin\left(\frac{\pi x}{\ell}\right)$$

$$U = \frac{EI}{2} \int\limits_0^l \left[\left(\frac{\pi}{\ell}\right)^2 a \, \sin\left(\frac{\pi x}{\ell}\right)\right]^2 dx$$

$$= \frac{EI}{2} \int\limits_0^l \left(\frac{\pi^2}{\ell^2}\right)^2 a^2 \sin^2\left(\frac{\pi x}{\ell}\right) dx$$

$$\text{let } \frac{\pi x}{\ell} = \theta; \cos 2\theta = 1 - 2\sin^2\theta;$$

$$\sin^2\theta = \frac{1}{2}\left[\frac{1-\cos 2\theta}{2}\right] = \frac{1}{2}\left[1-\cos\left(\frac{2\pi x}{\ell}\right)\right] = \frac{1}{2}\int_0^l\left[1-\cos\left(\frac{2\pi x}{\ell}\right)\right]dx$$

$$U = \frac{EI}{2}\left(\frac{\pi^4}{\ell^4}\right)a^2\frac{1}{2}\int_0^l\left[1-\cos\left(\frac{2\pi x}{\ell}\right)\right]dx$$

$$U = \frac{EI}{2}\left(\frac{\pi}{\ell}\right)^4\ell a^2$$

(a) Kinetic energy due to moment

Deflection at middle = a

Let the displacement $x = a\cos\omega t$; velocity = $-a\omega\sin\omega t$; max velocity = $|-a\omega|$

KE due to concentrated mass $M = \frac{1}{2}MV^2 = \frac{1}{2}M(a^2\omega^2)$

(b) Due to mass of the beam m

$$T = \frac{1}{2}\left(\frac{m}{\ell}\right)\int_0^\ell y^2 dx = \frac{1}{2}\left(\frac{m}{\ell}\right)\omega^2\int_0^\ell y^2 dx = \frac{1}{2}\left(\frac{m}{\ell}\right)\omega^2\left(\frac{a^2}{2}\right)\int_0^\ell 1-\cos\left(\frac{2\pi x}{\ell}\right)dx$$

$$T = \frac{m\omega^2 a^2}{4}$$

where m is the total mass of the entire beam.

$$\text{Total KE} = \frac{1}{2}Ma^2\omega^2 + \frac{1}{4}M(\omega^2 a^2) = \frac{1}{2}\omega^2 a^2\left(M + \frac{M}{2}\right)$$

$$(KE)\text{max} = (PE)\text{max}$$

$$\omega^2 = \frac{EI(\ell/2)(\pi/\ell)^4}{\left(M + \frac{M}{4}\right)}$$

Comparison by Dunkerley's Method

(a) Deflects due to central load, M

$$y_{11} = \frac{48EI}{M\ell^3}$$

(b) Deflects due to total load,

$$y_{22} = \frac{48EI}{m\ell^3}$$

$$\left(\frac{1}{\omega^2}\right) = \frac{M\ell^3}{48EI} + \frac{m\ell^3}{\pi^4 EI}$$

$$\omega^2 = \frac{EI(\pi/\ell)^4 \ell/2}{\left(1.013M + \frac{M}{2}\right)}$$

Exercise

1. All bodies possess _____and _____ which results in vibration of the body.
2. At equilibrium, whole of elastic energy is converted into _____ and the body continues to move in opposite direction because of it.
3. Whole of the kinetic energy is converted into _____ due to which the body again returns to the equilibrium position.
4. Any motion which repeats itself after an interval of time is called _____.
5. A motion which repeats itself after equal interval of time is called _____.
6. Number of cycles per unit time is called _____.
7. Maximum displacement of a vibrating body from the equilibrium position is called _____.
8. When system vibrates without any external force it is called _____.
9. Natural frequency is expressed in _____ (units).
10. Minimum number of _____ required to specify the motion of system at any instant is known as _____.
11. Degree of freedom may vary between _____.
12. _____ beam is an example for infinite degrees of freedom.
13. Motion of simple pendulum is an example for _____.
14. Resistance offered to the motion of the vibrating body is called _____.
15. When there is phase difference in the system, the vibrating motion can be expressed as _____(*Hint*: Equation of response).

16. When the frequency of external excitation is equal to natural frequency of the vibrating body, then the system is in _____ and amplitude of vibration becomes extensively _____.
17. Mechanical system consists of _____, _____ and _____ .
18. Continuous system is also called _____.
19. In a vibrating system, there is an exchange of energy from _____.
20. Energy is stored by mass in the form _____ and spring in the form of _____.
21. Sketch the basic vibratory system with SDOF.
22. In the vibratory system, if the amount of external excitation is known in magnitude, it is called _____.
23. If system vibrates indefinitely and the amplitude decays because of _____ and vanishes continuously, such kind of vibration is called _____.
24. _____ occurs as a result of interference between two waves of slightly different frequencies moving along the same straight line in the same direction.
25. If springs with stiffness k_1 and k_2 are connected in parallel, their effective stiffness is equal to _____.
26. "Mass develops an inertia force proportional to its acceleration and opposite in direction." This is stated by _____.
27. The Tension leg platform is heave restrained by _____
28. Match the design wave height for various regions is tabulated below:

I. Bay of Bengal	(a) 11 m for 1 year and 24 m for 100 years
II. Gulf of Mexico	(b) 6 m for 1 year and 12 m for 100 years
III. South China Sea	(c) 5 m for 1 year and 12 m for 100 years
IV. Arabian Sea	(d) 14 m for 1 year and 22 m for 100 years
V. Gulf of Thailand	(e) 12 m for 1 year and 24 m for 100 years
VI. Persian Gulf	(f) 8 m for on 1 yr and 18 m for 100 yrs
VII. North Sea	(g) 8 m for 1 year and 18 m for 100 years

29. Growth of marine algae increases the _____ and _____which in turn increase the wave or current loading.
30. In P-M spectrum fetch and duration are considered _____.
31. Algebraic sum of wave and current loads is different from calculation of load by adding the horizontal water particle velocity with the current velocity and computing the loads. This is because of _____.
32. Seismic loads are arising from derived type _____.

Key to Exercise

1. Mass; restoring capacity (elasticity)
2. Kinetic energy
3. Elastic or strain energy
4. Vibration or oscillation
5. Periodic motion
6. Frequency
7. Amplitude
8. Free vibration
9. rad/s or hertz
10. Independent coordinates; degrees of freedom
11. Zero to infinity
12. Cantilever
13. Simple harmonic motion
14. Damping (friction)
15. $x = A \sin(\omega t + \varphi)$
16. Resonance; large
17. Mass, stiffness, and damping
18. Distributed systems
19. One form to another (PE to KE or vice versa)
20. Kinetic energy $= 1/2 m \dot{x}^2$; Potential energy $= 1/2 k x^2$

21.
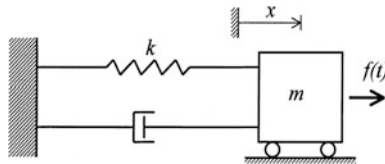
22. Deterministic vibration
23. Damping; transient vibration
24. Beating phenomenon
25. $k_{\text{eff}} = k_1 + k_2$
26. D'Alembert's Principle
27. Vertical tendons or tethers
28. I (f/g); II (e); III (a); IV (f/g); V (b); VI (c); VII (d)
29. Diameter and roughness of members
30. Infinite
31. Nonlinear term in the drag equation
32. Gravity loads

Solved Numerical Examples

1. Determine the natural frequency of the mass m placed at one end of the cantilever beam of negligible mass. (*Hint*: deflection = $Wl^3/3EI$)

   Deflection = $WL^3/3EI$;   stiffness = load/deflection; $k = 3EI/L^3$; $\omega = \sqrt{\frac{k}{m}} =$

   $\sqrt{\frac{3EI}{L^3m}}$ rad/s or $\frac{1}{2\pi}\sqrt{\frac{3EI}{L^3m}}$ Hz

2. Determine the natural frequency of the mass m placed at middle of the fixed beam of length (L m) negligible mass. (Hint: deflection = $Wl^3/192EI$)

   Deflection = $WL^3/3EI$;   stiffness = load/deflection; $k = 3EI/L^3$; $\omega = \sqrt{\frac{k}{m}} =$

   $\sqrt{\frac{3EI}{L^3m}}$ rad/s or $\frac{1}{2\pi}\sqrt{\frac{3EI}{L^3m}}$ Hz.

3. List the types of damped system and sketch the responses neatly.
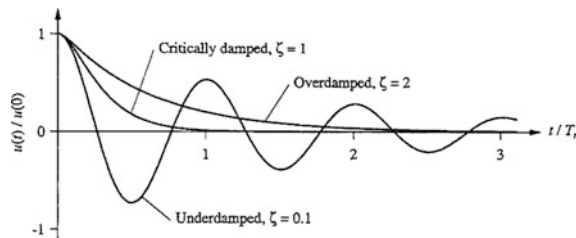
4. Unknown mass m is attached to the one end of the spring of stiffness k having the natural frequency of 12 Hz. When 1 kg mass is attached with the m and the natural frequency of the system is lowered by 25%, determine the value of unknown mass m and stiffness k.

   Let $f1 = 12\,\text{Hz} = \dfrac{1}{2\pi}\sqrt{\dfrac{k}{m}}\,\text{Hz};\quad f2 = 12 \times (75/100) = \dfrac{1}{2\pi}\sqrt{\dfrac{k}{m+1}}\,\text{Hz};$

   $f1/f2 = 12/9 = \left(\sqrt{\dfrac{k}{m}}\right)\Big/\left(\sqrt{\dfrac{k}{m+1}}\right) = (1.333)2 = \dfrac{\frac{k}{m}}{\frac{k}{m+1}} = \dfrac{m+1}{m}; m$

   $= 1.2857\,\text{kg}$

   $12 = \dfrac{1}{2\pi}\sqrt{\dfrac{k}{m}}; 12 \times 2\pi = \sqrt{\dfrac{k}{m}}; 5684.89 = \dfrac{k}{m};$

   $$k = 7276.6592\,\text{N/m}$$

5. Cylinder of diameter D and mass m floats vertically in a liquid of mass density ρ. It is made to oscillate by giving some initial displacement. Find the period of oscillation. What will be the frequency if salty liquid of specific gravity 1.2 is used?

Let us assume x is the displacement of the cylinder

Restoring force = $(\rho Ax)g$;

According to Newton's law, $mx + \ddot{\rho} Axg = 0$

$$\omega_n = \sqrt{\frac{\rho Ag}{m}}; \quad T = \frac{2\pi}{\omega} = \frac{2\pi}{\sqrt{\frac{\rho Ag}{m}}}\ \text{s}$$

if salt water $\rho = 1.2$; $\omega_n = \sqrt{\frac{1.2\rho Ag}{m}}$ rad/s where $A = \frac{\pi}{4}d^2$.

6. Find the natural frequency of the system
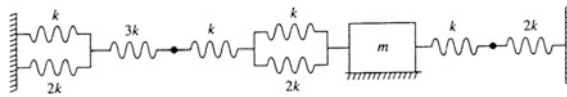
Take $m = 20$ kg; $k = 1000$ N/m
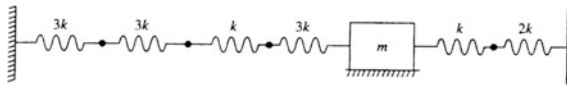
(a)
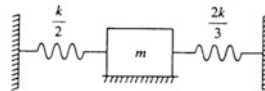
(b)
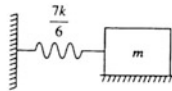
(c)

$$\omega = \sqrt{\frac{k}{m}} = \sqrt{\frac{7 \times 1000}{6 \times 20}} = 7.637 \ \text{rad/s}$$

7. Find the natural frequency of the system
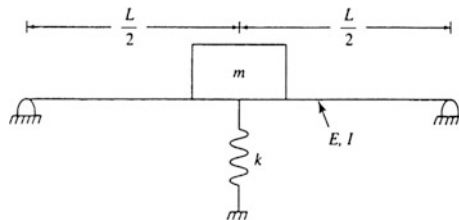
Take $E = 210 \times 10^9$ N/m^2; $I = 1.5 \times 10^{-5}$ m^4; $k = 1500$ N/m; $L = 3$ m

(*Hint:* displacement $x = \frac{PL^3}{48EI}$).

Displacement $x = \frac{PL^3}{48EI}$; Take $E = 210 \times 10^9$ N/m^2; $I = 1.5 \times 10^{-5}$ m^4; $k = 1500$ N/m; $m = 100$ kg
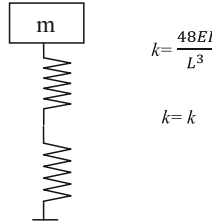
$$\frac{1}{K\text{eff}} = \frac{1}{k} + \frac{L^3}{48EI}$$

$$K_{\text{eff}} = 1450.657\,\text{N/m}; \quad \omega = \sqrt{\frac{k}{m}} = \sqrt{\frac{1450.657}{100}} = 3.809\,\text{rad/s}$$

8. Find the natural frequency of the system
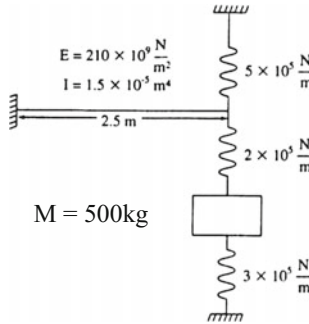
$$k\,\text{beam} = \frac{3EI}{L^3} = \frac{3 \times 210 \times 10^9 \times 1.5 \times 10^{-5}}{2.5^3} = 6.05 \times 10^5\,\text{N/m};$$

$$K_{\text{eff}} = \left(\frac{1}{\frac{1}{(6.05 \times 10^5 + 5 \times 10^5)} + \frac{1}{2 \times 10^5}} \right) + 3 \times 10^5 = 4.693 \times 10^5\,\text{N/m};$$

$$\omega = \sqrt{\frac{k}{m}} = \sqrt{\frac{4.693 \times 10^5}{500}} = 30.6366\,\text{rad/s}$$

9. Sketch the simple SDOF mathematical model and explain the components of it.
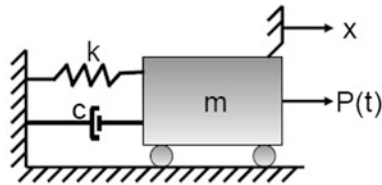
Mass element ,m	- representing the mass and inertial characteristic of the structure
Spring element ,k	- representing the elastic restoring force and potential energy capacity of the structure.
Dashpot, c	- representing the frictional characteristics and energy losses of the structure
Excitation force, P(t)	- represents the external force acting on structure.

10. Draw the mathematical model of the system
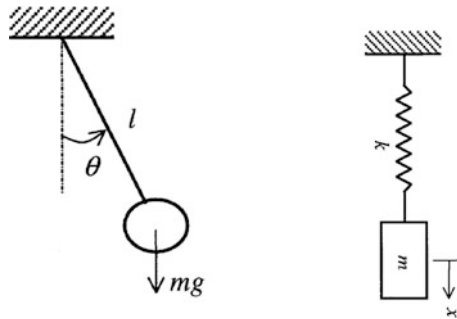
11. Draw the free body diagram of the system
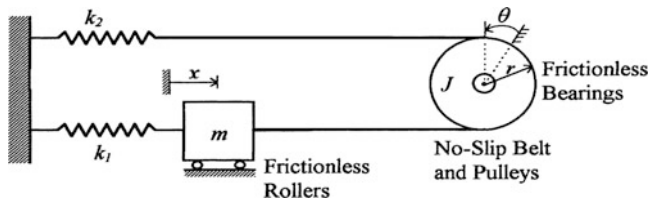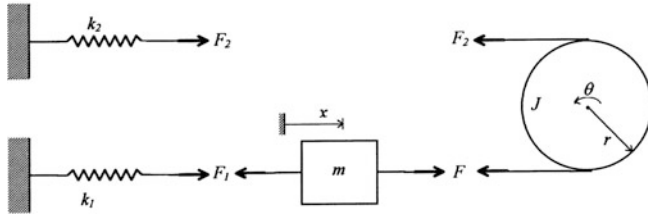
12. Sketch the periodic loading and non-periodic loading

Periodic Loading   Non-Periodic Loading
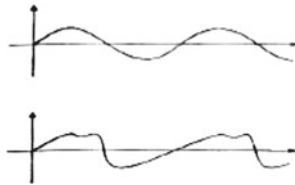
13. Write the equation of motion for the system given below:
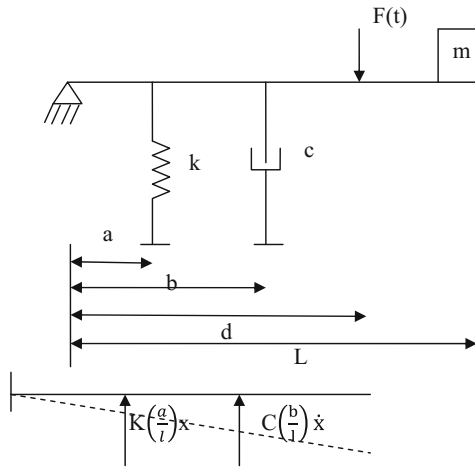
$$m\ddot{x} + c\left(\frac{b}{l}\right)^2 \dot{x} + \left(\frac{a}{l}\right)^2 x = \frac{d}{L}P(t)$$

14. A damper offers resistance 0.05 N at constant velocity 0.04 m/s .The damper is used with stiffness of 9 N/m. Determine the damping ratio and frequency of the system when the mass of the system is 0.10 kg.

$$\text{Damping force } F = C\dot{x}$$
$$\dot{x} = 0.04 \, \text{m/s,}$$
$$F = 0.05 \, \text{N}$$
$$C = F/\dot{x} = 0.05/0.04 = 1.25 \, \text{N s/m}$$
$$C_c = 2\sqrt{km} = 2\sqrt{9*0.1} = 1.897 \, \text{N s/m}$$
$$\xi = \frac{C}{C_c} = \frac{1.25}{1.897} = 0.658$$

The system is under-damped. The frequency of damped vibration is given by

$$\omega = \sqrt{\frac{k}{m}} = \sqrt{\frac{9}{0.1}} = 9.487 \, \text{rad/s}$$
$$\omega_d = \omega\sqrt{1-\xi^2} = 9.487\sqrt{1-0.658^2} = 5.379 \, \text{rad/s}$$

15. A vibrating system is defined by the following parameters: M = 3 kg, k = 100 N/m, C = 3 N s/m. Determine (a) the damping factor, (b) the natural frequency of damped vibration, (c) logarithmic decrement, (d) the ratio of two consecutive amplitudes, and (e) the number of cycles after which the original amplitude is reduced to 20%.
Critical damping is given by

$$C_c = 2\sqrt{km} = 2\sqrt{100*3} = 34.64 \, \text{N s/m}$$
$$\xi = \frac{C}{C_c} = \frac{3}{34.64} = 0.086$$
$$\omega = \sqrt{\frac{k}{m}} = \sqrt{\frac{100}{3}} = 5.773 \, \text{rad/s}$$
$$\omega_d = \omega\sqrt{1-\xi^2} = 5.773\sqrt{1-0.086^2} = 5.730 \, \text{rad/s}$$
$$\delta = \frac{2\pi\xi}{\sqrt{1-\xi^2}} = \frac{2\pi(0.086)}{\sqrt{1-0.086^2}} = 0.5424$$

The ratio of two consecutive amplitudes is given by

$$e^\delta = \frac{x_n}{x_{n+1}}$$
$$\frac{x_n}{x_{n+1}} = e^{0.5424} = 1.72$$
$$\delta = \frac{1}{n}\ln\left[\frac{x_n}{x_{n+1}}\right]$$
$$n = 2.96 \, \text{cylces}$$

The amplitude of the response will decay by 20% in about 3 cycles.

16. A mass of 7 kg is kept on two slabs of isolators placed one over the other. One of the isolators is synthetic rubber with stiffness of 5 kN/m and damping coefficient of 100 N s/m; second isolator is fibrous felt of 10 kN/m and damping coefficient of 400 N s/m. If the assembly is vibrated in the vertical direction actuating the series of isolators, determine the damped and undamped natural frequencies of the system.

    Isolators are connected in series and hence equivalent stiffness and damping coefficients can be readily determined.

$$\frac{1}{k_e} = \frac{1}{5000} + \frac{1}{10000}$$

$$k_e = 3333.33 \, \text{kN/m}$$

$$C_e = \frac{1}{100} + \frac{1}{400} = 80 \, \text{N s/m}$$

$$\omega_n = \sqrt{\frac{k_e}{m}} = 21.822 \, \text{rad/s}$$

$$\xi = \frac{C_e}{2\sqrt{k_e m}} = \frac{80}{2\sqrt{(3333.33 * 7)}} = 0.26$$

$$\omega_d = \omega_n \sqrt{1 - \xi^2} = 21.822 \sqrt{(1 - 0.26^2)} = 21.07 \, \text{rad/s}$$

17. A vibrating system having mass 1 kg is suspended by a spring of stiffness 1000 N/m and it is put to harmonic excitation of 10 N. Assuming viscous damping determine the following: (i) resonant frequency; (ii) amplitude at resonance; (iii) frequency corresponding to the peak amplitude; and (iv) damped frequency. Take C = 40 N s/m.

    (a) Frequency at resonance

$$\omega = \omega_n = \sqrt{(k/m)} = \sqrt{(1000/1)} = 31.62 \, \text{rad/s}$$

    Damping factor ξ is given by

$$\xi = c/2m\omega_n = 40/(2 * 2 * 31.62) = 0.632$$

    (b) Amplitude at resonance

$$x_{\text{resonance}} = \frac{F}{C\omega_n} = \frac{10}{40 * 31.62} = 7.91 \, \text{mm}$$

    (c) frequency corresponding to the peak amplitude is given by

$$\omega_{\text{peak}} = \omega_n \sqrt{1 - 2\xi^2} = 31.62 \, 8 * \sqrt{1 - (2 * 0.632^2)} = 14.185 \, \text{rad/s}$$

(d) Damped frequency is given by

$$\omega_d = \sqrt{(1 - \xi^2)}\omega_n = 31.62 * \sqrt{(1 - 0.632^2)}$$
$$= 24.5 \, \text{rad/s}$$

18. A body of mass 70 kg is suspended from a spring which deflects 2 cm under the load. It is subjected to damping whose value is tuned to be 0.23 times of the value that required for critical damping. Find the natural frequency of the undamped and damped vibrations and ratio of successive amplitudes for damped vibrations. If the body is subjected to a periodic disturbing force of 700 N and of frequency equal to 0.78 the natural undamped frequency, find the amplitude of forced vibrations and the phase difference with respect to the disturbing force.

Spring stiffness $k = \text{force/deflection} = (70 * 9.81)/(2 * 10^{-2}) = 34335 \, \text{N/m}$

$$\xi = C/C_c = 0.23$$

Undamped natural frequency is given by

$$\omega_n = \sqrt{\frac{k}{m}} = \sqrt{\frac{(34.335 * 10^3)}{70}} = 22.15 \, \text{rad/s}$$

Damped natural frequency is given by

$$\omega_d = \sqrt{(1 - \xi^2)}\omega_n$$
$$= 22.15 * \sqrt{(1 - 0.23^2)} = 21.57 \, \text{rad/s}$$

Logarithmic decrement is given by

$$\delta = 2\pi\xi/\sqrt{(1 - \xi^2)}$$
$$= 2\pi * 0.23/\sqrt{(1 - 0.23^2)} = 1.48$$

Ratio of successive amplitudes is given by

$$\frac{A_1}{A_2} = e^{\delta} = e^{1.48} = 4.39$$

The relation is valid. Hence,

$$A/(F/k) = \frac{1}{\sqrt{\left(1 - \beta^2\right)^2 + (2 * \xi * \beta)^2}}$$

Given that $F = 700$ N, $k = 34.335 * 10^3$ N/m, $\beta = 0.78$

$$A = \frac{\frac{700}{34335}}{\sqrt{(1 - 0.78^2)^2 + (2 * 0.23 * 0.78)^2}} = 0.038 \text{ m}$$

Phase difference is given by

$$\tan \theta = \frac{2 * \xi * \beta}{1 - \beta^2} = \frac{2 * 0.23 * 0.78}{1 - 0.78^2} = 0.916$$
$$\theta = 42° 29'$$

19. Determine the effect of mass suspended on the spring–mass system shown
below
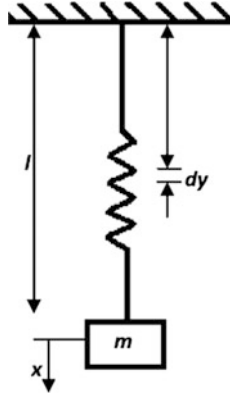
Let x and $\dot{x}$ be the displacement and velocity of mass. Velocity of spring
element at a distance y from the fixed end may be written as $\frac{\dot{x}y}{l}$ where ℓ is the
total length of spring. Kinetic energy of spring element dy is given by

$$\frac{1}{2}(\rho \, dy)\left(\frac{\dot{x}y}{l}\right)^2$$

where ρ is the mass of spring per unit length. Total kinetic energy of the system
is then given by

$$KE = \frac{1}{2}m\dot{x}^2 + \int_0^l \frac{1}{2}(\rho \, dy)\left(\frac{\dot{x}y}{l}\right)^2$$
$$= \frac{1}{2}m\dot{x}^2 + \frac{1}{2}\rho\dot{x}^2\frac{l}{3} = \frac{1}{2}m\dot{x}^2 + \frac{1}{6}m_s\dot{x}^2$$

where mass of spring is $m_s = \rho l$.

Potential energy of the system $= \frac{1}{2}kx^2$.

Total energy of the system = K.E + P.E

$$\frac{1}{2}m\dot{x}^2 + \frac{1}{2}m_s\frac{\dot{x}^2}{3} + \frac{1}{2}kx^2 = \text{constant}$$

Differentiating the above equation w.r.t. time

$$m\ddot{x} + \frac{m_s\ddot{x}}{3} + kx = 0$$

$$\left(m + \frac{m_s}{3}\right)\ddot{x} + kx = 0$$

$$\omega_n = \sqrt{\frac{k}{m + \frac{m_s}{3}}}\ \text{rad/s}$$

20. Circular cylinder of mass 4 kg and radius 15 cm is connected to a spring of stiffness 4000 N/m as shown in the below figure. It is free to roll on horizontal rough surface without slipping. Determine the natural frequency.
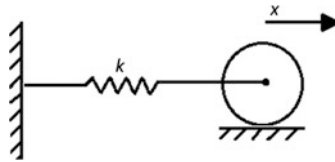
Total energy of the system

$T = $ K.E. due to translator motion $+$ K.E. due to rotary motion $+$ P.E. of spring

$$= \frac{1}{2}m\dot{x}^2 + \frac{1}{2}I\dot{\theta}^2 + \frac{1}{2}kx^2$$

$$= \frac{1}{2}mr^2\dot{\theta}^2 + \frac{1}{2}\cdot\frac{1}{2}mr^2\dot{\theta}^2 + \frac{1}{2}kr^2\theta^2 \ (\text{since } x = r\theta)$$

$$T = \frac{3}{4}m^2r^2\dot{\theta}^2 + \frac{1}{2}kr^2\theta^2 = \text{constant}$$

Differentiating with respect to time, we get

$$0 = \frac{3}{4}\cdot 2mr^2\ddot{\theta}\dot{\theta} + kr^2\dot{\theta}\theta = 0$$

$$\frac{3}{2}mr^2\ddot{\theta} + kr^2\theta = 0$$

$$\omega_n = \sqrt{\frac{kr^2}{(3/2)mr^2}} = \sqrt{\frac{2k}{3m}} \ \text{rad/s}$$

21. In a two-degrees of freedom system shown in the below figure, let $m1 = m2 = m$ and $k1 = k2 = k$. Determine both the natural frequencies of vibration and their amplitude ratios.
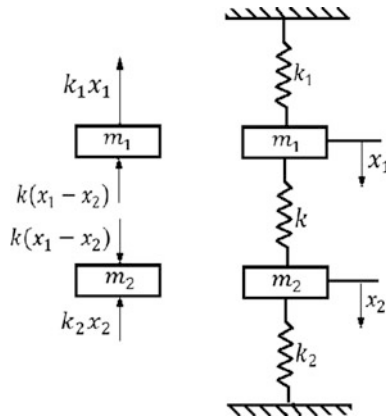
Equations of motion of the system can be written using Newton's law.
From the free body diagrams shown above, following equations can be written as follows:

$$m_1\ddot{x}_1 = -k_1x_1 - k(x_1 - x_2)$$
$$m_2\ddot{x}_2 = k_1(x_1 - x_2) - k_2x_2$$

Rearranging in matrix form,

$$\begin{bmatrix} m_1 & 0 \\ 0 & m_2 \end{bmatrix} \begin{Bmatrix} \ddot{x}_1 \\ \ddot{x}_2 \end{Bmatrix} + \begin{bmatrix} k_1 + k & -k \\ -k & k + k_2 \end{bmatrix} \begin{Bmatrix} x_1 \\ x_2 \end{Bmatrix} = \begin{Bmatrix} 0 \\ 0 \end{Bmatrix}$$

Solving the above equation using the classical eigen solver and substituting $m_1 = m_2 = m$ and $k_1 = k_2 = k$, we get:

$$\omega^2 = \frac{1}{2}\left[\frac{4k}{m} \pm \sqrt{0 + \frac{4k^2}{m^2}}\right] = \frac{3k}{m}, \frac{k}{m}$$

Therefore, the natural frequencies are

$$\omega_{1,2} = \sqrt{\frac{3k}{m}}, \sqrt{\frac{k}{m}}$$

For the first principle mode of vibration, for $\omega = \sqrt{\frac{3k}{m}}$, we get

$$\left(\frac{X_1}{X_2}\right)_1 = \frac{1}{k}\left[k + k - m\left(\frac{3k}{m}\right)\right] = -1$$

Also for the second mode of vibration $\omega = \sqrt{\frac{k}{m}}$, we get

$$\left(\frac{X_1}{X_2}\right)_1 = \frac{1}{k}\left[k + k - m\left(\frac{k}{m}\right)\right] = +1$$

Thus the two amplitude ratios are +1 and –1.

22. For the system shown in the below figure, find out the natural frequencies of vibration and principal modes of vibration.
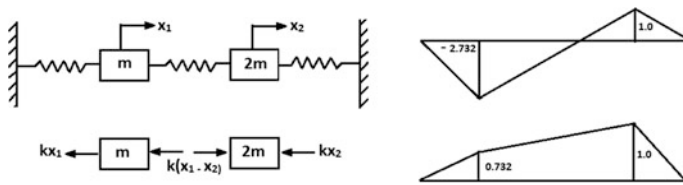
Let the displacement of the two masses be x_1 and x_2 from mean equilibrium positions. Assuming $x_1 > x_2$, for the free body diagrams shown, the differential equations of motion as obtained by applying Newton's law are given by

$$m\ddot{x}_1 = -k(x_1 - x_2) - kx_1$$

$$2m\ddot{x}_2 = k(x_1 - x_2) - kx_2$$

Let the assumed solutions be $x_1 = A\sin\omega t$ and $x_2 = B\sin\omega t$.
Substituting for x_1 and x_2 and their derivatives in the differential equations of motion, we have

$$(2k - m\omega^2)A - kB = 0$$

$$-kA + (2k - 2m\omega^2)B = 0$$

The amplitude ratios from above two equations are

$$\frac{A}{B} = \frac{k}{2k - m\omega^2} = \frac{2k - 2m\omega^2}{k}$$

or

$$(2k - 2m\omega^2)(2k - m\omega^2) = k^2$$

Simplifying further, the quadratic equation in ω^2 is

$$\omega^4 - \left(\frac{3k}{m}\right)\omega^2 + \left(\frac{3k^2}{2m^2}\right) = 0$$

The roots of quadratic equation are

$$\omega^2 = \left(\frac{3 \pm \sqrt{3}}{2}\right)\frac{k}{m}$$

Therefore, $\omega_1^2 = 2.366k/m$ and $\omega_2^2 = 0.634k/m$.
So

$$\omega_1 = \sqrt{2.366k/m} \text{ and } \omega_2 = \sqrt{0.634k/m}$$

To obtain the first principal mode of vibration, substitute $\omega^2 = 2.366k/m$ in the expression for amplitude ratio. We get

$$\left(\frac{A}{B}\right)_1 = \frac{2k - (2m)(2.366)(k/m)}{k} = \frac{2k - 4.732k}{k} = -2.732$$

The second principal mode of vibration is obtained by substituting $\omega^2 = 0.634k/m$

$$\left(\frac{A}{B}\right)_2 = \frac{2k - (2m)(0.634)(k/m)}{k} = \frac{0.732k}{k} = 0.732$$

Mode shapes are shown in the figure.

23. One type of seismograph, a device that records earthquakes, can be modeled as shown in the below figure. Determine (a) the differential equations of motion, (b) the frequency equation and the natural frequencies.
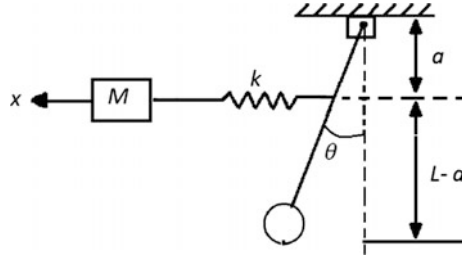
The figure shows the model of the seismograph in displaced position. Let the displacement of the mass M be x and that of the oscillating pendulum be θ from static equilibrium position. Let us assume θ to be small. Applying Newton's law to the free body diagram of the mass, we have

$$M\ddot{x} = -k(x - a\theta)$$

Similarly, applying Newton's law to free body diagram of the pendulum by taking moments of inertia about the pivot O, we get

$$I_0\ddot{\theta} = -mgL\theta + ka(x - a\theta)$$

Neglecting the mass moment of inertia of the bob about its own centre of gravity, we get

$$I = mL^2$$

For obtaining solutions to the differential equations of motion, let us assume that

$$x = A\,\sin \omega t \text{ and } = B\,\sin \omega t$$

$$\left(k - M\omega^2\right)A - kaB = 0$$

$$-kaA + \left(mgL + ka^2 - I_0\omega^2\right)B = 0$$

Amplitude ratios are given by

$$\frac{A}{B} = \frac{ka}{k - M\omega^2} = \frac{mgL + ka^2 - mL^2\omega^2}{ka}$$

This leads to the quadratic equation in ω^2 as given below:

$$\left(\omega^2\right)^2 - \left[\frac{k}{M} + \frac{mgL + ka^2}{mL^2}\right]\omega^2 + \frac{kg}{ML} = 0$$

$$\omega_{1,2}^2 = \frac{1}{2}\left[\frac{k}{M} + \frac{mgL + ka^2}{mL^2}\right] \pm \frac{1}{2}\sqrt{\left[\frac{k}{M} + \frac{mgL + ka^2}{mL^2}\right]^2 - 4\frac{kg}{ML}}$$

24. Find the flexibility influence coefficients of the system shown below

(a)   (b)   (c)   (d)
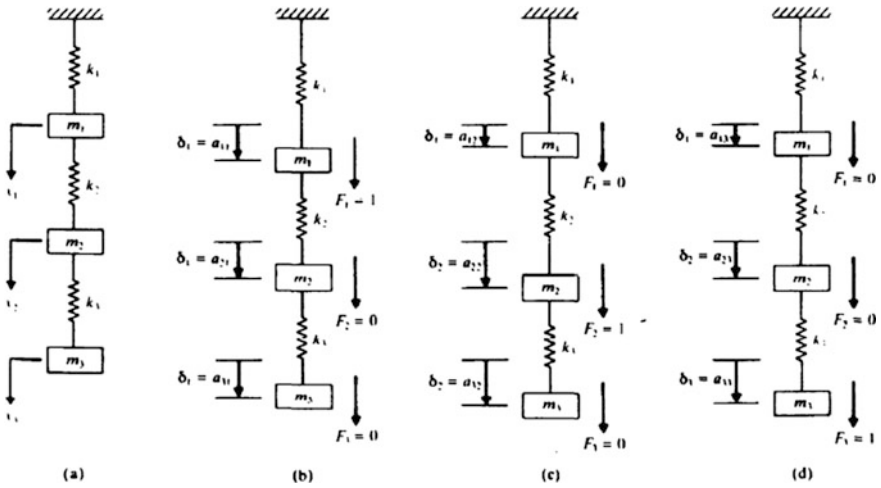
Let $x_1, x_2, \ldots$ and x_n denote the displacements of the masses $m_1, m_2, \ldots$ and m_n, respectively. The flexibility influence coefficients of the system can be determined in terms of the spring stiffness k_1, k_2, and k_n, as follows. If we apply a unit force at mass m_1, and no force at the other masses ($F1= 1$, $F2 = 0$, $F3 = 0$), as shown in Figure (b). The deflection of the mass m_1, is equal to $\delta 1$, $=1/k_1$, $=a_{11}$. Since the other two masses m_2, and m_3, move undergo rigid body translation) by the same amount of deflection δ_1. We have, by definition the following:

$$a_{21} = a_{31} = \delta 1 = \frac{1}{k_1}$$

Next we apply a unit force at mass m_2 and no force at masses m_1 and m_3. As shown in Figure (c) since the two springs k_1 and k_2 offer resistance. The deflection of mass is given by

$$\delta_2 = \frac{1}{k_{eq}} = \frac{1}{k_1} + \frac{1}{k_2} = \frac{k_1 + k_2}{k_1 k_2} = a_{22}$$

The mass m_3, undergoes the same displacement δ_2 (rigid body translation) while the mass m_1, moves through a smaller distance given by $\delta_1 = 1/k_1$, Hence

$$a_{32} = \delta_2 = \frac{k_1 + k_2}{k_1 k_2} \quad \text{and} \quad a_{12} = \delta_1 = \frac{1}{k_1}$$

Finally, when we apply a unit force to mass m_3 and no force to masses m_1, and m_2. as shown in Figure (d). The displacement of mass m_3 is given by

$$\delta_3 = \frac{1}{k_1} + \frac{1}{k_2} + \frac{1}{k_3} = \frac{k_1 + k_2 + k_3}{k_1 k_2 k_3} = a_{33}$$

While the displacements of masses m_2 and m_1 are given by

$$\delta_2 = \frac{1}{k_1} + \frac{1}{k_2} = \frac{k_1 + k_2}{k_1 k_2} = a_{23}$$

and

$$a_{13} = \delta_1 = \frac{1}{k_1}$$

According to Maxwell's reciprocity theorem, we have

$$a_{ij} = a_{ji}$$

Thus the flexibility matrix of the system is given by

$$[a] = \begin{bmatrix} \frac{1}{k_1} & \frac{1}{k_1} & \frac{1}{k_1} \\ \frac{1}{k_1} & \left(\frac{1}{k_1} + \frac{1}{k_2}\right) & \left(\frac{1}{k_1} + \frac{1}{2}\right) \\ \frac{1}{k_1} & \left(\frac{1}{k_1} + \frac{1}{k_2}\right) & \left(\frac{1}{k_1} + \frac{1}{k_2} + \frac{1}{k_3}\right) \end{bmatrix}$$

The stiffness matrix of the system can be found from the relation $[k] = [a] - 1$ or can be derived by using the definition of k_{ij}.

$$[k] = \begin{bmatrix} (k_1 + k_2) & -k_2 & 0 \\ -k_2 & (k_2 + k_3) & -k_3 \\ 0 & -k_3 & k_3 \end{bmatrix}$$

25. Determine the natural frequency coefficient of the spring–mass system shown below by Dunkerley's method?
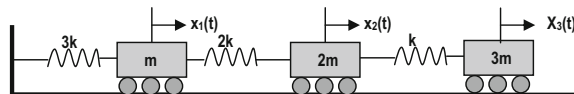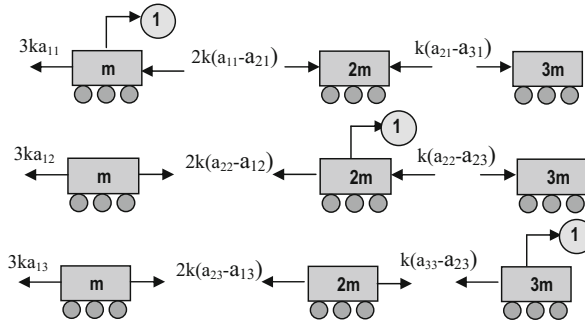
$$a_{11} = a_{12} = a_{13} = 1/3k$$

$$a_{21} = a_{31} = 1/3k$$

$$a_{22} = 1/3k + 1/2k = 5/6k$$

$$a_{22} = a_{32} = a_{23}$$

$$a_{33} = 1/3k + 1/2k + 1/k = 11/6k$$

Influence coefficient matrix is given by

$$\begin{bmatrix} a_{11} & a_{12} & a_{13} \\ a_{21} & a_{22} & a_{23} \\ a_{31} & a_{32} & a_{33} \end{bmatrix}$$

as compared with the Dunkerley's matrix $1/m \begin{bmatrix} 1/\omega_1^2 & \dots & \dots \\ \dots & 1/\omega_2^2 & \dots \\ \dots & \dots & 1/\omega_3^2 \end{bmatrix}$

Dunkerley's frequency is given by

$$1/\omega^2 = 1/\omega_1^2 + 1/\omega_2^2 + 1/\omega_3^2$$

On substituting we get

$$1/\omega^2 = 23m/6k$$

$$\omega = 0.511\sqrt{k/m}$$

26. Determine the natural frequencies and modes shapes of the system shown in the above figure by matrix iteration method? The influence coefficients are given below

$$a_{11} = a_{12} = a_{13} = a_{21} = a_{31} = \frac{1}{2k}$$

$$a_{22} = a_{23} = a_{32} = \frac{3}{2k}$$

$$a_{33} = \frac{5}{2k}$$

The equations for the above system in terms of influence coefficients can be written as

$$x_1 = 2ma_{11}x_1\omega^2 + 2ma_{12}x_2\omega^2 + 2ma_{13}x_3\omega^2$$

$$x_2 = 2ma_{21}x_1\omega^2 + 2ma_{22}x_2\omega^2 + 2ma_{23}x_3\omega^2$$

$$x_3 = 2ma_{31}x_1\omega^2 + 2ma_{32}x_2\omega^2 + 2ma_{33}x_3\omega^2$$

The equation can be written in matrix form as

$$\begin{Bmatrix} x_1 \\ x_2 \\ x_3 \end{Bmatrix} = m\omega^2 \begin{bmatrix} 2a_{11} & 2a_{12} & 2a_{13} \\ 2a_{21} & 2a_{22} & 2a_{23} \\ 2a_{31} & 2a_{32} & 2a_{33} \end{bmatrix} \begin{Bmatrix} x_1 \\ x_2 \\ x_3 \end{Bmatrix}$$

$$= m\omega^2 \begin{bmatrix} \frac{1}{k} & \frac{1}{k} & \frac{1}{2k} \\ \frac{1}{k} & \frac{3}{k} & \frac{3}{2k} \\ \frac{1}{k} & \frac{3}{k} & \frac{5}{2k} \end{bmatrix} \begin{Bmatrix} x_1 \\ x_2 \\ x_3 \end{Bmatrix}$$

$$\begin{Bmatrix} x_1 \\ x_2 \\ x_3 \end{Bmatrix} = \frac{m\omega^2}{k} \begin{bmatrix} 1 & 1 & 1/2 \\ 1 & 3 & 3/2 \\ 1 & 3 & 5/2 \end{bmatrix} \begin{Bmatrix} x_1 \\ x_2 \\ x_3 \end{Bmatrix}$$

First iteration

Let us assume $\begin{Bmatrix} x_1 \\ x_2 \\ x_3 \end{Bmatrix} = \begin{Bmatrix} 1 \\ 1 \\ 1 \end{Bmatrix}$

$$\begin{Bmatrix} 1 \\ 1 \\ 1 \end{Bmatrix} = \frac{m\omega^2}{k} \begin{bmatrix} 1 & 1 & 1/2 \\ 1 & 3 & 3/2 \\ 1 & 3 & 5/2 \end{bmatrix} = 2.5\frac{m\omega^2}{k} \begin{Bmatrix} 1 \\ 2.2 \\ 2.6 \end{Bmatrix}$$

Second iteration

$$\begin{Bmatrix} 1 \\ 2.2 \\ 2.6 \end{Bmatrix} = \frac{m\omega^2}{k} \begin{bmatrix} 1 & 1 & 1/2 \\ 1 & 3 & 3/2 \\ 1 & 3 & 5/2 \end{bmatrix} \begin{Bmatrix} 1 \\ 2.2 \\ 2.6 \end{Bmatrix} = 4.5 \frac{m\omega^2}{k} \begin{Bmatrix} 1 \\ 2.555 \\ 3.133 \end{Bmatrix}$$

Third iteration

$$\begin{Bmatrix} 1 \\ 2.555 \\ 3.133 \end{Bmatrix} = \frac{m\omega^2}{k} \begin{bmatrix} 1 & 1 & 1/2 \\ 1 & 3 & 3/2 \\ 1 & 3 & 5/2 \end{bmatrix} \begin{Bmatrix} 1 \\ 2.555 \\ 3.133 \end{Bmatrix} = 5.12 \frac{m\omega^2}{k} \begin{Bmatrix} 1 \\ 2.61 \\ 3.22 \end{Bmatrix}$$

Fourth iteration

$$\begin{Bmatrix} 1 \\ 2.61 \\ 3.22 \end{Bmatrix} = \frac{m\omega^2}{k} \begin{bmatrix} 1 & 1 & 1/2 \\ 1 & 3 & 3/2 \\ 1 & 3 & 5/2 \end{bmatrix} \begin{Bmatrix} 1 \\ 2.61 \\ 3.22 \end{Bmatrix} = 5.22 \frac{m\omega^2}{k} \begin{Bmatrix} 1 \\ 2.61 \\ 3.23 \end{Bmatrix}$$

So

$$1 = 5.22 \frac{m\omega^2}{k}, \quad \omega^2 = \frac{1}{5.22} \frac{k}{m}$$

Thus $\omega_1 = 0.437 \sqrt{\frac{k}{m}}$.

To find the second principle mode, the orthogonality relation is used as

$$\begin{Bmatrix} x_1 \\ x_2 \\ x_3 \end{Bmatrix} = \frac{m\omega^2}{k} \begin{bmatrix} 1 & 1 & 1/2 \\ 1 & 3 & 3/2 \\ 1 & 3 & 5/2 \end{bmatrix} \begin{bmatrix} 0 & \frac{-m_2}{m_1}\left(\frac{x_2}{x_1}\right) & \frac{-m_3}{m_1}\left(\frac{x_3}{x_1}\right) \\ 0 & 1 & 0 \\ 0 & 0 & 1 \end{bmatrix} \begin{Bmatrix} x_1 \\ x_2 \\ x_3 \end{Bmatrix}$$

$$= \frac{m\omega^2}{k} \begin{bmatrix} 1 & 1 & 1/2 \\ 1 & 3 & 3/2 \\ 1 & 3 & 5/2 \end{bmatrix} \begin{bmatrix} 0 & -\left(\frac{2.61}{1}\right) & -\frac{1}{2}(3.23) \\ 0 & 1 & 0 \\ 0 & 0 & 1 \end{bmatrix} \begin{Bmatrix} x_1 \\ x_2 \\ x_3 \end{Bmatrix}$$

$$= \frac{m\omega^2}{k} \begin{bmatrix} 0 & -1.61 & -1.11 \\ 0 & 0.39 & -0.11 \\ 0 & 0.39 & 1.89 \end{bmatrix} \begin{Bmatrix} x_1 \\ x_2 \\ x_3 \end{Bmatrix}$$

First iteration

Let us say $\begin{Bmatrix} x_1 \\ x_2 \\ x_3 \end{Bmatrix} = \begin{Bmatrix} 1 \\ 0 \\ -1 \end{Bmatrix}$

$$\begin{Bmatrix} 1 \\ 0 \\ -1 \end{Bmatrix} = \frac{m\omega^2}{k} \begin{bmatrix} 0 & -1.61 & -1.11 \\ 0 & 0.39 & -0.11 \\ 0 & 0.39 & 1.89 \end{bmatrix} \begin{Bmatrix} 1 \\ 0 \\ -1 \end{Bmatrix} = 0.11 \frac{m\omega^2}{k} \begin{Bmatrix} 10.9 \\ 1 \\ -17.18 \end{Bmatrix}$$

Second iteration

$$\begin{Bmatrix} 10.9 \\ 1 \\ -17.18 \end{Bmatrix} = \frac{m\omega^2}{k} \begin{bmatrix} 0 & -1.61 & -1.11 \\ 0 & 0.39 & -0.11 \\ 0 & 0.39 & 1.89 \end{bmatrix} \begin{Bmatrix} 10.9 \\ 1 \\ -17.18 \end{Bmatrix}$$
$$= 2.28 \frac{m\omega^2}{k} \begin{Bmatrix} 7.65 \\ 1 \\ -14 \end{Bmatrix}$$

Third iteration

$$\begin{Bmatrix} 7.65 \\ 1 \\ -14 \end{Bmatrix} = \frac{m\omega^2}{k} \begin{bmatrix} 0 & -1.61 & -1.11 \\ 0 & 0.39 & -0.11 \\ 0 & 0.39 & 1.89 \end{bmatrix} \begin{Bmatrix} 7.65 \\ 1 \\ -14 \end{Bmatrix} = 1.93 \frac{m\omega^2}{k} \begin{Bmatrix} 7.2 \\ 1 \\ -13.5 \end{Bmatrix}$$

Fourth iteration

$$\begin{Bmatrix} 7.2 \\ 1 \\ -13.5 \end{Bmatrix} = \frac{m\omega^2}{k} \begin{bmatrix} 0 & -1.61 & -1.11 \\ 0 & 0.39 & -0.11 \\ 0 & 0.39 & 1.89 \end{bmatrix} \begin{Bmatrix} 7.2 \\ 1 \\ -13.5 \end{Bmatrix}$$
$$= 1.875 \frac{m\omega^2}{k} \begin{Bmatrix} 7.13 \\ 1 \\ -13.4 \end{Bmatrix}$$

Fifth iteration

$$\left\{\begin{array}{c} 7.13 \\ 1 \\ -13.4 \end{array}\right\} = \frac{m\omega^2}{k} \begin{bmatrix} 0 & -1.61 & -1.11 \\ 0 & 0.39 & -0.11 \\ 0 & 0.39 & 1.89 \end{bmatrix} \left\{\begin{array}{c} 7.13 \\ 1 \\ -13.4 \end{array}\right\}$$

$$= 1.864 \frac{m\omega^2}{k} \left\{\begin{array}{c} 7.11 \\ 1 \\ -13.37 \end{array}\right\}$$

So

$$1 = 1.864 \frac{m\omega^2}{k}$$

$$\omega_2 = 0.73 \sqrt{k/m} \text{ rad/s}$$
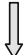
Similarly using Orthogonality relation, we can find ω_3 which is found to be $\omega_3 = 1.41 \sqrt{k/m}$.

27. Determine fundamental frequency of the system using Stodola method.
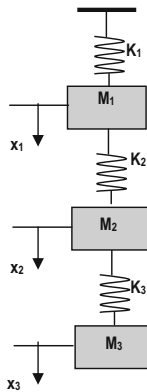
Force is necessary to cause deflection in the elastic system. In case of free vibration, only imaginary force responsible for causing deflection is the inertia force. Let Mr be the mass and Δr be the maximum deflection of the mass. ω be the vibrating frequency. Maximum inertia force is $m\ddot{x} = mr\omega^2 \Delta r$.

Let us assume that $m_1 = m_2 = m_3 = m$ and $k_1 = k_2 = k_3 = k$.

Description	k_1	m_1	k_2	m_2	k_3	m_3
Assumed deflection		1		1		1
Inertia force		$m_1\omega^2(1)$		$m_2\omega^2(1)$		$m_3\omega^2(1)$
Spring force						
	$3\,m\omega^2$		$2\,m\omega^2$		$m\omega2$	
Spring deflection	$3\,m\omega^2/k_1 =$ $3\,m\omega^2/k$		$2\,m\omega^2/k_2$ $=$ $2\,m\omega^2/k$		$m\omega^2/k_3 =$ $m\omega^{2/}k$	
Calculated deflection $(m\omega^2/k)$		3		5		6
		1		1.67		2
Assumed deflection		1		1.67		2
Inertia force		$m\omega^2$		$1.67\,m\omega^2$		$2\,m\omega^2$
Spring force	$4.67\,m\omega^2$		$3.67\,m\omega^2$		$2\,m\omega^2$	
Spring deflection	$4.67\,m\omega^2/k$		3.67 $m\omega^2/k$		$2\,m\omega^2/k$	
Calculated deflection $(m\omega^2/k)$		4.67		8.34		10.34
		1		1.79		2.21
Assumed deflection		1		1.79		2.21
Inertia force		$m\omega^2$		$1.79\,m\omega^2$		$2.21\,m\omega^2$
Spring force	$5\,m\omega^2$		$4\,m\omega^2$		$2.21\,m\omega^2$	
Spring deflection	$5\,m\omega^2/k$		$4\,m\omega^2/k$		$2.21\,m\omega^2/k$	
Calculated deflection $(m\,\omega^2/k)$		5		9		11.21
CONVERGED VALUES		1		1.80		2.24

$(1.0 + 1.8 + 2.24) = (5 + 9 + 11.21)\ m\omega^2/k$. Therefore, fundamental frequency is given by

$$\omega = \sqrt{\frac{k}{m}} \sqrt{\frac{(1+1.8+2.24)}{(5+9+11.21)}} = 0.447 \sqrt{\frac{k}{m}} \, \text{rad/s.}$$

Corresponding mode shape is given by the following vector: $\left\{ \begin{array}{c} 1 \\ 1.8 \\ 2.24 \end{array} \right\}$

28. For coulomb damping system with mass m = 200 kg, k = 1500 N/m, and μk = 0.1 and calculate the decay per cycle. Take g = 9.81 m/s^2.

The decay per cycle is $4\dfrac{f_d}{k} = \dfrac{4\mu_k mg}{k} = \dfrac{4*0.1*200*9.81}{1500} = 0.5232$ m.

29. Consider the harmonic oscillator described by $m\ddot{x} + \omega_n^2 x = 0$. Let m = 20 kg and k = 1800 N/m and calculate the response $x(t)$ for initial condition $x_0 = x(0) = 0.1$ m, $v_0 = \dot{x}(0) = 0.2$ m/s.

The natural frequency of the oscillator is $\omega_n = \sqrt{\frac{k}{m}} = \sqrt{\frac{1800}{20}} = 9.487$ rad/s

Amplitude is $\sqrt{x_0^2 + \left(\frac{v_o}{\omega_n}\right)^2} = \sqrt{0.1^2 + \left(\frac{0.2}{9.487}\right)^2} = 0.1022$ m

The phase angle is $\varphi = \tan^{-1}\left(\frac{v_o}{x_o \omega_n}\right) = \tan^{-1}\left(\frac{0.2}{0.1 \times 9.487}\right) = 11.9045$ rad

$$x(t) = A\cos(\omega t - \varphi) = 0.1022 \, \cos(9.487t - 11.9045) \, \text{m}$$

30. It was observed that vibration amplitude of a damped SDOF system has fallen by 50% after five complete cycles. Assume that the system is viscous damped and calculate the damping factor ζ. Let the no of cycles be 5 nos.

$$M = 5; \quad \delta = \frac{1}{m}\ln\left(\frac{x_n}{x_{m+n}}\right) = \frac{1}{5}\ln\left(\frac{x_n}{0.5x_n}\right) = 0.1386$$

Considering the maximum $\zeta = \frac{\delta}{2\pi} = \frac{0.1386}{2\pi} = 0.0221 = 2.2064\%$.

31. Define damping ratio.

$$\text{Damping ratio} = \zeta = \frac{\text{damping constant}}{\text{damping constant for crtically damped system}} = \frac{C}{C_{cr}}$$

32. For SDOF system, m = 4 kg, k = 1.6 × 103 N m^{-1} and the two cases of damping: (a) c_1 = 80 N m^{-1} s^{-1}; (b) c_2 = 320 N m^{-1} s^{-1}. Calculate the damping ratio for the two cases.

$$\omega_n = \sqrt{\tfrac{k}{m}} = \sqrt{\tfrac{1.6\times10^3}{4}} = 20 \text{ rad/s}; \quad \zeta_1 = \tfrac{C_1}{C_{cr}} = \tfrac{80}{2\times4\times20} = 0.5;$$

$$\zeta_2 = \tfrac{C_2}{C_{cr}} = \tfrac{320}{2\times4\times20} = 2$$

33. A 200-kg machine is placed at the end of 1.8-m long steel cantilever beam. The machine is observed to vibrate with natural frequency of 21 Hz. What is the moment of inertia of the beam's cross section about its neutral axis.

$$\omega_n = 21 \text{ Hz} = \left(21\frac{\text{cycles}}{s}\right)\left(2\pi \frac{\text{rad}}{\text{cycle}}\right) = 131.9469 \text{ rad/s};$$

$k_{equ} = m\omega^2 = (200\,\text{kg} \times (131.9\,\text{rad/s})^2) = 3.4820 \times 10^6 \text{ N/m}; \quad k_{equ} = 3EI/L^3;$

$\quad I = (k_{equ} * L^3)/(3E); \quad I = (3.4820 \times 10^6 \text{ N/m} * 1.8^3 \text{ m}^3)/(3 \times 210 \times 10^9 \text{ N/m}^2)$

$\quad = 3.2215 \times 10^{-5} \text{ m}^4.$

34. A 60 kg drum of the diameter 40 cm containing the waste material of mass density 1100 kg/m^3 is being hoisted by a 30-mm diameter steel ($E = 210 \times 109$ N/m^2) cable. When the drum is to be hoisted 10 m, the system natural frequency is measured as 40 Hz. Determine the volume of the drum. (*Hint*: $K_{equ} = AE/L$).

$$K_{equ} = \frac{AE}{L} = \frac{(\pi \times 0.015^2 \text{ m}^2)(210 \times 10^9 \text{ N/m}^2)}{10\,\text{m}} = 1.4844 \times 107 \text{ N/m};$$

$\omega_n = \sqrt{\tfrac{k_{equ}}{m}}; \quad \left[\left(40\frac{\text{cycles}}{S}\right)\left(2\pi\frac{\text{rad}}{S}\right)\right]^2 = \frac{1.4844\times10^7}{M}; \quad M = 235.0018 \text{ kg};$

$Mw = M - M_d = 235.0018 - 60 = 175.0018 \text{ kg};$

Volume of the drum = Mass/Mass density = 175.0018 kg/1100 kg/m^3 = 0.1591 m^3

35. For what value of *m* will resonance occur for the system shown below:
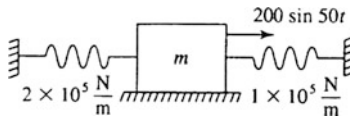
Springs are in parallel as the block is fixed and the equivalent stiffness of 3×105 N/m. Resonance occurs when excitation frequency 50 rad/s is equal to natural frequency. 50 rad/s $= \omega_n = \sqrt{\tfrac{k_{equ}}{m}}; \ m = \tfrac{k_{equ}}{\omega_n^2} = \tfrac{3\times10^5 N/m}{(50\,rad/S)^2} = 120$ kg.

36. A 35-kg electric motor that operates at 60 Hz is mounted on the elastic foundation of stiffness 3×106 N/m. The phase difference between the excitation and steady-state response is $21°$. What is the damping ratio of system?

$$\omega_n = \sqrt{\frac{k}{m}} = \sqrt{\frac{3 \times 10^6 \text{ N/m}}{35 \text{ kg}}} = 292.77 \text{ rad/s};$$

$$\beta = \frac{\omega}{\omega_n} = \left[\frac{(60 \text{ cycles/s})(2\pi \text{ rad/cycle})}{292.77 \text{ rad/s}}\right] = 1.2877;$$

$$\tan\theta = \frac{2\zeta\beta}{1 - \beta^2}; \quad \tan(180 - 21) = \frac{2 \times \zeta \times 1.2877}{1 - 1.2877^2}; \quad \zeta = 0.0982 = 9.8154\%$$

37. Evaluate the Frequency and mode shape for the MDOF system using Influence coefficient method. Use Dunkerley's method to evaluate natural frequency of the system.
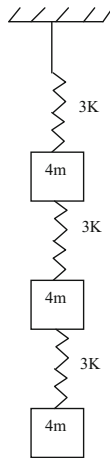
$$[\alpha] = \frac{1}{3k}\begin{bmatrix} 1 & 1 & 1 \\ 1 & 2 & 2 \\ 1 & 2 & 3 \end{bmatrix}$$

$\omega_{\text{Dunkerley}}$

$$\frac{1}{\omega^2} = 4m\left(\frac{1}{3k}\right) + 4m\left(\frac{2}{3k}\right) + 4m\left(\frac{3}{3k}\right) = \frac{24m}{3k}$$

$$\omega^2 = \frac{3k}{24m}$$

$$\omega = 0.354 \sqrt{\frac{k}{m}} \text{ rad/s}$$

Influence coefficient method

$$\begin{Bmatrix} x_1 \\ x_2 \\ x_3 \end{Bmatrix} = \frac{m\omega^2}{3k} \begin{bmatrix} 4 & 4 & 4 \\ 4 & 8 & 8 \\ 4 & 8 & 12 \end{bmatrix} \begin{Bmatrix} x_1 \\ x_2 \\ x_3 \end{Bmatrix}$$

Assuming $\begin{Bmatrix} x_1 \\ x_2 \\ x_3 \end{Bmatrix} = \begin{Bmatrix} 1 \\ 2 \\ 3 \end{Bmatrix}$;

$$\begin{Bmatrix} x_1 \\ x_2 \\ x_3 \end{Bmatrix} = \frac{24m\omega^2}{3k} \begin{bmatrix} 4 & 4 & 4 \\ 4 & 8 & 8 \\ 4 & 8 & 12 \end{bmatrix} \begin{Bmatrix} 1 \\ 1.83 \\ 2.33 \end{Bmatrix}$$

$$\begin{Bmatrix} x_1 \\ x_2 \\ x_3 \end{Bmatrix} = \frac{20.64m\omega^2}{3k} \begin{bmatrix} 4 & 4 & 4 \\ 4 & 8 & 8 \\ 4 & 8 & 12 \end{bmatrix} \begin{Bmatrix} 1 \\ 1.81 \\ 2.26 \end{Bmatrix}$$

$$\begin{Bmatrix} x_1 \\ x_2 \\ x_3 \end{Bmatrix} = \frac{20.28m\omega^2}{3k} \begin{bmatrix} 4 & 4 & 4 \\ 4 & 8 & 8 \\ 4 & 8 & 12 \end{bmatrix} \begin{Bmatrix} 1 \\ 1.80 \\ 2.25 \end{Bmatrix}$$

$$\begin{Bmatrix} x_1 \\ x_2 \\ x_3 \end{Bmatrix} = \frac{20.20m\omega^2}{3k} \begin{bmatrix} 4 & 4 & 4 \\ 4 & 8 & 8 \\ 4 & 8 & 12 \end{bmatrix} \begin{Bmatrix} 1 \\ 1.80 \\ 2.25 \end{Bmatrix}$$

$$\frac{20.20\, m\, \omega^2}{3k} = 1$$

$$\omega^2 = \frac{3k}{20.20m}$$

$$\omega = 0.385 \sqrt{\frac{k}{m}} \text{ rad/s}$$

38. Evaluate the Frequency and mode shape for the MDOF system using influence coefficient method. Use Dunkerley's method to evaluate natural frequency of the system.
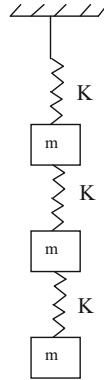
$$[\alpha] = \frac{1}{k} \begin{bmatrix} 1 & 1 & 1 \\ 1 & 2 & 2 \\ 1 & 2 & 3 \end{bmatrix}$$

$\omega_{\text{Dunkerley}}$

$$\frac{1}{\omega^2} = m\left(\frac{1}{k}\right) + m\left(\frac{2}{k}\right) + m\left(\frac{3}{k}\right) = \frac{6m}{k}$$

$$\omega^2 = \frac{k}{6m}$$

$$\omega = 0.408 \sqrt{\frac{k}{m}} \text{ rad/s}$$

Influence coefficient method

$$\begin{Bmatrix} x_1 \\ x_2 \\ x_3 \end{Bmatrix} = \frac{m\omega^2}{k} \begin{bmatrix} 1 & 1 & 1 \\ 1 & 2 & 2 \\ 1 & 2 & 3 \end{bmatrix} \begin{Bmatrix} x_1 \\ x_2 \\ x_3 \end{Bmatrix}$$

Assuming $\begin{Bmatrix} x_1 \\ x_2 \\ x_3 \end{Bmatrix} = \begin{Bmatrix} 1 \\ 2 \\ 3 \end{Bmatrix}$;

$$\begin{Bmatrix} x_1 \\ x_2 \\ x_3 \end{Bmatrix} = \frac{6m\omega^2}{k} \begin{bmatrix} 1 & 1 & 1 \\ 1 & 2 & 2 \\ 1 & 2 & 3 \end{bmatrix} \begin{Bmatrix} 1 \\ 1.83 \\ 2.33 \end{Bmatrix}$$

$$\begin{Bmatrix} x_1 \\ x_2 \\ x_3 \end{Bmatrix} = \frac{5.16m\omega^2}{k} \begin{bmatrix} 1 & 1 & 1 \\ 1 & 2 & 2 \\ 1 & 2 & 3 \end{bmatrix} \begin{Bmatrix} 1 \\ 1.81 \\ 2.26 \end{Bmatrix}$$

$$\begin{Bmatrix} x_1 \\ x_2 \\ x_3 \end{Bmatrix} = \frac{5.07m\omega^2}{k} \begin{bmatrix} 1 & 1 & 1 \\ 1 & 2 & 2 \\ 1 & 2 & 3 \end{bmatrix} \begin{Bmatrix} 1 \\ 1.81 \\ 2.25 \end{Bmatrix}$$

$$\begin{Bmatrix} x_1 \\ x_2 \\ x_3 \end{Bmatrix} = \frac{5.05m\omega^2}{k} \begin{bmatrix} 1 & 1 & 1 \\ 1 & 2 & 2 \\ 1 & 2 & 3 \end{bmatrix} \begin{Bmatrix} 1 \\ 1.80 \\ 2.25 \end{Bmatrix}$$

$$\frac{5.05m\omega^2}{k} = 1$$

$$\omega^2 = \frac{k}{5.05m}$$

$$\omega = 0.445 \sqrt{\frac{k}{m}} \text{ rad/s}$$

39. Evaluate the fundamental frequency and mode shape for the MDOF system using Dunkerley's method, influence coefficient method, Stodola method, and Rayleigh–Ritz method.
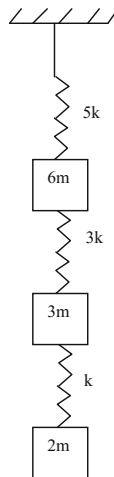
Dunkerley's Method

$$[\alpha] = \frac{1}{15k} \begin{bmatrix} 3 & 3 & 3 \\ 3 & 8 & 8 \\ 3 & 8 & 23 \end{bmatrix}$$

ω Dunkerley

$$\frac{1}{\omega^2} = 6m\left(\frac{13}{15k}\right) + 3m\left(\frac{8}{15k}\right) + 2m\left(\frac{23}{15k}\right) = \frac{88m}{15k}$$

$$\omega^2 = \frac{15k}{88m}$$

$$\omega = 0.41\sqrt{\frac{k}{m}} \text{ rad/s}$$

Influence Coefficient Method

$$\begin{Bmatrix} x_1 \\ x_2 \\ x_3 \end{Bmatrix} = \frac{m\,\omega^2}{15k} \begin{bmatrix} 18 & 9 & 6 \\ 18 & 24 & 16 \\ 18 & 24 & 46 \end{bmatrix} \begin{Bmatrix} x_1 \\ x_2 \\ x_3 \end{Bmatrix}$$

Assuming $\begin{Bmatrix} x_1 \\ x_2 \\ x_3 \end{Bmatrix} = \begin{Bmatrix} 1 \\ 2 \\ 3 \end{Bmatrix}$;

$$\begin{Bmatrix} x_1 \\ x_2 \\ x_3 \end{Bmatrix} = \frac{54m\omega^2}{15k} \begin{bmatrix} 18 & 9 & 6 \\ 18 & 24 & 16 \\ 18 & 24 & 46 \end{bmatrix} \begin{Bmatrix} 1 \\ 2.11 \\ 3.78 \end{Bmatrix}$$

$$\begin{Bmatrix} x_1 \\ x_2 \\ x_3 \end{Bmatrix} = \frac{59.67m\omega^2}{15k} \begin{bmatrix} 18 & 9 & 6 \\ 18 & 24 & 16 \\ 18 & 24 & 46 \end{bmatrix} \begin{Bmatrix} 1 \\ 2.16 \\ 4.06 \end{Bmatrix}$$

$$\begin{Bmatrix} x_1 \\ x_2 \\ x_3 \end{Bmatrix} = \frac{61.855 m\omega^2}{15k} \begin{bmatrix} 18 & 9 & 6 \\ 18 & 24 & 16 \\ 18 & 24 & 46 \end{bmatrix} \begin{Bmatrix} 1 \\ 2.18 \\ 4.15 \end{Bmatrix}$$

$$\begin{Bmatrix} x_1 \\ x_2 \\ x_3 \end{Bmatrix} = \frac{62.549 m\omega^2}{15k} \begin{bmatrix} 18 & 9 & 6 \\ 18 & 24 & 16 \\ 18 & 24 & 46 \end{bmatrix} \begin{Bmatrix} 1 \\ 2.19 \\ 4.18 \end{Bmatrix}$$

$$\begin{Bmatrix} x_1 \\ x_2 \\ x_3 \end{Bmatrix} = \frac{62.79 m\omega^2}{15k} \begin{bmatrix} 18 & 9 & 6 \\ 18 & 24 & 16 \\ 18 & 24 & 46 \end{bmatrix} \begin{Bmatrix} 1 \\ 2.19 \\ 4.19 \end{Bmatrix}$$

$$\begin{Bmatrix} x_1 \\ x_2 \\ x_3 \end{Bmatrix} = \frac{62.85 m\omega^2}{15k} \begin{bmatrix} 18 & 9 & 6 \\ 18 & 24 & 16 \\ 18 & 24 & 46 \end{bmatrix} \begin{Bmatrix} 1 \\ 2.19 \\ 4.19 \end{Bmatrix}$$

$$\frac{62.85\, m\, \omega^2}{15k} = 1$$

$$\omega^2 = \frac{15k}{62.85m}$$

$$\omega = 0.49 \sqrt{\frac{k}{m}}\,\text{rad/s}$$

Stodola Method

Description	$k_1 = 5k$	$m_1 = 6m$	$k_2 = 3k$	$m_2 = 3m$	$k_3 = k$	$m_3 = 2m$
Assumed deflection		1		2		4
Inertia force		$m\omega^2(6)$		$m\omega^2(6)$		$m\omega^2(8)$
Spring force	$20\omega^2$		$14m\omega^2$		$8m\omega^2$	
Spring deflection	$4m\omega^2/k$		$4.67m\omega^2/k$		$8m\omega^2/k$	
Calculated deflection $(m\omega^2/k)$		4		8.67		16.67
		1		2.17		4.17
Assumed deflection		1		2.17		4.17

(continued)

Description	$k_1 = 5k$	$m_1 = 6m$	$k_2 = 3k$	$m_2 = 3m$	$k_3 = k$	$m_3 = 2m$
Inertia force		$6m\omega2$		$6.51m\omega^2$		$8.34m\omega^2$
Spring force	$20.85m\omega^2$		$14.85m\omega^2$		$8.34m\omega^2$	
Spring deflection	$4.17m\omega^2/k$		$4.95\ m\omega^2/k$		$8.34\ m\omega^2/k$	
Calculated deflection ($m\omega^2/k$)		4.17		9.12		17.47
		1		2.19		4.19
Assumed deflection		1		2.19		4.19
Inertia force		$6m\omega^2$		$6.57m\omega^2$		$8.38m\omega^2$
Spring force	$20.95m\omega^2$		$14.95m\omega^2$		$8.38m\omega^2$	
Spring deflection	$4.19m\omega^2/k$		$4.98m\omega^2/k$		$8.38m\omega^2/k$	
Calculated deflection ($m\omega^2/k$)		4.19		9.17		17.55
Converged values		1		2.19		4.19

$$(1 + 2.19 + 4.19) = (4.19\omega^2 + 9.17\omega^2 + 17.55\omega^2)m/k$$

$$\omega^2 = \frac{7.38k}{30.91m}$$

$$\omega = 0.49\sqrt{\frac{k}{m}}\ \text{rad/s}$$

Rayleigh–Ritz Method

(1) m	(2) $\varphi r'$	(3) $FI = m\,\varphi r'$	(4)	(5) $\varphi r''/X_1$	(6) $= (3) \times (5)$ $FI \times \varphi r''$	(7) $= (1) \times (5)^2$ $m \times \varphi r''$
$6m$	1	$6m \times 1 = 6m$	$X_1 = \left(\dfrac{(6m+6m+8m)}{5k}\right) = \dfrac{4m}{k}$	1	$\dfrac{6m}{k}$	$6 \times (1)^2 = 6$
$3m$	2	$3m \times 2 = 6m$	$X_2 = \dfrac{4m}{k} + \left(\dfrac{(6m+8m)}{3k}\right) = \dfrac{8.67m}{k}$	2.17	$\dfrac{13.02m}{k}$	$3 \times (2.17)^2 = 14.13$
$2m$	4	$2m \times 4 = 8m$	$X_3 = \dfrac{8.67m}{k} + \left(\dfrac{8m}{k}\right) = \dfrac{16.67m}{k}$	4.17	$\dfrac{33.36m}{k}$ $\Sigma = \dfrac{52.38m}{k}$	$2 \times (4.17)^2 = 34.78$ $\Sigma = 54.91$
$6m$	1	$6m \times 1 = 6m$	$X_1 = \left(\dfrac{(6m+6.51m+8.34m)}{5k}\right) = \dfrac{4.17m}{k}$	1	$\dfrac{6m}{k}$	$6 \times (1)^2 = 6$
$3m$	2.17	$3m \times 2 = 6.51m$	$X_2 = \dfrac{4.17m}{k} + \left(\dfrac{(6.51m+8.34m)}{3k}\right) = \dfrac{9.12m}{k}$	2.19	$\dfrac{14.26m}{k}$	$3 \times (2.19)^2 = 14.39$
$2m$	4.17	$2m \times 4 = 8.34m$	$X_3 = \dfrac{9.12m}{k} + \left(\dfrac{8.34m}{k}\right) = \dfrac{17.46m}{k}$	4.19	$\dfrac{34.94m}{k}$ $\Sigma = \dfrac{45.46m}{k}$	$2 \times (4.19)^2 = 35.11$ $\Sigma = 55.5$
$6m$	1	$6m \times 1 = 6m$	$X_1 = \left(\dfrac{(6m+6.57m+8.38m)}{5k}\right) = \dfrac{4.19m}{k}$	1	$\dfrac{6m}{k}$	$6 \times (1)^2 = 6$
$3m$	2.19	$3m \times 2 = 6.57m$	$X_2 = \dfrac{4.19m}{k} + \left(\dfrac{(6.57m+8.34m)}{3k}\right) = \dfrac{9.17m}{k}$	2.19	$\dfrac{14.39m}{k}$	$3 \times (2.19)^2 = 14.39$
$2m$	4.19	$2m \times 4 = 8.38m$	$X_3 = \dfrac{9.17m}{k} + \left(\dfrac{8.38m}{k}\right) = \dfrac{17.55m}{k}$	4.19	$\dfrac{35.11m}{k}$ $\Sigma = \dfrac{55.5m}{k}$	$2 \times (4.19)^2 = 35.11$ $\Sigma = 55.5$

40. Evaluate the fundamental frequency and mode shape for the MDOF system using Stodola method.
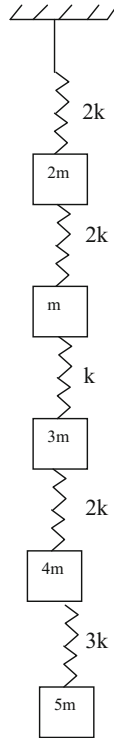
Description	k_1 $2k$	m_1 $2m$	k_2 $2k$	m_2 m	k_3 k	m_3 $3m$	k_4 $2k$	m_4 $4m$	k_5 $3k$	M_5 $5m$
Assumed deflection		1		2		3		4		5
Inertia force $m\omega^2$		2		2		9		16		25
Spring force $m\omega^2$	54		52		50		41		25	
Spring deflection $m\omega^2/k$	27		26		50		20.5		8.33	
Calculated deflection $(m\omega^2/k)$		27		53		103		123.5		131.83
		1		1.96		3.81		4.57		4.88
Assumed deflection		1		1.96		3.81		4.57		4.88

(continued)

Description	k_1 $2k$	m_1 $2m$	k_2 $2k$	m_2 m	k_3 k	m_3 $3m$	k_4 $2k$	m_4 $4m$	k_5 $3k$	M_5 $5m$
Inertia force $m\omega^2$		2		1.96		11.43		18.28		24.4
Spring force $m\omega^2$	58.07		56.07		54.11		42.68		24.4	
Spring deflection $m\omega^2/k$	29.04		28.04		54.11		21.34		8.13	
Calculated deflection $(m\omega^2/k)$		29.04		57.08		111.19		132.53		140.66
		1		1.97		3.83		4.56		4.84
Assumed deflection		1		1.97		3.83		4.56		4.84
Inertia force $m\omega^2$		2		1.96		11.49		18.24		24.2
Spring force $m\omega^2$	57.9		55.9		53.93		42.44		24.2	
Spring deflection $m\omega^2/k$	28.95		27.95		53.93		21.22		8.07	
Calculated deflection $(m\omega^2/k)$		28.95		56.9		110.83		132.05		140.12
Converged values		1		1.97		3.83		4.56		4.84

$$(1 + 1.97 + 3.83 + 4.56 + 4.84) = (28.95 + 56.9 + 110.83 + 132.05 + 140.12)\omega^2 m/k$$

$$\omega^2 = \frac{16.2k}{468.85m}$$

$$\omega = 0.19\sqrt{\frac{k}{m}}\ \text{rad/s}$$

41. Obtain all mode shapes and corresponding frequency of the system shown below:
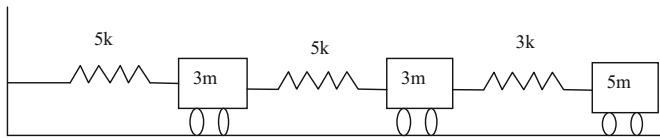
$$[\alpha] = \frac{1}{15k} \begin{bmatrix} 3 & 3 & 3 \\ 3 & 6 & 6 \\ 3 & 6 & 11 \end{bmatrix}$$

Influence coefficient method

$$\begin{Bmatrix} x_1 \\ x_2 \\ x_3 \end{Bmatrix} = \frac{m\omega^2}{15k} \begin{bmatrix} 9 & 9 & 15 \\ 9 & 18 & 30 \\ 3 & 18 & 55 \end{bmatrix} \begin{Bmatrix} x_1 \\ x_2 \\ x_3 \end{Bmatrix}$$

Assuming $\begin{Bmatrix} x_1 \\ x_2 \\ x_3 \end{Bmatrix} = \begin{Bmatrix} 1 \\ 2 \\ 3 \end{Bmatrix}$;

$$\begin{Bmatrix} x_1 \\ x_2 \\ x_3 \end{Bmatrix} = \frac{72m\omega^2}{15k} \begin{bmatrix} 9 & 9 & 15 \\ 9 & 18 & 30 \\ 3 & 18 & 55 \end{bmatrix} \begin{Bmatrix} 1 \\ 1.88 \\ 2.92 \end{Bmatrix}$$

$$\begin{Bmatrix} x_1 \\ x_2 \\ x_3 \end{Bmatrix} = \frac{69.72m\omega^2}{15k} \begin{bmatrix} 9 & 9 & 15 \\ 9 & 18 & 30 \\ 3 & 18 & 55 \end{bmatrix} \begin{Bmatrix} 1 \\ 1.87 \\ 2.92 \end{Bmatrix}$$

$$\begin{Bmatrix} x_1 \\ x_2 \\ x_3 \end{Bmatrix} = \frac{69.63m\omega^2}{15k} \begin{bmatrix} 9 & 9 & 15 \\ 9 & 18 & 30 \\ 3 & 18 & 55 \end{bmatrix} \begin{Bmatrix} 1 \\ 1.87 \\ 2.92 \end{Bmatrix}$$

$$\frac{69.63m\omega^2}{15k} = 1$$

$$\omega^2 = \frac{15k}{69.63m}$$

$$\omega = 0.22\sqrt{\frac{k}{m}} \; \text{rad/s}$$

II. Mode shape

$$\begin{Bmatrix} A_1 \\ B_1 \\ C_1 \end{Bmatrix} = \begin{Bmatrix} 1 \\ 1.87 \\ 2.92 \end{Bmatrix}$$

$$m_1 A_1 A_2 + m_2 B_1 B_2 + m_3 C_1 C_2 = 0$$

$$3mA_2 + 5.61mB_2 + 14.6mC_2 = 0$$

$$A_2 = -1.87B_2 - 4.87C_2$$

$$\begin{Bmatrix} A_2 \\ B_2 \\ C_2 \end{Bmatrix} = \begin{bmatrix} 0 & -1.87 & -4.87 \\ 0 & 1 & 0 \\ 0 & 0 & 1 \end{bmatrix} \begin{Bmatrix} A_2 \\ B_2 \\ C_2 \end{Bmatrix}$$

$$\begin{Bmatrix} x_1 \\ x_2 \\ x_3 \end{Bmatrix} = \frac{m\omega^2}{15k} \begin{bmatrix} 9 & 9 & 15 \\ 9 & 18 & 30 \\ 3 & 18 & 55 \end{bmatrix} \begin{bmatrix} 0 & -1.87 & -4.87 \\ 0 & 1 & 0 \\ 0 & 0 & 1 \end{bmatrix} \begin{Bmatrix} A_2 \\ B_2 \\ C_2 \end{Bmatrix}$$

$$\begin{Bmatrix} x_1 \\ x_2 \\ x_3 \end{Bmatrix} = \frac{m\omega^2}{15k} \begin{bmatrix} 0 & -7.83 & -28.83 \\ 0 & 1.17 & -13.83 \\ 0 & 1.17 & 11.17 \end{bmatrix} \begin{Bmatrix} x_1 \\ x_2 \\ x_3 \end{Bmatrix}$$

$$\text{Assuming} \begin{Bmatrix} x_1 \\ x_2 \\ x_3 \end{Bmatrix} = \begin{Bmatrix} 1 \\ -1 \\ 1 \end{Bmatrix}$$

$$\begin{Bmatrix} x_1 \\ x_2 \\ x_3 \end{Bmatrix} = \frac{m\omega^2}{15k} \begin{bmatrix} 0 & -7.83 & -28.83 \\ 0 & 1.17 & -13.83 \\ 0 & 1.17 & 11.17 \end{bmatrix} \begin{Bmatrix} 1 \\ -1 \\ 1 \end{Bmatrix}$$

$$\begin{Bmatrix} x_1 \\ x_2 \\ x_3 \end{Bmatrix} = \frac{-21m\omega^2}{15k} \begin{bmatrix} 0 & -7.83 & -28.83 \\ 0 & 1.17 & -13.83 \\ 0 & 1.17 & 11.17 \end{bmatrix} \begin{Bmatrix} 1 \\ 0.71 \\ -0.48 \end{Bmatrix}$$

$$\begin{Bmatrix} x_1 \\ x_2 \\ x_3 \end{Bmatrix} = \frac{8.28m\omega^2}{15k} \begin{bmatrix} 0 & -7.83 & -28.83 \\ 0 & 1.17 & -13.83 \\ 0 & 1.17 & 11.17 \end{bmatrix} \begin{Bmatrix} 1 \\ 0.90 \\ -0.55 \end{Bmatrix}$$

$$\begin{Bmatrix} x_1 \\ x_2 \\ x_3 \end{Bmatrix} = \frac{8.81m\omega^2}{15k} \begin{bmatrix} 0 & -7.83 & -28.83 \\ 0 & 1.17 & -13.83 \\ 0 & 1.17 & 11.17 \end{bmatrix} \begin{Bmatrix} 1 \\ 0.98 \\ -0.58 \end{Bmatrix}$$

$$\begin{Bmatrix} x_1 \\ x_2 \\ x_3 \end{Bmatrix} = \frac{9.05m\omega^2}{15k} \begin{bmatrix} 0 & -7.83 & -28.83 \\ 0 & 1.17 & -13.83 \\ 0 & 1.17 & 11.17 \end{bmatrix} \begin{Bmatrix} 1 \\ 1.01 \\ -0.59 \end{Bmatrix}$$

$$\begin{Bmatrix} x_1 \\ x_2 \\ x_3 \end{Bmatrix} = \frac{9.10m\omega^2}{15k} \begin{bmatrix} 0 & -7.83 & -28.83 \\ 0 & 1.17 & -13.83 \\ 0 & 1.17 & 11.17 \end{bmatrix} \begin{Bmatrix} 1 \\ 1.03 \\ -0.59 \end{Bmatrix}$$

$$\begin{Bmatrix} x_1 \\ x_2 \\ x_3 \end{Bmatrix} = \frac{8.94m\omega^2}{15k} \begin{bmatrix} 0 & -7.83 & -28.83 \\ 0 & 1.17 & -13.83 \\ 0 & 1.17 & 11.17 \end{bmatrix} \begin{Bmatrix} 1 \\ 1.05 \\ -0.60 \end{Bmatrix}$$

$$\begin{Bmatrix} x_1 \\ x_2 \\ x_3 \end{Bmatrix} = \frac{9.08m\omega^2}{15k} \begin{bmatrix} 0 & -7.83 & -28.83 \\ 0 & 1.17 & -13.83 \\ 0 & 1.17 & 11.17 \end{bmatrix} \begin{Bmatrix} 1 \\ 1.05 \\ -0.59 \end{Bmatrix}$$

$$\frac{9.08m\omega^2}{15k} = 1$$

$$\omega^2 = \frac{15k}{9.08m}$$

$$\omega = 1.29\sqrt{\frac{k}{m}} \text{ rad/s}$$

III. Mode shape

$$\begin{Bmatrix} A_1 \\ B_1 \\ C_1 \end{Bmatrix} = \begin{Bmatrix} 1 \\ 1.87 \\ 2.92 \end{Bmatrix} \begin{Bmatrix} A_2 \\ B_2 \\ C_2 \end{Bmatrix} = \begin{Bmatrix} 1 \\ 1.05 \\ -0.59 \end{Bmatrix}$$

$$m_1 A_1 A_3 + m_2 B_1 B_3 + m_3 C_1 C_3 = 0$$

$$m_1 A_2 A_3 + m_2 B_2 B_3 + m_3 C_2 C_3 = 0$$

$$3mA_3 + 5.61B_3 + 14.6C_3 = 0$$

$$3mA_3 + 3.15mB_3 + 3mC_3 = 0$$

$$A_3 = -1.87B_3 - 4.87C_3; \quad B_3 = 7.16C_3; \quad C_3 = C_3$$

$$\begin{Bmatrix} A_3 \\ B_3 \\ C_3 \end{Bmatrix} = \begin{bmatrix} 0 & 0 & 45.04 \\ 0 & 0 & 7.16 \\ 0 & 0 & 1 \end{bmatrix} \begin{Bmatrix} A_3 \\ B_3 \\ C_3 \end{Bmatrix}$$

$$\begin{Bmatrix} x_1 \\ x_2 \\ x_3 \end{Bmatrix} = \frac{m\omega^2}{15k} \begin{bmatrix} 0 & -7.83 & -28.83 \\ 0 & 1.17 & -13.83 \\ 0 & 1.17 & 11.17 \end{bmatrix} \begin{bmatrix} 0 & 0 & 45.04 \\ 0 & 0 & 7.16 \\ 0 & 0 & 1 \end{bmatrix} \begin{Bmatrix} A_3 \\ B_3 \\ C_3 \end{Bmatrix}$$

$$\begin{Bmatrix} x_1 \\ x_2 \\ x_3 \end{Bmatrix} = \frac{m\omega^2}{15k} \begin{bmatrix} 0 & 0 & -84.89 \\ 0 & 0 & -5.45 \\ 0 & 0 & 19.55 \end{bmatrix} \begin{Bmatrix} x_1 \\ x_2 \\ x_3 \end{Bmatrix}$$

$$\text{Assuming} \begin{Bmatrix} x_1 \\ x_2 \\ x_3 \end{Bmatrix} = \begin{Bmatrix} 1 \\ -1 \\ 1 \end{Bmatrix}$$

$$\begin{Bmatrix} x_1 \\ x_2 \\ x_3 \end{Bmatrix} = \frac{84.89m\omega^2}{15k} \begin{bmatrix} 0 & 0 & -84.89 \\ 0 & 0 & -5.45 \\ 0 & 0 & 19.55 \end{bmatrix} \begin{Bmatrix} -1 \\ -1.06 \\ 0.23 \end{Bmatrix}$$

$$\begin{Bmatrix} x_1 \\ x_2 \\ x_3 \end{Bmatrix} = \frac{19.52m\omega^2}{15k} \begin{bmatrix} 0 & 0 & -84.89 \\ 0 & 0 & -5.45 \\ 0 & 0 & 19.55 \end{bmatrix} \begin{Bmatrix} -1 \\ -1.06 \\ 0.23 \end{Bmatrix}$$

$$\frac{19.52m\omega^2}{15k} = 1$$

$$\omega^2 = \frac{15k}{19.52m}$$

$$\omega = 0.88\sqrt{\frac{k}{m}} \text{ rad/s}$$

$$\varphi = \begin{bmatrix} 1 & 1 & -1 \\ 1.87 & 1.05 & -0.06 \\ 2.92 & -0.6 & 0.23 \end{bmatrix}$$

$$\omega_n^{(1)} = 0.46\sqrt{\frac{k}{m}} \text{rad/s}; \; \omega_n^{(2)} = 1.29\sqrt{\frac{k}{m}} \text{rad/s};$$

$$\omega_n^{(3)} = 0.88\sqrt{\frac{k}{m}} \text{ rad/s}$$

42. Find the equivalent stiffness matrix of the cantilever beam of length 'L' and flexural rigidity 'EI', with two degrees of freedom as shown in the figure:

Let,

k be the stiffness of the beam.
Δ be the deflection of the beam.
P be the total force acting on the beam.

$$[k]\{\Delta\} = \{P\}$$

$$\begin{bmatrix} k_{xx} & k_{x\theta} \\ k_{\theta x} & k_{\theta\theta} \end{bmatrix} \begin{Bmatrix} dx \\ d\theta \end{Bmatrix} = \begin{Bmatrix} P_x \\ P_\theta \end{Bmatrix}$$

Expanding the second row of the above matrix equation,

$$k_{\theta x}dx + k_{\theta\theta}d\theta = P_\theta$$

$$d\theta = k_{\theta\theta}^{-1}[P_\theta - k_{\theta x}dx]$$

Expanding the first row of the matrix equation,

$$k_{xx}dx + k_{x\theta}d\theta = P_x$$

Combining the above equations,

$$\left[k_{xx} - k_{x\theta}k_{\theta\theta}^{-1}k_{\theta x}\right]dx + k_{x\theta}k_{\theta\theta}^{-1}P_\theta = P_x$$

$$[\bar{k}]dx + k_{x\theta}k_{\theta\theta}^{-1}P_\theta = P_x$$

Thus, the equivalent stiffness matrix is given by

$$\bar{k} = \left[k_{xx} - k_{x\theta}k_{\theta\theta}^{-1}k_{\theta x}\right]$$

For a cantilever beam of length L and flexural rigidity EI, the stiffness matrix is given by

$$k = \begin{bmatrix} \frac{12EI}{L^3} & -\frac{6EI}{L^2} \\ -\frac{6EI}{L^2} & \frac{4EI}{L} \end{bmatrix}$$

Now, the equivalent stiffness/ lateral stiffness of the beam is given by

$$\bar{k} = \left[k_{xx} - k_{x\theta} k_{\theta\theta}^{-1} k_{\theta x} \right]$$
$$= \frac{12EI}{L^3} - \left[\left(-\frac{6EI}{L^2} \right) \left(\frac{L}{4EI} \right) \left(-\frac{6EI}{L^2} \right) \right]$$
$$= \frac{3EI}{L^3}.$$

43. Find the natural period of the fixed beam shown in the figure below

Since, the structure is statically indeterminate, moment distribution method is used to calculate the total stiffness of the member.

(i) **Distribution Factor**:

Section	Stiffness	Total stiffness	Distribution factor (DF)	Sum of DF
AB	$\frac{2EI}{L}$	$\frac{6EI}{L}$	0.333	1
BC	$\frac{4EI}{L}$		0.667	

(ii) **Fixed End Moments**:

$$M_{AB} = -\frac{24EI}{L^2}$$

$$M_{BA} = -\frac{24EI}{L^2}$$

$$M_{BC} = +\frac{48EI}{L^2}$$

$$M_{CB} = +\frac{48EI}{L^2}$$

(iii) **Moment Distribution**:

	AB	BA	BC	CB
Distribution factor		0.333	0.667	
End moments (EI/L)	−24	−24	+48	+48
Distribution		−7.92	−16.08	
Carry over	−3.96			−8.04
Sum	−27.96	−31.92		39.96

(iv) **Force Calculation**:

Force in $AB = \dfrac{(31.92 + 27.92)\frac{EI}{L^2}}{L/2} = \dfrac{119.76EI}{L^3}$

Force in $AB = \dfrac{(39.96 + 27.92)\frac{EI}{L^2}}{L/2} = \dfrac{143.76EI}{L^3}$

The total force at joint $B = \dfrac{263.52EI}{L^3}$.

(v) **Natural frequency**:

Stiffness of the beam, $= \dfrac{263.52EI}{L^3}$.

Natural frequency, $\omega_n = \sqrt{\dfrac{k}{m}} = \dfrac{16.233}{L}\sqrt{\dfrac{EI}{mL}}$.

44. Find the natural frequency of the truss shown in the figure. Ignore the self-weight of the truss.
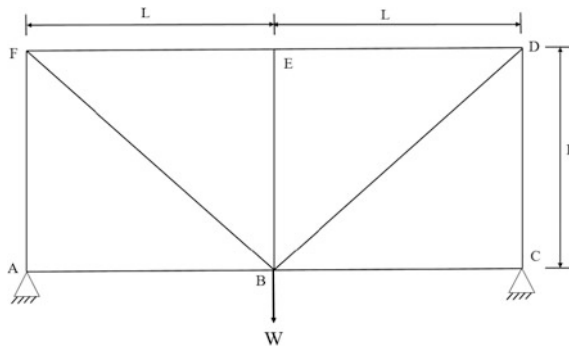
By using method of joints and unit force method,

Member	Length	P	p	PpL/AE
AB	L	0	0	0
BC	L	0	0	0
CD	L	−W/2	−1/2	WL/4AE
DE	L	−W/2	−1/2	WL/4AE

(continued)

(continued)

Member	Length	P	p	PpL/AE
EF	L	$-W/2$	$-1/2$	$WL/4AE$
AF	L	$-W/2$	$-1/2$	$WL/4AE$
BF	1.414L	$W/\sqrt{2}$	$1/\sqrt{2}$	$WL/\sqrt{2}AE$
BD	1.414L	$W/\sqrt{2}$	$1/\sqrt{2}$	$WL/\sqrt{2}AE$
EB	1.414L	0	0	0
Total =				$2.414WL/AE$

Total displacement at $B = 2.414\ WL/AE$

Stiffness, k = Force/displacement = 0.414 AE/L

Natural frequency, $\omega_n = \sqrt{\frac{k}{m}} = 0.643\sqrt{\frac{AE}{mL}}$.

45. Find the mass, stiffness, and force matrices for the wooden beam supported on two springs as shown in the figure:

(i) **Stiffness Matrix**:

Stiffness matrix is derived by applying unit displacements at nodes 1 and 2.
    Applying unit displacement at node 1,

$$k_{11} = k_1$$

$$k_{21} = 0$$

Applying unit displacement at node 2,

$$k_{12} = 0$$

$$k_{22} = k_2$$

Thus, the stiffness matrix is given by $k = \begin{bmatrix} k_1 & 0 \\ 0 & k_2 \end{bmatrix}$

(ii) **Force matrix**:

Force matrix is derived by finding the reaction at the fixed support.

$$F = \begin{bmatrix} -\frac{Pt}{2} & +\frac{P\theta}{L} \\ -\frac{Pt}{2} & -\frac{P\theta}{L} \end{bmatrix}$$

(iii) **Mass Matrix**:

Mass matrix is derived by applying unit acceleration at the nodes 1 and 2.
Applying unit acceleration at node 1,

$$m_{21}L = \frac{1}{2}\frac{m}{L}L\left(\frac{L}{3}\right)$$

$$m_{21} = \frac{M}{6}$$

$$m_{11} = \frac{M}{3}$$

Similarly, applying unit acceleration at node 2,

$$m_{12} = \frac{M}{6}$$

$$m_{22} = \frac{M}{3}$$

Thus, the mass matrix is given by,

$$M = \begin{bmatrix} \frac{M}{3} & \frac{M}{6} \\ \frac{M}{6} & \frac{M}{3} \end{bmatrix}$$

46. Using Lagrange's method, frame the equation of motion for the vibration isolator shown in the figure:

Kinetic energy $= \frac{1}{2}m_1\dot{x}_1^2 + \frac{1}{2}m_2\dot{x}_2^2$

Potential energy $= \frac{1}{2}k_1x_1^2 + \frac{1}{2}k_1(x_1 - x_2)^2$

Dissipation energy $= \frac{1}{2}C\dot{x}_1^2$

By using Lagrange's method,

$$\frac{d}{dt}\left(\frac{\partial(KE)}{\partial \dot{q}_i}\right) - \frac{\partial(KE)}{\partial q_i} + \frac{\partial(PE)}{\partial q_i} + \frac{\partial(DE)}{\partial \dot{q}_i} = Q_i$$

For the first degree of freedom,

$$\frac{\partial(KE)}{\partial \dot{x}_1} = m_1\dot{x}_1$$

$$\frac{d}{dt}\left(\frac{\partial(KE)}{\partial \dot{x}_1}\right) = m_1\ddot{x}_1$$

$$\frac{\partial(PE)}{\partial x_1} = (k_1 + k_2)x_1 - k_2x_2$$

$$\frac{\partial(DE)}{\partial \dot{x}_1} = C\dot{x}_1$$

Substituting in the above equation,

$$m_1\ddot{x}_1 + (k_1 + k_2)x_1 - k_2x_2 + C\dot{x}_1 = 0$$

Similarly, for the second degree of freedom,

$$m_2\ddot{x}_2 - k_2x_1 + k_2x_2 + C\dot{x}_1 = F_0e^{i\omega t}$$

Thus, the equation of motion is given by,

$$\begin{bmatrix} m_1 & 0 \\ 0 & m_2 \end{bmatrix} \begin{Bmatrix} \ddot{x}_1 \\ \ddot{x}_2 \end{Bmatrix} + \begin{bmatrix} C & 0 \\ 0 & C \end{bmatrix} \begin{Bmatrix} \dot{x}_1 \\ \dot{x}_2 \end{Bmatrix} + \begin{bmatrix} k_1 + k_2 & -k_2 \\ -k_2 & k_2 \end{bmatrix} \begin{Bmatrix} x_1 \\ x_2 \end{Bmatrix} = \begin{Bmatrix} 0 \\ F_0 e^{i\omega t} \end{Bmatrix}$$

47. Decouple the equation of motion of undamped two degree of freedom system and solve. Use the following data:

$$m = \begin{bmatrix} m & 0 \\ 0 & m \end{bmatrix}, \quad k = \begin{bmatrix} 2k & -k \\ -k & 2k \end{bmatrix}$$

The frequencies and corresponding mode shapes are identified as follows:

$$\omega_1 = \sqrt{\frac{k}{m}}, \quad \omega_2 = \sqrt{\frac{3k}{m}}$$

$$\varnothing_1 = \begin{Bmatrix} 1 \\ 1 \end{Bmatrix}, \quad \varnothing_2 = \begin{Bmatrix} -1 \\ 1 \end{Bmatrix}$$

(i) **Normalized Matrix**:

$$\varnothing_1^T M \varnothing_1 = \{ 1 \quad 1 \} \begin{bmatrix} m & 0 \\ 0 & m \end{bmatrix} \begin{Bmatrix} 1 \\ 1 \end{Bmatrix} = 2m.$$

$$\varnothing_1^* = \frac{1}{\sqrt{2m}} \begin{Bmatrix} 1 \\ 1 \end{Bmatrix}$$

$$\varnothing_2^T M \varnothing_2 = \{ -1 \quad 1 \} \begin{bmatrix} m & 0 \\ 0 & m \end{bmatrix} \begin{Bmatrix} -1 \\ 1 \end{Bmatrix} = 2m.$$

$$\varnothing_2^* = \frac{1}{\sqrt{2m}} \begin{Bmatrix} -1 \\ 1 \end{Bmatrix}$$

$$\tilde{P} = \frac{1}{\sqrt{2m}} \begin{bmatrix} 1 & -1 \\ 1 & 1 \end{bmatrix}$$

(ii) **Check**:

$\tilde{P}^T M \tilde{P} = \begin{bmatrix} 1 & 0 \\ 0 & 1 \end{bmatrix}$, which is an Identity matrix.

$\tilde{P}^T K \tilde{P} = \begin{bmatrix} \frac{k}{m} & 0 \\ 0 & \frac{3k}{m} \end{bmatrix}$. It is a diagonal matrix and the leading diagonal elements

gives the value of square of frequencies of the system.

(iii) **Equation of Motion**:

$$[M]\{\ddot{X}\} + [K]\{X\} = 0$$

$$\begin{bmatrix} m & 0 \\ 0 & m \end{bmatrix} \begin{Bmatrix} \ddot{x}_1 \\ \ddot{x}_2 \end{Bmatrix} + \begin{bmatrix} 2k & -k \\ -k & 2k \end{bmatrix} \begin{Bmatrix} x_1 \\ x_2 \end{Bmatrix} = 0$$

$$m_1 \ddot{x}_1 + 2kx_1 - kx_2 = 0$$

$$m_2 \ddot{x}_2 - kx_1 + kx_2 = 0$$

(iv) **Decoupling**:

The equation is expressed in the different domain by the following equation:

$$\{x\} = \tilde{P}\{y\}$$

$$\begin{Bmatrix} x_1 \\ x_2 \end{Bmatrix} = \tilde{P} \begin{Bmatrix} y_1 \\ y_2 \end{Bmatrix}$$

$$\begin{Bmatrix} x_1 \\ x_2 \end{Bmatrix} = \frac{1}{\sqrt{2m}} \begin{bmatrix} 1 & -1 \\ 1 & 1 \end{bmatrix} \begin{Bmatrix} y_1 \\ y_2 \end{Bmatrix}$$

(v) **Solution in Y Domain**:

$$[M]\{\ddot{X}\} + [K]\{X\} = 0$$

$$M\tilde{P}\ddot{Y} + K\tilde{P}Y = 0$$

Pre-multiplying with $\tilde{P}^T$,

$$\tilde{P}^T M \tilde{P}\ddot{Y} + \tilde{P}^T K \tilde{P}Y = 0$$

$$\begin{bmatrix} 1 & 0 \\ 0 & 1 \end{bmatrix} \begin{Bmatrix} \ddot{y}_1 \\ \ddot{y}_2 \end{Bmatrix} + \begin{bmatrix} \omega_1^2 & 0 \\ 0 & \omega_1^2 \end{bmatrix} \begin{Bmatrix} y_1 \\ y_2 \end{Bmatrix} = 0$$

$$\ddot{y}_1 + \omega_1^2 y_1 = 0$$

$$\ddot{y}_2 + \omega_2^2 y_2 = 0$$

The solution is given by

$$y_1(t) = y_1(0) \cos \omega_1 t + \frac{\dot{y}_1(0)}{\omega_1} \sin \omega_1 t$$

$$y_2(t) = y_2(0) \cos \omega_2 t + \frac{\dot{y}_2(0)}{\omega_2} \sin \omega_2 t$$

(vi) **X Domain**:

$$\begin{Bmatrix} x_1 \\ x_2 \end{Bmatrix} = \frac{1}{\sqrt{2m}} \begin{bmatrix} 1 & -1 \\ 1 & 1 \end{bmatrix} \begin{Bmatrix} y_1 \\ y_2 \end{Bmatrix}$$

$$x_1(t) = \frac{1}{\sqrt{2m}} [y_1(t) - y_2(t)]$$

$$x_2(t) = \frac{1}{\sqrt{2m}} [y_1(t) + y_2(t)]$$

(vii) **Transforming Initial Conditions from X Domain to Y Domain**:

$$\{x\} = \tilde{P}\{y\}$$

$$\{y\} = \tilde{P}^{-1}\{x\}$$

$$\tilde{P} = \frac{1}{\sqrt{2m}} \begin{bmatrix} 1 & -1 \\ 1 & 1 \end{bmatrix}$$

$$\tilde{P}^{-1} = \frac{\sqrt{2m}}{2} \begin{bmatrix} 1 & 1 \\ -1 & 1 \end{bmatrix}$$

$$\begin{Bmatrix} y_1 \\ y_2 \end{Bmatrix} = \sqrt{\frac{m}{2}} \begin{bmatrix} 1 & 1 \\ -1 & 1 \end{bmatrix} \begin{Bmatrix} x_1 \\ x_2 \end{Bmatrix}$$

Thus, the solution in Y domain is expressed as

$$y_1(t) = \sqrt{\frac{m}{2}}\left\{[(x_1(0)+x_2(0))\cos\omega_1 t] + \frac{1}{\omega_1}[(\dot{x}_1(0)+\dot{x}_2(0))\sin\omega_1 t]\right\}$$

$$y_2(t) = \sqrt{\frac{m}{2}}\left\{[(-x_1(0)+x_2(0))\cos\omega_2 t] + \frac{1}{\omega_2}[(-\dot{x}_1(0)+\dot{x}_2(0))\sin\omega_2 t]\right\}$$

48. For small damping, show that logarithmic decrement can be expressed in terms of vibration energy and energy dissipated per cycle.

$$\frac{x_2}{x_1} = e^{-\delta} = 1 - \delta + \frac{\delta^2}{2!}\cdots$$

Vibration energy is given by

$$U_1 = \frac{1}{2}kx_1^2, \quad U_2 = \frac{1}{2}kx_2^2$$

$$\text{Loss of energy} = \frac{U_1 - U_2}{U_1}$$

$$= \frac{x_1^2 - x_2^2}{x_1^2} = 1 - \frac{x_2^2}{x_1^2} = 1 - e^{-2\delta}$$

$$= 1 - \left[1 - 2\delta + \frac{2\delta^2}{2!}\cdots\right]$$

$$= 2\delta.$$

49. Find the maximum dynamic amplification factor for the rectangular impulse loading shown in the figure.

(i) **Phase 1: $0 \leq T \geq S$**

$$F(t) = F_0$$

$$x = \frac{\omega}{k} \int_0^T F_0 \sin \omega(T - t) dt$$

$$= \frac{\omega}{k} \left[-F_0 \frac{\cos \omega(T - t)}{\omega} \right]_0^T$$

$$= \frac{F_0}{k} \cos \omega(T - t) - \cos \omega T$$

$$= \frac{F_0}{k} [1 - \cos \omega T]$$

Since, $\frac{F_0}{k} = x_{st}$

$$\frac{x}{x_{st}} = 1 - \cos \omega T.$$

Thus, Dynamic Amplification Factor, $DAF = 1 - \cos \omega T$.
Let $\omega = \frac{2\pi}{\tau}$, where τ is the natural period of the system.

$$DAF = 1 - \cos \omega \frac{2\pi}{\tau} T.$$

For getting the maximum Dynamic Amplification Factor,

$$\frac{d}{dt}(DAF) = \frac{2\pi}{\tau} \sin \omega \frac{2\pi}{\tau} T = 0$$

Since $\omega \neq 0$,

$$\sin \omega \frac{2\pi}{\tau} T = 0$$

$$\frac{2\pi}{\tau} T = \pi$$

$$T = \frac{\tau}{2}$$

Hence, the Dynamic Amplification is maximum when the duration of loading is half of the maximum value.

$$DAF_{max} = 1 - \cos \omega \frac{2\pi}{\tau} \frac{\tau}{2} = 2.$$

(ii) **Phase 2**: **T > S**

According to the given loading condition, there is no loading in the second phase. But, the response will be due to the free vibration with the initial condition at $t = s$.

For phase 1,

$$\frac{x}{x_{st}} = 1 - \cos \omega T$$

$$x = x_{st}[1 - \cos \omega T]$$

$$\dot{x} = \omega x_{st} \sin \omega T$$

At $t = s$,

$$x_s = x_{st}[1 - \cos \omega s]$$

$$\dot{x}_s = \omega x_{st} \sin \omega s$$

For a free vibration response, the general response equation is given by

$$x = C_1 \cos \omega T + C_2 \sin \omega T$$

Applying the initial conditions,

(i) at $t = s$, $x = x_s$
(ii) at $t = s$, $\dot{x} = \dot{x}_s$

Thus, the general equation becomes

$$x = x_s \cos \omega T + \frac{\dot{x}_s}{\omega} \sin \omega T$$

By substituting the values of x_s and $\dot{x}_s$ in the above equation

$$x_s = x_{st}\{[1 - \cos \omega s] \cos \omega T + \sin \omega s \sin \omega T\}$$

The Dynamic Amplification Factor is given by

$$\frac{x}{x_{st}} = [1 - \cos \omega s] \cos \omega T + \sin \omega s \sin \omega T$$

Since, for a free vibration response, $x_{max} = \sqrt{(x_0)^2 + \left(\frac{\dot{x}_0}{\omega}\right)^2}$

From the equation of DAF,

$$x_0 = 1 - \cos \omega s$$

$$\frac{\dot{x}_0}{\omega} = \sin \omega s$$

Thus,

$$\text{DAF}_{\text{max}} = \sqrt{(1 - \cos \omega s)^2 + (\sin \omega s)^2} = \sqrt{2(1 - \cos \omega s)}$$

Since,

$$\cos 2\theta = 1 - 2\sin^2\theta$$

$$\text{DAF}_{\text{max}} = 2\sin\left(\frac{\omega s}{2}\right)$$

50. Find the response of the stepped pulse function shown in the figure:

(i) **Phase 1**: $\mathbf{0 \le T \le q}$

$$x = \frac{\omega}{k} \int_0^T 2Q \sin \omega(T - t)dt$$

$$= \frac{\omega}{k}\left[-2Q\frac{\cos \omega(T - t)}{\omega}\right]_0^T$$

$$= \frac{2Q}{k}\cos \omega(T - t) - \cos \omega T$$

$$= \frac{2Q}{k}[1 - \cos \omega T]$$

Since, $\frac{2Q}{k} = x_{st}$

$$\frac{x}{x_{st}} = 1 - \cos \omega T$$

Thus, Dynamic Amplification Factor, DAF $= 1 - \cos \omega T$.
Let $\omega = \frac{2\pi}{\tau}$, where τ is the natural period of the system.
DAF $= 1 - \cos \omega \frac{2\pi}{\tau} T$.
For getting the maximum Dynamic Amplification Factor,

$$\frac{d}{dt}(\text{DAF}) = \frac{2\pi}{\tau} \sin \omega \frac{2\pi}{\tau} T = 0$$

Since $\omega \neq 0$,

$$\sin \omega \frac{2\pi}{\tau} T = 0$$

$$\frac{2\pi}{\tau} T = \pi$$

$$T = \frac{\tau}{2}$$

Hence, the Dynamic Amplification is maximum when the duration of loading is half of the maximum value.

$$\text{DAF}_{\text{max}} = 1 - \cos \omega \frac{2\pi}{\tau} \frac{\tau}{2} = 2.$$

(ii) **Phase 2: q ≤ T ≤ 2q**

Here, the response is due to the initial conditions and loadings.
The response due to initial conditions is given by

$$x = x_{st}[1 - \cos \omega T]$$

$$\dot{x} = \omega x_{st} \sin \omega T$$

At $t = s$,

$$x_s = x_{st}[1 - \cos \omega s]$$

$$\dot{x}_s = \omega x_{st} \sin \omega s$$

For a free vibration response, the general response equation is given by

$$x = C_1 \cos \omega T + C_2 \sin \omega T$$

Applying the initial conditions,

(i) at $t = s$, $x = x_s$
(ii) at $t = s$, $\dot{x} = \dot{x}_s$

Thus, the general equation becomes

$$x = x_s \cos \omega T + \frac{\dot{x}_s}{\omega} \sin \omega T$$

By substituting the values of x_s and $\dot{x}_s$ in the above equation,

$$x_s = x_{st}\{[1 - \cos \omega s] \cos \omega T + \sin \omega s \, \sin \omega T\}$$

$$x_s = \frac{2Q}{k}\{[1 - \cos \omega s] \cos \omega T + \sin \omega s \, \sin \omega T\}$$

The response due to loading in the second phase is given by

$$x = \frac{\omega}{k} \int_0^T Q \sin \omega(T - t)\mathrm{d}t$$

$$= \frac{\omega}{k}\left[-Q\frac{\cos \omega(T - t)}{\omega}\right]_0^T$$

$$= \frac{Q}{k}\cos \omega(T - t) - \cos \omega T$$

$$= \frac{Q}{k}[1 - \cos \omega T]$$

Thus, the total response is

$$x = \frac{2Q}{k}\{[1 - \cos \omega s] \cos \omega T + \sin \omega s \, \sin \omega T\} + \frac{Q}{k}[1 - \cos \omega T]$$

51. Find the response of the triangular pulse function shown in the figure:

The solution for the function is given by

$$x(t) = A \sin \omega t + B \cos \omega t + \frac{F_0}{k}\left(1 - \frac{t}{T}\right)$$

Applying the initial conditions

(i)   at $t = 0$, $x_0 = 0$,

$$B = \frac{F_0}{k}$$

(ii)   at $t = 0$, $\dot{x}_0 = 0$,

$$\dot{x}(t) = \omega A \cos \omega t - \omega B \sin \omega t + \frac{F_0}{k}\left(-\frac{1}{T}\right)$$

$$A = \frac{F_0}{k}\frac{1}{\omega T}$$

The complete solution is

$$x(t) = \frac{F_0}{k}\left[\left(\frac{\sin \omega t}{\omega T}\right) - \cos \omega t - \frac{t}{T} + 1\right]$$

(i) **Phase 1**: $0 \leq \mathbf{T} \leq \mathbf{t}$

The response for the triangular pulse loading is

$$x(t) = \frac{F_0}{k} \left[\left(\frac{\sin \omega T}{\omega T} \right) - \cos \omega T \right]$$

The Dynamic Amplification Factor is

$$\frac{F_0}{k} = x_{st}$$

$$\text{DAF} = \frac{x}{x_{st}} = \left(\frac{\sin \omega T}{\omega T} \right) - \cos \omega T$$

(ii) **Phase 2**: $\mathbf{T} > \mathbf{t}$

According to the given loading condition, there is no loading in the second phase. But, the response will be due to the free vibration with the initial condition at $T = t$.

For phase 1,

$$\frac{x}{x_{st}} = (\sin \omega t) - \cos \omega t$$

$$x = x_{st}[(\sin \omega T) - \cos \omega T]$$

$$\dot{x} = x_{st} \left[\cos \omega T + \omega \sin \omega T - \frac{1}{\omega T} \right]$$

At $T = t$,

$$x = x_{st}[(\sin \omega t) - \cos \omega t]$$

$$\dot{x} = x_{st} \left[\frac{\cos \omega t}{t} + \omega \sin \omega t - \frac{1}{t} \right]$$

For a free vibration response, the general response equation is given by

$$x = C_1 \cos \omega T + C_2 \sin \omega T$$

Applying the initial conditions,

(i) at $T = t$, $x = x_T$
(ii) at $T = t$, $\dot{x} = \dot{x}_t$

Thus, the general equation becomes

$$x = x_t \cos \omega T + \frac{\dot{x}_t}{\omega} \sin \omega T$$

By substituting the values of x_t and $\dot{x}_t$ in the above equation,

$$x_t = x_{st} \left\{ [(\sin \omega t) - \cos \omega t] \cos \omega T + \left[\frac{\cos \omega t}{\omega t} + \sin \omega t - \frac{1}{\omega t} \right] \sin \omega T \right\}$$

The Dynamic Amplification Factor is given by

$$\frac{x}{x_{st}} = [(\sin \omega t) - \cos \omega t] \cos \omega T + \left[\frac{\cos \omega t}{\omega t} + \sin \omega t - \frac{1}{\omega t} \right] \sin \omega T$$

MATLAB Programs

1. **Eigen solver method**

(i) **Program**:

The following program will provide the frequency and mode shapes for the given system. It also includes the check for orthogonality followed by the normalization.

```
% Program for finding frequency and mode shape using EIGEN SOLVER METHOD
clc;
clear;
% Enter dof
dof=3;
% Enter mass values
m=[1 1 1]; % in kg
% Enter stiffness values
k=[1 1 1]; % in N/m
M=zeros(dof); %  Mass Matrix
K=zeros(dof); % Stiffness Matrix
%% formation of mass and stiffness matrices
for j=1:dof
    for i=1:dof
        M(i,i)=m(i); %Mass matrix
        if i<dof           K(i,i)=k(i)+k(i+1);%leading diagonal matrix
            K(i,i+1)=-k(i+1);
            K(i+1,i)=-k(i+1);
        elseif i==dof && length(k)>dof
            K(i,i)=k(i)+k(i+1);
        else
```

```
        K(i,i)=k(i);
      end
    end
end
fprintf ('Mass Matrix\n')
disp (M);
fprintf ('Stiffness Matrix\n')
disp (K);
%% eigen values and eigen vectors
[mode,w_square]=eig(K,M);
freq=sqrt(w_square);
for i=1:dof
    wn3(i)=freq(i,i);
    moden(:,i)= mode(:,i)/mode(1,i);
    fprintf('Frequency: wn = %6.3f rad/s \n',wn3(i));
end
fprintf('Modal Matrix\n x = \n');
disp(moden);
%% Check for orthogonality
for i=1:dof-1
    c1(i)=fix(moden(:,i)'*moden(:,i+1))*1000/1000;
end
if c1==0
    fprintf('The modes are orthogonal to each other. \n');
else
    fprintf('The modes are not orthogonal to each other. \n');
    break
end
%% Normalization and check
for i=1:dof
    mnew=moden(:,i)'*M*moden(:,i);
    modenor(:,i)=moden(:,i).*(sqrt(1/mnew));
end
for i=1:dof-1
    d1(i)=round((modenor(:,i)'*M*modenor(:,i))*1000/1000);
    d2(i)=fix((modenor(:,i)'*M*modenor(:,i+1))*1000)/1000;
end
s1=sum(d1)+1;
s2=sum(d2);
if s1==dof && s2==0
    fprintf ('The Normalized Modal Matrix \nx = \n');
    disp(modenor);
else
    break
end
```

(ii) **Sample Output**:

Mass Matrix

$$
\begin{matrix}
1 & 0 & 0 \\
0 & 1 & 0 \\
0 & 0 & 1
\end{matrix}
$$

Stiffness Matrix

$$
\begin{matrix}
2 & -1 & 0 \\
-1 & 2 & -1 \\
0 & -1 & 1
\end{matrix}
$$

Frequency: $w_n = 0.445$ rad/s
Frequency: $w_n = 1.247$ rad/s
Frequency: $w_n = 1.802$ rad/s
Modal Matrix

$$
x = \begin{matrix}
1.0000 & 1.0000 & 1.0000 \\
1.8019 & 0.4450 & -1.2470 \\
2.2470 & -0.8019 & 0.5550
\end{matrix}
$$

The modes are orthogonal to each other.
The normalized modal matrix

$$
x = \begin{matrix}
0.3280 & 0.7370 & 0.5910 \\
0.5910 & 0.3280 & -0.7370 \\
0.7370 & -0.5910 & 0.3280
\end{matrix}
$$

The mode shapes for the above sample problem is shown in the following figure:
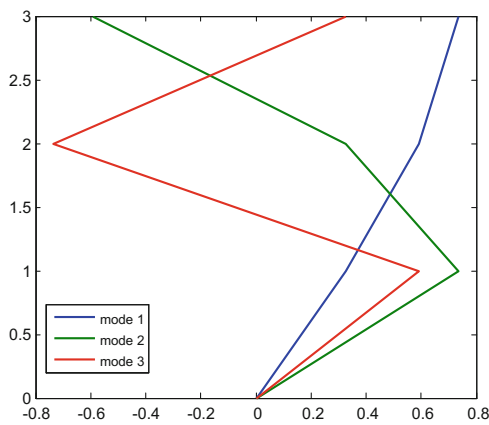
Normalized Mode Shapes of the MDOF system

2. **Fundamental frequency and mode shape**

(i) **Program**

From the following program, the fundamental frequency and mode shape of the MDOF system can be found by Dunkerley's method, Influence coefficient method, Stodola's method, and Eigen Solver method.

```
% Program for finding frequency and mode shape using different methods
% Dunkerley, Influence coeeffient, Stodola  and Eigen solver Methods
% Give the values for dof, mass and stiffness
clc;
clear;
% Enter dof
dof=3;
% Enter mass values
m=[1 1 1 ]; % in kg
% Enter stiffness values
k=[1 1 1 ]; % in N/m
M=zeros(dof); % Mass Matrix
K=zeros(dof); % Stiffness Matrix
A=zeros(dof); % Influence coefficient matrix
%% Dunkerley method
%This method gives only the fundamental frequency
k_inv=1./k; %matrix with 1/k values
k_new=cumsum(k_inv); %leading diagonal elements of influence coeffi-
cient matrix
wn=sqrt(1/(m*k_new'));
j=1;
for j=1:dof
    i=1;
    for i=1:dof
       M(i,i)=m(i); %Mass matrix
       x=min(i,j);
       A(i,j)=k_new(x); % Influence coefficient matrix
       i=i+1;
    end
    j=j+1;end
K=inv(A);% Stiffness matrix
fprintf('Mass Matrix:\n')
disp(M);
fprintf('Stiffness Matrix:\n')
disp(K);
fprintf('Influence Coefficient Matrix:\n')
disp(A);
fprintf('Dunkerley method: Fundamental frequency, wn = %6.3f rad/s \n \n',
```

```
wn);
%% Influence coefficient method
% for getting fundamental frequency and mode shape
x=ones(dof,1);% assumed modal matrix
xo=x;
for u=1:10000
    y=A*M*xo;
    xn=y/y(1);
    d=xo-xn;
    ch=1e-6.*x;
    if abs(d)<ch
     x=xn;
     wn1=sqrt(1/y(1));
     fprintf('Influence Coeffient method:
\nFundamental frequency and mode shape: wn = %6.3f rad/s \n x = \n',wn1);
     disp(x);
     break
    else
     xo=xn;
    end
end
%% Stodola's Method
% This method also gives fundamental frequency and mode shape
ad=ones(1,dof);% Asssumed deflection
ado=ad;
for u=1:10000
    fi=m.*ado; % Inertia force
    fs=flip(cumsum(flip(fi))); %spring force
    sd=fs./k; % Cumulative deflection
    cd=cumsum(sd); % Cumulative deflection
    r=cd/cd(1);%ratio
    d=abs(ado-r);
    ch=1e-6.*ado;
    if d<ch
       ad=r;
       wn2=sqrt(sum(r)/sum(cd));
       fprintf('Stodola method:
\nFundamental frequency and mode shape: wn = %6.3f rad/s \n x = \n',wn2);
       disp(r');
       break
    else
       ado=r;
    end
end
%% Eigen solver method
```

```
% This method gives mode shape and frequencies in pair
[mode,w_square]=eig(K,M);
freq=sqrt(w_square);
i=1;
for i=1:dof
   wn3(i)=freq(i,i);
   moden(:,i)= mode(:,i)/mode(1,i);
   i=i+1;
end
wn3n=min(wn3);
fprintf
('Eigen solver method: \nFundamental frequency and mode shape: wn = %
6.3f rad/s \n x = \n',wn3n);
disp(moden(:,1));
```

(ii) **Sample Output**

Mass Matrix:

$$
\begin{matrix}
1 & 0 & 0 \\
0 & 1 & 0 \\
0 & 0 & 1
\end{matrix}
$$

Stiffness Matrix:

$$
\begin{matrix}
2 & -1 & 0 \\
-1 & 2 & -1 \\
0 & -1 & 1
\end{matrix}
$$

Influence Coefficient Matrix:

$$
\begin{matrix}
1 & 1 & 1 \\
1 & 2 & 2 \\
1 & 2 & 3
\end{matrix}
$$

Dunkerley method: Fundamental frequency, $w_n = 0.408$ rad/s.

Influence Coefficient method:
Fundamental frequency and mode shape: $w_n = 0.445$ rad/s

$$
x = \begin{matrix}
1.0000 \\
1.8019 \\
2.2470
\end{matrix}
$$

Stodola method:
Fundamental frequency and mode shape: $w_n = 0.445$ rad/s

$$x = \begin{matrix} 1.0000 \\ 1.8019 \\ 2.2470 \end{matrix}$$

Eigen solver method:
Fundamental frequency and mode shape: $w_n = 0.445$ rad/s

$$x = \begin{matrix} 1.0000 \\ 1.8019 \\ 2.2470 \end{matrix}$$

Additional Exercise

1. Using the spring–mass system as an example, show that loss of potential energy of the mass due to displacement from the static equilibrium position will always be canceled by the work done by the equilibrium forces of the spring.
2. Ratio of (k/m) of a spring–mass system is given as 4.0. If the mass is deflected by 2 cm downwards, measured for its equilibrium position and given an upward velocity of 8 cm/s, determine its amplitude and maximum acceleration.
3. Derive an expression to obtain damping ratio using half-power band width method.
4. The following data are given for a vibrating system with viscous damping. Mass = 5 kg; $k = 40$ N/m; $C = 0.10$ N/ms. Find logarithmic decrement and ratio of any two successive amplitudes.
5. Draw the resonance response of a undamped system and write the inferences.
6. Show that in a damped system, amplitude of maximum displacement is bounded, even at resonance. What do you understand by this statement? Illustrate your answer with an appropriate figure.
7. Show that the log decrement is also given by the equation: $\delta = \frac{1}{n} \ln \left(\frac{x_0}{x_n} \right)$ where x_n represents amplitude after n cycles have elapsed. Plot also the curve showing the number of cycles elapsed against ξ for the amplitude to diminish by 50%.
8. In coulomb damping model, show that decay in the amplitude per cycle is constant.
9. A spring–mass system is excited by a force of $F_0 \sin (\omega t)$. At resonance, amplitude is measured as 0.58 cm. At 0.8 resonant frequency, amplitude measured is 0.46 cm. Determine the damping ratio ξ of the system.
10. In a damped system, damping limits the resonance response amplitude. Plot the number of cycles of the load versus resonance response and show that few cycles of excitations are required to reach the nearly full response amplitude.

11. Starting with the matrix equation, $K\phi_s = \omega_s^2 M\phi_s$, pre-multiply first with KM^{-1} and using orthogonality relation $\phi_r^T M\phi_s = 0$, show that $\phi_r^T KM^{-1} K\phi_s = 0$. Repeat this to show that $\phi_r^T [KM^{-1}]^h K\phi_s = 0$ for $h = 1, 2, 3, 4, \ldots$ n, where n is number of degrees of freedom.

12. Determine the influence coefficient matrix for the multi-degrees of freedom system shown in the below figure:
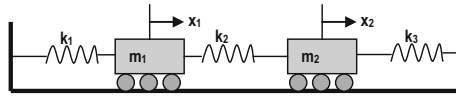
13. Determine the fundamental frequency of the system whose $[M]$ and influence coefficient matrix δ are given as below:

$$M = \begin{bmatrix} 60 & 0 & 0 \\ 0 & 100 & 0 \\ 0 & 0 & 80 \end{bmatrix}, \quad [\delta] = \begin{bmatrix} 6 & 5 & 3 \\ 5 & 7 & 4 \\ 3 & 4 & 6 \end{bmatrix}$$

14. What do you understand by mode shapes? Give its physical interpretation.
15. Why fundamental frequency is of great importance in structural dynamics?
16. A continuous structure has _____ number of degrees of freedom.
17. In structural dynamics, mass element represents _____ characteristics of the structure and _____ represents elastic restoring force.
18. A sketch of the body, isolated from all other bodies, in which all forces external to the body are shown is called _____.
19. An alternate approach which states that the system may be set in a state of dynamic equilibrium is called _____.
20. Degree of freedom of a system is the number of independent coordinates necessary to describe its position. True or false. If false, rewrite the correct statement.
21. It is observed experimentally that amplitude of free vibration of certain structure, modeled as single-degree of freedom decreases from 1 to 0.4 in 10 cycles. What is the % of critical damping?
22. The simplest form of periodic motion is _____.
23. What are the essential characteristics of a dynamic loading?
24. It is not always possible to obtain rigorous mathematical solutions for engineering problems. Should you agree to this statement, then which provides a reasonable link between the real physical system and mathematically feasible solution?
25. It is not always of freedom, damping element represents only dissipation of energy. Such pure elements do not exist in physical world this statement, then which provides a mathematical model.

26. Do both the figures shown below represent mathematical models that are dynamically equivalent? Explain your answer briefly.
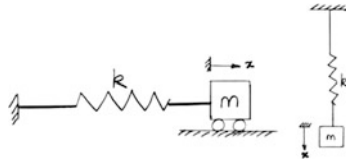
27. In a single-degree of freedom model, spring is considered a linear spring. In other words, force–displacement properties of the system are taken as linear. Is it a hypothetical situation compared to the real dynamic behavior of structures? Explain.

28. Find time period of the structure shown in the below figure. Cross section of the column is circular of 50 mm diameter, made of steel. Take E_{st} as 2×105 N/mm^2, mass as 100 kg, length of the column as 2 m.

29. A cantilever beam is shown in figure below has a lumped mass of 10 kg at its tip. Length of the beam is 1.5 m and stiffness of springs attached to the mass is 100 N/m. For initial displacement of 25 mm and initial velocity of 0.5 m/s, find the displacement and velocity of the system after 1 s. Take E_{st} as 2×105 N/mm^2. Neglect the self-weight of the beam. Beam is made of a steel flat of size 6 mm $\times$ 100 mm.
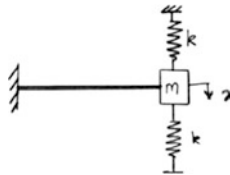
30. A vibrating system having mass of 4.5 kg and stiffness of 3500 N/m is viscously damped so that ratio of two consecutive peaks is reduced from 1.0 to 0.85. Determine natural frequency, logarithmic decrement, damping ratio, damping coefficient, and damped natural frequency.

31. What is the difference between vibration and oscillation?

32. What is negative damping? Explain it with an example.

33. Evaluate the frequency and mode shape for the MDOF system using Influence coefficient method. Use Dunkerley's method to evaluate natural frequency of the system.

$m = 3500$ kg; $K = 1500$ kN/m
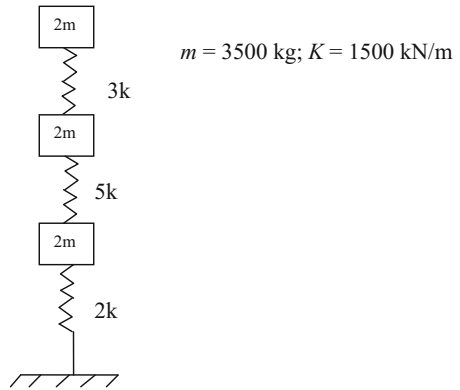
34. Evaluate the frequency and mode shape for the MDOF system using Influence coefficient method. Use Dunkerley's method to evaluate natural frequency of the system.
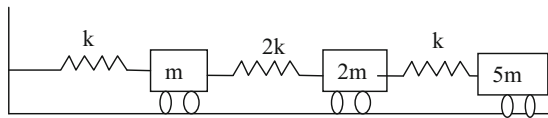
$m = 35$ kN; $K = 1000$

35. Evaluate the frequency and mode shape for the MDOF system using Influence coefficient method. Use Dunkerley's method to evaluate natural frequency of the system.
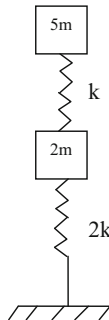
36. Evaluate the fundamental Frequency and mode shape for the MDOF system using Rayleigh–Ritz method and compare the frequency with Dunkerley's method.
37.
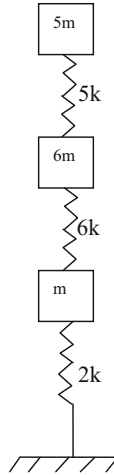
38. Evaluate the fundamental frequency and mode shape for the MDOF system using Stodola method.
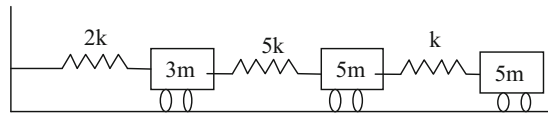
Additional Example Problems

1. Find the equivalent stiffness matrix of the cantilever beam of length 'L' and flexural rigidity 'EI', with two degrees of freedom as shown in the figure:

Let,

k be the stiffness of the beam.

Δ be the deflection of the beam.

P be the total force acting on the beam

$$[k]\{\Delta\} = \{P\}$$

$$\begin{bmatrix} k_{xx} & k_{x\theta} \\ k_{\theta x} & k_{\theta\theta} \end{bmatrix} \begin{Bmatrix} dx \\ d\theta \end{Bmatrix} = \begin{Bmatrix} P_x \\ P_\theta \end{Bmatrix}$$

Expanding the second row of the above matrix equation,

$$k_{\theta x}\mathrm{d}x + k_{\theta\theta}\mathrm{d}\theta = P_\theta$$

$$\mathrm{d}\theta = k_{\theta\theta}^{-1}[P_\theta - k_{\theta x}\mathrm{d}x]$$

Expanding the first row of the matrix equation,

$$k_{xx}\mathrm{d}x + k_{x\theta}\mathrm{d}\theta = P_x$$

Combining the above equations,

$$\left[k_{xx} - k_{x\theta}k_{\theta\theta}^{-1}k_{\theta x}\right]\mathrm{d}x + k_{x\theta}k_{\theta\theta}^{-1}P_\theta = P_x$$

$$[\bar{k}]\mathrm{d}x + k_{x\theta}k_{\theta\theta}^{-1}P_\theta = P_x$$

Thus, the equivalent stiffness matrix is given by,

$$\bar{k} = \left[k_{xx} - k_{x\theta}k_{\theta\theta}^{-1}k_{\theta x}\right]$$

For a cantilever beam of length L and flexural rigidity EI, the stiffness matrix is given by,

$$k = \begin{bmatrix} \frac{12EI}{L^3} & -\frac{6EI}{L^2} \\ -\frac{6EI}{L^2} & \frac{4EI}{L} \end{bmatrix}$$

Now, the equivalent stiffness/lateral stiffness of the beam is given by,

$$\bar{k} = \left[k_{xx} - k_{x\theta}k_{\theta\theta}^{-1}k_{\theta x}\right]$$
$$= \frac{12EI}{L^3} - \left[\left(-\frac{6EI}{L^2}\right)\left(\frac{L}{4EI}\right)\left(-\frac{6EI}{L^2}\right)\right]$$
$$= \frac{3EI}{L^3}.$$

2. Find the natural period of the fixed beam shown in the figure below:

Since, the structure is statically indeterminate, moment distribution method is used to calculate the total stiffness of the member.

(i) **Distribution Factor**:

Section	Stiffness	Total stiffness	Distribution factor (DF)	Sum of DF
AB	$\frac{2EI}{L}$	$\frac{6EI}{L}$	0.333	1
BC	$\frac{4EI}{L}$		0.667	

(ii) **Fixed End Moments**:

$$M_{AB} = -\frac{24EI}{L^2}$$

$$M_{BA} = -\frac{24EI}{L^2}$$

$$M_{BC} = +\frac{48EI}{L^2}$$

$$M_{CB} = +\frac{48EI}{L^2}$$

(ii) **Moment Distribution**:

	AB	BA	BC	CB
Distribution factor		0.333	0.667	
End moments (*EI/L*)	−24	−24	+48	+48
Distribution		−7.92	−16.08	
Carry over	−3.96			−8.04
Sum	−27.96	−31.92		39.96

(iv) **Force Calculation**:

$$\text{Force in } AB = \frac{(31.92 + 27.92)\frac{EI}{L^2}}{L/2} = \frac{119.76EI}{L^3}.$$

$$\text{Force in } AB = \frac{(39.96 + 27.92)\frac{EI}{L^2}}{L/2} = \frac{143.76EI}{L^3}.$$

$$\text{The total force at joint } B = \frac{263.52EI}{L^3}.$$

(v) **Natural Frequency**:

Stiffness of the beam, $= \frac{263.52EI}{L^3}$.

Natural frequency, $\omega_n = \sqrt{\frac{k}{m}} = \frac{16.233}{L}\sqrt{\frac{EI}{mL}}$.

3. Find the natural frequency of the truss shown in the figure. Ignore the self-weight of the truss.
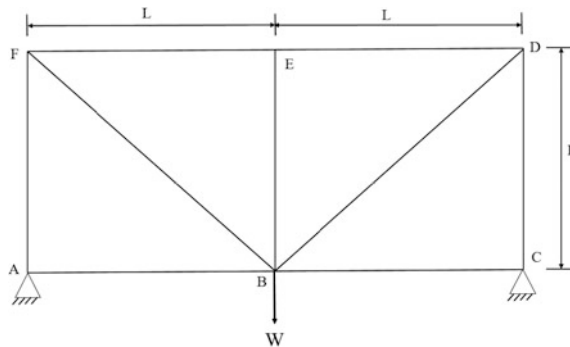
By using method of joints and unit force method,

Member	Length	P	p	PpL/AE
AB	L	0	0	0
BC	L	0	0	0
CD	L	−W/2	−1/2	WL/4AE
DE	L	−W/2	−1/2	WL/4AE
EF	L	−W/2	−1/2	WL/4AE
AF	L	−W/2	−1/2	WL/4AE
BF	1.414L	$W/\sqrt{2}$	$1/\sqrt{2}$	$WL/\sqrt{2}AE$
BD	1.414L	$W/\sqrt{2}$	$1/\sqrt{2}$	$WL/\sqrt{2}AE$
EB	1.414L	0	0	0
Total				2.414 WL/ AE

Total Displacement at B = 2.414 WL/AE

Stiffness, k = Force/Displacement = 0.414 AE/L

Natural frequency, $\omega_n = \sqrt{\frac{k}{m}} = 0.643 \sqrt{\frac{AE}{mL}}$.

4. Find the mass, stiffness and force matrices for the wooden beam supported on two springs as shown in the figure:

(i) **Stiffness Matrix**:

Stiffness matrix is derived by applying unit displacements at nodes 1 and 2.

Applying unit displacement at node 1,

$$k_{11} = k_1$$

$$k_{21} = 0$$

Applying unit displacement at node 2,

$$k_{12} = 0$$

$$k_{22} = k_2$$

Thus, the stiffness matrix is given by, $k = \begin{bmatrix} k_1 & 0 \\ 0 & k_2 \end{bmatrix}$

(ii) **Force Matrix**:

Force matrix is derived by finding the reaction at the fixed support.

$$F = \begin{bmatrix} -\frac{Pt}{2} & +\frac{P\theta}{L} \\ -\frac{Pt}{2} & -\frac{P\theta}{L} \end{bmatrix}$$

(iii) **Mass Matrix**:

Mass matrix is derived by applying unit acceleration at the nodes 1 and 2.

Applying unit acceleration at node 1,

$$m_{21}L = \frac{1}{2}\frac{m}{L}L\left(\frac{L}{3}\right)$$

$$m_{21} = \frac{M}{6}$$

$$m_{11} = \frac{M}{3}$$

Similarly, applying unit acceleration at node 2,

$$m_{12} = \frac{M}{6}$$

$$m_{22} = \frac{M}{3}$$

Thus, the mass matrix is given by,

$$M = \begin{bmatrix} \frac{M}{3} & \frac{M}{6} \\ \frac{M}{6} & \frac{M}{3} \end{bmatrix}$$

5. Using Lagrange's method, frame the equation of motion for the vibration isolator shown in the figure:

$$\text{Kinetic energy} = \frac{1}{2}m_1\dot{x}_1^2 + \frac{1}{2}m_2\dot{x}_2^2$$

$$\text{Potential energy} = \frac{1}{2}k_1x_1^2 + \frac{1}{2}k_1(x_1 - x_2)^2$$

$$\text{Dissipation energy} = \frac{1}{2}C\dot{x}_1^2$$

By using Lagrange's method,

$$\frac{d}{dt}\left(\frac{\partial(KE)}{\partial\dot{q}_i}\right) - \frac{\partial(KE)}{\partial q_i} + \frac{\partial(PE)}{\partial q_i} + \frac{\partial(DE)}{\partial\dot{q}_i} = Q_i$$

For the first degree of freedom,

$$\frac{\partial(KE)}{\partial\dot{x}_1} = m_1\dot{x}_1$$

$$\frac{d}{dt}\left(\frac{\partial(KE)}{\partial\dot{x}_1}\right) = m_1\ddot{x}_1$$

$$\frac{\partial(PE)}{\partial x_1} = (k_1 + k_2)x_1 - k_2x_2$$

$$\frac{\partial(DE)}{\partial\dot{x}_1} = C\dot{x}_1$$

Substituting in the above equation,

$$m_1\ddot{x}_1 + (k_1 + k_2)x_1 - k_2x_2 + C\dot{x}_1 = 0$$

Similarly, for the second degree of freedom,

$$m_2\ddot{x}_2 - k_2x_1 + k_2x_2 + C\dot{x}_1 = F_0e^{i\omega t}$$

Thus, the equation of motion is given by,

$$\begin{bmatrix} m_1 & 0 \\ 0 & m_2 \end{bmatrix}\begin{Bmatrix} \ddot{x}_1 \\ \ddot{x}_2 \end{Bmatrix} + \begin{bmatrix} C & 0 \\ 0 & C \end{bmatrix}\begin{Bmatrix} \dot{x}_1 \\ \dot{x}_2 \end{Bmatrix} + \begin{bmatrix} k_1 + k_2 & -k_2 \\ -k_2 & k_2 \end{bmatrix}\begin{Bmatrix} x_1 \\ x_2 \end{Bmatrix} = \begin{Bmatrix} 0 \\ F_0e^{i\omega t} \end{Bmatrix}$$

6. Decouple the equation of motion of undamped two degree of freedom system and solve. Use the following data:

$$m = \begin{bmatrix} m & 0 \\ 0 & m \end{bmatrix}, \quad k = \begin{bmatrix} 2k & -k \\ -k & 2k \end{bmatrix}$$

The frequencies and corresponding mode shapes are identified as follows:

$$\omega_1 = \sqrt{\frac{k}{m}}, \quad \omega_2 = \sqrt{\frac{3k}{m}}$$

$$\varnothing_1 = \left\{ \begin{matrix} 1 \\ 1 \end{matrix} \right\}, \varnothing_2 = \left\{ \begin{matrix} -1 \\ 1 \end{matrix} \right\}$$

(i) **Normalized Matrix**:

$$\varnothing_1^T M \varnothing_1 = \{ 1 \quad 1 \} \begin{bmatrix} m & 0 \\ 0 & m \end{bmatrix} \left\{ \begin{matrix} 1 \\ 1 \end{matrix} \right\} = 2m.$$

$$\varnothing_1^* = \frac{1}{\sqrt{2m}} \left\{ \begin{matrix} 1 \\ 1 \end{matrix} \right\}$$

$$\varnothing_2^T M \varnothing_2 = \{ -1 \quad 1 \} \begin{bmatrix} m & 0 \\ 0 & m \end{bmatrix} \left\{ \begin{matrix} -1 \\ 1 \end{matrix} \right\} = 2m.$$

$$\varnothing_2^* = \frac{1}{\sqrt{2m}} \left\{ \begin{matrix} -1 \\ 1 \end{matrix} \right\}$$

$$\tilde{P} = \frac{1}{\sqrt{2m}} \begin{bmatrix} 1 & -1 \\ 1 & 1 \end{bmatrix}$$

(ii) **Check**:

$\tilde{P}^T M \tilde{P} = \begin{bmatrix} 1 & 0 \\ 0 & 1 \end{bmatrix}$, which is an Identity matrix.

$\tilde{P}^T K \tilde{P} = \begin{bmatrix} \frac{k}{m} & 0 \\ 0 & \frac{3k}{m} \end{bmatrix}$. It is a diagonal matrix and the leading diagonal elements give the value of square of frequencies of the system.

(iii) **Equation of Motion**:

$$[M]\{\ddot{X}\} + [K]\{X\} = 0$$

$$\begin{bmatrix} m & 0 \\ 0 & m \end{bmatrix} \begin{Bmatrix} \ddot{x}_1 \\ \ddot{x}_2 \end{Bmatrix} + \begin{bmatrix} 2k & -k \\ -k & 2k \end{bmatrix} \begin{Bmatrix} x_1 \\ x_2 \end{Bmatrix} = 0$$

$$m_1 \ddot{x}_1 + 2kx_1 - kx_2 = 0$$

$$m_2 \ddot{x}_2 - kx_1 + kx_2 = 0$$

(iv) **Decoupling**:

The equation is expressed in the different domain by the following equation:

$$\{x\} = \tilde{P}\{y\}$$

$$\begin{Bmatrix} x_1 \\ x_2 \end{Bmatrix} = \tilde{P} \begin{Bmatrix} y_1 \\ y_2 \end{Bmatrix}$$

$$\begin{Bmatrix} x_1 \\ x_2 \end{Bmatrix} = \frac{1}{\sqrt{2m}} \begin{bmatrix} 1 & -1 \\ 1 & 1 \end{bmatrix} \begin{Bmatrix} y_1 \\ y_2 \end{Bmatrix}$$

(v) **Solution in Y Domain**:

$$[M]\{\ddot{X}\} + [K]\{X\} = 0$$

$$M\tilde{P}\ddot{Y} + K\tilde{P}Y = 0$$

Pre-multiplying with $\tilde{P}^{\mathrm{T}}$,

$$\tilde{P}^{\mathrm{T}} M \tilde{P} \ddot{Y} + \tilde{P}^{\mathrm{T}} K \tilde{P} Y = 0$$

$$\begin{bmatrix} 1 & 0 \\ 0 & 1 \end{bmatrix} \begin{Bmatrix} \ddot{y}_1 \\ \ddot{y}_2 \end{Bmatrix} + \begin{bmatrix} \omega_1^2 & 0 \\ 0 & \omega_1^2 \end{bmatrix} \begin{Bmatrix} y_1 \\ y_2 \end{Bmatrix} = 0$$

$$\ddot{y}_1 + \omega_1^2 y_1 = 0$$

$$\ddot{y}_2 + \omega_2^2 y_2 = 0$$

The solution is given by

$$y_1(t) = y_1(0) \cos \omega_1 t + \frac{\dot{y}_1(0)}{\omega_1} \sin \omega_1 t$$

$$y_2(t) = y_2(0) \cos \omega_2 t + \frac{\dot{y}_2(0)}{\omega_2} \sin \omega_2 t$$

(vi) **X Domain**:

$$\left\{ \begin{array}{c} x_1 \\ x_2 \end{array} \right\} = \frac{1}{\sqrt{2m}} \begin{bmatrix} 1 & -1 \\ 1 & 1 \end{bmatrix} \left\{ \begin{array}{c} y_1 \\ y_2 \end{array} \right\}$$

$$x_1(t) = \frac{1}{\sqrt{2m}} [y_1(t) - y_2(t)]$$

$$x_2(t) = \frac{1}{\sqrt{2m}} [y_1(t) + y_2(t)]$$

(vii) **Transforming Initial Conditions from X Domain to Y Domain**:

$$\{x\} = \tilde{P}\{y\}$$

$$\{y\} = \tilde{P}^{-1}\{x\}$$

$$\tilde{P} = \frac{1}{\sqrt{2m}} \begin{bmatrix} 1 & -1 \\ 1 & 1 \end{bmatrix}$$

$$\tilde{P}^{-1} = \frac{\sqrt{2m}}{2} \begin{bmatrix} 1 & 1 \\ -1 & 1 \end{bmatrix}$$

$$\left\{ \begin{array}{c} y_1 \\ y_2 \end{array} \right\} = \sqrt{\frac{m}{2}} \begin{bmatrix} 1 & 1 \\ -1 & 1 \end{bmatrix} \left\{ \begin{array}{c} x_1 \\ x_2 \end{array} \right\}$$

Thus, solution in Y domain is expressed as

$$y_1(t) = \sqrt{\frac{m}{2}}\left\{[(x_1(0)+x_2(0))\cos\omega_1 t] + \frac{1}{\omega_1}[(\dot{x}_1(0)+\dot{x}_2(0))\sin\omega_1 t]\right\}$$

$$y_2(t) = \sqrt{\frac{m}{2}}\left\{[(-x_1(0)+x_2(0))\cos\omega_2 t] + \frac{1}{\omega_2}[(-\dot{x}_1(0)+\dot{x}_2(0))\sin\omega_2 t]\right\}$$

7. For small damping, show that logarithmic decrement can be expressed in terms of vibration energy and energy dissipated per cycle.

$$\frac{x_2}{x_1} = e^{-\delta} = 1 - \delta + \frac{\delta^2}{2!}\cdots$$

Vibration energy is given by

$$U_1 = \frac{1}{2}kx_1^2, \quad U_2 = \frac{1}{2}kx_2^2$$

$$\text{Loss of energy} = \frac{U_1 - U_2}{U_1} = \frac{x_1^2 - x_2^2}{x_1^2}$$

$$= 1 - \frac{x_2^2}{x_1^2} = 1 - e^{-2\delta} = 1 - \left[1 - 2\delta + \frac{2\delta^2}{2!}\cdots\right]$$

$$= 2\delta.$$

8. Find the maximum dynamic amplification factor for the rectangular impulse loading shown in the figure.

(i) **Phase 1: 0 ≤ T ≥ S**

$$F(t) = F_0$$

$$x = \frac{\omega}{k} \int_0^T F_0 \sin \omega(T - t) dt$$

$$= \frac{\omega}{k} \left[-F_0 \frac{\cos \omega(T - t)}{\omega} \right]_0^T$$

$$= \frac{F_0}{k} \cos \omega(T - t) - \cos \omega T$$

$$= \frac{F_0}{k} [1 - \cos \omega T]$$

Since, $\frac{F_0}{k} = x_{st}$

$$\frac{x}{x_{st}} = 1 - \cos \omega T$$

Thus, Dynamic Amplification Factor, DAF $= 1 - \cos \omega T$.
Let $\omega = \frac{2\pi}{\tau}$, where τ is the natural period of the system.

$$DAF = 1 - \cos \omega \frac{2\pi}{\tau} T.$$

For getting the maximum Dynamic Amplification Factor,

$$\frac{d}{dt}(DAF) = \frac{2\pi}{\tau} \sin \omega \frac{2\pi}{\tau} T = 0$$

Since $\omega \neq 0$,

$$\sin \omega \frac{2\pi}{\tau} T = 0$$

$$\frac{2\pi}{\tau} T = \pi$$

$$T = \frac{\tau}{2}$$

Hence, the Dynamic Amplification is maximum when the duration of loading is half of the maximum value.

$$\mathrm{DAF_{max}} = 1 - \cos \omega \frac{2\pi}{\tau} \frac{\tau}{2} = 2.$$

(ii) **Phase 2**: **T > S**

According to the given loading condition, there is no loading in the second phase. But, the response will be due to the free vibration with the initial condition at $t = \mathbf{s}$. For phase 1,

$$\frac{x}{x_{st}} = 1 - \cos \omega T$$

$$x = x_{st}[1 - \cos \omega T]$$

$$\dot{x} = \omega x_{st} \sin \omega T$$

At t = s,

$$x_s = x_{st}[1 - \cos \omega s]$$

$$\dot{x}_s = \omega x_{st} \sin \omega s$$

For a free vibration response, the general response equation is given by,

$$x = C_1 \cos \omega T + C_2 \sin \omega T$$

Applying the initial conditions,

(i)   at $t = s$, $x = x_s$
(ii) at $t = s$, $\dot{x} = \dot{x}_s$

Thus, the general equation becomes,

$$x = x_s \cos \omega T + \frac{\dot{x}_s}{\omega} \sin \omega T$$

By substituting the values of x_s and $\dot{x}_s$ in the above equation,

$$x_s = x_{st}\{[1 - \cos \omega s] \cos \omega T + \sin \omega s \sin \omega T\}$$

The Dynamic Amplification Factor is given by

$$\frac{x}{x_{st}} = [1 - \cos \omega s] \cos \omega T + \sin \omega s \sin \omega T$$

Since, for a free vibration response, $x_{\max} = \sqrt{(x_0)^2 + \left(\frac{\dot{x}_0}{\omega}\right)^2}$

From the equation of DAF,

$$x_0 = 1 - \cos \omega s$$

$$\frac{\dot{x}_0}{\omega} = \sin \omega s$$

Thus,

$$\text{DAF}_{\max} = \sqrt{(1 - \cos \omega s)^2 + (\sin \omega s)^2} = \sqrt{2(1 - \cos \omega s)}$$

Since,

$$\cos 2\theta = 1 - 2 \sin^2 \theta$$

$$\text{DAF}_{\max} = 2 \sin \left(\frac{\omega s}{2} \right)$$

9. Find the response of the stepped pulse function shown in the figure:

(i) **Phase 1: $0 \leq T \leq q$**

$$x = \frac{\omega}{k} \int_0^T 2Q \sin \omega(T - t) dt$$

$$= \frac{\omega}{k} \left[-2Q \frac{\cos \omega(T - t)}{\omega} \right]_0^T$$

$$= \frac{2Q}{k} \cos \omega(T - t) - \cos \omega T$$

$$= \frac{2Q}{k} [1 - \cos \omega T]$$

Since, $\frac{2Q}{k} = x_{st}$

$$\frac{x}{x_{st}} = 1 - \cos \omega T$$

Thus, Dynamic Amplification Factor, DAF $= 1 - \cos \omega T$

Let, $\omega = \frac{2\pi}{\tau}$, where τ is the natural period of the system.

$$\text{DAF} = 1 - \cos \omega \frac{2\pi}{\tau} T.$$

For getting the maximum Dynamic Amplification Factor,

$$\frac{d}{dt} (\text{DAF}) = \frac{2\pi}{\tau} \sin \omega \frac{2\pi}{\tau} T = 0$$

Since $\omega \neq 0$,

$$\sin \omega \frac{2\pi}{\tau} T = 0$$

$$\frac{2\pi}{\tau} T = \pi$$

$$T = \frac{\tau}{2}$$

Hence, the Dynamic Amplification is maximum when the duration of loading is half of the maximum value.

$$\text{DAF}_{\text{max}} = 1 - \cos \omega \frac{2\pi}{\tau} \frac{\tau}{2} = 2.$$

(ii) **Phase 2: q $\leq$ T $\leq$ 2q**

Here, the response is due to the initial conditions and loadings.
The response due to initial conditions is given by

$$x = x_{st} [1 - \cos \omega T]$$

$$\dot{x} = \omega x_{st} \sin \omega T$$

At $t = s$,

$$x_s = x_{st} [1 - \cos \omega s]$$

$$\dot{x}_s = \omega x_{st} \sin \omega s$$

For a free vibration response, the general response equation is given by

$$x = C_1 \cos \omega T + C_2 \sin \omega T$$

Applying the initial conditions,

(i)   at $t = s$, $x = x_s$
(ii) at $t = s$, $\dot{x} = \dot{x}_s$

Thus, the general equation becomes

$$x = x_s \cos \omega T + \frac{\dot{x}_s}{\omega} \sin \omega T$$

By substituting the values of x_s and $\dot{x}_s$ in the above equation,

$$x_s = x_{st}\{[1 - \cos \omega s] \cos \omega T + \sin \omega s \sin \omega T\}$$

$$x_s = \frac{2Q}{k}\{[1 - \cos \omega s] \cos \omega T + \sin \omega s \sin \omega T\}$$

The response due to loading in the second phase is given by

$$\begin{aligned}
x &= \frac{\omega}{k} \int_0^T Q \sin \omega(T - t) \mathrm{d}t \\
&= \frac{\omega}{k} \left[-Q \frac{\cos \omega(T - t)}{\omega} \right]_0^T \\
&= \frac{Q}{k} \cos \omega(T - t) - \cos \omega T \\
&= \frac{Q}{k} [1 - \cos \omega T]
\end{aligned}$$

Thus, the total response is

$$x = \frac{2Q}{k}\{[1 - \cos \omega s] \cos \omega T + \sin \omega s \sin \omega T\} + \frac{Q}{k}[1 - \cos \omega T]$$

10. Find the response of the triangular pulse function shown in the figure:

The solution for the function is given by

$$x(t) = A \sin \omega t + B \cos \omega t + \frac{F_0}{k}\left(1 - \frac{t}{T}\right)$$

Applying the initial conditions

(i) at $t = 0$, $x_0 = 0$,

$$B = \frac{F_0}{k}$$

(ii) at $t = 0$, $\dot{x}_0 = 0$,

$$\dot{x}(t) = \omega A \cos \omega t - \omega B \sin \omega t + \frac{F_0}{k}\left(-\frac{1}{T}\right)$$

$$A = \frac{F_0}{k}\frac{1}{\omega T}$$

The complete solution is

$$x(t) = \frac{F_0}{k}\left[\left(\frac{\sin \omega t}{\omega T}\right) - \cos \omega t - \frac{t}{T} + 1\right]$$

(i) **Phase 1: $0 \leq T \leq t$**
The response for the triangular pulse loading is

$$x(t) = \frac{F_0}{k}\left[\left(\frac{\sin \omega T}{\omega T}\right) - \cos \omega T\right]$$

The Dynamic Amplification Factor is

$$\frac{F_0}{k} = x_{st}$$

$$\text{DAF} = \frac{x}{x_{st}} = \left(\frac{\sin \omega T}{\omega T}\right) - \cos \omega T$$

(ii) **Phase 2: T > t**

According to the given loading condition, there is no loading in the second phase. But, the response will be due to the free vibration with the initial condition at $T = t$.

For phase 1,

$$\frac{x}{x_{st}} = (\sin \omega t) - \cos \omega t$$

$$x = x_{st}[(\sin \omega T) - \cos \omega T]$$

$$\dot{x} = x_{st}\left[\cos \omega T + \omega \sin \omega T - \frac{1}{\omega T}\right]$$

At $T = t$,

$$x = x_{st}[(\sin \omega t) - \cos \omega t]$$

$$\dot{x} = x_{st}\left[\frac{\cos \omega t}{t} + \omega \sin \omega t - \frac{1}{t}\right]$$

For a free vibration response, the general response equation is given by

$$x = C_1 \cos \omega T + C_2 \sin \omega T$$

Applying the initial conditions

(i) at $T = t$, $x = x_T$
(ii) at $T = t$, $\dot{x} = \dot{x}_t$

Thus, the general equation becomes

$$x = x_t \cos \omega T + \frac{\dot{x}_t}{\omega} \sin \omega T$$

By substituting the values of x_t and $\dot{x}_t$ in the above equation,

$$x_t = x_{st}\left\{[(\sin \omega t) - \cos \omega t]\cos \omega T + \left[\frac{\cos \omega t}{\omega t} + \sin \omega t - \frac{1}{\omega t}\right]\sin \omega T\right\}$$

The Dynamic Amplification Factor is given by

$$\frac{x}{x_{st}} = [(\sin \omega t) - \cos \omega t]\cos \omega T + \left[\frac{\cos \omega t}{\omega t} + \sin \omega t - \frac{1}{\omega t}\right]\sin \omega T.$$

Chapter 4
Damping in Offshore Structures

Abstract This chapter deals with the methods of estimating damping in offshore structures. Different types of damping models, their comparison, and suitability to offshore structures are discussed in detail. Example problems are solved, and estimation of damping using different models is explained.

Keywords Structural damping · Viscous damping · Coulomb damping · Rayleigh damping · Caughey damping

4.1 Introduction

Under ideal conditions of no damping, if the system is set to vibration, it will be excited indefinitely at constant amplitude at its natural frequency. But in real time, any system set to vibration comes to rest, necessarily after passage of time; damping offered by the presence of air may be one of the reasons. As such, undamped systems are hypothetical, since damping is inherently present in the atmosphere. Further, ocean structures are under the influence of waves and current, which offers significant amount of damping to the structural system that is set in vibration. The basic types of damping are namely: (i) coulomb damping and (ii) viscous damping. Coulomb damping results from sliding of two surfaces; it is also called dry damping or friction damping. The damping force is the product of the normal force and the coefficient of friction between the body surface and the plane of motion. Note that the damping force in this case is independent of velocity of motion of the body which is under vibration. In case of viscous damping, the damping force accounts for the viscosity of the system. The presence of fluid medium around the body significantly influences the damping force acting on the body. Damping force will be proportional to the magnitude of the velocity and has the unit of N/(m s). Viscous damping seems to be more relevant to offshore structural systems due to the inherent presence of liquid medium around the body. Frictional forces are not conservative, as they cannot be derived from a potential function that is based on the displacement (response) of the vibrating system. However, these forces are

highly responsible for dissipation of energy or conversion of energy from one form to the other. This results in reduction in response of the structural system. The energy consumed by the friction forces is converted into heat energy and dissipated by conduction, by convection to the fluid surrounding the structure and by radiation.

Frictional forces in a system may arise due to any one of the following physical processes (Wilson 1984). There can be friction among the materials, leading to internal viscous damping. This is highly practical due to the use of modern materials like composites in offshore structures. At the connections or joints, due to the presence of materials of different composition, bimetallic coupling can result in friction forces. There can also be friction between two structural components, leading to structural damping. There can be friction between the structural members and fluid surrounding them, leading to external viscous damping. Lastly, there can be friction between the structural members at their supports which are in contact with them. This leads to coulomb damping. However, it is very difficult to quantify these damping forces in a given system, as the causes for such forces are diverse. Structural damping is usually considered to be 0.2–0.5% of that of the critical damping for steel platforms (Adams and Baltrop 1991). For concrete, this can be of the order of 0.5–1.5%. Hydrodynamic damping originates from the waves surrounding the offshore structures. They are found in two common forms namely: (i) radiation damping and (ii) viscous damping (Bearman and Russell 1996). Radiation damping is determined by potential theory. It exhibits a strong dependence on frequency and submergence effects. Literature shows that the drag damping is lower for larger diameter vertical column members in offshore structures; this is of the order 0.1%. Damping ratio of the marine structure, including the effect of added mass can be expressed as the ratio of the dry structure, as given below:

$$\xi_{\text{wet}} = \xi_{\text{dry}} \left[\frac{m^*_{\text{dry}} \omega^*_{\text{dry}}}{m^*_{\text{wet}} \omega^*_{\text{wet}}} \right], \tag{4.1}$$

where m^* and ω^* are generalized mass and frequency, respectively (Naess and Moan 2013). Literature also shows that the total damping ratio is about 2% for the first three modes for gravity platforms.

Classical damping is an approximate idealization if similar damping is distributed throughout the structure. However, in offshore structures, uniform distribution of damping throughout the structure is not applicable due to many reasons: (i) variation in material properties of members at connections; (ii) use of composites for variety of members; (iii) deck and the substructure shall be even isolated so that the large displacements of the deck under wind forces do not influence the substructure and that of the effects caused by waves do not influence the deck motion, etc. Three damping models are popular for offshore structures namely: (i) Rayleigh damping; (ii) Caughey damping; and (iii) modal damping. These are explained below with examples.

4.2   Damping Models: Rayleigh Damping

Consider a mass-proportional or a stiffness-proportional damping as given below:

$$C = a_0 M \qquad (4.2)$$

$$C = a_1 K, \qquad (4.3)$$

where a_0 and a_1 are constants having units as s^{-1} and s, respectively. In both the cases, C is diagonal by virtue of modal orthogonality properties; hence, these are classical damping matrices. Physically, they represent damping models as shown in Fig. 4.1.

In case of mass proportional damping, damping can be negligibly small due to air damping, but in offshore structures, this can be significantly high. In case of stiffness-proportional damping, dissipation of energy depends upon the relative displacement between the successive mass points. Keeping [C] as proportional to modal damping ratios, for the system with mass proportional damping, the damping ratio will be given by

$$
\begin{aligned}
C_n &= a_0 M_n \\
\xi_n &= \frac{C_c}{2 M_n \omega_n} = \frac{a_0 M_n}{2 M_n \omega_n} \\
\xi_n &= \frac{a_0}{2} \frac{1}{\omega_n}
\end{aligned}
\qquad (4.4)
$$

a) Mass proportional damping   b) Stiffness proportional damping
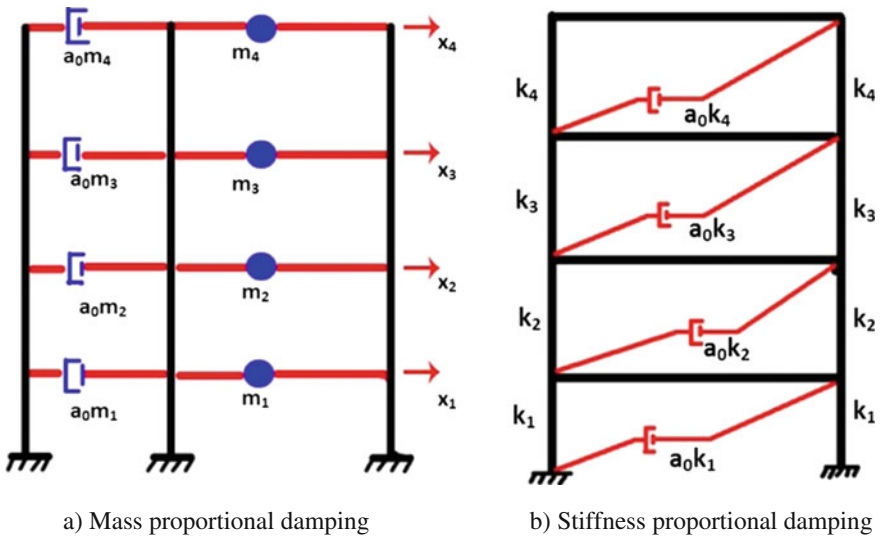
Fig. 4.1 Damping models

The damping ratio is inversely proportional to the natural frequency. Hence, a_0 can be settled to obtain a specified value of the damping ratio in nay mode, as given below:

$$a_0 = 2\xi_i \omega_i \tag{4.5}$$

With a_0 determined, damping matrix $[C]$ is known from Eq. (4.4). Similarly, for stiffness-proportional damping, we get the following relationships:

$$
\begin{aligned}
C_n &= a_1 K_n \\
\xi_n &= \frac{C_c}{2M_n \omega_n} = \frac{a_1 \omega_n^2 M_n}{2M_n \omega_n} \\
\xi_n &= \frac{a_1}{2} \omega_n
\end{aligned}
\tag{4.6}
$$

$$a_1 = \frac{2\xi_j}{\omega_j} \tag{4.7}$$

With a_1 determined from the above equation, damping matrix $[C]$ can be computed from Eq. (4.6). It is seen that both the damping models, being either mass proportional or stiffness proportional, are not validating the actual behavior of the offshore structures, experimentally. Hence to be consistent with the experimental observations, Rayleigh damping is proposed for offshore structures. The damping matrix will be proportional to both mass and stiffness as given below:

$$C = a_0 M + a_1 K \tag{4.8}$$

Damping ratio for nth mode of such a system is given by

$$\xi_n = \frac{a_0}{2} \frac{1}{\omega_n} + \frac{a_1}{2} \omega_n \tag{4.9}$$

Coefficients, a_0 and a_1 can be determined for a specific damping ratio (ξ_i, ξ_j) for ith and jth modes, respectively. For Fig. 4.2, one can pick up the damping ratio in such a manner that it is same for both the chosen frequencies (ω_i, ω_j).

Fig. 4.2 Rayleigh damping
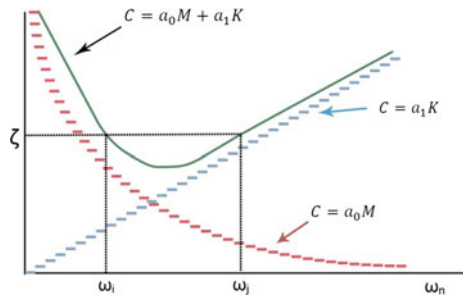
$$\xi_n = \frac{a_0}{2} \frac{1}{\omega_n} + \frac{a_1}{2} \omega_n$$

$$\xi_i = \frac{a_0}{2} \frac{1}{\omega_i}$$

$$\xi_j = \frac{a_1}{2} \omega_j \qquad (4.10)$$

$$\left\{ \begin{array}{c} \xi_i \\ \xi_j \end{array} \right\} = \frac{1}{2} \begin{bmatrix} \frac{1}{\omega_i} & \omega_i \\ \frac{1}{\omega_j} & \omega_j \end{bmatrix} \left\{ \begin{array}{c} a_0 \\ a_1 \end{array} \right\}$$

For $\xi_i, \xi_j = \xi$, then

$$\left\{ \begin{array}{c} a_0 \\ a_1 \end{array} \right\} = \frac{2\omega_i\omega_j}{\omega_j^2 - \omega_i^2} \begin{bmatrix} \omega_j & -\omega_i \\ -\frac{1}{\omega_j} & \frac{1}{\omega_i} \end{bmatrix} \left\{ \begin{array}{c} \xi_i \\ \xi_j \end{array} \right\}$$

$$a_0 = 2\xi \frac{\omega_i\omega_j}{\omega_i + \omega_j} \qquad (4.11)$$

$$a_1 = \frac{2\xi}{\omega_i + \omega_j}$$

Knowing the constants a_0 and a_1, damping matrix $[C]$ can be estimated using Eq. (4.8). Few critical observations in applying this procedure are as follows: (i) Modes (i, j) with specified damping ratios need to be chosen; and (ii) one must select reasonable value of damping ratios for all the modes. For example, if one wants to include third mode in the analysis with roughly the same damping ratio in all the modes (which is desired), then one should select the third frequency such that this condition is satisfied. Hence truncation of modes, in such cases, is also governed by the appropriate (nearly equal) damping ratios to the chosen frequencies.

4.2.1 Example Problem

Let us consider the spring-mass system shown in Fig. 4.3. Let m be 3500 kg and k be 1500 kN/m. Taking damping ratio for first two modes as 5%, compute the damping ratio for the third mode.
    Solution:
    Please note that for classical damping, it is essential that the damping in all the modes included in the analysis should be equal. Should we need to include the third mode also in the analysis, then it is essential to check whether the third mode has damping equivalent to that of the first two modes. By this way, it also necessitates the truncation of higher modes in the dynamic analysis.

Fig. 4.3 Example problem
4.2.1
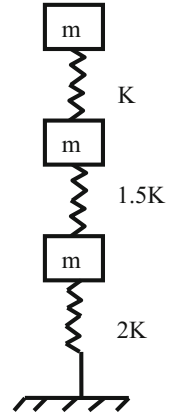
By following any standard procedure explained in the previous chapters, one can readily determine all the frequencies and their corresponding mode shapes. The computed values are given below.

$$\left[\omega_1 = 0.57\sqrt{\left[\frac{k}{m}\right]} \quad 01.414\sqrt{\left[\frac{k}{m}\right]} \quad 2.163\sqrt{\left[\frac{k}{m}\right]}\right]$$

After substituting for the values of mass and stiffness, we get

$[\omega] = [11.8\,\text{rad/s} \quad 29.27\,\text{rad/s} \quad 44.778\,\text{rad/s}]$. The corresponding mode shapes are as given below:

$$[\Phi] = \begin{bmatrix} 1 & 1 & 1 \\ 0.68 & -1 & -3.68 \\ 0.32 & 1 & 4.68 \end{bmatrix}$$

$$[M] = 3500 \begin{bmatrix} 1 & 0 & 0 \\ 0 & 1 & 0 \\ 0 & 0 & 1 \end{bmatrix}$$

$$[K] = 1500 \times 10^3 \begin{bmatrix} 1 & -1 & 0 \\ -1 & 2.5 & -1.5 \\ 0 & -1.5 & 3.5 \end{bmatrix}$$

$$a_0 = 2 \left[\frac{\omega_1 \omega_2}{\omega_1 + \omega_2} \right] (0.05) = 2 \left[\frac{11.8 \times 29.27}{(11.8 + 29.27)} \right] (0.05) = 0.841$$

$$a_1 = \frac{2\xi}{\omega_1 + \omega_2} = \frac{2 \times 0.05}{(11.8 + 29.27)} = 0.0024$$

$$[C] = a_0 M + a_1$$

$$[C] = (0.841 \times 3500) \begin{bmatrix} 1 & 0 & 0 \\ 0 & 1 & 0 \\ 0 & 0 & 1 \end{bmatrix} + 0.0024$$

$$\times 1500 \times 10^3 \begin{bmatrix} 1 & -1 & 0 \\ -1 & 2.5 & -1.5 \\ 0 & -1.5 & 3.5 \end{bmatrix}$$

$$= \begin{bmatrix} 6543.5 & -3600 & 0 \\ -3600 & 11943.5 & -5400 \\ 0 & -5400 & 15543.5 \end{bmatrix} \text{Ns/m}$$

To find the damping ratio in the third mode:

$$\xi_n = \frac{a_0}{2} \frac{1}{\omega_n} + \frac{a_1}{2} \omega_n$$

$$\xi_3 = \frac{a_0}{2} \frac{1}{\omega_3} + \frac{a_1}{2} \omega_3$$

$$\xi_3 = \frac{0.841}{2} \left[\frac{1}{44.778} \right] + \frac{0.0024}{2} \times 44.778 = 6.31\%$$

As the damping ratios in all the modes are almost equal, all the three modes shall be considered for the analysis.

4.3 Caughey Damping

If it is desired to specify the damping ratios in more than two modes, then a general formation of classified damping is interesting (Caughey 1960). Let the natural frequencies and mode shapes satisfy the following relationship:

$$K\varphi_r = \omega_r^2 M \varphi_r \tag{4.12}$$

Pre-multiplying Eq. (4.12) on both sides, we get:

$$\varphi_n^T [KM^{-1}K] \varphi_r = \omega_r^2 \varphi_n^T [KM^{-1}MK] \varphi_r = 0 \text{ for } n \neq r \text{ due to orthogonality} \tag{4.13}$$

Further, pre-multiplying Eq. (4.12) on both sides, we get:

$$
\begin{aligned}
\varphi_n^T[(KM^{-1})^2 K]\varphi_r &= \omega_r^2 \varphi_n^T[KM^{-1}KM^{-1}M]\varphi_r \\
&= \omega_r^2[KM^{-1}K]\varphi_r = 0 \text{ for } n \neq r
\end{aligned}
\tag{4.14}
$$

By repeated application of this procedure, a family of orthogonality relations can be obtained. This can be expressed in a compact form, as given below:

$$
\begin{aligned}
\varphi_n^T C_\ell \varphi_r &= 0 \text{ for } n \neq r \\
C_\ell &= [KM^{-1}]^\ell K \text{ for } \ell = 0, 1, 2, \ldots \infty
\end{aligned}
\tag{4.15}
$$

Now, pre-multiplying and rewriting the above equation as follows:

$$
\begin{aligned}
C_\ell &= M^{-1}M[KM^{-1}]^\ell K \text{ for } \ell = 0, 1, 2, 3, \ldots \infty \\
&= M[M^{-1}K][M^{-1}K]\ldots K \\
&= M[M^{-1}K]^\ell \text{ for } \ell = 0, 1, 2, 3 \ldots \infty
\end{aligned}
\tag{4.16}
$$

Alternatively, pre-multiplying Eq. (4.12) we get

$$
\varphi_n^T M K^{-1} K \varphi_r = \omega_r^2 \varphi_n^T[MK^{-1}]M\varphi_r
\tag{4.17}
$$

By following the same procedure as discussed above, we get

$$
C_\ell = M[M^{-1}K]^\ell \text{ for } \ell = -1, -2, -3, \ldots - \infty
\tag{4.18}
$$

Combining Eqs. (4.16) and (4.18), we get

$$
C_\ell = M \sum_{\ell=-\infty}^{\infty} a_\ell [M^{-1}K]^\ell
\tag{4.19}
$$

It can be shown that in the above equation, N terms in the infinite series will be independent. This shall lead to a general form of a classical damping matrix, which is given by

$$
C_\ell = M \sum_{\ell=0}^{N-1} a_\ell [M^{-1}K]^\ell,
\tag{4.20}
$$

where N is the number of degrees of freedom and a_l are constants. First three terms in the series are given by

$$a_0 M[M^{-1}K]^0 = a_0 M$$
$$a_1 M[M^{-1}K]^1 = a_1 K \qquad (4.21)$$
$$a_2 M[M^{-1}K]^2 = a_2 K M^{-1} K$$

It can be seen that the first two terms in the series are same as the Rayleigh damping. Suppose, if one wishes to specify the damping ratios for J modes of the N degrees-of-freedom system, then J terms need to be included in the Caughey series. They could be any J of the N terms of Eq. (4.20). Typically, first J terms included will be

$$C = M \sum_{\ell=0}^{J-1} a_\ell [M^{-1}K]^\ell \qquad (4.22)$$

For nth mode, generalized damping is given by

$$C_n = \varphi_n^T C \varphi_n = \sum_{\ell=0}^{N-1} \varphi_n^T C_\ell \varphi_n$$
$$C_\ell = M[M^{-1}K]^\ell$$
$$\text{For } \ell = 0 : \varphi_n^T C_0 \varphi_n = \varphi_n^T (a_0 M) \varphi_n = a_0 M_n \qquad (4.23)$$
$$\text{For } \ell = 1 : \varphi_n^T C_1 \varphi_n = \varphi_n^T (a_1 K) \varphi_n = a_1 \omega_n^2 M_n$$
$$\text{For } \ell = 2 : \varphi_n^T C_2 \varphi_n = \varphi_n^T (a_2 K M^{-1} K) \varphi_n$$
$$= a_2 \omega_n^2 \varphi_n^T K \varphi_n = a_2 \omega_n^2 (\omega_n^2 M_n) = a_2 \omega_n^4 M_n$$

Hence, we get

$$C_n = \sum_{\ell=0}^{N-1} a_\ell \omega_n^{(2\ell-1)} M_n \qquad (4.24)$$

Damping ratio is given by

$$\xi_n = \frac{C_n}{2M_n \omega_n}$$
$$\xi_n = \frac{1}{2} \sum_{\ell=0}^{N-1} a_\ell \omega_n^{(2\ell-1)} \qquad (4.25)$$

Coefficients, a_l can be determined from the damping ratios specified in any J modes, by solving J algebraic equations of Eq. (4.25), for unknowns of $a = 0, 1, \ldots, J-1$. With a_1 determined, damping matrix $[C_n]$ is known from Eq. (4.24) and the damping ratios are given by Eq. (4.25).

4.3.1 Critical Problems Associated with Caughey Damping

- The algebraic equations of Eq. (4.25) are numerically ill-conditioned because the coefficients $\omega_n^{-1}, \omega_n, \omega_n^3, \ldots$ can differ by orders of high magnitude.
- If more than two terms are included in the Caughey series, $[C]$ becomes a full matrix, although $[K]$ is banded, and lumped mass matrix is diagonal. This will increase the computational cost for analyzing large systems.

Hence, Rayleigh damping is preferred and assumed in most of the practical cases.

4.3.2 Example Problem

Let us consider the spring-mass system shown in Fig. 4.4. Let m be 3500 kg and k be 1500 kN/m. Evaluate classical damping matrix for all the three modes for damping ratio of 5%.

 Solution:

By following any standard procedure explained in the previous chapters, one can readily determine all the frequencies and their corresponding mode shapes.

The computed values are given below.

$$\left[\omega_1 = 0.57\sqrt{\left[\frac{k}{m}\right]} \quad 01.414\sqrt{\left[\frac{k}{m}\right]} \quad 2.163\sqrt{\left[\frac{k}{m}\right]}\right]$$

After substituting for the values of mass and stiffness, we get

$$[\omega] = [11.8\,\text{rad/s} \quad 29.27\text{rad/s} \quad 44.778\text{rad/s}].$$

Fig. 4.4 Example problem 4.3.2
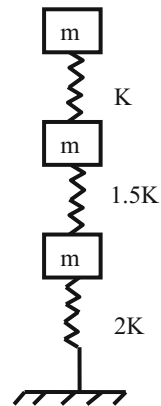
The corresponding mode shapes are as given below:

$$[\Phi] = \begin{bmatrix} 1 & 1 & 1 \\ 0.68 & -1 & -3.68 \\ 0.32 & 1 & 4.68 \end{bmatrix}$$

Caughey series for 3 degrees of freedom is given by

$$C = a_0 M + a_1 K + a_2 K M^{-1} K$$

$$\xi_n = \frac{1}{2} \sum_{\ell=0}^{2} a_\ell \omega_n^{(2\ell-1)}$$

$$\xi_n = \frac{a_0}{2}\left(\frac{1}{\omega_n}\right) + \frac{a_1 \omega_n}{2} + \frac{a_2 \omega_n^3}{2}$$

$$2\xi_n = \frac{a_0}{\omega_n} + a_1 \omega_n + a_2 \omega_n^3$$

$$2\begin{Bmatrix} 0.05 \\ 0.05 \\ 0.05 \end{Bmatrix} = \begin{bmatrix} 1/11.48 & 11.8 & 11.8^3 \\ 1/29.27 & 29.27 & 29.27^3 \\ 1/44.778 & 44.78 & 44.778^3 \end{bmatrix} \begin{Bmatrix} a_0 \\ a_1 \\ a_2 \end{Bmatrix}$$

Determine a_0, a_1 and a_2; then obtain $[C]$ using Eq. (4.24).

$$a_o = 0.772$$
$$a_1 = 0.003$$
$$a_2 = -5.812 \times 10^{-7}$$

$$C = \begin{bmatrix} 6454.743 & -3192.3 & -560.443 \\ -3192.3 & 10402.529 & -3387.343 \\ -560.443 & -3387.343 & 13034.386 \end{bmatrix}$$

4.4   Classical Damping Matrix by Damping Matrix Super-Positioning

We know that the damping matrix is given by the following equation:

$$\varphi^T c \varphi = C$$
$$C_n = \xi_n (2 M_n \omega_n) \qquad (4.26)$$
$$c = \left(\varphi^T\right)^{-1} C \varphi^{-1}$$

Determining $[C_n]$ using the above equation is inefficient because it requires inversion of two matrices of order N. Hence alternatively, using the orthogonality principle, we get

$$\varphi^T m \varphi = M$$

It can be shown that

$$\varphi^{-1} = M^{-1} \varphi^T m$$

$$(\varphi^T)^{-1} = m \varphi M^{-1}$$

(4.27)

From the Eq. (4.27), the required inverse matrices can be readily obtained because M is a diagonal matrix of generalized modal mass M_n; hence M^{-1} is easily computed as all the diagonal elements are $(1/M^n)$. Further, $[K]$ is a symmetric matrix and this property can be advantageous to perform the required operation. Substituting Eq. (4.27) in (4.26), we get

$$c = [m \varphi M^{-1}] C [M^{-1} \varphi^T m] \tag{4.28}$$

Since $[M]$ and $[C]$ are diagonal matrices, Eq. (4.28) can be rewritten as

$$c = m \left[\sum_{n=1}^{N} \frac{2 \xi_n \omega_n}{M_n} \varphi_n \varphi_n^T \right] m \tag{4.29}$$

nth term in the above summation is the contribution of the nth mode to the damping matrix $[C]$, with its damping ratio ξ_n, If this term in not included, then $[C]$ will imply zero damping ratio in the nth mode.

4.4.1   Critical Issues

- It is practical to include any first J modes even though N degrees of freedom exist.
- Lack of damping in modes $(J + 1)$ to N does not create any numerical problems in an unconditionally stable time-stepping procedure is chosen to integrate the equation of motion.

4.4.2 Example Problem

Let us consider the spring-mass system shown in Fig. 4.5. Let m be 3500 kg and k be 1500 kN/m. Determine damping matrix by superimposing the damping matrices for first two modes, each with 5% damping ratio.

Solution:

By following any standard procedure explained in the previous chapters, one can readily determine all the frequencies and their corresponding mode shapes.

The computed values are given below.

$$\left[\omega_1 = 0.57\sqrt{\left[\frac{k}{m}\right]} \quad 01.414\sqrt{\left[\frac{k}{m}\right]} \quad 2.163\sqrt{\left[\frac{k}{m}\right]}\right]$$

After substituting for the values of mass and stiffness, we get

$$[\omega] = [11.8\,\text{rad/s} \quad 29.27\text{rad/s} \quad 44.778\text{rad/s}].$$

The corresponding mode shapes are as given below:

$$[\Phi] = \begin{bmatrix} 1 & 1 & 1 \\ 0.68 & -1 & -3.68 \\ 0.32 & 1 & 4.68 \end{bmatrix}$$

The damping matrix is given by Eq. (4.29). Individual term of the matrix is now determined as below:

$$M = \varphi^T m \varphi$$

Fig. 4.5 Example problem 4.4.2
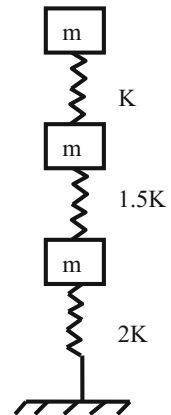
For the first mode,

$$M_1 = \{1 \quad 0.68 \quad 0.32\} \begin{bmatrix} 3500 & 0 & 0 \\ 0 & 3500 & 0 \\ 0 & 0 & 3500 \end{bmatrix} \begin{Bmatrix} 1 \\ 0.68 \\ 0.32 \end{Bmatrix}$$

$$= 5476.8.$$

$$C_1 = \frac{2\xi_1\omega_1}{M_1} m\varphi_1\varphi_1^T m$$

$$= \frac{2 \times 0.05 \times 11.8}{5476.8} \begin{bmatrix} 3500 & 0 & 0 \\ 0 & 3500 & 0 \\ 0 & 0 & 3500 \end{bmatrix} \begin{Bmatrix} 1 \\ 0.68 \\ 0.32 \end{Bmatrix}$$

$$\times \{1 \quad 0.68 \quad 0.32\} \begin{bmatrix} 3500 & 0 & 0 \\ 0 & 3500 & 0 \\ 0 & 0 & 3500 \end{bmatrix}$$

$$= \begin{bmatrix} 2640.228 & 1794.844 & 845.384 \\ 1794.844 & 1219.690 & 575.153 \\ 845.384 & 575.153 & 270.231 \end{bmatrix}$$

For the second mode,

$$M_2 = \{1 \quad -1 \quad -1\} \begin{bmatrix} 3500 & 0 & 0 \\ 0 & 3500 & 0 \\ 0 & 0 & 3500 \end{bmatrix} \begin{Bmatrix} 1 \\ -1 \\ -1 \end{Bmatrix}$$

$$= 10500.$$

$$C_2 = \frac{2\xi_2\omega_2}{M_2} m\varphi_2\varphi_2^T m$$

$$= \frac{2 \times 0.05 \times 29.27}{10500} \begin{bmatrix} 3500 & 0 & 0 \\ 0 & 3500 & 0 \\ 0 & 0 & 3500 \end{bmatrix} \begin{Bmatrix} 1 \\ -1 \\ -1 \end{Bmatrix}$$

$$\times \{1 \quad -1 \quad -1\} \begin{bmatrix} 3500 & 0 & 0 \\ 0 & 3500 & 0 \\ 0 & 0 & 3500 \end{bmatrix}$$

$$= 3414.833 \begin{bmatrix} 1 & -1 & -1 \\ -1 & 1 & 1 \\ -1 & 1 & 1 \end{bmatrix}$$

Now, the total damping matrix, after super-positioning two modes is given by

$$C = C_1 + C_2$$

$$= \begin{bmatrix} 2640.228 & 1794.844 & 845.384 \\ 1794.844 & 1219.690 & 575.153 \\ 845.384 & 575.153 & 270.231 \end{bmatrix}$$

$$+ 3414.833 \begin{bmatrix} 1 & -1 & -1 \\ -1 & 1 & 1 \\ -1 & 1 & 1 \end{bmatrix}$$

$$= \begin{bmatrix} 6055.466 & -1620.394 & -2569.854 \\ -1620.394 & 4634.928 & 3990.391 \\ -2569.854 & 3990.391 & 3685.469 \end{bmatrix}$$

Please note that the $[C]$, as computed from the above method, implies that there is no damping in the third mode, as only first two modes are considered.

4.5   Evaluation of Damping from Experimental Results

Free vibration experiment is carried out to determine the natural frequency and damping coefficient of the setup. Establishing the natural frequency and damping of the system is one of the important steps in the experiments and will help to determine the dynamic characteristics of the system. For heave free vibration, a weight approximately 7 kg is placed carefully at CG location of the TLP model. The weight is removed quickly and the resulting motions are recorded using accelerometers. A typical time history curve of the free vibration in heave direction is shown in Fig. 4.6. A small nudge is given to the TLP model in the surge direction, and the resulting motion is recorded. A time history plot of the free vibration in terms of surge acceleration is shown in Fig. 4.7. The black line in the figure is a 17-point moving average that depicts the variation of the surge acceleration without the high-frequency motions, making the overall surge variation and specifically the period easier to identify.

Based on the results of free vibration tests carried out on the scaled model, natural period and damping coefficient in heave and surge mode are obtained from the time series shown in the above figures. Logarithmic decrement method is used to determine the damping coefficient. Results obtained are shown in Table 4.1 for the TLP with and without perforated columns. TLP with perforated columns shows higher damping coefficient and higher time period in comparison to that without perforated columns (Chakrabarti and Hanna 1990).
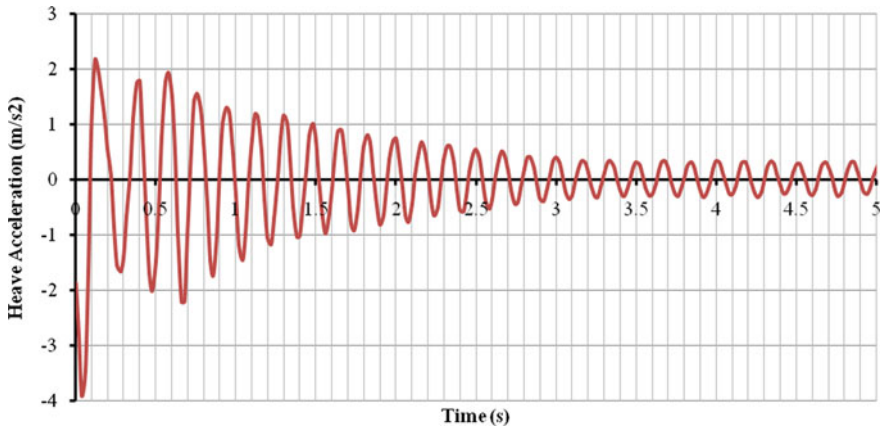
Fig. 4.6 Free vibration experiment—Heave acceleration of model with perforated column
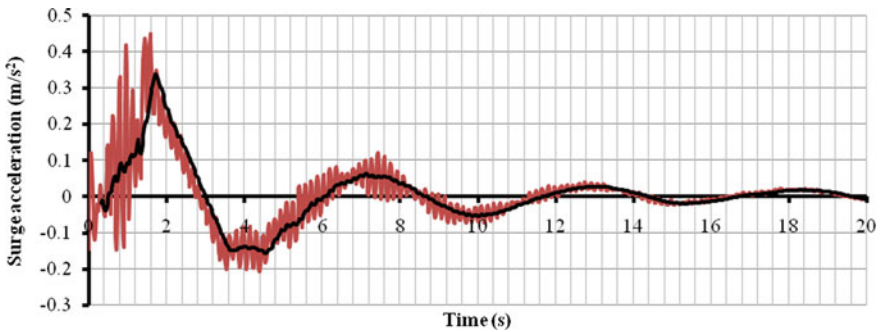
Fig. 4.7 Free vibration experiment—Surge acceleration of model with perforated column

Table 4.1 Results of free vibration experiment

Description	TLP without perforated column	TLP with perforated column
Heave damped time period	0.17	0.18
Surge damped time period	4.68	5.61
Heave damping coefficient	0.014	0.02
Surge damping coefficient	0.148	0.251

Example Problems

1. Determine the frequency and mode shapes for the following system and obtain
   the damping matrix using (i) Rayleigh damping, (ii) Caughey damping and
   (iii) matrix super-positioning. Let $m = 1000$ kg and $k = 1500$ kN/m. The
   damping ratio for all the three modes is 5%.
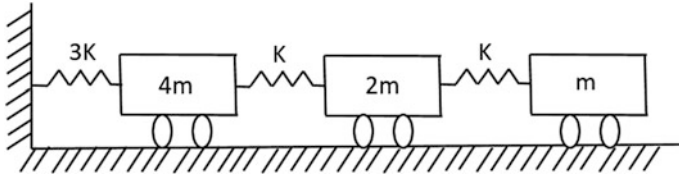
(i) **Frequency and mode shape**:

By following the standard procedure, the frequencies and mode shapes are identified as follows:

$$\omega_1 = 0.457\sqrt{\frac{k}{m}}$$

$$\omega_2 = \sqrt{\frac{k}{m}}$$

$$\omega_3 = 1.34\sqrt{\frac{k}{m}}$$

By substituting the values of m and k,

$$\omega_1 = 17.70\,\text{rad/s}$$
$$\omega_2 = 38.73\,\text{rad/s}$$
$$\omega_3 = 51.90\,\text{rad/s}$$

The corresponding mode shapes are given as

$$\varnothing = \begin{bmatrix} 1 & 1 & 1 \\ 3.162 & 0 & -3.162 \\ 4 & -1 & 4 \end{bmatrix}$$

(ii) **Rayleigh damping**:

$$\text{Mass matrix,}\, m = 1000 \begin{bmatrix} 4 & 0 & 0 \\ 0 & 2 & 0 \\ 0 & 0 & 1 \end{bmatrix} = \begin{bmatrix} 4000 & 0 & 0 \\ 0 & 2000 & 0 \\ 0 & 0 & 1000 \end{bmatrix}$$

$$\text{Stiffness matrix,}\, k = 1500 \times 10^3 \begin{bmatrix} 4 & -1 & 0 \\ -1 & 2 & -1 \\ 0 & -1 & 1 \end{bmatrix}$$

$$a_o = 2\xi\left[\frac{\omega_1\omega_2}{\omega_1+\omega_2}\right] = 2 \times 0.05\left[\frac{17.70 \times 38.73}{17.70+38.73}\right] = 1.215$$

$$a_1 = 2\xi\left[\frac{1}{\omega_1+\omega_2}\right] = 2 \times 0.05\left[\frac{1}{17.70+38.73}\right] = 0.0018$$

$$C = a_oM + a_1K$$

$$C = 1.215\begin{bmatrix} 4000 & 0 & 0 \\ 0 & 2000 & 0 \\ 0 & 0 & 1000 \end{bmatrix} + 2700\begin{bmatrix} 4 & -1 & 0 \\ -1 & 2 & -1 \\ 0 & -1 & 1 \end{bmatrix}$$

$$C = \begin{bmatrix} 15660 & -2700 & 0 \\ -2700 & 7830 & -2700 \\ 0 & -2700 & 3915 \end{bmatrix}$$

(iii) **Caughey damping**:

$$C = a_oM + a_1K + a_2KM^{-1}K$$

$$\xi_n = \frac{1}{2}\sum_{l=0}^{2} a_l\omega_n^{2l-1}$$

$$2\xi_n = \frac{a_o}{\omega_n} + a_1\omega_n + a_2\omega_n^3$$

$$2\begin{Bmatrix} 0.05 \\ 0.05 \\ 0.05 \end{Bmatrix} = \begin{bmatrix} 1/17.70 & 17.70 & 17.70^3 \\ 1/38.73 & 38.73 & 38.73^3 \\ 1/51.90 & 51.90 & 51.90^3 \end{bmatrix}\begin{Bmatrix} a_o \\ a_1 \\ a_2 \end{Bmatrix}$$

By solving the above matrix equation,

$$a_o = 1.083$$

$$a_1 = 0.0023$$

$$a_2 = -2.809 \times 10^{-7}$$

$$C = \begin{bmatrix} 15287.887 & -2185.950 & -316.013 \\ -2185.950 & 7011.919 & -2185.950 \\ -319.013 & -2185.950 & 3584.962 \end{bmatrix}$$

(iv) **Matrix super-positioning**

$$M = \varphi^T m \varphi$$

For the first mode,

$$M_1 = \{1 \quad 3.162 \quad 4\} \begin{bmatrix} 4000 & 0 & 0 \\ 0 & 2000 & 0 \\ 0 & 0 & 1000 \end{bmatrix} \begin{Bmatrix} 1 \\ 3.162 \\ 4 \end{Bmatrix}$$

$$= 399946.488$$

$$C_1 = \frac{2\xi_1 \omega_1}{M_1} m \varphi_1 \varphi_1^T mo$$

$$= \frac{2 \times 0.05 \times 17.70}{39996.488} \begin{bmatrix} 4000 & 0 & 0 \\ 0 & 2000 & 0 \\ 0 & 0 & 1000 \end{bmatrix} \begin{Bmatrix} 1 \\ 3.162 \\ 4 \end{Bmatrix}$$

$$\times \{1 \quad 3.162 \quad 4\} \begin{bmatrix} 4000 & 0 & 0 \\ 0 & 2000 & 0 \\ 0 & 0 & 1000 \end{bmatrix}$$

$$= \begin{bmatrix} 708.062 & 1119.446 & 708.062 \\ 1119.446 & 1769.845 & 1119.446 \\ 708.062 & 1119.446 & 708.062 \end{bmatrix}$$

For the second mode,

$$M_2 = \{1 \quad 0 \quad -1\} \begin{bmatrix} 4000 & 0 & 0 \\ 0 & 2000 & 0 \\ 0 & 0 & 1000 \end{bmatrix} \begin{Bmatrix} 1 \\ 0 \\ -1 \end{Bmatrix}$$

$$= 5000$$

$$C_2 = \frac{2\xi_2\omega_2}{M_2} m\varphi_2\varphi_2^T m$$

$$= \frac{2 \times 0.05 \times 38.73}{5000} \begin{bmatrix} 4000 & 0 & 0 \\ 0 & 2000 & 0 \\ 0 & 0 & 1000 \end{bmatrix} \begin{Bmatrix} 1 \\ 0 \\ -1 \end{Bmatrix}$$

$$\times \{1 \quad 0 \quad -1\} \begin{bmatrix} 4000 & 0 & 0 \\ 0 & 2000 & 0 \\ 0 & 0 & 1000 \end{bmatrix}$$

$$= \begin{bmatrix} 12393.60 & 0 & -3098.40 \\ 0 & 0 & 0 \\ -3098.40 & 0 & 774.6 \end{bmatrix}$$

For the third mode,

$$M_3 = \{1 \quad -3.162 \quad 4\} \begin{bmatrix} 4000 & 0 & 0 \\ 0 & 2000 & 0 \\ 0 & 0 & 1000 \end{bmatrix} \begin{Bmatrix} 1 \\ -3.162 \\ 4 \end{Bmatrix}$$

$$= 39996.488$$

$$C_3 = \frac{2\xi_3\omega_3}{M_3} m\varphi_3\varphi_3^T m$$

$$= \frac{2 \times 0.05 \times 51.90}{39996.488} \begin{bmatrix} 4000 & 0 & 0 \\ 0 & 2000 & 0 \\ 0 & 0 & 1000 \end{bmatrix} \begin{Bmatrix} 1 \\ -3.162 \\ 4 \end{Bmatrix}$$

$$\times \{1 \quad -3.162 \quad 4\} \begin{bmatrix} 4000 & 0 & 0 \\ 0 & 2000 & 0 \\ 0 & 0 & 1000 \end{bmatrix}$$

$$= \begin{bmatrix} 2076.182 & -3282.444 & 2076.182 \\ -3282.444 & 5189.544 & -3282.444 \\ 2076.182 & -3282.444 & 2076.182 \end{bmatrix}$$

Now, the total damping matrix is given by,

$C = C_1 + C_2 + C_3$

$$= \begin{bmatrix} 708.062 & 1119.446 & 708.062 \\ 1119.446 & 1769.845 & 1119.446 \\ 708.062 & 1119.446 & 708.062 \end{bmatrix} + \begin{bmatrix} 12393.60 & 0 & -3098.40 \\ 0 & 0 & 0 \\ -3098.40 & 0 & 774.6 \end{bmatrix}$$

$$+ \begin{bmatrix} 2076.182 & -3282.444 & 2076.182 \\ -3282.444 & 5189.544 & -3282.444 \\ 2076.182 & -3282.444 & 2076.182 \end{bmatrix}$$

$$= \begin{bmatrix} 151777.844 & -2162.998 & -314.156 \\ -2162.998 & 6959.389 & -2162.998 \\ -314.156 & -2162.998 & 3558.844 \end{bmatrix}$$

2. Determine the frequency and mode shapes for the MDOF system shown in figure:
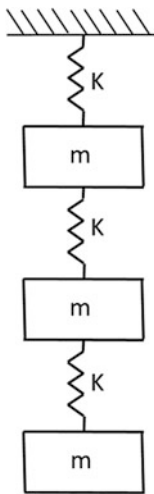
Find the normalized modal shapes and determine the damping matrix by matrix super-positioning. $M = 1000$ kg, $k = 1000$ kN/m and damping ratio is 4%.

(i) **Frequency and mode shape**:

By following the standard procedure, the frequencies and mode shapes are identified as follows:

$$\omega_1 = 0.445\sqrt{\frac{k}{m}}$$

$$\omega_2 = 1.247\sqrt{\frac{k}{m}}$$

$$\omega_3 = 1.802\sqrt{\frac{k}{m}}$$

By substituting the values of m and k,

$$\omega_1 = 14.072\,\text{rad/s}$$
$$\omega_2 = 39.434\,\text{rad/s}$$
$$\omega_3 = 56.98\,\text{rad/s}$$

The corresponding mode shapes are given as

$$\varnothing = \begin{bmatrix} 1 & 1 & 1 \\ 1.802 & 0.445 & -1.247 \\ 2.247 & -0.802 & 0.555 \end{bmatrix}$$

$$\text{Mass matrix, } m = 1000 \begin{bmatrix} 1 & 0 & 0 \\ 0 & 1 & 0 \\ 0 & 0 & 1 \end{bmatrix} = \begin{bmatrix} 1000 & 0 & 0 \\ 0 & 1000 & 0 \\ 0 & 0 & 1000 \end{bmatrix}$$

$$\text{Stiffness matrix, } k = 1000 \times 10^3 \begin{bmatrix} 2 & -1 & 0 \\ -1 & 2 & -1 \\ 0 & -1 & 1 \end{bmatrix}$$

For normalizing the modal vectors,

$$\varphi_1^T m \varphi_1 = \{1 \quad 1.802 \quad 2.247\} \begin{bmatrix} 1000 & 0 & 0 \\ 0 & 1000 & 0 \\ 0 & 0 & 1000 \end{bmatrix} \begin{Bmatrix} 1 \\ 1.802 \\ 2.247 \end{Bmatrix}$$

$$= 9296.216$$

$$\varphi_1^* = \frac{1}{\sqrt{9296.216}} \begin{Bmatrix} 1 \\ 1.802 \\ 2.247 \end{Bmatrix} = \begin{Bmatrix} 0.0104 \\ 0.0187 \\ 0.0233 \end{Bmatrix}$$

Similarly for second mode shape,

$$\varphi_2^T m \varphi_2 = \{1 \quad 0.445 \quad -0.802\} \begin{bmatrix} 1000 & 0 & 0 \\ 0 & 1000 & 0 \\ 0 & 0 & 1000 \end{bmatrix} \begin{Bmatrix} 1 \\ 0.445 \\ -0.802 \end{Bmatrix}$$

$$= 1841.229$$

$$\varphi_2^* = \frac{1}{\sqrt{1841.229}} \begin{Bmatrix} 1 \\ 0.445 \\ -0.802 \end{Bmatrix} = \begin{Bmatrix} 0.0233 \\ 0.0104 \\ -0.0187 \end{Bmatrix}$$

For the third mode shape,

$$\varphi_3^T m \varphi_3 = \{1 \quad -1.247 \quad 0.555\} \begin{bmatrix} 1000 & 0 & 0 \\ 0 & 1000 & 0 \\ 0 & 0 & 1000 \end{bmatrix} \begin{Bmatrix} 1 \\ -1.247 \\ 0.555 \end{Bmatrix}$$

$$= 2863.034$$

$$\varphi_3^* = \frac{1}{\sqrt{2863.034}} \begin{Bmatrix} 1 \\ -1.247 \\ 0.555 \end{Bmatrix} = \begin{Bmatrix} 0.0187 \\ -0.0233 \\ 0.0103 \end{Bmatrix}$$

The normalized modal matrix is given by,

$$\varnothing = \begin{bmatrix} 0.0104 & 0.0233 & 0.0187 \\ 0.0187 & 0.0104 & -0.0233 \\ 0.0233 & -0.0187 & 0.0103 \end{bmatrix}$$

(ii) **Damping Matrix**

$$M = \varphi^T m \varphi$$

Since the modes are normalized,

$$M_1 = M_2 = M_3 = 1$$

For the first mode,

$$C_1 = \frac{2\xi_1\omega_1}{M_1}m\varphi_1\varphi_1^T m$$

$$= \frac{2 \times 0.04 \times 14.072}{1} \begin{bmatrix} 1000 & 0 & 0 \\ 0 & 1000 & 0 \\ 0 & 0 & 1000 \end{bmatrix} \begin{Bmatrix} 0.0104 \\ 0.0187 \\ 0.0233 \end{Bmatrix}$$

$$\times \{0.0104 \quad 0.0187 \quad 0.0233\} \begin{bmatrix} 1000 & 0 & 0 \\ 0 & 1000 & 0 \\ 0 & 0 & 1000 \end{bmatrix}$$

$$= \begin{bmatrix} 121.762 & 218.938 & 272.794 \\ 218.938 & 393.667 & 490.505 \\ 272.794 & 490.505 & 611.164 \end{bmatrix}$$

For the second mode,

$$C_2 = \frac{2\xi_2\omega_2}{M_2}m\varphi_2\varphi_2^T m$$

$$= \frac{2 \times 0.04 \times 39.434}{1} \begin{bmatrix} 1000 & 0 & 0 \\ 0 & 1000 & 0 \\ 0 & 0 & 1000 \end{bmatrix} \begin{Bmatrix} 0.0233 \\ 0.0104 \\ -0.0187 \end{Bmatrix}$$

$$\times \{0.0233 \quad 0.0104 \quad -0.0187\} \begin{bmatrix} 1000 & 0 & 0 \\ 0 & 1000 & 0 \\ 0 & 0 & 1000 \end{bmatrix}$$

$$= \begin{bmatrix} 1712.666 & 764.452 & -1374.543 \\ 764.452 & 341.214 & -613.530 \\ -1374.543 & -613.530 & 1103.174 \end{bmatrix}$$

For the third mode,

$$C_3 = \frac{2\xi_3\omega_3}{M_3}m\varphi_3\varphi_3^T m$$

$$= \frac{2 \times 0.04 \times 56.98}{1} \begin{bmatrix} 1000 & 0 & 0 \\ 0 & 1000 & 0 \\ 0 & 0 & 1000 \end{bmatrix} \begin{Bmatrix} 0.0187 \\ -0.0233 \\ 0.0103 \end{Bmatrix}$$

$$\times \{0.0187 \quad -0.0233 \quad 0.0103\} \begin{bmatrix} 1000 & 0 & 0 \\ 0 & 1000 & 0 \\ 0 & 0 & 1000 \end{bmatrix}$$

$$= \begin{bmatrix} 1594.026 & -1986.140 & 877.993 \\ -1986.140 & 2474.709 & -1093.970 \\ 877.993 & -1093.970 & 483.601 \end{bmatrix}$$

Now, the total damping matrix is given by,

$$C = C_1 + C_2 + C_3$$

$$= \begin{bmatrix} 121.762 & 218.938 & 272.794 \\ 218.938 & 393.667 & 490.505 \\ 272.794 & 490.505 & 611.164 \end{bmatrix} + \begin{bmatrix} 1712.666 & 764.452 & -1374.543 \\ 764.452 & 341.214 & -613.530 \\ -1374.543 & -613.530 & 1103.174 \end{bmatrix}$$

$$+ \begin{bmatrix} 1594.026 & -1986.140 & 877.993 \\ -1986.140 & 2474.709 & -1093.970 \\ 877.993 & -1093.970 & 483.601 \end{bmatrix}$$

$$= \begin{bmatrix} 3428.454 & -1002.75 & -223.756 \\ -1002.75 & 3209.59 & -1216.995 \\ -223.756 & -1216.995 & 2197.939 \end{bmatrix}$$

Exercise

1. Explain basic types of damping?
2. Explain Coulomb damping?
3. Explain viscous damping?
4. Structural Damping for steel is in the range of _____ and for concrete is _____.
5. Rayleigh damping can be mathematically represented as _____.
6. _____ is proposed for offshore structures.
7. If more than _____ are included in the Caughey series, [C] becomes a full matrix.
8. Free vibration experiment is carried out to determine the _____ and _____ of the setup.
9. _____ method is used to determine the damping coefficient.
10. TLP with perforated columns shows _____ and _____ in comparison to that without perforated columns.

Answers

1. The basic types of damping are namely: (i) coulomb damping and (ii) viscous damping.
2. Coulomb damping results from sliding of two surfaces; it is also called dry damping or friction damping. The damping force is the product of the normal force and the coefficient of friction between the body surface and the plane of motion. Note that the damping force in this case is independent of velocity of motion of the body which is under vibration.
3. Viscous damping, the damping force accounts for the viscosity of the system. The presence of fluid medium around the body significantly influences the damping force acting on the body. Damping force will be proportional to the magnitude of the velocity and has the unit of N/(m s). Viscous damping seems to be more relevant to offshore structural systems due to the inherent presence of liquid medium around the body.

 4. 0.2–0.5% and 0.5–1.5%.
 5. $C = a_0 M + a_1 K$.
 6. Rayleigh damping.
 7. Two terms.
 8. Natural frequency and damping coefficient.
 9. Logarithmic decrement.
10. Higher damping coefficient and higher time period.

Chapter 5
Hydrodynamic Response of Perforated Members

Abstract This chapter deals with hydrodynamic response of perforated cylinders under regular waves through computational fluid dynamics (CFD). The chapter deals with a brief introduction of fluid–structure interaction and wave–structure interaction. Variations in water particle kinematics along the depth when encountered by perforated members are discussed in detail as they find many recent applications in the retrofitting and rehabilitation of offshore structural members.

Keywords Hydrodynamic response · Experimental studies · Perforated cylinders · Wave–structure interaction · Water particle kinematics · Retrofitting · Rehabilitation · Offshore structures · Tension leg platforms

5.1 Fluid–Structure Interaction

Fluid–structure interaction (FSI) plays an important role for structures placed in the path of flowing fluid. The presence of structure alters fluid flow field in its vicinity. Degree of compliance offered by the structure adds further complexity due to the reaction it offers to the excited force. Even though structures remain flexible (e.g., TLP) in certain degrees of freedom, dynamics become important. It is not their deformation capacity that is looked upon in this context. FSI becomes more important when the flow is a steady flow, may be in the form of current or a vertical shear. But in real sea state, structures experience large oscillating forces in the flow direction. When structures are placed in the flowing fluid, the flow pattern is altered. Restraints are developed in the fluid medium to maintain the position of the structure. Forces acting on the structures in fluid medium shall be classified as drag (acting in-line with the direction of flow) and lift (transverse to the direction of flow). Further, drag force can be classified as higher and smaller frequency components. These components will be functions of the geometry of the structure and flow conditions. Lift forces contain oscillatory components with multiple frequencies. On the downstream side, flow will return to its unaltered condition. This is due to fluid viscosity and damping. The region of altered flow directly behind the structure is called *wake region*. In the wake regions, there will be one-to-one

Table 5.1 Flow regimes in uniform flow

Flow region	Re range	Flow condition	Forces on cylinder
Laminar	0–40	No separation of flow	Drag forces occurring in the direction of flow
Subcritical	40–5E05	Broken stream lines	Lift forces depend on Strouhal number Steady drag force + smaller oscillating drag forces at double the frequency of lift force
Supercritical	5E05–7E05	Ill-defined vortices	Drag forces decrease rapidly lift and drag forces will be seen at higher frequencies
Trans-critical	>7E05	Vortices will be persistent turbulent flow due to randomness in fluid viscosity	Similar to subcritical range

relationship between the extent of wake region and restraint loads. This implies that in the wake region, frequency content is determinant and is same as that of the restraint loads, which enables the determination of FSI in a closed form.

The data shown in Table 5.1 represent the case for cylinder whose axis is normal to the flow direction. Flow is without turbulence and boundary effects.

5.2 Vertical Cylinders in Uniform Flow

Vertical cylinders experience loading from the flowing fluid, and the FSI will be defined by Reynolds number for cylinders that are infinitely long, smooth and fixed. Cylinder roughness and fluid turbulence reduce boundary value on either side of supercritical region. If the length of the cylinder is finite, this will introduce 3D aspect to the flow. Ends of cylinder will affect drag and lift coefficients; they are also dependent on the location of the cylinder. Vortex shedding pattern will also be affected (Table 5.2).

Table 5.2 Reduced velocity range

Flow region	Reduced velocity	Vortex shedding	Types of vibration caused
I	1.7–2.3	Symmetric shedding	In-line oscillation only
II	2.8–3.2	Alternate shedding of vortices	Predominantly in-line vibrations. Some transverse vibrations are also seen
III	4.5–8.0	Alternate shedding of vortices	Predominantly transverse vibration in-line vibrations are seen at frequency twice as that of the transverse vibration. This is called *figure eight motion*

Source Humphries and Walker (1987)

5.3 Flow in Deep Waters

In deep waters, flow is not uniform with depth and results in positive shear. Velocity will be greater than that near the surface. When the vertical cylinder is in shear flow condition, 3D flow regime will occur. Under positive shear, wake region experiences vertical upward flow. Variation in stagnation pressure causes downward flow along the length. The flow is *sheared* from upstream to downstream. There is downward flow on the U/S side and upward flow on the D/S side, as shown in Fig. 5.1.

The shear flow effect reduces the pressure coefficient at the top of the cylinder and increases the coefficient at the bottom. The pressure coefficient also changes with the strength of shear. In uniform flow, vertical cylinder will show vortices at the same frequency over its entire length, whereas in shear flow, frequency changes continuously.

5.4 Horizontal Cylinder in Uniform Flow

Examples of horizontal cylinders are subsea pipelines, members of floating break waters, pontoons, etc. These members will be influenced by current and waves. Under uniform flow field, horizontal cylinder will generate waves near upper boundary (free surface). Wave resistance depends upon Froude number:

Fig. 5.1 Flow in deep waters
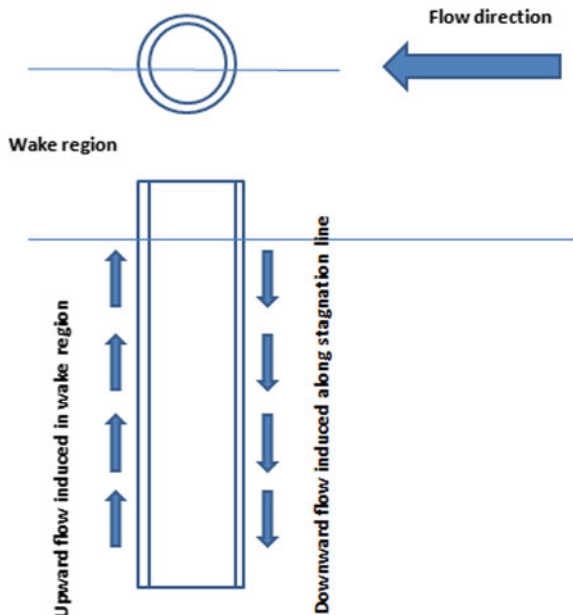
$$\text{Froude number } F_r = U_2/(2gy_1)$$

Y_1 is the depth of immersion, measured from the axis of the cylinder to free surface. When $Y_1 \gg$ radius, maximum wave resistance will occur, and minimum will occur when $F_r < 0.375$. Boundary effects and end effects of the cylinder introduce 3D effect in the flow past the cylinder of finite length. The major difference between horizontal and vertical cylinder is the appearance of lift force. When horizontal cylinder is located near boundary, flow will become unsymmetrical. Lift force will become a function of cylinder diameter and distance to the boundary. Horizontal cylinders will also be subjected to flow-induced vibrations.

5.5 Horizontal Cylinder in Shear Flow

Under shear flow, velocity variation across the face of the structure will be significant. Ratio of turbulence to velocity variation across horizontal cylinder is higher than that of a vertical cylinder. For increase in shear parameter, Strouhal number increases because of increase in vortex shedding frequency. With a fixed horizontal cylinder, load at a given velocity for a positive shear is more than that of uniform flow. At free surface, vertical load in both positive and negative shears increases significantly in comparison to uniform flow. Dynamic vertical loads on the cylinder at mid-depth under positive and negative shear contain higher energy at high frequencies. Near the surface, there is a significant reduction. Horizontal cylinder at free surface suppresses eddy shedding and wake formation. Steady component of vertical load increases significantly for horizontal cylinder at free surface.

5.6 Blockage Factor

Closely spaced members, connected in different orientations, cause distortion in the fluid field around them. For closely spaced members, the structure becomes dense. For dense structures, flow field slows down as it travels through the structure. This causes blockage effect and complicates the actual velocity field around the structure. Load on the structure increases due to this blockage. Drag force is summed for each member in the dense structure. In case of group of vertical cylinders present in the flow field, blockage factor CBF = 0.25S/D (for $0 < S/D < 4.0$) = 1.0 for S/D = 4.0, where S is c/c distance of the cylinder and D is diameter.

5.7 Wave–Structure Interaction (WSI)

When waves past cylinder, it causes oscillating in-line force on the cylinder. In addition, free surface also changes in case of a submerged cylinder. Large structures placed in wave field alter incident waves in its vicinity. If the dimension of the structure is large compared to the wave length, flow remains attached to the structure. When waves pass a cylinder, it causes oscillating in-line force on the cylinder. In addition, free surface also changes in case of a submerged cylinder. Several procedures can be used to explain the potential function generated in the vicinity, knowing the incident wave potential. Flow around the structure is assumed to remain attached. Separation is neglected and the fluid is assumed to be incompressible and irrotational, and structure is assumed to be rigid. Wave amplitude is assumed to be small. Fluid flow in the neighborhood is described by velocity potential. Velocity potential under linear theory is given by

$$\Phi = \varphi e^{(-i\omega t)}, \tag{5.1}$$

where φ is the spatial part of total velocity potential and ω is the incident wave frequency. Total potential is the sum of potential of incident wave component and potential of scattered wave component. Scattered wave component is normally represented by continuous distribution of waves. It is assumed as superposition of numerous waves. Boundary value problem, defined in terms of Laplace partial differential equations, is transformed into original partial differential equations, in potential theory. Boundary condition includes ocean floor, free surface, submerged surface of the structure, and radiation condition, as flow approaches infinity.

5.8 Perforated Cylinders

5.8.1 Wave Forces on Perforated Members

Several analytical studies are reported in the literature highlighting the wave forces on porous bodies. Wang and Ren (1994) are one of the earliest to study wave interaction with a concentric surface-piercing porous outer cylinder protecting an impermeable inner cylinder. Free surface elevation, net hydrodynamic forces, and wave-induced overturning moments on both cylinders are examined. Based on the analytical investigations carried out, it is seen that inner cylinder experienced more forces from long period waves in comparison to that from short period waves with decrease in annular spacing between the outer perforated cylinder and inner cylinder. Results showed that the existence of exterior porous cylinder reduces hydrodynamic force on the inner cylinder. Cylindrical breakwater is porous in the vicinity of the free surface and impermeable at some distance below the free surface; significant reduction is reported in wave field and hydrodynamic forces

experienced by the inner cylinder (William and Li 1998). Interaction of waves with arrays of bottom-mounted, surface-piercing circular cylinders is investigated through numerical studies (Williams and Li 2000). It is shown that the porosity of the structure results in a significant reduction in both the hydrodynamic loads experienced by the cylinders and the associated wave run-up. William et al. (2000) investigated the interaction of waves and free-floating circular cylinder with porous side walls. The porous region is bounded on top and bottom by impermeable end caps, which resulted in an enclosed fluid region within the structure. It is found that the permeability, size, and location of the porous region have a significant influence on the horizontal component of the hydrodynamic excitation and reaction loads, while their influence on the vertical components is relatively minor. Neelamani et al. (2002) carried out experimental investigations of seawater intake structure consisting of a perforated square caisson encircling a vertical suction through physical model studies. They found that the ratio of force on perforated caisson to the force on caisson with 10% porosity is reduced to a maximum of 60% with increase in the porosity of the caisson from 1.6 to 16.9%. This ratio is found to increase with the increase in relative wave height and decrease with increase in relative width. Neelamani and Muni (2002) examined wave forces on a vertical cylinder protected by vertical and inclined perforated barriers; numerical studies showed that there is a significant reduction in forces on the vertical cylinder due to perforated barriers.

Song and Tao (2007) studied 3D short-crested wave interaction with a concentric porous cylindrical structure. It is recommended that porous effect should be chosen lesser than 2 in order to provide meaningful protection to the interior cylinder from the wave impact. Vijayalakshmi et al. (2008) carried out experimental investigations on perforated circular cylinder encircling an impermeable cylinder at a constant water depth for regular and random waves. Porosity of the outer cylinder is varied from 4.54 to 19.15% to study its influence on variations in wave forces in the vicinity of the chosen twin cylinder system. Numerical method is developed on the basis of the application of boundary integral equation on a porous body with appropriate boundary conditions; porosity is modeled using the resistance coefficient and added mass coefficient for regular waves. It is seen that the resistance coefficient increased with the increase in porosity and wave height except for a porosity of 4.54%; added mass coefficient is almost negligible. Based on the experimental results, porosity of 10–15% is recommended to have significant effect on force reduction. Sankarbabu et al. (2007) investigated the influence of hydrodynamic wave forces on a group of cylinders, wave run-up, and free surface elevation in their vicinity. Results showed that the forces on inner cylinders are reduced in the presence of an outer porous cylinder when compared to that of the direct wave impact. Sankarbabu et al. (2007) investigated the hydrodynamic performance of a dual cylindrical caisson breakwater (DCBW) that is formed by a row of caissons; these caissons consist of porous outer cylinder circumscribing an impermeable inner cylinder. Based on the analytical studies carried out, it is seen that an optimum ratio of radius of inner cylinder to the outer exists as 0.5 for a satisfactory hydrodynamic performance of the DCBW; it shows improved stability

and wave transformation in its vicinity. Further, they concluded that the influence of porosity on the variation of forces, run-up on the caissons, and the surface elevation in the vicinity of the DCBW are found to be significant up to a value of 1.0; any further increase in this value results in lesser variation of the above parameters. Zhao et al. (2009) studied the interaction of waves and a porous cylinder with an inner horizontal porous plate; effects of porosity and position of the inner plate are investigated. It is shown that increase in porosity reduces wave exciting forces and efficiency of wave dissipation. Inner plate eliminates the sloshing mode in surge and pitch degrees of freedom. The arrangement is recommended for effective wave energy dissipation when located at still water surface.

5.8.2   Wave Forces on Offshore Structures with Perforated Members

Ker and Lee (2002) examined the coupling problems associated with wave–structure interaction of linear waves and porous tension leg platform (TLP), analytically. They found that the drag force in the porous body changes the response behavior of TLP significantly; at resonance frequencies, this change is significant. They also found that for long period waves, porous TLP remains relatively transparent and is similar to that of an impermeable one, while it dissipates most of the wave energy for short period waves. Zhong and Wang (2006) carried out analytical studies on solitary waves interacting with surface-piercing concentric porous cylinders. It was found that the hydrodynamic forces on inner cylinder increase and that of the exterior cylinder decrease with the decrease in the annular spacing. Forces on a single porous cylinder are reduced significantly in comparison to that of an impermeable cylinder of the same diameter. Further, it is also shown that for larger porosity of the outer cylinder, larger hydrodynamic forces are encountered on the inner cylinder and lesser on the outer cylinder. Existence of exterior porous cylinder reduces hydrodynamic force on the interior cylinder. Vijayalakshmi et al. (2007) verified this fact through experimental investigations by measuring wave forces and run-up on the twin, concentric perforated cylinders; results are compared with those predicted by the boundary integral method and found satisfactory. Porous effects on thin permeable plates are well quantified by Li et al. (2006); predicted values of porous effects of reflection and transmission coefficients that are estimated using analytical model are validated with experimental results. Jayalekshmi et al. (2010) investigated the dynamic response of a TLP under random waves and the effect of riser dynamics on platform behavior; an in-house finite element code is developed by the authors to perform the analysis. A random sea state is generated using the PM spectrum (Bringham 1974). Water particle kinematics are calculated using Airy's linear wave theory, and the load is evaluated using the relative form of the Morrison equation; variable submergence and current forces are also taken into account.

Adrezin et al. (1996) carried out dynamic analysis of complaint offshore structures and reiterated the fact that coupled motion analysis induces significant response in all active degrees of freedom of TLP under linear waves. Kim et al. (2007) discussed various nonlinearities associated with the analysis of TLPs under regular waves; the effect of these nonlinearities on the dynamic response and various strategies to solve the equation of motion for the fully coupled dynamic analysis are discussed in detail (Chakrabarti 1987, 1990, 2002). Zeng et al. (2007) conducted parametric studies of TLPs with large amplitude motion. Dynamic responses predicted by linear and nonlinear models are compared; they showed that the nonlinear responses of TLP, considering the effects induced by large amplitude motions, differ from that of the linear model, significantly. Two different approaches for response calculations are compared with wave approach angle as one of the primary factors in the parametric study. Kurian et al. (2008, 1993) conducted parametric studies on TLPs under random waves. Authors used PM spectrum, Airy wave theory, relative form of Morrison equation, and Newmark-Beta time integration scheme to obtain the response in time domain. Mass, damping, and stiffness matrices that are required to calculate the response are derived from the literature (Chandrasekaran and Jain 2002a, b; Chandrasekaran et al. 2004). Although coefficients used in the process of determining response are on the basis of recommendations made by other authors, both numerical and experimental investigations carried out by the authors are considered valid due to a close comparison of the same. Studies are also carried out by researchers to illustrate the influence of wave approach angle on the response of TLP in regular sea (Chandrasekaran et al. 2007a, b, c, d; Chen et al. 2006). Numerical studies carried out on triangular TLP under a variety of wave approach angles showed that nonlinear Stokes's fifth-order wave theory is well suited for deep-sea structures such as TLPs to estimate dynamic response. Significance of other nonlinearities caused by change in tether tension and variable submergence effect is on the dynamic response of TLPs that are also highlighted in the studies. Experimental studies carried out on the response analysis of TLPs showed the scale effect on the response quantities; variations between the analytical and experimental results are attributed to the boundary effect on the scaled model during experiments (Anita et al. 2004).

A detailed review of literature on wave interaction on porous cylinders shows a common agreement of significant force reduction on the inner cylinder with perforated outer cover (Chandrasekaran and Madhavi 2014b). Several studies highlighting the dynamic response of offshore TLPs under regular and random waves are also discussed; various nonlinearities associated with the response behavior of TLPs under waves are presented. Few experimental investigations carried out on dynamic response of TLP with perforated members will be discussed below.

5.9 Experimental Investigations on Perforated Cylinders

Perforated cylindrical structures reduce wave–structure interaction and scouring problems considerably (Chandrasekaran and Parameswara 2011; Chandrasekaran et al. 2012). Existence of exterior porous cylinder reduces the hydrodynamic forces on inner cylinder caused by the direct wave impact. It is seen from the literature that for reduced annular spacing, long waves impose larger forces on the inner cylinder than the short waves. Based on the experimental investigations carried out, researchers recommended porosity of about 10–15%. This is due to the fact that beyond this porosity ratio, no appreciable reduction in hydrodynamic response is observed. Preliminary experimental investigations are carried out to study the hydrodynamic response of perforated cylinders in regular waves. Variations of forces due to regular waves in a cylinder, with and without perforated cover, are measured. Experimental setup for the study is shown in Fig. 5.2. To evaluate the influence of porosity and diameter of perforations, three scaled models comprising outer cylinder of 315 mm diameter and inner impermeable cylinder of 110 mm in diameter are fabricated with uniform annular space. Steel frames are used for clamping the inner cylinder and the outer cylinder in the wave flume; model is suspended with a clear gap of about 50 mm above the seafloor, ensuring a cantilever action. Strain gauges are placed along the inner cylinder to determine the forces. Regular waves of height ranging from 5 to 25 cm for time periods of 1–2 s are generated for the tests.
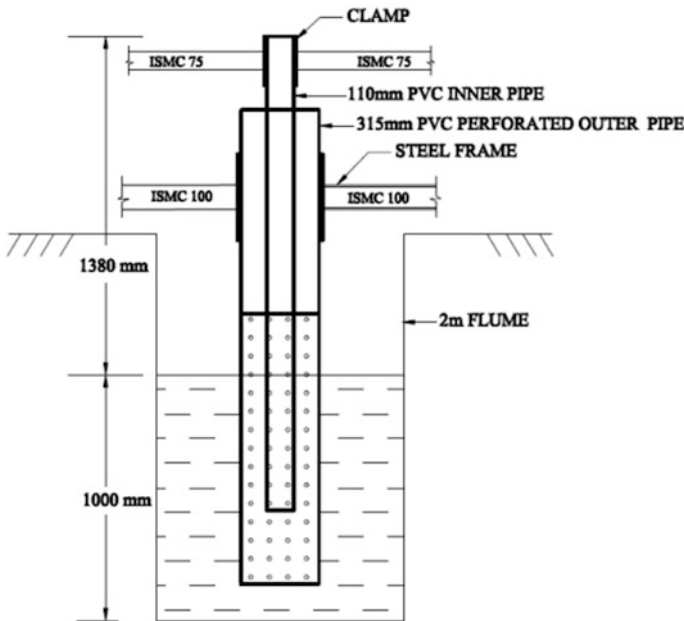
Fig. 5.2 Experimental setup to study response on perforated cylinder

Details of the inner and outer cylinders used for the study are given in Table 5.3. Diameters of perforations and length of perforations are varied to achieve different porosity ratios. Perforation ratios are in compliance with the Indian Standard Code of Practice IS 4985:2000. Figure 5.3 shows the inner and outer cylinders with different perforations; details of strain gauges affixed to the inner cylinder can also be seen.

Inner cylinder is fixed at one end, and the other end is set free to enable the cylinder to behave similar to that of cantilever beam. Known bending stresses are created by applying point load at a constant distance of 50 mm from the free end.

Table 5.3 Geometric details of cylinders considered for the study

Description	Inner cylinder	Outer cylinder		
		A	*B*	*C*
Diameter (mm)	110	315	315	315
Thickness (mm)	4.4	8.7	8.7	8.7
Perforation diameter (mm)	–	10	15	20
Length of the cylinder(mm)	1900	1930	1930	1930
Length of perforations (mm)	–	1450	1050	1050
Number of perforations along length	–	41	26	24
Number of perforations along circumference	–	28	24	24
Porosity (%)	–	6.3	10.6	16
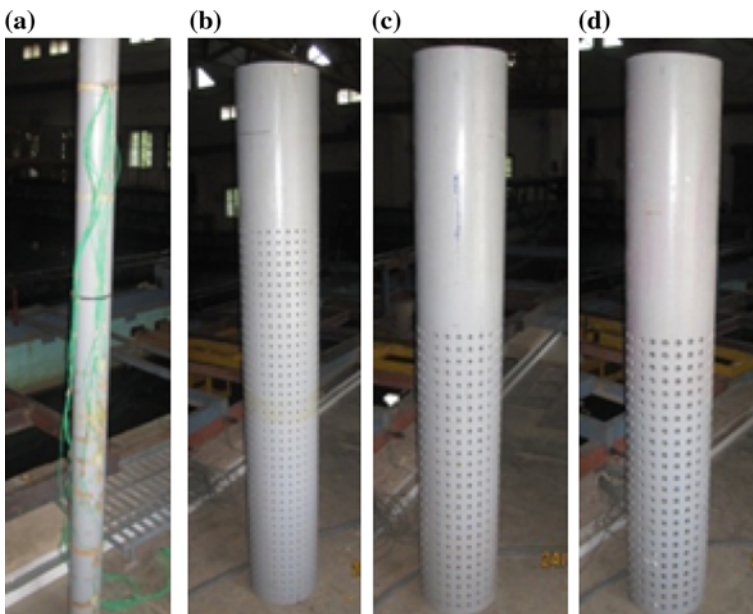
Fig. 5.3 Perforated cylinders considered for the study: **a** inner cylinder; **b** outer cylinder (A); **c** outer cylinder (B); **d** outer cylinder (C)

Bending strain in the inner cylinder, with and without perforated outer cylinders, is measured during the passage of regular waves. Regular waves with wave heights of 5–25 cm in the intervals of 5 cm and wave periods of 1–2 s in the intervals of 0.2 s are considered in the study. Bending strains are post-processed to determine hydrodynamic forces on the inner cylinder; their variations along its length are also studied. Maximum values of hydrodynamic forces computed on the inner cylinder encompassed by outer cylinders with different porosities are measured; a typical value for 25 cm wave height is given in Table 5.4. It can be seen that force reduction decreases with increase in porosity as the inner cylinder shall be exposed to more hydrodynamic load due to increased porosity. Further, force on the inner cylinder decreases significantly for short period waves compared to long period waves.

Figures 5.4 and 5.5 show the force variation in inner cylinder, encompassed with outer cylinders with different porosities; the plots are drawn for different wave heights varying from 5 to 25 cm, respectively. Wave periods are selected appropriately with respect to the cylinder diameter so that the model remains in Morison regime. It is seen from the figures that force variation in the inner cylinder is nonlinear; decrease in wave force is not proportional to increase in time period and wave height as well.

Table 5.4 Hydrodynamic forces for 25 cm wave height (N)

Wave period (s)	Inner cylinder	Outer cylinder		
		A	B	C
1.2	24.77	5.80	9.07	12.53
1.4	20.17	5.26	7.69	9.67
1.6	17.19	4.05	6.05	8.83
1.8	16.84	4.00	7.42	9.51
2.0	15.29	4.93	6.22	9.19
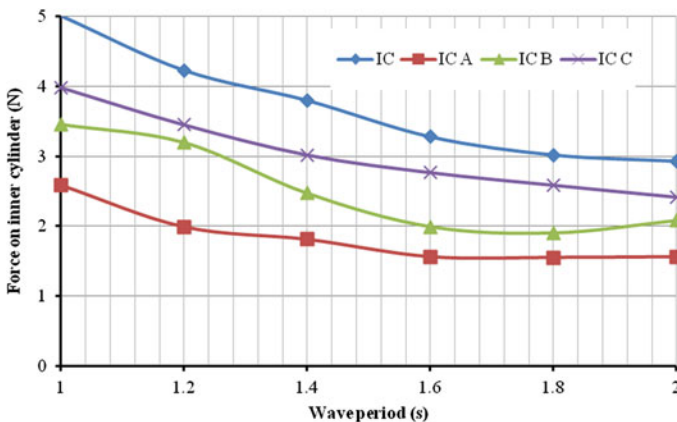
Fig. 5.4 Force variation in cylinders (WH = 5 cm)
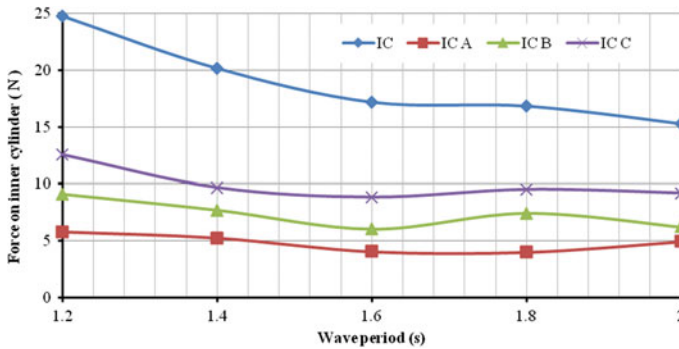
Fig. 5.5 Force variation in cylinders (WH = 25 cm)

The model investigated is built to a scale of 1:140, and the force reduction corresponding to the prototype cylinders with different porosities is shown in Table 5.5.

Based on the experiments conducted, it is seen that hydrodynamic forces on the inner cylinder decrease with the decrease in porosity. This reduction in the forces is significant for short period waves when compared to long period waves; variation is nonlinear and is not proportional to either the increase in wave height or wave period. The size of perforations and porosity influences hydrodynamic forces on cylindrical members significantly. It is also seen that the maximum force reduction is about 76% and minimum is about 17%. Presented study highlights the advantages of deploying perforated cylinders as outer cover on the impermeable inner cylinders. This has direct application of force reduction on the inner cylinders. However, the application is not desired for new design, but recommended as an alternative method of retrofitting of offshore structures.

Table 5.5 Force reduction in inner cylinder

S. No.	Description	Model (1:140)	Prototype
1	Water depth (m)	1.0	140
2	Diameter (inner cylinder) (m)	0.11	15.4
3	Force reduction (H = 25 cm; T = 1.2 s)		
	With outer cylinder A	18.97N (76.59%)	52.05MN
	With outer cylinder B	15.70N (63.38%)	43.08MN
	With outer cylinder C	12.24N (59.63%)	33.58MN
4	Force reduction (H = 5 cm; T = 2 s)		
	With outer cylinder A	1.37N (35.54%)	4.62MN
	With outer cylinder B	0.85N (29.02%)	2.86MN
	With outer cylinder C	0.51N (17.41%)	1.72MN

5.10   Experimental Investigations on Perforated TLP Model

Detailed experimental investigations carried out on impermeable inner cylinder encompassed by a larger outer cylinder with perforations along its length is discussed (Chandrasekaran and Madhavi 2014a, b, c, 2015a, b, c, d, e, f; Chandrasekaran 2015a; Chandrasekaran et al. 2014). By varying the porosity and diameter of perforations, their influence on the hydrodynamic response of the cylindrical member is examined. As an extended concept of the study, offshore TLPs with perforated members are experimentally investigated. Offshore TLPs are hybrid structures whose heave motion is highly damped, posing operational advantages; however, large surge, sway, and yaw motions cause inconvenience to people on board though the platform remains stable for operational sea state. In order to reduce the wave impact on pontoons and cylindrical members of TLPs, perforated cylinders shall be used as an outer cover to the members at highly stressed regions. It is one of the practical techniques to retrofit offshore coastal and offshore structures and also to improve their structural safety. In this present experimental study, a 1:150 scale model of a prototype TLP is fabricated with and without perforated outer column. Dynamic response in various active degrees of freedom and tether tension variations are studied under the regular waves of different time periods and wave heights. Details of the model are given in Table 5.6. Figure 5.6 shows the views of the TLP model considered for the study.

The outer perforated column is 150 mm in diameter with a height of 180 mm. The middle-third portion of the outer column is perforated with holes of 5 mm diameter spaced at 12-mm intervals, resulting in a porosity of 13.5%; outer column is connected to the inner column through a 10-mm-thick ring to maintain the required annular space. A reasonable comparison is possible through the attempted study as the static characteristics like mass and the center of gravity (KG) of the model remain nearly the same irrespective of the presence of the perforated cover. Table 5.7 shows the comparison of mass of acrylic and aluminum perforated covers. Figure 5.7 shows the experimental setup of the current study.

Table 5.6 Details of TLP model

Description	Notation	Units	Prototype TLP	Model (1:150)
Water depth	D	m	450	3
Material			Steel	Acrylic sheet
Unit weight of the material	ρ	kg/m^3	7850	1200
Side of the deck	S	m	70	0.47
Diameter of each leg	d	m	17	0.1
Draft	T	m	32	0.21
Total buoyancy	FB	kN	521,600	0.153
Self-weight of TLP + payload	W	kN	351,600	0.104
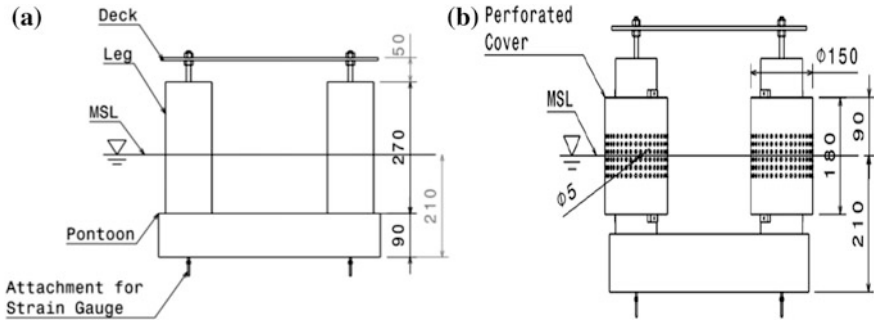
Fig. 5.6 Front view of TLP model: **a** without perforated cover; **b** with perforated cover

Table 5.7 Comparison of mass of acrylic and aluminum perforated covers

Component	Weight (kg)	Weight of cover (as percentage TLP)
TLP without perforated cover	9.04	–
Perforated cover (acrylic)	2.48	27.4%
Perforated cover (aluminum)	0.69	7.6%
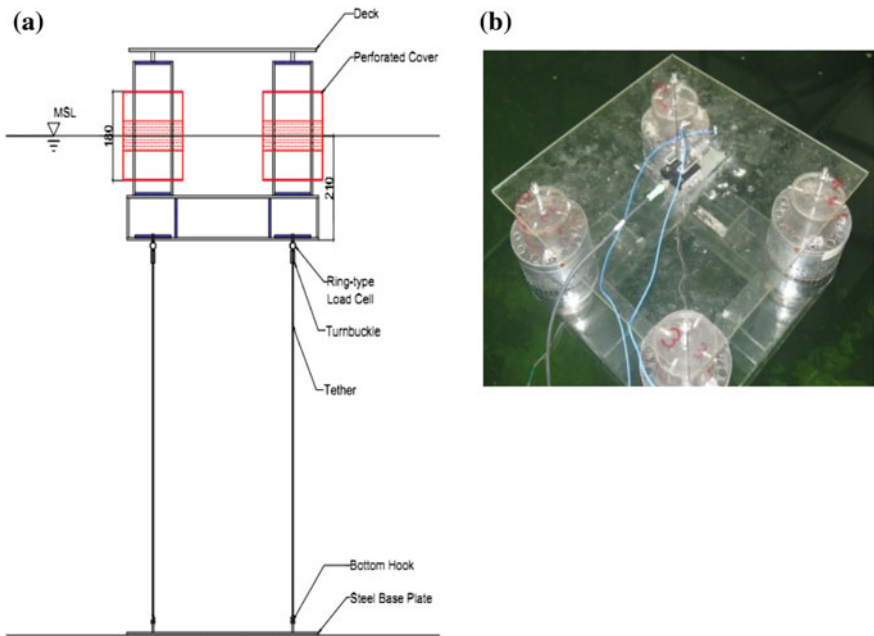
Fig. 5.7 Experimental setup: **a** components of the model; **b** instrumentation
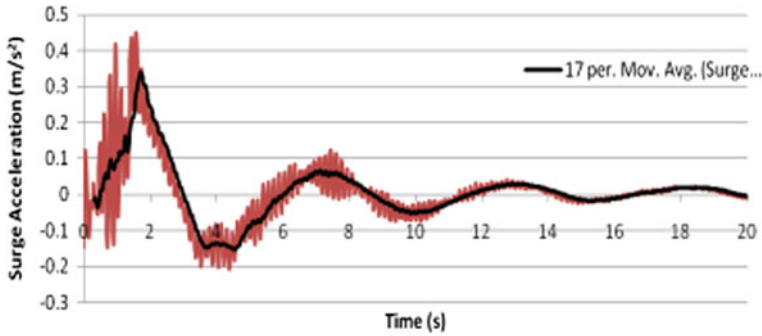
Fig. 5.8 Free surge acceleration with PC

Free vibration tests are carried out to determine the natural frequency and damping coefficient of the model. Figures 5.8 and 5.9 show the surge and heave acceleration of the free vibration tests of the model with perforated cover (PC); Table 5.8 shows the results of the test. Establishing the natural frequency of the system will help to determine the range of the wave periods.

The model was subjected to waves in the head sea direction whose time periods are varied in the range of 0.8–2.4 s; wave heights are varied in the range of 5–9 cm. Figures 5.10, 5.11, and 5.12 show the response of TLP model in surge and heave degrees of freedom and tether tension variation, respectively.

It is seen that response of TLP is reduced in the presence of outer perforated cover. Tether tension variation also shows a significant reduction in the presence of
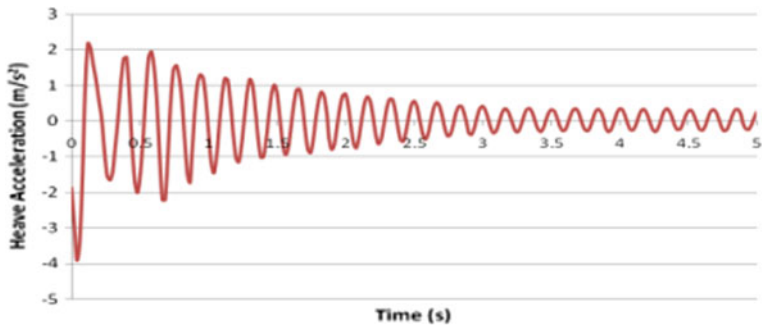
Fig. 5.9 Free heave acceleration with PC

Table 5.8 Results of free vibration experiment

Description	TLP without PC	TLP with PC
Heave damped time period	0.17	0.18
Surge damped time period	4.68	5.61
Heave damping coefficient	0.014	0.02
Surge damping coefficient	0.148	0.251
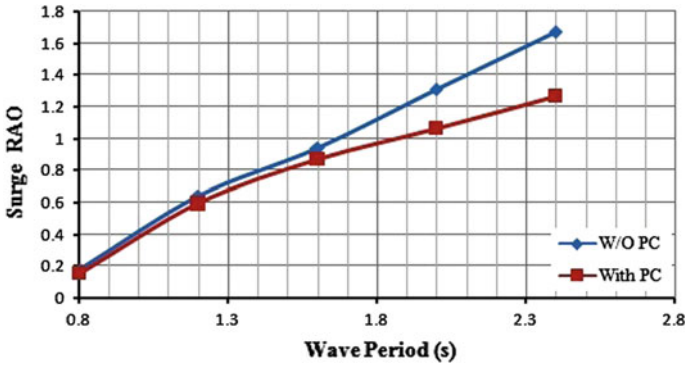
Fig. 5.10 Surge RAO for 7-cm wave
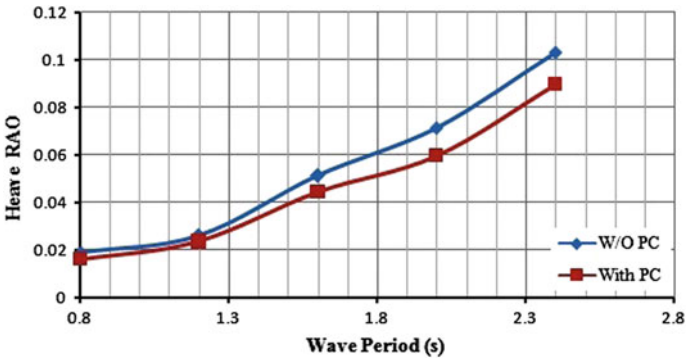
Fig. 5.11 Heave RAO for 7-cm wave
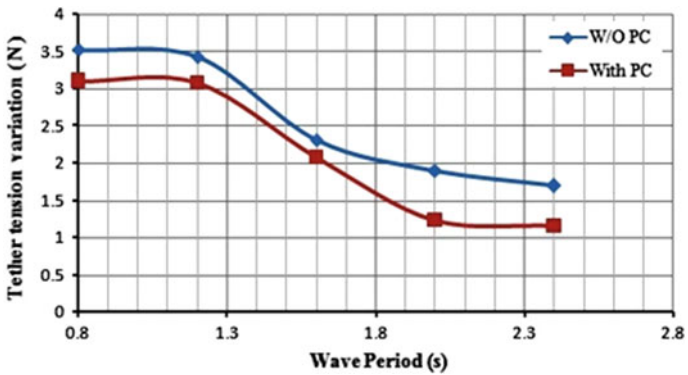
Fig. 5.12 Tether tension variation for 7-cm wave

Table 5.9 Average surge response reduction

Wave period (s)	Average response reduction (%)
0.80	13.35
1.20	7.07
1.60	6.78
2.00	18.01
2.40	24.84

outer perforated cover. Hydrodynamic response on TLPs with outer perforated covers is also investigated for different wave approach angles. Table 5.9 shows the average reduction in surge response for different wave periods; the maximum response reduction seen is about 24% due to the presence of outer perforated cylinders.

5.11   Numerical Studies on Perforated Cylinders

Numerical studies on perforated cylinders are carried out through simulation in STAR-CCM+ software. An attempt is made to simulate the hydrodynamic response of perforated cylinder with porosity 6.3%, which is similar to that of perforated outer cylinder, designated as A in the experimental studies. Simulation through STAR-CCM+ software is chosen due to the numerical capabilities enabled in different modules to simulate viscous drag and turbulence effects that are caused by perforations. Details of the simulation, as attempted through several stages of the numerical modeling, are discussed in steps; various settings such as mesh and physics models used in the study and their significance are also presented.

5.11.1   Development of the Numerical Models

A model of the perforated cylinder is CATIA V5. Figure 5.13 shows the model of the perforated outer cylinder generated in the software. Table 5.10 shows the details of both inner and perforated outer cylinders, while Table 5.11 shows the details of the perforations. Using "Pocket" tool, perforations are created along the circumference and length of the outer cylinder using "Circular pattern" and "Rectangular pattern" tools, respectively. Figures 5.14 and 5.15 show images of outer perforated cylinder and the assembly of inner with perforated outer cylinder, respectively.

Two different geometries namely (i) inner cylinder and (ii) inner cylinder with perforated outer cylinder are exported from CATIA V5, and new simulations are generated in STAR-CCM+ from the imported files. Figures 5.16 and 5.17 show the mesh generation of inner cylinder and inner cylinder with perforated outer cover, respectively; distribution of elements attained using the chosen volume control makes the mesh denser in the fluid region, as can be seen from the figures.
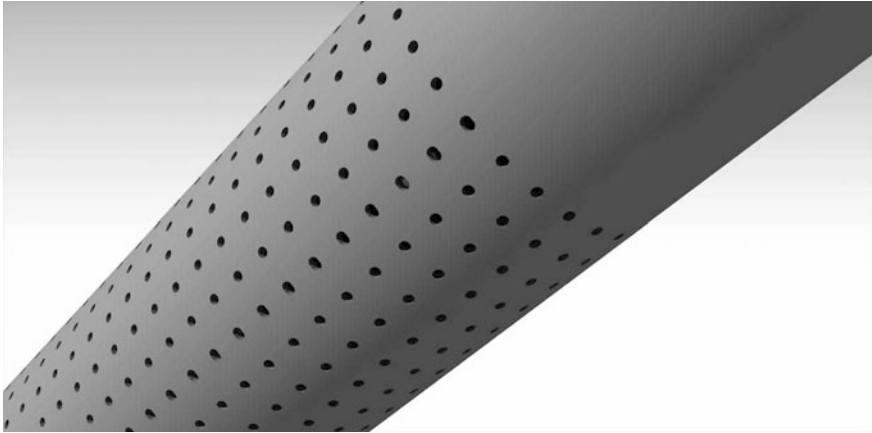
Fig. 5.13 Perforated outer cylinder

Table 5.10 Details of
cylinders

Details of cylinders	Inner cylinder (mm)	Outer cylinder *A* (mm)
Diameter	110	315
Length	1900	1930
Thickness	4.4	8.7

Table 5.11 Details of
perforations

Details of perforations	Outer cylinder *A*
Diameter of the perforation	10 mm
Length of perforation	1450 mm
Number of perforations along the length	41
Number of perforations along the circumference	28
Porosity	6.3%

Subsequently, "Generate volume mesh" tool is used to generate the mesh; 716,801 cells and 2,167,056 faces are generated for simulation of the inner cylinder, while 3,242,875 cells and 9,671,484 faces are generated for that of the inner cylinder with perforated outer cylinder, which is a fairly dense mesh. Several physics models are activated to simulate the wave forces on both the numerical models of inner cylinder and inner cylinder with perforated outer cylinder. A total of 16 physics models are used in the present simulation and activated. A new first-order wave is created under the "Waves" child node of the "VOF Waves" node in the list of chosen physics models. The "Point on Water Level" is set to 0.54 m for the simulation of inner cylinder and 0.8825 m for the simulation of inner cylinder with perforated outer cylinder; the chosen values also match the relevant values used in the experimental investigations. Wave amplitude is set to be 0.05 m.
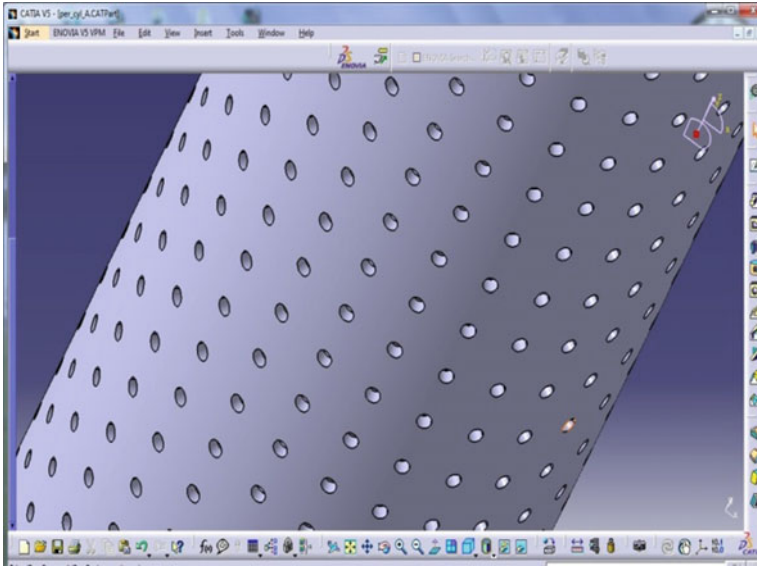
Fig. 5.14 Perforations along the circumference and length (Chandrasekaran et al. 2014a)
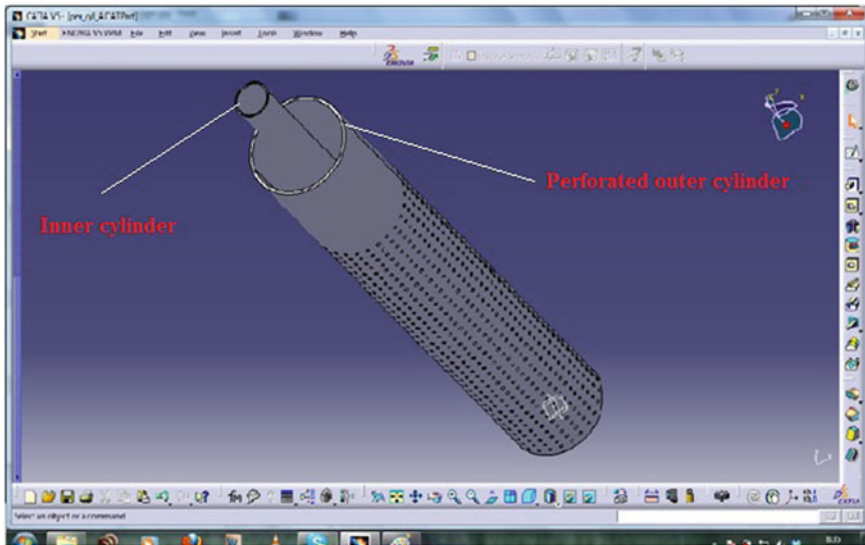
Fig. 5.15 Inner cylinder with perforated outer cylinder

Specification type is set to "Wave period" and numerical simulations are run for six waves for each model, for wave periods of 1.0–2 s with an interval of 0.2 s. The "Volume Fraction" is set to composite, and the method of each of the phases, water, and air is set to "Field Function". Boundaries in the region are set to match various

Fig. 5.16 Domain of inner cylinder generated with volumetric control (Chandrasekaran et al. 2014b)
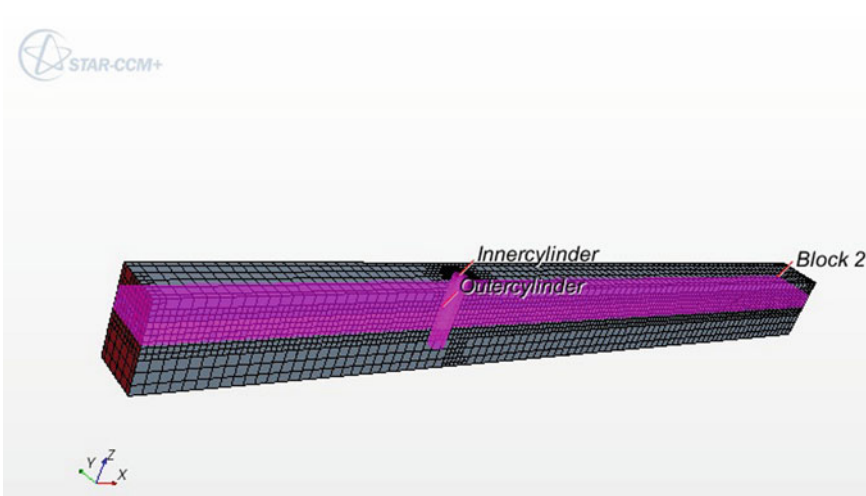
Fig. 5.17 Domain of inner cylinder with perforated outer cylinder generated with volumetric control (Chandrasekaran et al. 2014b)

types of boundary conditions namely (i) "Inlet" boundary is set as a velocity inlet; (ii) "Outlet" boundary is set as a pressure outlet; and (iii) "Inner cylinder" and "Outer perforated cylinder" are set as wall boundaries. The "Velocity Specification" method in the velocity inlet is changed to "Components", and the "Velocity" and "Volume Fraction" values are set identical to the experimental setup. Similarly, the "Volume Fraction" and "Pressure" settings of the pressure outlet are also set

accordingly. The "Time-Step" property of the "Implicit Unsteady" solver is set to 0.01 s. Under the "Stopping Criteria", the "Maximum Inner Iterations" property is set to 10, and the "Maximum Physical Time" is set to 10 s. The "Initialize Solution" tool is selected to activate the required simulation. An iso-surface with an iso-value of 0.5 and a scalar set to "Volume Fraction > Water" is used to visualize the free surface. Scalar is used to visualize both the inner cylinder and inner cylinder with perforated outer cylinder as shown in Figs. 5.18 and 5.19, respectively.

Both the simulated models namely inner cylinder and inner cylinder with perforated outer cylinder are subjected to unidirectional waves of 10 cm wave height. Wave periods are varied from 1 to 2 s with 0.2 s interval; Reynolds-Averaged Navier–Stokes equation is solved, which is assumed to be converged when the residuals decrease by multiple orders before settling around 0.001. Figures 5.20 and 5.21 show the variation of forces on inner cylinder with and without perforated outer cover, respectively, for wave height of 10 cm and wave periods ranging from 1 to 2 s.

Forces on inner cylinder with and without perforated outer cylinder are obtained from the numerical simulation for 10 cm wave height and wave periods ranging from 1 to 2 s; obtained results are shown in Tables 5.12 and 5.13 for inner cylinder with and without perforated outer cylinder, respectively; comparison with the results obtained from the experimental investigations is also shown.
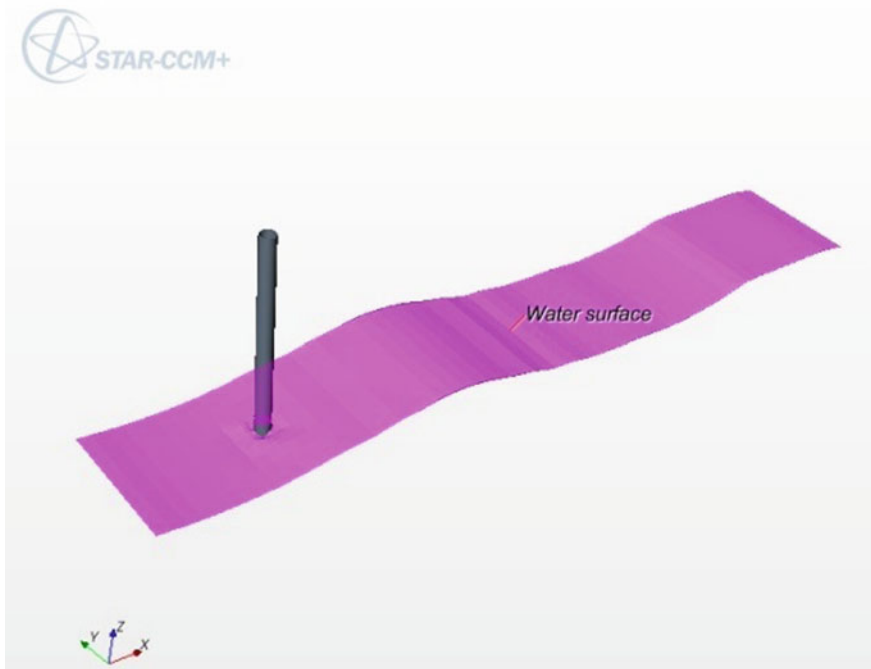
Fig. 5.18 Simulation of inner cylinder (Chandrasekaran et al. 2014a)
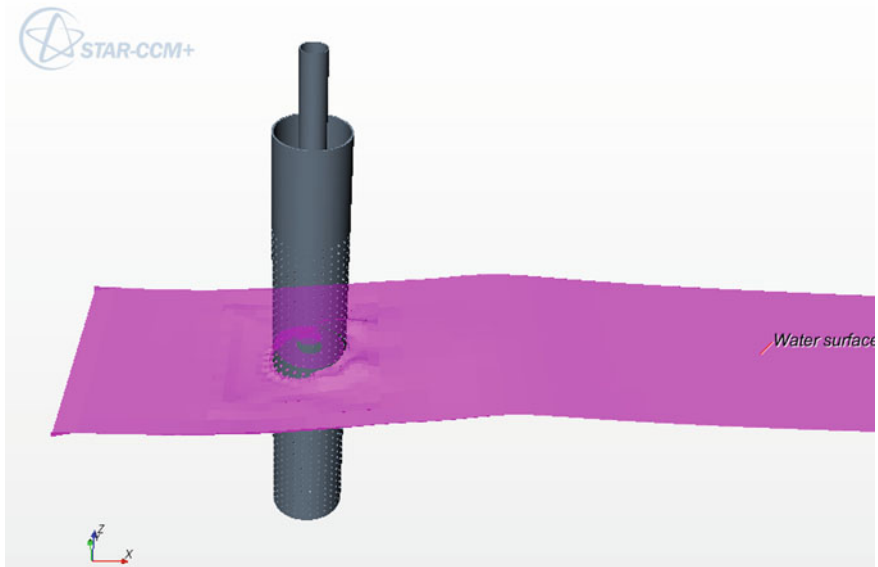
Fig. 5.19 Simulation of inner cylinder with perforated outer cylinder (Chandrasekaran et al. 2014a)
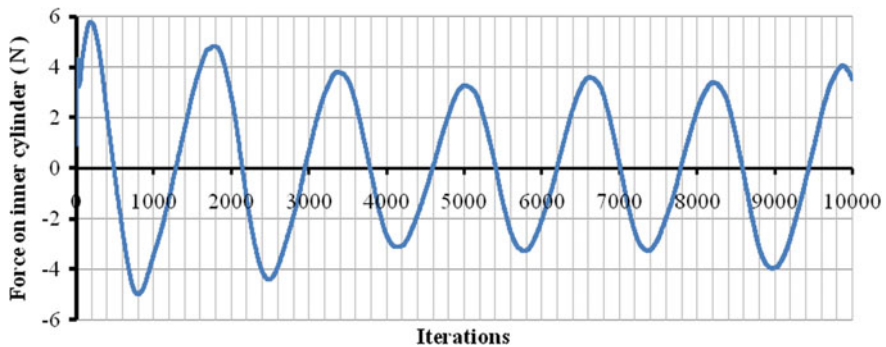
Fig. 5.20 Force on inner cylinder (WH = 10 cm; WP = 1.6 s) in numerical simulation

It can be seen from the tables that forces on inner cylinder without perforated outer cover, computed from both the numerical simulations and experimental results, are ranging from 1.99 to 13.63% with an average error of 7.08%. In case of forces computed on inner cylinder with perforated outer cylinder, errors between numerical simulations and experimental results range from 2.51 to 11.28%, with an average of 7.5%. Figure 5.22 shows the graphical comparison of the results obtained from numerical simulation and experimental investigations. It is also seen from the figure that both the results agree well within the acceptable error of tolerance for the chosen range of wave periods.
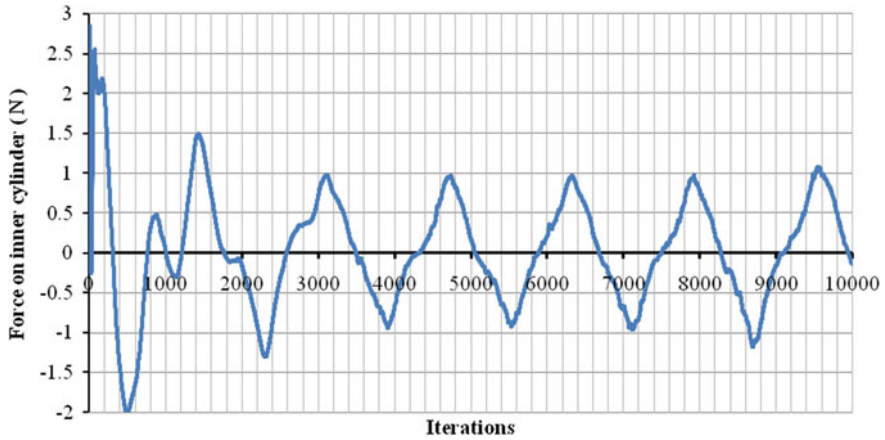
Fig. 5.21 Force on inner cylinder with perforated outer cylinder in numerical simulation (WH = 10 cm; WP = 1.6 s)

Table 5.12 Forces on inner cylinder (WH = 10 cm)

Wave period (s)	Numerical (N)	Experimental (N)	Error in %
1.0	11.06	10.11	8.59
1.2	10.2	8.81	13.63
1.4	8.45	7.69	8.99
1.6	6.84	6.65	2.78
1.8	6.52	6.39	1.99
2.0	6	5.61	6.50

Table 5.13 Forces on inner cylinder with perforated outer cylinder (WH = 10 cm)

Wave period (s)	Numerical (N)	Experimental (N)	Error in %
1.0	4.02	3.73	−7.81
1.2	3.65	3.28	−11.28
1.4	3.106	3.03	−2.51
1.6	2.75	2.85	3.51
1.8	2.51	2.77	9.39
2.0	2.32	2.59	10.42

Based on the experimental investigations and numerical studies carried out, it is seen that the force estimates between both the studies are in good agreement, validating the numerical procedure adopted in the study. Few problems associated with the simulation are (i) high cell numbers and (ii) larger domain attempted to simulate the conditions as that of the wave flume resulted in not yielding the velocity profile variation at the desired points along the cylinder. An attempt is made to simulate the numerical model for a 2D plate with relatively smaller domain
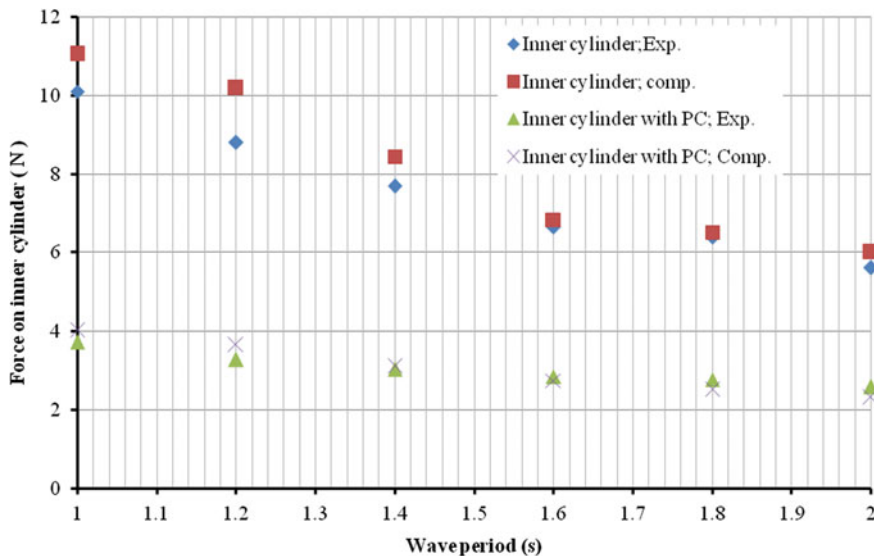
Fig. 5.22 Comparison of forces on inner cylinder with and without perforated outer cylinder

so as to trace the variation of velocity profile along the water depth; in addition, parametric studies like (i) size of perforation, (ii) perforation ratio, and (iii) location of perforation will be examined to derive the velocity profile variation under the influence of the chosen parameters. When the train of waves hits the cylinder, the energy gets dissipated due to back-and-forth movement causing a partial breaking of waves. Hence, this phenomenon acts as a good energy dissipation technique, which is an economical approach preferred by the design engineers. The reflection of the waves may also cause force on the outer porous cylinder. The horizontal velocity is a function of the following parameters:

$$V = f(\rho, g, D, H, a, \sigma, d), \tag{5.2}$$

where ρ is the mass density of water, g is the acceleration due to gravity, D is the diameter of the cylinder, H is the wave height, σ is the frequency of wave, a is the area of perforation, and d is the water depth. The present study is done for the perforation ratio between 10 and 15%. Hence, the above is transformed as given below:

$$V = f\left(\frac{H}{L} \text{ or } \frac{H}{d} \text{ or } \frac{d}{l} \text{ or } K_a, \frac{a}{D^2}, \sigma\sqrt{\frac{D}{g}}\right) \tag{5.3}$$

H/L parameter is generally used for the deepwater conditions. For clear understanding, the sea states are represented with H/L parameters. The sea states are grouped into three categories such as steep, medium, and low wave steepness. H/L ranging between 0.0051 and 0.0167 is categorized as waves with low

steepness; *H/L* ranging between 0.0198 and 0.0445 is categorized as medium wave; *H/L* ranging between 0.0491 and 0.1002 is categorized as steep waves. The cylinder is subjected to unidirectional waves of considered sea states. The horizontal velocity variation along the depth is derived. Figures 5.23, 5.24, and 5.25 show the horizontal velocity profile along the depth of cylinder for different sea states.

Zones of perforation are marked by a dotted line, and solid horizontal line indicates the mean sea level (MSL) of the cylinder. Velocity variations at few sections are plotted for discussion. For the all *H/L* considered, the profile of horizontal velocity along the water depth is highly nonlinear in the zone of perforation. It is also noted that there is a phase change in the velocity profile between the zones of perforation. As we know, the water particles try to take a shorter path during the flow; they try to escape through the nearby perforation, which leads to phase change in the perforation zones. The velocity variation along the depth of the cylinder with outer perforation cover is compared with the velocity profile without outer perforation cover; the plots show a significant deviation of the velocity vector with perforated cover. Hence, the study of water particle kinematics has become very important with the perforation cover. The peak also changes its phase for different perforation ratios, which is clearly shown in Fig. 5.26.

The variations of horizontal velocity at mean sea level for different perforation ratios for the considered sea states are non-proportional. This plot confirms that the range of perforation found optimum is between 11 and 12% with the considered
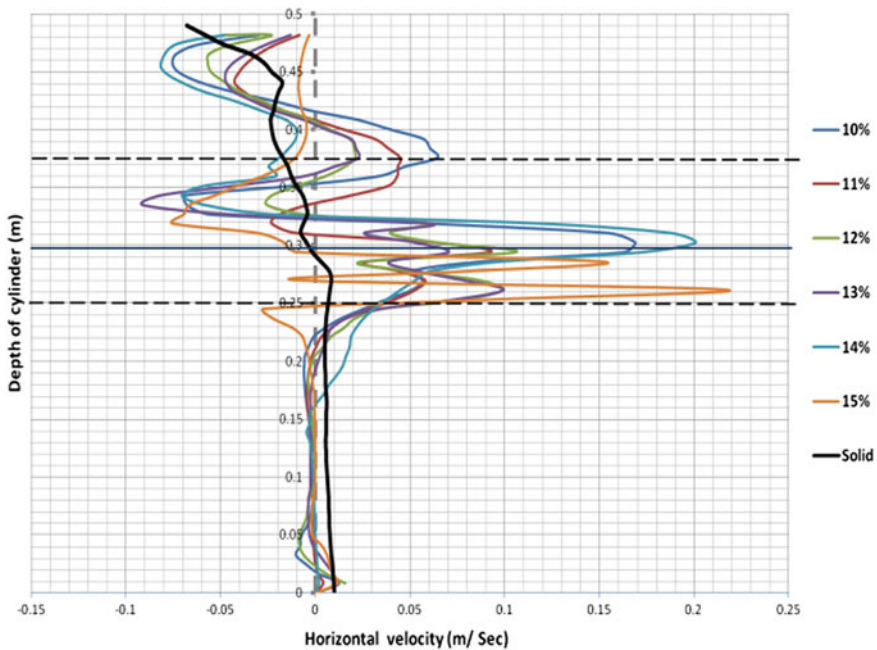
Fig. 5.23 Horizontal velocity variation for various percentages of perforation with wave steepness 0.0051
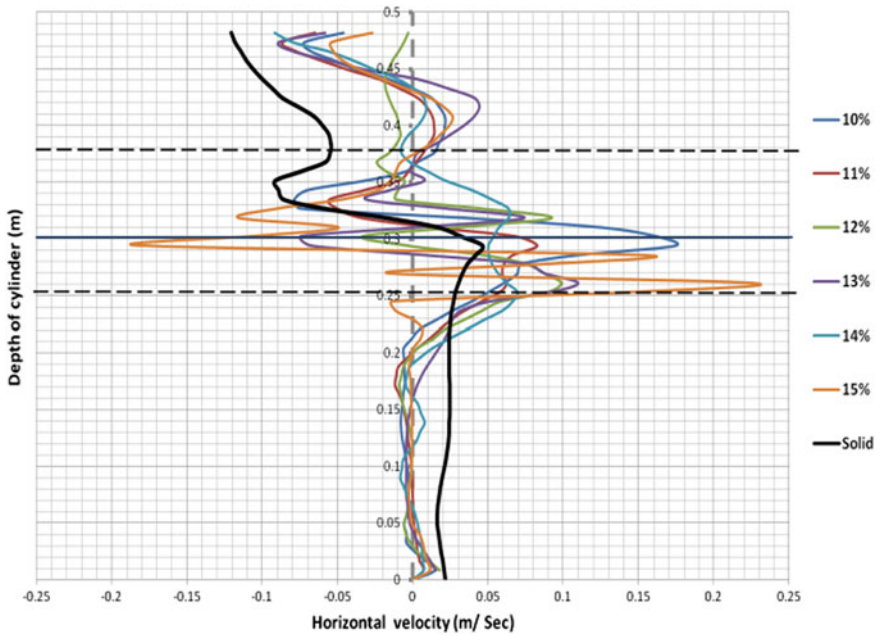
Fig. 5.24 Horizontal velocity variation for various percentages of perforation with wave steepness 0.0103
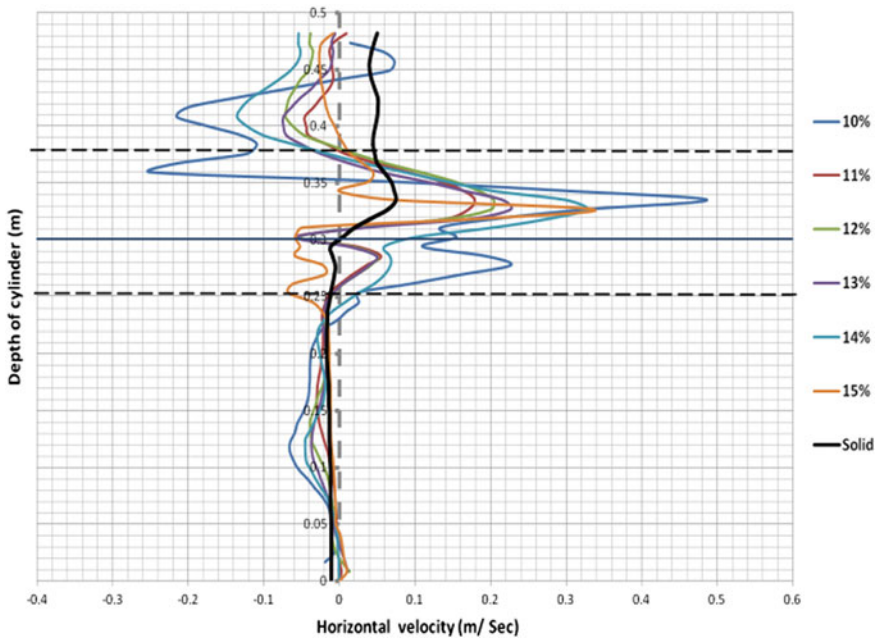
Fig. 5.25 Horizontal velocity variation for various percentages of perforation with wave steepness 0.0164
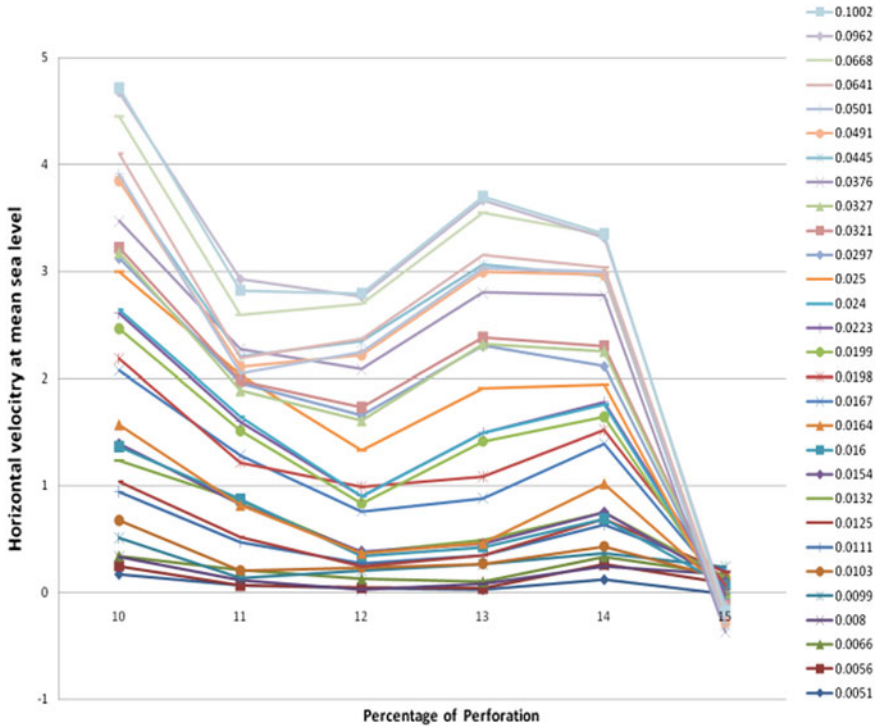
Fig. 5.26 Horizontal velocity at mean sea level for various wave steepnesses

geometrical parameters. Figure 5.26 shows the variation of horizontal velocity along the depth of the cylinder with and without perforation for different chosen sections such as section 1-1 and section 2-2, as shown in Fig. 5.27.

The plot indicates that there is significant reduction of horizontal velocity along the wave advancing direction. From the plot, it is also seen that the horizontal velocity which is associated directly to horizontal force increases in the region of perforation as it is placed just beneath the free surface. It is seen that the horizontal components of hydrodynamic characteristics are significantly influenced by the presence of porous zone. Figures 5.28, 5.29, and 5.30 show that the reduction in the horizontal velocity reduces with the reduction of wave steepness.

It is seen from the figures that there is no significant variation in the velocity component between the sections for the waves with low steepness. It is also seen that in the zone of perforation, the velocity profile is highly nonlinear. There is significant reduction in the horizontal velocity along the wave advancing direction. Steeper waves show higher reduction in the velocity than the waves with mild wave steepness. The design charts provided aids directly the design engineers to derive the horizontal velocity for different sea states and perforation ratio for the chosen geometric model. Based on the numerical studies conducted, the optimum percentage of perforation ratio for the chosen geometric model is recommended as 11–12%.
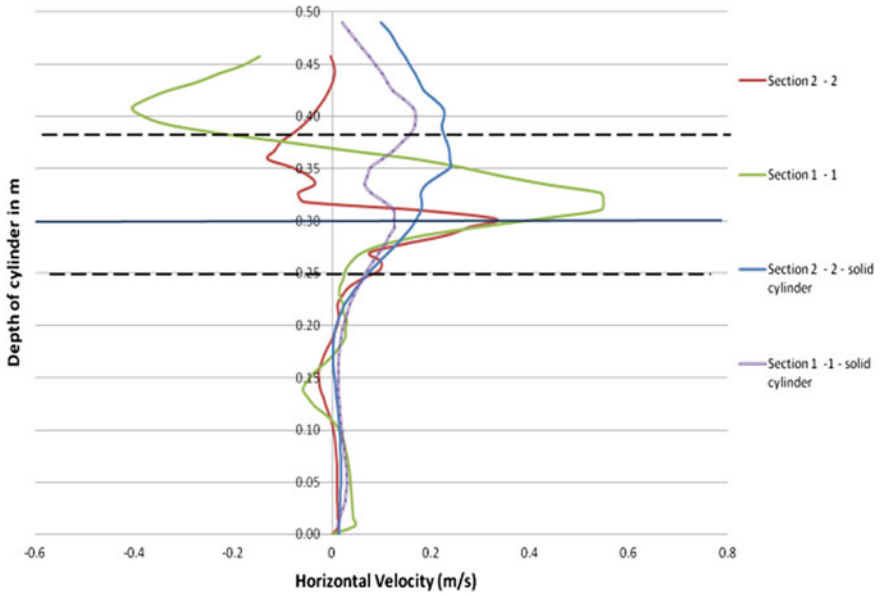
Fig. 5.27 Change in horizontal velocity between sections—perforation ratio 11% and *H*/*L* 0.0962
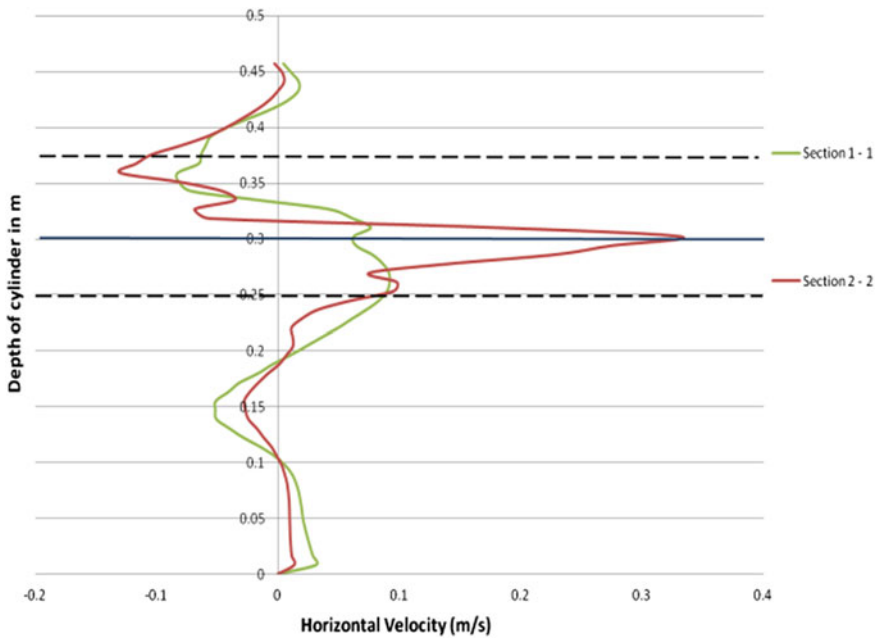
Fig. 5.28 Change in horizontal velocity between sections—steep wave
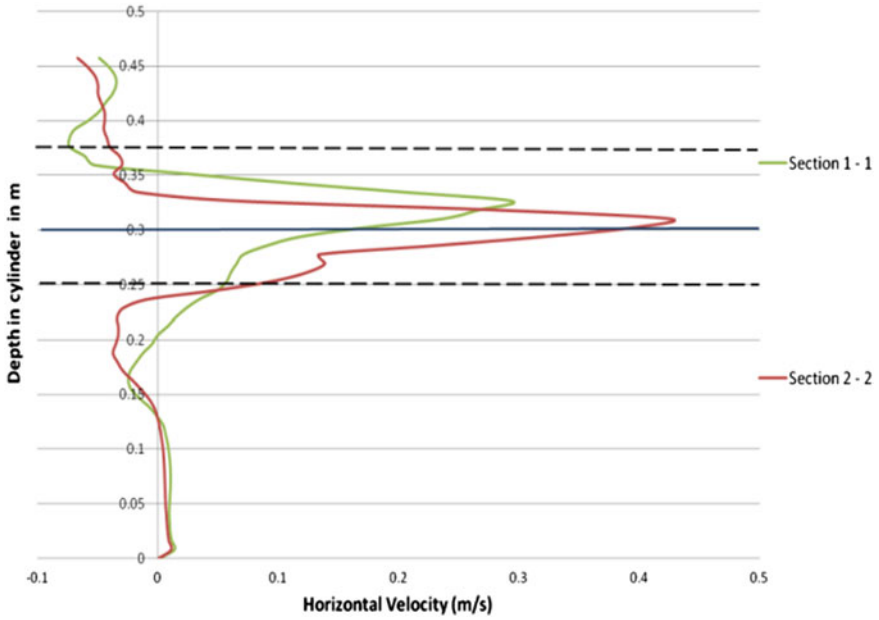
Fig. 5.29 Change in horizontal velocity between sections—medium steep wave
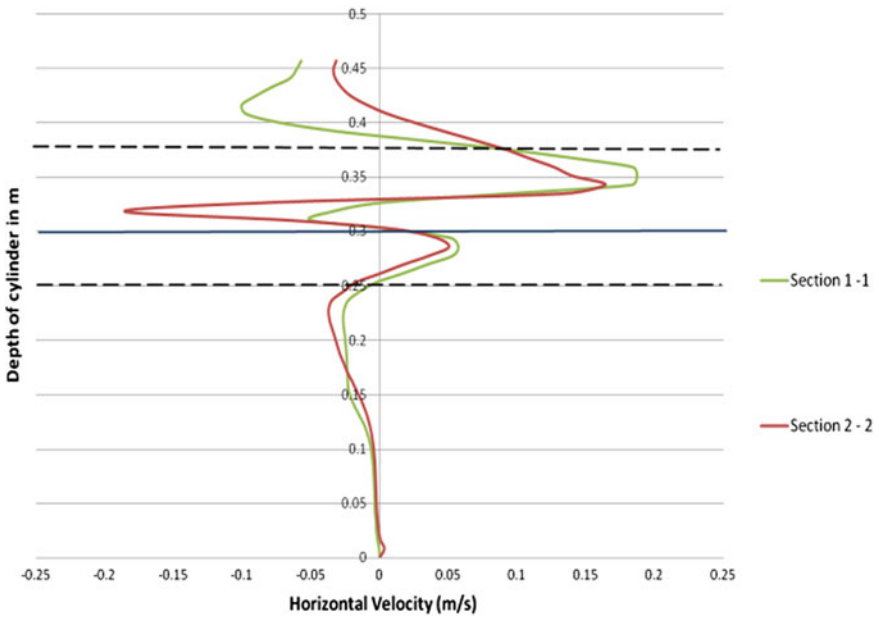
Fig. 5.30 Change in horizontal velocity between section—low steep wave

Exercise

1. List and explain briefly the forces acting on the structure.
2. In the_____, there will be one-to-one relationship between the extent of wake region and restraint loads.
3. Variation in _____causes downward flow along the length.
4. In_____, vertical cylinder will show vortices at the same frequency over its entire length, whereas in shear flow, frequency changes_____.
5. Horizontal cylinders will also be subjected to_____ _____.
6. Explain blockage factor?
7. _____ in porosity reduces wave exciting forces.
8. _____ in the porous body changes the response behavior of TLP significantly.
9. Perforated cylindrical structures reduce _____ and _____ _____ considerably.
10. Introduction of perforated member acts as a_____, which is an economical approach. And the profile of horizontal velocity along the water depth is highly _____ in the zone of perforation.

Answers

1. Forces acting on the structures in fluid medium shall be classified as drag (acting in-line with the direction of flow) and lift (transverse to the direction of flow). Further, drag force can be classified as higher and smaller frequency components. These components will be functions of the geometry of the structure and flow conditions. Lift forces contain oscillatory components with multiple frequencies. On the downstream side, flow will return to its unaltered condition. This is due to fluid viscosity and damping. The region of altered flow directly behind the structure is called *wake region*.
2. Wake regions.
3. Stagnation pressure.
4. Uniform flow; continuously.
5. Flow-induced vibrations.
6. Closely spaced members, connected in different orientations, cause distortion in the fluid field around them. For closely spaced members, the structure becomes dense. For dense structures, flow field slows down as it travels through the structure. This causes blockage effect and complicates the actual velocity field around the structure. Load on the structure increases due to this blockage.
7. Increase.
8. Drag force.
9. Wave–structure interaction and scouring problems.
10. Good energy dissipation technique; Nonlinear.

Chapter 6
Introduction to Stochastic Dynamics

Abstract This chapter deals with introduction to stochastic dynamics and its application to offshore structures. This chapter introduces the basics of reliability approach to the ultimate load design, levels of reliability, methods of reliability, reliability estimates, and limitation. The limitations and advantages of stochastic models are also explained. A quick preview about FOSM and advanced FOSM is also given in this chapter. Introduction to fatigue and fracture assessment is also provided.

Keywords Stochastic dynamics · Ultimate load · Reliability · FOSM · Advanced FOSM · Offshore structures

6.1 Introduction

In most of the cases, offshore structures are exposed to the environmental loads that can be modeled as a piecewise stationary process. A stationary process is one for which the statistical properties like mean value and standard deviation are same for all points in time (or) position (Wirsching and Ortiz 2006). Hence, the following equation holds good:

$$m_x = E[X(t)] = \text{constant} \tag{6.1}$$

For the condition $m_x = m_{x(t)}$ to be satisfied, autocorrelation function is given by

$$R_X(\tau) = E[X(t)X(t+\tau)] \text{ to remain function of } \tau \text{ only} \tag{6.2}$$

To check whether the following are independent of time,

$$\hat{m}_x(t) = \frac{1}{N} \sum_{j=1}^{N} x_j(t) \tag{6.3}$$

$$\hat{R}_x(t, t+\tau) = \frac{1}{N}\sum_{j=1}^{N} x_j(t)x_j(t+\tau) \tag{6.4}$$

If they remain independent of time, the process is said to be a stationary process. Stationary process is defined by satisfying the condition given in Eq. (6.1).

The auto-covariance function should be as follows:

$$C_X(\tau) = E[(X(t) - m_x)(X(t+\tau) - m_x)] = \text{function of } \tau \text{ only} \tag{6.5}$$

For a stationary process, transfer between the load and the response can be modeled as linear, time-invariant, while the system can be characterized by a transfer function. Hence, the relationship between variance spectrum of the response (called response spectrum) and variance spectrum of load (called load spectrum) is determined by a transfer function.

Let $F(t)$ denote a stochastic load process. Assuming that $F(t)$ acts as a linear, time-invariant system, which has an impulse response function $h_{FX(t)}$, for each realization $f(t)$ of $F(t)$, we get the corresponding realization $x(t)$ of the response $X(t)$. Hence,

$$
\begin{aligned}
x(t) &= \int_{-\infty}^{\infty} h_{FX(s)}f(t-s)\mathrm{d}s \\
&= \int_{0}^{\infty} h_{FX(s)}f(t-s)\mathrm{d}s
\end{aligned} \tag{6.6}
$$

$$\text{because} \quad h_{FX(s)} = 0 \quad \text{for} \quad s < 0$$

Equation (6.6) establishes the connection between the realization of the load process and the corresponding realization of the response process. This connection can also be described as below:

$$X(t) = \int_{0}^{\infty} h_{FX(s)}F(t-s)\mathrm{d}s \tag{6.7}$$

The above equation interprets that *there exists a relation between all the corresponding pairs of realization of $F(t)$ and $X(t)$*. It is important to note that the impulse response function or the transfer function, which determines the connection between the load and the response, is completely defined by the properties of the linear system. This remains independent of any given load. In the term of $h_{FX(t)}$, index FX is to be understood only as the visual indicator for the connection between $F(t)$ and $X(t)$. For example, if $Y(t)$ is the response of the load process $G(t)$, acting on the same linear system, then $h_{GY(t)} = h_{FX(t)}$.

6.1.1   *Mean Value of Response*

Assuming that $f_1(t), \ldots, f_N(t)$ is the sequence of realization of $F(t)$, let $x_1(t), \ldots, x_N(t)$, which denotes the corresponding response realization, then

$$\frac{1}{N}\sum_{j=1}^{N} x_j(t) = \frac{1}{N}\sum_{j=1}^{N} \int_0^\infty h_{FX(s)} f_j(t-s)\,ds \tag{6.8}$$

$$= \int_0^\infty h_{FX(s)} \left\{ \frac{1}{N}\sum_{j=1}^{N} \int_0^\infty f_j(t-s)\,ds \right\} \tag{6.9}$$

This leads to the following relationship:

$$E[X(t)] = \lim_{N\to\infty} \frac{1}{N}\sum_{j=1}^{N} x_j(t) = \int_0^\infty h_{FX(s)} \left\{ \lim_{N\to\infty} \frac{1}{N}\sum_{j=1}^{N} f_j(t-s) \right\} ds \tag{6.10}$$

$$= \int_0^\infty h_{FX(s)} E[F(t-s)]\,ds \tag{6.11}$$

If $F(t)$ is a stationary process, then $m_F = E[F(t)]$ is a constant. Then,

$$E[X(t)] = m_F \int_0^\infty h_{FX(s)}\,ds \tag{6.12}$$

It can be seen that the above equation is independent of time. Hence,

$$m_X = E[X(t)] = \text{constant} \tag{6.13}$$

Let $H_{FX}(\omega)$ be the transfer function that corresponds to the impulse response function of $h_{FX(t)}$. Then,

$$H_{FX}(0) = \int_0^\infty h_{FX(s)}\,ds \tag{6.14}$$

$$E[X(t)] = m_F H_{FX}(0) = m_X$$

For the system, whose equation of motion is given by

$$m\ddot{u} + c\dot{u} + ku = P_0 \cos(\omega t) \tag{6.15}$$

The transfer function for the linear system, described by the above equation of motion, is given by $H_{FX}(\omega)$. For the steady-state response of the system under the given excitation load, the dynamic amplification factor D is given by

$$D = \frac{1}{\sqrt{(1 - \beta^2)^2 + (2\xi\beta)^2}} \qquad (6.16)$$

For a weakly damped system, we also know that the maximum amplification factor is given by

$$D_{\max} = \frac{1}{2\xi} \qquad (6.17)$$

For $\xi = 2\%$, $D_{\max} = 25$, which implies that even small oscillating forces may lead to large responses. For the analysis of structural response to various forcing frequencies, it is therefore better to introduce a complex valued function as given below:

$$\begin{aligned} H(\omega) &= |H(\omega)|e^{-i\varphi} \\ u(t) &= |H(\omega)|P_0\cos(\omega t - \varphi) \end{aligned} \qquad (6.18)$$

In the above equation, $H(\omega)$ gives the amplitude amplification and φ gives the phase shift. For example, if $H(\omega) = 0.001$, for a particular frequency ω, then a force amplitude of 100 N will give rise to the displacement of 0.1 m at this frequency. The generalized expression for the steady-state response of the oscillating system is given by

$$\begin{aligned} u_p(t) &= \rho\cos(\omega t - \varphi) \\ \frac{\rho}{x_{\text{static}}} &= \frac{\rho}{(P_0/K)} = D \\ &\text{Hence,} \\ u_p(t) &= \frac{P_0}{K}\frac{1}{\sqrt{(1 - \beta^2)^2 + (2\xi\beta)^2}}\cos(\omega t - \varphi) \end{aligned} \qquad (6.19)$$

Comparing Eqs. (6.18) and (6.19), we get

$$H(\omega) = \frac{1}{K}\frac{1}{\sqrt{(1 - \beta^2)^2 + (2\xi\beta)^2}}, \qquad (6.20)$$

where $H(\omega)$ is called the transfer function or frequency response function, which maps the response behavior of the linear system to the external forcing function. It is seen that this function is proportional to the dynamic amplification factor. It

contains all relevant information about the dynamic amplification. Incorporating also the information related to the phase shift, transfer function is modified as

$$H(\omega) = \frac{1}{K}\frac{1}{\sqrt{(1-\beta^2)^2 + (2\xi\beta)^2}}e^{-i\varphi} \tag{6.21}$$

The reason, why it is easier to use $e^{-i\phi}$, in comparison to $\sin\phi$ or $\cos\phi$ is that

$$\frac{d}{dt}(e^{i\varphi}) = i\frac{d\varphi}{dt}(e^{i\varphi}), \quad \text{where } e^{i\varphi} \text{ factor does not change}$$

$$e^{i\varphi_1}e^{i\varphi_2} = e^{i(\varphi_1+\varphi_2)} = e^{i\varphi_3}, \quad \text{where the product of two factors are of the same kind}$$

The above two properties give many advantages in the derivations. Further, $H_{FX(0)} = (1/k)$ and $m_X = (m_F/K)$. This means that the mean value of the response is equal to the product of the mean value of the load and the system response to a static load of unit size; hence, the following equation holds good:

$$m_X = H_{FX(0)}m_F \tag{6.22}$$

It is seen from the above equation that, for the excitation force with zero mean value, response also has zero mean value.

6.2 Auto-covariance of Response

It is seen from the above section that for $m_F = 0$, m_X is also zero. Hence, for $F(t)$ to be a stationary process, it is convenient to assume $F'(t) = F(t) - m_F$, which also has zero mean value. Let $X'(t)$ be the response to the load process, $F'(t)$. Then,

$$
\begin{aligned}
X'(t) &= \int_0^\infty h_{FX(s)}F'(t-s)\,ds \\
&= \int_0^\infty h_{FX(s)}F(t-s)\,ds - \int_0^\infty h_{FX(s)}m_F\,ds \\
&= X(t) - m_X
\end{aligned}
\tag{6.23}
$$

For $X'(t)$ to have a zero mean value, $F(t)$ and $F'(t)$ have the same auto-covariance. Then, the following relation holds good:

$$x_j(t)x_j(t+\tau) = \int_0^\infty h_{FX(s_1)}f_j(t-s_1)ds_1 \cdot \int_0^\infty h_{FX(s_2)}f_j(t+\tau-s_2)ds_2$$

$$= \int_0^\infty \int_0^\infty h_{FX(s_1)}h_{FX(s_2)}f_j(t-s_1)f_j(t+\tau-s_2)ds_1ds_2$$

(6.24)

It is also known that

$$E[X(t)X(t+\tau)] = \lim_{N\to\infty}\frac{1}{N}\sum_{j=1}^N x_j(t)x_j(t+\tau) \qquad (6.25)$$

Hence, Eq. (6.24) can be rewritten as

$$= \int_0^\infty \int_0^\infty h_{FX(s_1)}h_{FX(s_2)}\lim_{N\to\infty}\frac{1}{N}\sum_{j=1}^N f_j(t-s_1)f_j(t+\tau-s_2)ds_1ds_2$$

$$= \int_0^\infty \int_0^\infty h_{FX(s_1)}h_{FX(s_2)}E[F(t-s_1)F(t+\tau-s_2)]ds_1ds_2 \qquad (6.26)$$

$$= \int_0^\infty \int_0^\infty h_{FX(s_1)}h_{FX(s_2)}C_F(\tau+s_1-s_2)ds_1ds_2$$

Since $F(t)$ is assumed to be stationary, $E[X(t)X(t+\tau)]$ will also be independent of time. The auto-covariance $C_X(\tau)$ will be as same as the autocorrelation $R_X(\tau)$, as the process is a zero mean process. Then, the following relation holds good:

$$C_X(\tau) = \int_0^\infty \int_0^\infty h_{FX(s_1)}h_{FX(s_2)}C_F(\tau+s_1+s_2)ds_1ds_2 \qquad (6.27)$$

6.3 Response Spectrum

Let $S_X(\omega)$ be the variance spectrum of the response of the process $X(t)$ and $S_F(\omega)$ be the variance spectrum of the load process $F(t)$, then variance spectrum of $X(t)$ will be defined by the Fourier transform of the auto-covariance of the response, which is given by

$$S_X(\omega) = \frac{1}{2\pi} \int\limits_{-\infty}^{\infty} C_X(\tau) e^{-i\omega\tau} d\tau$$

$$S_X(\omega) = \int\limits_{0}^{\infty} h_{FX(s_1)} \int\limits_{0}^{\infty} h_{FX(s_2)} \frac{1}{2\pi} \int\limits_{-\infty}^{\infty} C_F(\tau + s_1 - s_2) e^{-i\omega\tau} d\tau ds_2 ds_1 \qquad (6.28)$$

Put $\tau + s_1 - s_2 = \theta, \quad d\theta = d\tau, \quad$ then

$$S_X(\omega) = \int\limits_{0}^{\infty} h_{FX(s_1)} \int\limits_{0}^{\infty} h_{FX(s_2)} \frac{1}{2\pi} \int\limits_{-\infty}^{\infty} C_F(\theta) e^{-i\omega\theta} d\theta e^{i\omega(s_1 - s_2)} ds_2 ds_1$$

$S_X(\omega) = H_{FX}(-\omega) H_{FX}(\omega) S_F(\omega)$ because $e^{(-ix)*} = e^{ix}$ and $h_{FX(t)}$ is a real function.

Imposing the above condition, we get

$$H_{FX}(-\omega) = \int\limits_{0}^{\infty} h_{FX}(t) e^{i\omega t} dt = \int\limits_{0}^{\infty} h_{FX}(t) e^{-i\omega t^*} dt$$

$$\int\limits_{0}^{\infty} h_{FX}(t) e^{-i\omega t^*} dt = H_{FX}(\omega)^* \qquad (6.29)$$

$$S_X(\omega) = |H_{FX}(\omega)|^2 S_F(\omega)$$

The above equation gives the relationship between the response spectrum $S_X(\omega)$ and the load spectrum $S_F(\omega)$. Please note that Eq. (6.29) does not contain information about the phase shift between the load and the response; only amplitude amplification is known. From the response spectrum, one can compute several other statistical quantities that are important for assessing the response. For example, standard deviation of the response is obtained as follows:

$$m_X = H_{FX}(0) m_F$$

$$\sigma_X^2 = \int\limits_{-\infty}^{\infty} |H_{FX}(\omega)|^2 S_F(\omega) d\omega \qquad (6.30)$$

For $X(t)$ be the response of a linear system with transfer function $H_{FX}(\omega)$ to a stationary load process $F(t)$, RHS of Eq. (6.30) for standard deviation is to be computed numerically. For very less damping, $|H_{FX}(\omega)|^2$ becomes narrow around the resonance frequency, ω_r. This implies that the main contribution to the integral of Eq. (6.30) comes from a small interval around ω_r, which is evident from Fig. 6.1.

Fig. 6.1 Amplitude
amplification for various
damping ratios
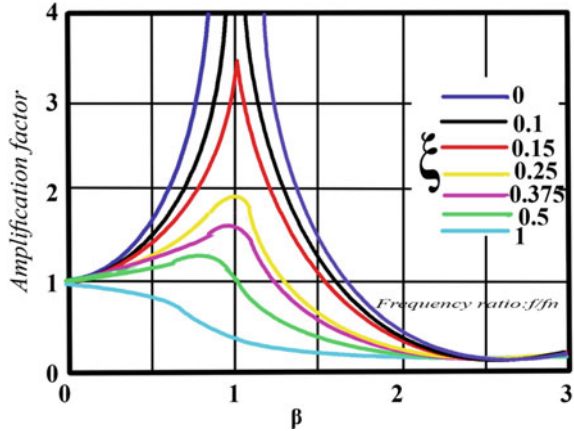
If $S_F(\omega)$ varies much slower than that of $|H_{FX}(\omega)|^2$, then it is often possible to replace $S_F(\omega)$ in Eq. (6.30) by $S_0 = S_F(\omega_r)$. Hence, Eq. (6.30) can be rewritten as

$$\sigma_X^2 = S_0 \int\limits_{-\infty}^{\infty} |H_{FX}(\omega)|^2 \mathrm{d}\omega \tag{6.31}$$

This procedure of replacing the input spectrum by a constant (S_0) is called *white noise approximation*. A typical feature of the response spectrum of a weakly damped system is that it is narrow banded. This follows the fact that the response spectrum, to a large extent, is determined by the value of $|H_{FX}(\omega)|^2$. With the *white noise approximation*, variance is given by Eq. (6.31).

6.4 Stochastic Process

Dynamic analyses can be carried out in two ways depending on the description of loads, namely (i) deterministic analysis, which requires the complete knowledge of load time history and (ii) stochastic analysis where statistical concepts are used to specify the loads. For example, when waves or wind loads are described in terms of statistical quantities, the response should also be described and analyzed in terms of same kind of quantities.

6.4.1 Example of Stochastic Modeling

Sea surface elevation, $X(t)$, is a good example of a random variable. A stochastic process is an abstract notion in a similar manner as that of a random variable. The

values of the variables that can be observed physically are the outcomes, which are usually referred as realizations. A sea surface time history that has a high randomness can be easily overcome by assuming the time history to be a realization of ergodic stationary process. The assumption implies that the statistical information about the process is in fact contained in a single realization of the process. For example, cumulative distribution function (CDF) $F_{X(t)}(x)$ assumes the values lesser than or equal to x, as given below:

$$F_{X(t)}(x) = \lim_{T \to \infty} \frac{T[x(t) \leq x]}{T}, \tag{6.32}$$

where T denotes the record length and $T[x(t) \leq x]$ denotes the total amount of time during T where $[x(t) \leq x]$. The quantity $X(t)$ is called as a stochastic process if $X(t)$ is a random variable for each value of t in an interval (a, b).

6.4.2 *Example of a Stochastic Process*

Assume X as a random variable, which is normally distributed with a mean value, m and standard deviation σ (> 0). Its probability density function is given by

$$f_X(x) = \frac{1}{\sqrt{2\pi}\sigma} \exp\left\{-\frac{1}{2}\left[\frac{x-m}{\sigma}\right]^2\right\} \tag{6.33}$$

If $g(t)$ is known, which is a real function defined for ($-\infty < t < \infty$), then

$$g(t) = \cos(\omega t), \tag{6.34}$$

where ω is a positive constant. Hence, $X(t) = Xg(t)$ is also a stochastic process defined for the same interval ($-\infty < t < \infty$). Realization of the process is then given as a product of $g(t)$ with an outcome x of the random variable X. In that case, the following equation holds good:

$$x(t) = xg(t) \tag{6.35}$$

Hence, if $g(t) = \cos(\omega t)$, its realization could be harmonic function of the same period, but with a different amplitude. Hence, the mean value is given by

$$m_X(t) = E[Xg(t)] = E[X]g(t) = mg(t)$$
$$\sigma_{X(t)} = \sqrt{E[X g(t)^2 - (m g(t)^2]}$$
$$= \sqrt{E[X^2]g(t)^2 - m^2 g(t)^2}$$
$$= \sqrt{E[X^2 - m^2|g(t)|]}$$
$$= \sigma|g(t)|$$

For each value of t, $g(t)$ is a constant. Hence, $X(t) = Xg(t)$ is also normally distributed if $g(t) \neq 0$.

The probability density function of $X(t)$ becomes

$$f_{X(t)}(x) = \frac{1}{\sqrt{2\pi}\sigma|g(t)|} \exp\left\{ -\frac{1}{2}\left(\frac{x - m\,g(t)}{\sigma|g(t)|} \right)^2 \right\} \tag{6.36}$$

6.5 Return Period

Let Z be a random variable. Then,

$$p = \mathrm{Prob}[Z > z] = 1 - F_Z(z) \tag{6.37}$$

Assuming that we can make series of observations of Z, mean number of observations to the first observed or measured value of X exceeds z is called the *return period* for exceedance of z, which is denoted by $\bar{R}(z)$:

$$\bar{R}(z) = \frac{1}{p} = \frac{1}{1 - F_Z(z)} \tag{6.38}$$

This equation can be described as an average of $(1/p)$ trails conducted before an event of probability p occurs. $\bar{R}(z)$ refers to the number of observations and these are assumed to be statistically independent. If return period needs to be explained in terms of time, one needs to know the time interval between the observations. If the observation interval is Δt, then the return period, in terms of time, is given by

$$R(z) = \Delta t \bar{R}(z) \tag{6.39}$$

The observation interval must be chosen sufficiently long such that individual observations become approximately independent. For example, a design load with a probability of 10^{-2} being exceeded during 1 year is often used in offshore structures. If we let $F(t)$ denote the relevant load process considered for the design and ξ denote the corresponding load level, then

Prob $(Z > \xi) = 0.01$, where $Z = \max (F(t))$; $0 \leq t) \leq 1$ year.

Return period of exceedance of ξ then becomes as follows:

$$\bar{R}(z) = \frac{1}{\mathrm{Pr\,ob}(Z > \xi)} = \frac{1}{0.01} = 100\,\text{years} \tag{6.40}$$

Reference period, in this case, is 1 year, and therefore return period of exceedance is 100 years. It is important to note that the time-varying loads, caused by waves, cannot be considered stationary over an extended period. This means that

the quantities such as yearly maxima must be computed using long-term statistics. Return periods are also computed based on the risk associated. This is a common practice in case of earthquake loads and seismic design of structures. For example, design basis earthquake (DBE) has a risk level of 10% at occurrence of 50 years, and that of maximum credible earthquake (MCE) is 2%. Based on the risk associated, return period is computed as below:

$$R = 1 - \left[1 - \frac{1}{T}\right]^n$$

$$\text{For DBE, } 0.1 = 1 - \left[1 - \frac{1}{T}\right]^{50} \text{ yields return period } (T) \text{ as } 475 \text{ years} \qquad (6.41)$$

$$\text{For MCE, } 0.02 = 1 - \left[1 - \frac{1}{T}\right]^{50} \text{ yields a retrun period of } 2500 \text{ years}$$

6.6   Safety and Reliability

Failure of engineering systems that occur under uncertain conditions is case-specific. It cannot be applied to all engineering systems in general. Hence, reliability is used to indicate the estimate of limit probabilities of the offshore structures under adverse conditions and safety is a measure used to indicate the reliability. But this demands a traditional way of analysis. Reliability offers probabilistic meaning to this traditional concept. Safety is a deterministic approach, which has a direct consequence to failure, whereas reliability is a probabilistic approach having a converse consequence of failure. Reliability is used as one of the design methods and its accuracy depends on the data from which the results are obtained. While reliability is based on engineering judgement, safety is based on statistical judgement. Thus, reliability is the probability of a system performing its required function adequately for a specified period under stated conditions. Reliability methods are very important in marine structures because it helps in estimating the degree of uncertainties and optimizing the design process (Chandrasekaran 2016a, b).

Extension of reliability analysis also includes the consequences of failure. Safety assessment and risk characterization are vital for offshore plants. Since risk is realization of hazard and hazard scenario is unavoidable in any process industry, the most important aspect of reliability is to account for all uncertainties that make the structure vulnerable to failure under a predefined limit state. Accuracy of the reliability studies depends on how accurately these uncertainties are accounted for in the analysis. It is an extremely difficult task to consider all the factors related to the reliability of the marine structures, due to the lack of information on the pertinent factors. Many assumptions are made during the reliability analyses, which influence the accuracy of the reliability studies. Uncertainties may arise due to the lack of

reliable information on the accidents in the offshore industry, load calculation, and the material properties. The important uncertainties are identified and engineering judgement is applied to them for better accuracy. Further, it is also important to note that analytical formulation of the limit state surface and integration of the probability density function within the domain of interest is very complex. In addition, methods of modeling and analysis are very complex in marine environment due to the interaction of many engineering systems and other environmental factors. Thus, modeling as an important aspect in reliability framework is always associated with certain uncertainties.

6.6.1   Uncertainties in Marine Structures

Uncertainties can be classified into two types: (i) aletory type that is associated with normal randomness and (ii) epistemic type that is associated with erroneous predictions and estimations of reality. The former type generally arises from the randomness in the environmental loads and is irreducible. The latter type can be reduced using appropriate prediction models and sampling techniques. Aletory-type uncertainties can be effectively handled by Bayesian approach and the epistemic type by the appropriate optimization procedures. The uncertainties in the marine structures can be grouped as follows: the first group in material properties such as the modulus of elasticity of concrete and steel in different loading conditions. The second group is related to the uncertainties in the estimation of loads especially in case of dynamic loads. The uncertainties in the estimation of static loads are negligible due to the strict quality control in the manufacturing of the construction materials. The third group consists of the uncertainties in mathematical modeling and methods of analysis, since each method of analysis is based on the number of assumptions leading to several uncertainties.

6.7   Reliability Framework

In the general sense, offshore platform should perform its intended function for a specified period of time under specific conditions. In the mathematical sense or narrow sense, reliability is estimating the probability of the structure for not attaining the limit state of collapse within the specified conditions, for the specified period:

$$\text{Reliability} = 1 - P_f, \tag{6.42}$$

which implies the fact that it is $(R - S)$, where R is the resistance of the structure and S is the load effects. For the resistance greater than the load effects, the structure is

always in the safe domain. If the load effects and resistance are expressed by their respective PDF as $f_s(S)$ and $f_s(R)$, respectively, then probability of failure is given by

$$P_f = \text{Prob}(R \le S) \tag{6.43}$$

$$
\begin{aligned}
&= \int_0^\infty f_R(s) - f_s(s)\mathrm{d}s \\
&= f_m(0)
\end{aligned}
\tag{6.44}
$$

where M is called the margin of safety, which is given by $(R - S)$. If the probability density function $\{f_m(m)\}$ and cumulative distribution function $F_m(m)$ are known, then probability of failure P_f can be computed analytically or numerically as given below:

(a) **R and S are normally distributed**

If R and S are normally distributed, then

$$p_f = \varphi(-\beta), \tag{6.45}$$

where the reliability index is given by

$$\beta = \frac{\mu_R - \mu_S}{\sqrt{\sigma_R^2 - \sigma_S^2}} \tag{6.46}$$

(b) **R and S are log-normally distributed**

In such cases, reliability index is given by

$$\beta = \beta_{LN} = \frac{\ln\left[\frac{\mu_R}{\mu_S}\sqrt{\frac{(1+V_S^2)}{(1+V_R^2)}}\right]}{\sqrt{\ln(1+V_R^2)(1+V_S^2)}} \tag{6.47}$$

$$\beta_{LN} \approx \frac{\left(\frac{\mu_R}{\mu_S}\right)}{\sqrt{V_R^2 + V_S^2}} \tag{6.48}$$

6.8 Ultimate Limit State and Reliability Approach

For an implicit failure probability in the design under random load effects, the following equations hold good:

$$\mu_S = B_S S_C \tag{6.49}$$

(a) For $B_S \leq 1.0$, $V_S = 0.15$–0.30 and $\mu_R = B_R R_C$,

where B_s reflects the ratio of the mean load if the period of variation is annual and then it should refer to the annual value of probability of failure. S_c is the characteristic value with 100 years return period. For (R, S) be log-normal, the following equation holds good:

$$\beta_{LN} = \frac{\ln \frac{\mu_R}{\mu_S}}{\sqrt{V_R^2 + V_S^2}} \tag{6.50}$$

For $(V_R V_S)$ be the partial safety factor of 1.5, $B_S = 0.8$, $B_R = 1.0$, $V_R = 0.15$, the above equation reduces to the following form:

$$= \frac{\ln \frac{1.1}{0.8}}{\sqrt{0.10^2 + 0.20^2}} = 13.5 \tag{6.51}$$

Ultimate limit state can affect the design since the method is based on the maximum load effect. It is also affected by the strength of the material, which is determined traditionally. Reliability framework is based on establishing a limit state function $g(x)$ for a single R and S, where the limit state function $g(x)$ is subjected to large uncertainties. The preferable design format is then given by

$$\frac{R_c}{V_R} \geq V_{s1} S_{1c} + V_{s2} S_{2c}, \tag{6.52}$$

where subscript stands for the characteristic value, R is the resistance, S is the load effect, γ_R is the resistance factor, and $V_{S1} V_{S2}$ are the load factors. Resistance refers to a characteristic strength of 5% of the fractal materials' strength, while load effect refers to the annual probability of exceedance of 10^{-2}. Design criterion is now given by g $(R_d, S_{1d}, S_{2d}) > 0$:

$$R_d = \frac{R_c}{V_R} \tag{6.53}$$

$$S_{1d} = V_{S1} S_{1C}$$

$$S_{2d} = S_{2c} V_{2c}$$

For multiple values of $(R$ and $S)$, the structure is subjected to different load combinations for which the bending failure criteria can be formulated as

$$g(R_1, R_2, R_3, S_{1j}, S_{2j}) := 1 - \left[\frac{S_{ij}}{R_1} + \frac{S_{2j}}{\left(1 - \frac{S_{1j}}{R_2}\right) R_3} \right] \tag{6.54}$$

The above equation can also be set as

$$= 1 - \left[\frac{X_1}{X_1} + \frac{X_3}{\left(1 - \frac{X_1}{R_4}\right)} \right],$$ (6.55)

where S_{1j}, S_{2j}, etc. are load effects for different combinations and R is the resistance (the count j stands for load type). The above equation is based on the Perry–Robertson approach in which R_1 and R_2 be the axial force and R_3 be the Euler load. In the partial design values of (R and S), they are represented by their respective characteristic values. But in the reliability study, they are considered random variables.

6.9   Short-Term Reliability of Single Load Effect

If the resistance (R) is constant over time and the load effect is the single load (S), then the characteristics value of the load effect can be obtained from the distribution of the individual maximum of the largest value in a given time period. The reliability problem can be arrived based on the extreme value of statistics to characterize $S_{\max}$.

Fracture probability in the short time period is given by

$$\begin{aligned} P_f(t) &= \text{Prob}(g(R, \max_{0 \le t \le T} S(Q(t)) \le 0 \\ &= \text{Prob}(g(R, S_{\max}(T) \le 0 \end{aligned}$$ (6.56)

where $g()$ is the limit state function, R is the structural resistance, and S is the load effect resulting from the load process $Q(t)$.

6.9.1   Up-Crossing Approach

The alternate approach is the up-crossing rate approach. This is time-dependent reliability, while the main interest lies in the time (t_f) to the first failure.

For a simple problem, following equation holds good:

$$M(t) = g(R, S(t)) = R - S(t)$$ (6.57)

t_f is the first time when $M(t) = 0$ that is when t_f is the time of first excursion of $M(t)$ from positive to negative value assuming $M(t)$ is a continuous process.

Probability of failure is the period $[0, T]$ and is equivalent to the probability that $t_f < T$:

$$P_f = 1 - \text{Prob}(t_f > T)$$

$$= 1 - \text{Prob}\left(N(t) = 0 \mathbin{\dot{:}} M(0) > 0\right)\text{Prob}(M(0) > 0) \tag{6.58}$$

where $N(t)$ is the number of up-crossing in $(0, t)$ or number of crossing from safe to failure design. $M(t) = R - S(t)$ is in the safe domain at zero time. If $M(0) > 0$ signifies the safety margin. In general, calculation of P_f is a complex task and approximate solution can be achieved by assuming $N(t)$ as a Poisson process that is uncertainty of level R by $s(t)$ is independent with the mean rate of $v_s^+(R) = v_m^-(0)$ per unit time:

$$\text{prob}(N(T) = 0) = \frac{\left(v_s^+(R)T\right)^0}{0!}e^{-v_s^{+}(R)T} = e^{-v_s^{+}(R)T} \tag{6.59}$$

Also, $\text{prob}(M(T) > 0) = 1 - P_f(0)$, which means that the probability of number of failure at $t = 0$. Hence, $P_f(o) = 0$, and then $P_f(t)$ is given by

$$P_f(T) \cong 1 - e^{-v_s^{+}(R)T} \cong v_s^+(R)T = v_m^-(o)T \tag{6.60}$$

As a special case, when $s(t)$ is a Gaussian process, then

$$v_s^+(R) = v_0^+ \exp\left(-\frac{(R - \mu_s)^2}{2\sigma_s^2}\right) \tag{6.61}$$

$$v_0^+ = v_s^+(0)$$

For the given value of random variable $X = (X_1, \ldots X_n)^{\text{T}}$ that represents those uncertainties, the conditioned failure probability is determined by down-crossing of 0 by $M(t; X)$ for $t \geq 0$:

$$P_f(x) = \text{prob}\left(\min_{0 \leq t \leq \text{T}} M\left(\dot{t} : x\right) \leq 0\right),$$

$$= 1 - \exp\left[-v_m^-(0; x)T\right] \tag{6.62}$$

where $v_m^-(0; x)$ is the zero down-crossing rate which depends on the parameter of vector x. The total failure probability considering the uncertainty in X can be calculated by unconditional probability, as given below:

$$P_f = \int_x P_f(x)f_x(x)\mathrm{d}x \tag{6.63}$$

The integral represents expected value of $P_f(x)$. Hence, P_f can be calculated as a random value, as shown below:

$$P_f \cong \frac{1}{N} \sum_{i=1}^{N} P_f(x_i) \tag{6.64}$$

6.10 Long-Term Reliability of Single Load Effect

For a nonstationary process $M(t; x)$ which could be for a long-term, failure probability is given by

$$P_f(x) = 1 - \exp\left\{ -\int_{0}^{T} v_m^-(0; t; x)\mathrm{d}t \right\}, \tag{6.65}$$

where $v_m^-(0; t; x)$ is the mean down-crossing rate which depends as the sea state and changes with time. For the given set of properties of the sea states, let W be the captured value, which is given by

$$W = \left(H_s, T_p, u_c, u_w, \vec{\text{wave}}, \vec{\text{wind}}, \vec{\text{current}} \right), \tag{6.66}$$

where H_s is the significant wave height, T_p is the spectral peak period, u_c is the current velocity, u_w is the mean wave speed, and $\vec{\text{wave}}, \vec{\text{wind}}, \vec{\text{current}}$ are the wave, wind, and current direction. Prerequisite of the long-term failure probability is to impose an ergodicity assumption on the environmental process $W = W(t)$, and then

$$P_f(x) = 1 - \exp\left\{ -T \int_{w} v_m^-(0; w; x) f_x(w)\mathrm{d}w \right\}, \tag{6.67}$$

where $v_m^-(0; w; x)$ derives mean zero down-crossing rate of M for the sea state $W = w$:

$$f_w(w) = \text{PDF of } W \tag{6.68}$$

The full long-term failure probability occurring for both environment variability and parameter uncertainty is given by

$$P_f = \int_{x} P_f(x) f_x(x)\mathrm{d}x \tag{6.69}$$

6.11   Levels of Reliability

Reliability studies are considered in different levels in the literature. Level I is focusing on the probability aspects of the problem. Suitable characteristic values of the random variables are introduced in the safety analysis. Main objective of this level of study is to minimize the deviation of the design values from that of the target value. For example, load-resistance factor design (LRFD) is of level I of reliability. Level II has two values for each parameter to be defined in the analysis namely mean and standard deviation. Level III is a complete analysis of the problem addressing the multidimensional probability density function of random variables, which is extended over the safety domain. Reliability is expressed in terms of suitable safety indices. In level IV, engineering economics is also applied in the reliability study. This level of reliability study is usually applied to structures of strategic importance. The study includes cost–benefit analysis, rehabilitation, consequence of failure, and return on capital investment.

Reliability methods offer many advantages: (i) they account for the uncertainties; (ii) they are rational methods to estimate safety; and (iii) they offer decision-making support for noneconomic and better-balanced design. Optimal distribution of material among various components of structure can be benefitted through a constant update mechanism, on the basis of which FEED function of engineering judgment is circumscribed. Reliability studies expand the knowledge of uncertainties in the response of the structure. There are few obstacles in implementing the reliability studies to the offshore plants in operation. They are classified as inertial, cultural, and philosophical. Different types of variables used in reliability study are, namely, (i) elementary variables (static variables) like material properties, (ii) geometry of the platform, (iii) boundary conditions, and (iv) issues related to the location and behavior dependent data.

Failure modes such as limit stress and limit displacement depend upon the system variables, which are in turn dependent on location behavior and failure modes. There are different steps of reliability namely elementary level, component level, system level, and detailed field investigation. The first step is handled by stochastic modeling, while the second step can be handled by probabilistic study of failure of components. In case of system-level studies, probabilistic studies on the failure of the whole system can be investigated. One of the serious limitations of reliability study is that it requires a large amount of data on the failure scenario. Other parameters that influence the accuracy of the results of the reliability studies are as follows:

1. Separation of two variables, namely safety domain and failure domain.
2. Nature of variables namely external or internal and whether they are independent or not.
3. Effect of time indicating the static content or the cyclic (dynamic) content.
4. Form of the performance function, which is dependent on the physical model of the system.

6.12   Reliability Methods

The main interest is to develop a reliability method in relation to modeling the materials and structures. The primary advantage of the reliability method in structures is to calculate the reliability estimates by nominal or conditional probability, reliability index, and serviceability of failure to stochastic date description. Three fields of application are particularly targeted; they are as follows:

1. Exceptionally highly innovative structures for which experience accumulated in last few certainties are inadequate. Reliability methods were first used for designing offshore platform.
2. Design of ordinary-type structures with codes whose current evolutions offer possibility of calibration of partial coefficients using reliability methods.
3. Monitoring of structures during the lifespan so that repair strategies can be optimized through reliability.

6.12.1   Advantages of Reliability Methods (ASC-83)

The advantages of reliability methods are as listed below:

- Offer a realistic procession of uncertainties and the methods for evaluating the safety factors that are often too arbitrary.
- Offer decision-making support for more economic and better-balanced design.
- Analyze failure modes and measure the reliability provided by application and regulations.
- Allow the optimal distribution of material and arrange various components of the structure.
- Benefit from the experience acquired in design by updating on the basis of feedback from the experience.
- Expand the knowledge of uncertainty in response to the structure.

There are some obstacles in the implementation of these advantages. They are as follows:

- These methods demand new approach and call to our thinking and working pattern.
- Because it is more of a probabilistic approach and lesser statistical approach, it demands more mathematical concepts rather than engineering skills.
- They explicitly underscore the acceptance of risk, and using safety coefficients, they demand the judgment and decision.
- One should have minimum statistical knowledge of elementary properties of variables, and we need to use these in modeling.

6.13   Stochastic Models

The stochastic modeling essentially helps to establish variability by best-suited probability density function. They can be done by two approaches namely naturalist's approach and physicist's approach. Reliability is also an observation of the sample that estimates μ, SD, and variance. This often gives ad hoc estimates or estimates by interval. These estimates are themselves a random variable, since based on this best judgment, PDF has to be determined. Alternatively, as per the physicist's approach, this seeks to understand the variability of the material's behavior on a microscopic scale. Results of reliability calculation depend on the quantity of data. But these data are always insufficient due to limitations that arise from the size of test samples, infinite domain, and distribution trails. Reliability analysis also requires failure scenario, which separates the situation that the designer decides as acceptable from those of the other. Complexities of reliability are mainly due to the nature of the random variables, effect of time, mechanical models, and the form of performance function chosen for the analysis.

6.13.1   First-Order Second Moment Method (FOSM)

In this case, first-order Taylor series approximation of the limit stat function is used for the analysis. Only second moments of the random variables are used to estimate the probability of failure. Limit state function is defined as

$$M = R - S, \tag{6.70}$$

where R and S are statistically independent and assumed to be normally distributed. Hence, the following relationship holds good:

$$\mu_m = \mu_R - \mu_S \tag{6.71}$$

$$\sigma_m = \sigma R_2 + \sigma S_2 \tag{6.72}$$

Probability of failure is given by

$$\begin{aligned} P_f &= P(M < 0) \\ &= P[(R - S) < 0] \end{aligned} \tag{6.73}$$

If M is the normal variant, then

$$P_f = \phi\left(\frac{-\mu_m}{\sigma m}\right) \tag{6.74}$$

Table 6.1 Merits and demerits of FOSM of reliability

Advantages	Disadvantages
It is easy to use	Results can cause serious errors. The tool used for the distribution function cannot be approximated by normal distribution
It does not require knowledge of distribution of random variables	Values of β depend on the specific form of the limit state function. This is an invariance problem

$$\beta = \text{reliability index} = \frac{\mu_m}{\sigma_m}, \qquad (6.75)$$

where ϕ is the case cumulative distribution function of standard normal variable. Probability of failure is given by

$$P_f = 1 - \phi\left(\frac{\mu_R - \mu_S}{\sigma_R^2 + \sigma_S^2}\right) \qquad (6.76)$$

If R and S are log-normal, then following relationship holds good:

$$P_f = 1 - \phi\left[\frac{\ln\left[\frac{\mu_R}{\mu_S}\sqrt{\frac{(1+V_S^2)}{(1+V_R^2)}}\right]}{\sqrt{\ln(1+V_R^2)(1+V_S^2)}}\right] \qquad (6.77)$$

Advantages and disadvantages of FOSM method are summarized in Table 6.1.

6.13.2 Advanced FOSM

As seen above, dependency of the reliability index on the chosen form of the limit function is one of the major drawbacks of FOSM. Further, the reliability index computed on the assumption that the random variables are statistically independent and normally distributed poses an additional complexity to FOSM. This makes its application limited to problems validating the above assumptions. In a more generic form, advanced FOSM gives reliability index; Hasofer–Lind method is one of the advanced FOSMs, which is discussed below.

The key point of the method is to estimate a *design point*, which is the minimum distance of failure from the origin. The minimum distance is the safety index (β_{HL}). The method actually transforms the random variable into a reduced form, which can be given as

$$X_i = \frac{x_i - x_i}{\sigma_{x_i}}\{\text{for } i = 1, 2, \ldots n\} \qquad (6.78)$$

This reduced variable will have a zero mean and unit standard deviation, which is a special process of distribution. Hence, the performance function $G(x) = 0$ is converted into $G(x') = 0$ to enable the mapping between the required domains. Reliability index β_{HL} is given by

$$\beta_{HL} = \sqrt{x_d x_d^T},\qquad(6.79)$$

where x_d is the minimum distance of the design point from the origin, which is also referred as a check point.

Following cases are specific:

Case 1: Limit state function is linear

Let us consider

$$M = R - S\qquad(6.80)$$

The reduced values are computed for the domain mapping, as discussed below:

$$R = \frac{R - \mu_R}{\sigma_R}\qquad(6.81)$$

$$S = \frac{S - \mu_S}{\sigma_S}\qquad(6.82)$$

$$M = (\sigma_R + \mu_R) - (\sigma_S + \mu_S)\qquad(6.83)$$

As the limit state function moves closer to the origin, failure region is mapped. Reliability index is given by

$$\beta = \frac{\mu_R - \mu_S}{\sqrt{\sigma_R^2 + R\sigma_R^2}}\qquad(6.84)$$

Case 2: Limit state function is nonlinear

In such cases, computing the minimum distance for calculating the reliability index actually becomes an optimization problem:

$$\beta_{HL} = D = \sqrt{(x)}t(x)\qquad(6.85)$$

The above function is to be minimized subject to the condition that $G(x) = 0$ for many random variables $(x_1, x_2, \ldots x_n)$, which originates from the safe state of the domain; $G(x) < 0$ indicates failure. Hence, $G(x) > 0$ denotes the minimum distance from the origin to a point on the limit state function, which is called design point. The problem is now reduced to determining the coordinates of the design point, geometrically or analytically. By this definition, reliability index becomes invariant as the minimum distance remains constant regardless of the shape of the limit state

function. Using the Lagrange multipliers, one can find the minimum distance as given below:

$$\beta HL = \frac{-\sum_{i=1}^{n} x'_{di} \frac{\partial G}{\partial' x_{di}}}{\sqrt{\sum_{i=1}^{n} \left(\frac{\partial G}{\partial X_{di}}\right)^2}}, \tag{6.86}$$

where $\frac{\partial G}{\partial X_{di}}$ is the partial derivative, evaluated at the design point with coordinates $(x_{di}, x_{d2}, \ldots)$.

6.14   Fatigue and Fracture

Environmental loads such as wave loads will cause long-term variation of local stresses, where fatigue designs of marine structures become very important (Wirsching and Light 1980). Fatigue design of marine structures requires a description of long-term variation of local stress caused by wave action, variable buoyancy, slamming, and vortex shedding (Kam and Dover 1988, 1989). Main contribution to fatigue damage is caused by the frequency of load occurring that are of the order of 10–20% of that of extreme load effects in the service life. Fatigue failures are catastrophic as they come without warning and cause significant damage. Physical process of fatigue consists of initiation of crack, stable crack growth, and unstable crack growth until rupture. Once the crack is initiated, it will tend to grow in a direction orthogonal to the direction of the oscillatory tensile stresses. Fatigue is a challenging failure mode to deal with because the initiation process of fatigue is unpredictable; difficulties exist in mapping the studies carried out in the lab scale to real structures. Fatigue failure is controlled by the following: (i) design, material, and structural detailing to address the probability of crack initiation; (ii) regular inspection during construction and operation; and (iii) following repair procedures as advised by the design loads. In case of design, the limiting conditions are already defined in advance, which are referred as limit states. This will include the case of failure at some defined extreme loads, which will include fatigue life requirements. Commonly checked limit state for marine structures is strength under extreme loading, fatigue life, fracture, and deflection. It is a common practice to present the results of strength, fatigue, and fracture as unity check.

Let $U = \frac{\text{actual or factored load}}{\text{Acceptable load}}$ which is used for strength check.

For fatigue, the unity check is $U = \sqrt[m]{\text{Design life damage}}$,

where $m = -\text{slope}^{-1}$ of $S - N$ curve

6.15   Fatigue Assessment

Fatigue damage occurs mainly due to the frequently occurring loads in the order of 10–20% of the effects caused due to the extreme loads in the service life of the structure. One category of fatigue assessment technique is based on the direct calculation of expected fatigue life or fatigue damage. By limiting a probabilistically defined stress range to be at or below a permissible stress range, an indirect fatigue assessment can also be performed by the simplified method. For the structural systems subjected to nonlinear loading, time history analyses are useful in estimating fatigue assessment. Methods of fatigue assessment include (i) simplified method, (ii) spectral method and (iii) deterministic method. Stress range that is produced by the variable loads imposed on the structure is stated as *Fatigue Demand.* Higher magnitude variable loadings are produced by waves with or without ocean current and the loads induced by the equipment. These variable loads cause dynamic response in the structure, which amplifies the fatigue-induced stresses. The fatigue demand should be determined by accomplishing appropriate structural analysis. The individual rules and guides for classification of particular types of mobile units and offshore structures specify the following: (i) Loads and load combinations, and (ii) sophistication levels required in terms of boundary conditions and structural modeling.

When the steel member is subjected to large fluctuating tensile stress, small cracks develop; these cracks grow in size and further progress, which make the structure to break. For machinery design where the stress fluctuation is similar throughout the design life, cyclic stresses are kept below the endurance limit. But for structures, this method is not permissible as the mixture of large-amplitude and small-amplitude stresses occur due to environmental loads. Hence, it becomes necessary to design the structures for intended fatigue life. Common design approach is nothing but the usage of *S–N* curve. These curves are based on experiments conducted on different types of structures. Fatigue failure can be detected by the occurrence of visible cracks, thickness of the crack, and complete loss of load-carrying capacity.

6.15.1   S–N Approach

Test on the steel specimen subjected to fluctuating loading showed that the number of cycles to failure (N) is inversely proportional to the stress range that is maximum and minimum stress, let it will be S, which is the power of m:

$$N \propto \frac{1}{S^m} \qquad\qquad (6.87)$$

$$N = ASm^{-1} \qquad\qquad (6.88)$$

If measures are taken to prevent corrosion, then for constant amplitude of stress cycling there is a cutoff stress below which no fatigue occurs. This is found to be 2×10^8 cycles. For variable amplitude stress cycling, which is the most general case with the marine structures, the cutoff value of stress decreases as the fatigue crack grows. The slope of S–N curve changes beyond 10^7 cycles from m to $m + 2$. This effect is significant if one is looking for the higher order of fatigue lives. Hence, for preliminary analysis, S–N curve can be taken as linear, which often simplifies the analysis. Over the range where m is constant, the S–N curves are plotted as straight line on log–log scale, whose slope is $(-1/m)$. Since S–N curves are experimentally plotted, for welded specimen, $m = 3$. Local stress concentration effect is caused by the shape of welds, and the specimen reduces the value of constant A. Increase in thickness reduces the fatigue life and hence A. Fatigue life decreases in freely corroding condition. Tubular joints have been subjected to a separate study, and a number of cycles are used for T-joints. One of the most proffered curves is UK T curve, which is given in Fig. 6.2.

S–N curve may be typically be formulated as

$$
\begin{aligned}
& N = ASm^{-1} \\
& N = ASm^{-1} \quad \text{for } s > s'; \\
& N = \infty \quad \text{for } s \leq s'; \\
& \quad \text{or} \\
& N = A_1 S^{-m_1} \quad \text{for } s > s'; \\
& N = A_2 S^{-m_2} \quad \text{for } s \leq s';
\end{aligned}
\tag{6.89}
$$

where the point of intersection between the two equations will be (N',S') with

$$
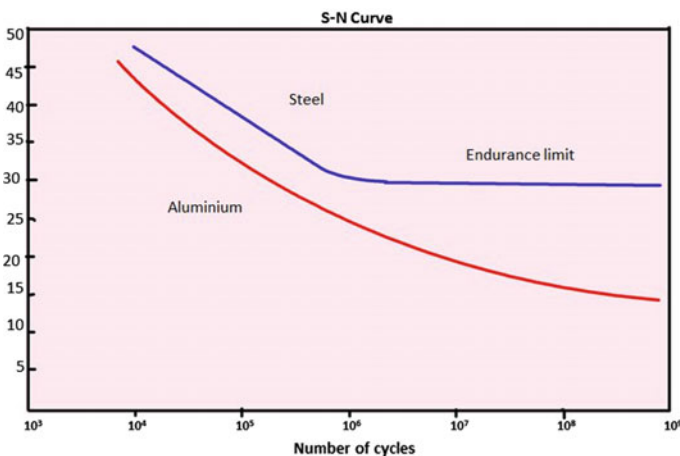N' = A_1(S')^{-m_1} = A_2(S')^{-m_2}
\tag{6.90}
$$

Fig. 6.2 Typical S–N curve

Alternatively S–N curve defined by $A = A_c$ is used to design the checks:

$$\log_{10} A_c = \mu - 2S, \tag{6.91}$$

where μ is the mean value of parameter of $\log_{10} N$ and S is the standard deviation of parameter of $\log_{10} N$.

Consider typical $\mu \approx 12$; $S \approx 0.2$; hence $\frac{A_c}{\mu_A} \approx 0.4$. It is noted that $A = A_{\text{ref}} \left(\frac{t_{\text{ref}}}{t} \right)^{m/4}$, where A_{ref} is the reference parameter in the S–N curve, t and t_{ref} are the plate thickness and the reference plate thickness, which are measured in mm.

S–N curves are traditionally determined by constant amplitude testing with large stress method:

$$R = \frac{\sigma_{\min}}{\sigma_{\max}} > 0.5 \tag{6.92}$$

Simplifying that stress, we can obtain the crack opening mode. Factors affecting S–N curve are relaxation of residual stresses, external loading with partly compression and crack closure effects, which would make the actual crack growth lesser than the implied load by the stress ranges used in the existing S–N curve.

6.16 Miner's Rule

For variable amplitude environmental loading, the S–N curve provides information on constant amplitude loading, which is supplemented by Miner's rule. This allows the number of drift amplitude cycle and concept of fatigue damage based on this rule. Fatigue damage for a joint, under n cycles of constant amplitude loading when it could be taken as $N = AS^{-m}$ cycles, is given by n/N. If the joint is subjected to variable amplitude loading, the load on the cycles can be divided into groups of approximately equal stress ranges. If there are g such groups with almost equal stress range in a given variable amplitude loading, then let s_g be the stress range in each group and n_g be the number of cycles in each group. Fatigue damage for each group will be

$$D_g = \frac{n_g}{N_g} \quad \text{where} \quad N_g = AS_g^{-m} \tag{6.93}$$

Miner's rule states that the failure under variable amplitude loading which will occur when

$$\sum_{g=1}^{G} D_g = 1 \tag{6.94}$$

Fatigue analysis will often refer to the values of n_g and S_g as the fatigue spectrum.

6.17   Fatigue Loading and Fatigue Analysis

Local stresses for fatigue design need to be determined for the temporal and spatial variation.

Figure 6.3 shows the spatial definition of notch, hotspot in the plane surface. Figure 6.4 shows the hotspot. For welded structures, the main parameter that represents the variation in time is called the stress range. This approach is based on the fact that tensile residual stresses are always present and that all stress cycles effectively derive the crack. The spatial stress variation can be accounted for by using nominal hotspot stress approach. Fatigue loading is a dynamic load such as wind, wave, and machine operation on marine structures. The primary source of the
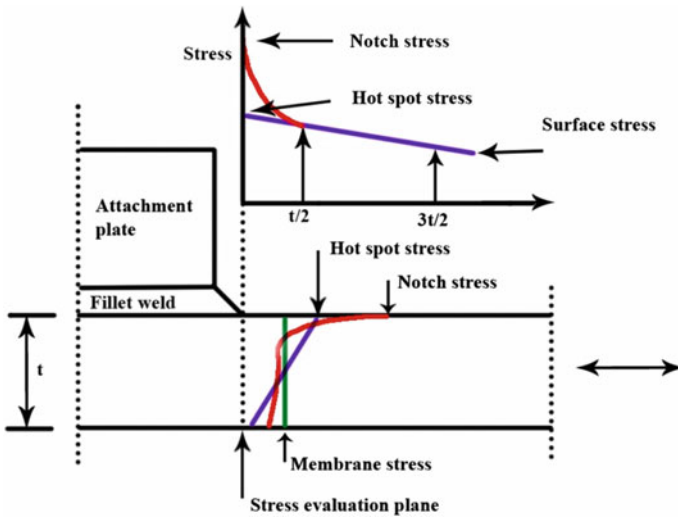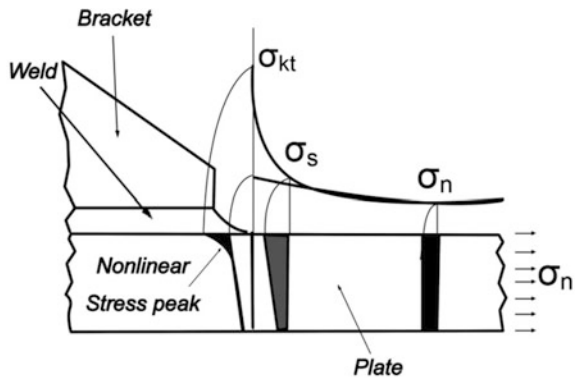

Fig. 6.3 Spatial definition of notch, hotspot, and surface in a plane surface

Fig. 6.4 Hotspot stresses

fatigue loading is the wave loads. Global analysis of the fatigue loading causes undesirable effects on the members. Local stress analysis is carried out to determine the hotspot stresses.

6.18   Time-Domain Fatigue Analysis

Time-domain fatigue analysis results in time series of stress. For narrowband Gaussian response, the cycles are well defined. For more general stress time histories, cycle counting methods have to be applied to all types of response time series. Time-domain methods use only the information provided by the series of peaks (local maximum) and valleys (local minima). According to different methods of constructing the effective stress ranges from these identified peaks and valleys, various cycle counting methods are used. The procedures are described by ASTM-1985. This includes peak counting, range counting, level crossing counting, and rainflow counting. Among these, rainflow counting is the best for fatigue damage estimates.

6.18.1   Rainflow Counting

This method was first proposed by Matsuishi and Endo (1968). Let us consider a stress time series of peaks and valleys with the time axis vertically downward. Lines connecting peaks and valley from a series of pagoda roofs are constructed. Each rainflow begins at the beginning of the time series at the inside every peak and valley. Rainflow initiating at a peak (or a valley) drop down until it reaches peak more positive (or a valley, more negative) than the peak (or the valley) from where it started. Rainflow also stops when it meets the rainflow roof assume. Rainflow must terminate at the end of the time series. Horizontal length of each rainflow is counted as half cycle with that stress range.

Methodology

1. Reduce the time history to a sequence of (tensile) peaks and (compressive) troughs.
2. Imagine that the time history is a pagoda.
3. Turn the sheet clockwise 90°, so the starting time is at the top.
4. Each tensile peak is imagined as a source of water that "drips" down the pagoda.
5. Count the number of half cycles by looking for terminations in the flow occurring when (a) it reaches the end of the time history, (b) it merges with a flow that started at an earlier tensile peak, or (c) it encounters a trough of greater magnitude.
6. Repeat Step 5 for compressive troughs.

7. Assign a magnitude to each half cycle equal to the stress difference between its start and termination.
8. Pair up half cycles of identical magnitude (but opposite sense) to count the number of complete cycles. Typically, there are some residual half cycles.

From Fig. 6.5, it is observed that rainflow starts at a valley point 1 drops down to 2 and 3 and so on. The cycle ends at 10, which is found to be a peak. There are nine half cycles that could be extracted. The rainflow initiates at valley point 1 and drops down to 2 and ends at 4 because the following valley has smaller value than initiating at point 1. Since the half cycle 1–2–4 is identified, the same rule is applied to half cycle 5–6. The second rainflow starts at 2 and ends at 3 because the success peak at 4 is larger than 2; similarly, half cycles 4–5–7 and 8–9 are extracted; half cycle 7–8–9 is found because time series end at 10. Half cycles 3–2′, 6–5′, and 9–8′ are determined because of rainflow starts at 3, 6, 9 peaks meets the rainflow at roofs above. When all half cycles are exhausted, the horizontal length of each cycle is used as an effective stress range to calculate the fatigue damage based on the linear damage accumulation law:

$$D_{RC} \leq D_{RFC} \leq D_{LCC}(= D_{NB}) \leq D_{PC} \tag{6.95}$$

D_{RC} be the fatigue damage estimated by range counting
D_{RFC} be the rainflow counting
D_{LCC} be the level crossing counting
D_{PC} be the peak counting
D_{NB} be the narrowband approximation (Table 6.2).
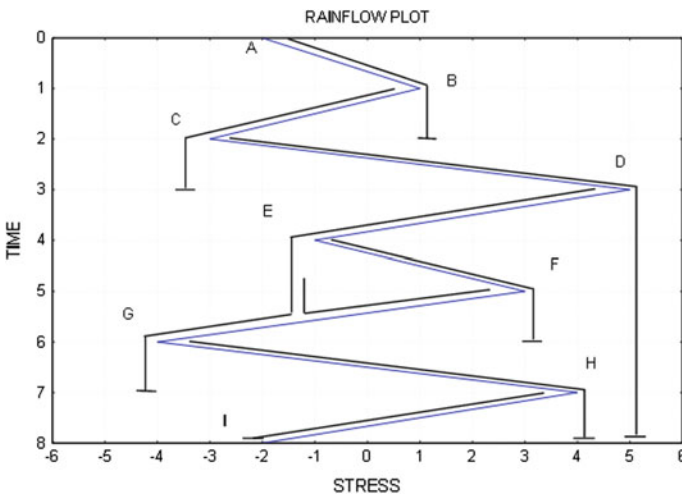
Fig. 6.5   Example of rainflow counting

Table 6.2 Rainflow counting

Rainflow cycles by path		
Path	Cycles	Stress range
A–B	0.5	3
B–C	0.5	4
C–D	0.5	8
D–G	0.5	9
E–F	1.0	4
G–H	0.5	8
H–I	0.5	6
Rainflow, total cycles		
Stress range	Total cycles	Path
10	0	–
9	0.5	D–G
8	1.0	C–D, G–H
7	0	–
6	0.5	H–I
5	0	–
4	1.5	B–C, E–F
3	0.5	A–B
2	0	–
1	0	–

6.19 Deterministic Fatigue Analysis

The deterministic fatigue analysis method applies Miner's rule. The loading of the structure is represented by loading cases $g = 1$ to G, each with a defined number of cycles (n_g) and time T. The structure is analyzed to determine the stress S_g for each group and hence the total damage D_t in time T. If the value of T is chosen as a year, then the fatigue life is $1/D_{\text{year}}$. When fatigue damage is high, the majority of damage occurs on the low cycle end of the curve, where M is typically 3. But when the structure is subjected to dynamic loading and the band of periods near the natural period, then the small change in an assumed period of the applied load changes the result significantly. Marine structures under wind and wave loading act as period-dependent filters. As a result, the number of cycles of stress response may differ from the number of loading cycles. This difficulty can be handled in spectral analysis. Deterministic fatigue analysis is often performed using semi-empirical relationship. When structures are subjected to waves, only one wave analysis is used to describe the lifetime stress history of the structure. For long-term exceedance to be a Weibull function,

$$n(\text{stress} > \sigma) = n_o \exp\left\{\left(\frac{\sigma}{\sigma_o}\right)^h \ln n_o\right\}, \tag{6.96}$$

where n is the number of stress cycles exceeding stress in n_o cycles, σ_o is stress that is exceeded once in n_o cycles, and h is the parameters (0.5–1.5) that depend on load and response characteristics of the structures. For long-term exceedance to be log-linear,

$$n(\text{Wave height} > H) = n_o \exp\left\{-\left(\frac{H}{H_0}\right) \ln n_o\right\}, \tag{6.97}$$

where H_o is the wave height exceeded once in the number of cycles known. H is the wave height exceeded n times in the number of cycles. The long-term exceedance can be considered with single-slope S–N curve to estimate the fatigue damage in n_L cycles.

For Weibull distribution,

$$D_L = \frac{n_L \sigma_o^m}{A} \left[\frac{\Gamma\left(1 + \frac{m}{h}\right)}{(\ln n_o)^{m/h}}\right] \tag{6.98}$$

For log-linear wave height exceedance is given by

$$D_L = \frac{n_L \left(aH_o^b\right)^m}{A} \left[\frac{\Gamma(1 + bm)}{(\ln n_o)^{bm}}\right] \tag{6.99}$$

Γ is a gamma function defined as

$$\Gamma(g) = \int_0^\infty x^{g-1} e^{-x} dx \tag{6.100}$$

This is a standard function and the values are available in standard tables.

6.20   Spectral Fatigue Analysis

Spectral fatigue analysis is applicable to structures that are executed by dynamic loading which has statistically stationary properties for a large number of stress cycles, for example, wind turbulence and wave load. The spectral method uses the shape of the stress spectrum to determine the number of stress cycles of various sizes. The stress spectrum can be narrow banded or broad banded.

6.20.1 Narrowband Spectrum

To perform fatigue calculation, we should compute zeroth and second moment of the spectrum about the line $f = 0$. It is common to assume Rayleigh distribution of the stress range in a given stress spectrum. m_0 and m_2 can be computed using numerical integration technique, that is, by trapezoidal rule. m_0 is the area under the spectrum which will correspond to variance of the signal and represented as the spectrum. For the spectrum with the Hz frequency axis, the square root of the ratio of the second moment (m_2) to the area (m_o) is the mean zero crossing period of the signal:

$$T_Z = \sqrt{\frac{m_o}{m_2}} \tag{6.101}$$

The number of stress cycles (n) in time (T) in seconds is given by

$$n = \frac{T}{T_z} \tag{6.102}$$

Rayleigh distribution assumes the plot of the shear range σ_r as

$$p(\sigma_r) = \frac{\sigma_r}{4m_0} \exp\left(-\frac{\sigma_r^2}{8m_o}\right) \tag{6.103}$$

In T seconds, the number of stress cycles (δ_n) in the band ($\delta\sigma_r$) cantered as σ_r is given by

$$\delta_n = n * p * (\sigma_r)(\delta\sigma_r) \tag{6.104}$$

Fatigue damage associated with that band of stress cycle is given by

$$\delta_D = \frac{\delta_n}{N} = \frac{\delta_n}{A\sigma_r^{-m}} = \frac{n\left(\frac{\sigma_r}{4m_0}\right)\exp\left[-\left(\frac{\sigma_r}{8m_o}^2\right)\right]\delta\sigma_r}{A\sigma_r^{-m}} \tag{6.105}$$

Fatigue damage of all σ cycles band is found by integration, which is given by

$$D = \int_0^\infty \frac{n\left(\frac{\sigma_r}{4m_0}\right)\exp\left[-\left(\frac{\sigma_r}{8m_o}^2\right)\right]\delta\sigma_r}{A\sigma_r^{-m}} \tag{6.106}$$

$$D = \frac{n}{4Am_0}\int_0^\infty \sigma_r^{(1+m)}\exp\left(-\frac{\sigma_r^2}{8m_o}\right)\delta\sigma_r$$

The integral has a standard solution of S–N curve, which is a gamma function:

$$\int_0^\infty x^a \exp\left(-bx^2\right) dx = \frac{\Gamma\left(\frac{a+1}{c}\right)}{C\left(B^{\left(\frac{a+1}{c}\right)}\right)}, \tag{6.107}$$

where

$$\Gamma(g) = \int_0^\infty x^{(g-1)} e^x dx \tag{6.108}$$

6.20.2   Broadband Spectrum

There are many methods available to explain how to count the stress range cycles in stationary broadband time history. Rainflow counts in largest cycles are extracted first. The smaller cycles are considered super-imposed on the larger cycle. This is considered the most reliable method for fatigue σ range counting. Each crest is matched with the following trays. Now the above definition is of use for frequency domain calculation because the definition of cycles was set up in terms, which were not amenable with statistical analysis. The spectral fatigue damage analysis of structures subjected to random loading assumes that the signal is stationary, Gaussian and random. Results are generally produced for mean period of zero crossing per unit time:

$$T_Z = \sqrt{\frac{m_0}{m_2}} \tag{6.109}$$

For mean time between the peaks or crests per unit,

$$T_c = \sqrt{\frac{m_2}{m_4}}, \tag{6.110}$$

where m_n is the nth moment of the PSD function:

$$m_n = \int_0^\infty f^n S_{\sigma\sigma}(f) df, \tag{6.111}$$

where $S_{\sigma\sigma}(f)$ is the one-sided stress spectrum, f is the frequency in Hz, and m_n values are obtained by numerical integration.

An irregularity factor, is defined as

$$\beta = \frac{T_c}{T_z} \tag{6.112}$$

β is an important factor in fatigue analysis because difficulty of prediction of σ cycle distribution from a σ spectrum is largely determined by whether its value lies between 0 and 1. As it approaches 1, the signal becomes narrowband, and probability density of the peak is given by

$$p(\sigma_p) = \frac{\sigma_p}{m_o} \exp\left(-\frac{\sigma_p^2}{2m_o}\right) \tag{6.113}$$

Cycle counting in this case is relatively easy. As approaches zero, signal becomes more like with noise. In this case, signal is said to be completely wideband. Probability density function peaks become Gaussian:

$$p(\sigma_p) = \frac{1}{\sqrt{2\pi m_0}} \exp\left(-\frac{\sigma_p^2}{2m_o}\right) \tag{6.114}$$

In reality, the response is neither narrow nor completely wideband. It is in between, so one can apply correction factors to the solution. Several researchers attempted to correct the narrowband fatigue damage calculation for the effects of a broad bandwidth. They are developed by generating sample time histories from stress spectra using inverse Fourier transform, and then a conventional rainflow cycle count can be obtained.

6.20.2.1   Wirsching's Correction Factor

$$D_{\text{RF}} = \lambda D_{\text{NB}}(M, \in) \tag{6.115}$$

D_{RF} = rainflow counted damage; D_{NB} = damage calculated using NB formula.

$$\lambda(M, \in) = a(m) + [1 - a(m)](1 - \in)^{c(m)} \tag{6.116}$$

$$a(m) = 0.926 - 0.333\,m \tag{6.117}$$

$$c(m) = 1.587 - 2.323\,m \tag{6.118}$$

$$\varepsilon = \sqrt{1 - \beta^2} \tag{6.119}$$

6.20.2.2   KAM and Doves Approach

This expression uses equivalent σ range parameter called σ_{efr}. The idea is to conceive total linearity cumulative fatigue damage caused by constant amplitude σ range using rainflow cycles extracted from the stress cycle:

$$\sigma_{\text{efr}} = \left[\int_0^\infty \sigma_r^m p(\sigma_r) \mathrm{d}\sigma_r \right] \tag{6.120}$$

$$\sigma_{\text{efr}} = 2\sqrt{2m_0} \left[\lambda(m, \varepsilon)\Gamma\left(\frac{m}{2} + 1\right) \right]^{1/m} \tag{6.121}$$

6.20.2.3   Chaudhary and Dover Approach

Based on the study of peak distribution in different sea state spectra, the following equation is proposed by Chaudhury and Dover (1985):

$$\sigma_{\text{efr}} = 2\sqrt{2m_0} \left[\frac{\varepsilon^{m+2}}{2\sqrt{\pi}} \Gamma\left(\frac{m+1}{2}\right) + \frac{\beta}{2}\Gamma\left(\frac{m+2}{2}\right) + \mathrm{err}\,(\beta)\frac{\beta}{2}\Gamma\left(\frac{m+2}{2}\right) \right]^{1/m}, \tag{6.122}$$

where

$$\mathrm{err}(\beta) = 0.3012(\beta) + 0.4916(\beta)^2 + 0.918(\beta)^3 - 2.3534(\beta)^4$$
$$- 3.3307(\beta)^5 + 15.654(\beta)^6 - 10.7846(\beta)^7$$

for $0.13 < \beta < 0.96$.

6.20.2.4   Hancock's Equation

Hancock and Gall (1985) proposed equations to include and ε into narrowband equation:

$$\sigma_{\text{efr}} = \sqrt[2]{2m_0} \left[\beta\Gamma\left(\frac{m}{2} + 1\right) \right]^{1/m} \tag{6.123}$$

$$\sigma_{\text{efr}} = \beta\sqrt[2]{2m_0}(2 - \varepsilon^2) \left[\Gamma\left(\frac{m}{2 - \varepsilon^2} + 1\right) \right]^{1/m} \tag{6.124}$$

The above factors are used to amend the traditional narrowband approach. An alternate approach is to avoid narrowband assumption and to develop fatigue life prediction in terms of rainflow ranges.

Probability density function of rainflow ranges $P_{RF}(\sigma_r)$ is given as

$$P_{RF}(\sigma_r) = \frac{(D_1/Q)e^{-z/Q} + (D_2 Z/R^2)e^{-z^2/2R^2} + D_3 Z\,e^{-z^2/2}}{2m_o^{1/2}} \tag{6.125}$$

$$\beta = \frac{T_c}{T_Z} = \sqrt{\frac{m_2^2}{m_0 m_4}} \tag{6.126}$$

$$x = \frac{T_c}{T_Z} = \frac{m_1}{m_0}\sqrt{\frac{m_2}{m_4}}; \quad Z = \frac{\sigma_r}{2\sqrt{m_0}} \tag{6.127}$$

$$D_1 = \frac{2(x_m - \beta^2)}{1 + \beta^2} \tag{6.128}$$

$$D_2 = \frac{1 - \beta - D_1 + D_1^2}{1 - R} \tag{6.129}$$

$$D_3 = 1 - D_1 - D_2 \tag{6.130}$$

$$R = \frac{\beta - x_m - D_1^2}{1 - \beta - D_1 + D_1^2} \tag{6.131}$$

$$Q = \frac{1.25(\beta - D_3 - RD_2)}{D_1} \tag{6.132}$$

$$m_n = \int_0^\infty f^n S_{\sigma\sigma}(f)\mathrm{d}f \tag{6.133}$$

which is given as nth moment used in the above equation:

$$\sigma_{\mathrm{efr}} = \int_0^\infty \sigma^m \beta(\sigma_r)\mathrm{d}\sigma_r \tag{6.134}$$

Now instead of $\beta(\sigma_r)$, substitute $P_{RF}(\sigma_r)$ in the above equation to obtain the effective stress range.

For $n = T/T_c$, damage can be estimated by

$$D = \left(\frac{T}{T_c}\right)\left(\frac{1}{A}\right)\int_0^\infty \sigma_r^m P_{RF}(\sigma_r)\mathrm{d}\sigma_r \tag{6.135}$$

A general solution for fatigue damage can be obtained for wideband case using the rainflow range probability density function. There is one stress range for each

peak stress in the response so that the number of the stress range in time T is T/T_C. The equation for damage in time T is given by

$$D = \left(\frac{T}{T_c}\right)\left(\frac{1}{A}\right) \int\limits_0^\infty \sigma_r^m P_{\mathrm{RF}}(\sigma_r)\mathrm{d}\sigma_r \qquad (6.136)$$

6.21   Stress Concentration Factor (SCF)

Fatigue damage estimates are highly dependent on the stress cycle range, which need to be considered in the S–N curve:

$$N = AS^{-m} \qquad (6.137)$$

However, in marine structures, stress concentration effects in the joints should be augmented for using them for fatigue damage estimates. For plated construction, the procedure is quite simple to determine the applied stress with an additional stress concentration factor by equations or graphs. But when the crack growth is expected from a sharp notch or corner, which is not a part of the geometry, stresses may show infinite enhancement that makes the S–N curve approach unsatisfactory. For example, tubular joints show stress changes rapidly near the joint, which has no reference stress in the S–N curve approach. This problem is solved by extrapolating the stress from 2 points away from the weld. Approximate stress concentration factor, as per the designer's choice can be used. In a tubular joint, fatigue is dominated by the stress perpendicular to weld, so the other stress components need to be considered in the damage estimates.

6.22   Crack Propagation

Application of fracture mechanics to the fatigue of the steel structures uses Paris and Erdogan (1983) Law. The law states that the crack growth (δ_a) in δN cycles in the applied stress range of (σ_r) is given by

$$\delta_a = C\left[y\,\sigma_r\sqrt{\pi a}\right]^m \delta N \qquad (6.138)$$

$$\delta a = C[\delta K]^m \delta N, \qquad (6.139)$$

where y is the crack- and geometry-dependent factor. For a through-thickness crack that occurs at the center of a very wide plate, $y = 1$; a is the crack length, which increases with the increase in the applied stress cycles; C and m are material-dependent constants. For example, typical mean values for C and m for BS

Table 6.3 Conversion table for material-dependent constant C

To convert	From to	Multiply C by
Crack size	m to mm	$10^{3(1\ -\ m/2)}$
Stress	MPa to kPa	10^{-3m}
Stress	MPa to Pa	10^{-6m}

Table 6.4 Fatigue crack propagation

a	σ_r	y	Δk	δN	δa
1	2	3	4	5	6

4360 grade 50D steel are $C = 5.2 \times 10^{-12}$ to 7.1×10^{-12} m/MPa$\sqrt{(\text{meters})}^{\text{m}}$, where $m = 3$. In the above expression, unit of C is complex, which makes the conversion difficult. Hence, the following table can be used (Table 6.3).

Fatigue crack propagation based on fracture mechanics is computed in a tabular form as given in Table 6.4.

Each row of the table calculates the crack growth in every δN cycle, which is chosen so that δa is reasonable small when compared with the value of crack length (a); this makes the crack length independent of the increment of the crack growth.

Step-by-Step Procedure to Compute the Fatigue Crack Propagation
Step 1: An initial value of the crack length (a) is known at the beginning of the calculation.
Step 2: Stress range σ_r may vary for the wave to wave case; hence, it is advisable to use σ_{efr}

$$\sigma_{\text{efr}} = m \sqrt{\frac{1}{N} \sum_{i=1}^{N} \sigma_{r_i}^m}$$

It is important to note that *growing crack leads to the reduction of stiffness and causes redistribution of stresses away from the crack. This would require computation of the effective stress for different crack lengths*. But for simplification, this need not be done.
Step 3: y is calculated at each stage of the crack growth.
Step 4: $\Delta k = y\sigma_r\sqrt{\pi a}$.
Step 5: δN is selected to give small changes in the crack length. Depending on the rate of crack growth, this value may be selected corresponding to the number of cycles in 1 year or 1 month, etc.
Step 6: $\delta a = C(y\sigma_r\sqrt{\pi a})^m$.
Step 7: Crack length (a) is increased from a to ($a + \delta a$).
Step 8: Use the effective stress, same as in Step 2.
Step 9: y is calculated now for the new crack length.
Step 10: Thus all the values in the above table will be filled up in a sequential manner.

Calculation is repeated for as many crack growth increments as that are required to reach a critical crack size. Computation is terminated until the defect may be then large enough to result in failure due to large stress values.

Example Problems

1. **Out of 1000 manufactured parts, 50 of them are substandard. Two parts are taken at random without replacement from the batch of 1000 parts. Determine the probability mass function and cumulative mass function**.

   Probability mass function:

   $$P(X = 0) = (950/1000) \times (949/999) = 0.902$$
   $$P(X = 1) = 2 \times (950/1000) \times (50/999) = 0.095$$
   $$P(X = 2) = (50/1000) \times (49/999) = 0.003$$

   Cumulative mass function:

   $$F(0) = P(X < {} = 0) = 0.902$$
   $$F(1) = P(X < {} = 1) = 0.997$$
   $$F(2) = P(X < {} = 2) = 1$$

2. **A, B, and C are candidates for placement in a company which has only one vacancy. Based on CV of A, B and C, A has 0.4 chance of that of B; B has chance of 0.8 of that of C. Find the probability of A, B, and C getting the job**.

   $$P(A) + P(B) + P(C) = 1$$

   Form the given data,

   $$P(A) = 0.4 \, P(B)$$
   $$P(B) = 0.8 \, P(C)$$

   Thus,

   $$0.32 \, P(C) + 0.8 \, P(C) + P(C) = 1$$
   $$P(C) = 0.4717$$
   $$P(B) = 0.3774$$
   $$P(A) = 0.1509$$

3. **In a test of concrete mix design, it is seen that 40% of coarse aggregate, 30% fine aggregate, 25% of cement, and 20% of water influence the strength of the concrete. What is the reliability of the above test results? The sample having the following mix proportion has to be assessed: coarse**

aggregate = 50%, **fine** **aggregate = 20%,** **cement = 20%,** **and** **water = 10%.**

Using the total probability theory,

$$P[A|B] = p[A]p[B|A]$$
$$P[\text{strength}|\text{proportion}] = (0.4 \times 0.5) + (0.3 \times 0.2) + (0.25 \times 0.2) + (0.2 \times 0.1)$$
$$= 0.33$$

4. **Consider a steel member of the deck in an offshore platform subjected to a bending moment of M = 300 kNm. The random variables considered are the yield stress, F and plastic section modulus, Z. The random variables follow a normal distribution with the following parameters:**

Random variable	Mean, μ	Standard deviation, σ
Yield stress	500 MPa	30 MPa
Section modulus	1×10^6 mm^3	5.5×10^3 mm^3

Estimate the reliability index based on strength formulation.
For strength formulation, the resistance is the random variable given by

$$R = FZ$$
$$S = M$$

The performance function is given by

$$g(F, Z) = R - S = FZ - M$$

Mean, $\mu_R = \mu_F \mu_Z = 500 \times 10^6 = 500$ kNm

Standard deviation,
$$\sigma_R = \left[Var(F) \left(\frac{\partial R}{\partial F} \right)^2 + Var(Z) \left(\frac{\partial R}{\partial Z} \right)^2 \right]^{\frac{1}{2}}$$
$$= [30^2 (1 \times 10^6)^2 + (5.5 \times 10^3)^2 500^2]$$
$$= 30.126 \text{ kNm}$$

The reliability index is given by

$$\beta = \frac{\mu_R - \mu_S}{\sqrt{\sigma_R^2 + \sigma_S^2}}$$

$$\beta = \frac{500 - 300}{\sqrt{30.126^2}}$$

$$\beta = 6.639$$

6. Estimate the reliability index using stress formulation for the previous problem.

This example illustrates reliability index using FOSM method and shows that it depends solely on the formulation of the performance function.

For the stress formulation, the resistance is given by

$$R = F$$
$$S = M/Z$$

The performance function is given by

$$g(F, Z) = R - S = F - M/Z$$

Mean, $\mu_s = M/\mu_z = (300 \times 10^6)/(1 \times 10^6) = 300$ MPa.

Standard deviation, $\sigma_S = \left[\text{Var}(Z) \left(\frac{\partial S}{\partial Z} \right)^2 \right]^{\frac{1}{2}}$

$$\sigma_S = \left[\text{Var}(Z) \left(-\frac{M}{\mu_Z^2} \right)^2 \right]^{\frac{1}{2}}$$

$$\sigma_S = \sigma_Z \left(-\frac{M}{\mu_Z^2} \right)$$
$$= 5.5 \times 10^3 \times (300 \times 10^6)/(1 \times 10^6)^2$$
$$= 1.65 \text{ MPa}$$

The reliability index is

$$\beta = \frac{\mu_R - \mu_S}{\sqrt{\sigma_R^2 + \sigma_S^2}}$$

$$\beta = \frac{500 - 300}{\sqrt{30^2 + 1.65^2}}$$

$$\beta = 6.657$$

Exercise 1

1. Reliability implies the estimate of _____ of the marine structures under adverse environmental conditions.
2. Safety is based on _____ judgement and reliability is based on _____ judgement.
3. Risk is an extension of _____ and also includes _____.
4. Mention any three uncertainties that arise in the reliability estimate of the marine structures.

5. The period of time during which the structure is unable to perform is called
   _____.
6. Reliability is a _____ of probability of failure.
7. _____ type of uncertainty generally arises from the randomness of the
   environmental loads.
8. _____ type of uncertainty corresponds to the erroneous predictions and
   estimations of reality.
9. Aletory-type uncertainties can be effectively handled by _____.
10. In Bayesian approach, models and model parameters are developed by
    _____.
11. Uncertainties associated with _____ are high in magnitude compared to
    the material properties.
12. In deterministic approach, _____ accounts for the uncertainties
    indirectly.
13. _____ is useful in describing the boundary between the safe and unsafe
    conditions.
14. Level I methods of reliability are equipped with _____ to account for the
    uncertainties.
15. In level II methods of reliability, the basic variables are described with
    _____.
16. Level IV method of reliability is appropriate for _____.
17. Mention any two advantages of reliability methods.
18. In FOSM method, _____ approximation is used.
19. _____ is the point of minimum distance of the performance function
    from the origin.
20. The _____ is an advanced improvement on FOSM method.
21. How fatigue failure is controlled in marine structures?
22. In marine structures, the cutoff stress is found to be _____.
23. The ratio of local stress to the nominal stress is called _____.
24. S–N approach is based on the fact that _____ are always present in
    the member that drives the crack formulation effectively.
25. The spatial stress variation can be accounted by using _____ approach.
26. The total stress at the weld toe is called _____.
27. The ratio of hotspot stress at the location to the nominal stress is called
    _____.
28. The spectral fatigue method uses _____ to determine the number of stress
    cycles of various magnitudes and ranges.
29. _____ is the stress in the immediate vicinity of a structural
    discontinuity.
30. _____ and _____ have considerable advantages in consistency
    and coverage for the estimation of stress concentration factors.

Key to Exercise 1

1. Limit state probabilities
2. Statistical, engineering
3. Reliability, consequences of failure
4. Load calculation, material properties, and methods of modeling.
5. Downtime of shutdown time.
6. Converse.
7. Aletory.
8. Epistemic.
9. Bayesian approach.
10. Likelihood function.
11. Dynamic loads.
12. Safety factors.
13. Reliability index.
14. Partial safety factors.
15. First-order statics.
16. Structures with strategic importance.
17. Rational method to estimate safety, they provide decision-making support for better-balanced design.
18. First-order Taylor series.
19. Design point
20. Hasofer–Lind method.
21. (i) by addressing the probability of crack propagation, (ii) scheduling regular inspection.
22. 2×10^8 cycles.
23. Stress concentration factor.
24. Tensile residual stresses.
25. Hotspot stress.
26. Notch stress.
27. Hotspot stress concentration factor.
28. Shape of the stress spectrum.
29. Hotspot stress.
30. Efthymiou equation and Lloyd's design equation.

Exercise 2

1. Explain stationary process?
2. Explain impulse response function or the transfer function?
3. $H(\omega)$ is called the transfer function or _____ function.
4. Write down the equation which gives the relationship between the response spectrum $S_X(\omega)$ and the load spectrum?
5. The procedure of replacing the input spectrum by a constant (S_0) is called _____.

6. Explain the two approaches in dynamic analysis?
7. Explain return period?
8. Safety is a measure used to indicate the_____.
9. Reliability offers _____ meaning to this traditional concept.
10. Explain the levels of reliability?
11. List the advantages of reliability methods?
12. The stochastic modeling essentially helps to establish variability by best-suited_____.
13. Differentiate merits and demerits of FOSM of reliability?
14. The reliability index computed on the assumption that the random variables are _____ and _____an additional complexity to FOSM.
15. _____ of marine structures requires a description of long-term variation of local stress caused by wave action, variable buoyancy, slamming, and vortex shedding.

Key to Exercise 2

1. A stationary process is one for which the statistical properties like mean value and standard deviation are same for all points in time (or) position. Hence, the following equation holds good. For a stationary process, transfer between the load and the response can be modeled as linear, time-invariant, while the system can be characterized by a transfer function. Hence, the relationship between variance spectrum of the response (called response spectrum) and variance spectrum of load (called load spectrum) is determined by a transfer function.
2. Impulse response function or the transfer function, which determines the connection between the load and the response, is completely defined by the properties of the linear system. This remains independent of any given load.
3. Frequency response.

$$H_{FX}(-\omega) = \int_0^\infty h_{FX}(t)e^{i\omega t}\mathrm{d}t = \int_0^\infty h_{FX}(t)e^{-i\omega t*}\mathrm{d}t$$

4.

$$\int_0^\infty h_{FX}(t)e^{-i\omega t*}\mathrm{d}t = H_{FX}(\omega)*$$

$$S_X(\omega) = |H_{FX}(\omega)|^2 S_F(\omega)$$

5. White noise approximation.
6. Dynamic analyses can be carried out in two ways depending on the description of loads namely: (i) deterministic analysis, which requires the complete knowledge of load time history and (ii) stochastic analysis where statistical concepts are used to specify the loads. For example, when waves or wind loads are described in terms of statistical quantities, then the response should also be described and analyzed in terms of same kind of quantities.

7. Return period of exceedance of ξ then becomes as follows:

$$\bar{R}(z) = \frac{1}{\operatorname{Prob}(Z > \xi)} = \frac{1}{0.01} = 100 \text{ years}$$

Reference period, in this case, is 1 year, and therefore return period of exceedance is 100 years. It is important to note that the time-varying loads, caused by waves, cannot be considered stationary over an extended period. This means that the quantities such as yearly maxima must be computed using long-term statistics. Return periods are also computed based on the risk associated. This is a common practice in case of earthquake loads and seismic design of structures.

8. Reliability.
9. Probabilistic.
10. Reliability studies are considered at different levels in the literature. Level I is focusing on the probability aspects of the problem. Suitable characteristic values of the random variables are introduced in the safety analysis. Main objective of this level of study is to minimize the deviation of the design values from that of the target value. For example, load-resistance factor design (LRFD) is of level I of reliability. Level II has two values for each parameter to be defined in the analysis namely mean and standard deviation. Level III is a complete analysis of the problem addressing the multidimensional probability density function of random variables, which is extended over the safety domain. Reliability is expressed in terms of suitable safety indices. In level IV, engineering economics is also applied in the reliability study. This level of reliability study is usually applied to structures of strategic importance. The study includes cost–benefit analysis, rehabilitation, consequence of failure, and return on capital investment.
11. The advantages of reliability methods are as listed below:

    - Offer a realistic procession of uncertainties and the methods for evaluating the safety factors that are often too arbitrary.
    - Offer decision-making support for more economic and better-balanced design.
    - Analyze failure modes and measure the reliability provided by application and regulations.
    - Allow the optimal distribution of material and arrange various components of the structure.
    - Benefit from the experience acquired in design by updating on the basis of feedback from the experience.
    - Expand the knowledge of uncertainty in response to the structure.

12. Probability density function.

13.

Advantages	Disadvantages
It is easy to use	Results can cause serious errors. The tool used for the distribution function cannot be approximated by normal distribution
It does not require knowledge of distribution of random variables	Values of β depend on the specific form of the limit state function. This is an invariance problem

14. Statistically independent and normally distributed poses.
15. Fatigue design.

Chapter 7
Applications in Preliminary Analysis and Design

Abstract This chapter deals with a few application problems in the design and development on new offshore structures based on the dynamic analyses. Studies presented in this chapter are based on the recent research conducted by the author, which are presented as a part of intuitive studies to the readers.

Keywords Design · Offshore structures · Preliminary design · Triceratops · Buoyant leg structure · Ball joints · Response isolation · Structural forms · Wave directionality · Springing · Ringing · Tension leg platforms · Vortex-induced vibration · VIV suppression · Re-gasification platforms

7.1 Free Vibration Response of Offshore Triceratops

Offshore triceratops is relatively a new type of compliant structure suitable for deep-water oil exploration. The structural form of the platform enables to counteract the encountered environmental loads efficiently. Triceratops consists of three or more buoyant leg structures (BLS) to achieve the required buoyancy, to support the deck structure, to restrain system and to serve storage requirements. The deck and BLS are connected by ball joints that transfer translational motion but restrain rotations from BLS to deck and vice versa. Free-decay studies are conducted on 1:150 scaled model, in free-floating and tethered conditions experimentally, analytically, and numerically; natural periods in heave and pitch/roll degrees of freedom are discussed for installation and decommissioning purposes. Experimental and analytical free-decay tests are conducted on the installed structure in surge and heave degrees of freedom; experimental, analytical, and numerical results are in good comparison. Based on the studies carried out, it is seen that the free-floating natural periods of both single BLS and tethered triceratops are away from the bandwidth of encountered wave periods, making the proposed platform safe and suitable for the chosen sea state and ultra-deepwaters.

7.2　New Structural Form

There exist many offshore structures for deepwaters such as compliant towers, tension leg platforms (TLPs), spars, semi-submersibles, and FPSOs. Recent developments focus on the optimization of structural form of compliant structures with respect to their cost, reduction in structural response, and enhancing their payload capacities. Operational features including the stability of tethered buoyant platforms are addressed by performing stochastic stability analysis (Muhuri and Gupta 1983). Buchner et al. (1999) discussed the complexities in model tests carried out on the new state-of-the-art deep-water offshore basin of Maritime Research Institute Netherlands (MARIN). Jayalekshmi et al. (2010) investigated the effect of tether-riser dynamics on the response characteristics of deepwater TLPs in water depths 900 and 1800 m under random waves in the time domain; statistical values of responses are found to increase with increase in water depth and a significant increase is observed when risers are included in the analysis. Comparative studies carried out on TLPs with two different geometries show that triangular TLPs are cost effective (Chandrasekaran and Jain 2002a, b). It is also shown that triangular TLPs exhibit lesser response in the surge and heave degrees of freedom than that of the four-legged (square) TLPs. Chandrasekaran et al. (2007) presented the response behavior of triangular TLP under regular waves using Stokes nonlinear wave theory, and results show that the response in surge and pitch degrees of freedom obtained using Stokes' theory is lesser than that obtained using the Airy's wave theory.

Offshore triceratops is relatively a new concept with respect to the structural form that is attempted for ultra-deepwaters (Charles et al. 2005); the chosen structural form enables reduction of response when compared with conventional deep-water offshore structures like TLPs, imparting economic and structural advantages in the design. Triceratops consists of BLS, deck structure, ball joint, and foundation system which is usually with tethers. BLS is a positively buoyant, floating, deep-draft structure intended for use in ultra-deep waters (Robert and Capanoglu 1995). It is simple cylindrical structure, which is used to provide required buoyancy to support deck structure, buoyant leg, and tethering system. BLS unit appears to resemble a spar due to its deep draft, but the restraining system resembles the behavior of a TLP; restraining system provides less rotational stiffness, and hence the pitch and roll responses are more than TLP but lesser than spar (Shaver et al. 2001). Capanoglu et al. (2002) showed a good comparison of the results of model tests with that of the analytical studies of a BLS. Chandrasekaran et al. (2010, 2011) carried out analytical and experimental studies on offshore triceratops under unidirectional regular waves; the influence of ball joint on the response of the deck in pitch and heave degrees of freedom are focused. Limitations of the experimental investigations on triceratops for ultra-deepwaters are also discussed in detail. In the present study, natural period of free-floating and tethered (600 m) triceratops is examined to analyze few critical features: (i) installation; (ii) operational; and (iii) decommissioning feasibility. Foundation system is chosen

Table 7.1 Mass properties of free-floating and tethered offshore triceratops

Details	Free-floating		Tethered	
	Prototype (ton)	Model (kg)	Prototype (ton)	Model (kg)
Payload	4059	1.2	4059	1.2
Ball joint	1013	0.3	1013	0.3
Leg weight	18,225	5.4	18,225	5.4
Ballast	21,032	6.23	21,032	6.23
Additional ballast	8635	2.56	–	–
Pretension	–	–	8635	2.56
Total	52,982	15.7	52,982	15.7
Displacement	52,982	15.7	52,982	15.7

as tethered system since flexible behavior is economical for ultra-deepwaters. Ball joint is placed between the BLS and deck to reduce the rotational response of the deck when the BLS is exposed to wave, current and impact loads; in addition, it reduces the rotational response of BLS units when the deck is exposed to aerodynamic loads. In the present study, triceratops consists of three BLS units whose geometric form and mass distribution are derived from Norwegian TLP at 600 m water depth; vertical center of gravity (VCG) to draft ratio is maintained as 0.5, as desired for deep-draft compliant structures. Free-decay oscillation studies are performed experimentally, analytically, and numerically on 1:150 scaled free-floating and tethered models; mass properties and structural details of both the models are given in Tables 7.1 and 7.2, respectively, while Fig. 7.1 shows the elevation of the scaled model considered for the study.

Table 7.2 Details of prototype and model of free-floating and tethered triceratops

Details	Free-floating		Tethered	
	Prototype (m)	Model (mm)	Prototype (m)	Model (mm)
Water depth	600	4000	600	4000
Draft	97.5	645.5[a]	97.5	650
Each buoyant leg structure				
Outer diameter	15	100.0	15	100.0
c/c distance	70	467.0	70	467.0
Cylinder height	120.0	800.0	120.0	800.0
VCG	−51.36	−337.8	−58.87	−392.5
	(m)	(mm)	(m)	(mm)
r_x, r_y	31.81	212.1	33.31	222.05
r_z	4.98	33.2	5.02	33.49
Deck	(m)	(mm)	(m)	(mm)
r_{Dx}, r_{Dy}	24.9	165.9	24.9	165.9

Table 7.2 (continued)

Details	Free-floating		Tethered	
	Prototype (m)	Model (mm)	Prototype (m)	Model (mm)
r_{Dz}	24.6	164.5	24.6	164.5
VCG	46.35	309.0	46.35	309.0
VCG of the whole structure	−55.39	−236.07[a]	−49.23	−328.22
Tethers[b]			(t)	(kg)
Pretension			8652	2.56
			kN/m	N/mm
AE/l			84,000	3.73

[a]Corrected to flume density
[b]Bare tether
l length of the tether; A_w water plane area
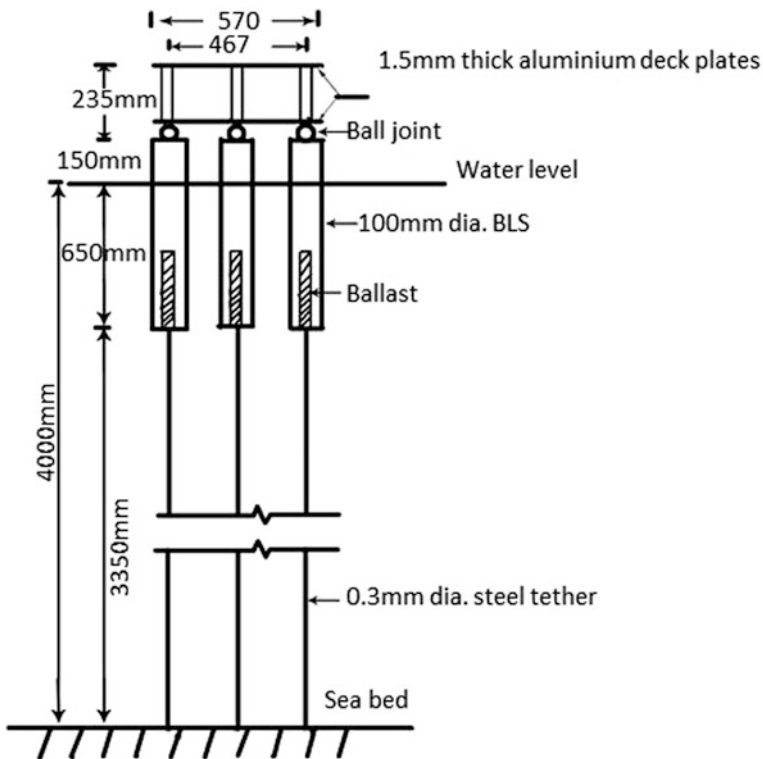
Fig. 7.1 Details of the scaled model
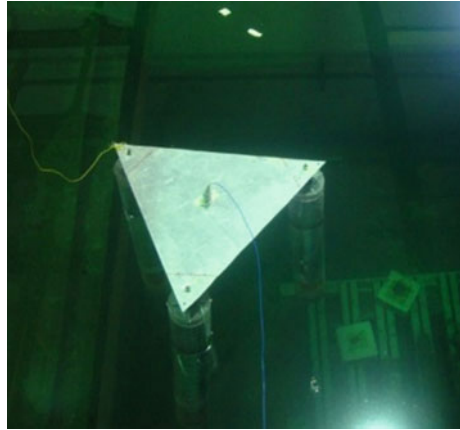
7.3   Model Details

BLS units are fabricated with acrylic cylinders of 100 mm diameter. Two-tier deck systems are fabricated with 1.5-mm thick aluminum sheets and placed at two different elevations to maintain the required VCG. Three tethers are connected to respective the BLS units using steel wire ropes of 0.3 mm diameter. Ball joints are made of Perspex material and placed between BLS units and the deck. Mild steel rods are used for the permanent ballast in each of the BLS unit so as to match the mass properties close to that of the prototype. Accelerometer and inclinometers are placed on the BLS units, while the deck is placed with the instruments to measure heave and pitch responses. Figure 7.2 shows the model commissioned in the wave flume.

7.4   Experimental Studies

7.4.1   Free-Floating Studies

This study is significant for installation and decommissioning purposes of the newly proposed triceratops. Though buoyancy of triceratops is more than the total mass of the structure, additional ballast is required to achieve the required buoyancy during installation. Free-floating heave and pitch periods are studied to avoid resonance during installation. As installation can be planned with each BLS unit separately or with the complete structure based on the capacity of the lifting equipment available, free-floating studies are carried out on both the single BLS unit and on the complete structure as well. As the displacement of single BLS unit is lesser than the complete triceratops, lifting equipment of larger capacity is not required for installation, which would result in significant saving of installation cost.

7.5   Analytical Studies

The analytical studies are performed in ANSYS AQWA software. The free-floating model is analyzed at 4 m water depth, while the tethered model of prototype is analyzed at 600 m water depth. Since BLS units are Morison elements, the line elements are modeled with segments, and the deck is modeled as quadratic plate elements; inbuilt ball joint is used in the analysis. Since BLS units do not have rigid body motion, each BLS unit is considered a separate structure (3 structures) and connected to deck structure (4th structure) with ball joints. The flume water density is also considered in the analysis. Prototype of tethered triceratops is modeled at 600 m water depth; tethers are modeled as steel wire ropes. Free-floating analytical models of single BLS, triceratops and tethered triceratops are shown in Fig. 7.3. Free-decay test is carried out analytically by subjecting the structure to zero wave amplitude and necessary initial conditions in the respective degree of freedom. Equation of motion for the free-decay test is as follows:

$$[M + Ma]\ddot{X} + [C]\dot{X} + [K]X = 0 \qquad (7.1)$$

where M is mass matrix; Ma is the added mass matrix, $[C]$ is the damping matrix, $[K]$ is the stiffness matrix at any instantaneous position and $\{\ddot{X}, \dot{X}, X\}$ are acceleration, velocity and displacement, respectively. Stiffness matrix of the structure, in free-floating condition is given by
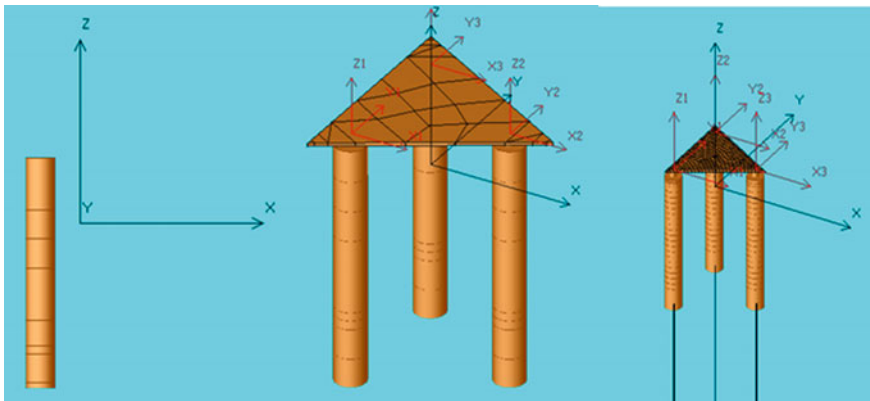

Fig. 7.3 Analytical model of single BLS, free-floating triceratops and tethered triceratops

$$\begin{bmatrix} 0 & 0 & 0 & 0 & 0 & 0 \\ 0 & 0 & 0 & 0 & 0 & 0 \\ 0 & 0 & \rho g A_w & \rho g A_p & -\rho g A_p & 0 \\ 0 & 0 & \rho g A_p & \Delta g GM_{La} & -\rho g A_p & -\Delta g GM_{La} \\ 0 & 0 & -\rho g A_p & -\rho g A_p & \Delta g GM_{Lo} & -\Delta g GM_{Lo} \\ 0 & 0 & 0 & 0 & 0 & 0 \end{bmatrix} \quad (7.2)$$

where $[K]$ is stiffness matrix, ρ is density of sea water, g is acceleration due to gravity, A_w is water plane area, A_p is projected area in respective degree of freedom, Δ is displacement, GM_{La} and GM_{Lo} are lateral and longitudinal meta-centric heights, respectively; stiffness matrix coefficients include changes in tether stiffness, hydrostatic stiffness and hydrodynamic stiffness.

7.6 Empirical Prediction

Heave natural period of single BLS and triceratops are predicted empirically. Added mass of the cylindrical BLS units is found by using semi-sphere volume whose radius is taken as same as that of the cylinder. The tethered surge natural period is also found empirically from the following equation (Faltinsen 1990; Faltinsen et al. 1995).

$$T = 2\pi \sqrt{\frac{(M + Ma)}{\left(\frac{p}{l}\right)}} \quad (7.3)$$

where p is pretension and l is the length of the tether. Table 7.3 shows the comparison of the results of model tests and empirical prediction.

Based on the studies carried out, it has been found that the installation of Triceratops can be done with each BLS unit separately or as a complete structure;

Table 7.3 Natural periods of the structure

DOF	Experimental	Analytical	Numerical
Single BLS			
Heave	1.6	1.6	1.59
Roll	1.59	1.38	
Pitch	1.59	1.38	
Free-floating triceratops			
Heave	1.66	1.65	1.65
Roll	8.04	8.57	
Pitch	8.04	8.57	
Tethered triceratops			
Surge	11.92	13.6	11.9
Heave	0.48	0.4	

free-floating periods are not matching with the wave periods in both the cases and hence no resonance during installation. Should the transportation be economical, installation cost can be minimized by installing each BLS unit separately. As the natural periods of tethered triceratops are also not matching with that of the wave periods, structural performance will be better during operational conditions. Permanent ballast in BLS units results in significant reduction in the pretension in tethers in comparison with that of TLPs. Hence, offshore triceratops does not require high-strength tethers as required for TLPs. Since it has vertical restraining system, heave response is lesser than that of spar, making offshore triceratops more economical for ultra-deepwaters.

7.7 Wave Directionality Effects on Offshore Triceratops

The primary objective of the current study is to investigate the nonlinear dynamic response characteristics of offshore triceratops under regular waves for different wave approach angles. In the present study, 1:150 scaled model of offshore triceratops is investigated under regular waves by varying the wave period. Geometric characteristics of the platform and mass distribution are derived from Norwegian TLP (Patel and Witz 1991) at a water depth of 600 m for equivalent buoyancy as that of the TLP. Buoyancy of pontoons of TLP is distributed to each BLS unit by increasing its draft; this is required to ascertain symmetric response in all BLS units for the considered wave approach angles. Mass distribution and geometric properties are given in Tables 7.4 and 7.5, respectively. BLS units are fabricated with acrylic material, and PVC ball joints are placed between the deck and the BLS units. Deck consists of two aluminum plates of 570 mm width and 1.5 mm thickness that are placed at two levels so as to obtain the representative value of center of gravity of the deck. In order to ensure equal payload distribution on each BLS unit, triangular geometry of the deck plate is chosen for the study; center of gravity of the BLS units and the deck is maintained on the same vertical axis. Components of the triceratops are shown in Fig. 7.4. Figure 7.5 shows the 1:150 scaled model considered for the study. The model is free-floated by ballasting each BLS unit; ballast mass is kept equivalent to the amount of pretension in each tether. Experimental studies are carried out in the wave flume of 4 m width, at a water depth of 4 m. Details of prototype and scaled wave data are given in the Tables 7.4 and 7.5. Dynamic response of the platform is measured for three different wave approach angles with reference to the axis of symmetry of the structure; details of instrumentation are shown in Fig. 7.6. Two accelerometers (surge/sway of BLS, heave of deck) and two inclinometers (pitch/roll of BLS and deck) are used to measure the acceleration and pitch responses. Surge, heave and pitch RAOs (response amplitude operators) of the model are scaled up to the prototype and plotted for BLS units and the deck under the regular wave loads; three wave approach angles namely 0°, 90°, and 180° are considered in the present study.

Table 7.4 Details of model and prototype of free-floating and tethered triceratops

Description	Free-floating		Tethered	
	Prototype (m)	Model (mm)	Prototype (m)	Model (mm)
Water depth	600	4000	600	4000
Draft	97.5	645.5[a]	97.5	650
Each buoyant leg structure				
Outer diameter	15	100.0	15	100.0
c/c distance	70	467.0	70	467.0
Length	120.0	800.0	120.0	800.0
VCG from MSL	−51.36	−337.8	−58.87	−392.5
VCB from MSL	−48.75	−322.8	−48.75	−325.0
	(m^2)	(mm^2)	(m^2)	(mm^2)
Water plane area	176.71	7854.0	176.71	7854.0
	(t m^2)	(kg mm^2)	(t m^2)	(kg mm^2)
I_{xx}, I_{yy}	16,550,362	217,947.2	14,892,025	196,109
I_{zz}	146,775.3	1932.8	81,067.6	1067.6
	(m)	(mm)	(m)	(mm)
r_x, r_y	31.81	212.1	33.31	222.05
r_z	4.98	33.2	5.02	33.49
Deck	(m^2)	(mm^2)	(m^2)	(mm^2)
Deck area	6330.86	281,372	6330.86	281,372
I_{Dxx}, I_{Dyy}	1,256,831	16,550.9	1,256,831	16,550.9
I_{Dzz}	1,236,483	16,282.9	1,236,483	16,282.9
r_{Dx}, r_{Dy}	24.9	165.9	24.9	165.9
r_{Dz}	24.6	164.5	24.6	164.5
VCG	−46.35	−309.0	−46.35	−309.0
VCG of the whole structure	−55.39	−236.07[a]	−49.23	−328.22
Tether			(t)	(kg)
Pretension			8652	2.56
			kN/m	N/mm
AE/l			84,000	3.73
Area of tether			0.211 m^2	0.07[b] mm^2
			(m)	(mm)
Length of the tether			502.5	3350.0
			kN/m^2	N/mm^2
Modulus of elasticity			2×10^8	2×10^5

[a]Corrected to flume density
[b]Bare tether

Table 7.5 Natural period of the structure(s)

1:150 Model			
Degree of freedom	Free-floating triceratops	Free-floating BLS	Tethered
Surge	–	–	11.92
Heave	1.66	1.60	0.48
Pitch	8.04	1.59	–
Prototype			
Surge			145.98
Heave	20.33	19.59	5.88
Pitch	98.47	19.47	

Fig. 7.4 Components of triceratops
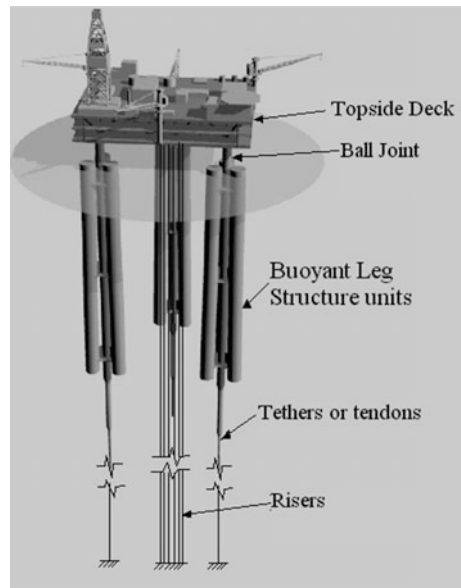
7.8   Discussions of Experimental Studies

Free oscillation tests are conducted on free-floating and tethered models of the structure to determine their natural periods of vibration. These tests are conducted in two stages: (i) each BLS is freely floated by ballasting, while free oscillation tests are conducted on single BLS in heave and pitch degrees of freedom; and (ii) deck is connected to BLS units through ball joints for the desired draft of 650 mm, and subsequently free oscillation tests are conducted on the whole platform. Tethers are then connected to the model, and the platform is de-ballasted to enable the desired pretension in tethers. Free-floating natural periods and their scaled-up values of the prototype are given in Table 7.3. It is seen that natural periods of the platform are
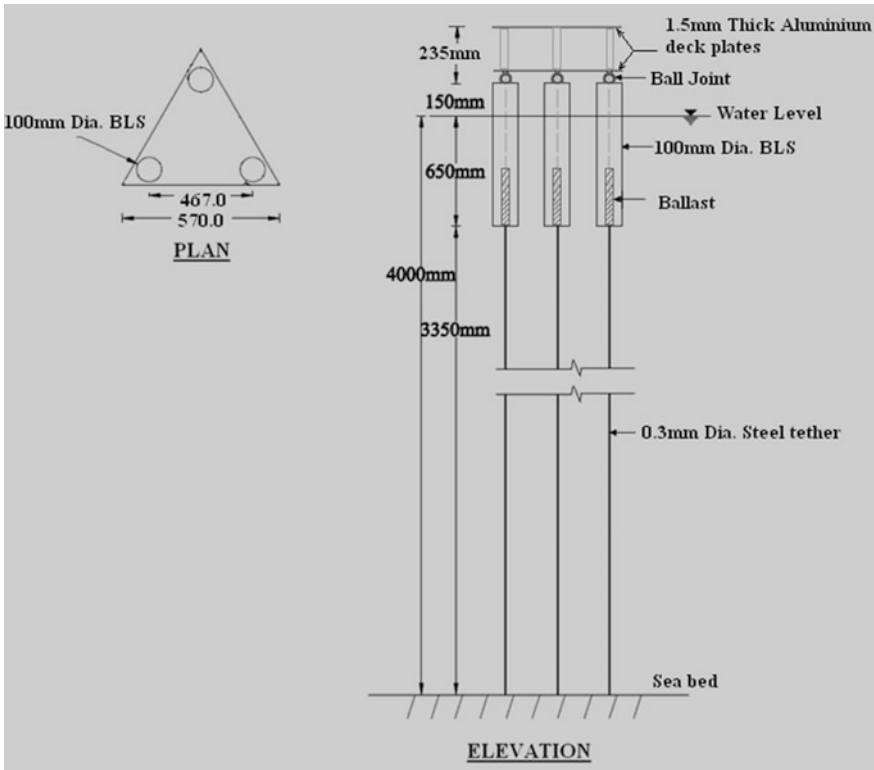
Fig. 7.5 Plan and elevation of the scaled model

A1 — Accelerometer 1 (Surge/Sway of BLS)
IM1 — Inclinometer1 (Pitch/Roll of BLS)
A2 — Accelerometer 2 (Surge/Sway of Deck)
IM2 — Inclinometer2 (Pitch/Roll of Deck)
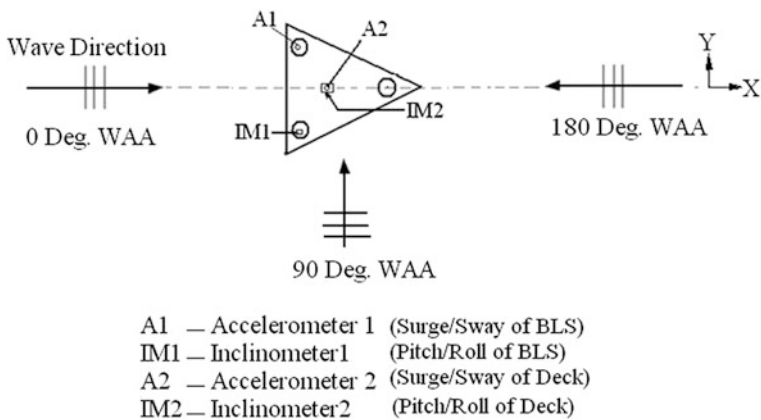
Fig. 7.6 Instrumentation for different wave approach angles
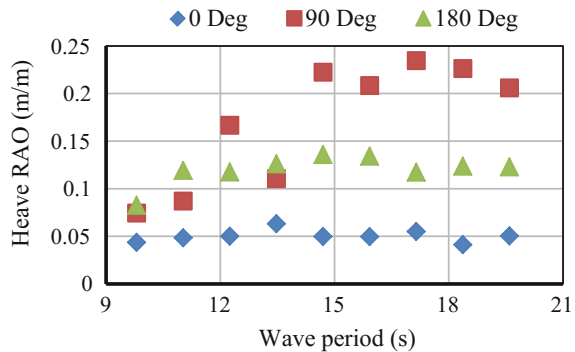
Fig. 7.7 Surge/sway RAOs
of triceratops
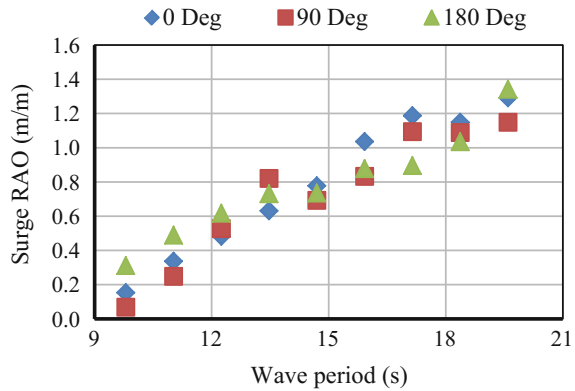
Fig. 7.8 Heave RAO of
triceratops

away from the bandwidth of the operation wave periods; this is advantageous
during installation, operation and decommissioning as well.

Surge/sway and heave RAOs are shown in Figs. 7.7 and 7.8, respectively. It is
seen from Fig. 7.7 that the variations in surge/sway responses are not significant for
different wave approach angles; however, it shows maximum variation for 180°
wave approach angle. Figure 7.8 shows a significant influence of wave direction-
ality on heave RAO; variation is minimum at 0° and maximum at 90°. Variations in
heave response for different wave approach angles shall be attributed to the phase
lag of BLS legs when compared with that of the approaching waves. Pitch RAOs of
BLS and deck are shown in Figs. 7.9 and 7.10. It is seen from the figures that there
are no significant variations in the pitch response of both the deck and BLS units for
different wave approach angles; compliancy offered by the ball joints shall be seen
as a major contributing factor to this behavior. Pitch in the deck is observed mainly
due to the transfer of heave from BLS to deck. Pitch/roll response of BLS is similar
in all wave approach angles, indicating circular mass distribution in the BLS.

Experimental investigations are carried out on the scaled model of offshore
Triceratops to ascertain the influence of wave directionality on its response
behavior. Experimental results show that the wave directionality does not influence

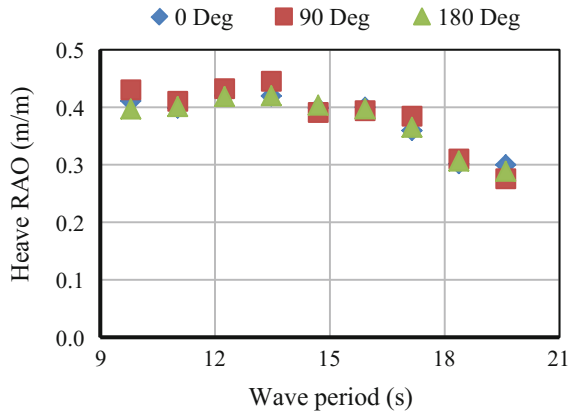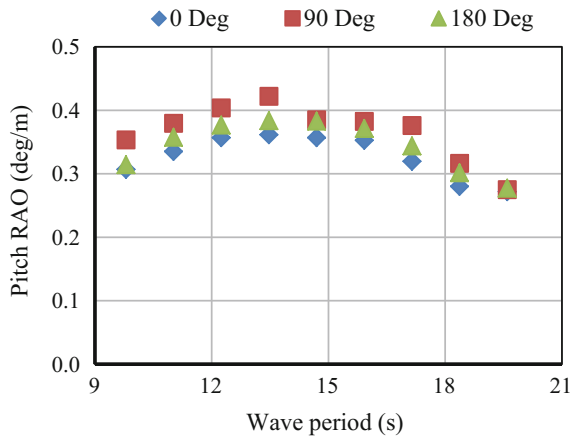**Fig. 7.9** Pitch/roll RAOs of BLS

Fig. 7.10 Pitch/roll RAO of deck

surge/sway response of the platform significantly. Comparison of surge/sway RAO with that of heave shows that the structure is restrained in heave degree of freedom, which is expected for a compliant platform. Wave directionality does not influence pitch response of both the deck and BLS units; compliancy offered by the ball joints shall be seen as a major contributing factor to this behavior. For the chosen deck of triangular geometry, reduced rotational response under different wave approach angles reinforces the suitability of triceratops for irregular sea states; insensitivity of pitch/roll response for different wave approach angles indicates circular mass distribution in the BLS. Presented studies validate the suitability of offshore triceratops for ultra-deepwater; however, more detailed analytical investigations are preferable to strengthen the present experimental observations.

7.9　Springing and Ringing Responses of Tension Leg Platforms

Certain class of offshore structures exhibits highly intense nonlinear behavior called springing and ringing. Dynamic response of compliant structures like tension leg platforms (TLPs) under impact and non-impact waves responsible for ringing and springing phenomenon is of large interest to marine engineers (Buchner and Bunnik 2007; Chandrasekaran and Yuvraj 2013). This section describes the mathematical formulation of impact and non-impact waves and discusses the method of analysis of TLPs of triangular geometry under these wave effects. Responses of square and equivalent triangular TLPs are compared. Heave response in square TLPs show bursts, but there are no rapid buildups; gradual decays are seen in most cases looking like a beat phenomenon, while such results are not predominantly noticed in case of equivalent triangular TLPs. Ringing caused by impact waves in pitch degree of freedom and springing caused by non-impact waves in heave degree of freedom in both the platform geometries are undesirable, as they pose a serious threat to the platform stability. Analytical studies conducted show that equivalent triangular TLPs positioned at different water depth are less sensitive to these undesirable responses, thus making it as a safe alternative for deep-water oil explorations. The study presented is a prima-facie to understand the geometric design and form development of offshore structures for deep-water oil exploration.

7.9.1　Springing and Ringing

Springing and ringing is shown by a certain class of compliant offshore structures namely TLPs and gravity-based structures (GBSs) gained research focus since they were first observed in a model test of the Hutton TLP in the North Sea in 1980s (Mercier 1982, 1997). Springing is caused in the vertical/bending modes by second-order wave effects at the sum frequencies; this behavior is common in both mild and severe sea states. Ringing is attributed to the strong transient response observed in these modes under severe loading conditions triggered presumably by the passage of a high, steep wave. This transient response further decays to steady state at a logarithmic rate depending on the system damping (Chandrasekaran and Jamshed 2015). Figure 7.11 shows a schematic view of springing and ringing. TLPs are generally designed to keep their natural frequencies in heave, pitch and roll degrees of freedom, several times above the dominant wave frequency, whereas structural frequencies in surge, sway and yaw degrees of freedom are designed to be lower than the dominant wave frequency as shown in Fig. 7.12. Though TLPs are designed with this kind of shift in their structural frequencies, springing and ringing still become important when the range of structural frequency is several times higher than the dominant wave frequencies. As a result, ringing can not only cause a total breakdown of these platforms even in moderate storms but can also hamper
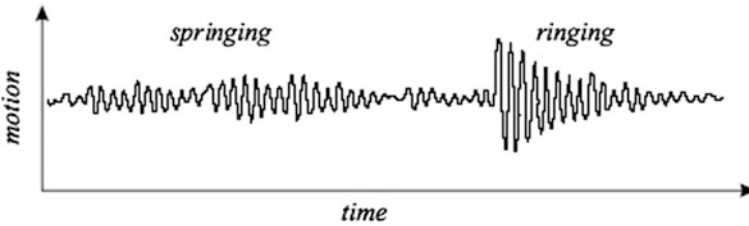
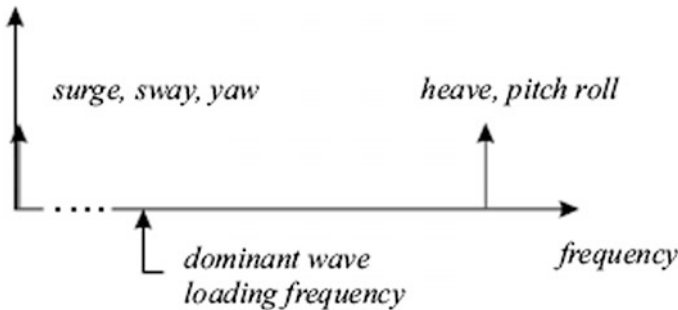**Fig. 7.11**   Schematic view of springing and ringing waves

Fig. 7.12   Frequency range of TLPs relative to dominant wave frequency

daily operations and lead to fatigue failure (Winterstein 1998; Ude et al. 1994; Marthinsen et al. 1992). Studies on ringing and springing response had a primary focus on large volume structures that are dominated by wave diffraction inertial-type loading and minimally affected by drag forces (Natvig 1994, 1996; Jeffereys and Patel 1982; Jefferys and Rainey 1994; Faltinsen et al. 1995); these studies discussed the response of TLPs and GBS with slender cylinders. Kim and Zou (1995) and Kjeldsen and Myrhaug (1979) observed that waves causing ringing response are highly asymmetric. Gurley and Kareem (1998) showed that viscous loads are also capable of inducing ringing response of members with large wavelength-to-diameter ratios, where instantaneous moment acting on the cylinder is a quadratic function of wave elevation. The precursors of ringing and springing phenomenon are (i) the generation of high-frequency force necessitating the presence of steep, near-vertical wave fronts; and (ii) resonant buildup due to subsequent loading within the range of the time period of TLP. This could be realized by setting the dominant wave frequency as several times as the natural frequency of the structure. Also frequency at which ringing occurs is well above the incident wave frequency and is close to the natural frequency of the structure.

7.10   Evolution of Platform Geometry

Natvig and Vogel (1995) reported several advantages of TLPs with triangular geometry namely: (i) no tether tension measurements required on day-to-day operation; (ii) increased tolerances for the position of foundation; and (iii) increased draught and heel tolerances, making it more advantageous than four-legged square TLPs. Triangular TLPs that are statically determinate can have foundations placed with larger tolerances without affecting tether behavior. With the near-equal load sharing of all tethers of triangular TLP despite weather directions, the maximum load level in one group reduces, thus resulting in decreased cross-sectional material of tethers, which is an important area for cost savings in TLPs while they show lesser response under regular and random waves as well (Chandrasekaran and Jain 2002a, b). Stability analysis performed on triangular TLPs under impact loading and influence of wave approach angle showed that they are more stable in the first mode of vibration in comparison to square TLPs, while impulse loading acting on their corner column affects their performance behavior significantly (Chandrasekaran et al. 2006, 2007a, b). The aspects of platform geometry that affect tether loading and tether system thus become the focus on the design of future TLPs (Booton et al. 1987).

7.11   Mathematical Development

A *ringing* event involves the excitation of transient structural deflections at/close to the natural frequency of the platform arising at third harmonic of the incident wave field, whereas *springing* effect involves excitation of motion in vertical degree of freedom, for example, in heave in TLPs due to nonlinear forces arising at the second harmonic of the incident waves. The shape of the impact wave generating ringing is hence crucial and is experimentally observed that these waves are steep and asymmetric with respect to both horizontal and vertical axes; Kim et al. (1997) recommended to use laboratory generated ringing waves in case of non-availability of any analytical wave models. Therefore, the generation of impact wave time histories from currently available wave theories and random wave elevation spectrums suffer from potential difficulties such as the following: (i) shape of experimentally observed ringing waves being different from analytical ones; (ii) absence of a systematic method to categorize such steep, irregular, and asymmetric waves; and (iii) insufficiency of these theories to generate extreme waves that could cause impact forces. These limitations restrict the use of existing theories for generation of impact waves that are associated with the onset of ringing (see for example, Son 2006). Thus, the necessity of steep waves conforming to experimentally generated waves calls for implementation of a higher order nonlinear wave kinematic theory and nonlinear fluid model. On the other hand, this could lead to complicated mathematical formulations that will become computationally inefficient when solved numerically (Bathe and Wilson 1987). Because of these reasons, several researchers (Soding et al. 1990) successfully simulated ringing and springing waves using Airy's wave theory and used dynamic Morison equation for force evaluation. Also in the current study, water particle kinematics for ringing

and springing waves is obtained using Airy's wave theory from a randomly generated sea surface elevation using Pierson Moskowitz (PM) spectrum. The original PM spectrum, a function of wind velocity, is modified as a function of modal frequency and later modified again as a function of significant wave height and modal frequency (Michel 1999). For ringing to be present in the considered sea state, dominant wave frequency should be several times higher than surge natural frequency. Therefore, the modal frequency used in the PM spectrum is chosen to be about five times of the surge frequency. The modified one parameter formula given by Eq. (7.4) is employed in the present study. Figure 7.13a shows the PM spectrum.
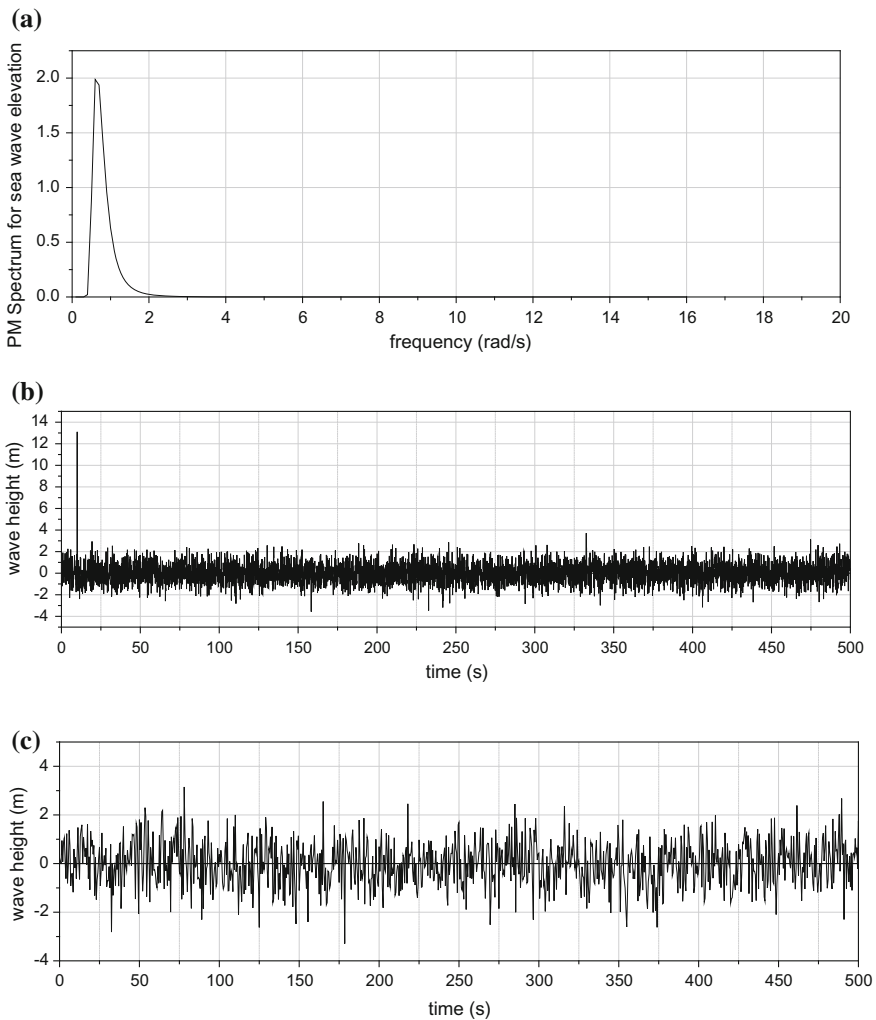
Fig. 7.13 a PM spectrum for wave height elevation **b** impact wave profile with impact wave at $t = 10$ s **c** non-impact wave profile

$$S_{\eta\eta}(\omega) = \frac{8.1 \times 10^{-3} g^2}{\omega^5} \exp\left[-1.25\left(\frac{\omega_m}{\omega}\right)^4\right] \tag{7.4}$$

where g is acceleration due to gravity, ω_m is the modal frequency and $S_{\eta\eta}$ is the power spectral density of wave height. Wave elevation, $\eta(t)$ realized as a discrete sum of many sinusoidal functions with different angular frequencies and random phase angles is given by

$$\eta(t) = \sum_{i=1}^{n} \sqrt{2S_{\eta\eta}(\omega_i)\Delta\omega_i} \cdot \cos(\omega_i t - \varphi_i) \tag{7.5}$$

where ω_i are discrete sampling frequencies $(\Delta\omega_i = \omega_i - \omega_{i-1})$, n is the number of data points and φ_i are random phase angles. Range of random phase angles are set to decide the generated wave to be an impact or a non-impact wave. Impact waves shall have wave profile with a peak at a particular time (t_0) that will be distinctly higher than other wave heights; wave heights that become comparable at all time periods and lie within the prescribed limits are termed as non-impact waves. For generating a non-impact wave profile, phase angles φ_i are chosen as random numbers within the range $[0, 2\pi]$. For an impact wave at an arbitrary time t_0, φ_i is chosen in the range $[0, 0.01]$ at time $t = t_0$; Eq. (7.5) is subsequently modified as given below:

$$\eta(t) = \sum_{i=1}^{n} \sqrt{2S_{\eta\eta}(\omega_i)\Delta\omega_i} \cdot \cos(\omega_i(t - t_0) - \varphi_i) \tag{7.6}$$

A sample impact and non-impact wave thus generated using the above equations is shown in Fig. 7.13b, c, respectively.

7.12   Analytical Model of TLP

Equivalent geometrical configuration of triangular TLP is evolved on the basis of equation of equilibrium applied in the static sea conditions. For TLPs of square and triangular geometry, the respective equations are given as

$$F_B = 4(T_0)_{\text{square}} + W \tag{7.7}$$

$$F_B = 3(T_0)_{\text{square}} + W \tag{7.8}$$

where F_B is the buoyant force, T_0 is the initial pretension in each tether, and W is the total weight of the platform. Equivalent triangular TLP is arrived by considering two cases namely: (i) buoyant force and initial pretension per tether are considered equal for both the geometries resulting in reduced total pretension in triangular
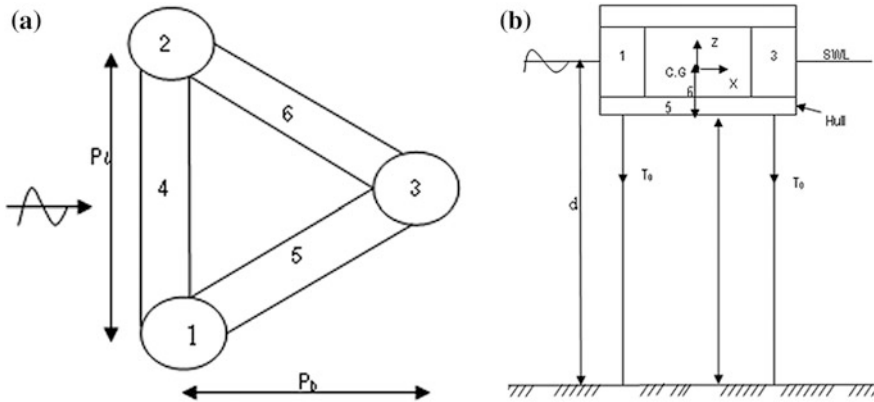
Fig. 7.14 **a** Plan and **b** elevation of example TLP

TLP; and (ii) total initial pretension, weight, and buoyancy are kept the same for both geometries thereby increasing the initial pretension per tether in the triangular TLP. The platform considered in the study is a rigid body having six degrees of freedom. Figure 7.14 shows the plan and elevation of the triangular TLP having plan dimension as P_l used in the study.

Unidirectional waves with incident angle normal to one of the pontoons are considered. Maximum absolute response in pitch degree of freedom is obtained when the waves are normally impinged; other degrees of freedom namely sway, roll and yaw that are activated by a non-normal wave show minimal effects. Four square TLPs at different water depths, reported in the literature (Chandrasekaran and Jain 2002a, b; Buchner et al. 1999), are considered for the analysis, and their geometric properties are given in Table 7.6, whereas Table 7.7 shows time periods of equivalent triangular TLPs with initial pretension same as that of these square ones. The hydrodynamic coefficient of drag (C_d) and inertia (C_m) used in Morison equation are asserted to be independent of the wave frequencies (Burrows et al. 1992). C_d is taken as unity, while C_m is assumed to vary along the water depth (Chandrasekaran et al. 2004) and is interpolated for the entire water depth using a second-degree polynomial as given below:

$$C_m(y) = p_1 \cdot y^2 + p_2 \cdot y + p_3 \tag{7.9}$$

where y is the water depth measured from sea bed; p_1, p_2 and p_3 are coefficients used for interpolation and given in Table 7.8. Tethers are modeled as elastic cables with axial AE/l when taut, and zero when they slack.

Table 7.6 Geometric properties of square TLPs considered

Property	TLP$_1$	TLP$_2$	TLP$_3$	TLP$_4$
Weight (kN)	351,600.00	330,000.00	330,000.00	370,000.00
F_B (kN)	521,600.00	465,500.00	520,000.00	625,500.00
T_0 (kN)	170,000.00	135,500.00	190,000.00	255,500.00
Tether length, l (m)	568.00	269.00	568.00	1166.00
Water depth (m)	600.00	300.00	600.00	1200.00
CG (m)	28.44	27.47	28.50	30.31
AE/l (kN/m)	84,000.00	34,000.00	82,000.00	45,080.00
Plan dim (m)	70.00	75.66	78.50	83.50
D and D_c (m)	17.00	16.39	17.00	18.80
r_x (m)	35.10	35.10	35.10	35.10
r_y (m)	35.10	35.10	35.10	35.10
r_z (m)	35.10	42.40	42.40	42.40

Table 7.7 Natural wave periods and frequencies of equivalent triangular TLPs with T_0 per tether same

Case	Natural time period (s)			Natural frequency (Hz)		
	Surge	Heave	Pitch	Surge	Heave	Pitch
TLP$_1$	98.00	1.92	2.110	0.0102	0.5208	0.4739
TLP$_2$	87.20	1.96	2.155	0.0115	0.5102	0.4640
TLP$_3$	97.00	1.92	2.060	0.0103	0.5208	0.4854
TLP$_4$	132.0	3.11	3.120	0.0076	0.3215	0.3205

Table 7.8 Values of coefficients for interpolation of C_m

Description	p1	p2	p3
TLP$_1$	7.780×10^{-7}	-9.667×10^{-4}	1.8
TLP$_2$	3.111×10^{-6}	-1.933×10^{-3}	1.8
TLP$_3$	7.778×10^{-7}	-9.667×10^{-4}	1.8
TLP$_4$	1.944×10^{-7}	-4.833×10^{-4}	1.8

7.13 Hydrodynamic Forces on TLP

Modified Morison's equation accounting for the relative motion between the platform and waves is used to estimate hydrodynamic force per unit length $f(t)$ on the members of TLP and is given by

$$f(t) = \frac{\pi D_c^2}{4} \rho C_m \ddot{u} + \frac{1}{2} \rho C_d D_c (\dot{u} - \dot{x})|\dot{u} - \dot{x}| \pm \frac{\pi D_c^2}{4}(C_m - 1)\rho \ddot{x} \qquad (7.10)$$

where $\dot{x}, \ddot{x}$ are horizontal structural velocity and acceleration, $\dot{u}, \ddot{u}$ are horizontal water particle velocity and acceleration, ρ is mass density of sea water, C_d and C_m

are hydrodynamic drag and inertia coefficients and D_c is diameter of pontoons, respectively. As there is no significant variation in water depth for the pontoons at the bottom, constant C_d (as 1.0) and C_m (as 2.0) values are used for them. The last term in Eq. (7.10) is the added mass term and is taken as positive when the water surface is below mean sea level. The hydrodynamic force vector $F(t)$ is given by

$$\{F(t)\} = \{\, F_1 \quad F_2 \quad F_3 \quad F_4 \quad F_5 \quad F_6 \,\}^{\mathrm{T}} \tag{7.11}$$

where F_1, F_2, and F_3 are total force in surge, sway, and heave degrees of freedom and F_4, F_5, and F_6 are moments of these forces about X, Y, and Z axes, respectively.

7.14   Dynamics of Triangular TLP

Equation of motion describing the dynamic equilibrium between the inertia, damping, restoring and exciting forces can be assembled as follows:

$$[M]\{\ddot{x}\} + [C]\{\dot{x}\} + [K]\{x\} = \{F(t)\} \tag{7.12}$$

where $[M]$ is the mass matrix, $[C]$ is the damping matrix, $[K]$ is the stiffness matrix, and $\{F(t)\}$ is the force vector as defined by Eq. (7.11).

7.14.1   Mass Matrix

The structural mass is assumed to be lumped at each degree of freedom. Hence, it is diagonal in nature and constant. The added mass M_a due to the water surrounding the structural members is also been considered up to MSL. The presence of off-diagonal terms in the mass matrix indicates contribution of added mass due to the hydrodynamic loading in the activated degrees of freedom due to unidirectional wave load.

$$[M] = \begin{bmatrix} M_1 + M_{a11} & 0 & 0 & 0 & 0 & 0 \\ 0 & M_2 & 0 & 0 & 0 & 0 \\ 0 & 0 & M_3 + M_{a33} & 0 & 0 & 0 \\ 0 & 0 & 0 & M_4 & 0 & 0 \\ M_{a51} & 0 & M_{a53} & 0 & M_5 & 0 \\ 0 & 0 & 0 & 0 & 0 & M_6 \end{bmatrix} \tag{7.13}$$

where $M_{11} = M_{22} = M_{33} =$ total mass of the structure, M_4 is mass moment of inertia about the x axis $= Mr_x^2$, M_5 is mass moment of inertia about the y axis $= Mr_y^2$, M_6 is mass moment of inertia about the z axis $= Mr_z^2$, and r_x, r_y, and r_z are radius of gyration about the x, y and z axis, respectively. M_{a11}, M_{a33} are added

mass terms in surge and heave degrees of freedom, M_{a51}, M_{a53} are added mass moment of inertia due to the additional mass in surge and heave degrees of freedom, respectively. The presence of off-diagonal terms indicates the contribution of added mass due to hydrodynamic loading. The contribution of added mass up to MSL has already been considered along with the force vector. The added mass terms are given by

$$M_{a11} = 0.25\pi\rho D^2[C_{\mathrm{m}} - 1]x_{\text{surge}} \tag{7.14}$$

$$M_{a33} = 0.25\pi\rho D^2[C_{\mathrm{m}} - 1]x_{\text{heave}} \tag{7.15}$$

7.14.2 Stiffness Matrix

The coefficients K_{ij} of the stiffness matrix of triangular TLP are derived from the first principles, as presented in the literature (Chandrasekaran and Jain 2002a, b), and the same has been used in the current study.

$$[K] = \begin{bmatrix} K_{11} & 0 & 0 & 0 & 0 & 0 \\ 0 & K_{22} & 0 & 0 & 0 & 0 \\ K_{31} & K_{32} & K_{33} & K_{34} & K_{35} & K_{36} \\ 0 & K_{42} & 0 & K_{44} & 0 & 0 \\ K_{51} & 0 & 0 & 0 & K_{55} & 0 \\ 0 & 0 & 0 & 0 & 0 & K_{66} \end{bmatrix} \tag{7.16}$$

The coefficients of the stiffness matrix have nonlinear terms due to cosine, sine, square root, and square terms of the structural displacements. Furthermore, tether tension changes due to TLP motion making $[K]$ response dependent. Off-diagonal terms reflect the coupling effect between various degrees of freedom. Change in tether tension updates $[K]$ at every time step and also changes buoyancy of TLP. It is interesting to note that coefficients of $[K]$ continuously vary at every time step and are replaced by new values based on the structural response of TLP.

7.14.3 Damping Matrix

Damping matrix $[C]$ is assumed to be proportional to initial values of $[M]$ and $[K]$ and is given by (Chopra 2003):

$$[C] = a_0[M] + a_1[K] \tag{7.17}$$

where a_0 and a_1 are, respectively, the stiffness and mass proportional damping constants. Damping matrix given by the above equation is orthogonal as it permits modes to be uncoupled by eigenvectors associated with the undamped eigen problem. Damping constants a_0 and a_1 are determined by choosing the fractions of critical damping (ξ_1 and ξ_2) at two different frequencies (ω_1 and ω_2) and solving simultaneous equations for a_0 and a_1.

$$a_0 = 2(\xi_2\omega_2 - \xi_1\omega_1)/(\omega_2^2 - \omega_1^2) \tag{7.18}$$

$$a_1 = 2\omega_1\omega_2(\xi_1\omega_2 - \xi_2\omega_1)/(\omega_2^2 - \omega_1^2) \tag{7.19}$$

Damping attributable to a_0 [K] increases with increasing frequency, whereas damping attributable to a_1 [M] increases with decreasing frequency. In the current study, value of these coefficients is obtained using the above equations by taking damping ratio $\zeta = 0.05$ in surge and yaw degrees of freedom. Free vibration analysis is performed to find out natural frequencies of the platform corresponding to these degrees of freedom and found that damping ratios maintain reasonable values for all the other modes which are contributing significantly to the response. Initial pretension in all tethers is assumed to be equal and total pretension changes with the motion of platform. The equation of motion is solved in the time domain by employing Newmark's integration scheme by taking $\alpha = 0.25$ and $\beta = 0.5$. The solution procedure incorporates the changes namely: (i) stiffness coefficients varying with tether tension; (ii) added mass varying with sea surface fluctuations; and (iii) evaluation of wave forces at instantaneous position of the displaced platform considering the fluid–structure interaction. Behavior under wave loading becomes nonlinear, and components of the equation of motion at each step components are updated. Ten terms in the power series are found to be sufficient to give convergence in the iterative scheme. The time step Δt has been taken as 0.1 s, which is a relatively small value in comparison with the natural period (T_n) and hence yields accurate values for the response.

7.15   Ringing Response

Ringing is usually a phenomenon attributed to the response of compliant structures like TLPs under impact waves. Figures 7.15, 7.16 and 7.17 show heave, pitch, and surge responses of all four cases of TLPs under impact waves namely (i) square TLPs; (ii) equivalent triangular TLPs with T_0 per tether same as that of square; and
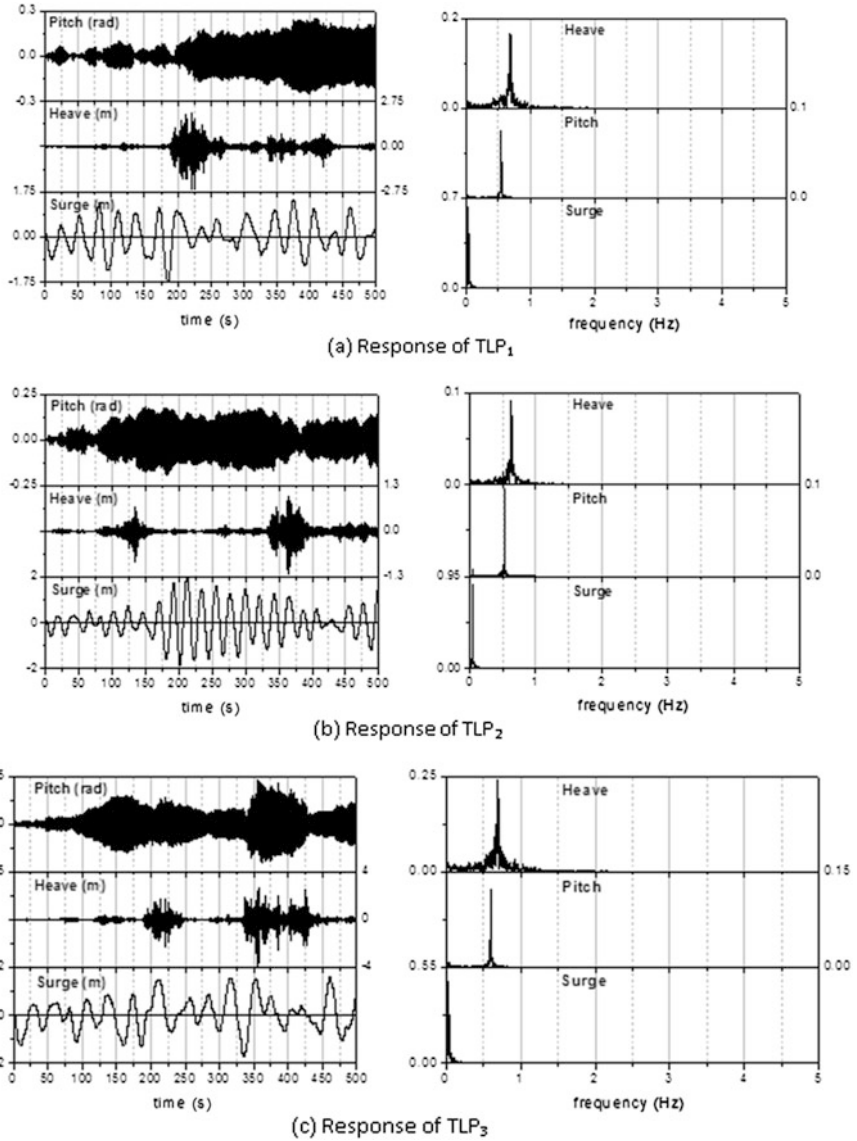
(a) Response of TLP$_1$

(b) Response of TLP$_2$

(c) Response of TLP$_3$

Fig. 7.15 Response of square TLPs to impact waves
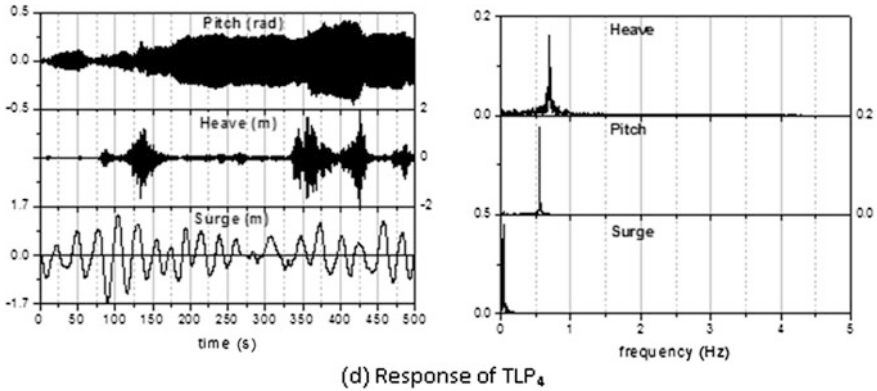
(d) Response of TLP$_4$

Fig. 7.15 (continued)

(iii) equivalent triangular TLPs with total T_0 same as that square, respectively. It can be seen that the response is primarily triggered in pitch degree of freedom for a wide range of period similar to the response of a bell vibrating for a longer time when struck by a large impact force. This is noticed in both the geometries of TLPs, which shall be attributed to a ringing response. Though a similar response is noticed under the influence of non-impact waves also, it can be seen that the intensity of pitch response caused by the latter is less compared to that caused by impact waves. By comparing the ringing response in pitch degree of freedom of TLP$_1$ and TLP$_3$ at the same water depth but with different tether tension, it can be seen that increased tether tension enhances pitch response due to impact waves in both the geometries; however, pitch response of triangular TLPs of both cases (i and ii) is lesser than the square ones. Further comparison of pitch response of TLP$_2$, TLP$_3$, and TLP$_4$ under impact waves shows increase in water depth from 300 to 600 m increases the response by about 50%, and further increase to 1200 m enhances the response by 100%. This behavior is seen in both the geometries, but it is interesting to note that increase in water depth does not enhance the ringing response in pitch degree of freedom in triangular TLP (with T_0 per tether same case) as much as the square ones (see for example, pitch response of TLP$_3$ and TLP$_4$ of triangular TLP with same T_0 per tether case). It is also important to note that the influence of increase in water depth on pitch response of triangular TLPs with total T_0 same as that of square is even lesser. By considering TLPs as most suitable for deep-water situation, it can be seen that ringing response in pitch degree of freedom in triangular TLPs (T_0 per tether same case) under impact waves are lesser that of the square ones, and it is further reduced for triangular TLP with total T_0 same as square (for example, TLP$_4$). While attributing pitch response to impact waves, which is clearly a ringing phenomenon, as undesirable, triangular TLPs showing lesser response in this front makes them a focus for futuristic design of TLPs in deepwater.
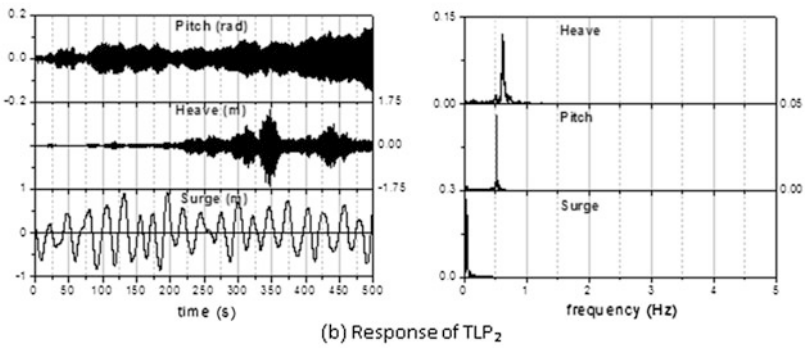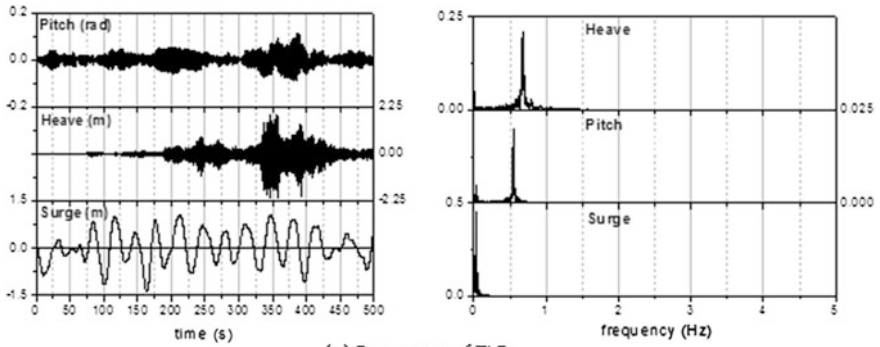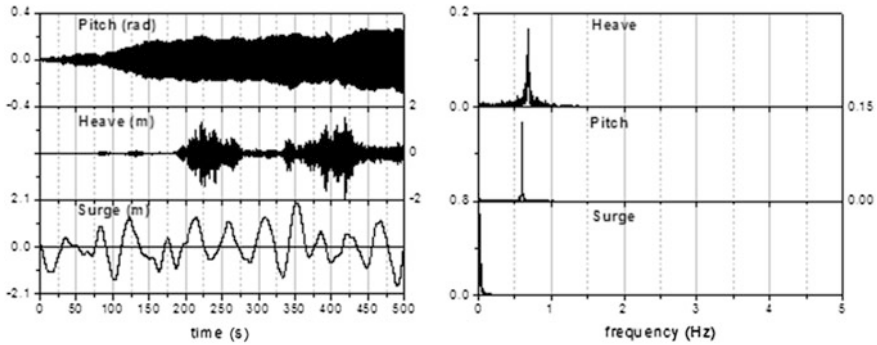
(a) Response of TLP$_1$

(b) Response of TLP$_2$
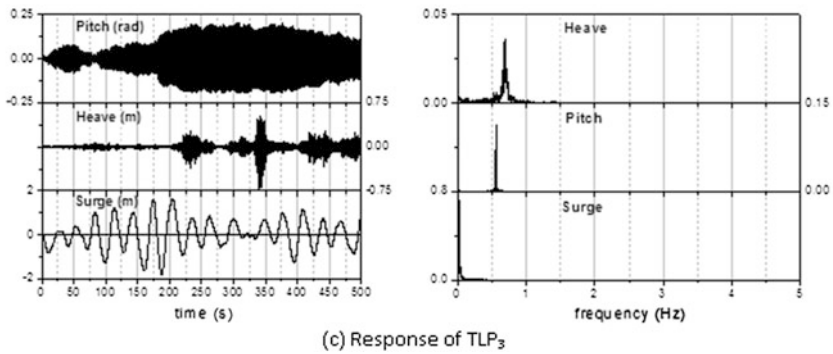
(c) Response of TLP$_3$

Fig. 7.16 Response of equivalent triangular TLPs to impact waves (T_0 per tether same)
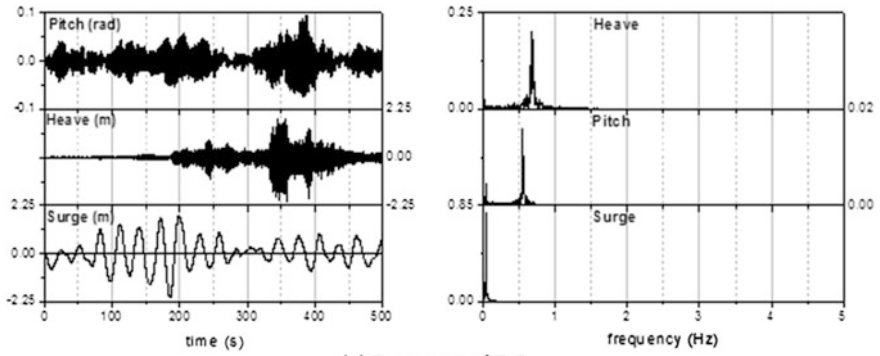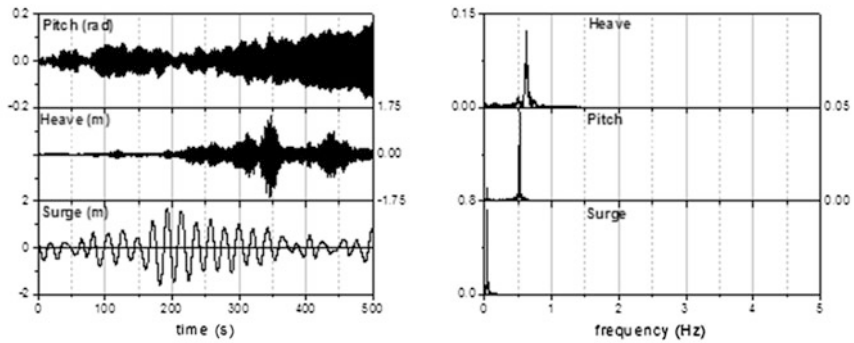
(d) Response of TLP$_4$

Fig. 7.16 (continued)

7.16   Springing Response

The response behavior of TLPs with different geometry shows a near resonating case of heave response under non-impact waves. This phenomenon is usually known as springing. Figures 7.18, 7.19 and 7.20 show heave, pitch and surge responses of all four cases of TLP under non-impact waves namely (i) square TLPs; (ii) equivalent triangular TLPs with T_0 per tether same as that of square; and (iii) equivalent triangular TLPs with total T_0 same as that square, respectively. It can be seen that heave response is triggered at a frequency near to that of its natural frequency causing springing response. The broad band in frequency response commonly noticeable in both the geometries indicates more energy concentration near the natural frequency of heave degree of freedom. By comparing springing response in heave degree of freedom of TLP$_1$ and TLP$_3$ at same water depth but with different tether tension, it is seen that heave response under non-impact waves decreases with increase in tether tension for same water depth in both the geometries; however, heave response of triangular TLPs of both the equivalence cases is lesser than the square ones. Further, increase in water depth from 300 to 600 m increases the heave response by about 45%, and further increase in water depth to 1200 m increases it to about 100%. Though this behavior is common to both the geometries, increase in water depth does not enhance heave response in both equivalent cases of triangular TLPs (for example, TLP$_2$, TLP$_3$, and TLP$_4$). It is quite interesting to note that the response in case of triangular TLPs with total T_0 same as that of square is even lesser. It can be seen that springing response in heave degree of freedom of triangular TLPs (of both equivalence case) under non-impact waves is lesser than that of square ones (for example, TLP$_4$). Further, almost heave response in all square TLPs show bursts, but there are no rapid build-ups and gradual decays in most cases, looking like a beat phenomenon. This is possibly due to the superimposition of waves of nearly same frequency, while such results are not predominantly noticed in case of equivalent triangular TLPs. This type of

(a) Response of TLP$_1$
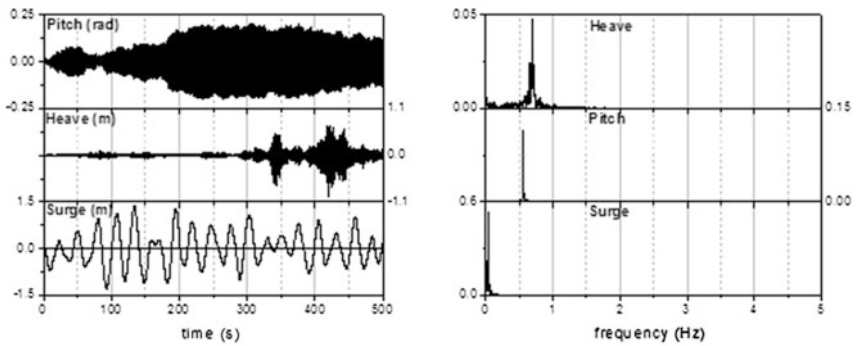
(b) Response of TLP$_2$

(c) Response of TLP$_3$

Fig. 7.17 Response of equivalent triangular TLPs to impact waves (total T_0 same)
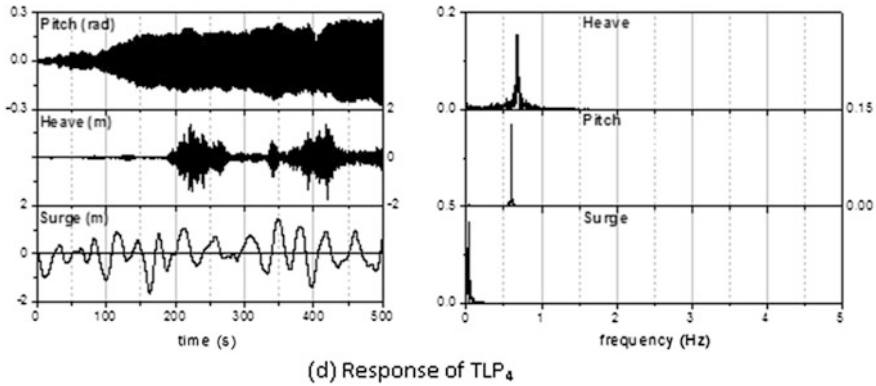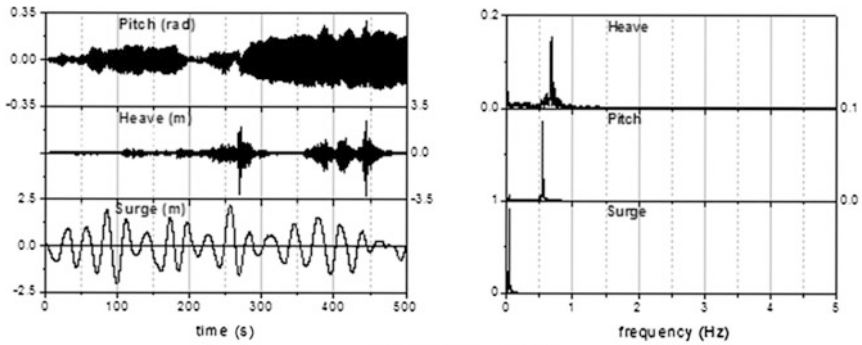
(d) Response of TLP₄

Fig. 7.17   (continued)

response makes square TLPs more prone also to fatigue failure due to repeated build-up and decay of tether forces. Heave response under non-impact waves, which is clearly a springing response, poses a threat to the platform stability since they occur closer to the natural frequency of heave degree of freedom causing a near resonating case. Triangular TLPs showing lesser response in comparison to square in this front make them more attractive for deepwater conditions. The response in surge degree of freedom does not show any such undesirable phenomenon under the influence of impact and non-impact waves as well probably because of its high degree of compliancy.

7.17   Significance of Springing and Ringing Response

As such, ringing and springing response, occurring at the natural frequency of one of the stiff degree of freedom, say heave, can endanger the stability of the platform (Pilotto et al. 2002, 2003; Pilotto and Ronalds 2003). In addition, ringing can not only cause a total breakdown of these platforms even in moderate storms but also can hamper daily operations and lead to fatigue failure. The variations in dynamic response with respect to water depth and tether tension are presented by showing their influence on springing and ringing response. While some of these observations are already noticed in case of square TLPs, the amount of change in the response has been quantified in this study apart from presenting their influence on platform geometry. Note that the choice of equivalent triangular TLPs as an example highlights the vulnerability of heave motion characteristics of the stiff system.
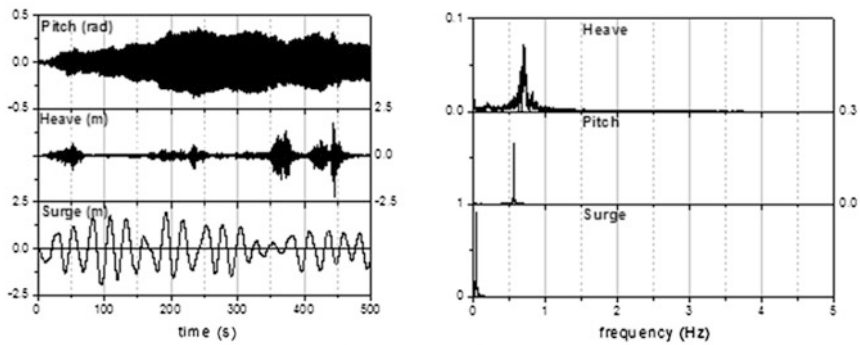
Some of the specific conclusions that can be drawn from the study are as follows: (i) impact waves cause ringing response in pitch degree of freedom in both the geometries; (ii) increased tether tension enhances pitch response in both the geometries under impact waves, but this enhancement is less in triangular TLP

(a) Response of TLP$_1$
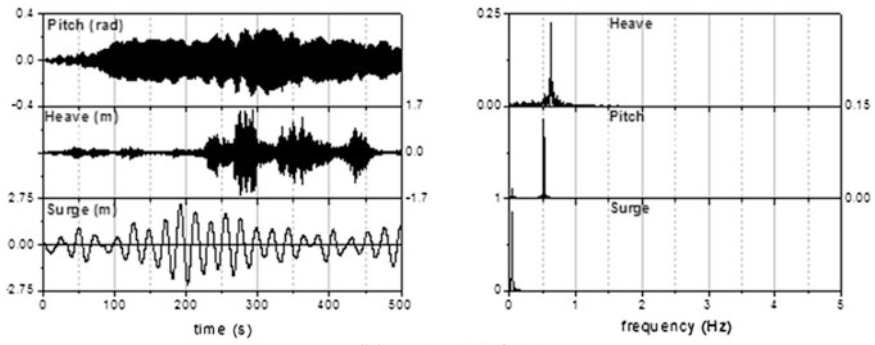
(b) Response of TLP$_2$

(c) Response of TLP$_3$

Fig. 7.18 Response of square TLPs to non-impact waves (total T_0 same)
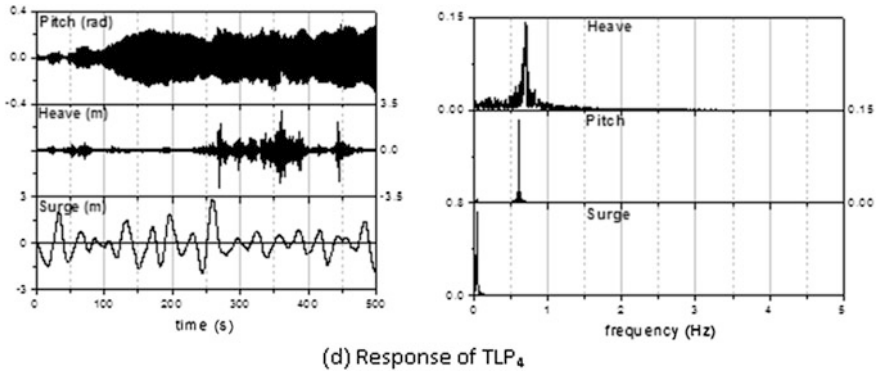
(d) Response of TLP$_4$

Fig. 7.18 (continued)

(with same T_0 case) compared with square; (iii) increase in water depth enhances pitch response due to impact waves for both geometries of TLPs, but this increase is less in triangular TLPs compared to square ones; (iv) pitch response in triangular TLPs (T_0 per tether same case) under impact waves are much reduced as compared to square, and it is further reduced for triangular TLP with total T_0 same as square; (v) the broad band in frequency response of heave degree of freedom under non-impact waves, occurring near to its natural frequency of TLPs of both geometries, is attributed to springing; (vi) heave response under non-impact waves decreases with increase in tether tension for same water depth in both the geometries, but it is further less in case of triangular TLPs; and (vii) beat phenomenon noticed in heave response of square TLPs under non-impact waves is not seen in triangular TLPs.

7.18 Stability Analysis of Offshore Triceratops

Mathieu stability equations are very commonly used to assess conditions of stability of several systems namely: (i) flexible structures; (ii) circuits with varying resistance in electrical field; (iii) moored compliant structures; and (iv) columns under varying axial forces, etc. (Simos and Pesce 1997; Mathieu 1868). Stability chart proposed by them represents a conditional solution for Mathieu's equation as general solution cannot be obtained. This is due to the fact that Mathieu parameters are case-specific. Patel and Park (1991) investigated Mathieu stability of tethers considering them as simply supported columns with constant tension along its length. They excluded nonlinear damping and formulated the governing equation using Galerkin's technique, which resulted in Mathieu equation. Even though
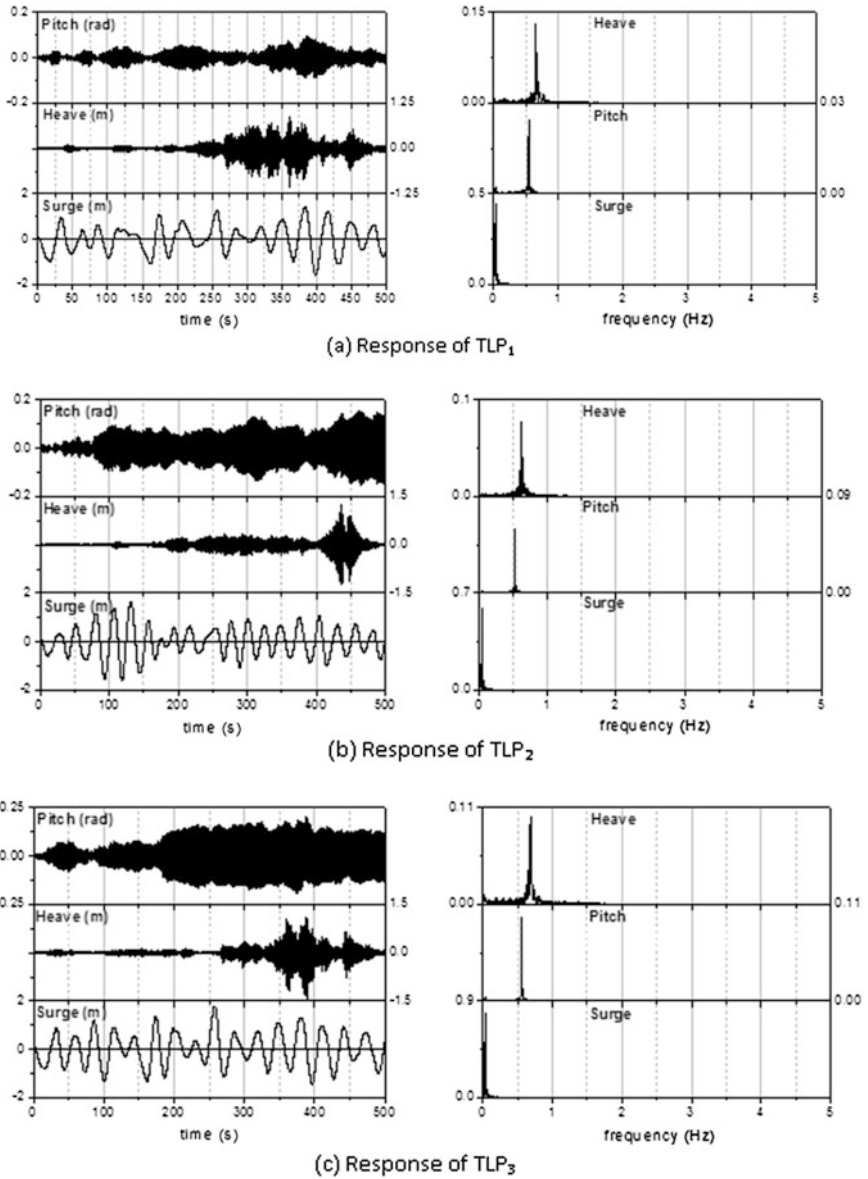
(a) Response of TLP$_1$

(b) Response of TLP$_2$

(c) Response of TLP$_3$

Fig. 7.19 Response of equivalent triangular TLPs to non-impact wave (total T_0 same)
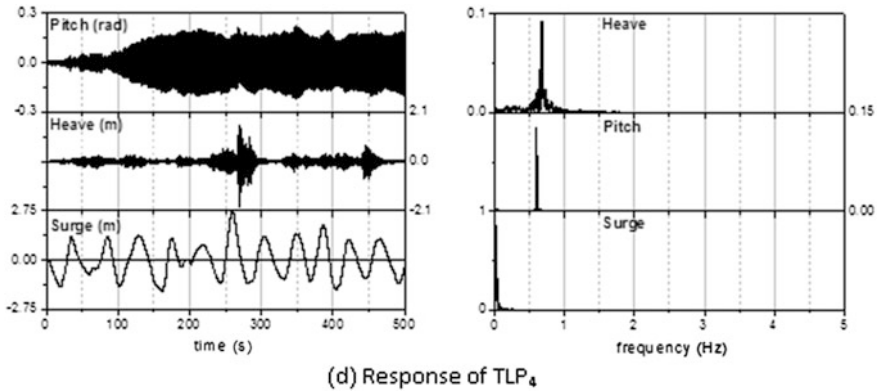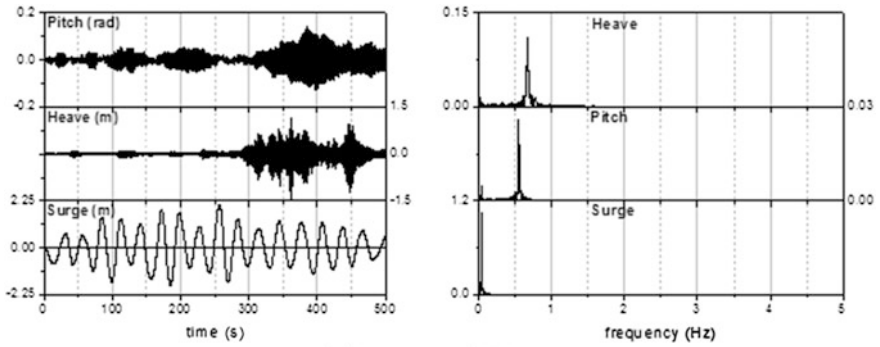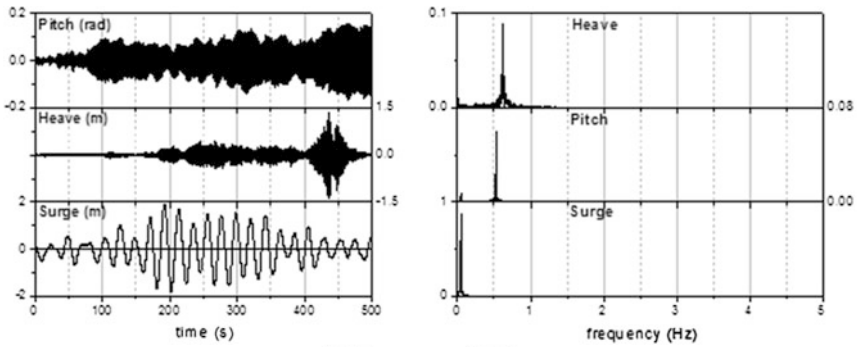
(d) Response of TLP₄

Fig. 7.19 (continued)

stability charts for small parameters exists (Ince 1925; Goldstein 1929), Mathieu stability charts are extended to large parameters using perturbation method and Runge-Kuttta method as compliant structures exhibit large range of values for Mathieu functions.

Stability analysis of Hutton TLP is presented using this extrapolation technique, which showed the satisfactory application of Mathieu stability (Haslum and Faltinsen 1999). Recent studies on Mathieu stability of spar platforms showed that instability occurs when the pitch natural period is twice of that of the heave period (Rho et al. 2002, 2003; Koo et al. 2004). Simos and Pesce (1997) generated a dynamic model for Mathieu equation for TLP tethers using a linear cable equation. They considered tension variation due to the submerged mass as a vital input for the lateral vibration of tethers. Stability analysis of Auger and Hutton TLP were carried out and compared with the constant tension model by Patel and Park (1991). Auger TLP tethers are found to be unstable in the first mode of vibration. Chandrasekaran and Jain (2002) presented the dynamic model of the coupled degree of freedoms for triangular and square configuration TLPs under regular waves. They showed the necessity for detailed tether analysis to assess the suitability of modified geometric form under deepwater. Chandrasekaran et al. (2006) illustrated the stability of TLPs of different geometric configurations under varied water depth. They also highlighted the effect of coefficient of inertia (C_m) in Mathieu stability and showed that lesser pretension in tethers shall lead to instability. It is also explicitly shown that triangular configuration TLPs are more stable compared to that of square TLPs in the first mode of vibration. It was also concluded that increase in the inertia coefficient leads to more hydrodynamic mass and hence increase the stability.
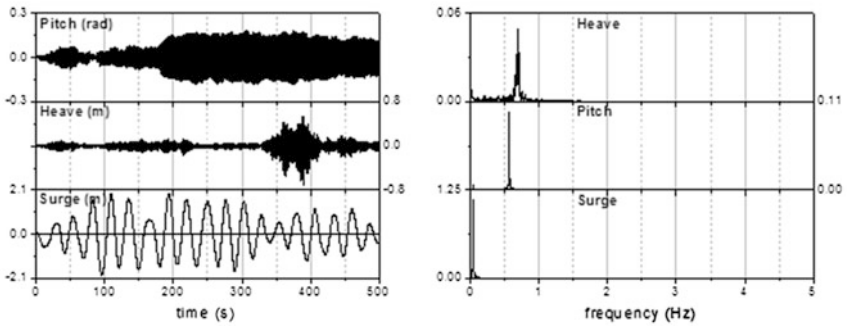
Triceratops consists of a triangular deck and three buoyant legs, which are position restrained using group of high pretensioned tethers. Buoyant legs are connected to the deck using ball joints, which restrains transfer of rotational degrees of freedom from the buoyant legs to the deck. White et al. (2005) introduced the

(a) Response of TLP₁

(b) Response of TLP₂

(c) Response of TLP₃

Fig. 7.20 Response of equivalent triangular TLPs to non-impact waves (total T_0 same)

new concept of triceratops in offshore platforms. Chandrasekaran et al. (2010) studied the Recent studies showed that dynamic response of the deck of triceratops under environmental loads is lesser than that of the buoyant legs, making it suitable for deepwaters (Chandrasekaran et al. 2010; White et al. 2005). Chandrasekaran et al. (2013) showed that triceratops exhibit more stiffness in the
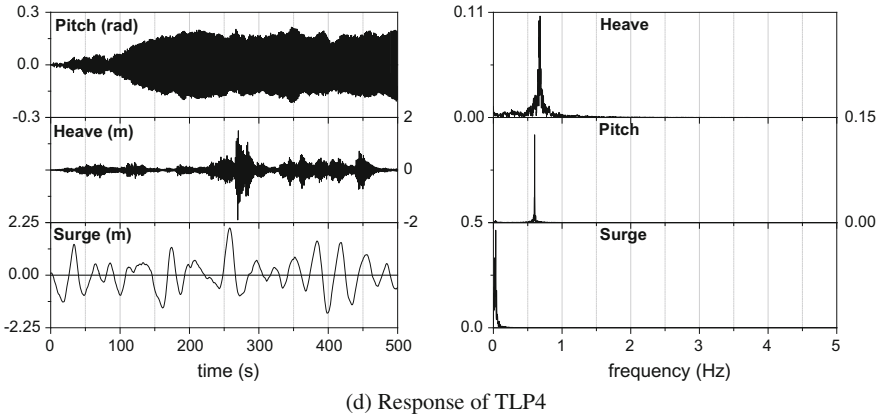
(d) Response of TLP4

Fig. 7.20 (continued)

vertical plane (heave motion) under aerodynamic loads; yaw motion is significantly low due to the ball joints. Numerical investigations on the response of triceratops under seismic loads using Kanai-Tajimi power spectrum showed that tension variation in tethers imposed significant response in deck and BLS (Chandrasekaran and Madhuri 2013). Stability analysis of TLP tethers under vortex-induced oscillation under lock-in condition is efficiently handled using incremental harmonic balance method to assess the stability using Floquet theory.

Dynamic equation of tether vibration is formulated using an idealized linear model. This is similar to that of the straight slender column, which is simply supported at ends under varying axial tension caused due to its varying submerged mass. Ignoring flexural rigidity and current effects, dynamic equation for the lateral movement of tether is given by

$$M\frac{\partial^2 y}{\partial t^2} - \frac{\partial}{\partial x}\left[T(x).\frac{\partial y}{\partial x}\right] + Bv\left|\frac{\partial y}{\partial t}\right|.\frac{\partial y}{\partial t} = 0 \tag{7.20}$$

where M is the total mass of the tether, which is the sum of added mass and physical mass (m) per unit length. $T(x)$ is the total tension in the tether, which is the sum of static tension (due to pretension (P) and submerged weight). Bv is the viscous damping coefficient. A is the tension amplitude from the heave motion of the hull due to wave and ω is the wave frequency. Dynamic tension due to the heave motion of the hull is given by

$$T(x) = P + \mu g(L - x) - A\cos(\omega t) \tag{7.21}$$

In the above equation, static tension is indicated by the first two terms and dynamic tension by the last term. Equation (7.21) is similar to the Sturm–Liouville problem, which can be solved by transforming into a Bessel equation by
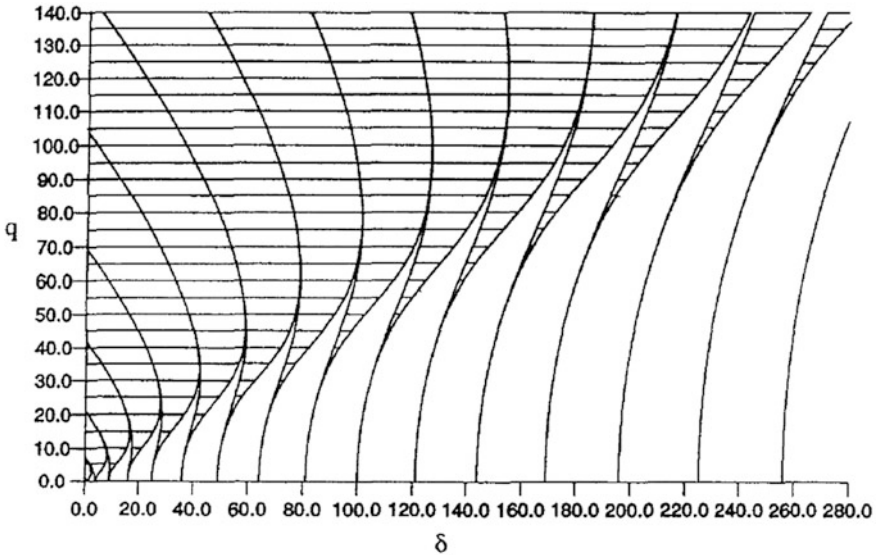
Fig. 7.21 Mathieu stability chart up to large parameters

introducing a variable (η). Solutions are obtained in terms of Bessel functions and Mathieu parameters are obtained for nth mode of vibration. Tether stability depends on the region in which the Mathieu functions lies; shaded regions show instability. Figure 7.21 shows the stability chart extended to large parameters (Patel and Park 1991).

Figure 7.22 shows details of numerical model of offshore triceratops considered for the study. A set of 12 tethers is used to anchor the structure to the seabed, which is grouped into three. Ball joints are used to connect the buoyant legs with that of the deck. Ball joints are capable of restraining rotational displacements but transfer translational displacements from the buoyant legs to the deck. Hence, stiffness in the vertical plane, similar to that of a TLP is achieved (by not restraining heave transfer) and compliancy in the horizontal plane is maintained (by not restraining surge/sway transfer). Table 7.9 shows the structural details of the platform.

7.18.1 Postulated Failure

Postulated failure case of allowing increase in payload, to ascertain its influence on tether tension variation and its possible failure is one of the ways of estimating the stability loss of the platform using Mathieu's stability charts. Six different cases with the increased payload are analyzed for tether tension variation using ANSYS AQWA under regular waves for (5 m, 6.8 s), which corresponds to the operational sea state of deep-water platforms. Maximum tension in each tether is
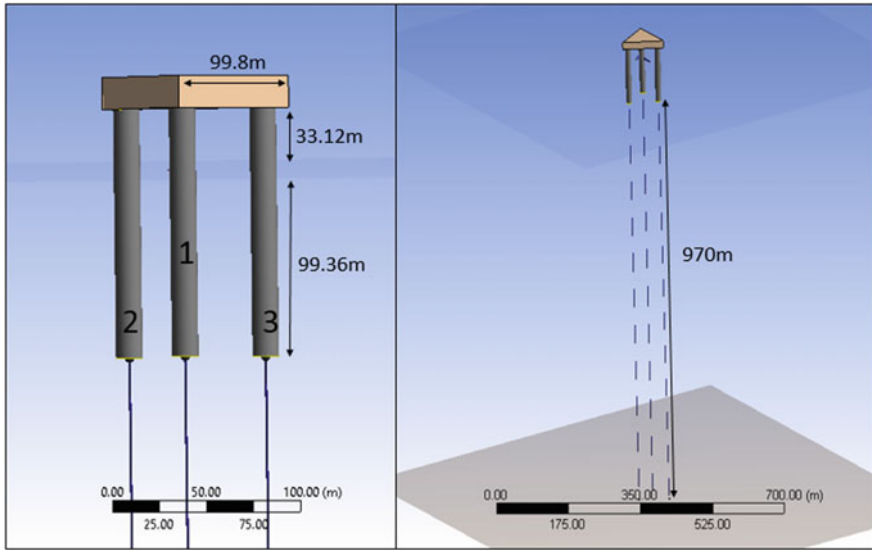
Fig. 7.22 Numerical model of offshore triceratops

Table 7.9 Properties of
triceratops

Description	Triceratops	Units
Water depth	1069.36	m
Total mass	320,500	kN
Buoyant force	470,440	kN
Diameter of buoyant leg	14.14	m
Plan dimension	99.40	m
Freeboard	33.12	m
Draft	99.36	m
Length of buoyant leg	132.48	m
Total tether force	149,940	kN
Pretension in one tether	12,495	kN
Tether length	970	m
No of tethers	12	
AE/L	57,623	kN/m

obtained and given in Table 7.10. Table 7.11 shows the maximum tension variation
in each buoyant leg of triceratops due to additional payload cases. It is seen from
the table that tension variation for Case 1 (with no additional increase in the
payload) is about 11%, which is within the desired tension variation limits. It is also
seen that tension variation increases with the increase in payload. For increase in
payload more than 15%, tension variation is close to double of its original value.
A maximum of 3.53 times of that of the initial pretension is observed for Case 6,
which has an additional payload of about 25%.

Table 7.10   Total mass and reduced pretension

Description	Case 1	Case 2	Case 3	Case 4	Case 5	Case 6
Payload added	–	5%	10%	15%	20%	25%
Total mass (kN)	320,500	336,525	352,550	368,575	384,600	400,625
Total tether force (kN)	149,940	133,915	117,890	101,865	85,840	69,815
Tether force in one leg (kN)	49,980	44,638.33	39,296.67	33,955	28,613.33	23,271.67
Pretension in each tether (kN)	12,495	11,159.58	9824.17	8488.75	7153.33	5817.92
% reduction in pretension	–	10.69	21.37	32.06	42.75	53.44

Table 7.11   Maximum tension variation

Description	Maximum cable force in each leg (4 tethers on each leg) (kN)			Initial tension in each leg (kN)	% Tension variation
	1	2	3		
Case 1	52,553.79	55,597.19	54,621.80	49,980.00	11.24
Case 2	50,654.59	63,001.71	62,499.94	44,638.33	41.14
Case 3	58,246.68	62,917.30	58,818.79	39,296.67	60.11
Case 4	66,335.85	78,912.74	72,455.49	33,955.00	132.40
Case 5	101,928.18	83,372.34	90,697.14	28,613.33	256.23
Case 6	105,323.30	94,725.30	92,779.21	23,271.67	352.58

Reduction in pretension resulted from the increased payload for Case 1 is about 10.69%. Decrease in pretension induces more response in the structure, which is reflected in the tether tension variation. Similarly, 25% increase in payload leads to a reduction of pretension by about 53% (as seen in Case 6), which resulted in maximum response and tether tension variation. It is evident from these preliminary set of studies that even accidental increase in payload can result in significant change in tether tension, causing instability to the platform. Apart from challenging its complaint features, operability will also be challenged. To determine whether tethers undergo parametric oscillation, Mathieu parameters are estimated under different postulated failure cases to assess the stability condition.

7.18.2   Mathieu Stability Under Postulated Failure

Dynamic analysis of the platform under postulated failure cases is carried out to obtain Mathieu parameters. Dynamic tension amplitude is estimated from the maximum tension variation for each case and Mathieu parameters are obtained; results are given in Table 7.12 while the corresponding points are also plotted in the stability chart, as shown in Fig. 7.23. Points lie within the shaded region show that

Table 7.12 Mathieu parameters under postulated failure	Description	Mathieu parameters		Stability condition
		δ	Q	
	Case 1	73.96	3.73	Stable
	Case 2 (5%)	66.86	12.21	Stable
	Case 3 (10%)	59.77	15.73	Stable
	Case 4 (15%)	52.69	30.01	Unstable
	Case 5 (20%)	45.62	49.12	Unstable
	Case 6 (25%)	38.46	55.18	Unstable
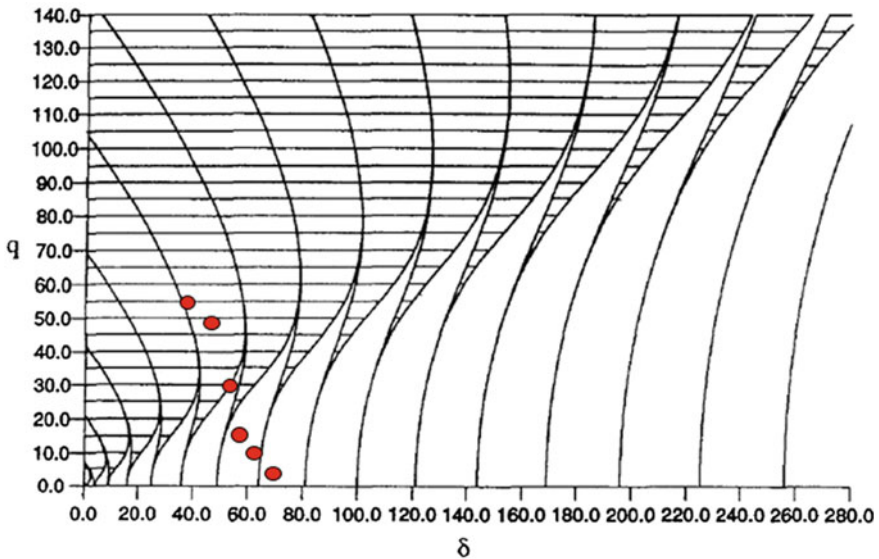
Fig. 7.23 Stability chart for triceratops tether under postulated failure

they are stable. From the Mathieu stability analysis, it is seen that for the postulated failure Case 1, platform is under stable condition. This is also in good agrement with that of the interpretation made from the numerical studies. For Case 2, stability analysis shows stable condition where as phase plots show instability. 5% increase in payload decreased the stability parameter (δ) by 9.6% and increased the stability parameter (q) by 3.27 times. As payload increases, stability parameters move toward the lower regions of instability as seen in Case 4. Even small changes in the stability parameters lead to a significant stable or unstable region. For Case 3 and Case 4, the increase in stability parameter (δ) is 11.85% where as another parameter (q) is increased by 90%. This shows a nonlinear dependence of both the parameters under the postulated failure cases considered for the study.

7.18.3   Summary

Stability assessment of triceratops is presented for the postulated failure cases by increasing the payload on the deck. Detailed numerical analyses are carried out to obtain the Mathieu stability parameters for triceratops, which is novel. It is seen from the studies carried out that increase in payload reduces the pretension in cables, which leads to instability. Since tether tension variation is significant for determining the stability of tethers, it is necessary to do Mathieu stability analysis for tethers under postulated failure cases. It is also interesting to note that unstable response of the platform may or may not cause Mathieu instability in tethers. A few cases under consideration showed that the platform was unstable even before tethers showed instability. It is therefore vital to ascertain stability of platform, independent of tether instability under the postulated failure cases.

7.19   Design of Suppression Systems for Vortex-Induced Vibration (VIV)

Vortex-shedding is a phenomenon that occurs over bluff bodies subjected to sustained currents, which might result in large transverse motions (Humphries and Walker 1987). When a flowing medium strikes a non-streamlined bluff object, it moves around the object generating alternating pressure forces on either side of the bluff body. This results in the formation of vortices, causing periodic forces, which are strong enough to set the body into oscillatory motion. Vortex-Induced Vibration (VIV) are the outcome of such exciting forces that are generated by vortex-shedding on hull of a bluff body, causing response closer to the resonant period (Anagnostopoulos and Bearman 1992; Bearman 1984). Experimental investigations carried out on elastically mounted cylinder showed wake formation with the maximum amplitude occurring near lower limit of lock-in region. Due to VIV, structure undergoes a number of stress cycles leading to fatigue damage. Based upon the significant consequences of VIV on several mechanical systems and ocean engineering structures, VIV suppression configurations are encouraged (Sarpkaya 1978). Observation of large amplitude responses of systems that used water as working fluid necessitates the importance of VIV suppression by design (Khalak and Williamson 1991; Zdravkovich 1981). While a number of suppression techniques of VIV suppression are successfully developed, cost and difficulty of implementation restricted their applications (Owen and Masa 2003). In view of suppressing VIV, use of helical strakes proved to be effective in strengthening the cylinder to resist larger bending moments that result from the increased drag. Under close examination of flow behind a pair of cylinder, pair of anti-phase streets and in-phase shedding can cause the formation of a single wake in large scale (Govardhan and Williamson 2000; Brika and Laneville 1993). Their applications in marine risers by modeling them, as flexible cylinders are quite successful.

Normalized vortex-shedding frequency, which is represented by Strouhal number is affected by various flow velocities (Lesage and Garthshore 1987). An application example on experimental investigations of a rigid cylinder, resembling hull of a Spar platform is presented.

Flow around a cylinder is one of the classical topics in field of hydrodynamics (Mutlu and Jorgen 2003). Models proposed by several researchers consider rigid circular cylinder with a single degree of freedom in the cross-flow direction (Gabbai and Benaroya 2005; Rodolfo et al. 2011). Experimental investigations carried out on long, flexible cylinders indicated the formation of vortex-induced motion in the form of hysteresis loop motion in which contributions are seen from each of the vortex-shedding modes (Chandrasekaran and Marin 2016). Amongst various methods proposed to suppress VIV, strakes and shrouds are found to be effective regardless the orientation of structure to waves and current; but showed a substantial increase in drag, resulting in high drift. When strakes or bumps are fixed, no regular shedding is observed on the wake side of the cylinder, while major advantage is effective suppression of amplitude of vibration of the cylinder. Recent studies also show the possibilities of suppression of vibration of multiple cylinders using rough strip (Blevins 1994). A few analytical and numerical investigations of VIV on cylinders with low mass and aspect ratio are helpful in modeling wake oscillations and force decomposition, resulting from VIV suppression systems. Alternatively, force reduction is also achieved by providing an outer perforated cover, which alters fluid flow around cylinders in flow regime.

7.19.1 Experimental Investigations

Experimental investigations are carried out by idealizing cylinder as a single degree of freedom system; model is set free along the left direction. While mooring system is modeled as a spring system in the towing tank, scaled model is fabricated and tested to evaluate to fluid–oscillator interaction. Total length of specimen is 1080 mm including a draft of 917 mm and clear height. The experimental setup is shown in Fig. 7.24. A cylinder of diameter 101.6 and 2 mm thickness is sealed at the bottom to make it watertight. The Test setup is connected to the carriage of towing tank, where the specimen is clamped to the carriage. Towing tank carriage is moved at the required velocity in a still water medium. Considering the fact that motion amplitude and drag force rely on the relative motion between the test section and fluid medium and not on the physical fluid flow, test section is moved during experimental studies while water remains stationary. First set of tests are conducted on a plain cylinder of unit mass ration, without any VIV suppression systems. Tests are conducted for velocities ranging from 0.2 to 1.2 m/s at an interval of 0.02 m/s. Amplitude of transverse vibration is measured using LVDT with its probe connected to the towing carriage on which cylinder is clamped.

A passive method of VIV suppression is attempted. Two steel wires are fixed parallel to the axis of the cylinder to miniature turnbuckles and stretched over small
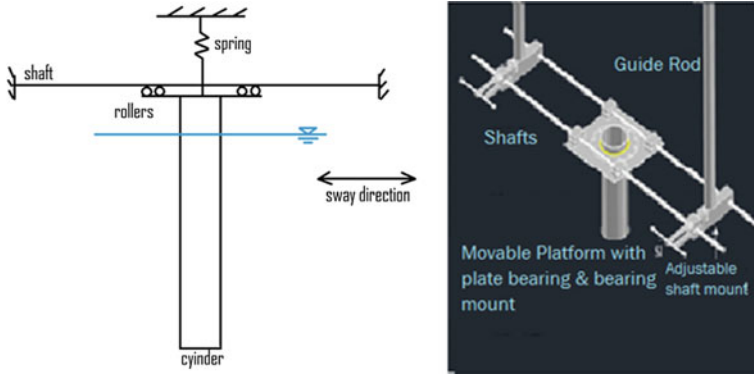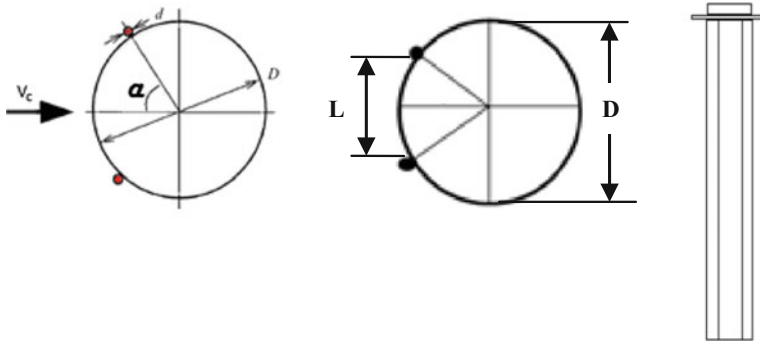
Fig. 7.24 Experimental set up

Fig. 7.25 Vertical stripping wires attached to cylinder

notches at the ends of the cylinder. Sufficient tensile load is applied to keep the wire in tension so that it rests against the cylinder wall; no glue or other adhesive is used to fix the wire against the cylinder, see Figure 7.25 for details. Steel wires of 0.3 mm in diameter are fixed at different angles (α) with respect to the stagnation point to achieve diameter ratio (d/D) of 0.003. Tests are repeated by attaching wires at different angles varying from 40° to 80° at an interval of 10°. Alternatively, helical wires of diameter 0.3 mm are wrapped around the cylinder in a helical configuration, as shown in Fig. 7.26. Experimental investigations are then carried out to assess the influence of pitch of helical strakes on VIV suppression; strakes are fixed to the cylinder at different pitch of 5D, 7D, and 10D, where D is the diameter of the cylinder.

Response amplitude of bare cylinder over a wide range of reduced velocity is shown in Fig. 7.27. It is seen from the figure that at lower reduced velocity, cylinder barely moves. With the increase in reduced velocity, lock-in phenomenon occurs and response of cylinder increases significantly. It is seen that at a reduced

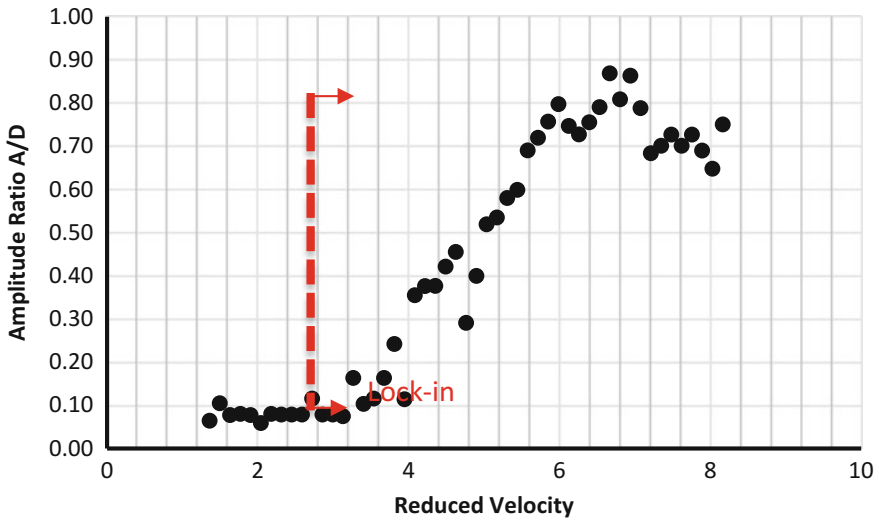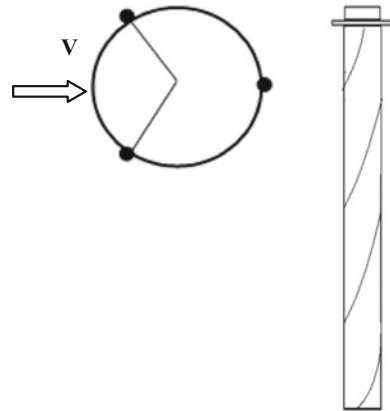Fig. 7.26 Helical stripping
wires attached to cylinder

Fig. 7.27 Amplitude ratio of bare cylinder for different velocity

velocity of 6.668 (current velocity 0.98 m/s) maximum response occurred ($A/D = 0.87$). This is attributed to the fact that the cylinder undergoes vibration in the transverse direction, whose magnitude is almost equal to its own diameter. By attaching tripping wires, turbulence is generated within the laminar boundary layer. Such protrusions or attachments on the surface of the bluff body have considerable effect on vortex-induced formation process and resulting oscillations of the cylinder. Figure 7.28 shows the response behavior of cylinder attached with the vertical wires. Satisfactory results are achieved when tripping wires are attached 50° with respect to the stagnation point. It is seen that maximum response ratio (A/D) is reduced to about 71% in comparison to that of a bare cylinder. It is also seen that
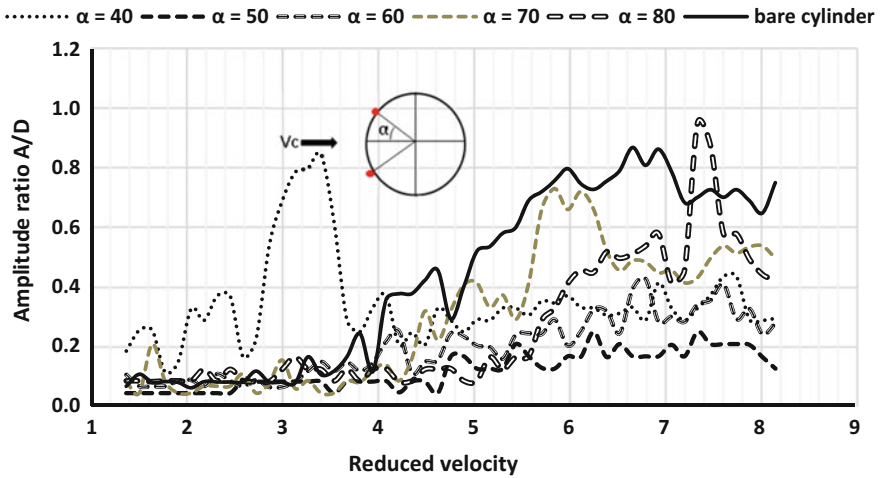
Fig. 7.28 Comparison of VIV suppression using vertical tripping wires

vibration is suppressed effectively throughout the chosen range of velocity. Tripping wires fixed at 40° show response at higher end of reduced velocity whereas cylinders attached with 80° show low response at the lower end of reduced velocity.

Since vertical wires are unidirectional with respect to the flow direction, investigations are also carried out by attaching helical wires at different pitch. It is expected to have a better suppression under all flow directions. Figure 7.29 shows the comparison of VIV suppression using helical wires at different pitch. Plots show
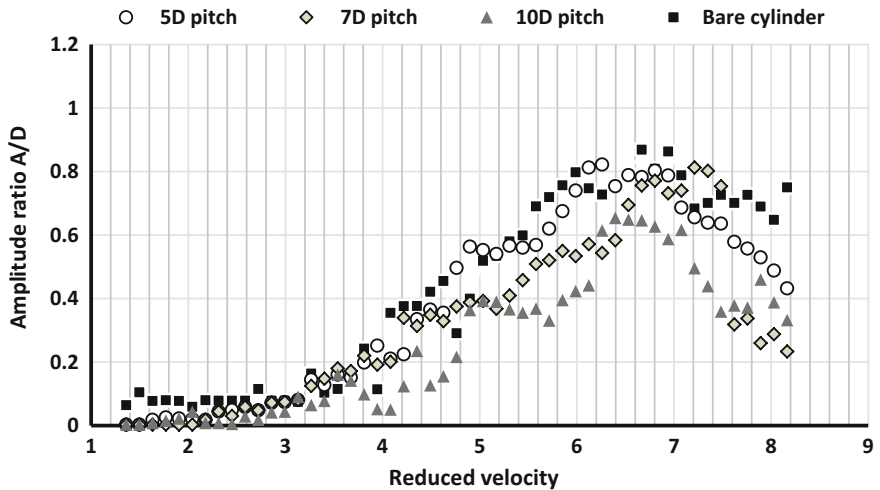

Fig. 7.29 Comparison of VIV suppression using helical wires

Table 7.13 Comparison of VIV suppression systems

Description	Area under the curves	Maximum amplitude ratio
Bare cylinder	2.970	0.8685
VIV suppression using vertical tripping wires		
40°	2.378	0.8454
50°	0.818	0.2478
60°	1.356	0.4259
70°	2.069	0.7304
80°	1.79	0.9499
VIV suppression using helical wires		
5D pitch	2.7691	0.8221
7D pitch	2.2728	0.8124
10D pitch	1.807	0.6538

a common trend of behavior but the peak response and the velocity, at which lock in occurs, vary slightly. As seen from the plots, one of the most effective arrangements shall be a set of three wires wound at a pitch of 10D. In this case, response amplitude is reduced about 25% in comparison to that of a bare cylinder. Lock-in region starts at a reduced velocity of 4.89. As each configuration has a different pattern of suppression, overall benefits of different modifications are quantified by considering area under the curve. Table 7.13 shows comparison of both the suppression systems considered in the study. It is seen that vertical wires attached at 50° show the best reduction in amplitude while in helical arrangement, wires wrapped at 10D showed the minimum response.

7.19.2   Summary

Presented example study demonstrated the necessity of VIV suppression and methods of force response reduction of cylinders under vortex-induced motion. Under the action of steady flow, bare cylinder undergoes a transverse vibration whose amplitude becomes almost equal to its diameter. Presented example study confirms the effectiveness of tripping wires in VIV suppression through detailed experimental investigations. When wires are arranged vertically, flow separation point has an important role in vibration. As the angle between wires with respect to that of the stagnation point increases, lock-in point is shifted toward higher reduced velocity. Vertical wires, when placed at 50° and 60° are found to be effective in VIV suppression. This has a practical application where a prominent current direction prevails. Helical configuration is symmetric with respect to the wave approach, which can therefore provide effective suppression irrespective of the flow direction. Out of helical configurations tested, wires placed at pitch equals 10 times of the diameter of the cylinder showed maximum suppression.

7.20 Dynamic Analyses of Buoyant Leg Storage and Re-gasification Platform: Experimental Investigations

Environmental loads encountering offshore compliant structures are more severe in deepwater in addition to the complexities that arise during their installation. As existing platforms showed serious limitations in terms of storage space, geometric form of offshore compliant platforms needs special attention (ABS 2014). Recent studies showed that transporting LNG for longer distance to onshore imposes heavy penalty in terms of cost and other environmental issues (Lloyd's Register 2005). It is therefore imperative to reduce the transport cost by processing LNG offshore by deploying large storage and re-gasification units adjacent to the production wells. Buoyant Leg Storage and Re-gasification Platform (BLSRP) is relatively a new structural form proposed to store and process LNG offshore (Lognath 2017). Proposed platform consists of a deck, which is connected to six buoyant legs through the hinged joints while the buoyant legs are connected to the seabed using taut mooring tethers. The conceived structural form is a hybrid concept, which restrains transfer of both rotational and translational responses from the buoyant legs to deck and vice versa. Taut moored tethers and deep-draft buoyant legs resemble the behavior of Tension Leg Platform (TLP) and Spar, respectively. Present research deals with the analysis, design, and development of BLSRP.

In the offshore location, gas is liquefied and transported near shore for re-gasification, which is an alternative to transporting through pipelines. Transfer of natural gas through subsea pipelines s expensive and hazardous to ocean environment; they have high probability of oil spill and pipeline leaks (ABS 2004). Buoyant legs are alternate structural forms of Spar platforms as they are positively buoyant with deep draft. The proposed platform consists of a deck, which is connected to six Buoyant Leg Structures (BLS) through the hinged joints. Buoyant legs are connected to the seabed using taut mooring tethers. The conceived structural form is a hybrid concept, which restrains transfer of both rotational and translational responses from the buoyant legs to the deck and vice versa. One of the main advantages is the improved functionality in terms of increase in the storage and processing facility of LNG. BLSRP is novel by its design (Chandrasekaran et al. 2015a, b). Deck is isolated from the buoyant legs by hinged joints. Advantages of hinged joints on compliant offshore structures are well demonstrated by various researchers in the recent past (Chandrasekaran et al. 2013; Chandrasekaran and Senger 2016). Hinged joints restrain the rotational motion from the buoyant legs to the deck, which enables a better recentering under wave loads (Chandrasekaran 2015a, b). On the other hand, larger response of the deck in the compliant degree of freedom like surge, sway, and yaw under wind loads shall not influence additional rotation to the buoyant legs due to the presence of hinged joints (Lognath 2017). One of the main operational requirements of LNG tankers is that degree of compliancy on the top side should be restrained to a larger extent (Chandrasekaran 2016a, b; Chandrasekaran and Jain 2016).

7.20.1 Experimental Investigations

Experimental investigations are carried out on a scaled model of BLSRP (1:150) under regular waves for 0° and 90° incident wave directions. Figure 7.30 shows the geometric view of the platform while the scaled model in its installed position is shown. Major components of BLSRP are deck, LNG tank, buoyant legs, hinged joint, and tethers. Structural details of BLSRP Prototype are shown in Table 7.14.

Initial pretension imposed on tethers is about 12% of that of the design draft, which is similar to that of any taut moored compliant structure like tension leg platform (TLP). Deck is connected to the buoyant legs by hinged joints. While the deck and hinged joints are of stainless steel, buoyant legs are fabricated using PVC, which is ballasted with sand to achieve the required draft and pretension in tethers. Stainless steel wire ropes are used as tethers, which are uniformly pretensioned to the desired level. A mild steel base plate, placed at the flume bed is used as the template to anchor the tethers.

While one end of tethers is connected to each buoyant leg and other end is connected to the base plate with top-tensioned taut mooring system. Six rollers are attached to the circumference of the base plate for guiding the mooring lines during installation and commissioning. Separate load cells are used to measure the tether tension variation in each leg. While piezoelectric accelerometers are used to measure translational responses, inclinometers are used to measure the rotational responses. A set of accelerometers and inclinometers are placed both on the deck and on each buoyant legs to record the responses under wave loads. Responses in all active degrees of freedom are measured at their local center of gravity of buoyant legs and deck.

Table 7.15 shows the results of free vibration tests carried out on the scaled model and prototype, during experimental and numerical studies, respectively. It is seen from the table that natural periods of BLSRP resemble any typical tethered compliant structure like TLP except showing relatively higher stiffness in yaw degree-of-freedom. Higher stiffness in yaw motion is attributed to the symmetric
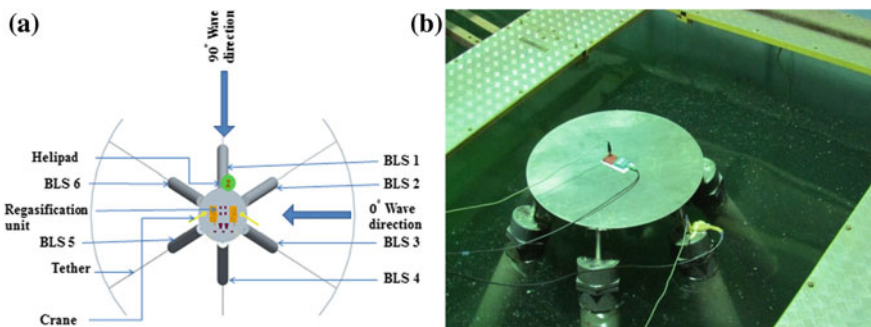

Fig. 7.30 Buoyant leg storage and re-gasification platform: **a** plan; **b** installed condition

Table 7.14 Structural details of BLSRP (Lognath 2017)

Description	Prototype	Units	Model	Units
Water depth	600	m	4000	mm
Mass of the structure	400,000	ton	118.51	kg
Utilities	10,000	ton	2.93	kg
Secondary deck plate	1250	ton	0.37	kg
Stainless steel tank	1800	ton	0.53	kg
LNG	25,000	ton	7.40	kg
Main deck plate	2500	ton	0.74	kg
BLS (6 no)	25,500	ton	7.55	kg
Ballast	333,950	ton	98.94	kg
Diameter of the BLS	22.50	m	150	mm
Length of the BLS	200	m	1333.33	mm
Diameter of the deck	100	m	666.66	mm
Draft	163.57	m	1117.73	mm
Meta-centric height	15.18	m	114.86	mm
Length of the tether	470.84	m	3138.93	mm
Initial Tether tension	8715.89	ton	2.50	kg
Deck				
I_{XX}, I_{YY}	2,530,725.50	ton m^2	33,326.42	kg mm^2
I_{ZZ}	4,729,752	ton m^2	62,284.8	kg mm^2
r_{XX}, r_{YY}	7.90	m	50.66	mm
r_{ZZ}	10.80	m	72	mm
Single buoyant leg				
I_{XX}, I_{YY}	85,147,115	ton m^2	1,121,278.81	kg mm^2
I_{ZZ}	1,159,825.3	ton m^2	15,273.41	kg mm^2
r_{XX}, r_{YY}	37.70	m	251.33	mm
r_{ZZ}	4.40	m	29.33	mm
Tether diameter	0.05	m	0.33	mm
Tether stiffness	875,741	N/m	0.03	N/mm
Height of the LNG tank	7	m	46.66	mm
Modulus of tether	2.1E+11	N/m^2	1400	N/mm^2

layout of the buoyant legs, which are independently spread at the bottom but closely connected to the deck. As hinged joints are under high axial force imparted by tethers, their moment-rotation characteristics vary compared to their behavior in the absence of axial force. It is very complex to capture this time-dependent behavior and incorporate it into the numerical model, which is influenced by the variable buoyancy of the legs. Discrepancies between the experimental and numerical studies, as seen in the estimate of natural periods and damping ratios are attributed to this effect.

Table 7.15 Natural periods of BLSRP

Description	Tethered BLSRP (experimental)			Numerical studies (prototype)			
	Natural period (s)		Damping ratio (%)	Free-floating		Tethered	
	Model	Prototype		Natural period (s)	Damping (%)	Natural period (s)	Damping (%)
Surge	9.21	112.76	8.12	–	–	118.50	8.55
Sway	9.26	113.37	8.30	–	–	121.00	8.45
Heave	0.28	3.42	3.50	3.21	3.64	3.18	3.65
Roll	0.33	4.04	6.44	4.15	6.50	–	–
Pitch	0.35	4.34	6.63	4.25	6.60	–	–
Yaw	4.90	59.97	7.12	–	–	–	–

Figure 7.31 shows the response of the platform for all the complete range of wave periods. It is seen from the figures that the deck response is significantly lesser than that of the maximum response in all active degrees of freedom. It can also be observed that responses of the deck and buoyant legs are symmetric with respect to abscissa with lesser residue indicating high recentering capabilities. This behavior is attributed to the restraint offered by the hinged joint, in both translational and rotational degrees of freedom. Differences in the responses of buoyant legs are due to the variable submergence effect, which is one of the primary sources of non-linearity in the excitation force. Table 7.16 shows the maximum values of response in all degrees of freedom for (0°, 0.1 m) wave data. By comparing the response amplitudes, it is seen that the response in the deck is appreciably lower than the maximum response of the buoyant legs in all degrees of freedom. Presence of hinged joints at each BLS unit isolates the deck from the legs and thus improves the operational comfort and safety of the platform. Presence of rotational responses in the deck, despite the presence of hinged joint, is due to the differential heave response that occurred from the dynamic tether tension variations. As buoyant legs are symmetrically spread with respect to the vertical axis of the platform, it is imperative to envisage a non-uniform phase lag in the recentering process; this causes the yaw motion on the deck. Roll response of the deck is about 60% lesser than that of the maximum response of the buoyant leg while heave response is about 40% lesser. Quantitative comparison of responses with that of the permissible values of that of compliant structures is not done due to the novelty of the chosen geometric form. Besides the rotational responses of the deck being lesser than that of the buoyant legs, still it remains a design challenge, which needs detailed investigations. It is also seen that the maximum tether tension variation is about 20%, which is within permissible limits (American Petroleum Institute 2005)
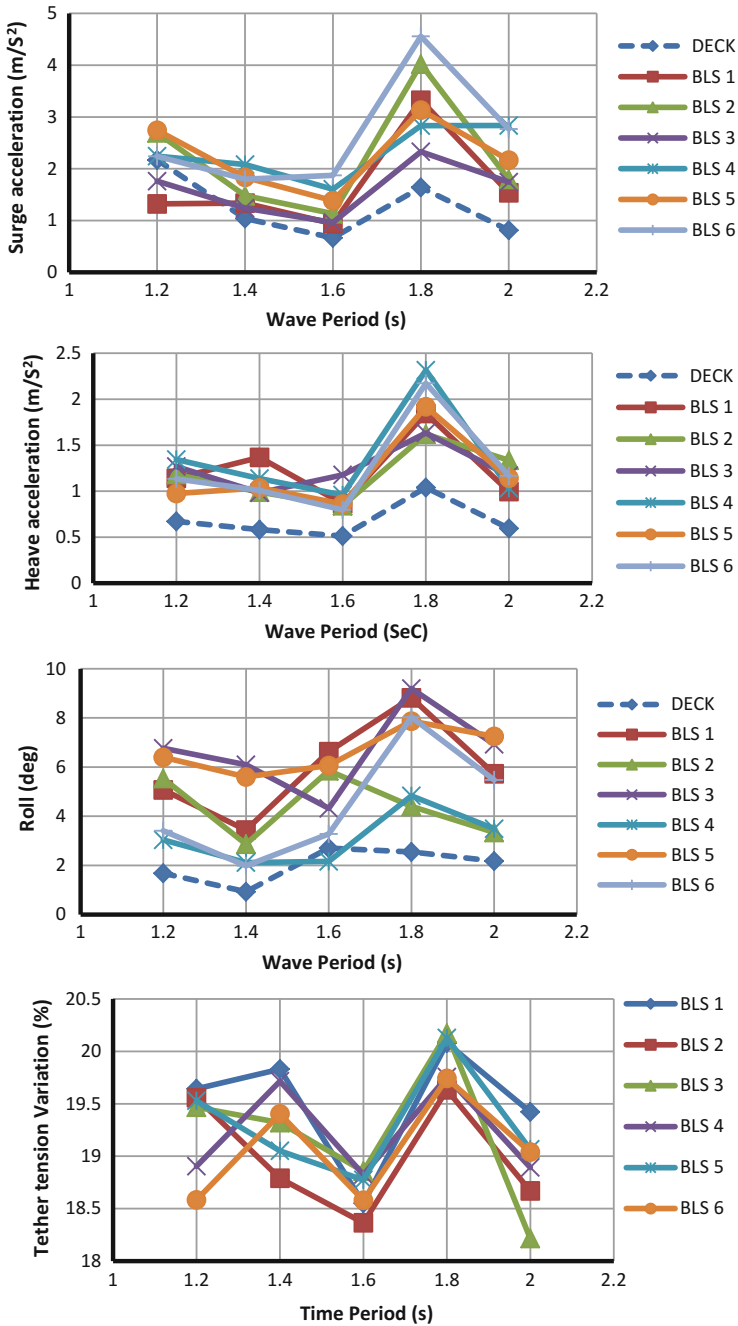
Fig. 7.31 Dynamic response of BLSRP under 90° wave heading

Table 7.16 Maximum response of BLSRP model (0°, WH = 0.1 m)

Description	Deck	BLS 1	BLS 2	BLS 3	BLS 4	BLS 5	BLS 6
Surge (m/s^2)	1.36	3.09	2.48	3.23	2.86	3.93	4.20
Sway (m/s^2)	1.27	3.03	1.82	2.46	2.18	2.73	3.62
Heave (m/s^2)	0.92	1.52	1.53	1.21	1.15	1.42	1.36
Roll (deg)	4.77	9.68	9.78	11.34	8.72	8.53	10.41
Pitch (deg)	6.05	9.31	9.31	11.22	10.31	8.72	12.02
Yaw (deg)	4.13	4.24	5.87	5.94	4.52	5.91	5.94

7.20.2   Summary

The conceived structural form is a hybrid concept, which restrains transfer of both rotational and translational responses from the buoyant legs to the deck and vice versa. The main advantage is the improved functionality in terms of increase in the storage and re-gasification capacity of the liquefied natural gas. Detailed experimental investigations showed that heave response of the deck is lesser in comparison with that of the buoyant legs. Presence of roll and pitch responses of the deck, despite the hinged joint at each Buoyant legs, is due to the differential heave response that occurred from the dynamic tether tension variations. Response of the deck is less influenced by the wave action on buoyant legs due to the presence of hinged joints. Hinged joints isolate the deck from buoyant legs and thereby improve operational comfort and safety of the platform. It is also observed that maximum variation in tether tension is within the permissible limits.

Exercise

1. Triceratops consists of _____ to achieve the required buoyancy, to support the deck structure, to restrain system and to serve storage requirements.
2. BLS   is   a   _____,   _____, _____ intended for use in ultra-deepwaters.
3. _____ is placed between the BLS and deck to reduce the rotational response of the deck when the BLS is exposed to wave, current and impact loads.
4. _____ is carried out analytically by subjecting the structure to zero wave amplitude and necessary initial conditions in the respective degree of freedom.
5. Write the Equation of motion for the free-decay test?
6. _____ in BLS units results in significant reduction in the pretension in tethers in comparison with that of TLPs.
7. Offshore   structures   exhibit   highly   intense   nonlinear   behavior   called _____ and _____.
8. Explain Springing and Ringing response of TLP's?

9. _____ of compliant structures like tension leg platforms (TLPs) under impact and non-impact waves responsible for ringing and springing phenomenon is of large interest to Marine Engineers.

10. A _____ event involves the excitation of transient structural deflections at/close to the natural frequency of the platform arising at third harmonic of the incident wave field.

Key to Exercise

1. Three or more buoyant leg structures (BLSs).
2. Positively buoyant, floating, deep-draft structure.
3. Ball joint.
4. Free-decay test.
5. Equation of motion for the free-decay test is as follows:

$$[M + Ma]\ddot{X} + [C]\dot{X} + [K]X = 0$$

where M is mass matrix; Ma is the added mass matrix, $[C]$ is the damping matrix, $[K]$ is the stiffness matrix at any instantaneous position and $\{\ddot{X}, \dot{X}, X\}$ are acceleration, velocity and displacement, respectively.

6. Permanent ballast.
7. Springing and Ringing.
8. Springing is caused in the vertical/bending modes by second-order wave effects at the sum frequencies; this behavior is common in both mild and severe sea states. Ringing is attributed to strong transient response observed in these modes under severe loading conditions triggered presumably by passage of a high, steep wave. This transient response further decays to steady state at a logarithmic rate depending on the system damping.
9. Dynamic response.
10. Ringing.

References

ABS (2014) LNG bunkering: technical and operational advisory. American Bureau of Shipping, Houston, TX, USA

ABS (2004) Offshore LNG terminals. American Bureau of Shipping, Houston, TX, USA

Adams AJ, Baltrop NDP (1991) Dynamics of fixed marine structures. Butterworth-Helneman Ltd., London

Adrezin R, Bar-Avi P, Benaroya H (1996) Dynamic response of compliant offshore structures-review. J Aerosp Eng 9(4):114–131

American Petroleum Institute (2005) Design and analysis of station keeping systems for floating structures, API recommended practice 2SK, 3rd edn. USA

Anagnostopoulos P, Bearman PW (1992) Response characteristics of a vortex-excited cylinder at low reynolds numbers. J Fluids Struct 6:39–50

Anagnostopoulos SA (1982) Dynamic response of offshore structures to extreme waves including fluid-structure interaction. Eng Struct 4:179–185

API-RP 2A-WSD (2000) Recommended practice for planning, designing and constructing fixed offshore platforms. American Petroleum Institute, Washington, D.C.

ASTM (2005) Rain-flow counting method. ASTM E 1049-85

Bai Y (2001) Pipelines and risers. In: Elsevier ocean engineering book series, vol 3. Elsevier, Amsterdam

Bar-Avi P (1999) Nonlinear dynamic response of a tension leg platform. J Offshore Mech Arct Eng 121:219–226

Basim MB, Johnson C, Philip J, Roesset M (1996) Implication of tendon modeling on nonlinear response of TLP. J Struct Eng 122(2):142–149

Bathe KJ, Wilson EL (1987) Numerical methods in finite element analysis. Prentice Hall, New Delhi

Bea RG, Xu T, Stear J, Ramas R (1999) Wave forces on decks of offshore platforms. J Waterw Port Coast Ocean Eng 125(3):136–144

Bearman PE, Russell MP (1996) Viscous damping of TLP hulls. In: Managed program on uncertainties and loads on offshore structures (ULOS), Project Report, Imperial College

Bearman PW (1984) Vortex shedding from oscillating bluff bodies. Annu Rev Fluid Mech 16:195–222

Bhattacharyya SK, Sreekumar S, Idichandy VG (2003) Coupled dynamics of Sea Star mini tension leg platform. Ocean Eng 30:709–737

Blevins RD (1994) Flow induced vibration, 2nd edn. Krieger Publishing, Malabar, FL

Boaghe OM, Billings SA, Stansby PK (1998) Spectral analysis for non-linear wave forces. J Appl Ocean Res 20:199–212

Booton M, Joglekar N, Deb M (1987) The effect of tether damage on tension leg platform dynamics. J Offshore Mech Arct Eng 109:186–192

Brika D, Laneville A (1993) Vortex-induced vibrations of a long flexible circular cylinder. J Fluid Mech 250:481–508

Bringham EO (1974) The fast fourier transform. Prentice Hall, Englewood Cliffs, NJ

Buchner B, Bunnik T (2007) Extreme wave effects on deepwater floating structures. In: Proceedings of offshore technology conference, OTC 18493, Houstan, Texas, 30 Apr–3 May

Buchner B, Wichers JEW, de Wilde JJ (1999) Features of the state-of-the-art deepwater offshore basin. In: Proceedings of offshore technology conference, OTC 10841, Houstan, Texas, 3–6 May

Burrows R, Tickell RG, Hames D, Najafian G (1992) Morison wave forces co-efficient for application to random seas. J Appl Ocean Res 19:183–199

Capanoglu CC, Shaver CB, Hirayama H, Sao K (2002) Comparison of model test results and analytical motion analyses for buoyant leg structure. In: Proceedings of 12th international offshore and polar engineering conference, Kitakushu, Japan, 26–31 May, pp 46–53

Caughey TK (1960) Classical normal modes in damped linear dynamic systems. J App Mech ASME 27:269–271

Chakarabarti SK, Hanna SY (1990) Added mass and damping of a TLP column model. In: Proceedings of the international offshore technology conference No. 4643, pp 533–545

Chakrabarti SK (2002) The theory and practice of hydrodynamics and vibration. World Scientific, Singapore

Chakrabarti SK (1987) Hydrodynamics of offshore structures: computational mechanics. WIT Press, Southampton

Chakrabarti SK (1990) Non-linear method in offshore engineering. Elsevier Science Publisher, The Netherlands

Chakrabarti SK (1994) Offshore structure modeling. World Scientific, Singapore

Chandrasekaran S, Jain AK, Madhuri S (2013) Aerodynamic response of offshore triceratops. Ship Offshore Struct 8(2):123–140. doi:10.1080/17445302.2012.691271

Chandrasekaran S (2015a) Dynamic analysis and design of ocean structures, 1st edn. Springer, India. ISBN 978-81-322-2276-7

Chandrasekaran S (2015b) Advanced marine structures. CRC Press, Florida (USA). ISBN 9781498739689

Chandrasekaran S (2015c) Dynamic analysis of offshore structures, video course on MOOC, NPTEL portal at https://onlinecourses.nptel.ac.in/noc15_oe01/preview

Chandrasekaran S (2016a) Offshore structural engineering: reliability and risk assessment. CRC Press, Florida. ISBN 978-14-987-6519-0

Chandrasekaran S (2016b) Risk and reliability of offshore structures, video course on MOOC, NPTEL portal at https://onlinecourses.nptel.ac.in/noc16_oe01/preview

Chandrasekaran S, Jain AK (2016) Ocean structures: construction, materials and operations. CRC Press, Florida. ISBN 978-14-987-9742-9

Chandrasekaran S, Jamshed N (2015) Springing and ringing response of offshore triceratops. In: Proceedings of 34th international conference on ocean, offshore and arctic engineering (OMAE 2015), St. John's, NL, Canada, 31 May–5 June 2015, OMAE2015-41551

Chandrasekaran S, Nannaware M (2013) Response analyses of offshore triceratops to seismic activities. Ship Offshore Struct 9(6):633–642. doi:10.1080/17445302.2013.843816

Chandrasekaran S, Madavi N (2014a) Retrofitting of offshore structural member using perforated cylinders. SFA Newsletter 13:10–11

Chandrasekaran S, Madhavi N (2014b) Hydrodynamic performance of retrofitted structural member under regular waves. Int J Forensic Eng Inder Sci 2(2):100–121

Chandrasekaran S, Madhavi N (2014c) Numerical study on geometrical configurations of perforated cylindrical structures. J Perform Constr Facil, ASCE 30(1):04014185. doi:10.1061/(ASCE)CF.1943-5509.0000687

Chandrasekaran S, Madhavi N (2014d) Variation of water particle kinematics with perforated cylinder under regular waves In: Proceedings of ISOPE 2014, 15–20 June, Busan, South Korea

Chandrasekaran S, Madhavi N (2015a) Estimation of force reduction on ocean structures with perforated members. In: Proceedings of 34th international conference on ocean, offshore and arctic engineering (OMAE2015), St. John's, NL, Canada, 31 May–5 June 2015, OMAE2015-41153

Chandrasekaran S, Madhavi N (2015b) Flow field around a outer perforated circular cylinder under regular waves: numerical study. Int J Marine Syst Ocean Technol. doi:10.1007/s40868-015-0008-1

Chandrasekaran S, Madhavi N (2015c) Design aids for offshore structures with perforated members. Ship Offshore Struct 10(2):183–203. doi:10.1080/17445302.2014.918309

Chandrasekaran S, Madhavi N (2015d) Retrofitting of offshore cylindrical structures with different geometrical configuration of perforated outer cover. Int J Shipbuild Prog 62(1–2):43–56. doi:10.3233/ISP-150115

Chandrasekaran S, Madhavi N (2015e) Variation of flow field around twin cylinders with and without outer perforated cylinder: numerical studies. China Ocean Eng 30(5):763–771

Chandrasekaran S, Madhuri S (2015) Dynamic response of offshore triceratops: numerical and experimental investigations. Ocean Eng 109(15):401–409. doi:10.1016/j.oceaneng.2015.09.042

Chandrasekaran S, Parameswara PS (2011) Response behavior of perforated cylinders in regular waves. In: Proceedings of 30th international conference on ocean, offshore and arctic engineering, OMAE 2011, Rotterdam, The Netherlands, 19–24 June 2011, OMAE 2011-49839

Chandrasekaran S, Senger M (2016) Dynamic analyses of stiffened triceratops under regular waves: experimental investigations. Ships Offshore Struct T&F, http://www.tandfonline.com/doi/full/10.1080/17445302.2016.1200957

Chandrasekaran S, Yuvraj K (2013) Dynamic analysis of a tension leg platform under extreme waves. J Naval Arch Mar Eng 10:59–68. doi:10.3329/jname.v10i1.14518

Chandrasekaran S, Lognath RS, Jain A (2015a) Dynamic analysis of buoyant leg storage and regasification platform under regular waves. In: Proceedings of 34th international conference on ocean, offshore and arctic engineering (OMAE 2015), St. John's, NL, Canada, 31 May–5 June 2015, OMAE2015-41554

Chandrasekaran S, Mayank S, Jain A (2015b) Dynamic response behavior of stiffened triceratops under regular waves: experimental investigations. In: Proceedings of 34th international conference on ocean, offshore and arctic engineering (OMAE 2015), St. John's, NL, Canada, 31 May–5 June 2015, OMAE2015-41376

Chandrasekaran S, Madhavi N, Natarajan C (2014) Variations of hydrodynamic characteristics with the perforated cylinder. In: Proceedings of 33rd international conference on ocean, offshore and arctic engineering, OMAE 2014, 8–13 June, San Francisco, USA

Chandrasekaran S, Merin T (2016) Suppression system for offshore cylinders under vortex induced vibration. Vibroeng Procedia 7:01–06

Chandrasekaran S (2013a) Dynamic of ocean structures. Web-based course on national program on technology enhanced learning, IIT Madras. Available at nptel.ac.in/courses/114106036

Chandrasekaran S (2013b) Ocean structures and materials. Web-based course on national program on technology enhanced learning, IIT Madras. Available at: nptel.ac.in/courses/114106035

Chandrasekaran S (2013c) Advanced marine structures. Web-based course on national program on technology enhanced learning, IIT Madras. Available at nptel.ac.in/courses/114106037

Chandrasekaran S (2014) Advanced theory on offshore plant FEED engineering. Changwon National University Press, Replublic of South Korea, p 237, ISBN 978-89-969792-8-9

Chandrasekaran S (2016) Offshore structural engineering: reliability and risk assessment. CRC Press, Florida. ISBN 978-14-987-6519-0

Chandrasekaran S, Jain AK (2002a) Dynamic behavior of square and triangular offshore tension leg platforms under regular wave loads. Ocean Eng 29(3):279–313

Chandrasekaran S, Jain AK (2002b) Triangular configuration tension leg platform behavior under random sea wave loads. Ocean Eng 29(15):1895–1928

Chandrasekaran S, Jain AK (2004) Aerodynamic behavior of offshore triangular tension leg platforms. In: Proceedings of ISOPE, Toulon, France, pp 564–569

Chandrasekaran S, Pannerselvam R (2009) Offshore structures: materials, analysis, design and construction. In: Proceedings of short course on offshore structures and materials, IITM, Chennai, 14–18 Dec, p 156

Chandrasekaran S, Gaurav (2008) Offshore triangular tension leg platform earthquake motion analysis under distinctly high sea waves. J Ships Offshore Struct 3(3):173–184

Chandrasekaran S, Bhaskar K, Hashim M (2010a) Experimental study on dynamic response behavior of multi-legged articulated tower. In: Proceedings of 29th international conference on ocean, offshore and arctic engineering, OMAE 6–11 June 2010 Shanghai, China

Chandrasekaran S, Bhaskar K, Harilal Lino Brijit R (2010b) Dynamic response behavior of multi-legged articulated tower with and without TMD, In: Proceedings of international conference of marine technology MARTEC–2010, 11–12 Dec, Dhaka, Bangladesh, pp 131–136

Chandrasekaran S, Jain AK, Chandak NR (2004) Influence of hydrodynamic coefficients in the response behavior of triangular TLPs in regular waves. Ocean Eng 31:2319–2342

Chandrasekaran S, Chandak NR, Gupta A (2006a) Stability analysis of TLP tethers. Ocean Eng 33 (3):471–482

Chandrasekaran S, Jain AK, Chandak NR (2006b) Seismic analysis of offshore triangular tension leg platforms. Int J Struct Stab Dyn 6(1):1–24

Chandrasekaran S, Jain AK, Chandak NR (2007) Response behavior of triangular tension leg platforms under regular waves using Stokes nonlinear wave theory. J Waterw Port Coast Ocean Eng, ASCE 133(3):230–237

Chandrasekaran S, Jain AK, Gupta A (2007a) Influence of wave approach angle on TLP's response. Ocean Eng 8–9(34):1322–1327

Chandrasekaran S, Jain AK, Gupta A, Srivastava A (2007b) Response behavior of triangular tension leg platforms under impact loading. Ocean Eng 34:45–53

Chandrasekaran S, Pannerselvam R, Saravanakumar S (2012) Retrofitting of offshore tension leg platforms with perforated cylinders. In: 3rd Asian conference on mechanics of functional materials and structures (ACFMS), 8–9 Dec, IIT Delhi

Chandrasekaran S, Seeram M, Jain AK, Gaurav (2010) Dynamic response of offshore triceratops under environmental loads. In: Proceedings of international conference of marine technology MARTEC, 11–12 Dec, Dhaka, Bangladesh, pp 61–66

Chandrasekaran S, Sharma A, Srivastava S (2007) Offshore triangular TLP behavior using dynamic Morison equation. J Struct Eng 34(4):291–296

Chandrasekaran S, Sundaravadivelu R, Pannerselvam R, Madhuri S (2011) Experimental investigations of offshore triceratops under regular waves. In: Proceedings of 30th international conference on ocean, offshore and arcticengineering, OMAE 2011, 19–24 June, Rotterdam, The Netherlands

Chandrsaekaran S, Bhattacharyya SK (2011) Analysis and design of offshore structures. HRD center for offshore and plant engineering (HOPE), Changwon National University, Republic of Korea, p 285

Charles WN, Robert CW, Capanoglu C (2005) Triceratops: an effective platform for developing oil and gas fields in deep and ultra deep water. In: Proceedings of 15th international offshore and polar engineering conference, 19–24 June, Seoul, Korea, pp 133–139

Chaudhury G, Dover W (1995) Fatigue analysis of offshore platforms subjected to sea wave loading. Int J Fatigue 7(1):13–19

Chen X, Ding Y, Zhang J, Liagre P, Neidzwecki J, Teigen P (2006) Coupled dynamic analysis of a mini TLP: comparison with measurements. Ocean Eng 33:93–117

Choi HS, Lou Jack YK (1991) Nonlinear behavior of an articulated offshore loading platform. Appl Ocean Res 13(2):63–74

Chopra AK (2003) Dynamics of structures: theory and applications to earthquake engineering, 2nd edn. Person Education, Singapore

Clauss GF, Birk L (1996) Hydrodynamic shape optimization of large offshore structures. J Appl Ocean Res 18:157–171

Clauss GT et al (1992) Offshore Structures, vol 1—conceptual design and hydromechanics. Springer, London

Copple RW, Capanoglu CC (1995) A buoyant leg structure for the development of marginal fields in deep water. In: Proceedings of fifth international offshore and polar engineering conference, 16–11 June, The Hague, The Netherlands, p 163

Davenport AG (1961) The Spectrum of horizontal gustiness near the ground in high winds. J Roy Meteorol Soc 87:194–211

Dawson TH (1983) Offshore structural engineering. Prentice-Hall, Englewood Cliffs, NJ

de Boom WC, Pinkster JA, Tan PSG (1984) Motion and tether force prediction of a TLP. J Waterw Port Coast Ocean Eng 110(4):472–486

Demirbilek Z (1990) Design formulae for offset, set down and tether loads of a tension leg platform (TLP). Ocean Eng 17(5):517–523

Devon R, Jablokow K (2010) Teaching FEED. In: Proceedings of Mid-Atlantic ASEE Conference, 15–16 Oct, Villanova University, Pennsylvania, USA.

DNV (1982) Rules for the design. Construction and Inspection of Offshore Structures, Det Norske Veritas, Oslo

DOE-OG (1985) Offshore installation: guidance on design and construction. U.K. Department of Energy, London

Dyrbe C, Hansen SV (1997) Wind loads on structures. John Wiley and Sons, U.K.

Ertas A, Eskwaro-Osire S (1991) Effect of damping and wave parameters on offshore structure under random excitation. Nonlinear Dyn 2:119–136

Ertas A, Lee JH (1989) Stochastic response of tension leg platform to wave and current forces. J Energy Res Technol 111:221–230

Faltinsen OM (1990) Sea loads on ships and offshore structures. Cambridge University Press, New York

Faltinsen OM, Newman JN, Vinje T (1995) Nonlinear wave loads on a slender vertical cylinder. J Fluid Mech 289:179–198

Gabbai RD, Benaroya H (2005) An overview of modeling and experiments of vortex-induced vibration of circular cylinders. J Sound Vib 282:575–616

Gadagi MM, Benaroya H (2006) Dynamic response of an axially loaded tendon of a tension leg platform. J Sound Vib 293:38–58

Gerwick BC Jr (1986) Construction of offshore structures. John Wiley, New York

Goldstein S (1929) Mathieu functions, Trans Cambridge Philosophical Society 23:303–36

Govardhan R, Williamson CHK (2000) Modes of vortex formation and frequency response of a freely vibrating cylinder. J Fluid Mech 420:85–130

Govardhan R, Williamson CHK (2002) Resonance forever: existence of a critical mass and an infinite regime of resonance in vortex-induced vibration. J Fluid Mech 473:147–166

Graff WJ (1981a) Introduction to offshore structures. Gulf Publishing Co., Houston

Graff WJ (1981b) Introduction to offshore structures: design. Fabrication and Installation. Gulf Publishing Co., Tokyo

Guo B, Song S, Chacko J, Ghalamber A (2005) Offshore pipelines. Gulf Professional Publishing, MA, USA

Gurley Kurtis R, Ahsan K (1998) Simulation of ringing in offshore systems under viscous loads. J Eng Mech ASCE 124(5):582–586

Gusto MSC (2010) The exploration market. InSide 15:4–7

Halkyard JE, Davies RL, Glanville RS (1991) The tension buoyant tower: a design for deep water. In: 23rd Annual Offshore Technology Conference, OTC 6700, 6–9 May, Houston, Texas, pp 41–55

Hancock JW, Gall DS (1985) Fatigue under narrow and broad band stationary loading. Final report of cohesive program of R&D in fatigue of offshore structures, Marine Tech. Directorate Ltd., Texas, USA

Haritos N (1985) Modeling the response of tension leg platforms to the effects of wind using simulated traces. Math Comput Simul 27:231–240

Haslum HA, Faltinsen OM (1999) Alternative shape of spar platforms for use in hostile areas. In: Proceedings of the 31st offshore technology conference, Houston, 217–228, (OTC 10953)

Helvacioglu IH, Incecik A (2004) Dynamics of double articulated towers, integrity of offshore structures 4. Elsevier, London

Hitchings GA, Bradshaw H, Labiosa TD (1976) Planning and execution of offshore site investigations for North Sea gravity platform. In: Proceedings of offshore technology conference, Paper No. 2430

Hoeg K (1976) Foundation engineering for fixed offshore structures. In: Proceedings first international conference behaviour of offshore structures vol 1. pp 39–69

Hove K, Foss I (1974) Quality assurance for offshore concrete gravity structures. In: Proceedings of offshore technology conference, Paper No. 2113

Hsu HT (1981) Applied offshore structural engineering. Gulf Publishing Co., Houston

Humphries JA, Walker DH (1987) Vortex excited response of large-scale cylinders in shear flow. Proc Sixth OMAE, Houston, TX 2:139–143

Ince EL (1925) Researches into the characteristic numbers of the Mathieu equation. In: Proceedings royal society of Edinburgh, vol 46. pp 20–29

Islam N, Ahmad S (2003) Nonlinear seismic response of articulated offshore tower. Defense Sci J 53(1):105–113

Issacson M, Det St Q (1982) Non-linear wave effects on fixed and floating bodies. J Fluid Mech 120:267–281

Iwaski H (1981) Preliminary design study of tension leg platform. MIT University

Jayalekshmi R, Sundaravadivelu R, Idichandy VG (2010) Dynamic analysis of deep water tension leg platforms under random waves. J Offshore Mech Arctic Eng 132(4):041605

Jefferys ER, Patel MH (1982) Dynamic analysis models of tension leg platforms. J Energy Res Technol 104:217–223

Jefferys ER, Rainey RCT (1994) Slender body models of TLP and GBS 'ringing'. BOSS, McGraw-Hill Inc., New York, NY

Anitha J, Idichandy VG, Bhattacharyya SK (2004) Experimental and numerical study of coupled dynamic response of a mini tension leg platform. J Offshore Mech Arctic Eng 126(4):318–330

Kam JCP, Dover WD (1988) Fast fatigue assessment procedure under random time history. Proc Inst Civil Eng Part 2 85:689–700

Kam JCP, Dover WD (1989) Advanced tool for fast assessment of fatigue under offshore random wave stress history. Proc Inst Civil Eng Part 2 87:539–556

Kawanishi T, Ohashi S, Takamura H, Koboyashi H (1993) Earthquake response of tension leg platform under unbalanced initial tension. Proc ISOPE, Singapore, pp 319–325

Kawanishi T, Katoh W, Furuta H (1987) Tension leg platform earthquake motion analysis. Oceans 19:543–547

Ker W-K, Lee C-P (2002) Interaction of waves and a porous tension leg platform. J Waterw Port Coast Ocean Eng 128(2):88–95

Khalak A, Williamson CHK (1991) Motions, forces and mode transitions in vortex induced vibrations at low mass-damping. J Fluids Struct 13:813–851

Kim C-H, Zou J (1995) A universal linear system model for kinematics and forces affected by nonlinear irregular waves. Int J Offshore Polar Eng 5(3):166–170

Kim C-H, Kim MH, Liu YH, Zhao CT (1994) Time domain simulation of nonlinear response of a coupled TLP system. Int J Offshore Polar Eng 4(4):281–291

Kim C-H, Lee C-H, Goo J-S (2007) A dynamic response analysis of tension leg platform including hydrodynamic interaction in regular waves. Ocean Eng 34(11–12):1680–1689

Kim C-H, Zhao CT, Zou J, Xu Y (1997) Springing and ringing due to laboratory-generated asymmetric waves. Int J Offshore Polar Eng 7(1):30–35

Kjeldsen SP, Myrhaug D (1979) Wave-wave interactions and wave-current interactions in deep water. In: Proceedings of 5th POAC conference Trondheirn, Norway, vol 111, p 179

Kobayashi M, Shimada K, Fujihira T (1987) Study on dynamic responses of a TLP in waves. J Offshore Mech Arctic Eng 109:61–66

Koo BJ, Kim MH, Randall RE (2004) Mathieu instability of a spar platform with mooring and risers. Ocean Eng 31(17–18):2175–2208

Kurian et al (2008) Parametric study of TLPs subjected to random waves. In: Proceedings of international conference on construction and building technology, Kuala Lumpur, Malaysia, pp 1–9

Kurian VJ, Idichandy VG, Ganapathy C (1993) Hydro dynamic response of tension leg platforms: a model. Exp Mech 33(3):212–217

Leffler WL, Pattarozzi R, Sterling G (2011) Deep-water petroleum: exploration and production. Pennwell Corp., Oklahoma, pp 350

Lesage F, Garthshore LS (1987) A method of reducing drag and fluctuating side force on bluff bodies. J Wind Eng Ind Aerodyn 25:229–245

Li Y, Liu Y, Teng B (2006) Porous effect parameter of thin permeable plates. Coast Eng 48 (4):309–336

Lloyd's Register (2005) Rules and regulations for the classification of mobile offshore units, London

Lognath RS (2017) Dynamic analyses of Buoyant leg storage and regasification platform under environmental loads. Ph.D thesis submitted to IIT Madras

Low YM (2009) Frequency domain analysis of a tension leg platform with statistical linearization of the tendon restoring forces. Mar Struct 22:480–503

Marthinsen T, Winterstein SR, Ude TC (1992) TLP fatigue due to second-order springing. Probabilistic methods and structural and geotechnical reliability. In: Proceedings of specialty conference, pp 455–458

Mather A (2000) Offshore engineering: an introduction, 2nd edn. Witherby & Co Ltd., London

Mathieu E (1868) Memoire sur le movement vibratoire d'une membrane de forme elliptique. Jour. de math.Pures et Appliquees (Jour.de Liouville) 13,137.

Matsuishi M, Endo T (1968) Fatigue of metals subjected to varying stresses. Japan Soc Mech Eng 3:37–40

Mercier JA (1982) Evolution of tension leg platform technology. In: Proceedings of 3rd international conference on the behaviour of offshore structures, MIT

Mercier RS (1997) Mars tension leg platform: use of scale model testing in the global design. In: Proceedings of offshore technology conference, OTC 8354-MS, 5–8 May, Houston, Texas

Michel WH (1999) Sea spectrum revisited. Mar Technol 36(4):211–227

Moe G, Verley RLP (1980) Hydrodynamic damping of offshore structures in wave and currents. In: Offshore technology conference, 12th annual OTC, Houston, Texas, pp 37–44

Muhuri PK, Gupta AS (1983) Stochastic stability of tethered buoyant platforms. Ocean Eng 10 (6):471–479

Mutlu Sumer B, Fredsoe J (2003) Hydrodynamics around cylindrical, revised edition. World Scientific Publishing Co. Pte. Ltd

Naess A, Moan T (2013) Stochastic dynamics of marine structures. Cambridge University Press, New York

Nagamani K, Ganapathy C (2000) Dynamic response of three leg articulated tower. Ocean Eng 27:1455–1471

Natvig BJ (1996) TLP installation without motion compensation. Proc ISOPE, Los Angeles, CA, USA 1:228–231

Natvig BJ (1994) A proposed ringing analysis model or higher order tether response. In: Proceedings of 4th international offshore and polar engineering conference, ISOPE, Golden, CO, pp 40–51

Natvig BJ, Vogel H (1995)TLP design philosophy—past, present, future. In: Proceedings of international conference offshore and polar engineers, The Hague, pp 64–69

Neelamani S, Muni Reddy MG (2002) Wave forces on a vertical cylinder defenced by a perforatedvertical and inclined barriers. Indian J Mar Sci 31(3):179–187

Neelamani S, Uday Bhaskar N, Vijayalakshmi K (2002) Wave forces on a seawater intake caisson. Ocean Eng 29(10):1247–1263

Nordgren RP (1987) Analysis of high frequency vibration of tension leg platforms. J Offshore Mech Arctic Eng 109:119–125

Owen JC (2003) Masa Brankovic experimental studies of passive control of vortex-induced vibration. J Fluids Struct 15:597–605

Paik JK, Thayamballi AK (2007) Ship-shaped offshore installations: design, building and operations. Cambridge University Press, New York

Paik I, Roesset JM (1996) Use of quadratic transfer functions to predict response of tension leg platforms. J Eng Mech 122(9):882–889

Patel MH, Park HI (1991) Dynamics of tension leg platform tethers at low tension. Part I—Mathieu stability at large parameters. Mar Struct 4(3):257–273

Patel MH (1989) Dynamics of offshore structures. Butterworth, London

Patel MH, Witz JA (1991) Compliant offshore structures. Butterworth-Heinemann Ltd., Oxford

Perryman SR, Horton EE, Halkyard JE (1995) Tension buoyant tower for small fields in deep waters. Offshore technology conference, OTC 7805, 1–4 May, Houston, Texas, pp 13–22

Pilotto BMR, Stocker R (2002) Dynamic response of shallow water mono-pod platforms. In: Proceedings of international conference offshore mechanics and arctic engineering, Oslo, Norway, vol 1, pp 113–120

Pilotto BMR, Stocker R (2003) Nonlinear dynamic analysis with deterministic and random seas. Oceans Conf Record (IEEE) 5:2908–2915

Pilotto BMR (2003) Dynamic behavior of minimum platforms under random loads. In: Proceedings of international conference offshore mechanics and arctic engineering, vol 1, Cancum, Mexico, pp 441–449

Reddy DV, Arockiasamy M (1991) Offshore structures, vol I. Kriger Publishing Co., Malabar, Florida

Rho JB, Choi HS, Lee WC, Shin HS, Park IK (2002) Heave and pitch motion of a spar platform with damping plate. In: Proceedings of the 12th international offshore and polar engineering conference, vol 1, Kitakyshu, pp 198–201

Rho JB, Choi HS, Lee WC, Shin HS, Park IK (2003) An experimental study for mooring effects on the stability of spar platform. In: Proceedings of the 13th international offshore and polar engineering conference, vol 1, Honolulu, HI, pp 285–288

Rijken OR, Niedzwecki JM (1991) A knowledge base approach to the design of tension leg platform. Center for Offshore Technology, Offshore Technology Research Center, Texas, pp 24–100

Robert WC, Capanoglu CC (1995) Buoyant Leg Structure for the development of marginal fields in deep water. In: Proceedings of international offshore and polar engineering conference, 11–16 June, The Hague, The Netherlands, pp 163

Rosetti GF, Gonçalves1 RT, Fujarra ALC (2011) Experimental comparisons to assure the similarity between VIM (vortex-induced motion) and VIV (vortex-induced vibration) Phenomena. doi:10.1115/OMAE2011-49011

Ney R, Andrade RFM, Batista RC (1992) Dynamic response analysis of small-scale model tension leg platform. Mar Struct 5:491–513

Sadehi K (1989) Design and analysis of marine structures. Khajeh Nasirroddin Tsi University of Technology, Tehran, Iran

Sadehi K (2001) Coasts, ports and offshore structures engineering. Power and Water University of Technology, Tehran, Iran

Sadehi K (2007) Offshore and petroleum platforms for cyprus oil/gas fields. J Soc Appl Sci 2(4):1–16

Sankarbabu K, Sannasiraj SA, Sundar V (2007) Interaction of regular waves with a group of dual porous circular cylinders. Appl Ocean Res 29(4):180–190

Sarpkaya T, Isaacson M (1981) Mechanics of wave forces on offshore structures. Van Nostrand Reinhold, New York

Sarpkaya T (1978) Fluid forces on oscillating cylinders. ASCE J Waterw Port Coast Ocean Div 104:275–290

Shaver CB, Capanoglu CC, Serrahn CS (2001) Buoyant leg structure preliminary design, constructed cost and model test results. In: Proceedings of 11th international offshore and polar engineering conference, Stavanger, Norway, 17–22 June, pp 432–439

Simos AN, Pesce CP (1997) Mathieu stability in the dynamics of TLP tether considering variable tension along the length. Trans Built Environ 29:175–186

Soding H, Blok JJ, Chen HH, Hagiwara K, Issacson M, Jankowski J, Jefferys ER, Mathisen J, Rask I, Richer JP, Romeling JU, Varsta P (1990) Environmental forces on offshore structures: a state-of-art review. Mar Struct 3:59–81

Son S (2006) Design of ocean platforms against ringing response. MS Thesis, Mechanical Engineering Department, Texas Tech University, Lubbock, TX, USA

Song H, Tao L (2007) Short-crested wave interaction with a concentric porous cylindrical structure. Appl Ocean Res 29(4):199–209

Stansberg CT, Ormberg H, Oritsland O (2002) Challenges in deep water experiments: hybrid approach. J Offshore Mech Arctic Eng 124:90–96

Stoke's GG (1880) On the theory of oscillatory waves. Math Phys Papers 1:225–228

Tabeshpour MR, Golafshani AA, Seif MS (2006) Comprehensive study on the results of tension leg platform responses in random sea. J Zhejiang University Sci 7(8):1305–1317

Tromans P, Swan C, Masterton S (2006) Nonlinear potential flow forcing: the ringing of concrete gravity based structures. Research Report No. 468, Ocean Wave Engineering Ltd, Health & Safety Executive Publication, Norwich, UK

Ude TC, Winterstein SR, Marthinsen T (1994) Volterra models for ocean structures: extreme and fatigue reliability. J Eng Mech ASCE 120(6):1369–1385

Vannucci P (1996) Simplified optimal design of tension leg platform TLP. Struct Optim 12:265–268

Vijayalakshmi K, Neelamani S, Sundaravadivelu R, Murali K (2007) Wave run up on a concentric twin perforated circular cylinder. Ocean Eng 34(2):327–336

Vijayalakshmi K, Sundaravadivelu R, Murali K, Neelamani S (2008) Hydrodynamics of a concentric twin perforated circular cylinder system. J Waterw Port Coast Ocean Eng 134 (3):166–177

Wang K-H, Ren X (1994) Wave interaction with a concentric porous cylinder system. Ocean Eng 21(4):343–360

White NC, Copple WR, Capanoglu C (2005) Triceratops: an effective platform for developing oil and gas fields in deep and ultra-deep water. In: Proceedings of 15th international offshore and polar engineering conference, 19–24 June, Seoul, Korea, pp 133–139

William AN, Li W (1998) Wave interaction with a semi-porous cylindrical breakwater mounted on a storage tank. Ocean Eng 25(2–3):195–219

William AN, Li W, Wang K-H (2000) Water wave interaction with a floating porous cylinder. Ocean Eng 27(1):1–28

Williams AN, Li W (2000) Water wave interaction with an array of bottom-mounted surface-piercing porous cylinders. Ocean Eng 27(8):841–866

Wilson JF (1984) Dynamics of offshore structures. Wiley Inter Science Publications, New York

Winterstein SR (1988) Nonlinear vibration models for extremes and fatigue. J Eng Mech ASCE 114(10):1772–1790

Wirsching P, Ortiz PK (2006) Random vibrations: theory and practice. Dover, NY

Wirsching PH, Light MC (1980) Fatigue under wide band random loading. J Str Div ASCE 1593–1607

Witz JA, Patel MH, Harrison JH (1986) On the hydrodynamics of semisubmersibles with articulated members. Proc Roy Soc London Ser A Math Phys Sci 403:81–109

Yan, F-S, Zhang D-G, Sun, L-P, Dai Y-S (2009) Stress verification of a TLP under extreme wave environment. J Mar Sci Appl 8:132–136

Yoneya T, Yoshida K (1982) The dynamics of tension leg platforms in waves. J Energy Res Technol 104:20–28

Yoshida K, Ozaki M, Oka N (1984) Structural response analysis of tension leg platforms. J Energy Res 106:10–17

Young AG, Kraft LM, Focht JA (1975) Geotechnical considerations in foundation design of offshore gravity structures. In: Proceedings of offshore technology conference, Paper No. 2371

Zdravkovich MM (1981) Review. classification of various aerodynamic and hydrodynamic means for suppressing vortex shedding. J Wind Eng Ind Aerodyn 7:145–189

Zeng X et al (2007) Parametric studies of tension leg platform with large amplitude motions. In: Proceedings of 17th international offshore and polar engineering conference, Lisbon, Portugal, pp 202–209

Zhao F, Bao W, Kinoshita T, Itakura H (2009) Interaction of waves and a porous cylinder with an inner horizontal porous plate. Appl Ocean Res 32(2):252–259

Zhong Z, Wang KH (2006) Solitary wave interaction with a concentric porous cylinder system. Ocean Eng 33(7):927–949

Index